National Library
of Canada

Canadian Theses Service

Ottawa, Canada
K1A 0N4

Bibliothèque nationale
du Canada

Services des thèses canadiennes

CANADIAN THESES

THÈSES CANADIENNES

NOTICE

The quality of this microfiche is heavily dependent upon the quality of the original thesis submitted for microfilming. Every effort has been made to ensure the highest quality of reproduction possible.

If pages are missing, contact the university which granted the degree.

Some pages may have indistinct print especially if the original pages were typed with a poor typewriter ribbon or if the university sent us an inferior photocopy.

Previously copyrighted materials (journal articles, published tests, etc.) are not filmed.

Reproduction in full or in part of this film is governed by the Canadian Copyright Act, R.S.C. 1970, c. C-30.

AVIS

La qualité de cette microfiche dépend grandement de la qualité de la thèse soumise au microfilmage. Nous avons tout fait pour assurer une qualité supérieure de reproduction.

S'il manque des pages, veuillez communiquer avec l'université qui a conféré le grade.

La qualité d'impression de certaines pages peut laisser à désirer, surtout si les pages originales ont été dactylographiées à l'aide d'un ruban usé ou si l'université nous a fait parvenir une photocopie de qualité inférieure.

Les documents qui font déjà l'objet d'un droit d'auteur (articles de revue, examens publiés, etc.) ne sont pas microfilmés.

La reproduction, même partielle, de ce microfilm est soumise à la Loi canadienne sur le droit d'auteur, SRC 1970, c. C-30.

THIS DISSERTATION
HAS BEEN MICROFILMED
EXACTLY AS RECEIVED

LA THÈSE A ÉTÉ
MICROFILMÉE TELLE QUE
NOUS L'AVONS REÇUE

NL-339 (r.86/06)

Canada

THE UNIVERSITY OF ALBERTA

# Synoptic Cloud Analysis and Development

by

© Farouk Mohamed Helmy Safwat

A THESIS

SUBMITTED TO THE FACULTY OF GRADUATE STUDIES AND RESEARCH

IN PARTIAL FULFILMENT OF THE REQUIREMENTS FOR THE DEGREE

OF Master of Science

IN

Meteorology

Geography

EDMONTON, ALBERTA

Spring 1986

Permission has been granted to the National Library of Canada to microfilm this thesis and to lend or sell copies of the film.

L'autorisation a été accordée à la Bibliothèque nationale du Canada de microfilmer cette thèse et de prêter ou de vendre des exemplaires du film.

The author (copyright owner) has reserved other publication rights, and neither the thesis nor extensive extracts from it may be printed or otherwise reproduced without his/her written permission.

L'auteur (titulaire du droit d'auteur) se réserve les autres droits de publication; ni la thèse ni de longs extraits de celle-ci ne doivent être imprimés ou autrement reproduits sans son autorisation écrite.

ISBN 0-315-30294-1

THE UNIVERSITY OF ALBERTA

RELEASE FORM

NAME OF AUTHOR Farouk Mohamed Helmy Safwat

TITLE OF THESIS Synoptic Cloud Analysis and Development

DEGREE FOR WHICH THESIS WAS PRESENTED Master of Science

YEAR THIS DEGREE GRANTED Spring 1986

Permission is hereby granted to THE UNIVERSITY OF ALBERTA LIBRARY to reproduce single copies of this thesis and to lend or sell such copies for private, scholarly or scientific research purposes only.

The author reserves other publication rights, and neither the thesis nor extensive extracts from it may be printed or otherwise reproduced without the author's written permission.

(SIGNED) Farouk Safwat

PERMANENT ADDRESS:

12 Menasha Street,
Moharem Bay, Alexandria
Egypt

DATED 11 December 1985

THE UNIVERSITY OF ALBERTA

FACULTY OF GRADUATE STUDIES AND RESEARCH

The undersigned certify that they have read, and recommend to the Faculty of Graduate Studies and Research, for acceptance, a thesis entitled Synoptic Cloud Analysis and Development submitted by Farouk Mohamed Helmy Safwat in partial fulfilment of the requirements for the degree of Master of Science in Meteorology.

E R Reinelt

Supervisor

Keith A. Hage

Date 11 December 1985

# Dedication

To my loving wife *Hanan*

whose support and

encouragement were

behind the success

of this work

## Abstract

Based on Spring and Summer 1983 satellite and synoptic data over Western Canada, two synoptic studies are presented. The first involves a synoptic classification of cloud patterns, and the second is a model of cyclogenesis and development for the upper-level cold low.

Based on results of the first study, a definition and a revised classification for synoptic patterns have been proposed. Three characteristics are used to classify cloud systems into four groups: cloud bands, vortex clouds, cellular clouds, and uniform cloud areas. Each group includes a number of specific cloud patterns and different meteorological parameters. The proposed classification adds to, and extends previous models introduced by other investigators.

In the second study, a new analysis of the mechanism of upper-level development, based on cloud pattern structure, has been carried out and a definition for weakening and strengthening has been introduced. The different stages of cloud pattern cyclogenesis and development are discussed in relation to the low-level synoptic pattern, to the topography of the 500-mb surface, the vorticity field, the thickness field of the layer 1000/500 mb, and to the jet-stream system at 250-mb. The model compares well with other models suggested by other authors.

Upper-level cyclone developments can be classified into two regimes, termed modified and pure. A modified system is associated with a low-level frontal system, while a pure system is not. It was found that upper-level cyclone intensification, (based on cloud pattern structure) within the vorticity contour greater than 16 X $10^{-5}$ $s^{-1}$, may be expected in 82 per cent of the cases, while weakening within a vorticity contour of less than 16 X $10^{-5}$ $s^{-1}$ is likely in 74 per cent of the cases.

## Acknowledgments

I would like to thank my supervisor, Dr. E. R. Reinelt, for his support and guidance during the course of this work. I would like, also, to thank Dr. K. Hage and Dr. R. Gerard who served on my examining committe.

Many thanks are due to a number of people; Mr. J. Ballus and Mr. L. Walker in Alberta Weather Centre; Mr. R. Pakan, Mr. J. Chesterman, and Mr. P. Hof in Geography Department. My sincere gratitude goes to Dr. J. Roesseler whose help and assistance are appreciated. At last, I would like to thank Mrs. Laura Smith for her time and help.

This work was completed while on leave of absence from the Meteorological Authority of Egypt.

## Table of Contents

Chapter Page

1. A Review of Synoptic Scale Studies ..... 1

1.1 Introduction ..... 1

1.2 Synoptic Scales of Motion ..... 2

1.3 General Characteristics of Cloud Systems ..... 2

1.3.1 Introduction ..... 2

1.3.2 Definitions ..... 3

1.4 Anderson's Classification of Cloud Systems ..... 3

1.4.1 Meso-scale Cloud System ..... 3

1.4.2 Sub-synoptic Scale Cloud System ..... 4

1.4.3 Synoptic-Scale Cloud System ..... 4

1.4.3.1 Cloud Band Pattern ..... 5

1.4.3.2 Spiral Cloud Pattern ..... 5

1.4.3.3 Cellular Cloud Pattern ..... 5

1.4.4 Planetary-Scale Cloud System ..... 5

1.5 Anderson's Classification of Synoptic Scale Cloud System ..... 5

1.5.1 Cloud Band Group ..... 5

1.5.1.1 Frontal Bands ..... 6

1.5.1.2 Non-Frontal Bands ..... 6

1.5.1.3 Jet-Stream Bands ..... 6

1.5.2 Vortices Cloud Group ..... 7

1.5.2.1 Low-Level Vortices ..... 7

1.5.2.2 Enhanced Cumuli-Comma Shaped Cloud Areas ..... 7

1.5.2.3 Upper-Level Vortices ..... 7

1.5.3 Cellular Cloud Group ..... 8

1.5.3.1 Open Cellular Cloud Pattern ..... 8

1.5.3.2 Closed Cellular Cloud Pattern ..... 8

1.6 Zwatz-Meise's Classification of Synoptic-Scale Cloud System ........................ 9
1.6.1 Cloud Band Group ........................ 9
1.6.1.1 Frontal Band Pattern ........................ 9
1.6.1.2 Non-Frontal Cloud Band Pattern ........................ 11
1.6.2 Vortices Cloud Group ........................ 12
1.6.2.1 Low-Level Vortex ........................ 13
1.6.2.2 Upper-Level Vortex ........................ 13
1.6.2.3 Comma Configuration Cloud Pattern ........................ 13
1.6.3 Cellular Cloud Group ........................ 14
1.6.3.1 Open Cellular Pattern ........................ 14
1.6.3.2 Closed Cellular Pattern ........................ 15
1.6.4 Uniform Cloud Area Group ........................ 15
1.7 The Purpose Of The Study ........................ 16
2. Data Analysis ........................ 18
2.1 Introduction ........................ 18
2.2 Satellite Data ........................ 18
2.2.1 Factors Affecting Satellite Images ........................ 18
2.2.1.1 Image Resolution ........................ 18
2.2.1.2 Frequency Range ........................ 19
2.2.1.3 The Time Of The Day And The Viewing Angle ........................ 21
2.2.1.4 The Sector Of The Satellite Image ........................ 21
2.2.1.5 Accuracy of Gridding ........................ 21
2.2.2 Satellite Image Enhancement ........................ 23
2.2.2.1 Different Enhancement Curves ........................ 26
2.2.2.2 Examples Of Enhanced Curves ........................ 28
2.2.3 Polar Orbiting Satellite ........................ 28
2.2.3.1 Satellite Parameters ........................ 34

2.2.3.2 Satellite Characteristics ........ 34

2.2.3.3 Satellite Scanning ........ 35

2.2.3.4 Satellite Gridding ........ 35

2.2.3.5 Satellite Resolution ........ 38

2.2.4 Geostationary Satellites ........ 38

2.2.4.1 GOES Satellite Parameters ........ 38

2.2.4.2 Satellite Characteristics ........ 40

2.3 Synoptic Data ........ 40

2.3.1 Methods Of Analysis ........ 41

2.4 Selection Of Samples ........ 41

2.5 Synoptic Scale Cloud System Classification ........ 44

2.5.1 Introduction ........ 45

2.5.2 Cloud Bands Group ........ 45

2.5.2.1 The Frontal Cloud Band ........ 46

2.5.2.2 Pre-Frontal Cloud Band ........ 47

2.5.2.3 Post-Frontal Cloud Band ........ 52

2.5.2.4 Convergence Cloud Band ........ 57

2.5.2.5 Orographic Cloud Band ........ 60

2.5.2.6 Shear Cloud Band ........ 60

2.5.2.7 Jet Cloud Band ........ 66

2.5.2.8 Non-Frontal Cloud Band ........ 72

2.5.3 Vortex Cloud Group ........ 72

2.5.3.1 Low-Level Vortex ........ 74

2.5.3.2 Upper-Level Vortex ........ 75

2.5.3.3 Comma Cloud Pattern ........ 79

2.5.4 Cellular Cloud Group ........ 79

2.5.4.1 Open Cellular Pattern ........ 81

2.5.4.2 Closed Cellular Pattern ........ 82

2.5.4.3 Non-Organized Pattern ........ 82

2.5.5 Uniform Area Cloud Group ........ 83

2.5.5.1 Fog or Stratus Cloud Pattern ........ 83

2.5.5.2 Mid-Level Stratified Cloud Pattern ........ 84

3. Cyclogenesis and Upper-Level Development ........ 87

3.1 Cyclogenesis ........ 87

3.1.1 The definition Of Synoptic Cyclogenesis ........ 87

3.1.2 Early Studies ........ 87

3.1.3 Divergence Theories ........ 88

3.1.4 Pattern of Cyclogenesis on Satellite Images ........ 88

3.1.4.1 Baroclinic-Zone Cyclogenesis ........ 89

3.1.4.2 Split-Flow Cyclogenesis ........ 93

3.1.4.3 Cold-Air Vortex Cyclogenesis ........ 97

3.1.4.4 Induced-Wave Cyclogenesis ........ 100

3.2 Diffluence-Confluence And Jet Streams ........ 105

3.2.1 Confluence-Diffluence ........ 105

3.2.2 Jet Stream And Cyclogenesis ........ 107

3.2.2.1 Definition ........ 107

3.2.2.2 Early Studies ........ 107

3.3 Petterssen's Model of Upper-Level Development ........ 111

3.3.1 Petterssen-Smebye Hypothesis ........ 111

3.3.2 An Example of a Pure Case of Upper-Level Cyclogenesis ........ 112

3.3.3 An Example of a Modified Case of Upper-Level Cyclogenesis ........ 116

3.4 Zwatz-Meise's Model of Upper-Level Lows ........ 120

3.4.1 The Trough Stage ........ 121

3.4.2 The Pinch-Off Stage ........ 122

3.4.3 The Split-Off Stage .......... 122

3.4.4 The Cut-Off Stage .......... 123

3.4.5 The Decay Stage .......... 124

3.4.6 Summary and General Remarks .......... 124

4. Upper-Level Low Case Studies .......... 128

4.1 Introduction .......... 128

4.2 Case #1 .......... 131

4.3 Case #2 .......... 161

4.4 Case #3 .......... 189

4.5 Case #4 .......... 209

4.6 Case #5 .......... 230

4.7 Case #6 .......... 247

5. Results of the Study .......... 270

5.1 General Outline .......... 270

5.2 Synoptic Scale Cloud Pattern Classification .......... 270

5.3 The Upper-Cold Low Model .......... 271

5.3.1 The Troughing Stage .......... 272

5.3.2 The Splitting Stage .......... 272

5.3.3 The Pinching-off Stage .......... 273

5.3.4 The Cutting-off Stage .......... 273

5.3.5 The Mature Stage .......... 274

5.3.6 The Decay Stage .......... 274

5.4 Results and Conclusions .......... 278

5.5 Suggestions for Future Studies .......... 281

Bibliography .......... 282

# List of Figures

Figure Page

2.1 Attenuation effect. ........ 20

2.2 Contamination effect. ........ 20

2.3 Sun angle effect, a) May 11, 1983, 2107Z, NOAA-7. b) May 11, 1983, 2248Z, NOAA-7 ........ 22

2.4 Infrared calibration data (adapted from Clark 1983). ........ 24

2.5 Enhancement graph and equivalent temperature transfomations. ........ 25

2.6 Different enhancement curves. ........ 27

2.7 Infrared wrapped enhancement (adapted from Clark 1983). ........ 29

2.8 Enhancement curve MB. ........ 30

2.9 Enhancement curve ZA. ........ 30

2.10 Infrared steep sliced enhancement (adapted from Clark 1983). ........ 31

2.11 Polar orbital satellite main parts. ........ 32

2.12 A descending node orbit. ........ 33

2.13 An ascending node orbit. ........ 33

2.14 Satellite orbital path and system. ........ 36

2.15 Satellite paths overlapping. ........ 36

2.16 Computer produced overlay for NOAA-7 satellite pass #N (adapted from Alberta Weather Centre). ........ 37

2.17 Computer produced overlay for NOAA-7 satellite pass #N+1 (adapted from Alberta Weather Centre). ........ 37

2.18 GOES-E and GOES-W (geostationary satellites) overlap area coverage (adapted from Clark 1983). ........ 39

2.19 GOES satellite area coverage. ........ 39

2.20 Reconstructed satellite overlay. ........ 42

2.21 NOAA-6 satellite image, a) visible, b) infrared, 1635 GMT, 01 April 1983. ........ 48

Figure Page

2.21.1 01 April 1983, 1200 GMT dashed line: zero isolpeth of relative vorticity at 500-mb, dashed-dotted line: thermal front parameter for the layer 1000/500 mb. .......... 49

2.24.1 01 July 1983, 1200 GMT dashed line: zero isopleth of relative vorticity at 500 mb, dashed-dotted line: thermal front parameter for the layer 1000/500 mb. .......... 49

2.22 NOAA-8 satellite image, a) infrared, b) visible, 1501 GMT, 18 September 1983. .......... 50

2.23 NOAA-7 satellite image, a) visible, b) infrared, 2306 GMT, 23 April 1983. .......... 53

2.23.1 24 April 1983, 0000 GMT, CMC 500-mb analysis, dashed lines: thickness contours for the layer 500/1000 mb. .......... 54

2.24 NOAA-8 satellite image, a) visible, b) infrared, 1642 GMT, 01 July 1983. .......... 55

2.24.2 01 July 1983, 1200 GMT, CMC 500-mb analysis, dashed lines: thickness contours for the layer 500/1000 mb. .......... 56

2.25 NOAA-7 satellite image, a) visible, b) infrared, 2316 GMT, 14 April 1983. .......... 58

2.26 NOAA-7 satellite image, a) infrared, b) visible, 2321 GMT, 27 June 1983. .......... 58

2.25.1 15 April 1983, 0000 GMT, dashed lines: thickness contours for the layer 850/700 mb, solid lines: thickness contours for the layer 500/250 mb. .......... 59

2.26.1 28 June 1983, 0000 GMT, dashed lines: thickness contours for the layer 850/700 mb, solid lines: thickness contours for the layer 500/250 mb. .......... 59

2.27 NOAA-7 satellite image, a) infrared, b) visible, 2316 GMT, 14 April 1983. .......... 61

2.28 NOAA-7 satellite image, a) visible, b) infrared, 1650 GMT, 13 April 1983. .......... 61

2.27.1 15 April 1983, 0000 GMT, CMC 500-mb analysis, dashed lines: thickness contours for the layer 500/1000 mb. .......... 62

2.28.1 13 April 1983, 1200 GMT, CMC 500-mb analysis, dashed lines: thickness contours for the layer 500/1000 mb. .......... 63

Figure Page

2.29 NOAA-8 satellite image, infrared, 0258 GMT, 10 July 1983. ........ 64

2.30 NOAA-7 satellite image, infrared, 1035 GMT, 03 April 1983. ........ 64

2.29.1 10 July 1983, 0000 GMT, CMC 500-mb analysis, dashed lines: thickness contours for the layer 500 / 1000 mb, dashed-dotted lines: absolute vorticity field ( $*10^{-5}$ $s^{-1}$ ). ........ 65

2.30.1 03 April 1983, 0000 GMT, CMC 500-mb analysis, dashed lines: thickness contours for the layer 500 / 1000 mb, dashed-dotted lines: absolute vorticity field ( $*10^{-5}$ $s^{-1}$ ). ........ 65

2.31 NOAA-7 satellite image, a) infrared, b) visible, 2351 GMT, 03 April 1983. ........ 67

2.32 NOAA-8 satellite image, a) visible, b) infrared, 1434 GMT, 10 September 1983. ........ 68

2.32.1 10 September 1983, 1200 GMT, dashed lines: thickness contours for the layer 700 / 300 mb, arrows: jet stream at 250-mb surface. ........ 69

2.33 NOAA-6 satellite image, a) visible, b) infrared, 1615 GMT, 04 June 1983. ........ 70

2.34 NOAA-8 satellite image, a) visible, b) infrared, 1527 GMT, 06 August 1983. ........ 70

2.33.1 04 June 1983, 1200 GMT, CMC 250-mb analysis, dashed lines: isotaches, arrows: jet stream. ........ 71

2.34.1 06 June 1983, 1200 GMT, CMC 250-mb analysis, dashed lines: isotaches, arrows: jet stream. ........ 71

2.35 NOAA-7 satellite image, infrared, 0039 GMT, 25 July 1983. ........ 73

2.36 NOAA-7 satellite image, infrared, 0015 GMT, 02 July 1983. ........ 73

2.37 NOAA-8 satellite image, a) visible, b) infrared, 0358 GMT, 23 June 1983. ........ 73

2.38 NOAA-6 satellite image, a) visible, b) infrared, 1521 GMT, 12 May 1983. ........ 76

2.39 NOAA-8 satellite image, a) visible, b) infrared, 1756 GMT, 27 August 1983. ........ 77

Figure Page

2.40 NOAA-6 satellite image, a) visible, b) infrared, 1457 GMT, 13 May 1983. .......... 78

2.41 NOAA-8 satellite image, a) infrared, b) visible, 1458 GMT, 12 August 1983. .......... 80

2.42 NOAA-8 satellite image, a) visible, b) infrared, 1757 GMT, 13 August 1983. .......... 85

2.43 NOAA-6 satellite image, a) visible, b) infrared, 1617 GMT, 27 April 1983. .......... 85

2.44 NOAA-6 satellite image, a) visible, b) infrared, 1536 GMT, 24 May 1983. .......... 86

2.45 NOAA-8 satellite image, a) visible, b) infrared, 1717 GMT, 21 September 1983. .......... 86

3.1 The early stage of baroclinic-zone cyclogenesis .......... 91

3.2 The second stage of development .......... 91

3.3 The third stage of development .......... 92

3.4 The fourth stage of development .......... 92

3.5 The last stage of development .......... 95

3.6 The first stage of split-flow cyclogenesis .......... 95

3.7 The second stage of development .......... 96

3.8 The third stage of development .......... 96

3.9 The last stage of split-flow development .......... 98

3.10 The first stage of cold-air vortex cyclogenesis .......... 98

3.11 The second stage of development .......... 99

3.12 The third stage of development .......... 99

3.13 The last stage of cold-air vortex cyclogenesis .......... 102

3.14 The first stage of induced-wave cyclogenesis .......... 102

3.15 The second stage of development .......... 103

3.16 The third stage of development .......... 103

Figure Page

3.17 The last stage of development ........ 104

3.18 Contour confluence is due to southerly warm flow with northerly cold flow ........ 104

3.19 Different possible flow patterns and the associated orthogonal radius of curvature for each pattern ........ 106

3.20 Jet-stream upper level model and the associated low-level development (adapted from Reiter, 1963) ........ 109

3.21 Different models of upper-level flow patterns (adapted from Riehl, 1954) ........ 109

3.22 500-mb chart, adapted from Petterssen and Smebye (1971) ........ 113

3.23 500-mb chart, adapted from Petterssen and Smebye (1971) ........ 113

3.24 500-mb chart, adapted from Petterssen and Smebye (1971) ........ 113

3.25 500-mb chart, adapted from Petterssen and Smebye (1971) ........ 113

3.26 Isallobaric analysis, adapted from Petterssen and Smebye (1971) ........ 114

3.27 Thickness analysis for the layer 850/500 mb, adapted from Petterssen and Smebye (1971) ........ 114

3.28 Thickness analysis for the layer 850/500 mb, adapted from Petterssen and Smebye (1971) ........ 114

3.29 Thickness analysis for the layer 850/500 mb, adapted from Petterssen and Smebye (1971) ........ 114

3.30 The kinetic energy anslysis for different layers during the lifetime of the system, SFC: surface, adapted from Petterssen and Smebye (1971) ........ 115

3.31 The horizontal kinetic energy distribution, adapted from Petterssen and Smebye (1971) ........ 115

3.32 The vertical kinetic energy distribution, adapted from Petterssen and Smebye (1971) ........ 115

3.33 500-mb chart, adapted from Petterssen and Smebye (1971) ........ 117

Figure Page

3.34 500-mb chart, adapted from Petterssen and Smebye (1971) ........ 117

3.35 500-mb chart, adapted from Petterssen and Smebye (1971) ........ 117

3.36 500-mb chart, adapted from Petterssen and Smebye (1971) ........ 117

3.37 Thickness analysis for the layer 850/500 mb, adapted from Petterssen and Smebye (1971) ........ 118

3.38 Thickness analysis for the layer 850/500 mb, adapted from Petterssen and Smebye (1971) ........ 118

3.39 Thickness analysis for the layer 850/500 mb, adapted from Petterssen and Smebye (1971) ........ 118

3.40 Thickness analysis for the layer 850/500 mb, adapted from Petterssen and Smebye (1971) ........ 118

4.41 The kinetic energy anslysis for different layers during the lifetime of the system, SFC: surface, adapted from Petterssen and Smebye (1971) ........ 119

3.42 The horizontal kinetic energy distribution, adapted from Petterssen and Smebye (1971) ........ 119

3.43 The vertical kinetic energy distribution, adapted from Petterssen and Smebye (1971) ........ 119

3.44 The troughing stage, solid lines: 500-mb contours, dashed line: stability index, F: frontal band, B: comma developed area, and *: surface low centre ........ 125

3.45 The pinching-off stage, solid lines: 500-mb contours, dashed line: stability index, F: frontal band, B: comma developed area, and *: surface low centre ........ 125

3.46 The splitting-off stage, solid lines: 500-mb contours, dashed line: stability index, F: frontal band, B: comma developed area, D: cellular cloud area, and *: surface low centre ........ 126

3.47 The cutting-off stage, solid lines: 500-mb contours, dashed line: stability index, B: comma developed area, D: cellular cloud area, A and C: stratiform cloud areas, and *: surface low centre ........ 126

Figure Page

3.48 The decay stage, solid lines: 500-mb contours, dashed line: stability index, B: comma developed area, D: cellular cloud area, and *: surface low centre ..... 127

4.1 NOAA-7 satellite image, a) visible, b) infrared, 2301 GMT, 10 May 1983. ..... 135

4.2 CMC 500-mb analysis, 11 May 1983, 0000 GMT, solid lines: height contours, dashed lines: thickness field (500/1000 mb), dash-dotted: absolute vorticity ($*10^{-5}$ $s^{-1}$) and arrows: jet stream (250-mb). ..... 136

4.3 CMC 850-mb analysis, 11 May 1983, 0000 GMT, solid lines: height contours, dashed lines: isotherms. ..... 137

4.4 NOAA-6 satellite image, a) visible, b) infrared, 1545 GMT, 11 May 1983. ..... 138

4.5 NOAA-7 satellite image, infrared, 1115 GMT, 11 May 1983. ..... 138

4.6 The same as in Figure 4.2 except for 11 May 1983, 1200 GMT. ..... 139

4.7 The same as in Figure 4.3 except for 11 May 1983, 1200 GMT. ..... 140

4.8 NOAA-7 satellite image, a) visible, b) infrared, 2106 GMT, 11 May 1983. ..... 141

4.9 GOES-E satellite image, 100.0 W, visible, 0001 GMT, 12 May 1983. ..... 142

4.12 NOAA-7 satellite image, infrared, 1102 GMT, 12 May 1983. ..... 142

4.10 The same as in Figure 4.2 except for 12 May 1983, 0000 GMT. ..... 143

4.11 The same as in Figure 4.3 except for 12 May 1983, 0000 GMT. ..... 144

4.13 The same as in Figure 4.2 except for 12 May 1983, 1200 GMT. ..... 145

4.14 The same as in Figure 4.3 except for 12 May 1983, 1200 GMT. ..... 146

4.15 NOAA-7 satellite image, a) visible, b) infrared, 2055 GMT, 12 May 1983. ..... 147

Figure Page

4.16 NOAA-6 satellite image, a) visible, b) infrared, 0109 GMT, 13 May 1983. .......... 148

4.17 The same as in Figure 4.2 except for 13 May 1983, 0000 GMT. .......... 149

4.18 The same as in Figure 4.3 except for 13 May 1983, 0000 GMT. .......... 150

4.19 NOAA-7 satellite image, infrared, 1050 GMT, 13 May 1983. .......... 151

4.20 The same as in Figure 4.2 except for 13 May 1983, 1200 GMT. and dashed-lines: isotherms. .......... 152

4.21 The same as in Figure 4.3 except for 13 May 1983, 1200 GMT. .......... 153

4.22 NOAA-7 satellite image, a) visible, b) infrared, 2043 GMT, 13 May 1983. .......... 154

4.23 NOAA-6 satellite image, a) visible, b) infrared, 0046 GMT, 14 May 1983. .......... 155

4.24 The same as in Figure 4.2 except for 14 May 1983, 0000 GMT. .......... 156

4.25 The same as in Figure 4.3 except for 14 May 1983, 0000 GMT. .......... 157

4.26 NOAA-7 satellite image, infrared, 1038 GMT, 14 May 1983. .......... 158

4.27 NOAA-6 satellite image, visible, 1434 GMT, 14 May 1983. .......... 158

4.28 The same as in Figure 4.2 except for 14 May 1983, 1200 GMT. .......... 159

4.29 The same as in Figure 4.3 except for 14 May 1983, 1200 GMT. .......... 160

4.30 The same as in Figure 4.2 except for 22 June 1983, 1200 GMT. .......... 164

4.31 The same as in Figure 4.3 except for 22 June 1983, 1200 GMT. .......... 165

4.32 NOAA-8 satellite image, a) visible, b) infrared 1636 GMT, 22 June 1983. .......... 166

Figure Page

4.33 NOAA-7 satellite image, a) visible, b) infrared 2240 GMT, 22 June 1983. .......... 167

4.34 The same as in Figure 4.2 except for 23 June 1983, 0000 GMT. .......... 168

4.35 The same as in Figure 4.3 except for 23 June 1983, 0000 GMT. .......... 169

4.36 NOAA-7 satellite image, infrared, 1236 GMT, 23 June 1983. .......... 170

4.37 NOAA-8 satellite image, infrared, 1614 GMT, 23 June 1983. .......... 170

4.38 The same as in Figure 4.2 except for 23 June 1983, 1200 GMT. .......... 171

4.39 The same as in Figure 4.3 except for 23 June 1983, 1200 GMT. .......... 172

4.40 NOAA-8 satellite image, a) visible, b) infrared 0202 GMT, 24 June 1983. .......... 173

4.41 The same as in Figure 4.2 except for 24 June 1983, 0000 GMT. .......... 174

4.42 The same as in Figure 4.3 except for 24 June 1983, 0000 GMT. .......... 175

4.43 The same as in Figure 4.2 except for 24 June 1983, 1200 GMT. .......... 176

4.44 The same as in Figure 4.3 except for 24 June 1983, 1200 GMT. .......... 177

4.45 NOAA-8 satellite image, a) visible, b) infrared, 1552 GMT, 24 June 1983. .......... 178

4.46 NOAA-7 satellite image, a) visible, b) infrared, 2215 GMT, 24 June 1983. .......... 179

4.47 The same as in Figure 4.2 except for 25 June 1983, 0000 GMT. .......... 180

4.48 The same as in Figure 4.3 except for 25 June 1983, 0000 GMT. .......... 181

4.49 NOAA-7 satellite image, a) visible, b) infrared, 1211 GMT, 25 June 1983. .......... 182

Figure Page

4.50 The same as in Figure 4.2 except for 25 June 1983. 1200 GMT. .................... 183

4.51 The same as in Figure 4.3 except for 25 June 1983. 1200 GMT. .................... 184

4.52 NOAA-7 satellite image, a) visible, b) infrared. 2203 GMT. 25 June 1983. .................... 185

4.53 The same as in Figure 4.2 except for 26 June 1983. 0000 GMT. .................... 186

4.54 The same as in Figure 4.3 except for 26 June 1983. 0000 GMT. .................... 187

4.55 NOAA-8 satellite image, a) visible 0119 GMT, b) infrared 0119-0259 GMT, 26 June 1983. .................... 188

4.56 The same as in Figure 4.2 except for 16 August 1983. 0000 GMT. .................... 191

4.57 The same as in Figure 4.3 except for 16 August 1983. 0000 GMT. .................... 192

4.58 NOAA-8 satellite image, a) visible, b) infrared. 0324 GMT. 16 August 1983. .................... 193

4.59 The same as in Figure 4.2 except for 16 August 1983. 1200 GMT. .................... 194

4.60 The same as in Figure 4.3 except for 16 August 1983. 1200 GMT. .................... 195

4.61 NOAA-8 satellite image, a) visible, b) infrared. 1658 GMT. 16 August 1983. .................... 196

4.62 NOAA-7 satellite image, a) visible, b) infrared. 2315 GMT. 16 August 1983. .................... 197

4.63 The same as in Figure 4.2 except for 17 August 1983. 0000 GMT. .................... 198

4.64 The same as in Figure 4.3 except for 17 August 1983. 0000 GMT. .................... 199

4.65 NOAA-8 satellite image, a) visible, b) infrared. 0240 GMT. 17 August 1983. .................... 200

4.66 The same as in Figure 4.2 except for 17 August 1983. 1200 GMT. .................... 201

Figure Page

4.67 The same as in Figure 4.3 except for 17 August 1983, 1200 GMT. .......... 202

4.68 NOAA-8 satellite image, a) visible, b) infrared, 1630 GMT, 17 August 1983. .......... 203

4.69 NOAA-7 satellite image, a) visible, b) infrared, 2302 GMT, 17 August 1983. .......... 204

4.70 The same as in Figure 4.2 except for 18 August 1983, 0000 GMT. .......... 205

4.71 The same as in Figure 4.3 except for 18 August 1983, 0000 GMT. .......... 206

4.72 NOAA-8 satellite image, a) visible, b) infrared, 0218 GMT, 18 August 1983. .......... 207

4.73 NOAA-8 satellite image, a) visible, b) infrared, 1609 GMT, 18 August 1983. .......... 208

4.74 The same as in Figure 4.2 except for 18 August 1983, 1200 GMT. .......... 211

4.75 The same as in Figure 4.3 except for 18 August 1983, 1200 GMT. .......... 212

4.76 GOES-W satellite image, visible, 1515 GMT, 18 August 1983. .......... 213

4.77 NOAA-7 satellite image, infrared, 1257 GMT, 18 August 1983. .......... 213

4.78 NOAA-7 satellite image, a) visible, b) infrared, 2250 GMT, 18 August 1983. .......... 214

4.79 The same as in Figure 4.2 except for 19 August 1983, 0000 GMT. .......... 215

4.80 The same as in Figure 4.3 except for 19 August 1983, 0000 GMT. .......... 216

4.81 NOAA-8 satellite image, infrared, 0338 GMT, 19 August 1983. .......... 217

4.82 NOAA-7 satellite image, infrared, 1245 GMT, 19 August 1983. .......... 217

4.83 The same as in Figure 4.3 except for 19 August 1983, 1200 GMT. .......... 218

Figure Page

4.84 The same as in Figure 4.3 except for 19 August 1983, 1200 GMT. ........ 219

4.85 NOAA-8 satellite image, a) visible, b) infrared, 1547 GMT, 19 August 1983. ........ 220

4.86 NOAA-7 satellite image, a) visible, b) infrared, 2237 GMT, 19 August 1983. ........ 221

4.87 The same as in Figure 4.2 except for 20 August 1983, 0000 GMT. ........ 222

4.88 The same as in Figure 4.3 except for 20 August 1983, 0000 GMT. ........ 223

4.89 NOAA-8 satellite image, a) visible, b) infrared, 0136 GMT, 20 August 1983. ........ 224

4.90 The same as in Figure 4.2 except for 20 August 1983, 1200 GMT. ........ 225

4.91 The same as in Figure 4.3 except for 20 August 1983, 1200 GMT. ........ 226

4.92 The same as in Figure 4.2 except for 21 August 1983, 0000 GMT. ........ 227

4.93 The same as in Figure 4.3 except for 21 August 1983, 0000 GMT. ........ 228

4.94 NOAA-7 satellite image, a) visible, b) infrared, 2225 GMT, 20 August 1983. ........ 229

4.95 NOAA-7 satellite image, a) visible, b) infrared, 2247 GMT, 08 April 1983. ........ 232

4.96 The same as in Figure 4.2 except for 09 April 1983, 0000 GMT. ........ 233

4.97 The same as in Figure 4.3 except for 09 April 1983, 0000 GMT. ........ 234

4.98 The same as in Figure 4.2 except for 09 April 1983, 1200 GMT. ........ 235

4.99 The same as in Figure 4.3 except for 09 April 1983, 1200 GMT. ........ 236

4.100 NOAA-6 satellite image, a) visible, b) infrared, 1644 GMT, 09 April 1983. ........ 237

Figure Page

4.101 NOAA-7 satellite image, infrared, 2253 GMT, 09 April 1983. ........ 238

4.102 NOAA-6 satellite image, infrared, 0232 GMT, 10 April 1983. ........ 238

4.103 The same as in Figure 4.2 except for 10 April 1983, 0000 GMT. ........ 239

4.104 The same as in Figure 4.3 except for 10 April 1983, 0000 GMT. ........ 240

4.105 The same as in Figure 4.2 except for 10 April 1983, 1200 GMT. ........ 241

4.106 The same as in Figure 4.3 except for 10 April 1983, 1200 GMT. ........ 242

4.107 NOAA-6 satellite image, a) visible, b) infrared, 1623 GMT, 10 April 1983. ........ 243

4.108 NOAA-7 satellite image, a) visible, b) infrared, 2223 GMT, 10 April 1983. ........ 244

4.109 The same as in Figure 4.2 except for 11 April 1983, 0000 GMT. ........ 245

4.110 The same as in Figure 4.3 except for 11 April 1983, 0000 GMT. ........ 246

4.111 The same as in Figure 4.2 except for 23 July 1983, 0000 GMT. ........ 249

4.112 The same as in Figure 4.3 except for 23 July 1983, 0000 GMT. ........ 250

4.113 NOAA-8 satellite image, a) visible, b) infrared, 0319 GMT, 23 July 1983. ........ 251

4.114 The same as in Figure 4.2 except for 23 July 1983, 1200 GMT. ........ 252

4.115 The same as in Figure 4.3 except for 23 July 1983, 1200 GMT. ........ 253

4.116 NOAA-8 satellite image, visible, 1709 GMT, 23 July 1983. ........ 254

4.117 NOAA-7 satellite image, infrared, 1312 GMT, 23 July 1983. ........ 254

Figure Page

4.118 The same as in Figure 4.2 except for 24 July 1983, 0000 GMT. .......... 255

4.119 The same as in Figure 4.3 except for 24 July 1983, 0000 GMT. .......... 256

4.120 NOAA-8 satellite image, a) visible, b) infrared, 0257 GMT, 24 July 1983. .......... 257

4.121 The same as in Figure 4.2 except for 24 July 1983, 1200 GMT. .......... 258

4.122 The same as in Figure 4.3 except for 24 July 1983, 1200 GMT. .......... 259

4.123 NOAA-8 satellite image, a) visible, b) infrared, 1648 GMT, 24 July 1983. .......... 260

4.124 NOAA-7 satellite image, visible, 2253 GMT, 24 July 1983. .......... 261

4.125 NOAA-8 satellite image, infrared, 0236 GMT, 25 July 1983. .......... 261

4.126 The same as in Figure 4.2 except for 25 July 1983, 0000 GMT. .......... 262

4.127 The same as in Figure 4.3 except for 25 July 1983, 0000 GMT. .......... 263

4.128 The same as in Figure 4.2 except for 25 July 1983, 1200 GMT. .......... 264

4.129 The same as in Figure 4.3 except for 25 July 1983, 1200 GMT. .......... 265

4.130 NOAA-8 satellite image, a) visible, b) infrared, 1625 GMT, 25 July 1983. .......... 266

4.131 NOAA-7 satellite image, a) visible, b) infrared, 2240 GMT, 25 July 1983. .......... 267

4.132 The same as in Figure 4.2 except for 26 July 1983, 0000 GMT. .......... 268

4.133 The same as in Figure 4.3 except for 26 July 1983, 0000 GMT. .......... 269

5.1 The troughing stage .......... 275

Figure Page

5.2 The splitting stage ........ 275

5.3 The pinching-off stage ........ 276

5.4 The cutting-off stage ........ 276

5.5 The mature stage ........ 277

5.6 The decay stage ........ 277

# 1. A Review of Synoptic Scale Studies

## 1.1 Introduction

In the last two decades dramatic changes have taken place in the world of weather analysis and forecasting with the advent of numerical weather prediction, weather radars, and weather satellites. The wealth of information available to the operational forecaster makes it difficult to reach prognostic decisions within a limited time. Aids are needed to help the forecaster in the decision-making process. One of the most successful is the "decision tree" method. It is a systematic, step-wise process which incorporates different meteorological parameters from different sources into a decision-making process leading toward a prognostic conclusion. The use of the "decision-tree" method in weather forecasting eliminates subjective judgements and personal bias in a weather forecast. By using this approach, in a logical and orderly manner, the process of forecasting becomes more objective and more soundly scientific.

The reader will ask: "what is the relation between what was said above and the topic of the thesis?". The answer resides in the "decision-tree" building process. To construct a decision tree one has to assign first the area and degree of risk, as well as, meteorological parameters describing a particular weather event, and then rank the most significant parameters in a decreasing order of importance. Once the basic decision tree has been developed, it can be updated and fine tuned, by adding modifications and incorporating other meteorological parameters deduced from subsequent studies. This leads one to study the association between significant weather events, e.g. heavy precipitation, flash floods, etc. and the size of weather systems, such as synoptic scale systems, subsynoptic scale systems, etc.. It also leads one to study the relation between the development of weather systems and the significant meteorological parameters likely involved. The last two objectives will be discussed in detail in section 1.7.

## 1.2 Synoptic Scales of Motion

The integration of the equations of motion gives discrete sets of waves, such as long waves, gravity waves and sound waves. All of them satisfy the differential equations, but not all are meteorologically significant.

In 1948, Charney suggested scales for different meteorological parameters which, when applied, eliminate the lesser waves and preserve only the large atmospheric motion. The scales of these parameters are:

-Horizontal dimension, L, of the order of $10^6$ meters, is approximately the mean horizontal distance between two consecutive ridges or troughs in a stream-line pattern.

-Vertical dimension, H, of the order of $10^4$ meters, is roughly the height of the tropopause.

-Speed of propagation, C, of the order of 10 m/s, is the speed of a moving weather system such as a cyclonic storm.

-Time dimension, $T = L/C$, is of the order of $10^5$ s. or 1 day.

The above parameters have been chosen because they are the basic criteria used to gauge the weather phenomena examined in the present study.

## 1.3 General Characteristics of Cloud Systems

### 1.3.1 Introduction

The examination of extensive cloud systems has shown that certain systems are persistent and tend to reoccur. The early investigators recognized this and classified them according to specific configuration. Cloud characteristics used to identify and classify these cloud systems are brightness, pattern, structure, texture, shape, and size.

### 1.3.2 Definitions

-Pattern: refers to the organized variations of light density, i.e. arrangements of white, grey and black specks.

-Size: indicates the scale of a cloud area as compared with a geographical land mark.

-Shape: denotes the overall organization of a cloud area, e.g. banded, circular or isolated.

-Shadow: is the characteristic that gives an estimate of the cloud area depth by the illumination angle; it helps in identifying the cloud structure.

-Tone: is the degree of brightness due to the change of the scanning angle with respect to the Sun, e.g. the tone of the same cloud area on two successive images may be different.

-Texture: is the ability of a cloud area to absorb or reflect light, e.g. smooth cloud areas are uniform and flat while striated or cellular areas are not.

## 1.4 Anderson's Classification of Cloud Systems

In 1973, Anderson et. al. attempted to classify cloud systems, shown in satellite images in mid-latitudes, according to the scale characteristic, especially the length dimension. They classified cloud systems into: meso-scale, sub-synoptic, synoptic, and planetary-scale systems.

### 1.4.1 Meso-scale Cloud System

The size of meso-scale systems ranges from the smallest discernable cloud area up about 250 km.,This system includes:

-Cloud lines of convective cloud elements stretching in one direction 30 to 100 km. in length.

-Cloud cells, either open or closed, arranged in a specific pattern of size range 10 to 100 km.

-Striations are narrow or curved streaks 50 to 150 km. in length, and usually occurring in overcast cloud decks.

-Wave clouds, caused by mountain barriers, range from 20 to 100 km. in size.

-Ship trails are persisting cloud lines produced by ship smoke and range from 50 to 250 km. in length.

-Mesoscale vortices, formed from different amounts of clouds, range in size from 50 to 200 km.

-Stratified clouds such as fog and stratus are characterized by a smooth flat texture, grey to bright in tones. Frequently, they have sharp edges bounded by topographical features. They form in the planetary boundary layer by physical processes common to fog and stratus. The size is highly variable, ranging from hundreds of meters up to hundreds of kilometers.

### 1.4.2 Sub-synoptic Scale Cloud System

Sub-synoptic scale cloud group includes different cloud areas with size ranges between 100 and 2500 km. It includes:

-Vortices in stratiform clouds and weak circulation of sizes up to 300 km.

-Vortices in cumuliform clouds, with stronger circulation and bigger in size, about 600 km. in extent.

-Squall lines, which often appear ahead of cold fronts, are usually formed of Cu and Cb clouds and typically some 200 km. long.

-Cb clusters, or what have been defined later by Maddox (1980) as Mesoscale Convective Complexes, are clusters of Cb cells of size up to 2500 km..

### 1.4.3 Synoptic-Scale Cloud System

The classification of synoptic-scale systems is one of the main objectives of this study and will be discussed in detail later. Synoptic-scale cloud system includes three groups, classified as follows:

#### 1.4.3.1 Cloud Band Pattern

This pattern includes frontal bands, non-frontal bands, and jet-stream bands.

#### 1.4.3.2 Spiral Cloud Pattern

This class includes low-level vortices, upper-level vortices, and commas within cold air.

#### 1.4.3.3 Cellular Cloud Pattern

It includes open and closed cloud pattern.

### 1.4.4 Planetary-Scale Cloud System

Planetary-scale cloud areas may extend for thousands of kilometers over the globe. Mostly banded, they include:

-Extratropical planetary bands, within which cyclone disturbances are embedded. They are associated with Rossby waves.

-Subtropical cloud bands are often found in the upper levels, e.g. bands associated with subtropical jet-streams. They may extend for thousands of kilometers.

-Intertropical cloud bands form near the equator. They may also extend for thousands of kilometers but they tend to be in segments.

## 1.5 Anderson's Classification of Synoptic Scale Cloud System

In 1974, Anderson, et. al. introduced a classification for the synoptic-scale cloud system, based on characteristic size. It includes the following groups:

### 1.5.1 Cloud Band Group

A cloud band is defined as a nearly continuous cloud formation with a distinct long axis where the length is about four times the width. This group is subdivided, in turn, into:

### 1.5.1.1 Frontal Bands

Frontal bands are formed, generally, from multilayered clouds topped with cirriform cloud areas. They extend for several thousands of kilometers, have a weak cyclonic curvature, and are about 500 kilometers in width. They are associated with fronts, cold, warm, occluded, or stationary. Also, they can be active or inactive, depending on their width, continuity and brightness.

### 1.5.1.2 Non-Frontal Bands

Non-frontal bands have the appearance of frontal bands but they are not associated with fronts. Sometimes they are associated with areas of confluence or areas of meridional advection of tropical moist air, and sometimes they are formed in a north-south convergent flow as a low pressure field approaches a high pressure field. Again their activity could be deduced from the width of the band, brightness, and continuity.

### 1.5.1.3 Jet-Stream Bands

In an attempt to locate and identify the jet stream axis near a cirrus cloud area, Anderson et. al. found that the jet stream is located on the cloud-free area north of the cirrus cloud band, identified as the jet-stream band, where the change is abrupt. Jet-stream bands, which are located slightly equator-ward from the jet axis, tend to have an anticyclonic curvature and very small width compared to their length. Over the ocean, with an abundance of moisture, cellular cloud systems may form on the cyclonic side of a jet band. A jet cirrus band with a cyclonic curvature will be very narrow in width and has a faint shade.

### 1.5.2 Vortices Cloud Group

Cloud vortices have spirals of bands around a common centre, identifying areas of cyclonic development. This group includes extra-tropical cloud systems, upper cold lows and comma clouds. In general, dynamic processes play an important role in system formation, such as vertical motion in the early stages of development. Vortex clouds, in turn, are subdivided into three subgroups, as follows:

#### 1.5.2.1 Low-Level Vortices

Low-level vortices develop within a frontal band system as a wave and become well defined in the mature stage. The dynamical triggering process is the positive vorticity advection over a disturbance on a baroclinic frontal zone.

#### 1.5.2.2 Enhanced Cumuli-Comma Shaped Cloud Areas

Comma shaped patterns develop within a cellular cloud area, especially over the ocean. They are formed from brighter cumulus clusters, and are associated with vorticity maxima at the 500-mb surface. They may also show spiral configuration shape in the early stages of development. In later stages, comma-like cloud areas form, and become associated mostly with positive vorticity advection.

#### 1.5.2.3 Upper-Level Vortices

Upper-level vortices develop within cold air in an area of enhanced cumuli, form a spiral pattern and appear like the occlusion stage of low-level vortices. The cold dome of air and the cut-off process play an important role in developing such patterns.

### 1.5.3 Cellular Cloud Group

Cellular cloud patterns forms from convective clouds, organized as either open or closed cells. The physical processes are ,generally, the same in both cases, and include cold air advection, subsidence, and stability. The pattern represents a mesoscale convective mixing interacting with a large-scale flow. On the other hand, the thermodynamic processes involve the temperature difference between the air and the underlying surface, the mixing of moist air in the planetary boundary, and the intensity of heating from below. The cellular pattern breaks down when the vertical wind shear becomes significant. Open cells are associated with cyclonic flow and closed cells with anticyclonic flow.

#### 1.5.3.1 Open Cellular Cloud Pattern

Open cellular pattern is found in the rear areas of cold fronts within cold unstable air. It is made up of individual convective cells within otherwise clear areas. In polar air masses, it consists mainly of towering cumulus clusters, while in subtropical air it forms mainly stratocumulus clusters. Open cells indicate warming from below and conditional instability in the lower layers. They most readily develop over the ocean, but they may also form over land in the presence of large bodies of water and adequate surface heating on the surrounding terrain. Land based patterns are of less duration, usually persisting for some 12 hours on the average.

#### 1.5.3.2 Closed Cellular Cloud Pattern

Usually, closed cellular patterns are found to the rear area of a cold front and close to the next up-stream ridge. In this group the convective cells tend to merge, leaving very little clear air between the cloud elements, while the whole pattern is bounded by regions largely free of clouds. Covection is not intense as in the case of open cellular pattern. The convection process is driven either by weak surface heating, or by upper radiation cooling. The convective cells are made up, mainly, of stratocumulus in polar and subtropical air. The closed cellular pattern is due to weak low level instability. It also forms over the ocean and, with lesser persistance over the land.

### 1.6 Zwatz-Meise's Classification of Synoptic-Scale Cloud System

In 1981 Zwatz-Meise made a few modifications to Anderson's, 1974, classification of synoptic scale cloud system by introducing another group and new patterns. Details within specific groupings have been changed considerably. Zwatz-Meise and her collegues have also added another important feature by attempting to incorporate both conventional and satellite data into one system. Thorough examination of their study reveals how solid and consistent their results are. The following sections describe the general features of their classification.

### 1.6.1 Cloud Band Group

The main features remain the same as in Anderson's regime. The cloud bands are extended, linear features and several times as long as wide. Most of the bands are thick and layered, and may extend to great heights. This group includes:

#### 1.6.1.1 Frontal Band Pattern

The frontal band has the same features as described before in Anderson's classification. The cloud band area is associated with a frontal system, defined in synoptic data. This pattern includes cold frontal bands, warm frontal bands, occluded frontal bands and stationary frontal bands. Several derived meteorological parameters were used to assist in identifying a frontal band. These parameters are:

-Thermal frontal parameter TPF, defined as the gradient field of the temperature gradient field at the 850-mb surface taken in the direction of the temperature gradient field.

$$\mathrm{TPF} = -\nabla|\nabla T| \cdot \frac{\nabla T}{|\nabla T|} \qquad (1.1)$$

,where T is the temperature field at the 850-mb surface, $\frac{\nabla T}{|\nabla T|}$ is the direction vector of the temperature gradient field.

-The zero isopleth of the relative vorticity at the 500-mb surface.

$$\zeta_5 = 0 \qquad (1.2)$$

,where $\zeta_5$ is the relative geostrophic vorticity at the 500-mb surface defined by

$$\zeta_5 = \frac{g}{f}\nabla^2 Z \qquad (1.3)$$

,where g is the acceleration due to gravity, f is the coriolis parameter, and Z is the geopotential height of the 500-mb surface.

-The zero contour of the relative vorticity of the thermal field of the 850/500 mb. layer.

$$\zeta_{th} = 0 \qquad (1.4)$$

,where $\zeta_{th}$ is the relative geostrophic vorticity of the thermal field defined as

$$\zeta_{th} = \frac{g}{f}\nabla^2 h \qquad (1.5)$$

,where h is the thickness field of the 850/500 mb. layer.

### 1.6.1.2 Non-Frontal Cloud Band Pattern

In this subgroup, Zwatz-Meise included several bands not well defined before. She also showed how this general classification may be extended to other cloud bands.

This pattern now includes:

#### Jet Band

In addition to the main features described before in Anderson's classification ,the jet band shows a fibrous structure, banded orientation, and is located at very high levels. The band is most easily recognized and identified on the visible images. Since the fibrous clouds are indicative of horizontal wind shear, such bands are either jet bands or shear bands, Zwatz-Meise and Hailzl (1980-b). Jet bands are less intense than shear bands, but since both may merge, it may be very difficult to distinguish between them. Jet bands are most frequently found over the sea, but they can be observed also over land.

#### Shear Band

This band was first studied and defined by Zwatz-Meise and Hailzl in 1980-b. Having first examined the possible reasons for the development of such bands they erased the old misinterpretation that these bands are features of cold or stationary-fronts. The shear band is characterized by a well-marked anticyclonic curvature. The cyclonic side is associated with the thermal wind field of the 700/300 mb. layer. The orientation of the fibrous elements is the same as, and parallel to the thermal wind field. Shear bands move faster than jet bands and still faster than frontal bands. This is the reason for misinterpreting them as frontal bands, since all the bands, (jet, frontal and shear) may merge into a single band in the late stages of development.

Convergence Band

Although some examples of this band were shown early in Anderson's study (1974), it was not then well established nor defined. In 1980, Hailzl carried out several studies and came out with a satisfactory explanation for the formation, development, and motion of convergence bands. Hailzl found that, as the remnants of an old frontal band, which had moved away from the baroclinic zone, came under the influence of a mid-level convergence field only, they tend to redevelop into a new band. He also found that, such convergence fields may exist throughout a layer e.g. 850/500 mb.. In such cases an estimate of the vertical motion field can be made and consequently of the band thickness.

Pre-Frontal Band

This band had a great interest in Zwatz-Meise's study, 1981. She found that, the band is associated with but not directly connected to the frontal band, especially not to the cold frontal band. It has almost the same structure as a frontal band but it has a different orientation. Again, the use of satellite data combined with synoptic data has a great advantage. While it is very difficult to distinguish this band from a cold frontal band, a pre-frontal band is always associated with the flat ridge of a thickness field of the 850/500 mb. layer.

### 1.6.2 Vortices Cloud Group

The vortices group is sometimes called the non-banded cloud group. The principal feature common to this group is a spiral shape of synoptic size at some stage of development. Such spiral shapes may be simple or complex. The group includes the following patterns:

### 1.6.2.1 Low-Level Vortex

The low-level vortices are usually associated with the centre of an extra-tropical cyclone where two different air masses, one warm and moist, and the other cold and dry, interact to form a spiral-like area of white, dense cloudiness. The other features are very similar to those described, before, in Anderson's classification, (1974).

### 1.6.2.2 Upper-Level Vortex

The cloud pattern of this vortex develops independently of any other cloud area. Superficially it looks like the cloud area of an occluded stage of a low-level vortex. The centre of the vortex is usually covered with cellular clouds bounded by one or two very dense white cloud bands. The physical process behind the formation of upper-level vortices is quite different from that in low-level vortices. A pool of cold air at the core of an upper-level low is surrounded by warm moist air which ascends the cold pool and forms a spiral band. Satellite images are of great aid in identifying the first signs of formation in this pattern, as well as showing the subsequent stages of development and decay .

### 1.6.2.3 Comma Configuration Cloud Pattern

This distinctive configuration forms mostly within regions of cold air and assumes the shape of a comma. Commas exist in different sizes, but they represent the stage of mature development, and they are not characterized by areas of dry-air intrusion, as noted by Zwatz-Meise (1981). The physical process behind the formation and development is also different from that of the low-level and upper vortex groups. This is so because comma development takes place within an area of cyclonic vorticity advection.

### 1.6.3 Cellular Cloud Group

Although this group is formed from individual smaller-scale cloud areas, yet the overall configuration is of synoptic scale. Patterns of regular configuration always form over oceans, with outbreaks of cold air. Cellular groups form either as a closed-type or as an open-type pattern. For example, a pattern behind cold frontal bands is often open, while that located behind jet bands is often of the closed type. But again, both types may form over land or ocean. While a cellular pattern over land tends to be short lived, that formed over oceans persists longer because of more vigorous convective activity, see Zwatz-Meise (1981). The different parameters that play an important role are: (i) the temperature difference between the air and the underlying surface, (ii) the lapse rate (specially in the lower levels), (iii) the moisture field distribution, and (iv) the surface roughness.

#### 1.6.3.1 Open Cellular Pattern

In this pattern, development takes place because of the large temperature difference between the cold air advected over a warm surface (sea or land) and also because of the pronounced instability in the lower levels. Such patterns tend to form in regions of cyclonic curvature. Orderly cellular patterns are usually found over sea and quite irregular distributions over land. They tend to persist for several days over the sea but only for about one day over land. Where a comma pattern forms in an area of maximum cyclonic vorticity, the cellular cloud pattern has a unique shape of dense white convective clouds, usually called 'enhanced cumuli'. The regularity of pattern, in open systems, is a reflection of the distribution of the vorticity field aloft. Over land the open pattern forms as a result of the temperature difference between the air and the Earth's surface, and in the presence of strong instability.

### 1.6.3.2 Closed Cellular Pattern

As mentioned above, the temperature difference between the air and the underlying surface plays an important role. In this pattern such temperature differences are quite small, and often less than 1° C. Again, cold air advected over a warm surface leads to convective cloudiness that breaks up into cells where the air descends. The resulting pattern will be more regular than the open pattern. Two other favourable conditions for development are: weak instability and anticyclonic curvature of the stream-line field. This pattern may also exist over land and sea.

### 1.6.4 Uniform Cloud Area Group

It is in this group that differences between Anderson's classification and Zwatz-Meise's are most marked. This is hardly surprising when one remembers that in 1974 Anderson considered uniform cloud areas such as fog and low stratus as a local mesoscale system, whereas Zwatz-Meise's (1981) classification recognized that, this group displays marked differences. Any attempt to incorporate the wide range of dimensions into a single class will be very difficult. However, Zwatz-Meise has managed to include all clouded areas that have a uniform texture, definite pattern and similar horizontal size into one distinct group. The justification for this differentiation resides in the contrast between the uniform group and the cellular group. One may say that both (the cellular and the uniform groups) have similar horizontal dimensions, yet the patterns and the textures are quite different. This group contains the vast white or light grey uniform cloud areas with sharp well defined edges and topographically bounded such as a wide expanse of fog cut up by mountains. The physical process behind the development of uniform cloud area is low-level stability, often marked by a pronounced inversion.

### 1.7 The Purpose Of The Study

The study will concentrate on two main objectives . The first objective is concerned with the examination and analysis of the "Synoptic Scale Cloud System Classification" in the light and guidance of the previous studies carried out by Anderson 1969-1974, Weldon 1975-1979, and Zwatz-Meise 1981. Different sources of data will be used, e.g. satellite data will include all possible satellite images available from polar-orbiting and geostationary satellites. On the other hand, conventional data on which most of the early studies are based, will receive a good share of attention in an attempt to explain how a synoptic-scale cloud system fits the current classification, proposed by Zwatz-Meise (1981). Within this main objective, attempts will be made to seek a logical approach to such classification.

The second part of the study will consider a new synoptic model of cyclogenetic development for what is known as "the upper cold low". Knowing that the previous extensive studies, carried out over Western Canada and U. S. A., have concentrated on conventional data or satellite data alone, a determined attempt will be made to incorporate both synoptic and satellite data into one scheme. Because of the limited time available for the project, only a preliminary study could be carried out, and thus definitive results are not to be expected. The satellite data used will consist mainly of images from polar-orbiting satellites, while the geostationary satellite data will be considered only whenever more details are needed. The use of satellite data does not pre-empt any possible information that conventional data may provide. Hence pertinent surface maps, 850-mb., 700-mb., 500-mb., and 300-mb. or 250-mb., surfaces will be examined carefully. Within the second objective, the role of significant meteorological parameters, which show good evidence of association with the development problem, will be discussed at length. Special attention will be given to the role of the absolute vorticity field.

The area of study is over Western Canada bounded by the 90° W meridian in the east, by the 150° W meridian in the west, and by the 40° N and 60° N parallels to the south and north, respectively. A margin of five degrees latitudinally and longitudinally will be allowed and considered in order to include all cases and phases of interest adjacent to, or just outside, the domain of the study area. Finally, the study will be carried out for the period from April 1st, 1983 to September 30th, 1983.

# 2. Data Analysis

## 2.1 Introduction

Two sources of data will be considered in the study, namely satellite data and conventional data. Each source will be examined and analysed in an attempt to identify synoptic cloud systems and whether or not they can be sub-classified. The approximations and limitations of the method of analysis, and the sources of error will be considered also. Then data from both sources will be incorporated into a composite definitive classification.

## 2.2 Satellite Data

Satellite data come in digital and image forms processed according to requirements with linear or non-linear enhancement. The main source of data are the polar orbiting satellites NOAA-6, NOAA-7 and NOAA-8. The geostationary satellites (GOES-E, GOES-W) provide supplementary sources of data. Both satellite systems will be discussed very briefly. The reports by Schwalb (1978), "The Office of the System Engineering" (1979), and Clark (1983) should be consulted for more details.

### 2.2.1 Factors Affecting Satellite Images

Before examining cloud systems shown on a satellite image, a number of factors must be considered, as pointed out by Weber and Wilderotter (1981), and in the WMO Technical Note #473 (1977). Ignoring these factors may lead to gross misinterpretations. The most important factors to be considered are:

#### 2.2.1.1 Image Resolution

Satellite image resolution is defined as the capability of the imaging system to resolve and analyse the smallest element of spatial or temporal change. For example, the spatial resolution of a satellite image refers to the smallest horizontal diameter of a cloud area that should be resolved. High spatial resolution means that the image possesses much fine detail while one with low spatial resolution reveals only the grosser features. The image resolution depends on different factors such as:

- Sensor Resolution

This term denotes the scanner device resolution. The scanner width is the threshold limit between what is visible and what is not. Cloud areas located away from the subpoint, the point on the Earth's surface directly beneath the satellite sensor, will suffer from inferior resolution due to the distance and the angle of view.

- System Resolution

System resolution refers to the net resolution of a satellite image resulting from the scanner, the electronics on the satellite, the electronic noise due to signal modulation and atmospheric dust. For example, GOES-W sensor resolution is approximately one kilometer while a full disk satellite image resolution is eight kilometers.

- Effective Resolution

The effective resolution is resolution recorded on satellite image photopaper and discernable by the human eye. It depends on photo processing, quality and condition of the photographic paper, printing process (focusing), and the amount of image reduction. It is thus the net sum of all factors described above.

### 2.2.1.2 Frequency Range

In the visible band, the scanner is sensitive to radiation between 0.4-0.7 μm, and in the infrared, between 10.5-12.5 μm. Attenuation and contamination, being functions of the frequency ranges, may affect clouds appearance in the satellite image. Figure 2.1 shows the effect of attenuation. For example, attenuation may cause clouds on infrared images to appear colder. Figure 2.2 shows the effect of contamination. In this example , cirrus clouds over low stratus clouds would appear like altostratus clouds.

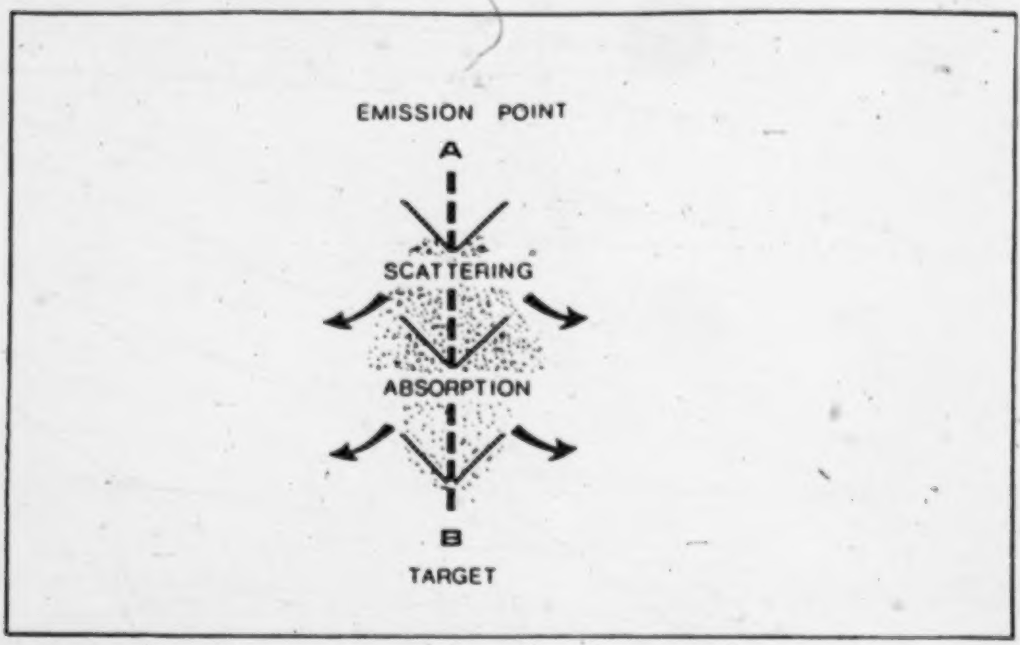
EMISSION POINT
A
SCATTERING
ABSORPTION
B
TARGET

Figure 2.1 Attenuation effect.

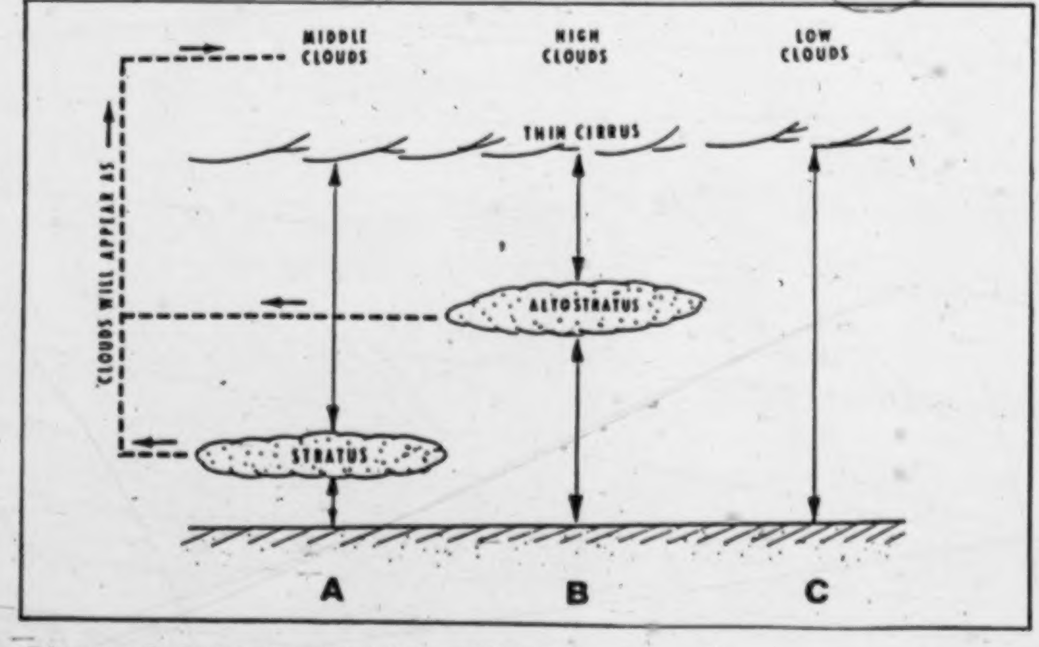
MIDDLE CLOUDS
HIGH CLOUDS
LOW CLOUDS
CLOUDS WILL APPEAR AS
THIN CIRRUS
ALTOSTRATUS
STRATUS
A
B
C

Figure 2.2 Contamination effect.

#### 2.2.1.3 The Time Of The Day And The Viewing Angle

These factors affect visible-range images only. On such images, areas under a high Sun tend to be brighter than areas illuminated by a low Sun. But, on the other hand, visible-range images at low Sun reveal more information about the cloud height (shadow character) than those under high Sun. This is important, especially in the case of clouds of vertical development such as cumulonimbus clouds, where the convective activity may appear more impressive under low Sun than under high Sun. Care should be taken when comparing a case viewed towards the Sun with a case viewed away from the Sun. In the case of polar-orbiting satellite images, a cloud system viewed away from the Sun on a given orbit will be less bright than the same system seen later on the next. Figure 2.3 is a good example for this case, where the difference in image brightness is due to the difference in solar elevation between the two consecutive orbital paths. Note in particular the difference in reflectivity over the Idaho-Wyoming border.

#### 2.2.1.4 The Sector Of The Satellite Image

The scanned picture becomes increasingly distorted with increasing distance from the subpoint. This distortion is proportional to the angle of scanning, an effect most obvious on geostationary images. Thus a cloud system shown at the edge of a GOES-E satellite image will be different in area and orientation when viewed on a GOES-W image. A good rule of thumb is: the closer the cloud area to the subpoint, the more faithful its representation.

#### 2.2.1.5 Accuracy of Gridding

Accurate gridding is very important in that it may affect all the calculations, if not done properly. In order to relate cloud systems to parametric fields such as vorticity, it is necessary to transform the data from the satellite image coordinate system to the synoptic map coordinate system. Accuracy in fitting a

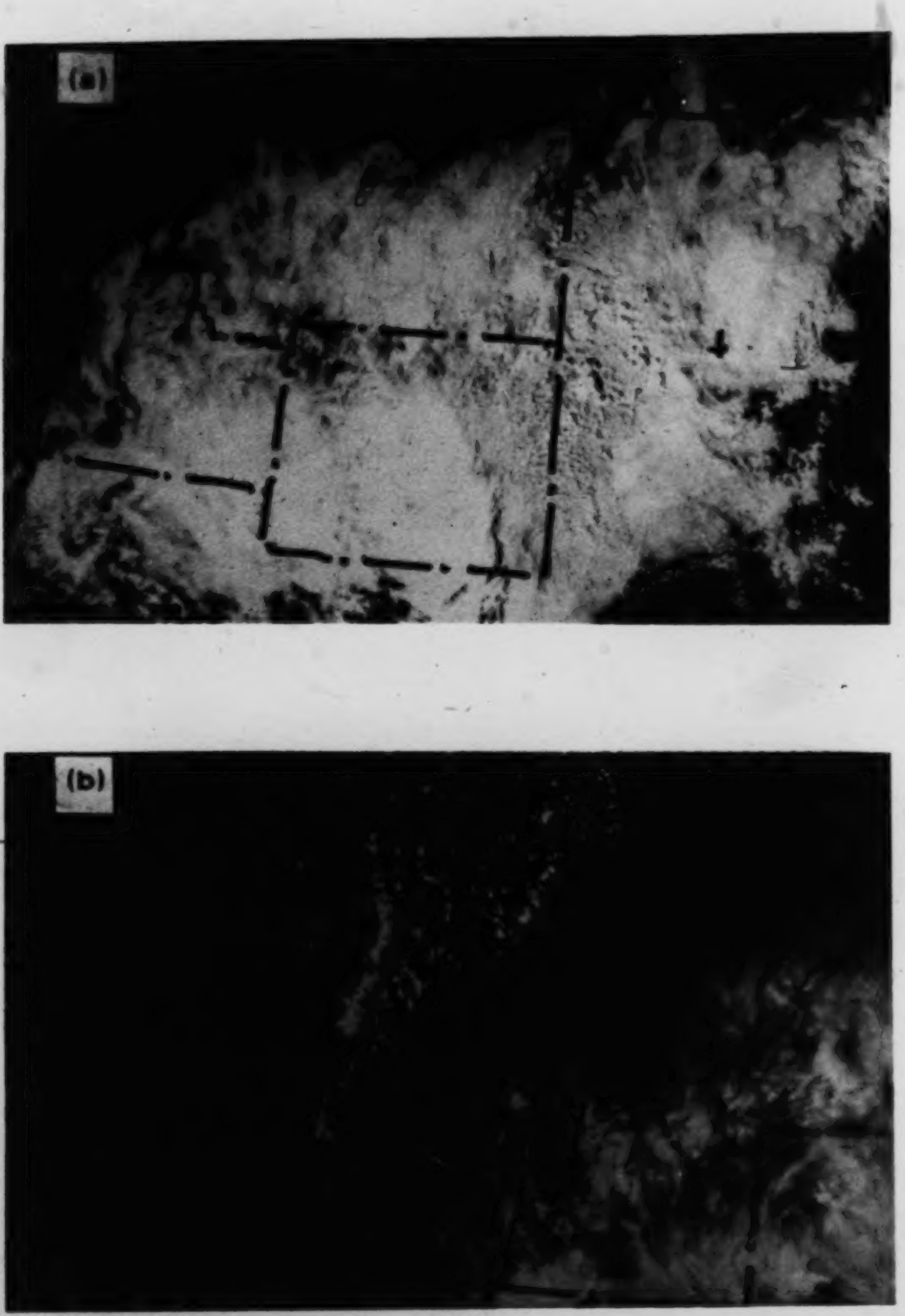

Figure 2.3 Sun angle effect. a)May 11,1983,2107Z, NOAA-7. b)May 11,1983,2248Z,NOAA-7.

latitude / longitude grid to a satellite image depends on several considerations:

(i) accurate knowledge of the satellite's position in space and time,

(ii) a good grid overlay produced and calculated for each satellite orbit, which in turn depends on the precision of the input information and orbital prediction parameters,

(iii) an image with as little distortion as possible otherwise, false variations in the size of a cloud area may occur, and

(iv) correct matching and marking of the grid overlay to the satellite image.

The analyst should do his best to fit the overlay grid to the nearest identifiable landmarks e. g. lakes, coast lines, etc.. If properly done, the gridding error will be less than the average near the subpoint and somewhat above average near the edges of the image. In Spring and Summer landmarks will be well defined in the visible image, while in Winter most landmarks will be poorly defined.

### 2.2.2 Satellite Image Enhancement

Enhancement curves show the linear or nonlinear relationships between the converted digital signal counts (0-255) and the gray scale-representation of reflectivity or temperature. The purpose of enhancement is to increase the degree of contrast within cloud areas in a satellite image. The following questions enable one to construct the desired enhancement curve.

-What will the image be used for?

-What specific information is required for best analysis?

-What is the time of the year?

-What is the geographical sector needed and what is the map scale?

In constructing the curve, specially for infrared data, it is useful to consider the standard calibration table and the enhancement graph paper, shown in Figures 2.4 and 2.5. The scanned calibrated imagery, is received on the form of digital counts ranging from 0 to 255. The scaling in the calibration table does not proceed in unifom steps, e.g. the

Page 24 has been removed because of the unavailability of copyright permission

The information contained a figure of "calibration data".
(adapted from Clark 1983)

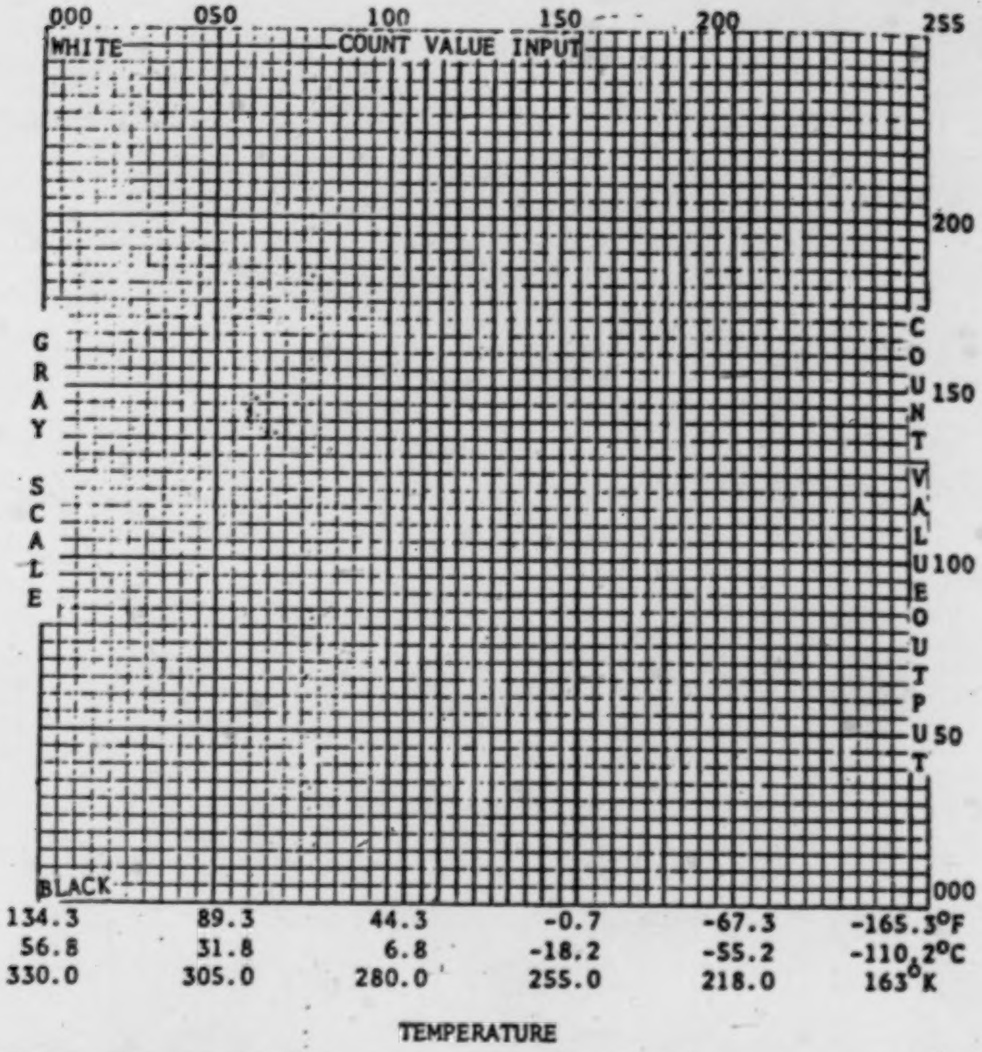

| SEGMENT NUMBER | °C TEMPERATURE<br>__________to_________ | COMMENTS<br>REASON FOR SEGEMENT ENHANCEMENT |
|---|---|---|
| | | |
| | | |
| | | |
| | | |
| | | |
| | | |
| | | |

Figure 2.5 Enhancement graph and equivalent temperature transfomations.

infrared scale increases in steps of 1° K within the range 163° K to 242° K, and only 0.5° K in the range 242° K to 330° K. In a study carried out by Reinelt et. al. (1975), four types of enhancement curves were used to transform digital data into shades of gray, in the manner described below.

### 2.2.2.1 Different Enhancement Curves

Considering Figure 2.6, enhancement curves may be classified into:

(i)-Linear enhancement curves, represented by the curve AB, at which the temperature range, 330-163° K, is transformed into continuous, uniformly changing shades of gray.

(ii)-Steep enhancement curves, represented by the curve AC, at which the temperature range, 330-275° K, is transformed into continuous but rapidly changing shades of gray, and the range 275-163° K is assigned to a single shade of gray.

(iii)-Sliced enhancement curves, represented by the curve DEFGHI, produce a monotonic stepwise sequences of shades of gray in ascending or descending order, in such a way that each temperature range is assigned to a specific gray shade. For example, the temperature range 287-267° K is converted to black, between 267-242° K is shaded dark gray, and the range 242-228° K is transformed to a light gray shade.

(iv)-Wrapped enhancement curves, represented by the curve DEFGHIJKLMB, are similar to sliced curves, except that the temperature ranges are transformed in special ways such as ascending, descending, inverted as required to display certain features.

Two important criteria should be considered when constructing an enhancement curve.

(i)- Only a limited number of enhanced features should be shown.

(ii)- As many as possible details without inviting confusion.

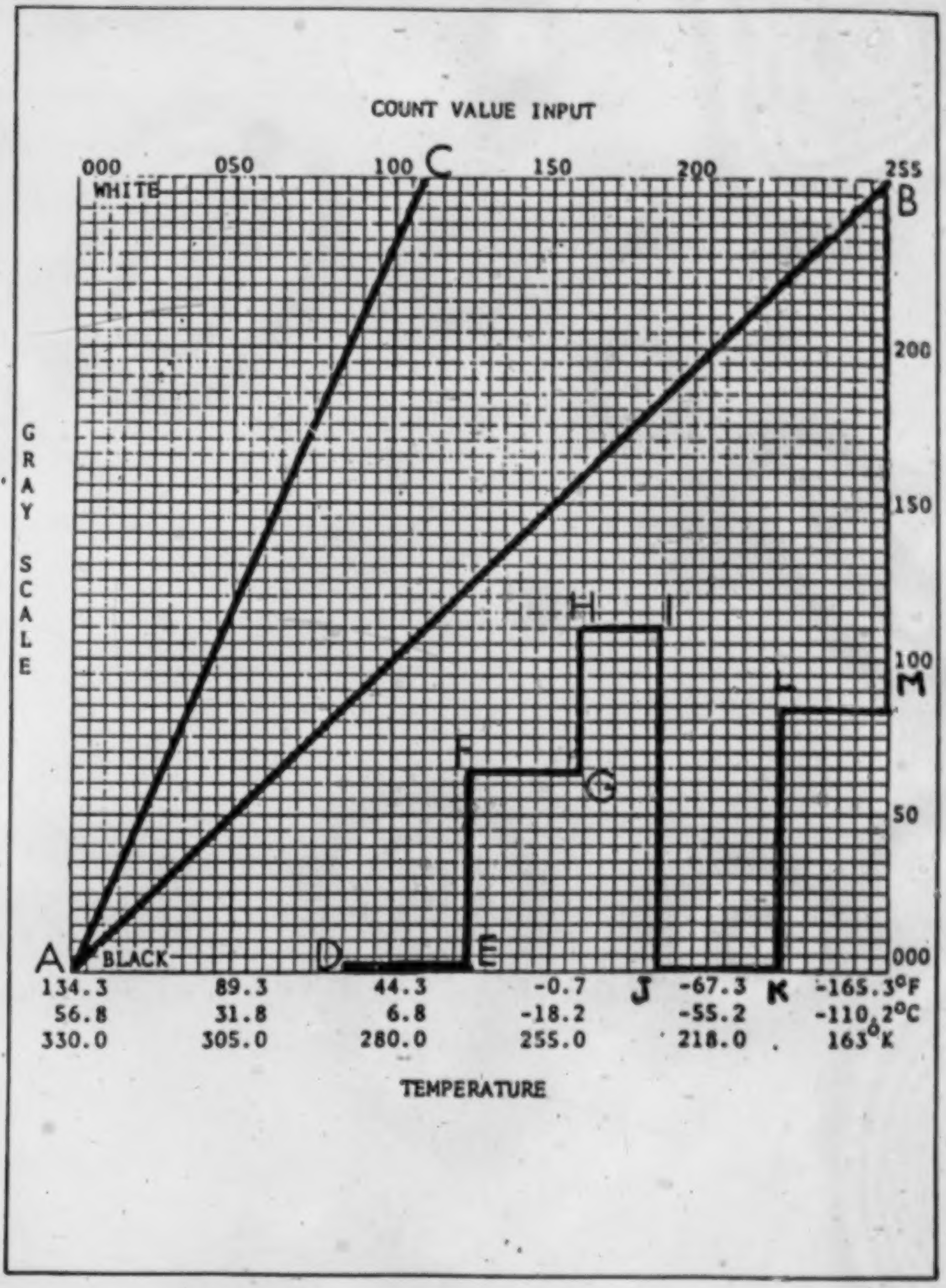

Figure 2.6 Different enhancement curves.

Each enhancement curve has its own function. For example, a steep enhancement curve is very useful in displaying deep vertically structured cloud areas such as towering cumulus and Cb clouds, but it tends to mask the cloud boundaries. Linear enhancement produces a good overview of clouds but without much detail.

On each satellite image two gray scales are shown, the first for a linear change, and the second for whatever special enhancement. Temperature ranges, chosen to approximate contours, can be identified without reference to the tabular values.

#### 2.2.2.2 Examples Of Enhanced Curves

Enhancement curve MB: Figure 2.7 shows an image enhanced according to curve MB in Figure 2.8. Segments 1-3 provide more distinct definition of low and mid-level clouds, segments 4-7 favour definition of convective clouds, and segment 8 enhances domes of very cold air.

Enhancement curve ZA : Figures 2.9 is an example of "slicing" curve applied to the global sector shown in Figure 2.10. This curve is specially useful to emphasize low, mid-level, and high clouds.

### 2.2.3 Polar Orbiting Satellite

The polar-orbit satellite NOAA-7 will be discussed briefly in the following. Figure 2.11 shows the main parts of the satellite vehicle. NOAA-7 is in Sun-synchronous orbit, i.e. the satellite orbit precesses at the same average rate as the Earth's annual revolution about the Sun. In other words, as the Earth rotates, each orbit is over an area experiencing the same local time as the area viewed in the previous orbit, and thus the satellite-SUN-Earth relationship system remains constant. Typical orbits of the satellite are shown in Figures 2.12 and 2.13. One half of each orbit is over the night side of the Earth and one half is over the Sun-lit side. About 12 orbits cover the entire globe. The principal NOAA-7 parameters and characteristics are described below.

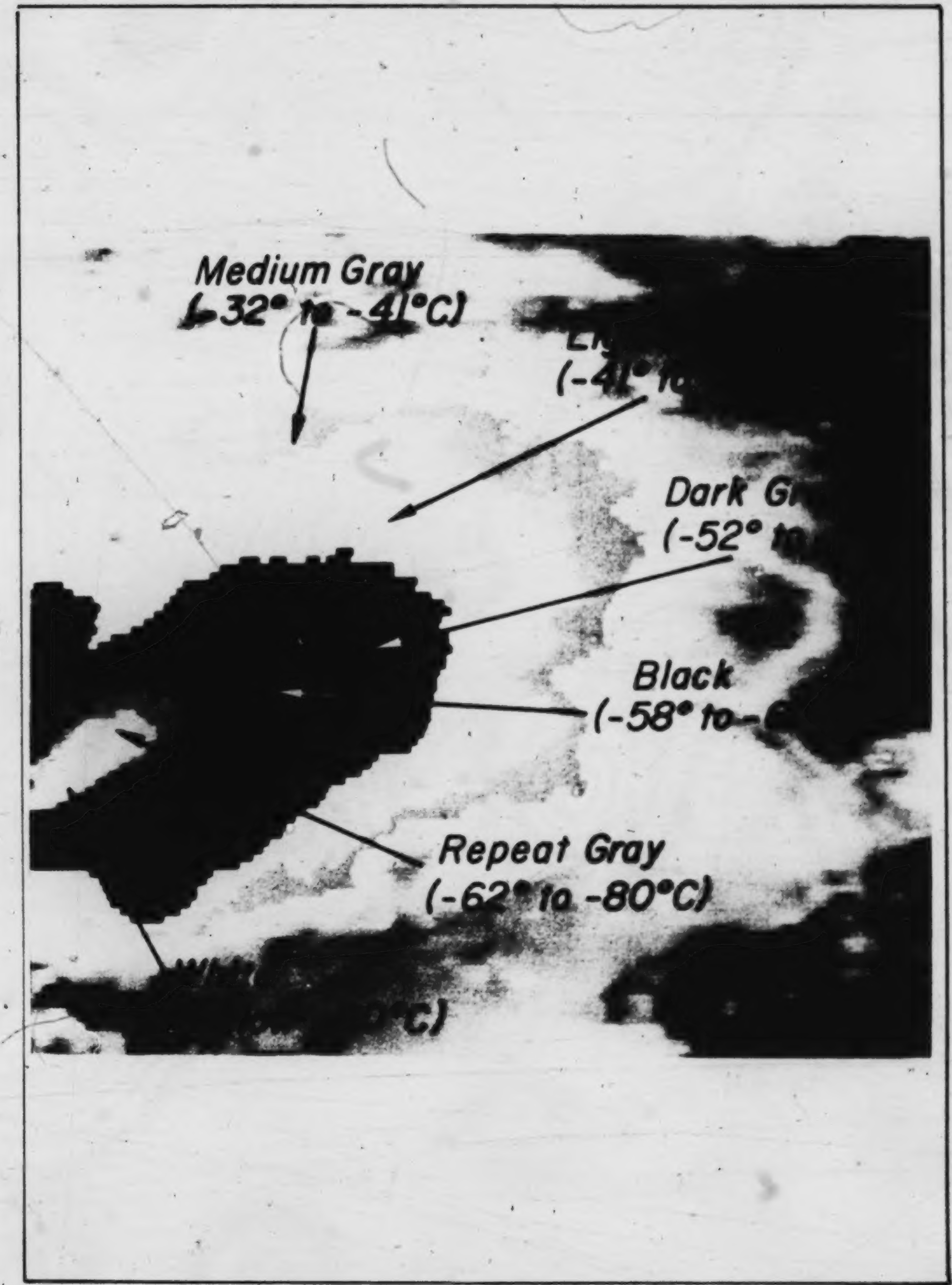
Medium Gray
(-32° to -41°C)
(-41° to
Dark Gr
(-52° to
Black
(-58° to -6
Repeat Gray
(-62° to -80°C)
°C)

Figure 2.7 Infrared wrapped enhancement (adapted from Clark 1983).

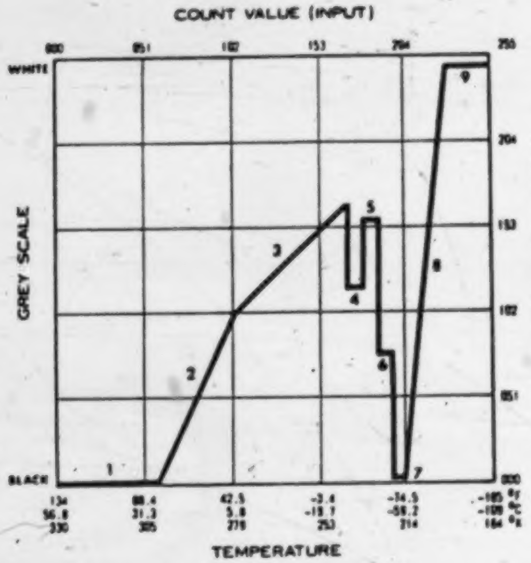

Figure 2.8 Enhancement curve MB.

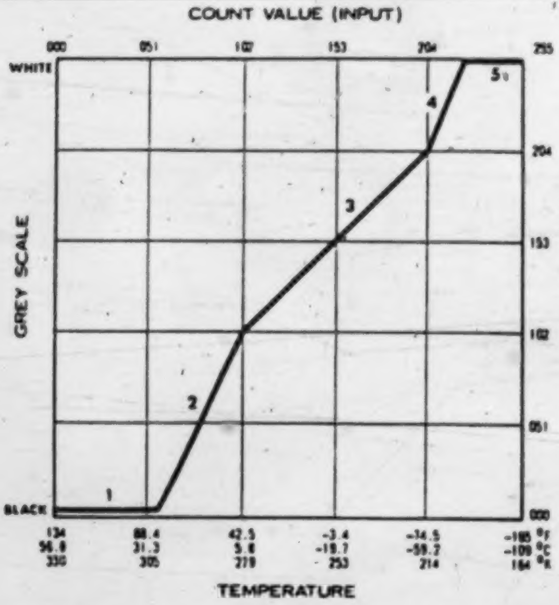

Figure 2.9 Enhancement curve ZA.

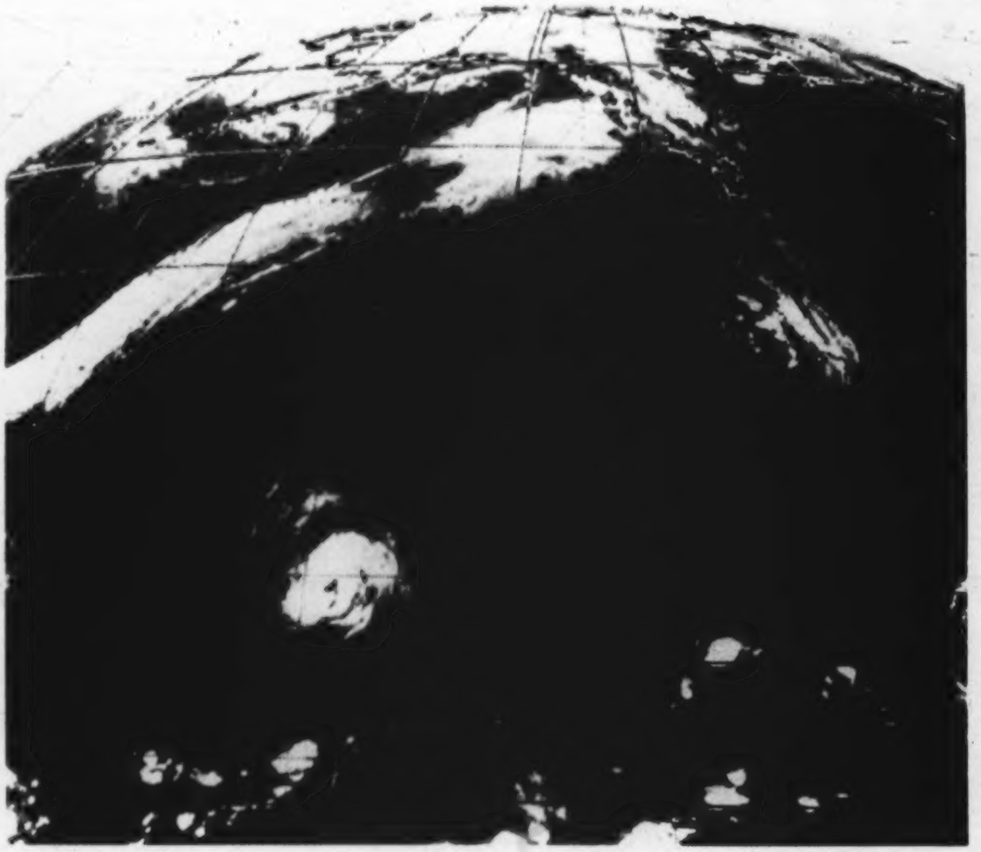

Figure 2.10 Infrared steep sliced enhancement (adapted from Clark 1983).

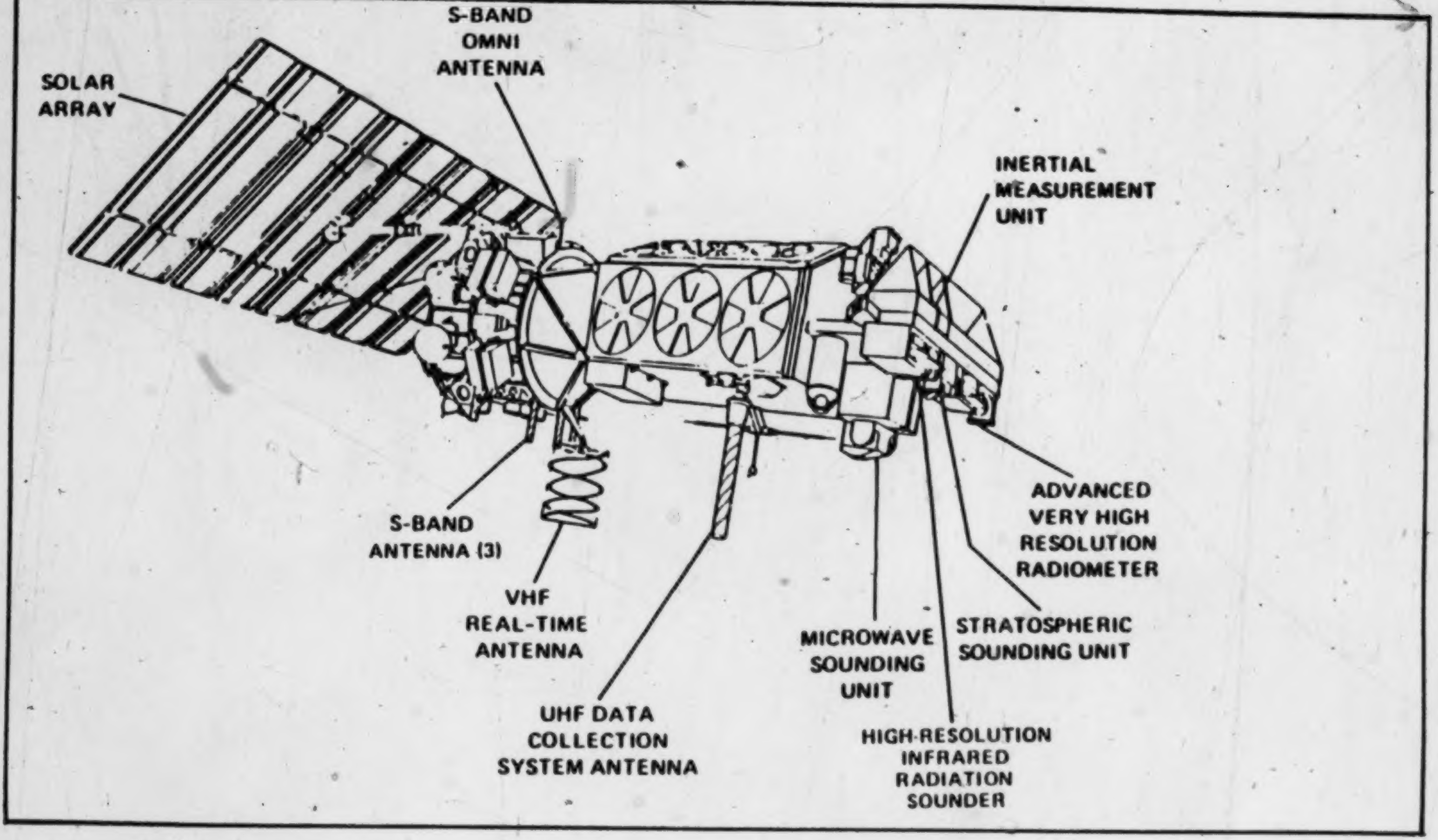
S-BAND
OMNI
ANTENNA
SOLAR
ARRAY
INERTIAL
MEASUREMENT
UNIT
ADVANCED
VERY HIGH
RESOLUTION
RADIOMETER
S-BAND
ANTENNA (3)
VHF
REAL-TIME
ANTENNA
STRATOSPHERIC
SOUNDING UNIT
MICROWAVE
SOUNDING
UNIT
UHF DATA
COLLECTION
SYSTEM ANTENNA
HIGH-RESOLUTION
INFRARED
RADIATION
SOUNDER

Figure 2.11 Polar orbital satellite main parts.

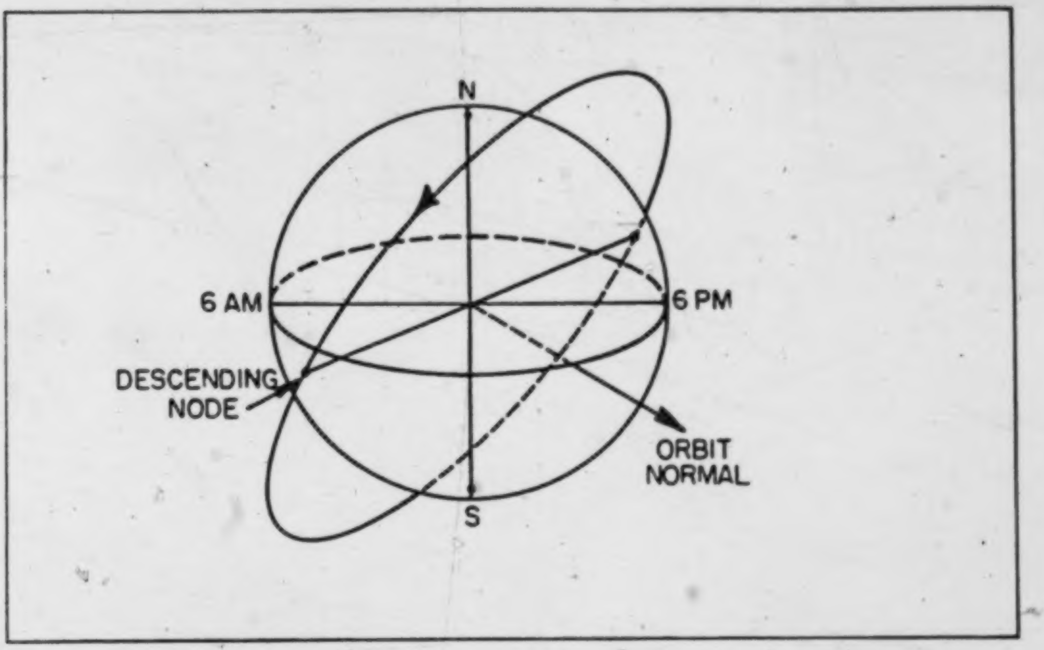
N
6 AM
6 PM
DESCENDING NODE
ORBIT NORMAL
S

Figure 2.12 A descending node orbit.

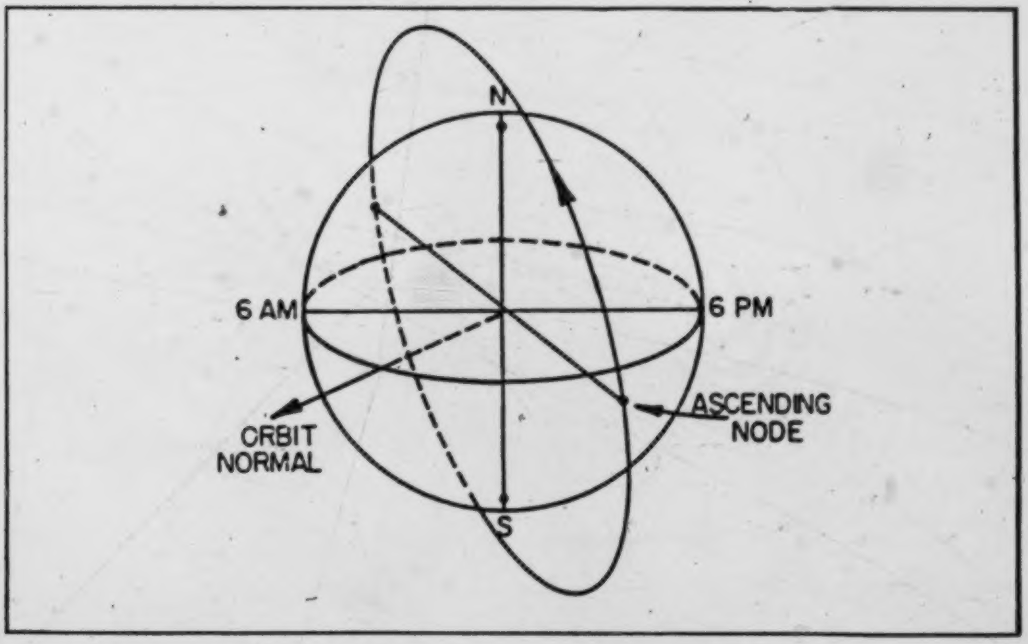
N
6 AM
6 PM
ASCENDING NODE
ORBIT NORMAL
S

Figure 2.13 An ascending node orbit.

### 2.2.3.1 Satellite Parameters

-Height above the Earth's surface: about 865 km.

-Orbital period is about 102 minutes.

-Inclination angle is about 99°.

-Westward nodal regression = 25°, i.e. the satellite regresses 25° of longitude per orbit at the equator.

-Angular speed is about 16.56 X $10^{-3}$ $s^{-1}$, and the orbital speed 25,000 km/hour.

### 2.2.3.2 Satellite Characteristics

-The satellite precesses at a constant rate of about one degree per day, maintaining thereby constant orientation with respect to the Sun over the course of the year.

-The satellite carries an AVHRR scanner (Advanced Very High Resolution Radiometer) in the visible and infrared bands with five channels giving a spatial resolution of 1 km.

-The scanner has five radiometer channels visible (0.55-0.68 μm), near infrared (0.725-1.1 μm, 3.55-3.93 μm) and far infrared (10.5-11.5 μm, 11.5-12.5 μm) regions.

-Both the visible and infrared band analog signals are converted to digital counts of 0-255. High counts represent low reflectivity and low temperature, while low counts represent high reflectivity and high temperature.

-Reflectivity is related to cloud thickness, while radiance in the infrared band is related to the temperature of the cloud top layer.

-In general, increased brightness in the visible band is associated with cloud thickness, and in the infrared it is associated with colder clouds.

-Brightness character in the visible band is variable, since it is a function of viewing angle and the Sun angle. For example, the cases to be examined are distributed over a period of six months, and hence under different Sun angle viewing. Special care should, therefore, be taken when comparing different cases and different studies.

-A schematic diagram of a scanning satellite in orbit is shown in Figure 2.14.

-Under similar conditions of illumination, water clouds (cumulus, stratocumulus and stratus) tend to appear brighter than ice clouds (cirrus, cirrostratus, cumulonimbus). However, different cloud areas may appear with equal brightness, under different atmospheric conditions.

### 2.2.3.3 Satellite Scanning

The output data must be corrected for geometric distortions. These corrections are performed in order to maintain an almost constant resolution along the scan line. Each scan line consists of 700 individual picture elements ("pixels"), at which scanning is restricted to be within 55 degree of the satellite subpoint, i.e. 27 degrees of longitude at the equator. Since the satellite regresses 25 degrees of longitude per orbit, there is a 2° longitude overlap between each two consecutive orbits at the equator. This overlap increases with latitude increase as shown in Figure 2.15. The AVHRR contains a mirror which rotates at the rate of 360 degrees per minute or 6 scans per second. Since the scan of the mirror is perpendicular to the satellite track, its sweep combined with the motion of the satellite provides complete coverage of the area of view. This can be seen in Figure 2.14.

### 2.2.3.4 Satellite Gridding

For each satellite path, a latitude / longitude intersection grid overlay is applied to the satellite image. The analyst adjusts it according to the available landmarks. Due to the Earth's rotation and curvature, the latitude / longitude intersections are not orthogonal in all parts of an image. Figures 2.16 and 2.17 show this clearly, where 120° W meridian is curved on both figures and in different directions. This, in turn, produces areal distortion across the whole image, which increases with the size of the area viewed. In other words, it is quite difficult to overlay two consecutive images with adequate accuracy since there is distortion in the North-South direction, as well as, in the East-West direction and of different amount. Wieler (1981) has

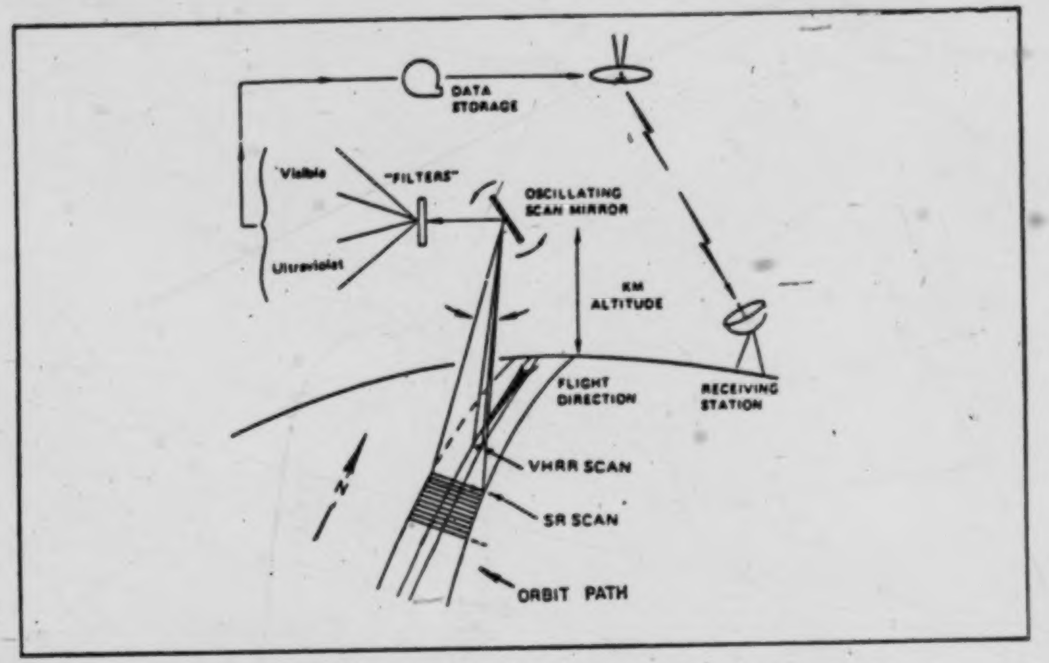
DATA
STORAGE
Visible
"FILTERS"
OSCILLATING
SCAN MIRROR
Ultraviolet
KM
ALTITUDE
FLIGHT
DIRECTION
RECEIVING
STATION
N
VHRR SCAN
SR SCAN
ORBIT PATH

Figure 2.14 Satellite orbital path and system.

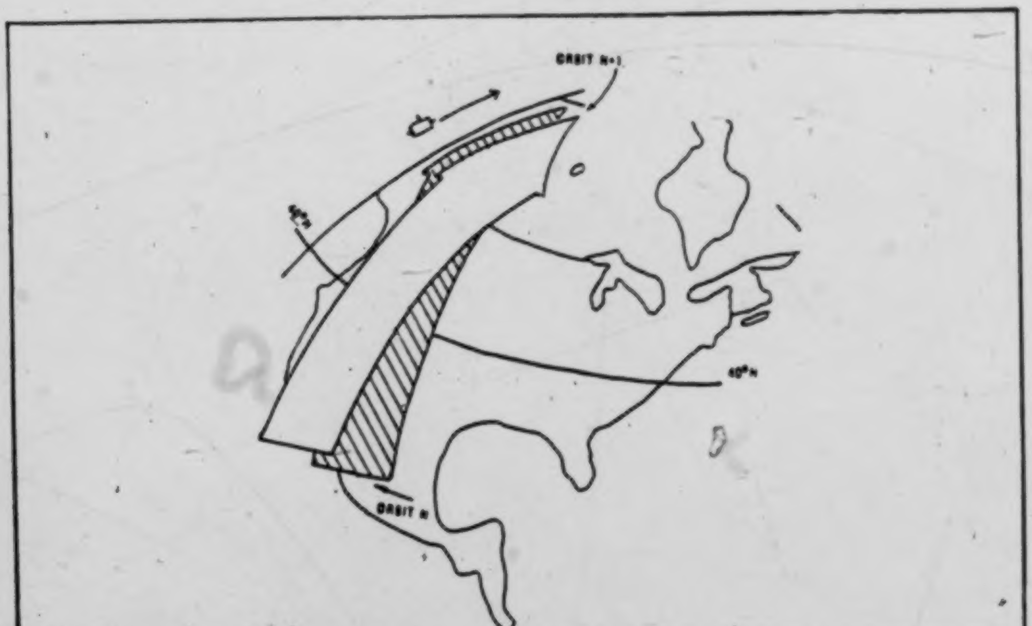
ORBIT N+1
40°N
ORBIT N

Figure 2.15 Satellite paths overlapping.

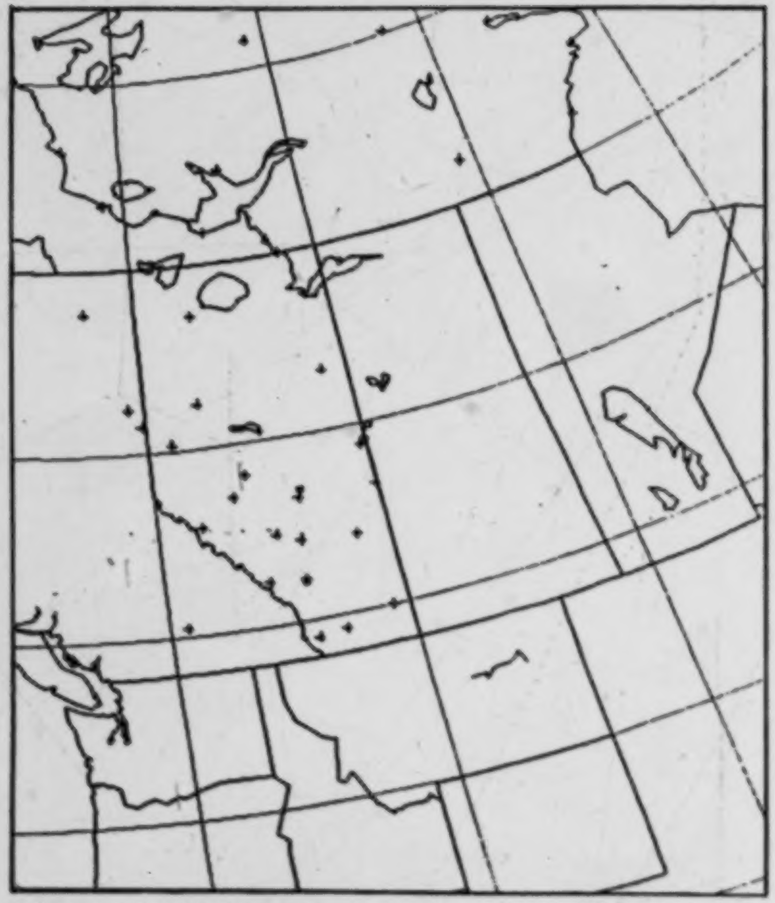

Figure 2.16 Computer produced overlay for NOAA-7 satellite pass #N (adapted from Alberta Weather Centre).

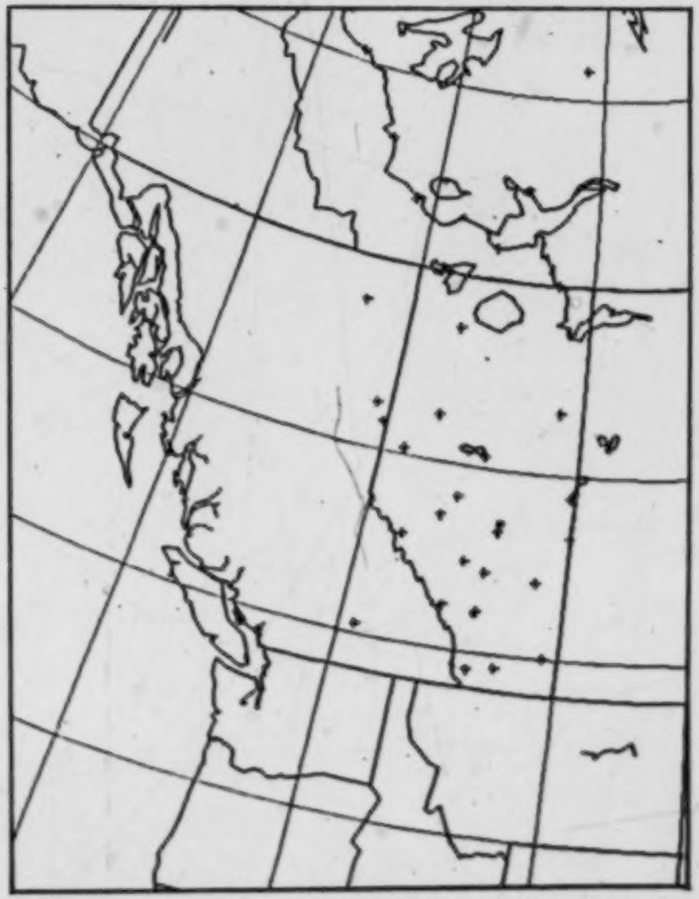

Figure 2.17 Computer produced overlay for NOAA-7 satellite pass #N+1 (adapted from Alberta Weather Centre).

shown that the total gridding error is due to both satellite altitude and time error. The total error is approximately 10 km at the satellite subpoint. Since this error is only 1% of the synoptic-scale horizontal parameter, it can be neglected in the current study.

#### 2.2.3.5 Satellite Resolution

By satellite resolution one means the ability to differentiate between small objects. The NOAA-7 AVHRR sensor data are corrected along the scan line in such a way that the spatial resolution is, nearly, constant and equal to about 1 km. in both the visible and infrared band. The spatial resolution between two adjacent scans is 1.1 km. Hence, the spatial resolution error can be neglected when one considers synoptic-scale systems.

### 2.2.4 Geostationary Satellites

Figure 2.18 shows the areal coverage of two geostationary satellites. Only GOES-W satellite (135° W) will be described in some detail. A GOES satellite is in an Earth-synchronous orbit, i.e. it moves in an orbit with angular speed equal to that of the Earth. Hence, GOES remains in a nearly fixed position relative to the Earth, i.e. geostationary relative to a particular longitude and the equator. Thus, the satellite views the same area of the Earth at all times. The areal coverage is shown schematically in Figure 2.19.

#### 2.2.4.1 GOES Satellite Parameters

-Height above the Earth's surface: approximately 35,800 km.

-The orbital period: 24 hours.

-Plane of rotation: the equatorial plane.

-Satellite motion: from west to east.

-The angular speed: 7.29 X $10^{-5}$ $s^{-1}$.

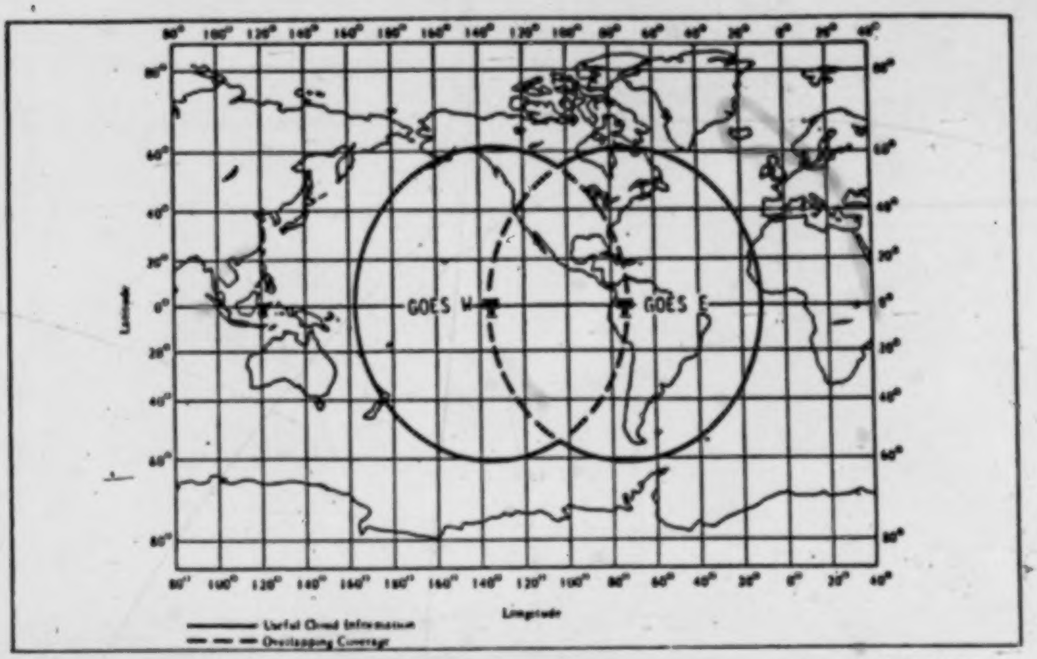
80° 100° 120° 140° 160° 180° 160° 140° 120° 100° 80° 60° 40° 20° 0° 20° 40°
80°
60°
40°
20°
0°
20°
40°
60°
80°
Latitude
GOES W
GOES E
Longitude
Useful Cloud Information
Overlapping Coverage

Figure 2.18 GOES-E and GOES-W (geostationary satellites) overlap area coverage (adapted from Clark 1983).

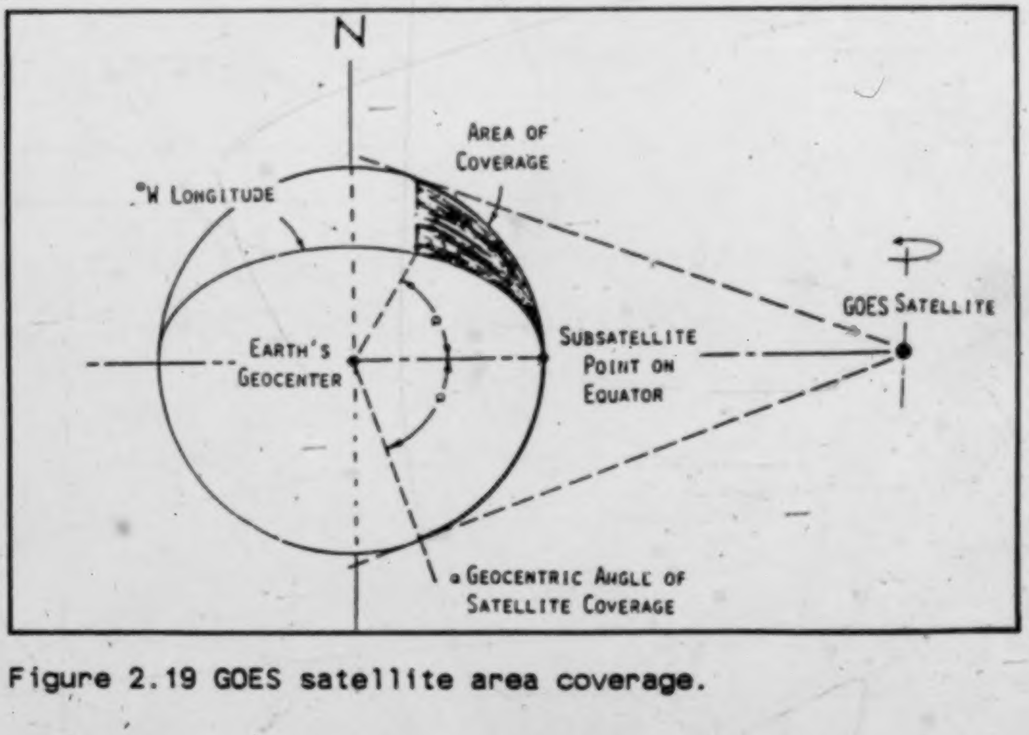
N
AREA OF COVERAGE
°W LONGITUDE
GOES SATELLITE
EARTH'S GEOCENTER
SUBSATELLITE POINT ON EQUATOR
ø GEOCENTRIC ANGLE OF SATELLITE COVERAGE

Figure 2.19 GOES satellite area coverage.

-The scanning mirror spin: 100 rotations per minute.

-The geometric scanning angle of the satellite coverage: 77 degrees.

-The frequency of coverage: once every 30 minutes .

### 2.2.4.2 Satellite Characteristics

The GOES-W satellite maintains a constant position with respect to 130° W longitude and the equatorial plane. It carries a VAS scanner (VISSR Atmospheric Sounder), VISSR stands for Visible and Infrared Spin Scan Radiometer. The primary VISSR scanner has a two-channel radiometer operating in visible (0.55-0.75 $\mu$m), and infrared (10-12.5 $\mu$m). Both the visible and infrared data are represented by digital counts (0-255) in a manner similar to that in NOAA satellites. In operational mode, data are transmitted on every scan line. The subpoint spatial resolution is 0.9 km. for the visible band and 6.9 km. for the infrared. Errors in spatial resolution can be neglected compared to the horizontal scale of synoptic-cloud systems.

## 2.3 Synoptic Data

Synoptic data are plotted on charts of different scales, but all are of polar stereographic projection true at 60° N and with map factor:

$$\text{map factor} = \frac{1 + \sin 60}{1 + \sin \phi} \qquad (2.1)$$

,where $\phi$ is the latitude angle. The original map scale of these charts is 1:20X$10^{6}$, where the mapping is conformal, i.e. the angle between latitude circles and meridians is constant and equal to 90 degrees. Since the overlay map of the satellite image does not coincide with the synoptic chart, a special map was constructed from several overlays for an area bounded by 90-150° W and 40-70° N. A sample of this chart is shown in Figure 2.20. The resulting map coincides exactly with the synoptic charts within an area of 10 degrees of longitude by 5 degrees of latitude. Outside this area distortion increases with increasing viewing area. The synoptic maps include the surface, 850-mb, 700-mb, 500-mb, 300-mb and 250-mb. They were obtained from Alberta Weather Centre archive and CMC (Canadian Meteorological Centre) microfilm archive.

### 2.3.1 Methods Of Analysis

Finite-difference and spectral methods are used for analysing synoptic data and their derived parameters. In the finite-difference method the solution of the basic atmospheric equations is represented at discrete grid points in space and time. In the spectral method the field variables (geopotential height , vorticity,... etc. ) are expanded in a series of coefficients and multiplied by orthogonal basis functions. Both methods are used in operational analysis and prognosis, but the solutions differ to some extent, e.g. in the numerical value of the vorticity field.

## 2.4 Selection Of Samples

In the process of selecting a sample, certain points should be considered namely; (i) the criteria of selection, (ii) the sources of data, (iii) the limitations of the data, and (iv) the available methods of analysis.

According to Anderson (1973, 1974) and Zwatz-Meise (1981), cloud systems can be classified according to characteristic dimensions. This general classification includes the synoptic-scale cloud system as a major group, which in turn is sub-classified into four sub-groups. However, these studies did not provide a theoretical basis for such classification, but it relied mainly on the subjective examination of satellite image cases. Although Zwatz-Meiŝe has used surface and upper-level synoptic maps, her classification lacks the dimensional scaling thought necessary to such classification. It is the objective of this project to examine separate cases over Western Canada in an attempt to justify the usefulness of their models and to apply the dimensional analysis to these cases.

Case studies are chosen on the basis of cloud systems observed on satellite images. Satellite data in Spring and Summer seasons do not involve complexities, so, data

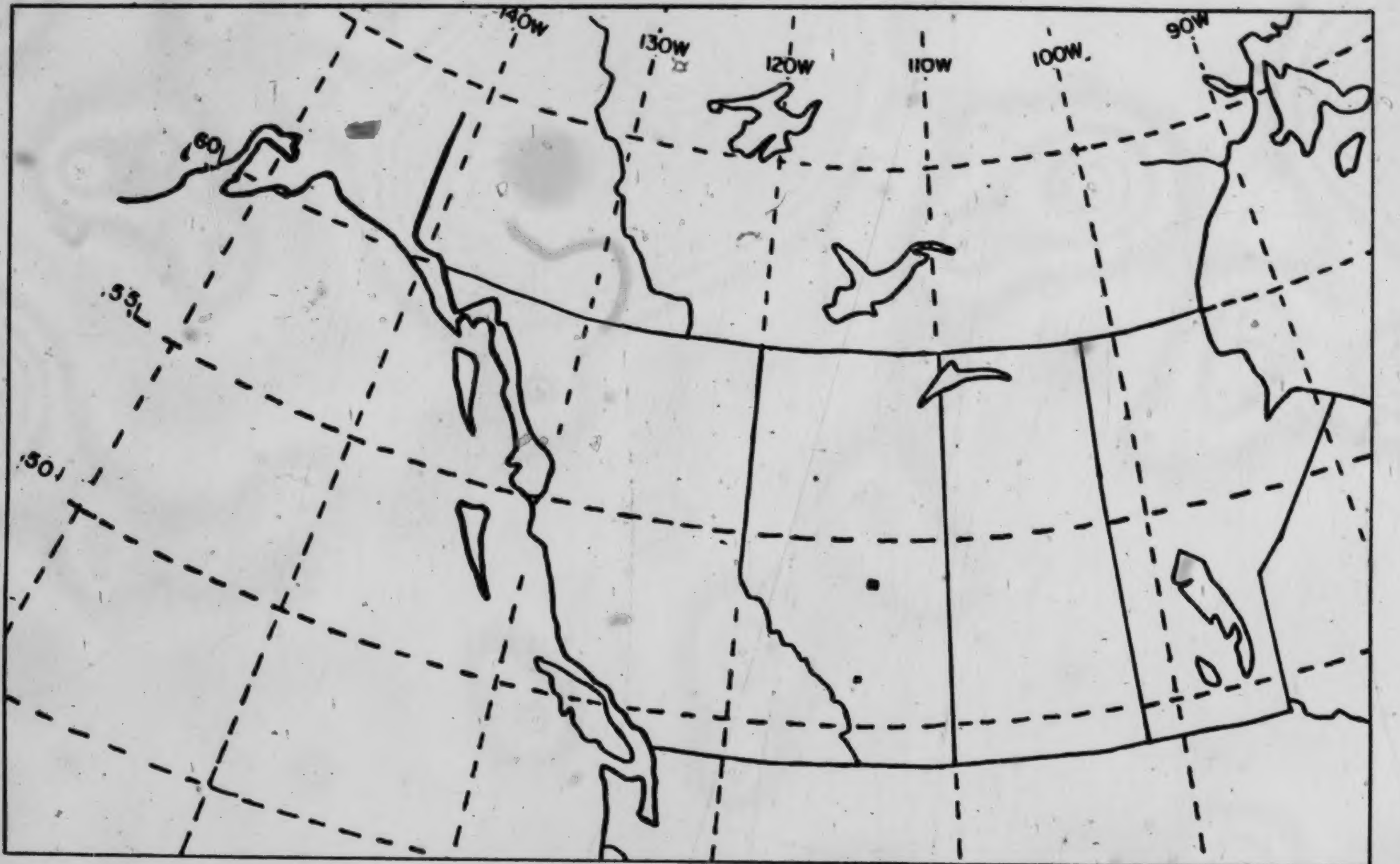
140W
130W
120W
110W
100W
90W
60
55
50

Figure 2.20 Reconstructed satellite overlay.

from April to September 1983 are to be examined. According to Orlaniski (1975), the horizontal scale dimension, being of synoptic scale, can be chosen as the main criterion for classifying weather systems. The second criterion for selection is the following: if a cloud system which, for the most part of its existence, is sub-synoptic in scale, but attains synoptic-scale size at some stage during its development, it will be considered synoptic-scale cloud system.

The principal sources of data are satellite images from NOAA-6,7 and 8. Additional satellite images from GOES-W and GOES-E are used whenever more details are needed. After different synoptic systems have been identified on satellite images, synoptic charts are used to support that classification. Since conventional radio-sonde data are issued only twice a day, time differences between satellite data and conventional data of +3 or -3 hours will be considered in the analysis. however, any approximations, in time and space do not present a serious problem, but rather introduce elements of reality into the classification process by tending to eliminate spurious accuracy and preventing the formulation of an overly-idealized synoptic cloud model.

Limitations on the selection and analysis of the data:

(i)-The period for selection: April to September 1983 inclusive.

(ii)-Satellite data used: NOAA-6, NOAA-7, NOAA-8, and GOES-W satellite images.

(iii)-Topographic effect :To be limited by confining the study to areas of uncomplicated topography, as much as possible, since mountainous regions contribute to different weather processes and cloud system variations.

(iv)-Satellite data are studied first, then synoptic data. Finally, both sets of data are examined together.

(v)-The general features of the classification and its subgroups are presented.

## 2.5 Synoptic Scale Cloud System Classification

Charney's (1948) criterion for large scale motion systems is not easily applied to satellite data. As mention above in Section 1.2 Chapter 1, he considered basic dimensions with specified orders of magnitude, which when applied to synoptic data eliminate nonsignificant waves.

The application of Charney's criterion to satellite data may eliminate some synoptic cloud patterns. By synoptic cloud pattern, is meant, an area of cloud that extends over one or more synoptic dimensions. Cloud patterns on satellite images may show a region of cloudiness that satisfy only one or two synoptic dimensions and yet must be classified as a synoptic pattern configuration. Examination of synoptic cloud patterns shows that the horizontal dimension may be considered as the best measures of, and principal factor common to all synoptic-scale cloud patterns. Moreover, the horizontal dimension of a cloud system can be measured directly on gridded images, whereas other dimensions such as the vertical dimension are measured indirectly. Thus a practical criterion for cloud systems classification may be stated as follows: " any cloud system which satisfies, for a period of about 12 hours at least the synoptic-scale horizontal dimension will be considered as a synoptic system".

The above criterion is based on the observable characteristics of different cloud systems, as seen on satellite images and in connection with the corresponding conventional data. Of course, one should not ignore the fact that this criterion may have limited applicability because of the limited number of examined cases, and thus is of a probabilistic result. In other words, within the synoptic-scale domain, one may expect it to have highest probability of occurence. In any event, the results are limited to within the synoptic-scale order of magnitude, and do not apply to specific scales.

### 2.5.1 Introduction

The different dimensions of a synoptic cloud system, applied to satellite data, are defined as follows:

(i)-The horizontal dimension, L, which is of the order of 1000km, represents the length of a cloud area in the horizontal direction of expanding.

(ii)-The vertical dimension, H, which is of the order of 10 km, represents the thickness of a cloud area.

(iii)-The speed of propagation, C, which is of the order of 10 meters per second represents the horizontal speed of the centroid of a cloud area.

(iv)-The time dimension, T, which is of the order of 1 day, represents the time within which a cloud area attains synoptic size.

The examination of different synoptic cloud areas, on satellite images, suggests that they may be classified into four main groups. Each group possesses distinct but common features that differentiates it from the other groups The four groups are: (i) cloud bands group, (ii) vortex cloud group, (iii) cellular cloud group, and (vi) uniform cloud group. In the following pages, each group will be defined in terms of its specific characteristics and examples for each will be given.

### 2.5.2 Cloud Bands Group

A cloud band is defined as a nearly continous, relatively broad formation extended in one direction, and only slightly curved. The length of such a cloud pattern is typically five to eight times the width. The curvature of the band is of the order of $10^{-3}$ $km^{-1}$ or less, so that the radius of the band is greater than 1000 km. The curvature character may be used to differentiate between cloud bands and cloud vortices, which in all other aspects may be of the same order of magnitude in lateral and areal extent. As will be seen, the thickness dimension varies for the different cloud patterns included in this group. For example, a frontal band may have a thickness of 10 km, while for a jet band it is approximately 1 km. The variation in this dimension from one pattern to the other makes it difficult to consider the thickness as a necessary condition within the synoptic regime. A similar problem arises with the speed of propagation of cloud bands. For example, the speed of a frontal band is typically about 30 knots, while for a jet band it is about 100 knots, or about one order of magnitude greater. However, the variation in the dimension T is limited to a narrow range. It is of the order of one day, e.g. a jet band may persist for five days, while a frontal band may persist for seven days. This group includes eight bands, all having the same general characteristics but differing in lesser specific features. The eight subgroups are: (i) the frontal band, (ii) the pre-frontal band, (iii) the post-frontal band, (iv) the convergence band, (v) the orographic band, (vi) the shear band, (vii) the jet band, and (viii) the non-frontal band. Examples of each type are described below, illustrated with pertinent maps and satellite images.

#### 2.5.2.1 The Frontal Cloud Band

This band is, most easily, detected on a satellite image, even in weak cases. It has a length of about 3000 km on average, and a small width of about 500 km. This band appears very bright in the visible image, and very white in the infrared. Several examples are shown in Figures 2.21, 2.22, 2.23, 2.24, 2.25, 2.26, and 2.31. In each image the band is marked with the letter (A). In Figures 2.21 and 2.22 arrows delineate the back edge of each band. The bands are of considerable vertical extent, as can be deduced from both the visible and infrared images: very dense in the visible and very bright in the infrared. In Figure 2.21, at the area of the bulge over the West Coast at (A), the band is highly reflective in the visible and a very cold (black) in the infrared, wrapped and enhanced image. Another example is shown in Figure 2.22. The abrupt change, on the back edge of the band, indicates a rapid change in the vertical motion field, with ascending motion along the band, and subsidence in the cloud free-area.

Since the activity of a front is closely related to the brightness of the frontal cloud, it may be readily assessed from the satellite image. In Figures 2.21, 2.22, the band is active; in Figures 2.23, 2.26, it is less active; and in Figures 2.24, 2.31 it is inactive. Thorough investigation of several cases showed that the degree of activity of a frontal band depends at least on three parameters:

(i)- the surface front,

(ii)- the thermal front, a parameter marked by the line of maximum change in the gradient of the thickness field of the layer 500 / 1000 km., and

(iii)- the zero isopleth of the relative vorticity field at the 500-mb surface, which divides areas of anticyclonic vorticity from areas of cyclonic vorticity. Examination of these parameters suggests that the activity of a frontal band is a function of the distance between the isolines: the closer the parameter lines to each other the more active the band. Figures 2.21 and 2.21.1 show an active frontal band, where the front and isopleths are close together and intersect. On the other hand, Figures 2.24 and 2.24.1 depict an inactive case, where the isolines are far apart.

As noted before, the frontal band has a well-defined trailing edge which is bent into a smooth curve having a radius of the order of 1000 km. This curvature is always positive or cyclonic. Sometimes, an irregular pattern may develop on the trailing edge, as seen in Figure 2.21. This irregular formation may harbour an incipient wave which may later evolve into a separate cyclonic system. The frontal band can be associated with either a cold, warm, or stationary front. The cold frontal band is the most persisting and active, while the warm band can be identified only with difficulty because of its short lifetime.

### 2.5.2.2 Pre-Frontal Cloud Band

The pre-frontal band is associated, but not connected, with a frontal band. In all the cases examined, it was associated with either a stationary or cold-frontal band.

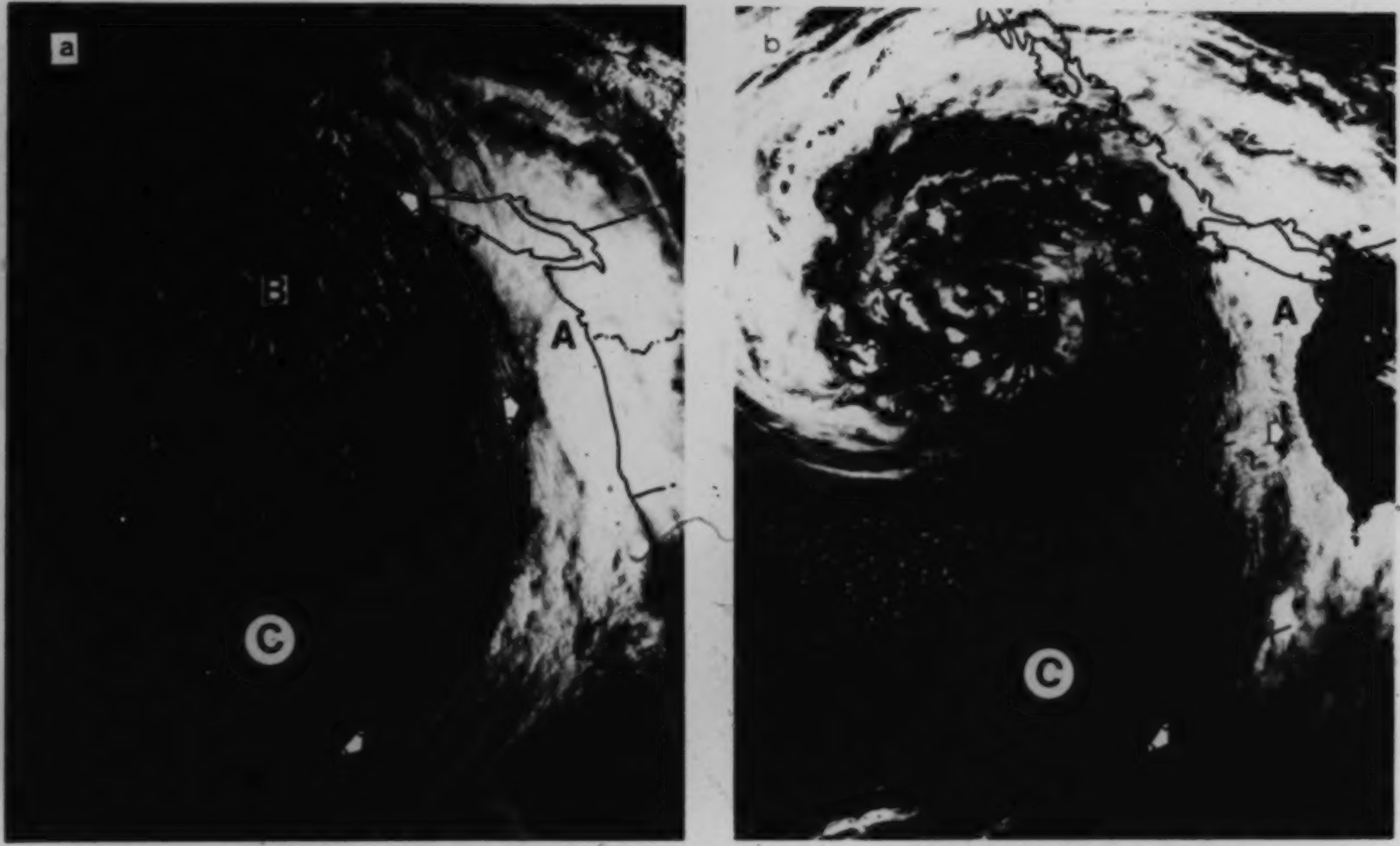

Figure 2.21 NOAA-6 satellite image, a) visible, b) infrared, 1635 GMT, 01 April 1983.

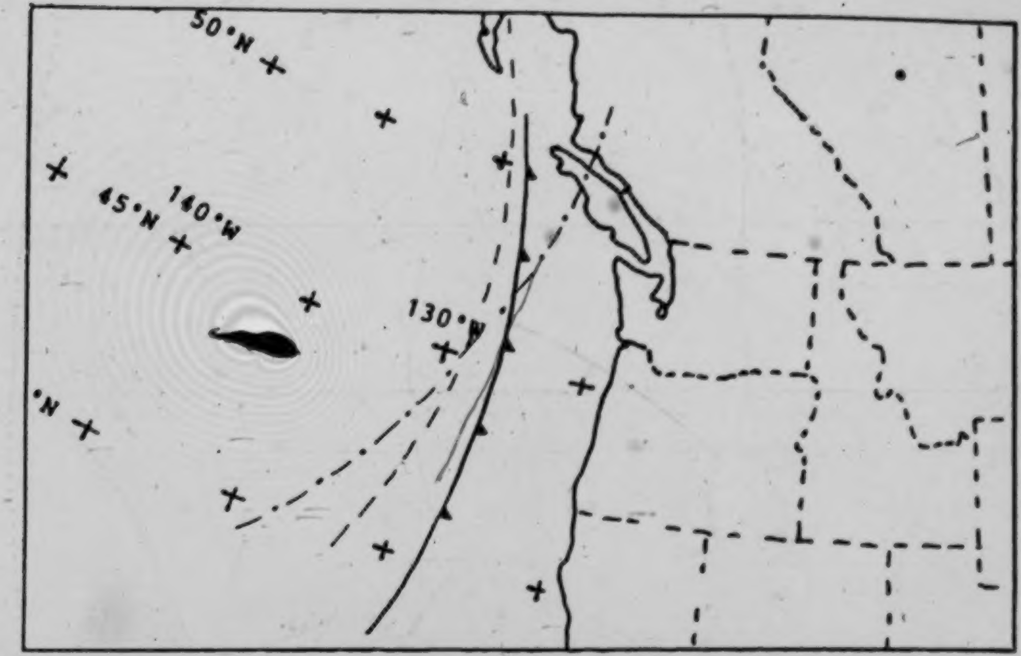

Figure 2.21.1 01 April 1983, 1200 GMT dashed line: zero isopleth of relative vorticity at 500 mb, dashed-dotted line: thermal front parameter for the layer 1000/500 mb.

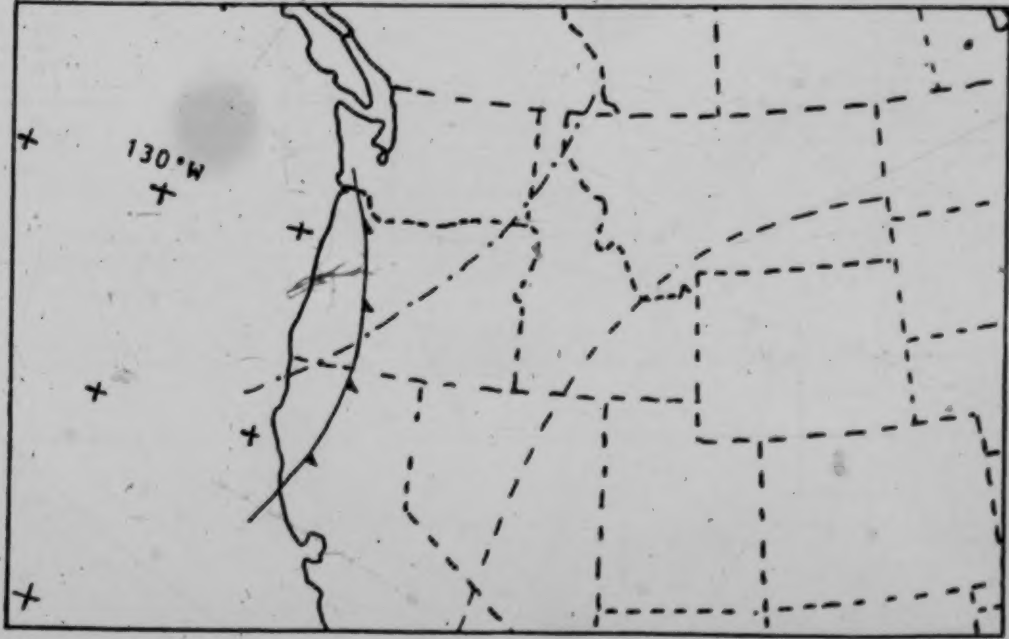

Figure 2.24.1 01 July 1983, 1200 GMT dashed line: zero isopleth of relative vorticity at 500 mb, dashed-dotted line: thermal front parameter for the layer 1000/500 mb.

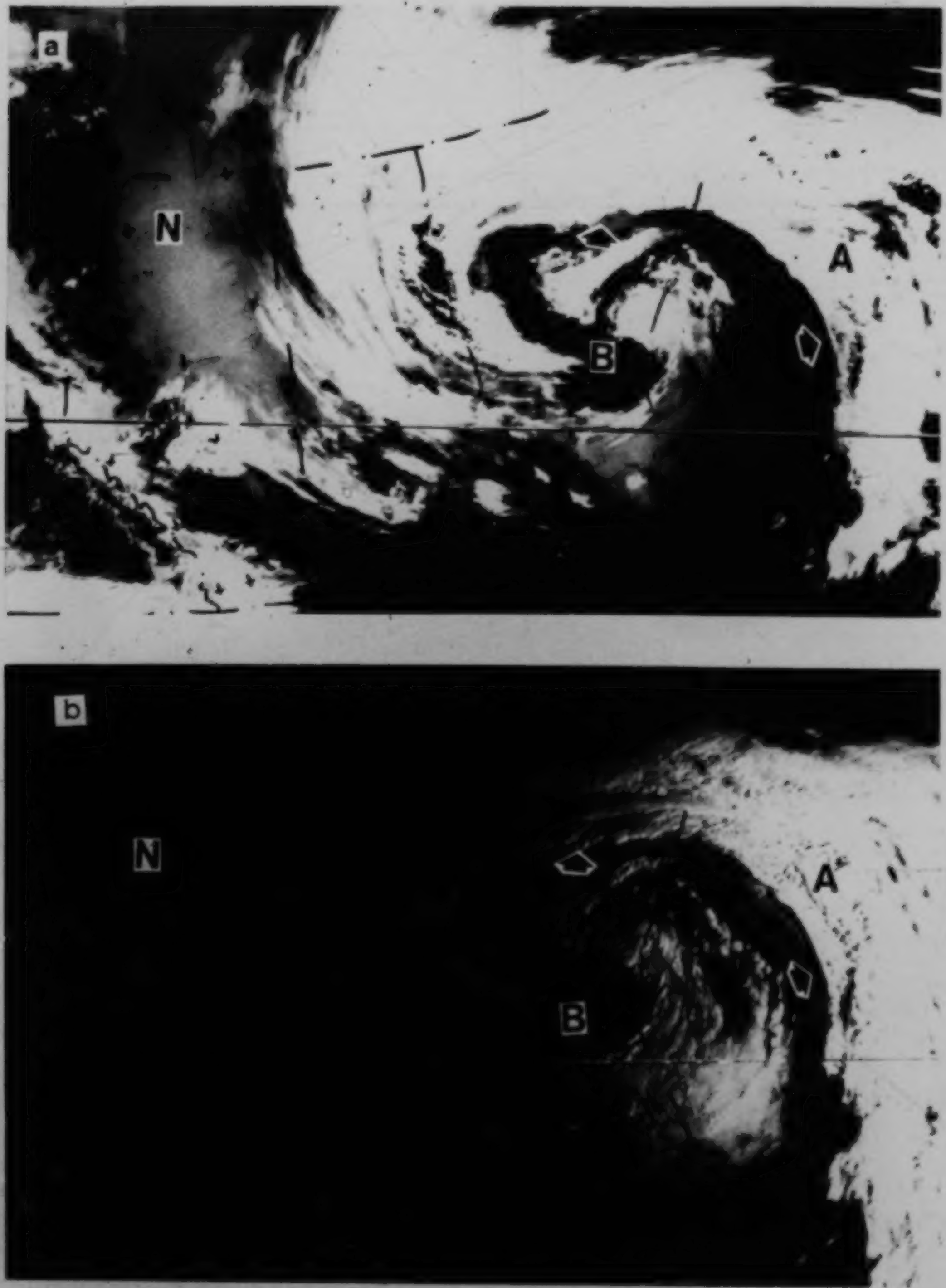

Figure 2.22 NOAA-8 satellite image, a) infrared, b) visible, 1501 GMT, 18 September 1983.

Kress and Zwatz-Meise (1980-a) were the first to define this band. Examples of the band structure are shown in Figures 2.23, 2.24; where the band is marked with the letter (E). In all the cases examined, the band stretched parallel to the frontal band. In Figure 2.23, one can detect two pre-frontal bands extending meridionally and parallel to the frontal band (A). The first band, not marked, extends southward over Idaho, and the second marked with (E), is also parallel to the band (A). The separate cloud bands can readily be discerned on high-resolution satellite images, such as Figure 2.23, where the cloud-free areas between (E) and (A) stand out clearly in both the visible and infrared. In mountainous regions, the clearing between bands may be enhanced by orographic effects. In other cases one may interpret those bands as warm frontal bands. Figure 2.24 is another example, where the black arrows show the separation between the different bands.

Satellite images provide the first clue for identifying pre-frontal bands. They are parallel to frontal bands and have the same orientation, and similar characteristic dimensions. At later stages of development, both the frontal and pre-frontal bands may merge in such a way that it will be difficult to differentiate between them. This is because the speed of propagation of the pre-frontal band is much less than that for a frontal band. Unless the development history is traced back to its origin, the band may be misinterpreted as a warm frontal band. However, one should remember that a warm frontal band has a different orientation and is not parallel to a cold frontal band.

Active bands are associated with sharp ridges in the 500 / 1000 mb thickness field, while inactive bands are not. Also, the use of the thickness field enables one to locate the band. In the cases examined, the band was located approximately 2° of latitude upstream of the thickness ridge, except in cases having more than one pre-frontal band. Examples are shown in Figures 2.23 and 2.24. Figure 2.23 is a case of active development, where the pre-frontal band is associated with the sharp ridge of the thickness lines as shown in Figure 2.23.1. Band (E) is also upstream of the thickness ridge, while the first pre-frontal band (not marked) is located on the thickness ridge.

Figure 2.24 represents an inactive case. Comparing the image in Figure 2.24 to the map in Figure 2.24.1 shows that the band (E) is also located upstream of a flat thickness ridge. In both cases, the frontal band (A) is located a few degrees downstream of the thickness trough. Checking the locations with respect to the thickness fields for other layers, e.g. 850/500 mb and 500/250 mb, did not change the spatial relationships.

The above findings are at variance with the results of Kress and Zwatz-Meise (1980-a). In their study of European systems they found that the pre-frontal band is located on the ridge of a flat thickness field and has a quite different orientation from that of the frontal band.

### 2.5.2.3 Post-Frontal Cloud Band

This band does not seem to have been recognized by other authors despite its being a readily identifiable distinct entity on satellite images. The post-frontal band forms to the rear of the frontal band; it is parallel to the frontal band, and conforms to it in orientation and cyclonic curvature. The frontal band is usually associated with cold occluded frontal system. The post-frontal band merges with the frontal band in the early stages of development, it may be identified by its structural difference. For example, in Figures 2.25 and 2.26 the post-frontal band is marked with the letter (F) and the arrows point out the different trailing edges. Both (F) and (A) are of comparable horizontal structure, but the vertical extents are different. The satellite images reveal that (F) is composed of thin high level clouds much less in depth than the clouds of band (A).

The post-frontal band is not associated with an upper-level shear field or a jet stream system. Moreover, it does not have the fibrous structure of jet or shear

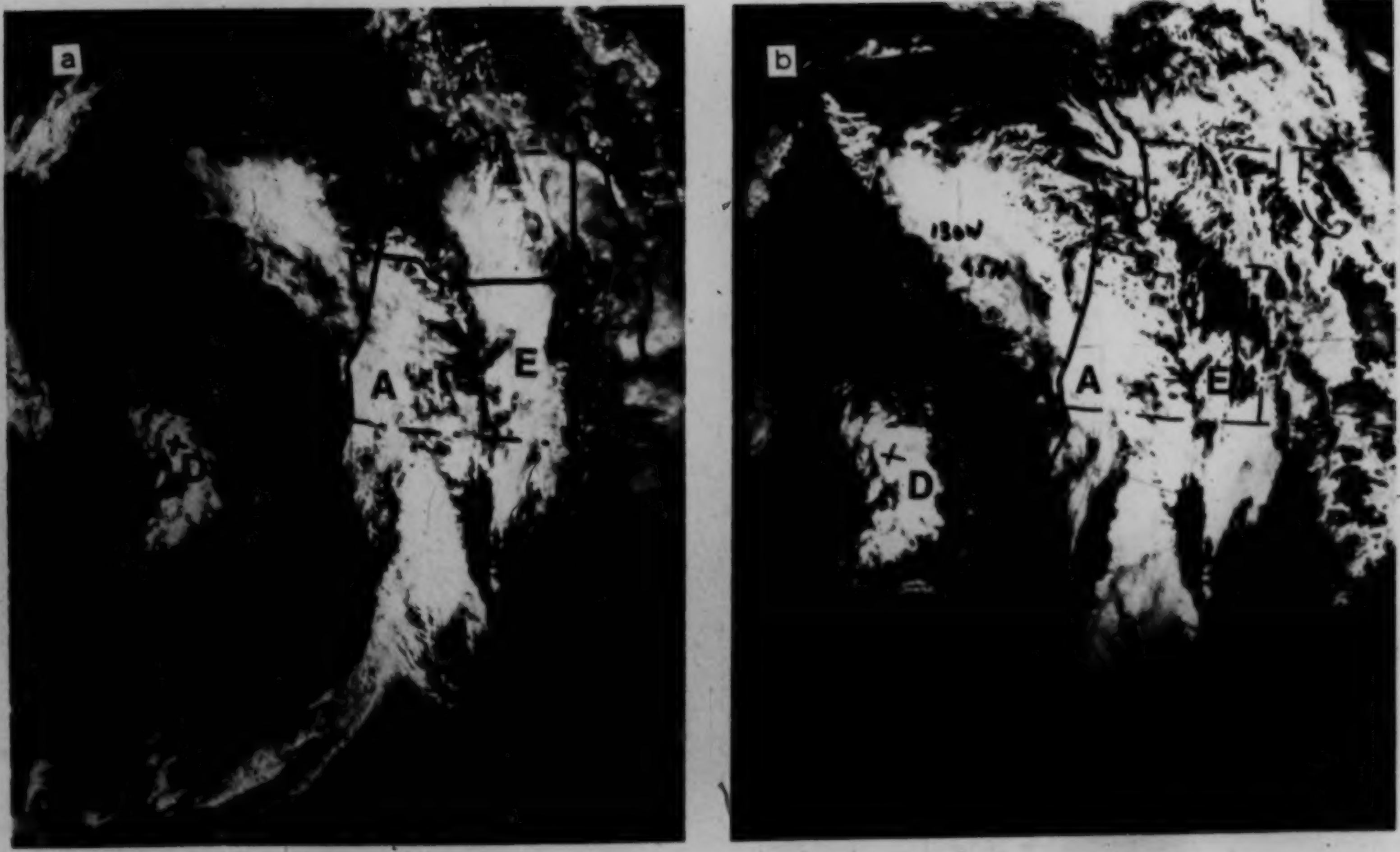
a
A
E
D
b
130W
45N
A
E
D

Figure 2.23 NOAA-7 satellite image, a) visible, b) infrared, 2306 GMT, 23 April 1983.

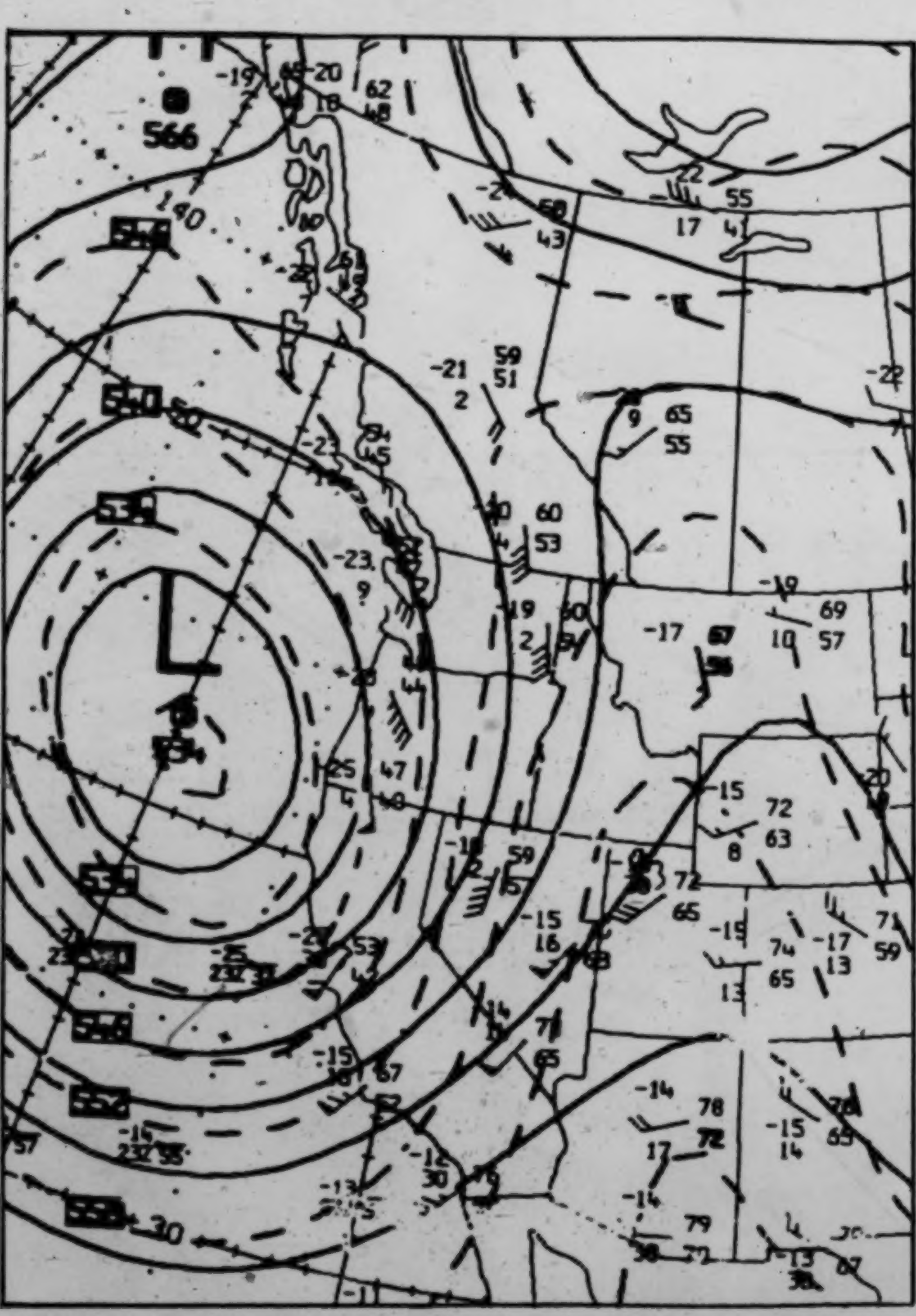
566
546
540
534
534
540
546
552
558
140
30
L

Figure 2.23.1 24 April 1983, 0000 GMT, CMC 500 mb analysis, dashed lines: thickness contours for the layer 500/1000 mb.

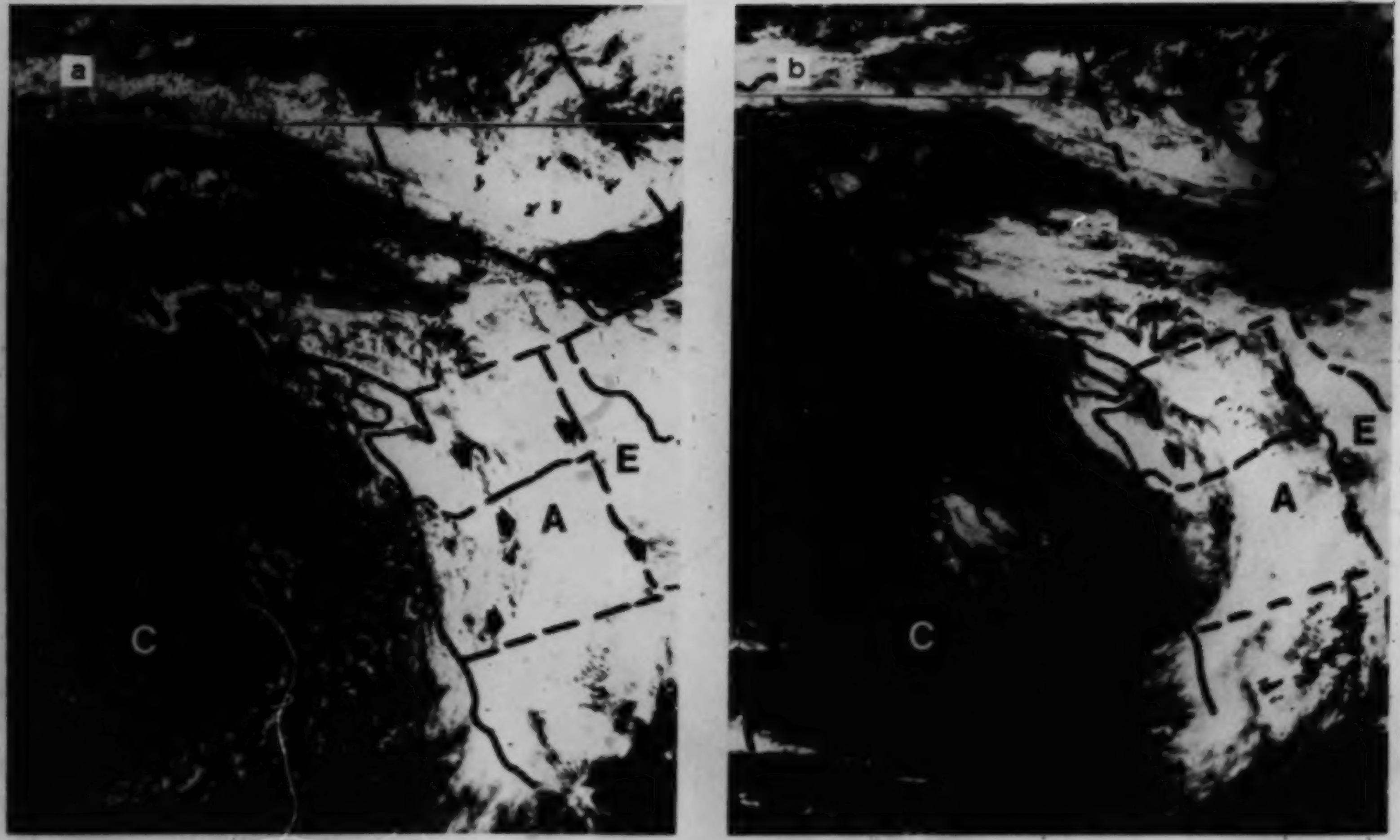

Figure 2.24 NOAA-8 satellite image, a) visible, b) infrared, 1642 GMT, 01 July 1983.

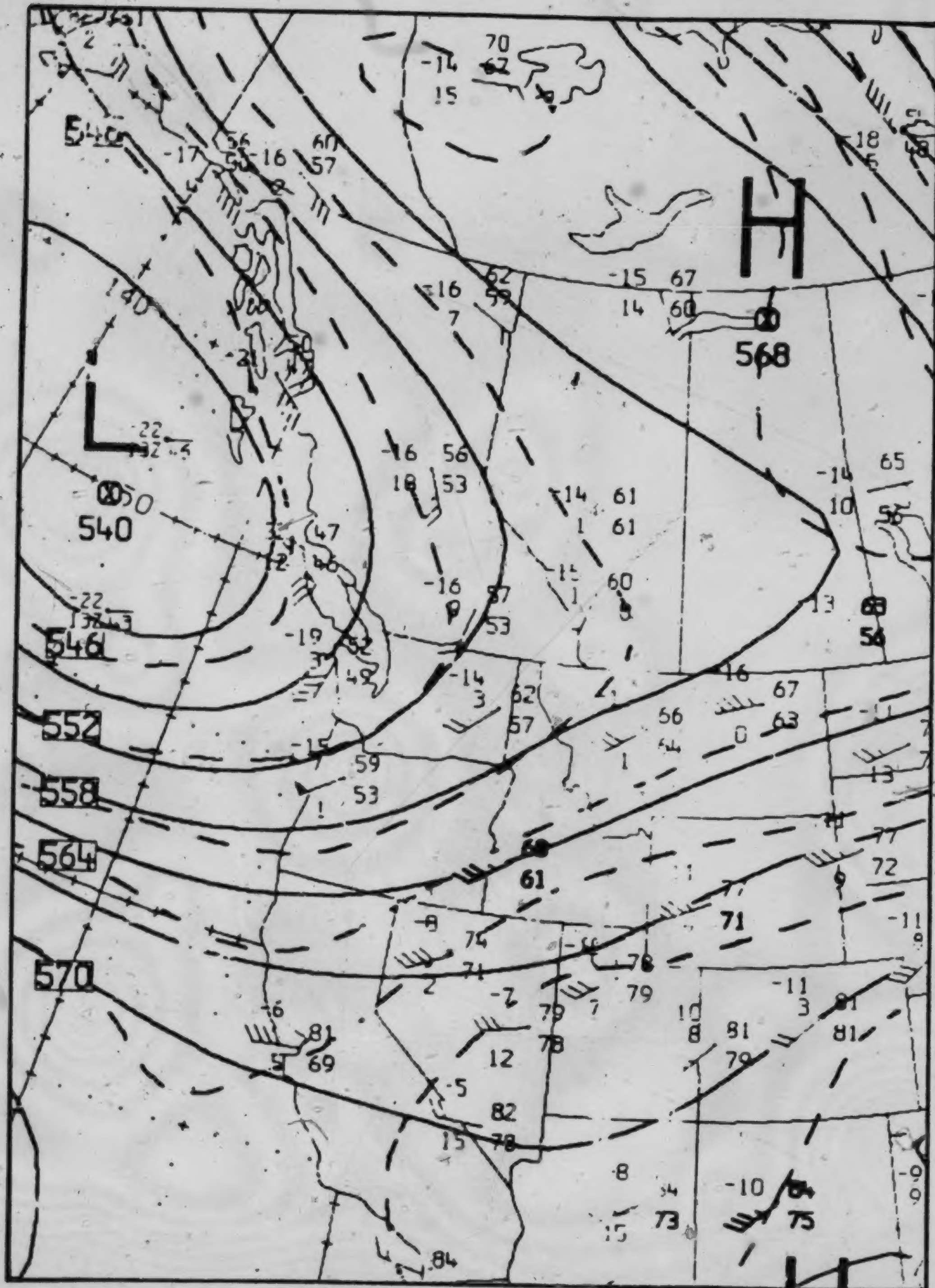
H
568
L
540
546
552
558
564
570

Figure 2.24.2 01 July 1983, 1200 GMT, CMC 500 analysis, dashed lines: thickness contours for the layer 500/1000 mb.

bands. The physical process behind the formation of this band is not fully understood but attempts were made to arrive to a tentative explanation by relating conventional data to satellite data. Visible and infrared images provide the first clue : the post-frontal band obviously is different from the frontal band in vertical structure. From the thickness field of 850 / 700 mb and 500 / 250 mb layers, one may deduce that a post-frontal band is associated with low-layer (850 / 700 mb) thickness ridge and an upper-layer (500 / 250 mb) thickness trough. These relationships may be examined by reference to the image of Figure 2.25 and the map in Figure 2.25.1. A full explanation of the formation of the post-frontal band is beyond the scope of the present study.

### 2.5.2.4 Convergence Cloud Band

A convergence band is an old frontal band which has lost some of its characteristic frontal parameters, and has come under the control of a horizontal convergence field at upper levels. Hailzl (1980) was the first to define and analyse the development process of this band. Early recognition of the band allows one to make a better estimate for its motion and development. The band has all the characteristics of a frontal band except its curvature and width. The curvature of the band becomes anticyclonic or zero, while its width decreases and becomes more uniform. Both edges of the band become sharper with the trailing edge defined mostly clearly.

It is difficult to identify a frontal band from a convergence band using satellite data only, especially if the band is in a transitional stage. However, the incorporation of both satellite data and the ( estimated ) 500-mb convergence fields makes it possible to identify the covergence band. Figures 2.27 and 2.28 show a case of transition from frontal to convergence band, where the band is marked with the letter (J). Figure 2.27 is the final stage, where (J) attained the character of a convergence band, while Figure 2.28 shows an intermediate stage. The synoptic

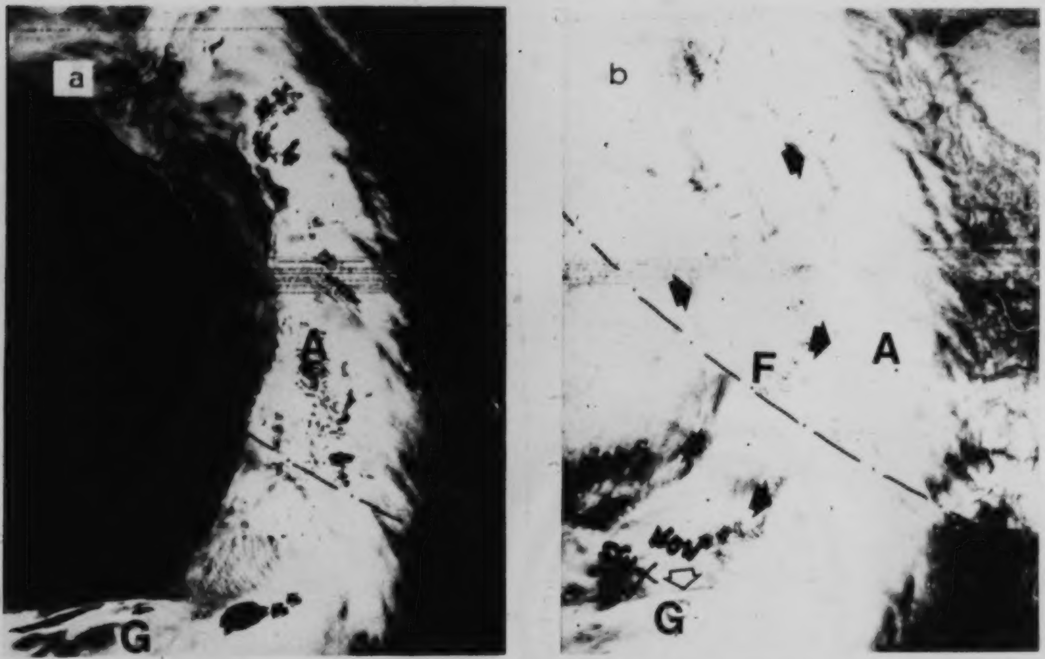

Figure 2.25 NOAA-7 satellite image, a) infrared, b) visible, 2316 GMT, 14 April 1983.

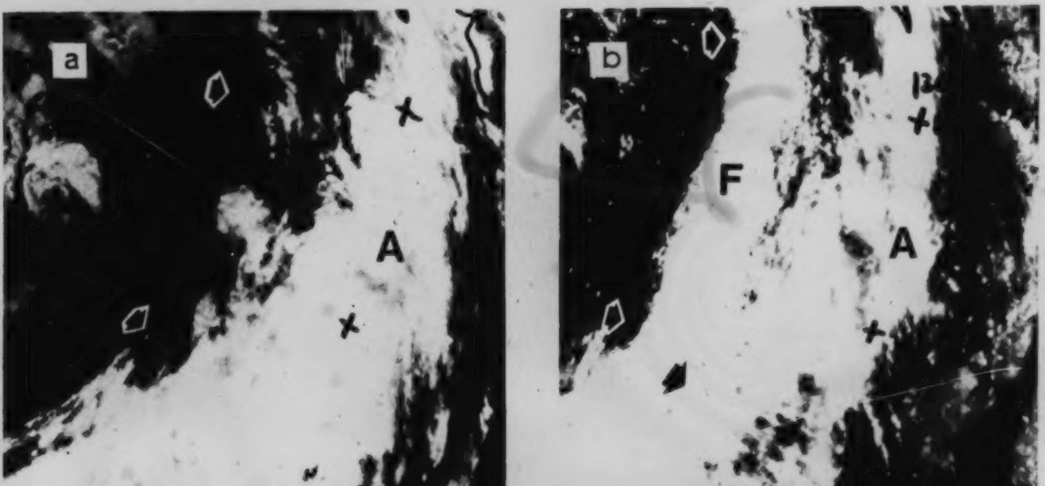

Figure 2.26 NOAA-7 satellite image, a) infrared, b) visible, 2321 GMT, 27 June 1983.

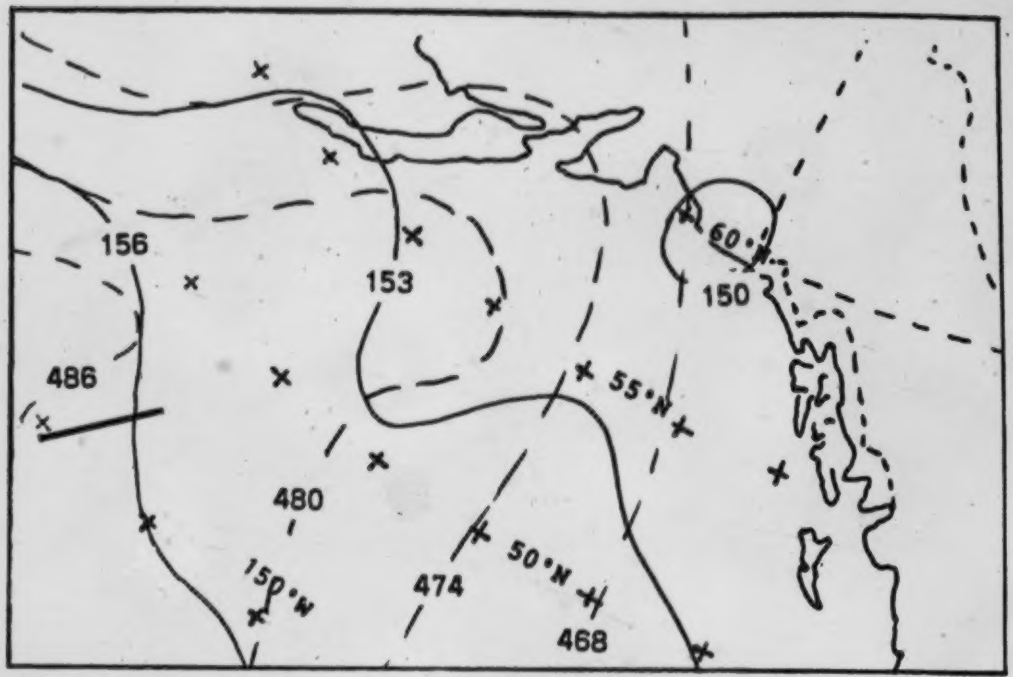
156
153
150
60°N
486
55°N
480
150°W
474
50°N
468

Figure 2.25.1 15 April 1983, 0000 GMT dashed lines: thickness contours for the layer 850/700 mb, solid lines: thickness contours for the layer 500/250 mb.

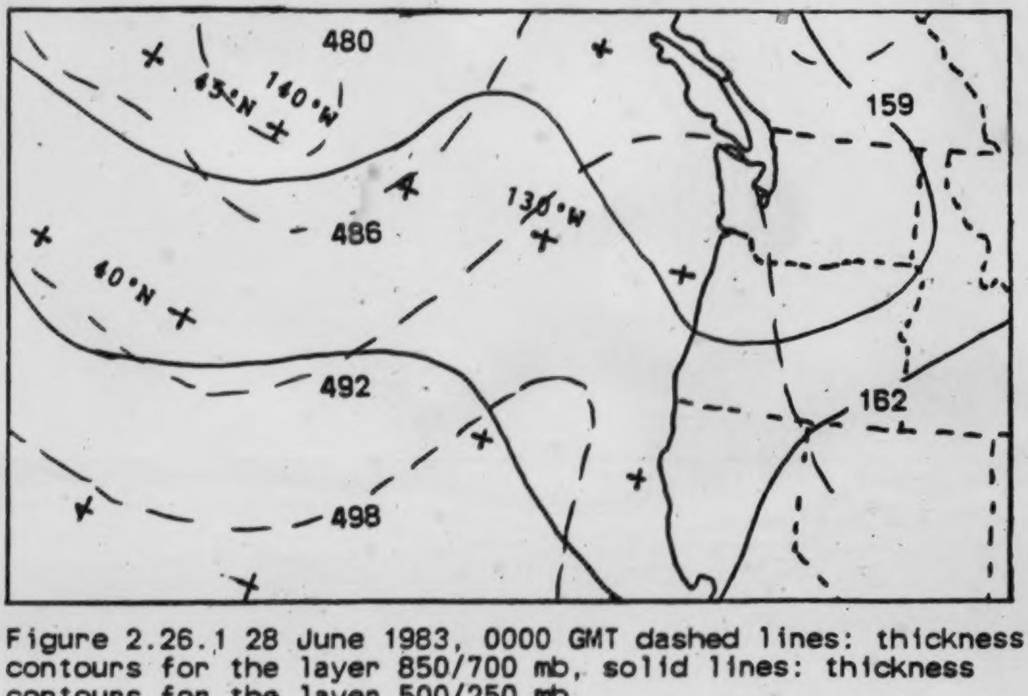
480
45°N
140°W
159
130°W
486
40°N
492
162
498

Figure 2.26.1 28 June 1983, 0000 GMT dashed lines: thickness contours for the layer 850/700 mb, solid lines: thickness contours for the layer 500/250 mb.

maps of Figures 2.27.1 and 2.28.1 correspond to the images in Figures 2.27 and 2.28, respectively. From Figures 2.27 and 2.27.1 one may conclude that (J) came under increasing influence of the horizontal field of confluence, especially in the southern part of the band.

### 2.5.2.5 Orographic Cloud Band

The orographic cloud band satisfies synoptic-scale conditions only partly. The examples given in Figures 2.29 and 2.30 are marked with the letter (I). The band is very bright in the infrared and very white in the visible image. This band is shorter than the other cloud bands, but since its other dimensions are of synoptic scale, one may consider it also as a synoptic band. Examination of the limited number of cases shows that the band is not part of a rotational or a thermal field, but rather under the influence of an anticyclonic relative vorticity field, within an upper ridge or col. In the following example, Figures 2.29 and 2.29.1, the band (I) lies within an area of anticyclonic relative vorticity ( the absolute vorticity field is dash-dotted), an upper ridge, and near zero thickness gradient field. In the second example, Figure 2.30 and 2.30.1, the band (I) is located within the domain of a col, largely a region of anticyclonic relative vorticity within a weak thermal ridge.

This band seems to develop only in mountainous regions. Since the band is not, apparently, associated with specific thermal or dynamical fields, one may assume that its development is largely due to orographic lift.

### 2.5.2.6 Shear Cloud Band

This is a very special pattern of cloud bands. It was examined and defined by Zwatz-Meise and Hailzl in (1980-b). The band develops on the anticyclonic side of a maximum-gradient shear change. This gradient is well defined in the layer 700/250 mb. Thepenier and Gruette (1980) found similar bands over Europe. However, their investigation of cloud formation and development makes no refrence to upper-level

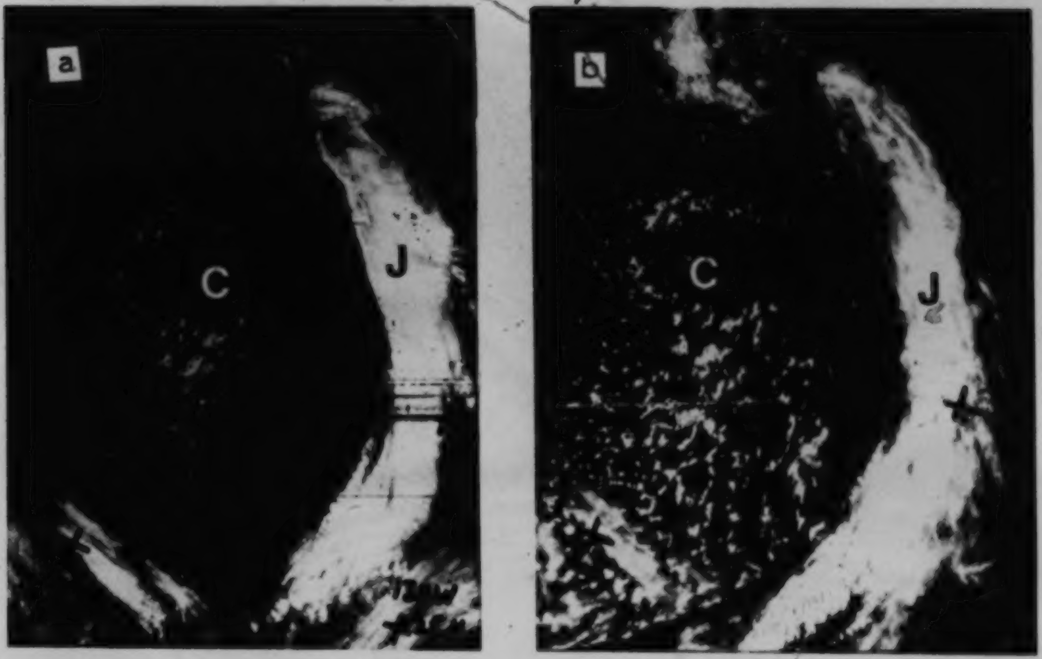

Figure 2.27 NOAA-7 satellite image, a) infrared, b) visible, 2316 GMT, 14 April 1983.

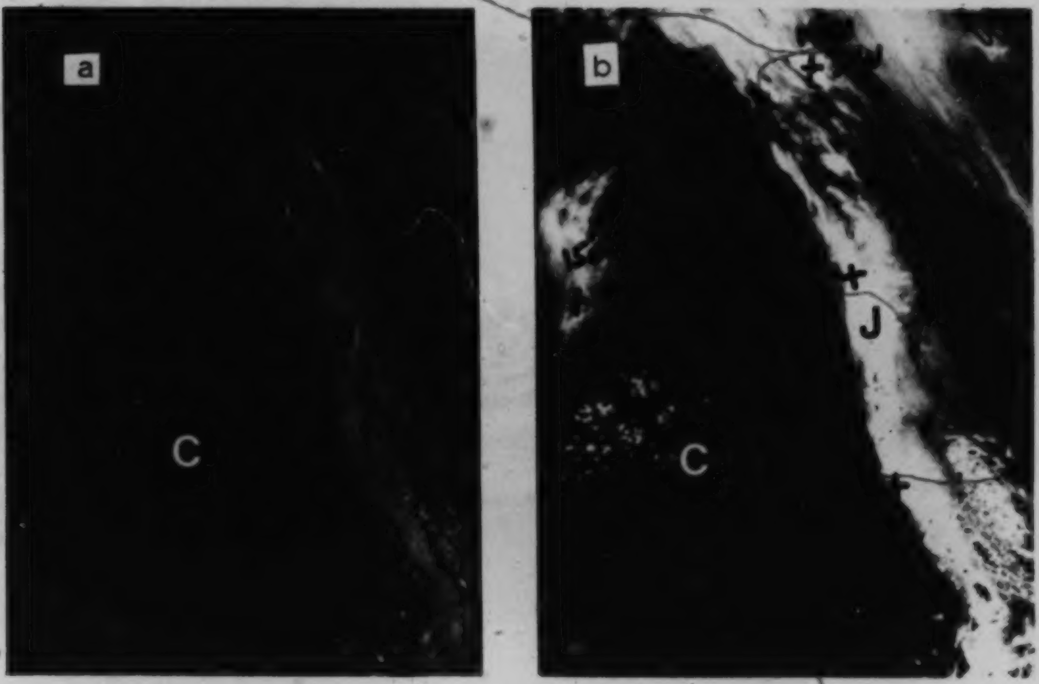

Figure 2.28 NOAA-7 satellite image, a) visible, b) infrared, 1650 GMT, 13 April 1983.

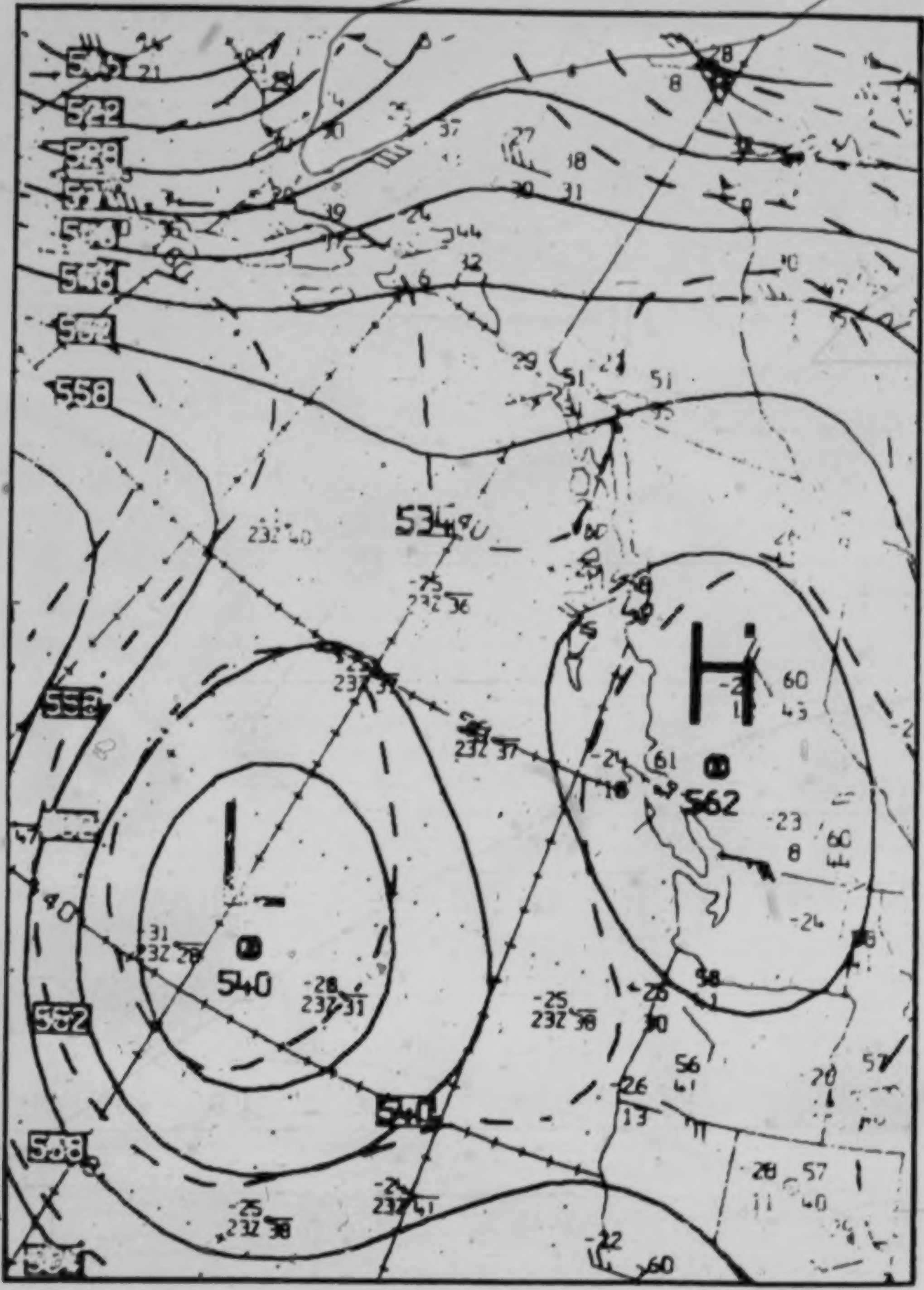
522
528
546
552
558
534
H
562
L
540
540
552
558
562
558

Figure 2.27.1 15 April 1983, 0000 GMT, CMC 500 mb analysis, dashed lines: thickness contours for the layer 500/1000 mb.

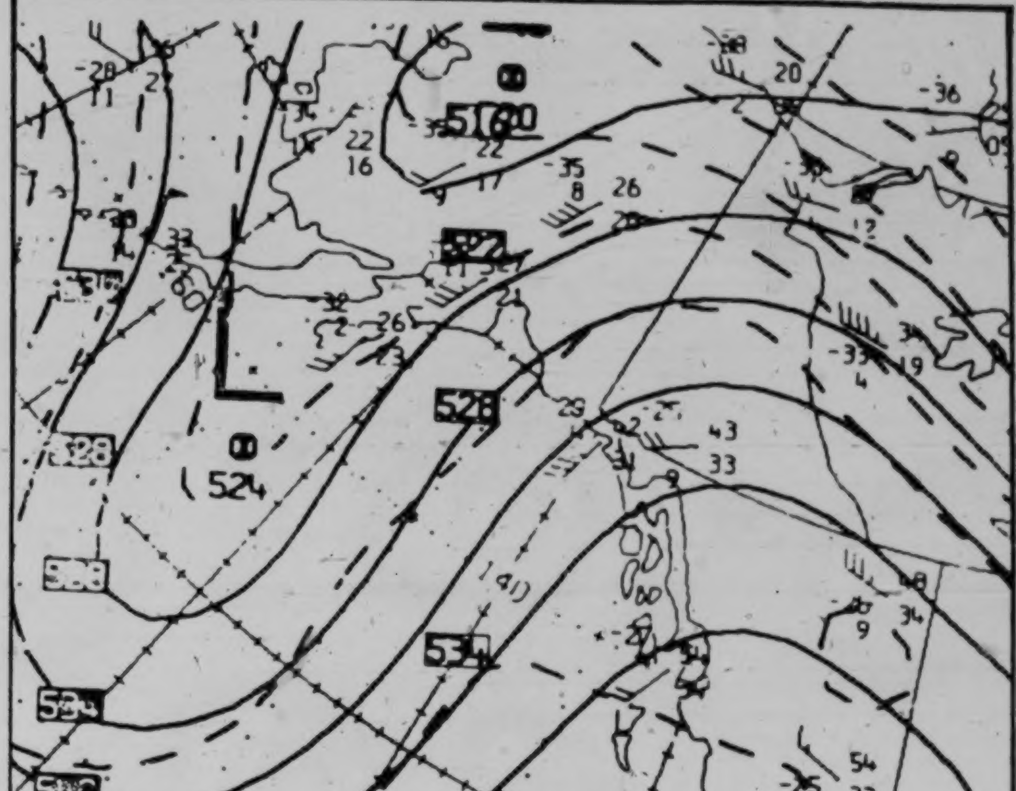

Figure 2.28.1 13 April 1983, 1200 GMT, CMC 500 mb analysis, dashed lines: thickness contours for the layer 500/1000 mb.

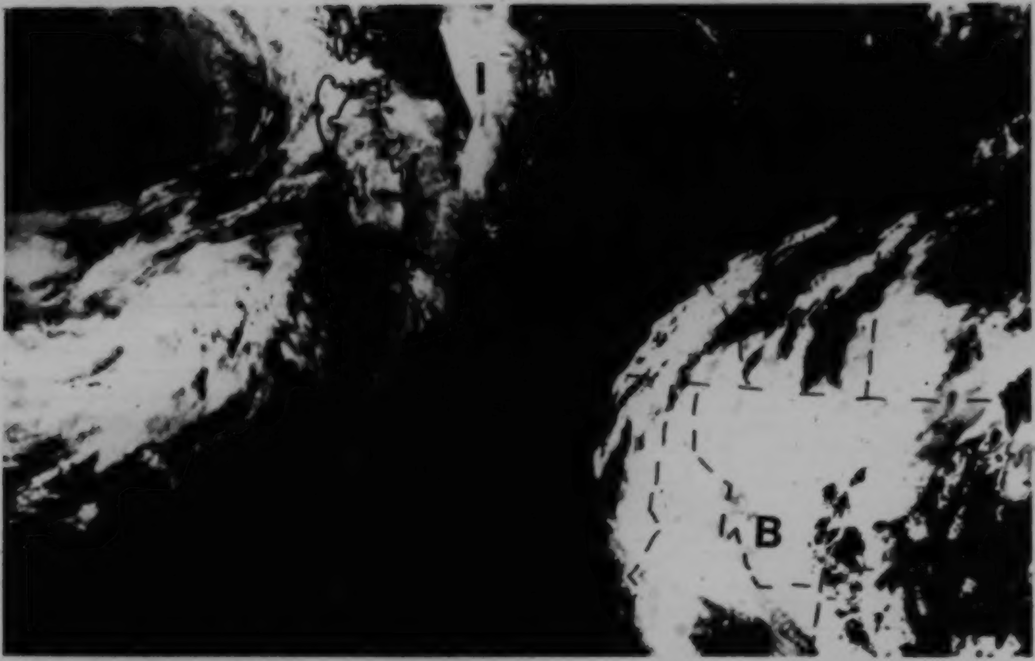

Figure 2.29 NOAA-8 satellite image, infrared, 0258 GMT, 10 July 1983.

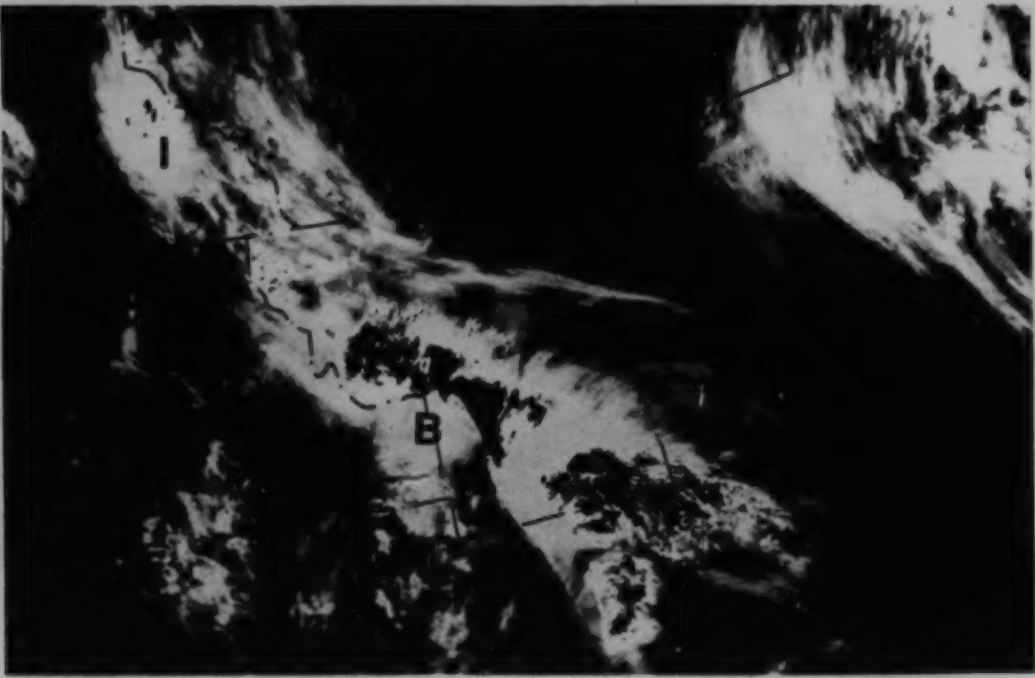

Figure 2.30 NOAA-7 satellite image, infrared, 1035 GMT, 03 April 1983.

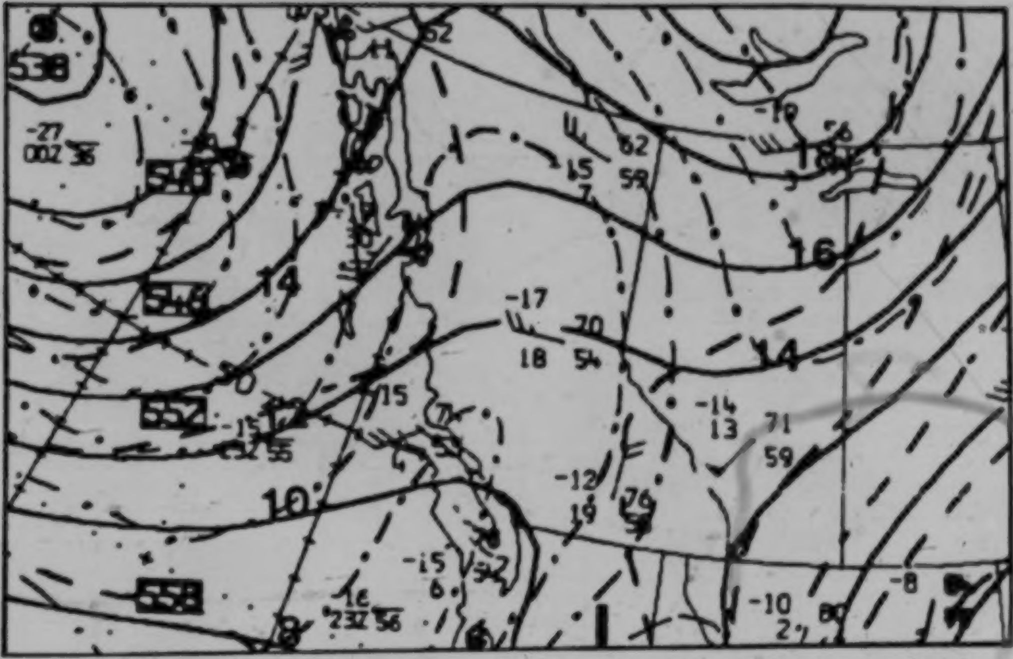
538
546
546
552
558
10
14
16
18
-17
18
54
-14
13
71
59

Figure 2.29.1 10 July 1983, 0000 GMT, CMC 500 mb analysis, dashed lines: thickness contours for the layer 500/1000 mb, dashed-dotted lines: absolute vorticity field ( $*10^{-5}$ $s^{-1}$ ).

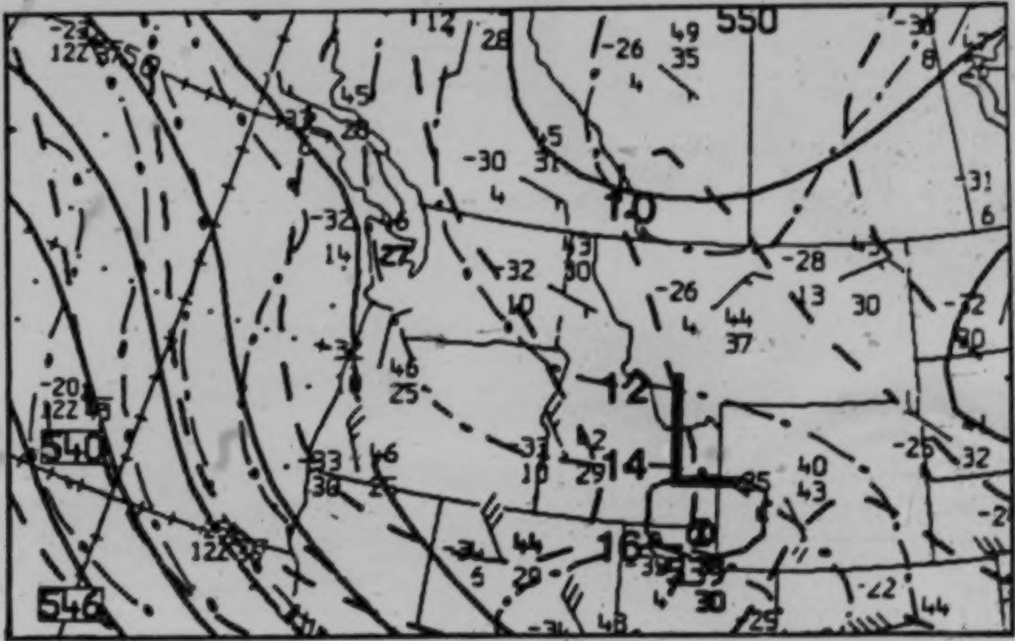
550
540
546
10
12
14
16
L

Figure 2.30.1 03 April 1983, 0000 GMT, CMC 500 mb analysis, dashed lines: thickness contours for the layer 500/1000 mb, dashed-dotted lines: absolute vorticity field ( $*10^{-5}$ $s^{-1}$ ).

meteorological parameters.

In this study, similar band developments were found over the Pacific Ocean and Western Canada. This band may have a north-south orientation or an east-west extension. Examples, of different cases are shown below. In each of the Figures 2.31, 2.32,and 2.40 the band is marked with the letter (G).

At first, these bands were , mistakenly, interpreted as frontal bands. Figure 2.31 shows both a frontal band (A) and a shear band (G). The shear band is simply not an extension of (A). It is clearly a separate entity and often more intense than (A). The examination of Figure 2.31.b shows that the band (G) is higher and thicker than band (A). Yet in most cases, the advance and over-ride of (G) on (A) make it difficult to distinguish between them. Figures 2.32 and 2.40 support this observation. Band (G) advances and overtakes the old frontal band (A) and masks it in the later stages.

This band is of a very great length and may extend for thousands of kilometers, specially over oceans. It is also of considerable width, has an anticyclonic curvature and is composed of middle and high clouds. The trailing edge is parallel to the thermal wind field of the layer 700/250 mb. In Figure 2.32 the trailing edge of (G) is parallel to the thermal wind field of the layer 700/250 mb. (dashed lines), and merges with the jet axis near the head of the band.

### 2.5.2.7 Jet Cloud Band

This band satisfies only the horizontal dimension criterion of synoptic cloud systems, since its vertical extent is very small and its speed of propagation is very large. The jet band consists entirely of high clouds having a fibrous structure. Accordingly, it is rather awkward to classify, but since it is of synoptic-scale length it may be considered a synoptic cloud system.

Examples of this band are shown in Figures 2.33, 2.34 and 2.36, where the band on every image is marked with the letter (H). The band is usually very narrow and, in most cases, not very dense as the case of a shear band. The life time of the

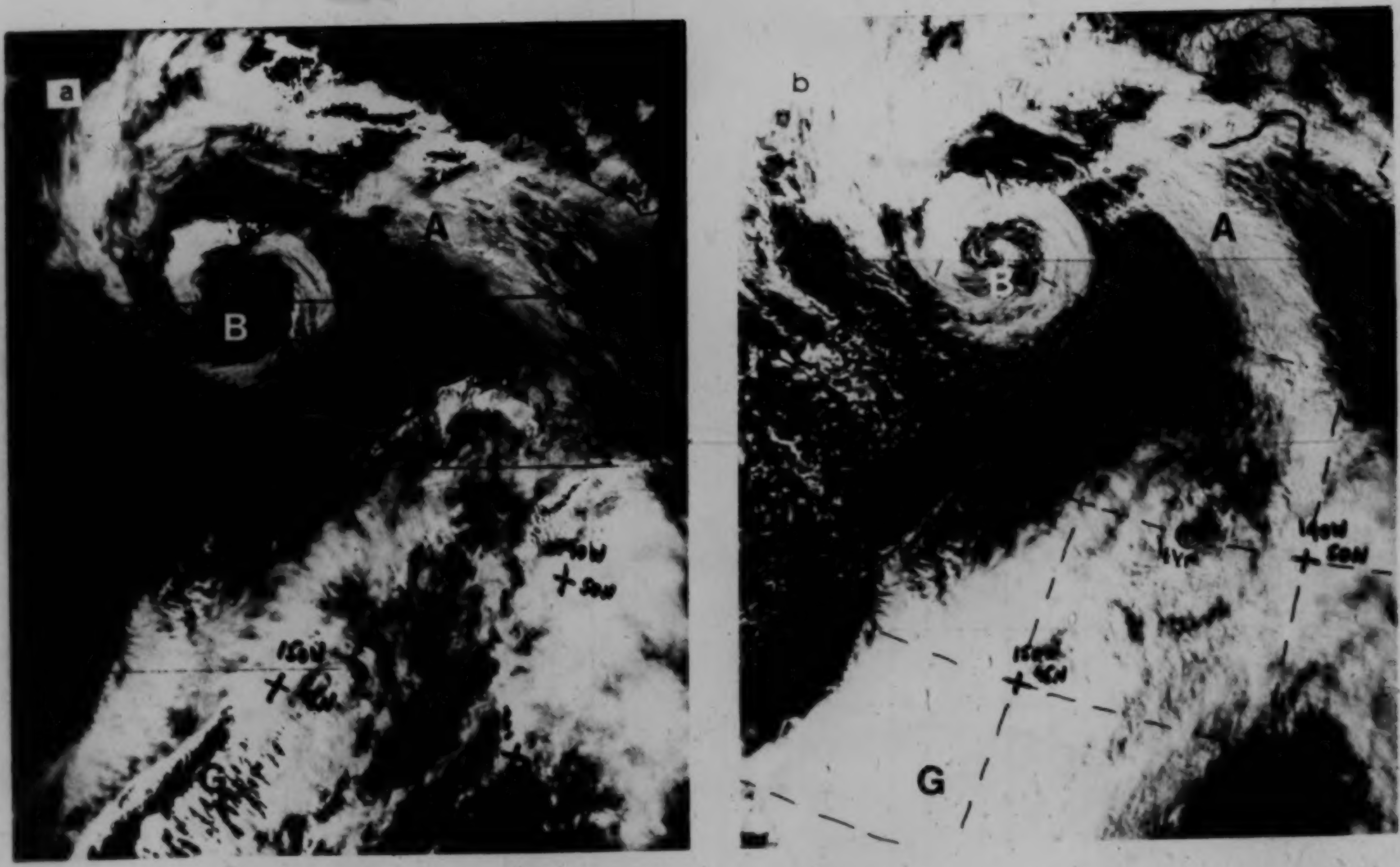
a
A
B
150W
40N
50N
G
b
A
B
140W
50N
150W
40N
G

Figure 2.31 NOAA-7 satellite image, a) infrared, b) visible, 2351 GMT, 03 April 1983.

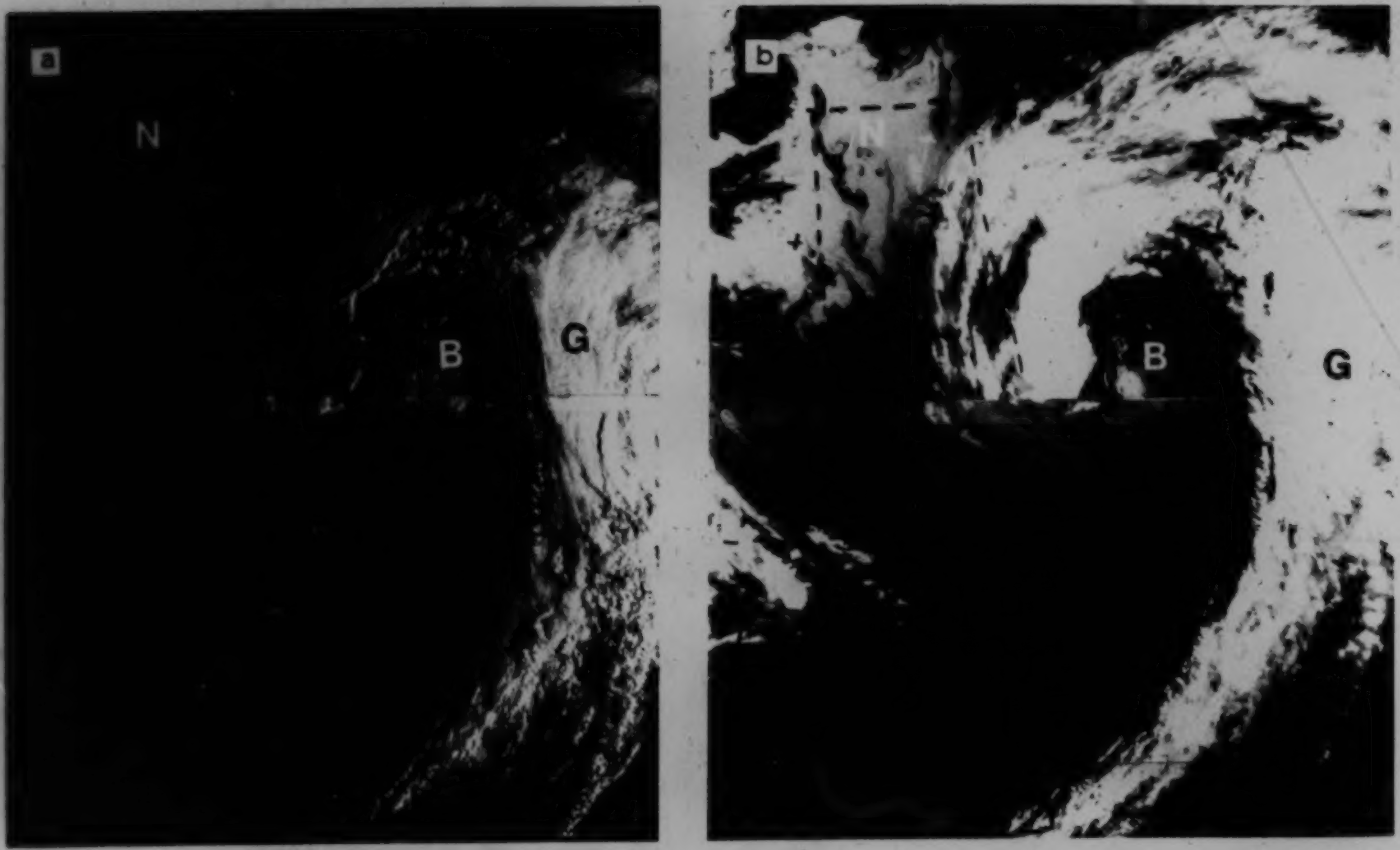

Figure 2.32 NOAA-8 satellite image, a) visible, b) infrared, 1434 GMT, 10 September 1983.

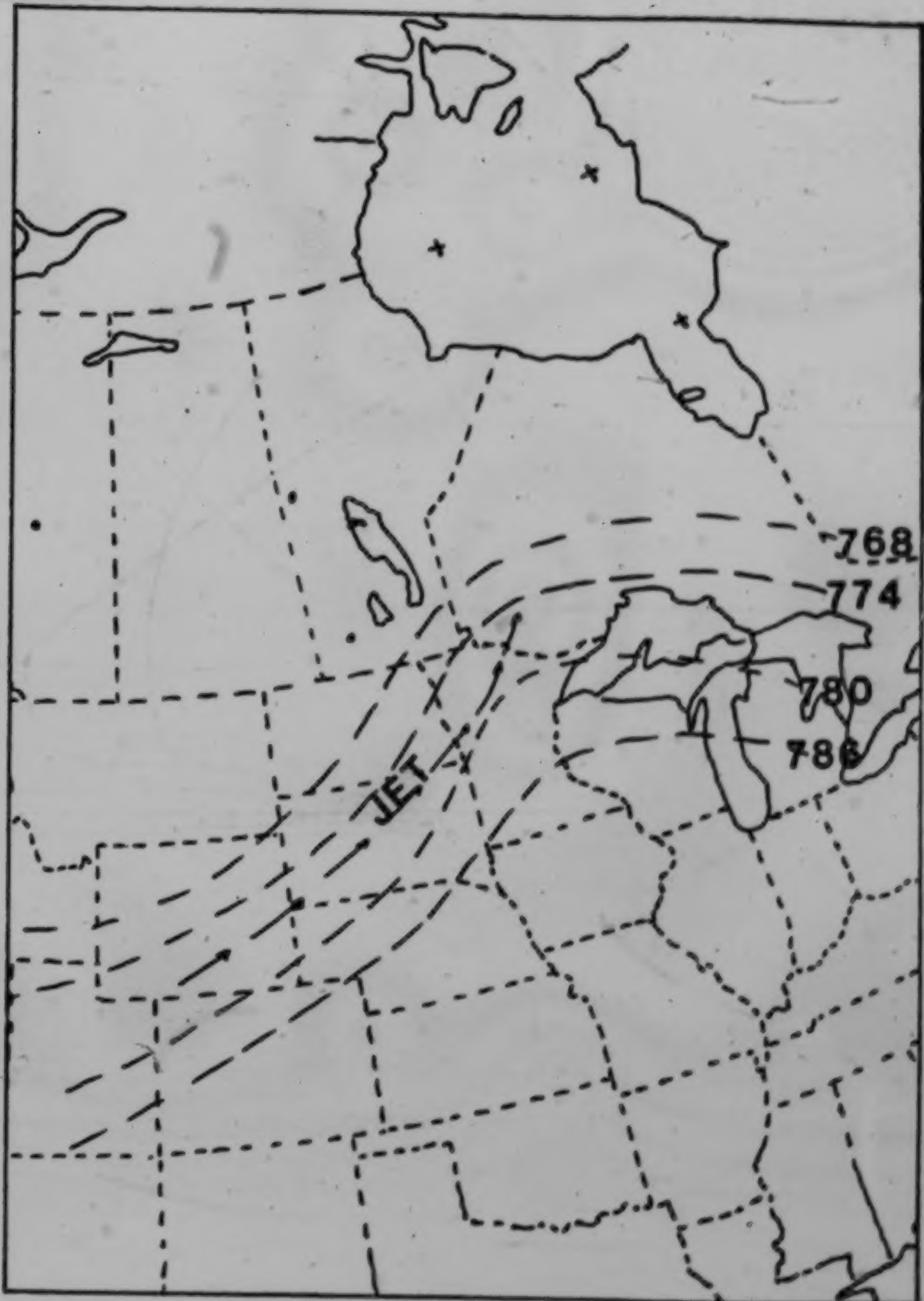
768
774
780
786
JET

Figure 2.32.1 10 September 1983, 1200 GMT, dashed lines: thickness contours for the layer 700/300 mb, arrows: jet stream at 250 mb surface.

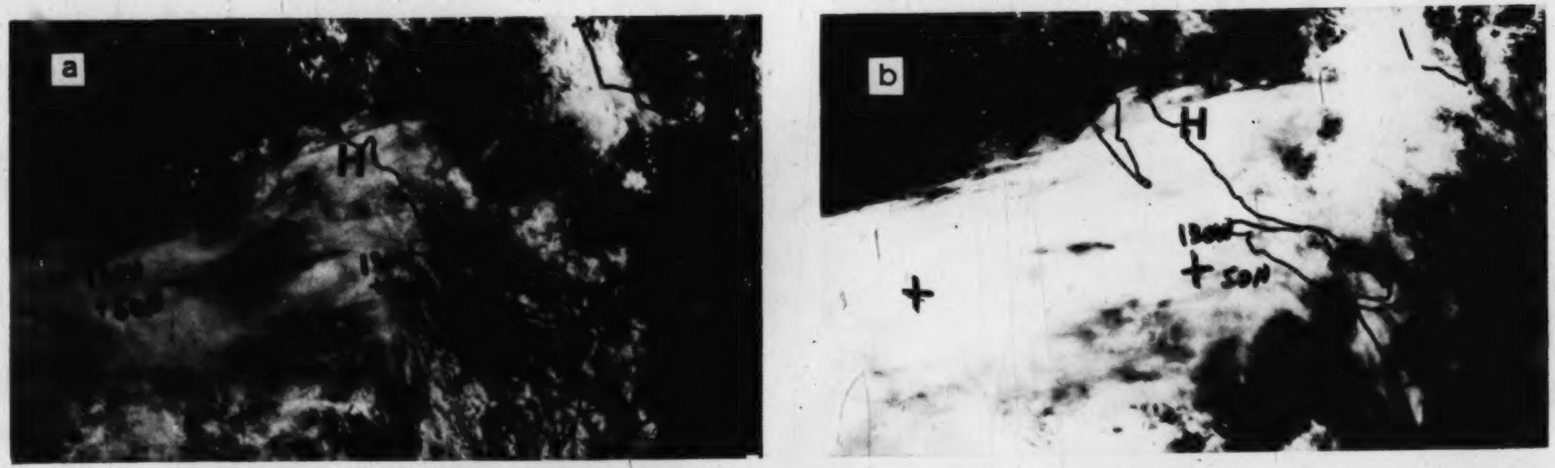

Figure 2.33 NOAA-6 satellite image, a) visible, b) infrared, 1615 GMT, 04 June 1983.

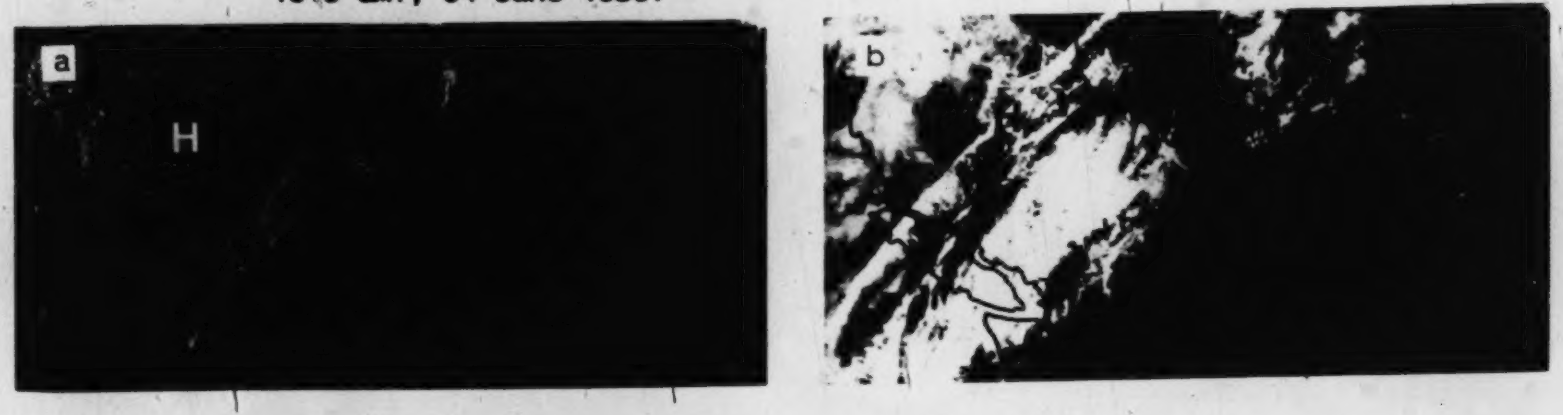

Figure 2.34 NOAA-8 satellite image, a) visible, b) infrared, 1527 GMT, 06 August 1983.

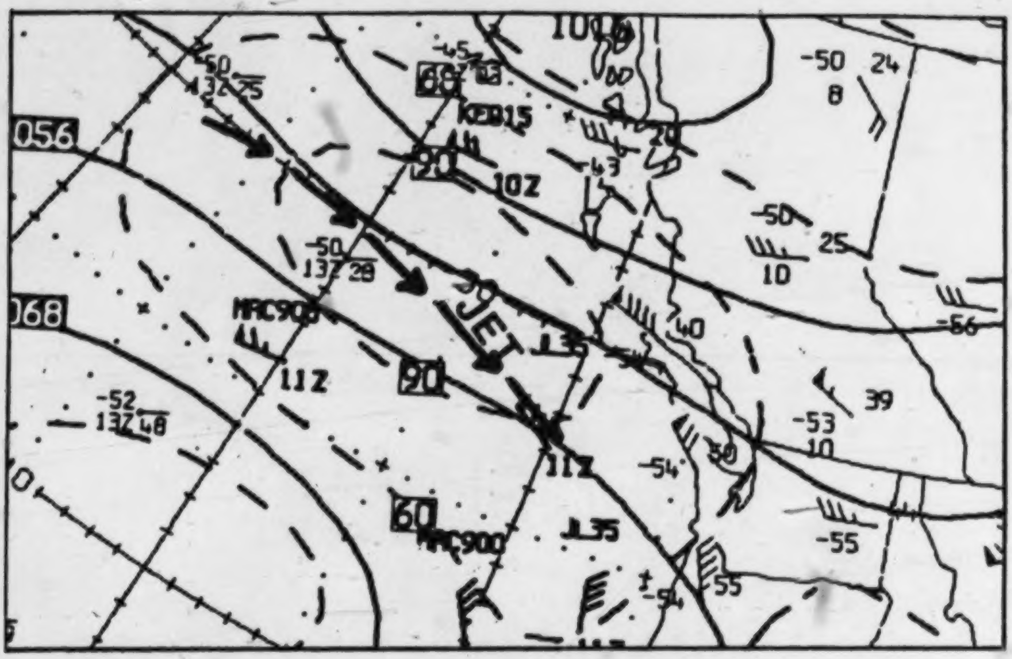
JET
056
068
-50
25
-50
24
10
-53
39
-54
-55
55
-52
60
90
MAC900
KEB15
11Z
10Z
J135

Figure 2.33.1 04 June 1983, 1200 GMT, CMC 250 mb analysis, dashed lines: isotaches, arrows: jet stream.

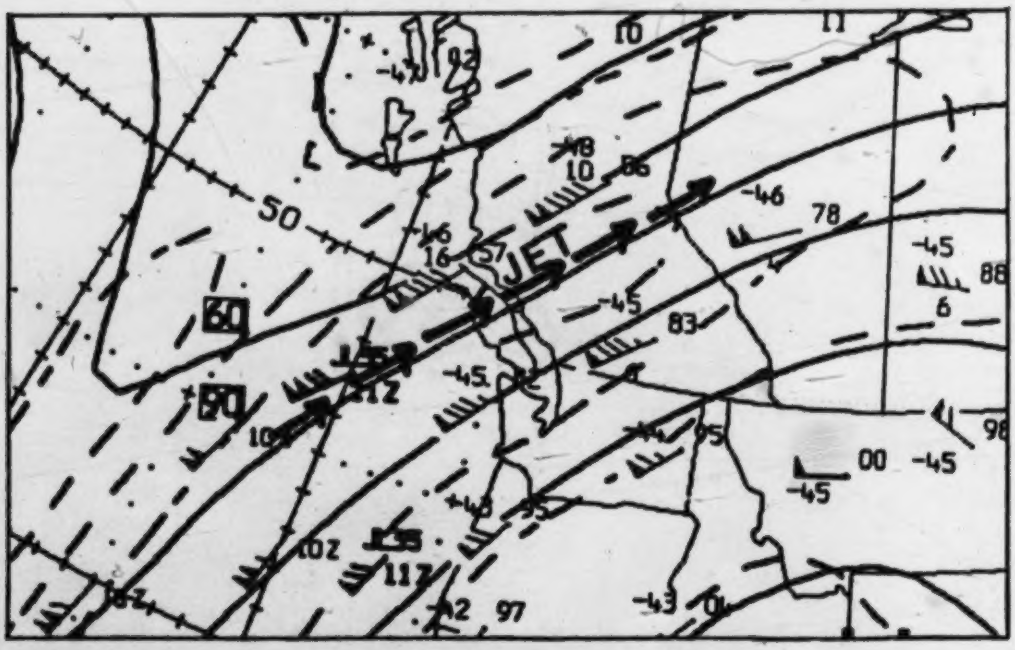
JET
50
60
90
10
-46
78
-45
88
83
-45
95
00
-45
97
-43
10Z
11Z
J135

Figure 2.34.1 06 June 1983, 1200 GMT, CMC 250 mb analysis, dashed lines: isotaches, arrows: jet stream.

band is rather short, 2 days on the average.

This cloud band can be found on the anticyclonic side of a jet axis. Sometimes, it is found alone as in Figure 2.34, or may merge with sheets of high clouds as in Figure 2.33. The band is always characterized with a weak anticyclonic curvature. Conventional and satellite data are often difficult to reconcile when attempting to locate the jet system. This problem is shown in Figures 2.33 and 2.33.1 where the jet axis has a different orientation on the map from the jet band on the image. In the other example, Figure 2.34, the jet band (H) is in alignment with the jet axis on the map, Figure 2.34.1. Time differences in observation, errors in analysis, and insufficient data over the ocean are likely reasons for differences in the band location.

#### 2.5.2.8 Non-Frontal Cloud Band

This subgroup includes all other unspecified cloud bands. These bands satisfy the horizontal synoptic-scale condition, but have not been subdivided further at this stage. The flexibility inherent in the classification process allows these clouds to be placed into the synoptic cloud classification even if not fully categorized to date.

Figures 2.35, 2.37 are examples of these bands, all marked with the letter (O). They have different curvatures, e.g. in Figure 2.35, the band is curved anticyclonically, while in Figure 2.37, it is curved cyclonically. All the examined cases were clearly not associated with a jet system or a shear structure, yet, they all look much like jet bands.

### 2.5.3 Vortex Cloud Group

A vortex cloud area is defined as a region of one or more spiral cloud bands of marked curvature, and converge toward one common center of revolution.

The vortex group includes three types of cloud configurations: (i) the low-level vortex, (ii) the upper-level vortex, and (iii) the comma vortex. All members of this group

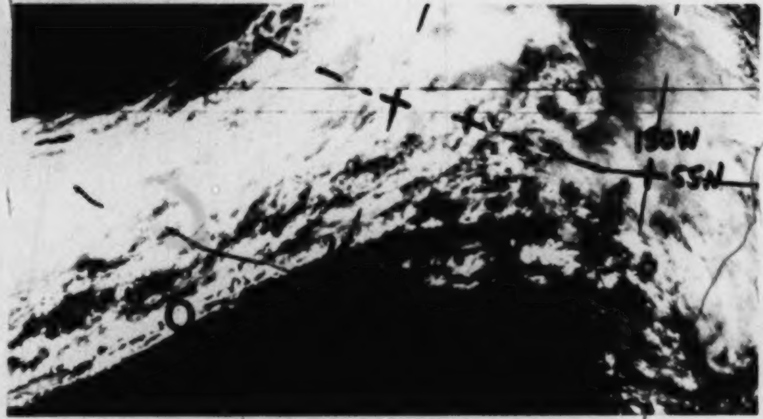

Figure 2.35 NOAA-7 satellite image ,infrared, 0039 GMT, 25 July 1983.

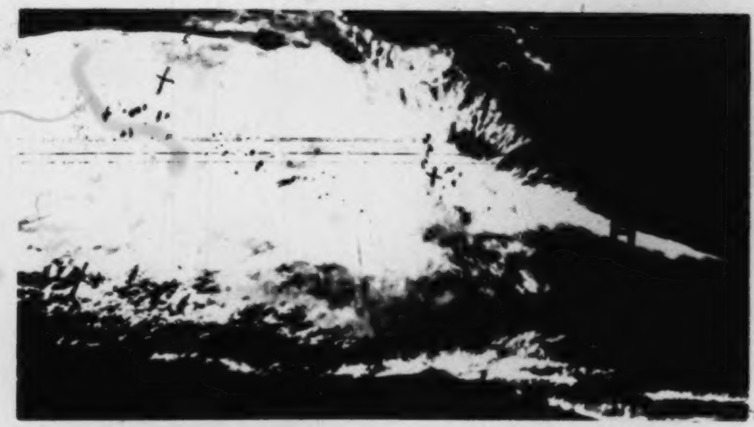

Figure 2.36 NOAA-7 satellite image ,infrared, 0015 GMT, 02 July 1983.

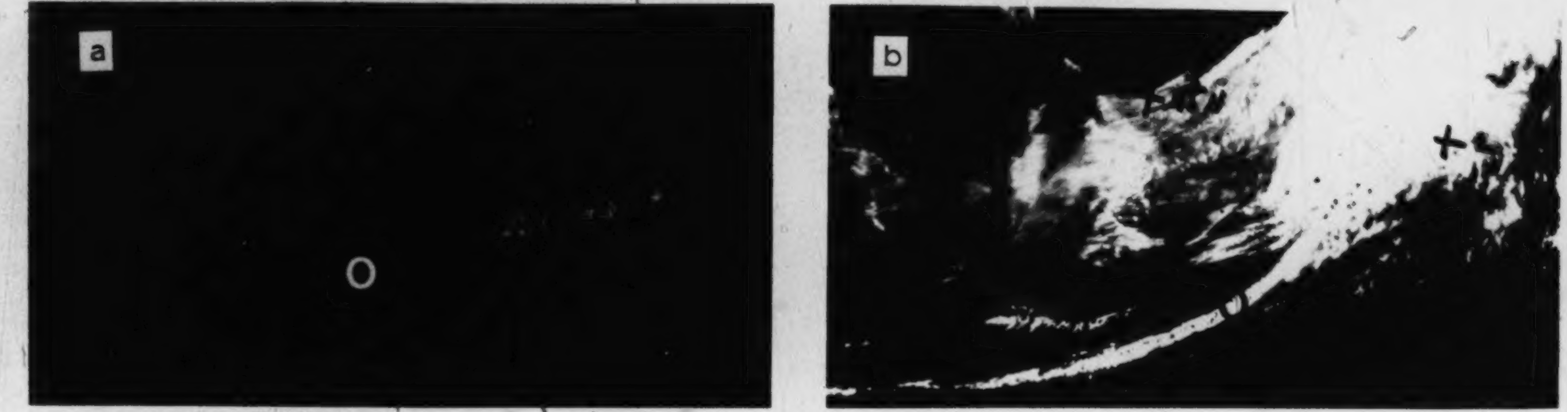

Figure 2.37 NOAA-8 satellite image, a) visible, b) infrared, 0358 GMT, 23 June 1983.

are dimensionally of synoptic-scale, although the comma configuration may not fully satisfy all the conditions at the early stages of development. Different examples of each type will be given.

One of the main differences between this group and the cloud band group is the radius of curvature. In this group the radius of curvature lies between 500 km at the upper limit and 200 km at the lower limit. This enables one to distinguish between different cloud areas within the general classification system. For example, in the case of extra-tropical cyclones, the vortex may merge with the frontal band, but, by considering their respective characteristic curvatures one can isolate both patterns from each other.

The vertical dimension of this group is of the order of 10 km. However, cloud areas in this group may reach higher levels than those in the cloud band group. This is because of the cumuliform nature of the cloud elements, and their intense convective development. On the other hand, the speed of propagation of spiral clouds is less than that of the cloud band group. Despite their great resemblance in overall configuration the three types develop in very different ways. This is true for low-level vortex and upper-level vortex.

### 2.5.3.1 Low-Level Vortex

Several examples of the low-level vortex, marked with the letter (B), are shown in Figures 2.21, 2.22, 2.31, and 2.32. In each case, the center of convergence is well defined and easily identifiable. The vortex passes through various stages of its life cycle, from a developing small wave through growth and maturity to ultimate dissipation. Figure 2.21, shown earlier, provides an example of the incipient wave stage. The wave bulges anticyclonically from the frontal band at (A). The areas marked with (B) in Figures 2.21, 2.22, and 2.32 are examples of the mature stage, whereas area (B) in Figure 2.31 is a case of dissipating stage.

The vortex is composed of intrusions of a dry, cold air (the black, cloud free strip) within a moist warm air mass (the dense, white, bright cloudness). This can be readily seen in Figure 2.31. In Figure 2.32 the central part of the vortex, consisting mainly of Cb clouds, is very cold and very dense indicating extreme vertical development.

It is difficult, in the early stages of development of a low-level synoptic system, to differentiate between the vortex cloud and an adjoining band. Care should be taken in calculating the radius of curvature of each cloud area. On the other hand, in the dissipating stage, the linkage between the cloud band and the vortex breaks down. In the late stages of life cycle, the vortex cloud area becomes fragmented and separated from the banded area. A good example, for this case, is shown in Figure 2.31.

### 2.5.3.2 Upper-Level Vortex

In this subgroup, the overall cloud configuration is similar to that of a low-level vortex. Moreover, in the late stages of development, it is very difficult to differentiate between the two configurations. This is the reason for marking the cloud area in this group with the letter (B) as well. In Figure 2.31, (B) denotes a low-level vortex, while in Figure 2.39 (B) denotes an upper-level vortex. The use of both synoptic and satellite data is very necessary in identifying the vortex cloud type. More details will be given in the subsequent chapters, when discussing the development of the upper cold low system. Other examples of upper-level vortex are given in Figures 2.38, 2.39, and 2.40.

There are several stages of development. The first is the troughing stage and the last is decay. Figures 2.29 and 2.30 are examples for the first stage, while Figures 2.38 and 2.39 are good examples for the mature stage. In figure 2.40 the vortex has reached the decay stage.

Despite the close similarity in appearance between the low-level vortex and the upper-level vortex, the physical process behind the development is different. In the upper-level vortex, the moist warm air ascends around a dry cold dome of air.

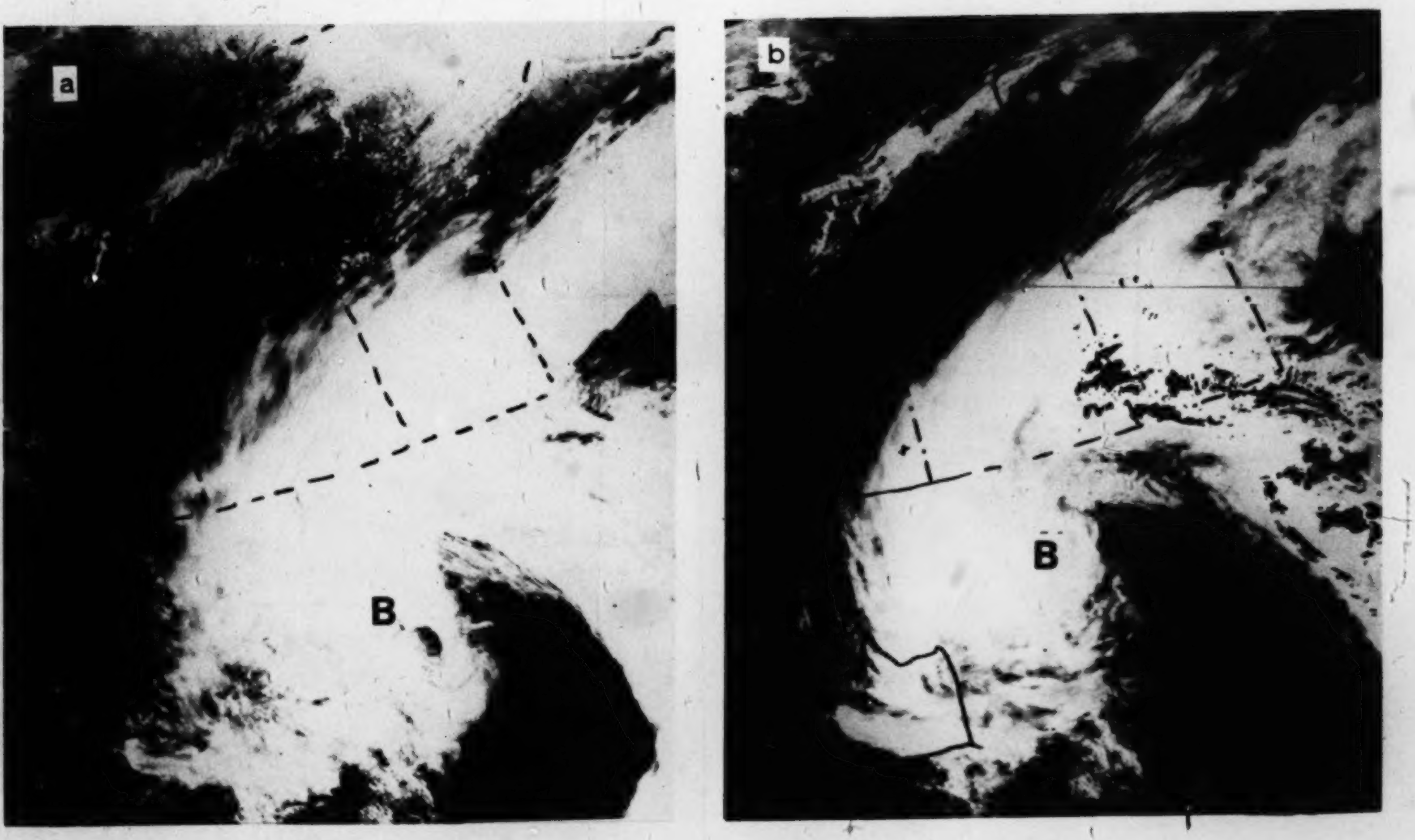

Figure 2.38 NOAA-6 satellite image, a) visible, b) infrared, 1521 GMT, 12 May 1983.

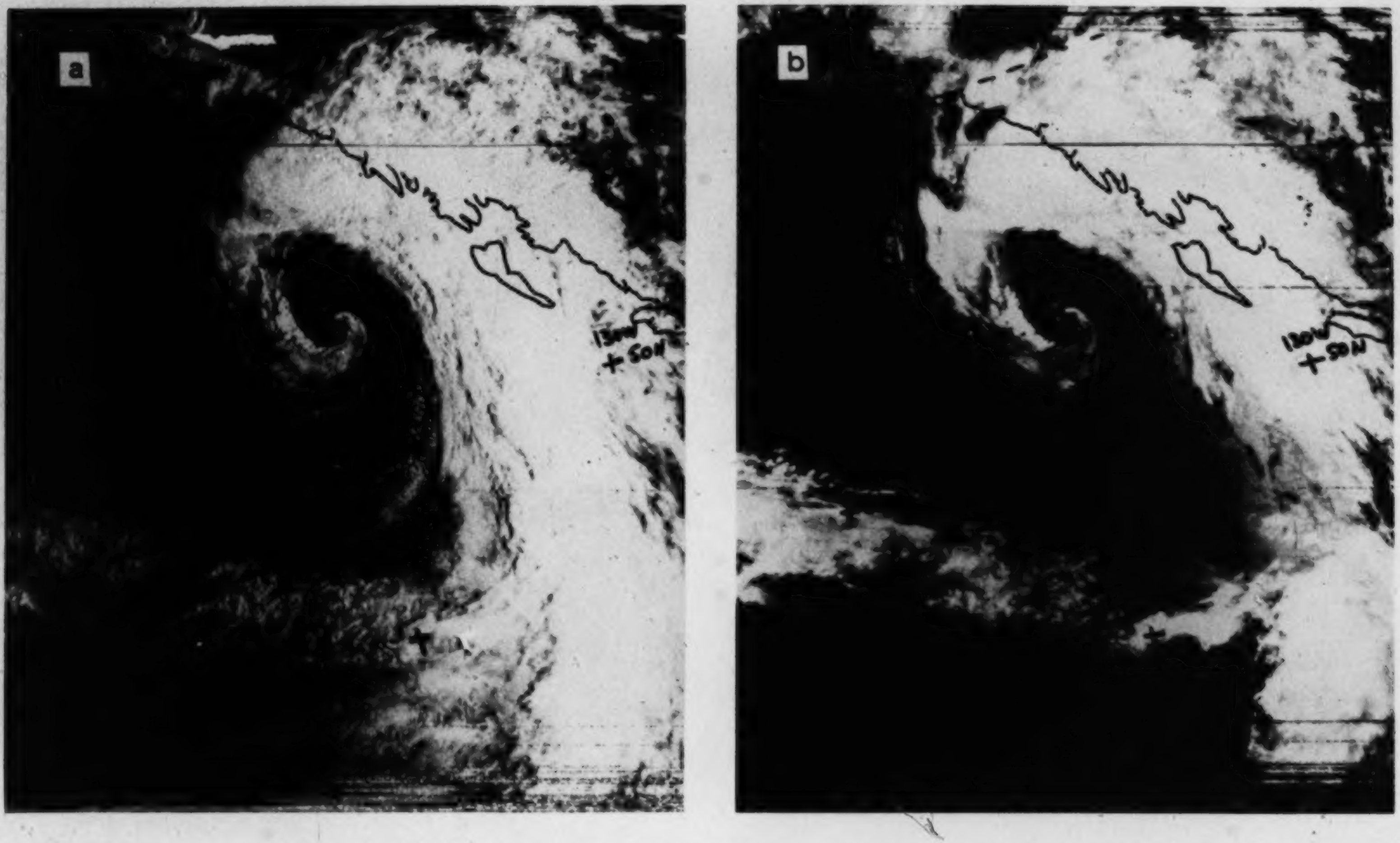
a
130W
+ 50N
b
130W
+ 50N

Figure 2.39 NOAA-8 satellite image, a) visible, b) infrared, 1756 GMT, 27 August 1983.

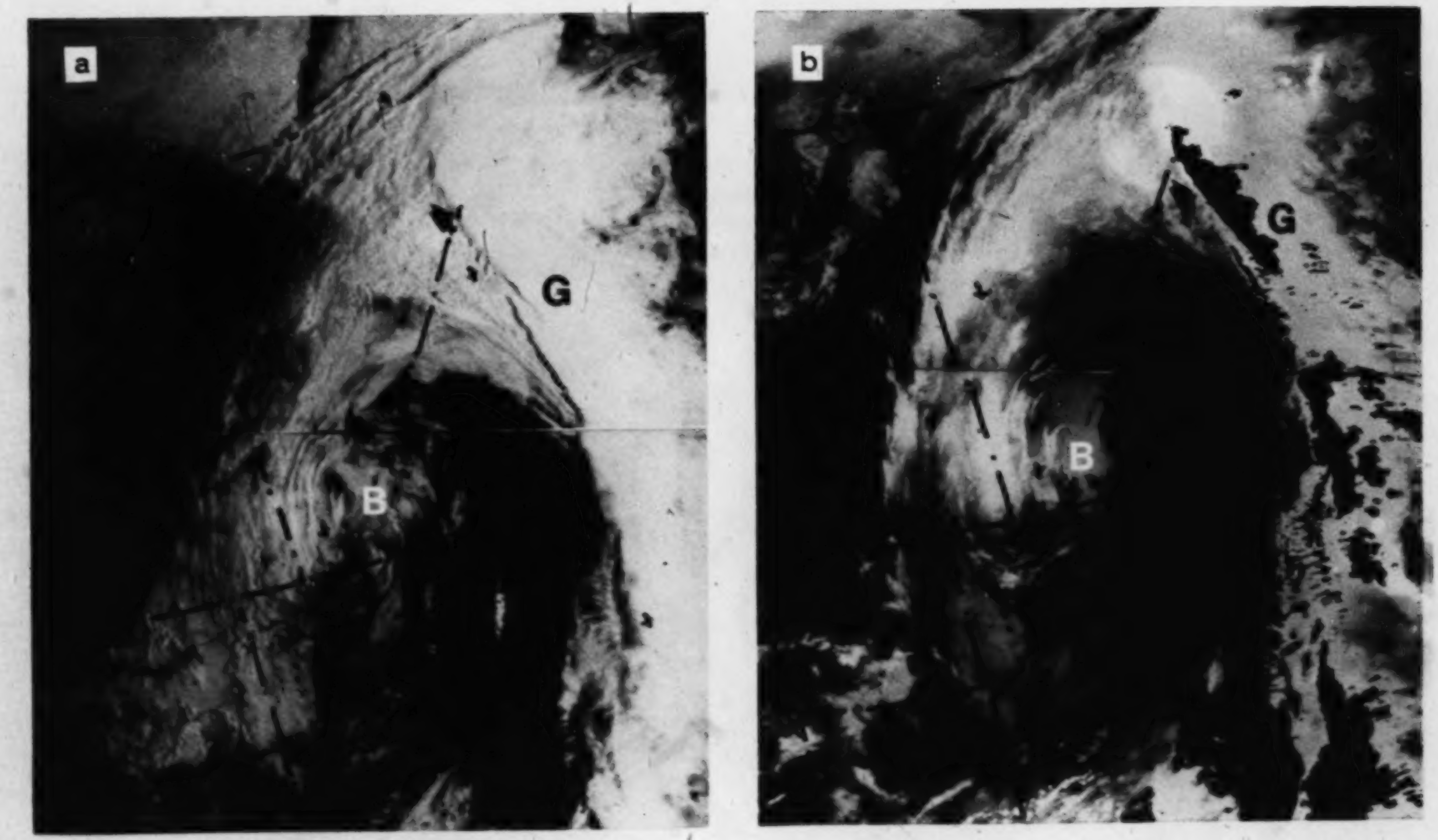

Figure 2.40 NOAA-6 satellite image, a) visible, b) infrared, 1457 GMT, 13 May 1983.

The result is the well shown vortex. The case of low-level vortex was described before. The cloud area vortex is mature and well developed. Its lifetime is longer than that of a low-level vortex.

#### 2.5.3.3 Comma Cloud Pattern

This is the third vortex configuration in this group. The overall configuration pattern is different from that in the other two cases. Examples of this case are shown in Figures 2.23 and 2.41, where the pattern is marked with the letter (D). As can be seen from all cases examined, the center of convergence is not identifiable as that in the case of a low-level vortex. Rather, the pattern has a comma-like configuration with a solid head.

The pattern may either form in a simple configuration, e.g. Figure 2.23 or, in a complex configuration, e.g. Figure 2.41. In the first case, the comma pattern is formed in a cold area, such as behind a frontal system. In the second, it is formed within cold air but not associated with any other specific systems.

Since the pattern is made up mainly of actively convective cloud elements, it forms most readily over ocean areas. The tail of a comma pattern stretches southwestward with respect to the head. Since the comma may evolve at any stage of development, it must be included in the synoptic classification.

### 2.5.4 Cellular Cloud Group

A cellular cloud area is defined as a discontinuous expanse of clouds made up of individual cumuliform cloud cells of variable vertical thickness. While the last two groups have a well defined horizontal length, the cellular group lacks the linear character. In other words, there is no prefered horizontal extension for a cellular cloud area. The group includes three types: (i) the open pattern, (ii) the closed pattern, and (iii) the non-organized pattern. The first two patterns have a geometrical configuration, regular or irregular. The last pattern has a small unorganized configuration.

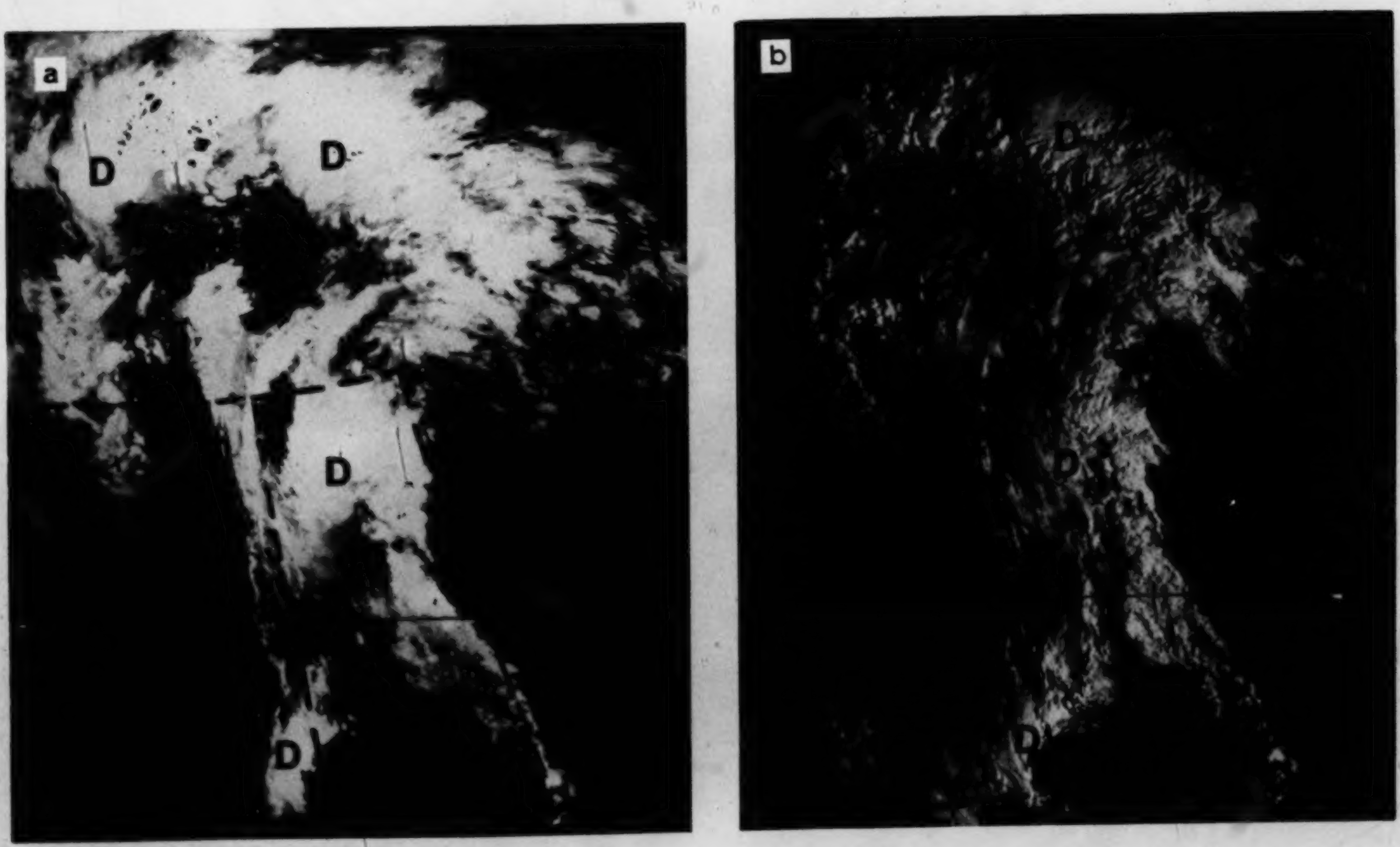

Figure 2.41 NOAA-8 satellite image, a) infrared, b) visible, 1458 GMT, 12 August 1983.

Other synoptic patterns may develop from any pattern in this group. For example, a comma cloud pattern may develop when a cellular cloud area comes under the effect of a rotational field, e.g. Figure 2.23 (cloud area D). This is, also, true for the non-organized pattern, where the resulting pattern will be of synoptic-scale and not subsynoptic such as the mesoscale convective complex described by Maddox (1980). This will be shown in detail in the section of "Non-Organized Pattern".

As to synoptic characteristics, this group satisfies most conditions: the horizontal dimension extends from 1000 to 3000 km, the vertical extent varies from 3 to more than 10 km. A cellular cloud area persists usually for five days, but its speed of propagation is very slow. Since the group has no banded shape, it does not have a specific curvature, yet its cloud elements may line up with a cyclonic or an anticyclonic curvature, according to the applied rotational field.

In this group the interaction between synoptic and subsynoptic system is clear. An upper air flow (synoptic) interacts with a convection process (meso-synoptic) resulting in the cellular pattern. For example, if an upper cold air mass, with pronounced subsidence, moves over a warm ocean, the convective activity results in a cellular synoptic pattern. Such an example is shown in Figure 2.21, where the cold air flows cyclonically over the Pacific Ocean, in the area marked with (C).

### 2.5.4.1 Open Cellular Pattern

Figures 2.21, 2.24, 2.27 and 2.28 show examples of the open cellular pattern. The pattern is marked with the letter (C). The vertical development is greater than that in closed cellular patterns. Comparison of Figures 2.21 with 2.24 shows this difference. In Figure 2.21, the cloud elements are white at (b) and bright at (a), while in Figure 2.24, they are bright at (a) and light gray at (b). Accordingly, one may conclude that the thickness of open cells is normally greater than that of closed cells.

The cloud elements of the pattern may line up in cyclonic curves, e.g. Figure 2.21, or in straight lines, as in Figure 2.27. Usually, these patterns form behind cold frontal bands over water surfaces. Moreover, regular configurations are more likely over sea than over land, with more persistence in the former case.

### 2.5.4.2 Closed Cellular Pattern

Figure 2.24 shows an example of the closed pattern, marked also with the letter (C). The closed pattern lies within an area bounded by 40° N to 45° N and 125° W to 130° W. The cloud elements of this pattern are strato-cumulus.

The physical process behind the pattern development is the same as that in open cells. The controlling factors are: (i) the stability in the lower layer, (ii) the vertical subsidence, and (iii) the wind field in the lower layer. However, in closed cells, the temperature difference between the surface and the lower-layer air is small. This leads to more limited thickness. In the same time, the low-level wind field smears out the cloud configuration.

### 2.5.4.3 Non-Organized Pattern

This pattern is different from the open and the closed patterns described above. The overall cloud area configuration of the pattern is made up of individual cumuli-form cloud cells, often Cb type. In the early stage of development, the pattern looks like a closed one. But, in the late stages, it may develop into a comma pattern (Vortex Cloud Group). It is difficult to assign this pattern to a definite group. However, since it is more nearly cellular, it was decided to include it in the cellular group. On the other hand, this pattern is different from both the open and closed patterns, even when it subsequently develops into an enhanced cumuli pattern. Figure 2.30 shows an early stage of such a development, located over Utah-Nevada. In Figures 4.40 and 4.45, the pattern is marked with the letter (K). In the last example, the pattern developed into a comma pattern as can be seen from both figures.

The non-organized pattern is different from the mesoscale convective complexs pattern, described by Maddox (1980). Nevertheless, both may have a similar appearance and configuration in the early stages of development. In time, a non-organized pattern may develop into a synoptic comma which may,in turn, play a significant role in the development of a synoptic storm. In the case of mesoscale convective complexes, the pattern does not develop into a comma configuration, but it may assume a circular or a linear pattern, of sub-synoptic scale.

### 2.5.5 Uniform Area Cloud Group

A cloud area with continuous, homogenous, stratiform pattern and of a uniform thickness is defined as a uniform cloud area. Typical examples are extensive areas of fog and stratus. As in the case of the cellular group, a uniform cloud area does not have a stretched or curved shape. There are two types in this group, (i) the fog or stratus pattern, and (ii) the mid-level pattern. An examination of the different types shows that the vertical extent of cloud areas in this group is limited to a thickness of about 500 meters. Yet, the areal coverage and persistence in time as such to allow one to consider the group as a synoptic-scale system.

Close examination of satellite images in the visible and infrared enables one to identify such areas. Topographical features, such as coast lines and valleys, help in outlining areas of fog and stratus patterns. In the several cases examined, the conventional data were of great help, specially over land, and with short duration patterns

#### 2.5.5.1 Fog or Stratus Cloud Pattern

Figures 2.42, 2.43, 2.44, and 2.45 show several examples of fog and stratus clouds. Such areas are marked with the letter (L). Synoptic cases of fog and stratus are shown in Figures 2.42, 2.43, and 2.44, while in Figure 2.45, the arrow points to a mesoscale case of valley fog. As can be seen from these figures, fog or stratus is readily identified from a satellite image, specially in the visible range. In

Figures 2.43 and 2.44 the west coast delineates the eastern boundary of the pattern, while arrows mark the sharp west boundary. Fog and stratus are not easily distinguishable in the satellite images, but proper enhancement enables one to identify them, if one remembers that fog will be near-black in the infrared, while stratus will be dark gray.

### 2.5.5.2 Mid-Level Stratified Cloud Pattern

This pattern has the same features as fog or stratus, but it is light gray in both the infrared and visible images. Figures 2.22 and 2.32 show two examples of this pattern. The cloud areas, marked with the letter (N), have a characteristic smooth, flat texture and sharp edges. The two patterns, shown, have formed in the cold air behind a frontal system without acquiring a pronounced curvature. The structure and characteristics of these patterns suggest that, they may be included in the "Uniform Cloud Area Group".

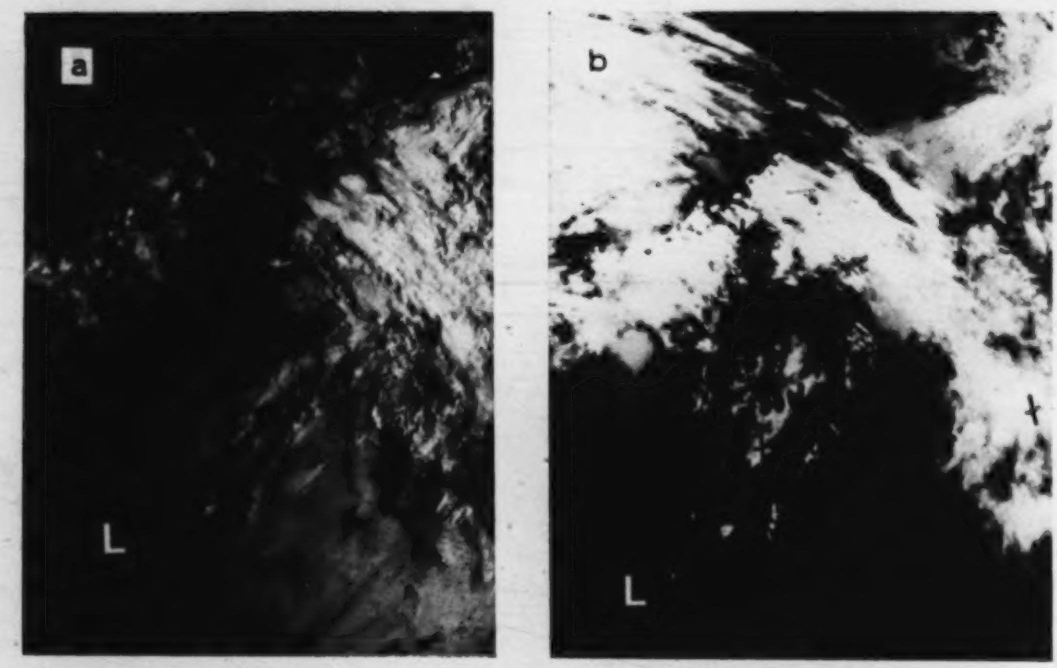

Figure 2.42 NOAA-8 satellite image, a) visible, b) infrared, 1757 GMT, 13 August 1983.

Figure 2.43 NOAA-6 satellite image, a) visible, b) infrared, 1617 GMT, 27 April 1983.

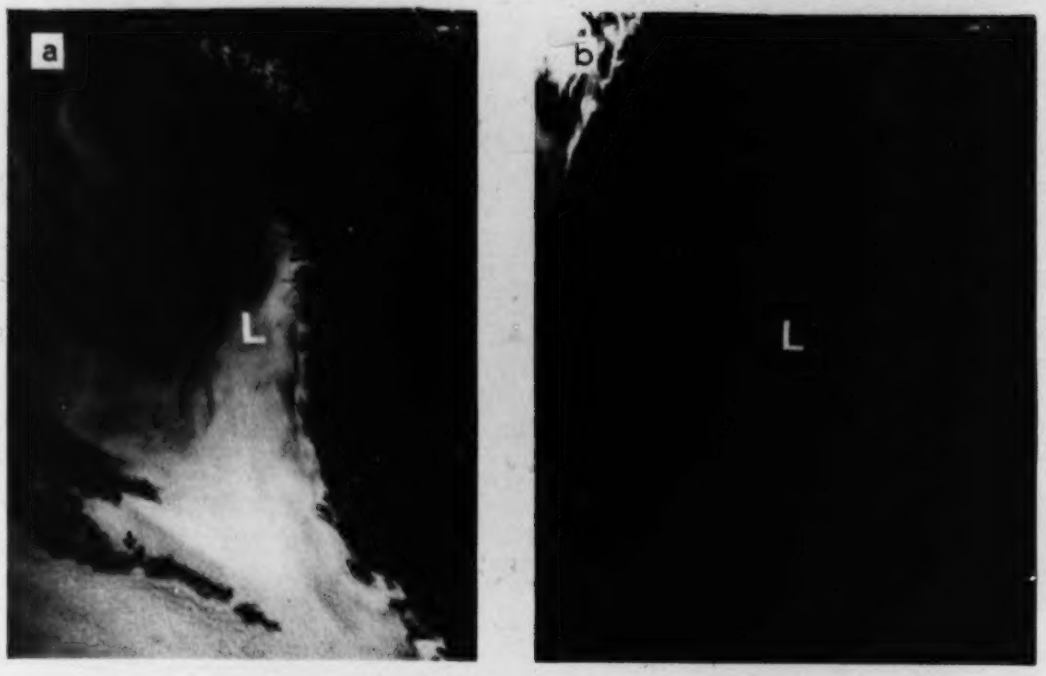

Figure 2.44 NOAA-6 satellite image, a) visible, b) infrared, 1536 GMT, 24 May 1983.

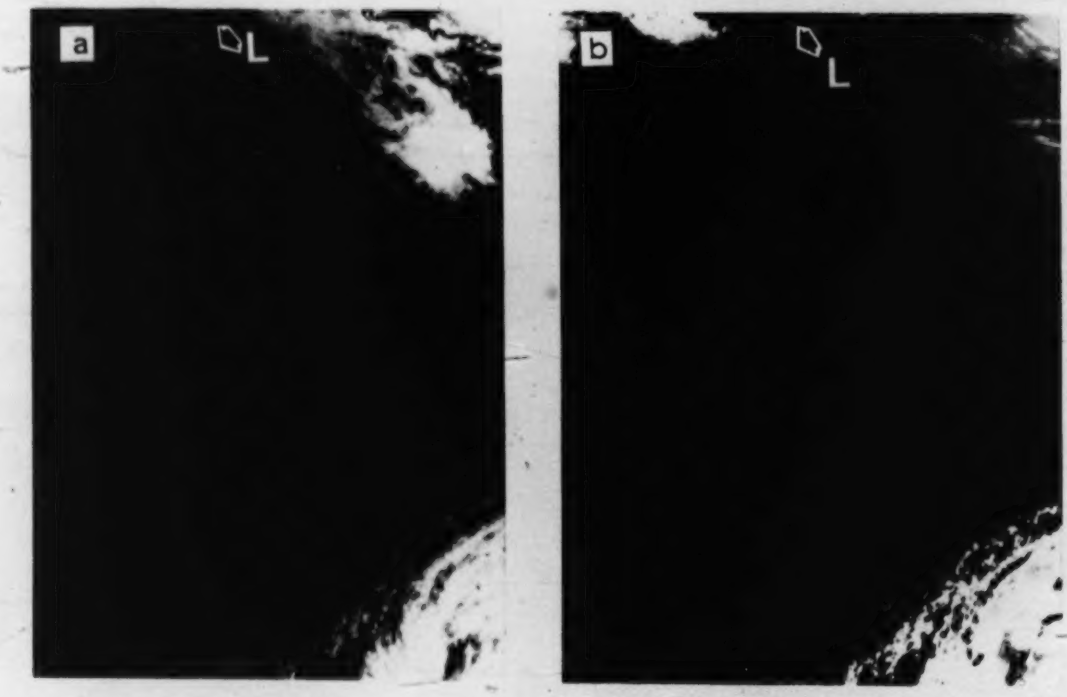

Figure 2.45 NOAA-8 satellite image, a) visible, b) infrared, 1717 GMT, 21 September 1983.

# 3. Cyclogenesis and Upper-Level Development

## 3.1 Cyclogenesis

### 3.1.1 The definition Of Synoptic Cyclogenesis

The initiation of a cyclonic circulation and its subsequent development into a low pressure area is referred to as cyclogenesis. From the Earth bound synoptic point of view, cyclogenesis is the term applied to the process of formation of closed circulation at the surface, while from a space-view of a satellite, cyclogenesis is seen as the initiation of an enhanced cumuli-form pattern with cyclonic circulation and its subsequent development into a well-defined comma. Details and related processes will be considered later.

### 3.1.2 Early Studies

In discussing the problem of development, the basic idea concentrates and revolves around the problem of how the air is removed from a column of air. The germinal idea came from Margules (1904), who stated that "a small net divergence or convergence is a measure of the surface pressure change". In 1922 J. Bjerknes and V. Solberg introduced their early model of low-level cyclogenesis, according to which the development of an unstable wave on a frontal surface resulted in the formation of low pressure area. The kinetic energy of development comes from the air mass difference across the surface of discontinuity. In 1919, W.H. Dines extended Margules' work and introduced the idea of atmospheric compensation, which requires that "divergence (convergence ) in the lower troposphere is compensated by convergence ( divergence ) in the upper troposphere".

### 3.1.3 Divergence Theories

The problem of cyclogenesis attracted the attention of several notable scientists in the followed years. In 1939, R. Scherhag introduced what has come to be known as the divergence theory. He postulated that the upper-level divergence will produce a pressure fall at the surface, if not compensated by low-level convergence. The net divergence is both a necessary and sufficient condition. In 1944 J. Bjerknes and J. Holmboe derived an equation which expresses the pressure tendency at any surface in terms of net mass divergence.

$$\left(\frac{\partial p}{\partial t}\right)_z = - \int_z^{\infty} \nabla \cdot (\rho \overline{V})\,dz + (\rho g\, w)_z \qquad (3.1)$$

where, z represents the height of some pressure level, $\overline{V}$ is the mean horizontal velocity, w is the vertical speed, and $\rho$ is the density of the air. The above equation indicates how the pressure tendency, at any level, is a consequence of the net horizontal mass flux.

### 3.1.4 Pattern of Cyclogenesis on Satellite Images

In 1975-1979,R. Weldon suggested a new classification of synoptic-scale cyclogenesis. Basing his work on GOES satellite data, he distinguished four groups which represent the main basic types of cyclogenesis, without including any sub-synoptic features or cloud systems:

-Baroclinic Zone Cyclogenesis.

-Split-Flow Cyclogenesis.

-Cold-Air Vortex Cyclogenesis.

-Induced-Wave Cyclogenesis.

In each group, the model of development includes several phases and all incorporate synoptic data, as well as satellite data. The synoptic data used are the geopotential height contours of the 500-mb surface, and the jet-stream axis extracted from the maximum wind speed at either the 250-mb or the 300-mb surfaces. In the following figures, the jet axis, which is in direct association with cyclogenesis, will be hatched and marked by the number (2). The four different cloud areas within the cloud system will be denoted by the capital letters: (A), (B), (C) and (D).

(i)-The Vorticity Comma, marked with the letter (B), is a comma-like shape of convective clouds, usually Cb or towering Cu. (B) may lack the comma shape in the early stages.

(ii)-The Baroclinic Cirrus Deck, marked with the letter (A), is a band-like shape of middle and high level clouds. When it develops, it has an anticyclonic curvature or "S" like pattern especially in the late stages of development.

(iii)-The Deformation Cirrus Deck, marked with the letter (C), has a band-like shape but it is thinner than the baroclinic deck (A). It also has a streaky structure. It is found in multiple bands with an anticyclonic curvature. It exits in an area of mass convergence.

(iv)-The Circular Cellular Cloud Area, marked with the letter (D), has, either, regular or irregular organization of low-level convective clouds and often form in late stages.

The highest common cloud area factor between all groups is the comma cloud area, (B).

### 3.1.4.1 Baroclinic-Zone Cyclogenesis

This is the least frequent type of cyclogenesis. It is the closest model to the well known "classical frontal wave model". The development process can be described in four phases. In general, it is characterized with a meridional troughing of a large amplitude and the upper-jet axis rounds the base of that troughing without splitting.

Phase # 1

Figure 3.1 shows the early stage of development, where the cloud area (B) is masked by the cloud area (A). Also, the northern edge of (A) coincides with the old jet axis (1). The cloud area (F), which has not been described before and found in this group, is a frontal cloud band.

Phase #2

Figure 3.2 illustrates the second stage, where both cloud areas (A) and (F) show marked anticyclonic curvature. The cloud area (B) develops into a comma-like shape and moves further northward with respect to the cloud area (A). The old jet (1) advances eastward with a pronounced anticyclonic curvature, while jet (2) advances toward the base of the trough. Also shown is the position of the surface front. It advances and moves with (B) to the northern edge of (A).

Phase #3

At this stage, shown in Figure 3.3, the development reaches a profound stage. The cloud area (B) develops vertically and expands horizontally. At the same time (B) moves partially out from the cloud area (A). Cloud area (A) continues to acquire more anticyclonic curvature and increases in area as well. Jet (1) moves very fast northeast-ward and jet (2) advances around the base of the tilted trough. The collective motion of the system is eastward but is not the same for each cloud area, e.g. (B) moves westward with respect to (A). This is because (A) is faster than (B). Also, the frontal band (F) becomes more anticyclonically curved as it moves closer to the northern edge of (A).

Phase #4

This is the mature stage of development, at which the cyclonic system reaches its storm stage. Figure 3.4 shows this phase. The closed contours of the circulation show up at the 500-mb surface and even at higher levels. The first sign of (C) appears at this stage. Soon thereafter, this cloud area reaches the maximum development. The old jet decays and the new jet controls the system development. The layers of clouds will be stacked nearly vertical as the system approaches phase #5.

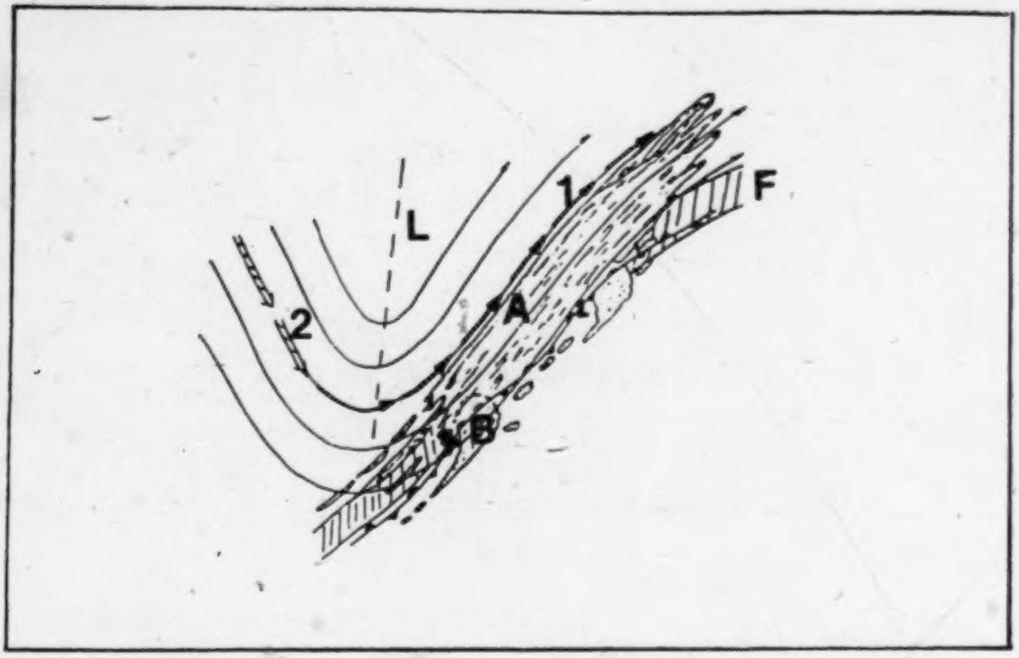

Figure 3.1 The early stage in baroclinic zone cyclogenesis.

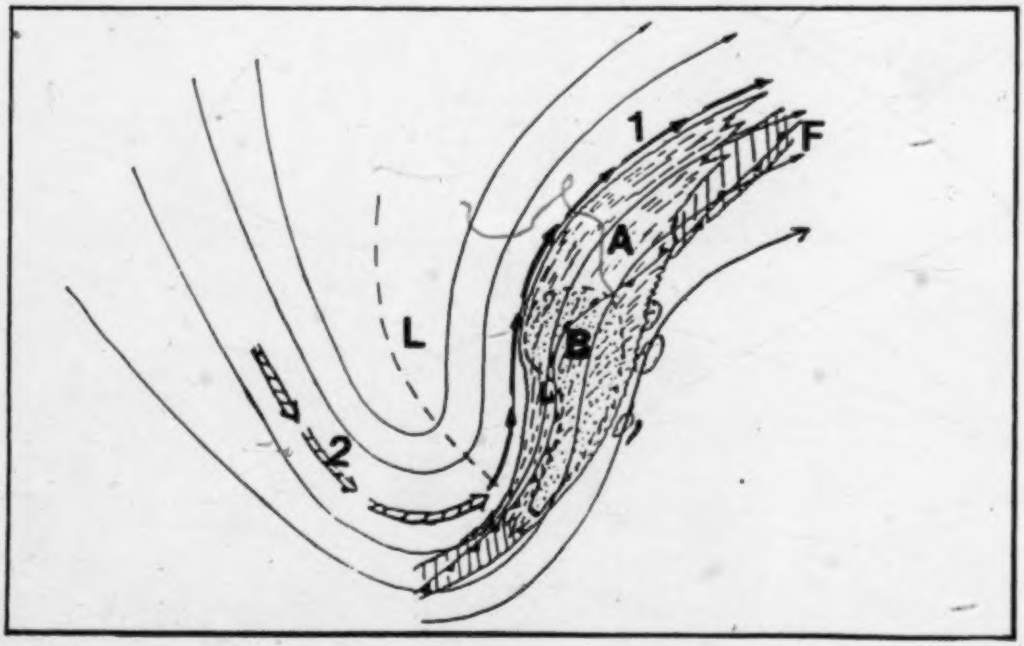

Figure 3.2 The second stage of development.

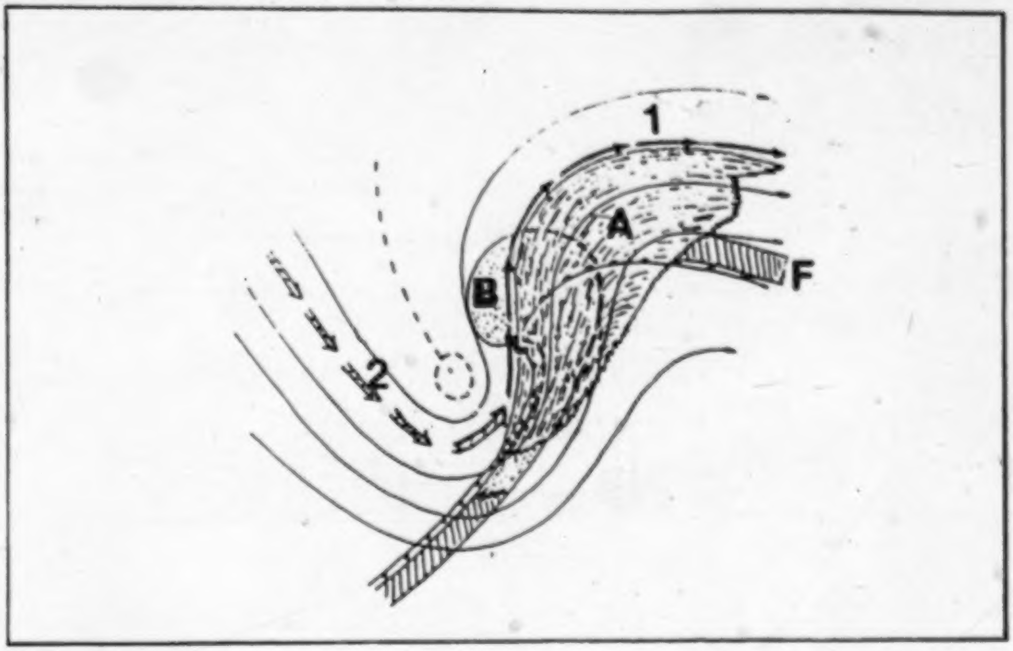

Figure 3.3 The third stage of development.

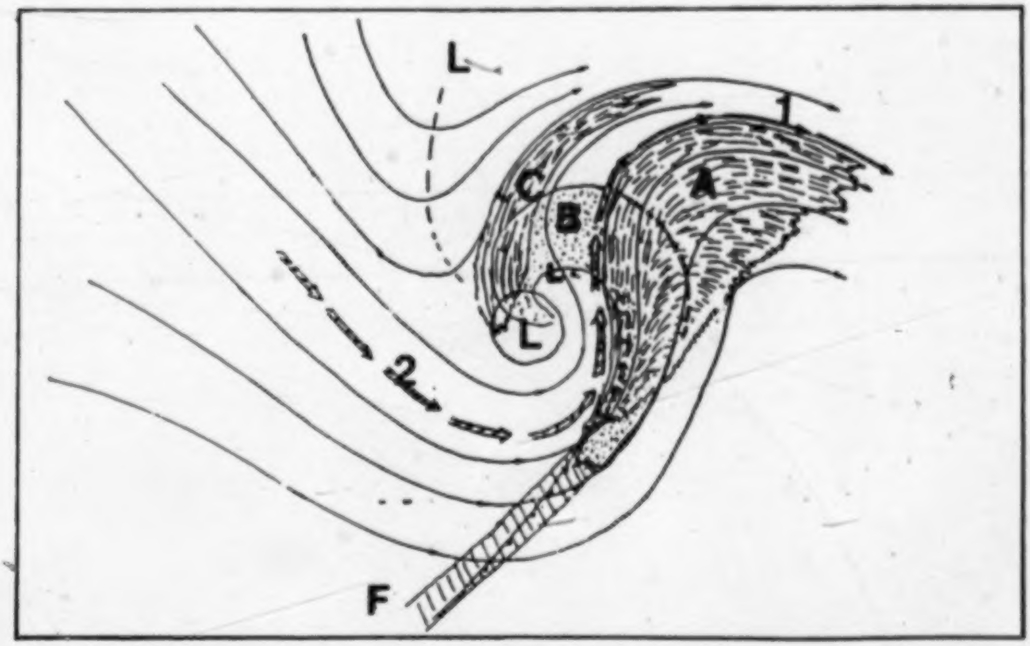

Figure 3.4 The fourth stage of development.

Phase #5

The system will reach this stage only if it is continually supported with energy. This stage will then represent the final stage of development, after which the pattern will not evolve, further, except for an increase in area. Figure 3.5 shows the main features at this stage. One also notices for the first time the existence of a new cloud area (D) and the amalgamation of (A) and (C) into one cloud area. Meanwhile, (B) moves farther westward with respect to (A) usually separating completely and moving out from (A).

### 3.1.4.2 Split-Flow Cyclogenesis

Split-flow cyclogenesis comprises the second most frequent type. It is very close to the well known "Upper-Cold Low model". The main characteristics of the flow at the 500-mb surface are well pronounced meridional troughing and a splitting jet stream. The following figures will illustrate the different phases of this development in detail.

Phase # 1

In Figure 3.6, the flow shows a well defined troughing and the splitting of an advancing jet into two streams. The first, jet (1), represents the old and stronger jet, while the second, jet (2) represents the new one. The triggering jet for development is jet (2), which advances toward the base of the troughing. Cloud areas (C) and (B) are the first signs of development at this stage. Often, (B) forms an enhanced cumuliform pattern rather than a comma-like shape. A closed circulation may show up at the base of the extended troughing at the 500-mb surface.

Phase #2

A dramatic change happens at this stage. The cloud area (B) develops very rapidly and assumes a comma-like shape of considerable size, sometimes referred to as "naked enhanced". Cloud area (C), which has a marked anticyclonic curvature, evolves and advances westward with respect to (B). The new jet (2) advances very fast towards the base of the trough. At this point the flow begins to separate as the lower part of the trough deepens and a cut-off, closed circulation develops at the base of the trough. The head of (B) moves farther northward and to the cyclonic side of the jet axis (2). Figure 3.7 shows the different cloud areas.

Phase #3

This stage represents the "adolescent" stage of development, where the cloud area (A) appears for first time and partly covers the tail of (B). The cloud area (C) advances westward and approaches the head of (B). Cloud area (B) evolves, attains a well-defined shape, and moves on farther to the cyclonic side of jet (2). Figure 3.8 shows this stage of development and the different cloud areas. The overall cloud pattern increases in area and becomes better defined. But, the low-level features of flow, e.g. at the 850-mb surface , are ill defined and show great variability. The new jet (2) continues to advance around the base and to the eastern side of the trough.

Phase #4

This is the mature stage of split-flow cyclogenesis. On synoptic maps, the closed circulation shows up at all levels from the surface to the 300-mb level. All cloud areas (A), (B), (C), and (D) become well-defined, as can be seen in Figure 3.9. The cloud shield spreads over a large area. The overall configuration is almost the same as in baroclinic cyclogenesis system. The surface features become organized and well defined. One important point is that cloud areas (A) and (B) are not extensions of each other but two separate overlapping cloud areas.

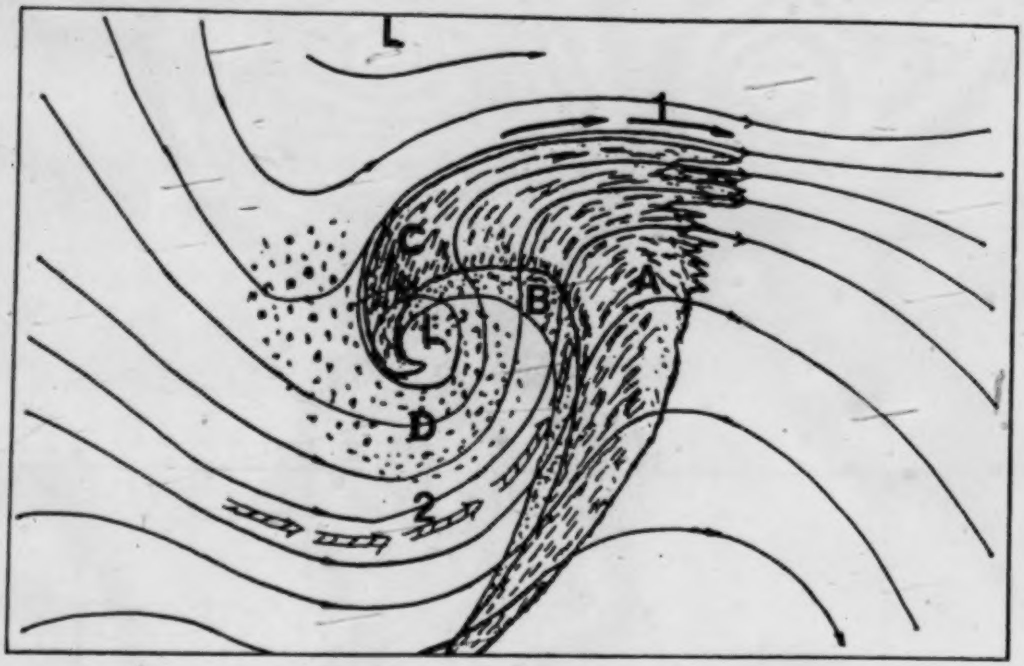

Figure 3.5 The last stage of development.

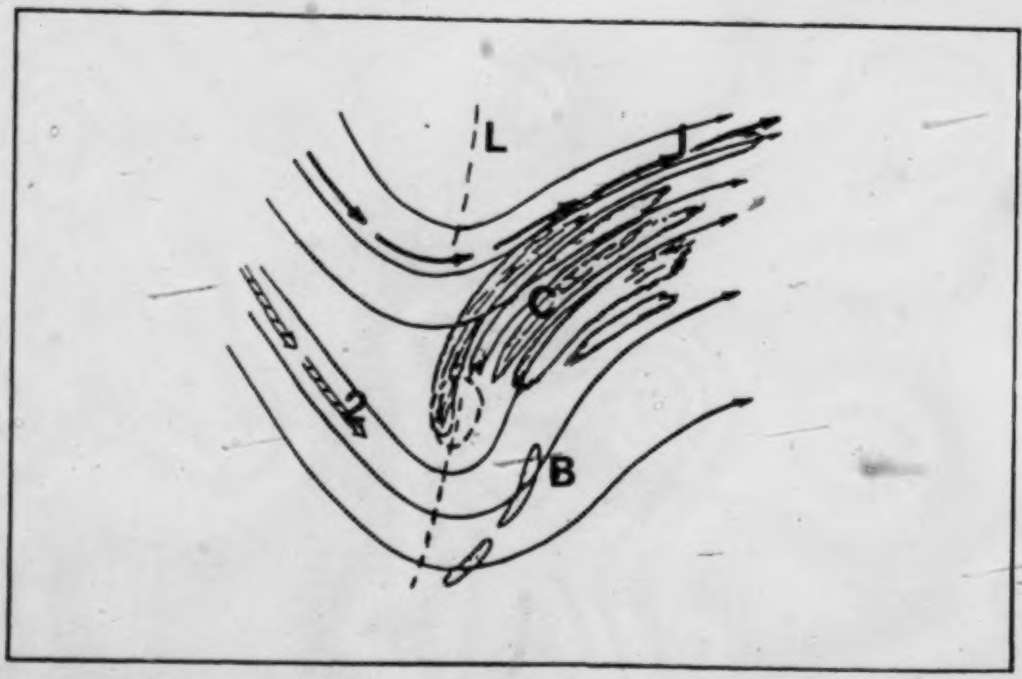

Figure 3.6 The first stage of split-flow cyclogenesis.

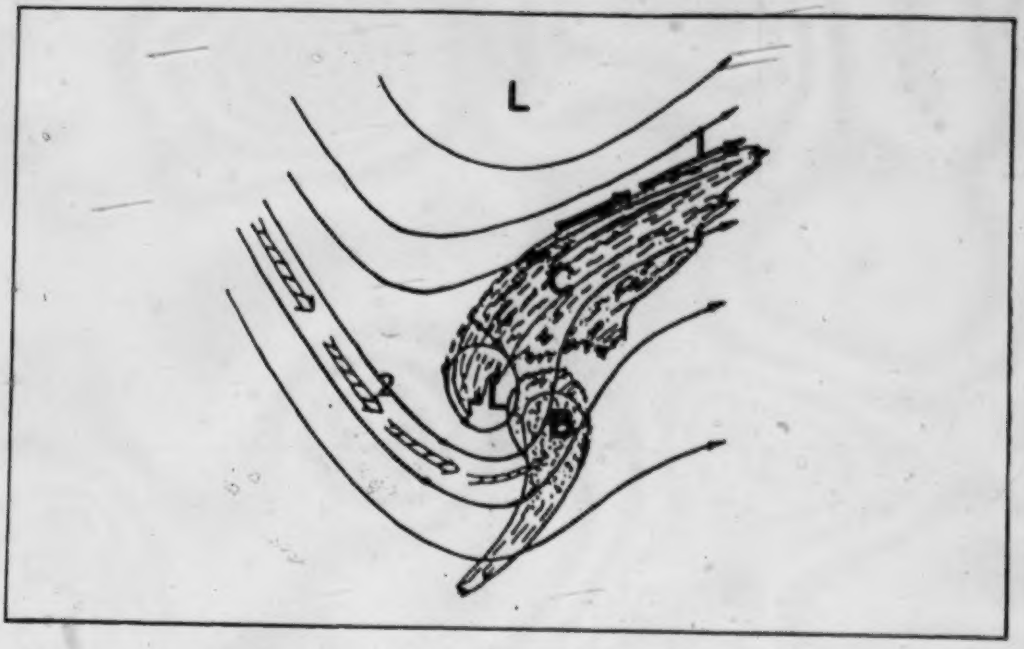

Figure 3.7 The second stage of development.

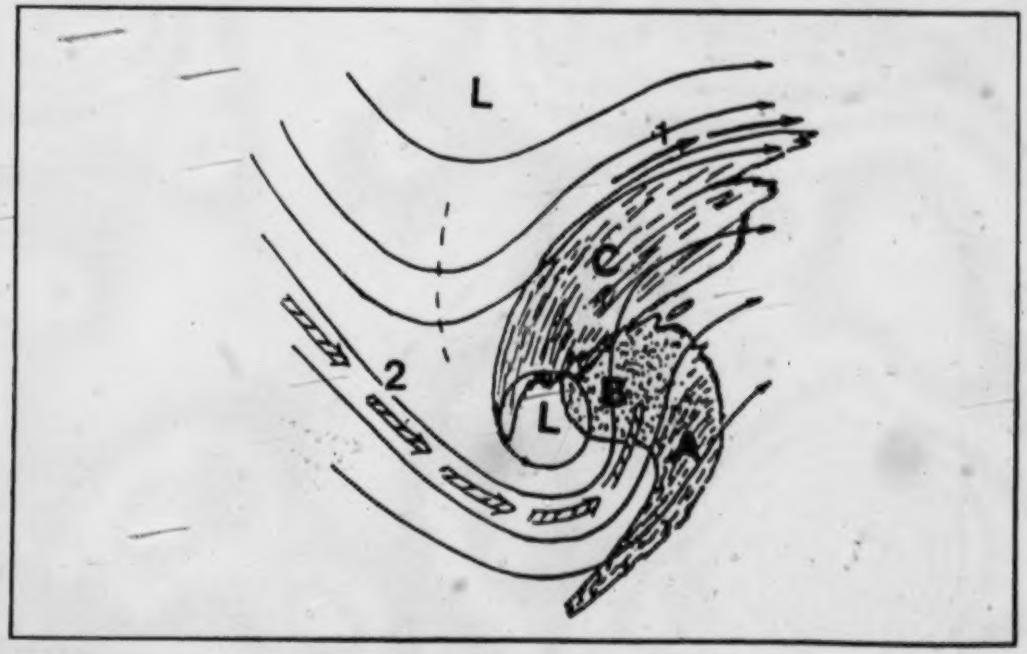

Figure 3.8 The third stage of development.

### 3.1.4.3 Cold-Air Vortex Cyclogenesis

Cold-air vortex and induced-wave cyclogenesis (to be described) are the most common mechanisms of cyclogenesis. They are often found over ocean areas, especially over the North-Atlantic and the North-Pacific. Cold-air cyclogenesis has been defined, lately, by others (e.g. Reed, 1979) under the name "Polar air stream cyclogenesis". In this type, a new distinct cyclone forms behind an old baroclinic frontal zone and produces its own circulation pattern. The overall configuration is governed by a confluent pattern rather than a splitting pattern. The following figures will illustrate the different phases of cyclogenesis.

#### Phase #1

Figure 3.10 shows the first stage of development. The system (A') is an old baroclinic system with an old jet axis (1) on its northern edge. The new system forms in the cold air behind the old system with a weak cloud area (B) and a well-defined cloud area (A). A new jet (2) advances between (A) and (B) and merges with the old jet (1) as seen in Figure 3.10. It should also be noted that the new jet approaches the base of the trough, which is of moderate amplitude. The new jet continues to advance and becomes parallel to the old jet (1).

#### Phase #2

While the old system persists, the new system continues to develop. The cloud area (B) becomes a comma-like shape, and moves further to the cyclonic side of jet (2). Cloud area (A) grows and extends zonally with a marked anticyclonic curvature. Jet (2) advances eastward and moves very close to jet (1). Figure 3.11 shows the details.

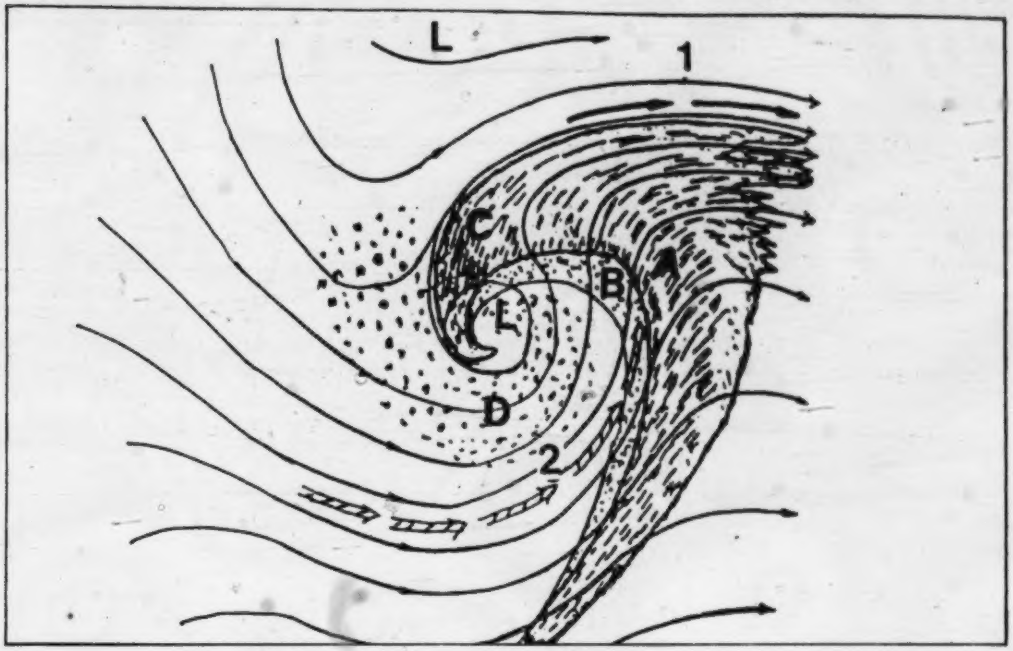

Figure 3.9 The last stage of split-flow development.

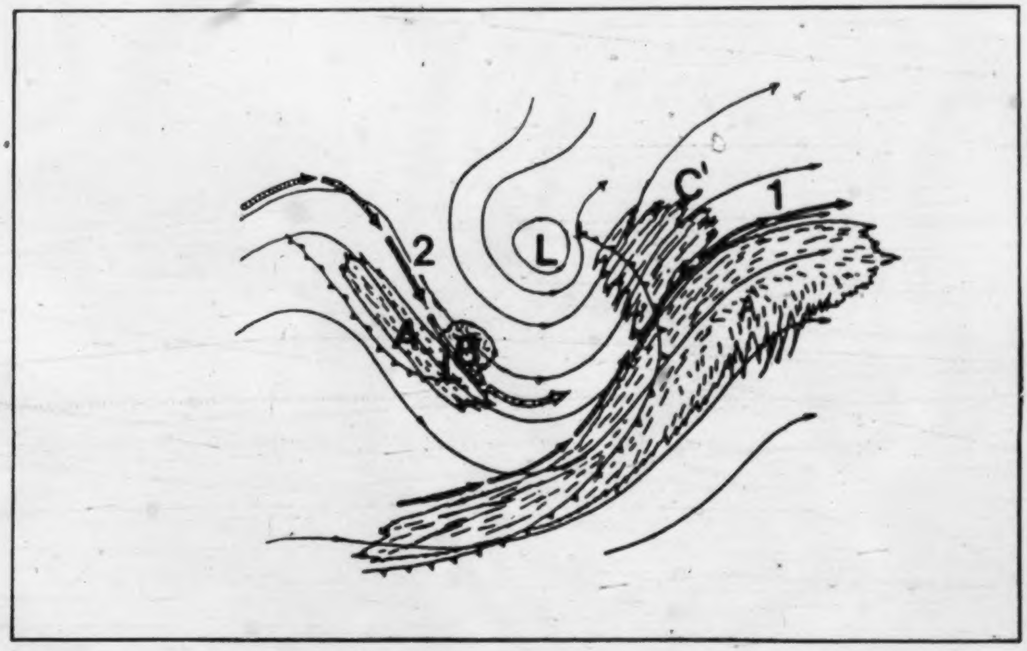

Figure 3.10 The first stage of cold-air vortex cyclogenesis.

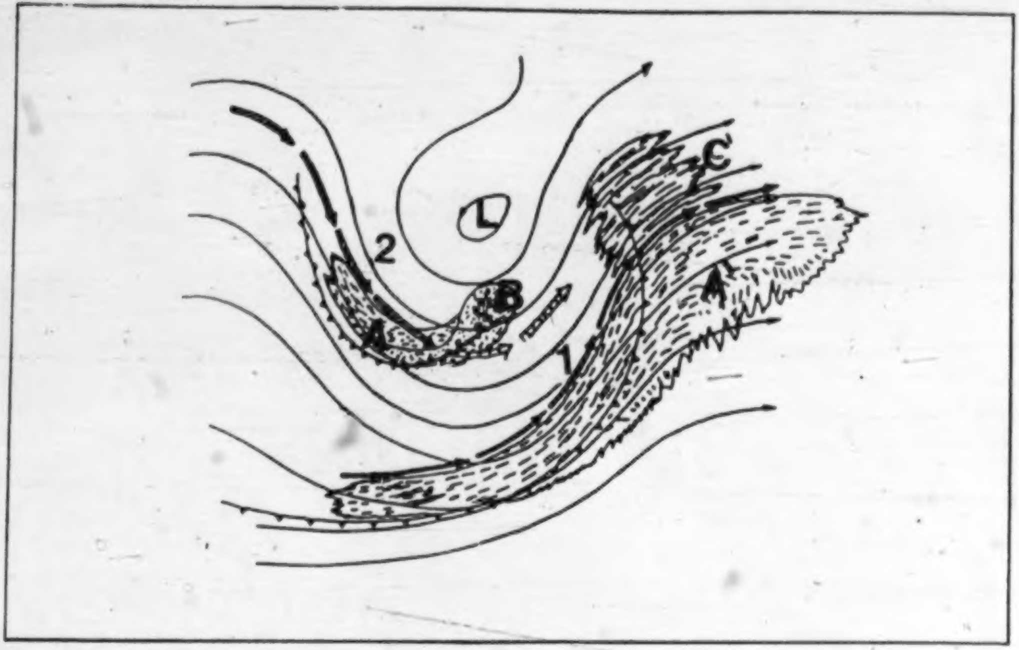

Figure 3.11 The second stage of development.

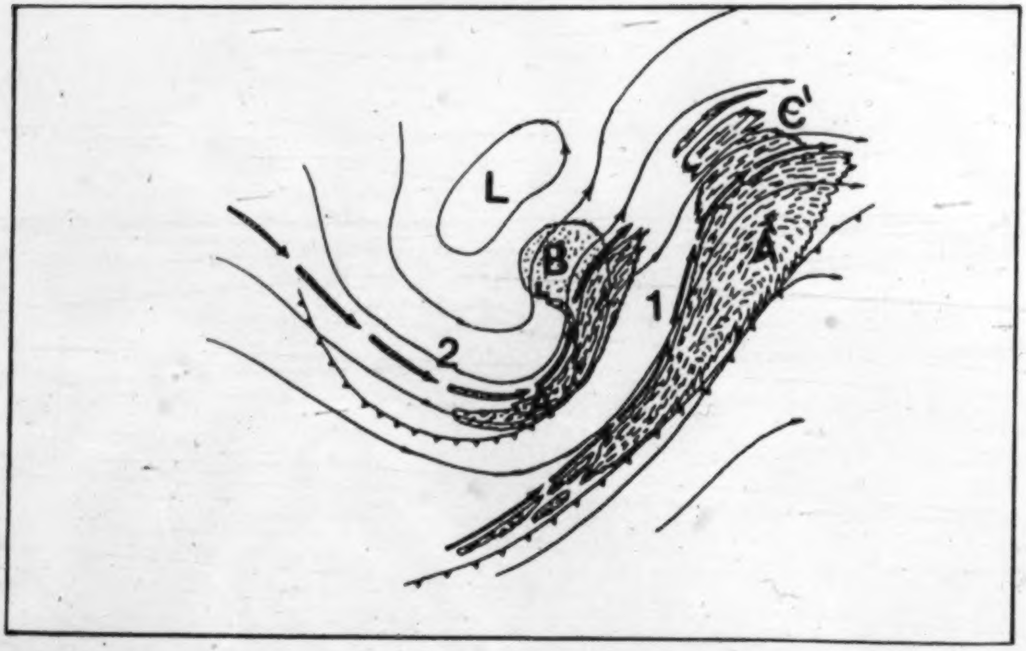

Figure 3.12 The third stage of development.

Phase #3

In Figure 3.12, the new system approaches the storm stage and, in the same time, it is completely separated from the old system, which begins to weaken considerably. The cloud area (B) moves away from (A) which masks only the tail of (B) and the frontal band. The new jet (2) advances, crosses (B), and moves to the eastern side of the trough. The old jet is still unchanged and nearly parallel to the new system.

Phase #4

This phase is well shown in Figure 3.13, where the storm stage of the new system can be seen very clearly. The new system has fully developed and is now well separated from the old and weaker system. The different cloud areas (A), (B), and (C) are seen and the tail of (B) extends southward as a frontal band. At this stage the new system is the dominant one.

### 3.1.4.4 Induced-Wave Cyclogenesis

The induced-wave cyclogenesis has almost the same features and phases as the cold-air vortex mode, but with a few differences. The new jet (2) advances to the eastern side of the 500-mb trough, and merges with the old jet rather than becoming parallel to it. The following figures illustrate the different phases. A new system develops within the cold air region and moves towards the baroclinic zone of the old system, in such a way that it appears to induce a wave on the old baroclinic zone (A'). The development of both systems continues thereafter as if they were one system.

Phase #1

In Figure 3.14, the old system moves away from the trough while the new system, composed mostly of the baroclinic zone (A), is located on the anticyclonic side of a new advancing jet (2). Jet (2) approaches jet (1) in a confluent configuration and merges with it at this stage of development. Sometimes, the new jet does not merge with the old but stays parallel to it. Also, the cloud area (B) may appear at this stage in advance of (A).

### Phase #2

This phase is quite different from phase #2 of the cold-air vortex mode. Figure 3.15 shows how the cloud areas (A) and (B) evolve and move toward the old system, which begins to conform to the new advancing system.

### Phase #3

At this stage of development, the cloud area (B) develops and becomes a well-defined comma, while the two jet axes merge into one system and no double-jet structure ensues. In Figure 3.16, for the sake of clarity, both jet axes are shown in close proximity. Meanwhile, the middle area of the cloud area (A'), the old baroclinic area, has weakened considerably.

### Phase #4

This is the last stage of cyclogenesis, where the new system attains maturity and all cloud areas are fully formed. In Figure 3.17, the tail of (B) moves under the old baroclinic zone (A') to form a lambda-like shape. Only one jet system is left rather than two. The old baroclinic zone (A') breaks down into two parts. The advancing part of (A') moves faster than the trailing part which decays quickly. This may be misinterpreted as the "adolescent" stage of the "Baroclinic-Zone Cyclogenesis" regime, if its history of development is not traced and examined carefully.

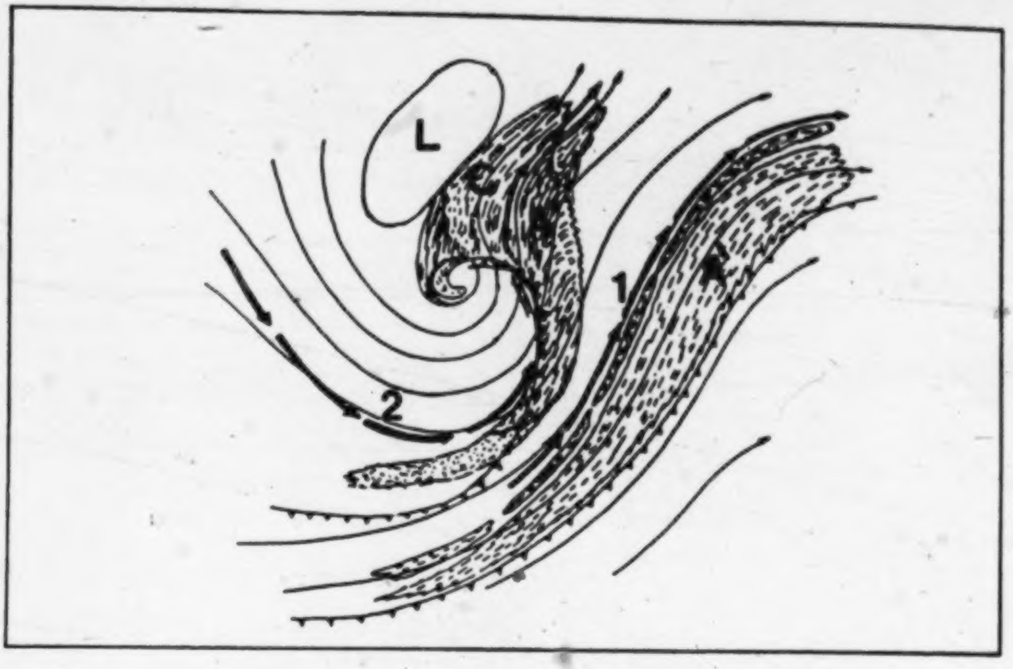

Figure 3.13 The last stage of cold-air vortex cyclogenesis.

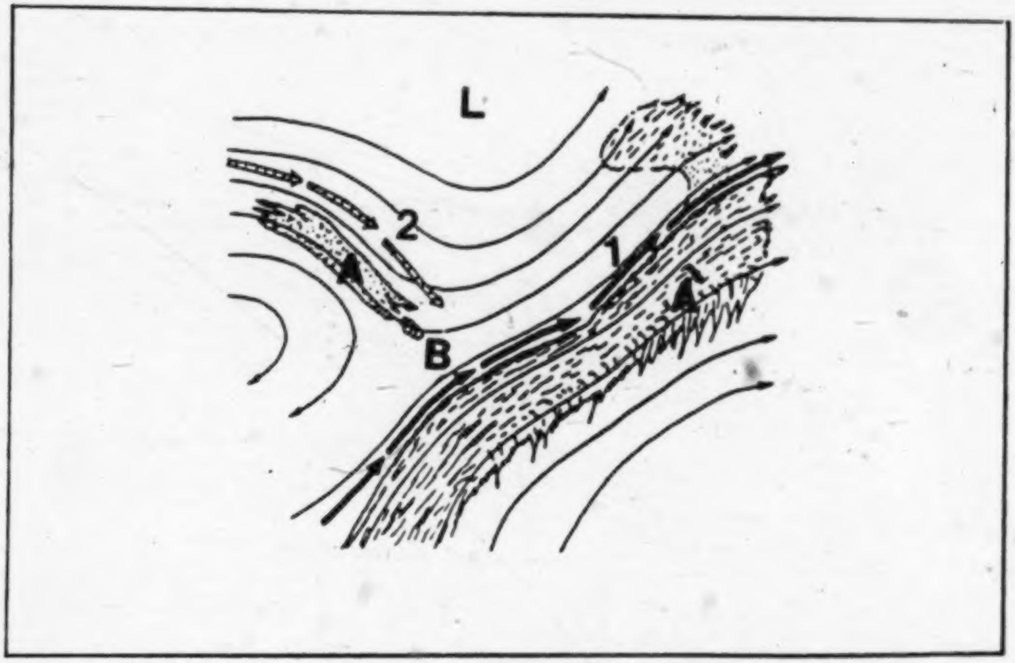

Figure 3.14 The first stage of induced wave cyclogenesis.

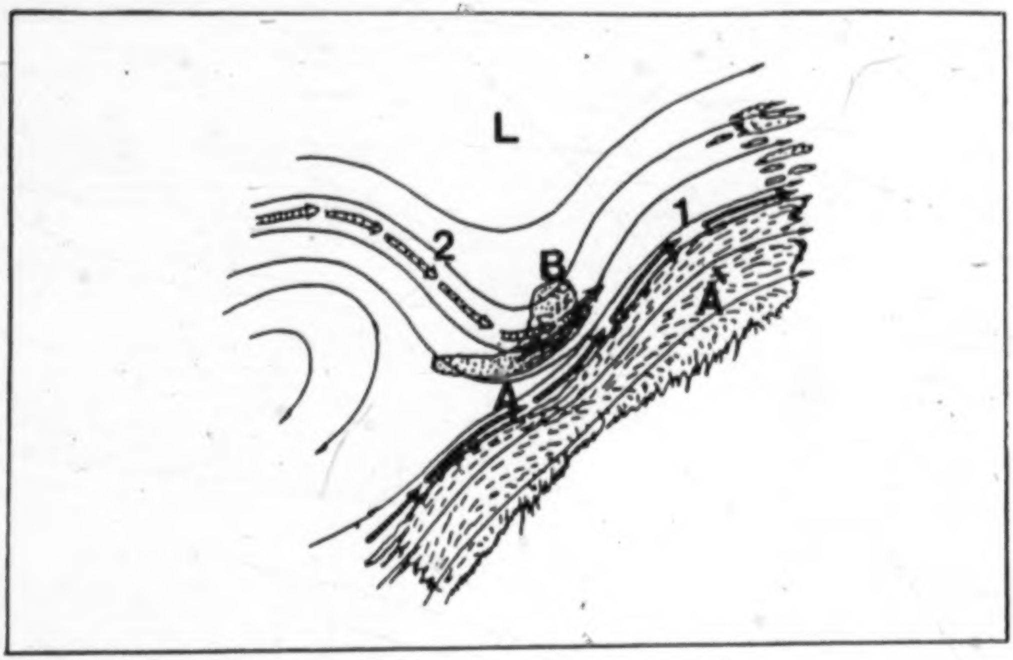

Figure 3.15 The second stage of development.

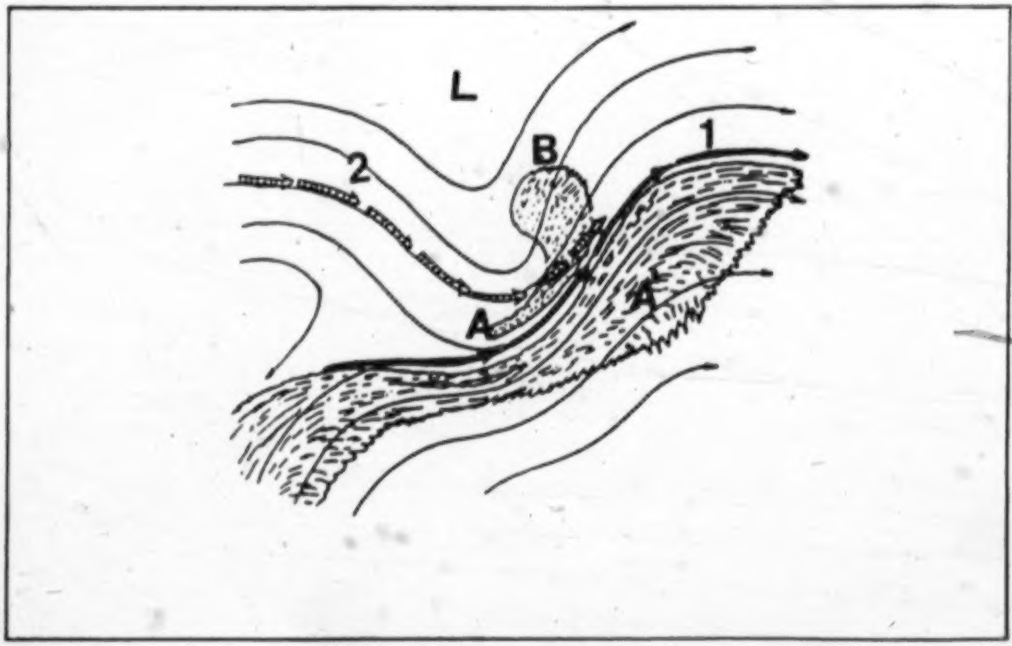

Figure 3.16 The third stage of devlopment.

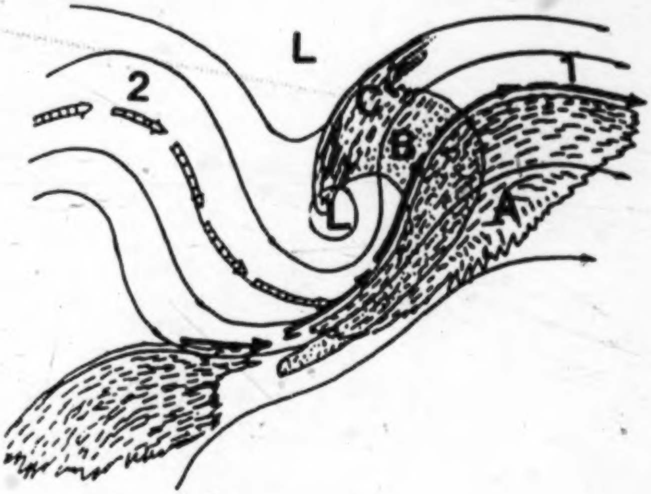

Figure 3.17 The last stage of development.

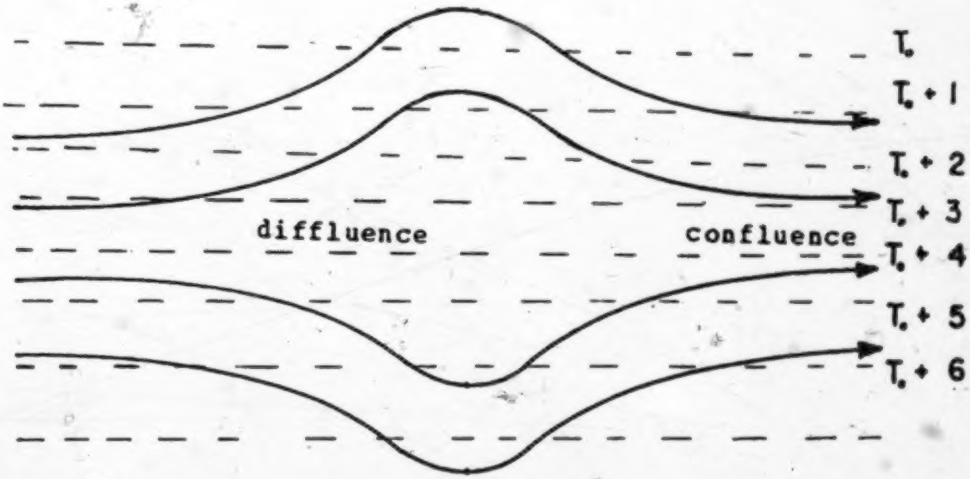
$T_0$
$T_0 + 1$
$T_0 + 2$
$T_0 + 3$
diffluence
confluence
$T_0 + 4$
$T_0 + 5$
$T_0 + 6$

Figure 3.18 Contour confluence is due to southerly warm flow with northerly cold flow.

## 3.2 Diffluence-Confluence And Jet Streams

### 3.2.1 Confluence-Diffluence

J. Namias and P. Clapp (1949) found that: " Confluence results most commonly where a stream of warm midtropospheric air from the south curves anticyclonically, gradually flowing beside a cold cyclonically curved stream from the north". This is illustrated schematically in Figure 3.18, where confluence results in meridional temperature gradient intensification, and diffluence leads to weakening of the thermal gradient. In other words, confluence concentrates the available energy into a narrow stream, where the flow attains its maximum speed, while diffluence has the reverse effect.

In 1956 S. Petterssen examined the problem of confluence and diffluence in more detail. A stream is said to be confluent if the streamlines converge toward a common axis, say in the direction of the geostrophic wind and it is diffluent if the streamlines diverge from the common axis of the flow. Care should be taken here, since confluence does not necessarily imply mass convergence, and vice versa. Also Petterssen showed that

$$\frac{\partial^2 z}{\partial x \partial y} = K_n \frac{\partial z}{\partial y} \qquad (3.2)$$

,where z is the height of an isobaric surface, $K_n$ is the curvature of the gradient of contours, sometimes called the orthogonal curvature of the contours. $K_n$ is thus a measure of the confluence or diffluence, e.g. regions of $K_n > 0$ are called confluent, and regions where $K_n < 0$ are said to be diffluent. Figure 3.19 illustrates this for four different cases of flow. Now the geostrophic wind component in the x-direction is given by.

$$u_G = -\frac{g}{f} \frac{\partial z}{\partial y} \qquad (3.3)$$

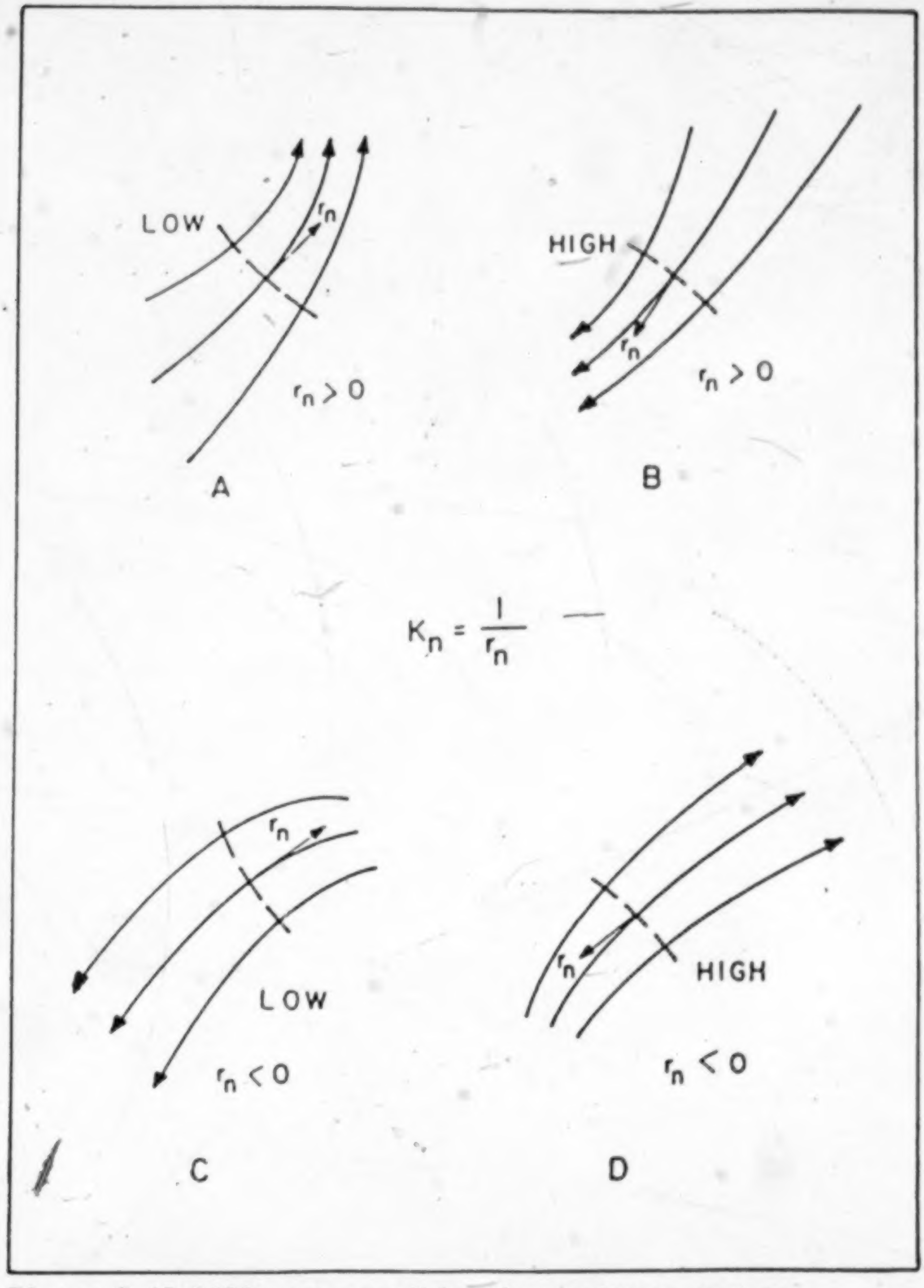
LOW
$r_n$
$r_n > 0$
A
HIGH
$r_n$
$r_n > 0$
B
$K_n = \frac{1}{r_n}$
$r_n$
LOW
$r_n < 0$
C
$r_n$
HIGH
$r_n < 0$
D

Figure 3.19 Different possible flow patterns and the associated orthogonal radius of curvature for each pattern.

,where g is the acceleration of gravity and f is the Coriolis parameter. Substituting in (3.2) results in

$$u_G K_n = -\frac{g}{f}\frac{\partial^2 z}{\partial x \partial y} \tag{3.4}$$

Taking x in the direction of the contour lines and y in the direction perpendicular and to the left of the contours one obtains

$$\frac{\partial u_G}{\partial s} = K_n \, u_G \tag{3.5}$$

,where s measures the distance along the contour lines. From the last equation, confluence is obtained by measuring the variation of the geostrophic wind along the contour lines.

### 3.2.2 Jet Stream And Cyclogenesis

#### 3.2.2.1 Definition

Jet stream is a fast narrow current concentrated along a quasi-horizontal axis in the upper troposphere and lower stratosphere, characterized by strong vertical and lateral wind shears. It is typically thousands of kilometers in length, hundreds of kilometers in width, and several kilometers in depth. The vertical shear is of order 10 m/sec. per km. and the lateral shear is of the order 10 m/sec. per 100 km. The arbitrary lower limit of wind speed along its axis is taken to be 30 m/sec..

#### 3.2.2.2 Early Studies

Jet streams were first encountered by high-flying pilots in the Second World War. With the subsequent development of jet stream theory in the late Forties and Fifties, it became known that maximum cyclonic vorticity (+) is located to the north of the jet axis and minimum cyclonic vorticity (0) is located to the south of the jet axis. This is shown in Figure 3.20, adapted from Reiter (1963).

The vorticity equation for a quasi-geostrophic frictionless flow can be written as,

$$\frac{1}{\zeta+f}\left[\frac{\partial \zeta}{\partial t} + V \cdot \nabla(\zeta+f)\right] = -\nabla \cdot V \qquad (3.6)$$

,where $\zeta$ is the relative vorticity as defined before, where V is the horizontal velocity, and f is the Coriolis parameter. From the above equation, one finds that the air masses flowing through this pattern ( Figure 3.20 ) experience divergence in the region of positive vorticity advection, i.e. in the left front quadrant (I) of a jet maximum. Similarly, for the other regions, one gets the distribution of divergence and convergence shown in Figure 3.20. In the above example, only the shear term of vorticity is considered. But when both the shear and curvature terms contribute to the vorticity, one finds the pattern shown in Figure 3.21.

According to the polar-front theory, the perturbation component in the wind field, acting normal to the frontal surface, causes a deformation of the front which amplifies through the stage of a wave disturbance into a cyclone. But, the polar-front theory contains a contradiction. Assume that near the ground a perturbation component has developed in the flow of warm air which initiates the formation of a warm sector. This perturbation would cause the warm air mass to move against the cold air, forming an indentation toward the cold side of the frontal surface. This process would result in a pressure rise. On the other hand, cyclogenesis is characterized by pressure falls. Hence, the pressure rise which is to be expected from the convergence of flow, would counteract the pressure fall. This would have a damping effect on development and favour frontolysis. In the real atmosphere, the development of a cyclonic vortex is always with surface pressure falls.

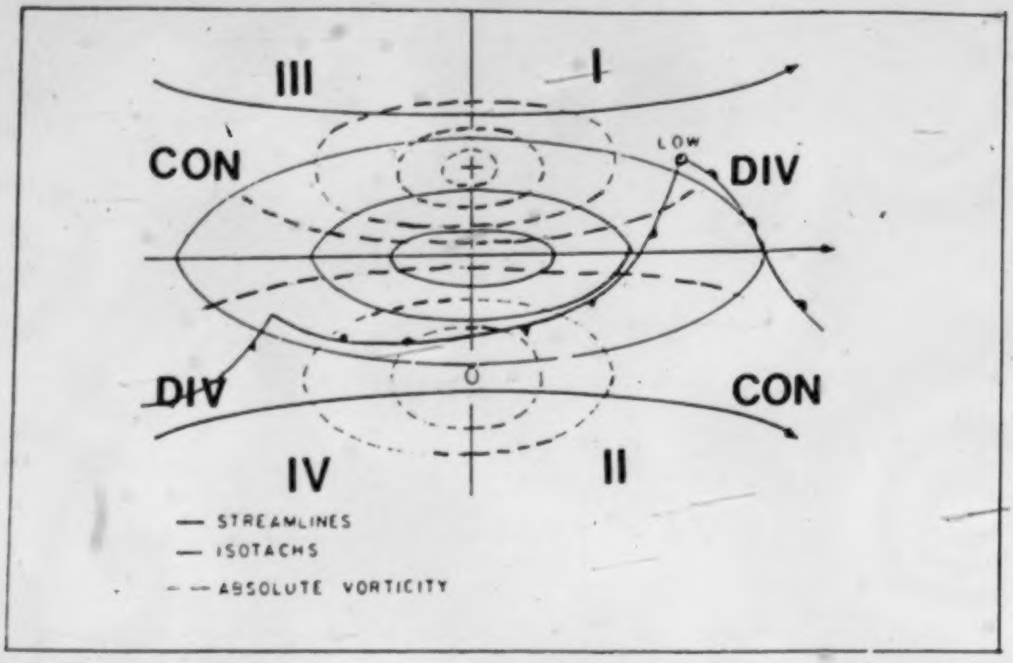
III
I
CON
LOW
DIV
+
DIV
0
CON
IV
II
STREAMLINES
ISOTACHS
ABSOLUTE VORTICITY

Figure 3.20 Jet-stream upper-level model and the associated low-level development (adapted from Reiter, 1963).

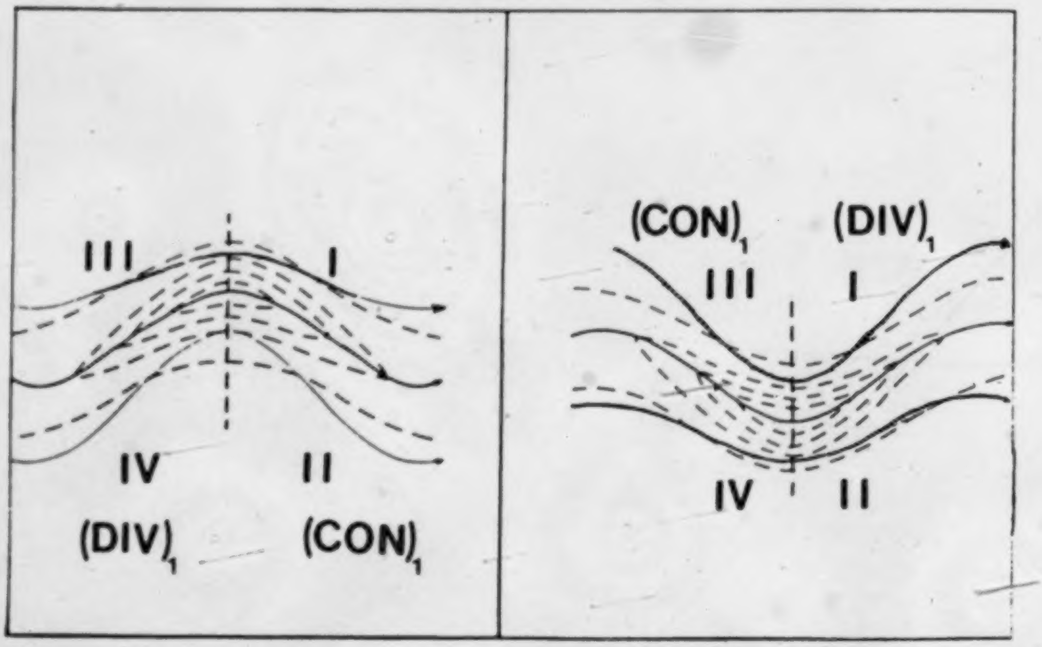
III
I
IV
II
(DIV)1
(CON)1
(CON)1
(DIV)1
III
I
IV
II

Figure 3.21 Different models of upper-level flow patterns(adapted from Riehl, 1954).

One is forced therefore to the conclusion that the cyclogenetic mechanism of pressure falls is caused by processes at high levels. Thus, cyclogenesis depends on a baroclinic structure in which the wind field is a function of height. Low-level convergence is superimposed by upper-level divergence, which attains maximum values in jet stream regions. Thus the upper divergence, which occurs in the left forward and in the right rear quadrant of a jet, brings about the pressure fall in the lower troposphere which, in turn, is a prerequisite for low-level convergence and cyclogenesis. Whether cyclogenesis actually occurs depends on several circumstances which may not all be fulfilled every time. Therefore, not every jet stream generates a cyclone, but every cyclone is associated with a jet stream .

In 1953, Riehl and Teweles examined the relationship between jet streams and upper cold-low cyclogenesis. In addition to the mechanism described above, strong cyclogenesis frequently follows the appearance of an elongated and nearly isolated cold dome aloft, best seen at 500-mb, surrounded by an advancing jet axis at the 300-mb surface. In addition, the thermal structure at the 500-mb surface is such as to produce a strong thermal gradient in the area of likely development, on the south-southwest side of the cold dome. Cyclonic development at the ground does not occur in the intense frontal zone but, surprisingly, far down stream. It is thus not possible to consider development to occur within the zone of strongest baroclinicity. When Riehl and Teweles (1953) examined the cold dome, they found its velocity to be practically the same as that of the wind vector at its center. They also noted that, the cold dome rises through the different stages of development, as confirmed by vertical cross-sections, and the horizontal area increase of the dome. Moreover, they regard the down stream propagation of the advancing jet as a link between the cold dome and the cyclone formation.

## 3.3 Petterssen's Model of Upper-Level Development

The theoretical and synoptic analysis of cyclone development, carried out by Petterssen and collaborators (1955, 1956 and 1971) has led to the well-known hypothesis that: "Cyclone development at low levels commences when and where an area of positive vorticity advection in the upper troposphere (normally on the forward side of an advancing trough) begins to spread over an area of warm advection (or near-absence of cold advection) in the lower troposphere". The experimental testing of the hypothesis has yielded good results. Nevertheless, and specially for cases over Europe, other observations suggest the existence of a cyclogenestic mechanism which does not strictly fit the famous hypothesis.

In 1971, Petterssen and Smebye introduced modifications, based on analyzed cases of a characteristic upper-level flows. The purpose of their study was to investigate storm development and the sources of energy necessary to augment the available potential energy.

### 3.3.1 Petterssen-Smebye Hypothesis

Cyclone development commences when a pre-existing upper trough, with strong positive vorticity advection on its forward side, spreads over low-level area of warm advection (or near-absence of cold advection) in which fronts may or may not be present. Synoptic development is initiated through a finite dynamic disturbance in the upper troposphere and intensifies due to importation of kinetic energy from the jet-stream region. Cases not associated with fronts are pure upper-level cyclones, whereas those associated with surface fronts are modified upper-level cyclones.

The distance of separation between the upper trough and the surface low decreases very rapidly during cyclone intensification. The amount of positive vorticity advection is very large at the onset of development, and decreases toward the time of peak intensity. The amount of warm advection is initially small, but increases as the cyclone intensifies. The final structure of the upper-level low looks like the occluded stage of a low-level cyclone.

### 3.3.2 An Example of a Pure Case of Upper-Level Cyclogenesis

Figure 3.22 shows the initial stage, where a deep cut-off low is centred over southern California. The positive vorticity advection on the forward side of the trough (not shown) is small. At the surface, a large anticyclone dominates the area of likely development and the (*) marks the centre of the surface low.

In Figure 3.23, the cut-off remains almost stationary and an advancing short wave, from the Gulf of Alaska, approaches the old trough. The net result is shown in Figure 3.24, where the new positive vorticity centre came around the base of the cut-off trough. As a result, a large area of strong positive vorticity advection has formed on the eastern side of the trough. Meanwhile, a large field of warm advection has formed in the same area (not shown in Figure 3.24) as well as a surface cyclone marked with *. Figure 3.25 shows the next stage, where the cut-off low reaches its maximum development and the surface low centre (*) approachs the upper troughing centre. Thereafter, the positive vorticity advection diminishes considerably, while the warm advection increases slowly.

Petterssen and Smebye used two approaches to investigate the baroclinicity within the storm area, referred to as, the thickness and the energy approach. Figure 3.26 indicates the possible time and area of low-level development (area of maximum negative barometric tendency). The frontal analysis within the area of impending cyclogenesis shows that the surface front is very shallow. Comparison between Figures 3.26 and 3.27 suggests that the expected development would take place within a barotropic area. As the cyclone matured, a baroclinic field of moderate intensity develops in the lower troposphere, as seen in Figures 3.28 and 3.29.

In the kinetic eneregy approach, the total kinetic energy over the area of concern, from the surface up to 100-mb level, is calculated during the life time of the storm.

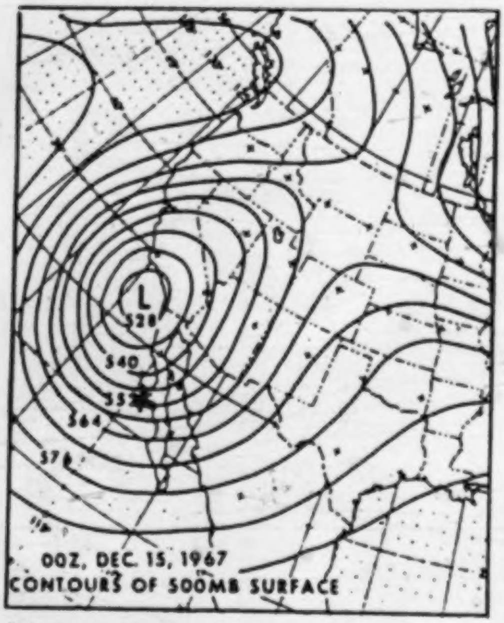
L
528
540
552
564
576
00Z, DEC. 15, 1967
CONTOURS OF 500MB SURFACE

Figure 3.22 500-mb chart, adapted from Petterssen and Smebye (1971).

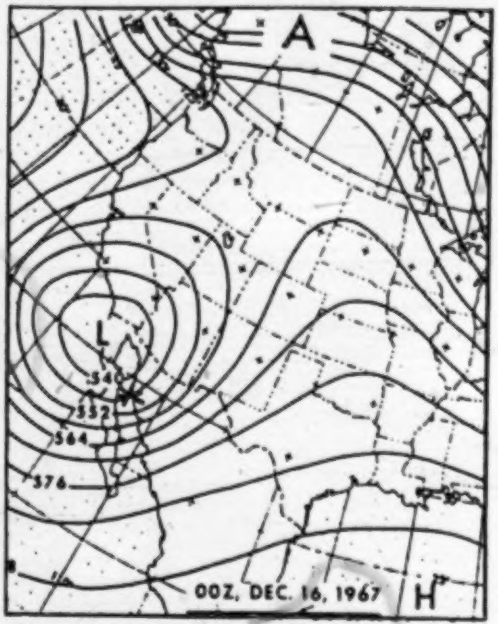
A
L
540
552
564
576
00Z, DEC. 16, 1967
H

Figure 3.23 500-mb chart, adapted from Petterssen and Smebye (1971).

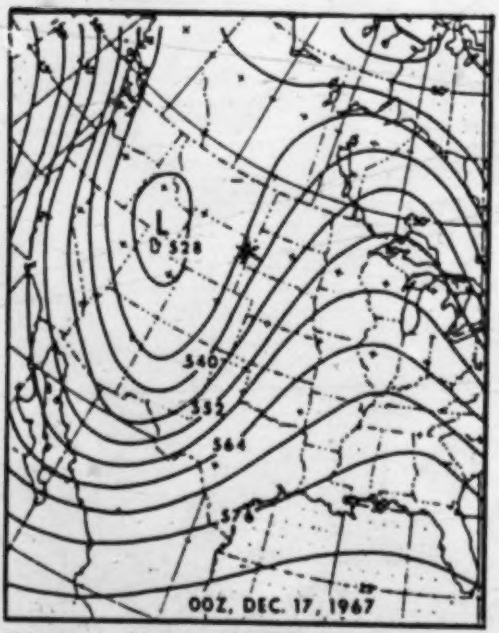
L
528
540
552
564
576
00Z, DEC. 17, 1967

Figure 3.24 500-mb chart, adapted from Petterssen and Smebye (1971).

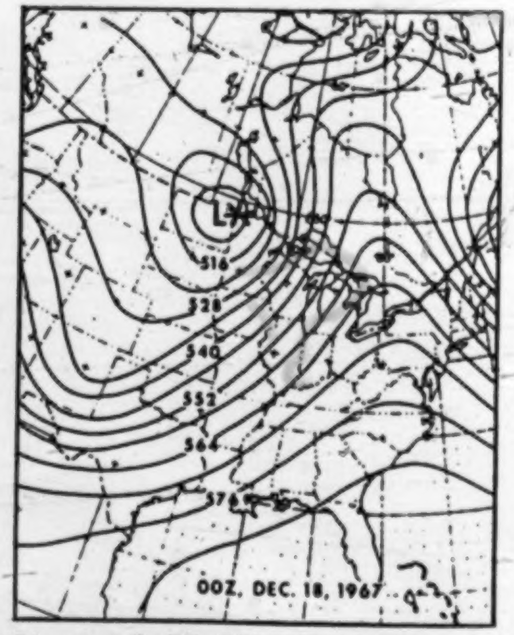
L
516
528
540
552
564
576
00Z, DEC. 18, 1967

Figure 3.25 500-mb chart, adapted from Petterssen and Smebye (1971).

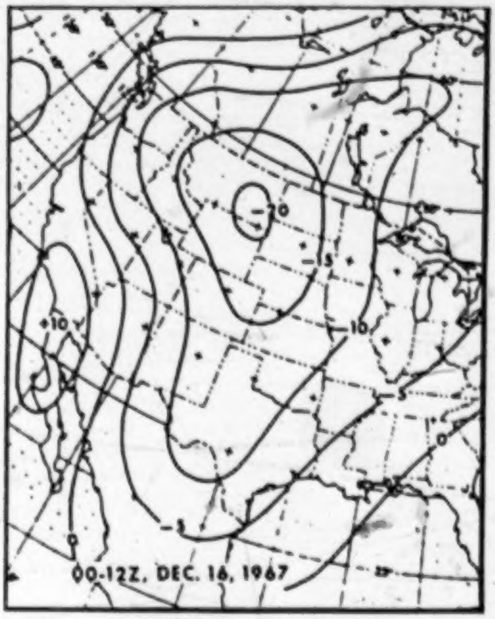
-10
-5
+10
10
5
0
-5
00-12Z, DEC. 16, 1967

Figure 3.26 Isallobaric analysis, adapted from Petterssen and Smebye (1971).

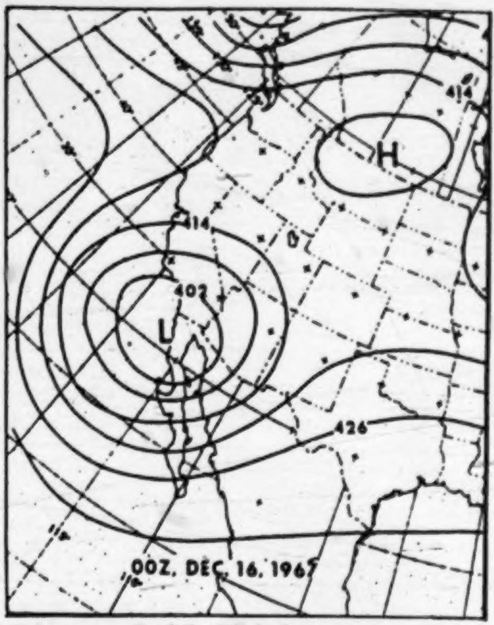
414
H
414
402
L
426
00Z, DEC. 16, 1967

Figure 3.27 Thickness analysis for the layer 850/500 mb, adapted from Petterssen and Smebye (1971).

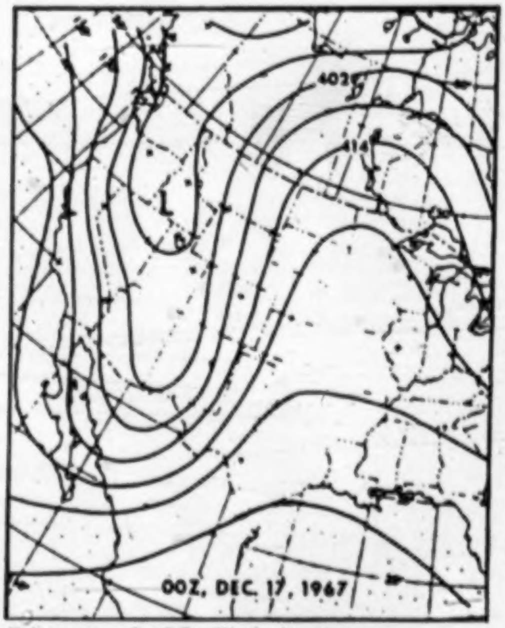
402
414
L
00Z, DEC. 17, 1967

Figure 3.28 Thickness analysis for the layer 850/500 mb, adapted from Petterssen and Smebye (1971).

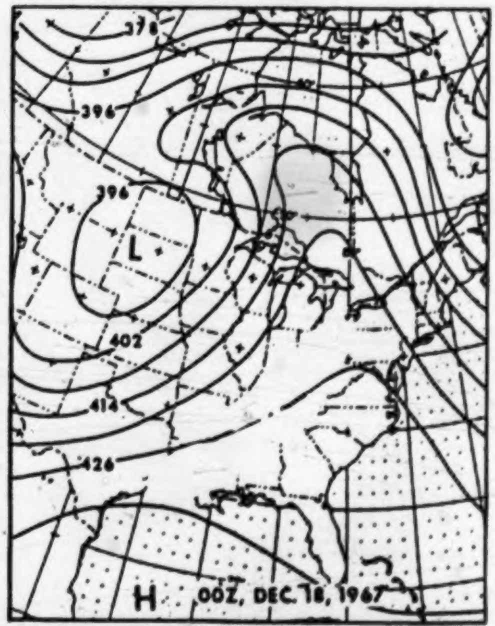
378
396
396
L
402
414
426
H
00Z, DEC. 18, 1967

Figure 3.29 Thickness analysis for the layer 850/500 mb, adapted from Petterssen and Smebye (1971).

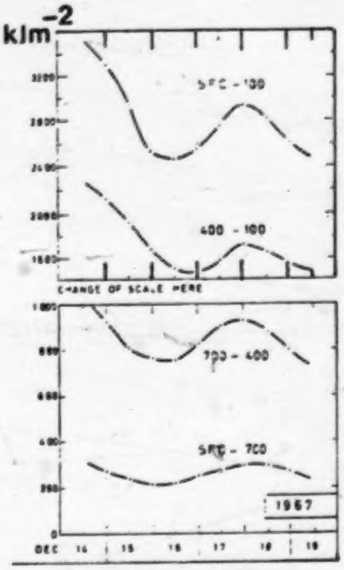

Figure 3.30 The kinetic energy analysis for different layers during the lifetime of the system, SFC : surface, adapted from Petterssen and Smebye (1971).

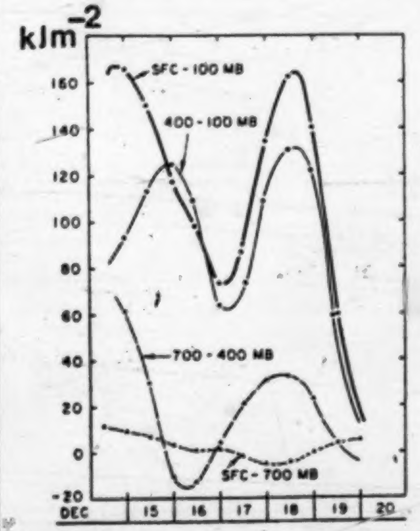

Figure 3.31 The horizontal kinetic energy distribution, adapted from Petterssen and Smebye (1971).

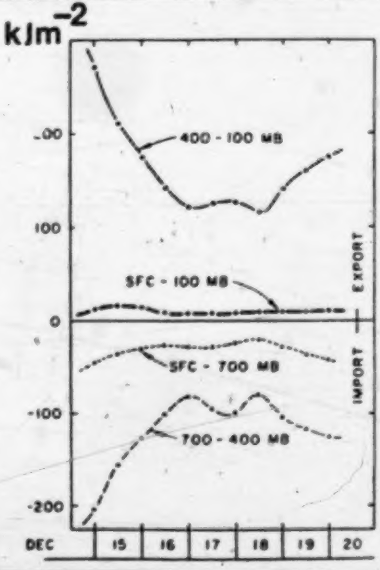

Figure 3.32 The vertical kinetic energy distribution, adapted from Petterssen and Smebye (1971).

Figure 3.30 shows the general features, where the system has a minimum value, at all levels on Dec. 16th (the time of development onset), and a maximum value on Dec. 18th (the time of maximum development). Comparison of Figures 3.31 and 3.32 shows the importance of the vertical export of kinetic energy. Figure 3.32 also shows that the export of kinetic energy from the top layer (400-100 mb) exceeds that developed in the lower layer (700-400 mb). In other words, cyclone development took place at the expense of baroclinicity within the jet stream region rather than at the expense of surface front baroclinicity.

### 3.3.3 An Example of a Modified Case of Upper-Level Cyclogenesis

Figures 3.33-3.36 show the different stages of development, where (*) marks the surface low centre. In Figure 3.33, a well-developed upper trough is shown over Texas, while on the surface a small wave disturbance has been initiated. In Figures 3.34-3.36, the elongated trough shows continued deepening as it moved southeast-ward first, then northeast-ward, where it weakened. A large amount of positive vorticity advection (not shown) has spread over an area of low-level warm advection in the vicinty of prospective cyclogenesis. Thereafter, a surface cyclone developed. Twenty-four hours later, (Figure 3.36) the approach of a new short wave led to the demise of the first system.

In the sequence of Figures 3.37-3.40, the general structure of the lower troposphere (850-500 mb) in the area of development was highly baroclinic, as can be seen from the thickness analysis. The baroclinicity was strong from the beginning and increased as the storm developed. The mode of the onset of development and the baroclinic structure suggest the existence of an upper-level system, while the surface frontal structure suggests a low-level development. Petteressen and Smebye considered this as a new mode of development, initiated by a modified upper-level low.

Figure 3.41, which corresponds to Figure 3.30 in the pure case, shows a maximum value of kinetic energy at the time of development onset which thereafter

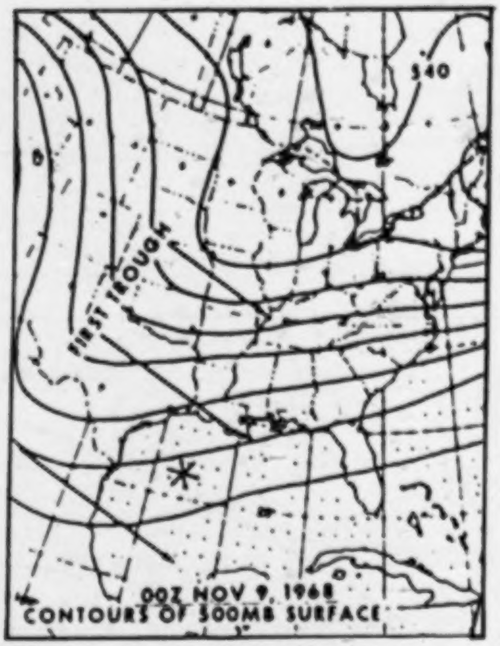
540
FIRST TROUGH
00Z NOV 9, 1968
CONTOURS OF 500MB SURFACE

Figure 3.33 500-mb chart, adapted from Petterssen and Smebye (1971).

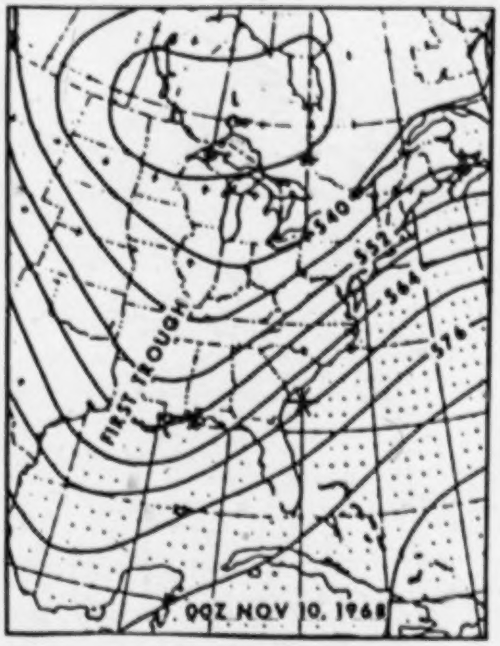
540
552
564
576
FIRST TROUGH
00Z NOV 10, 1968

Figure 3.34 500-mb chart, adapted from Petterssen and Smebye (1971).

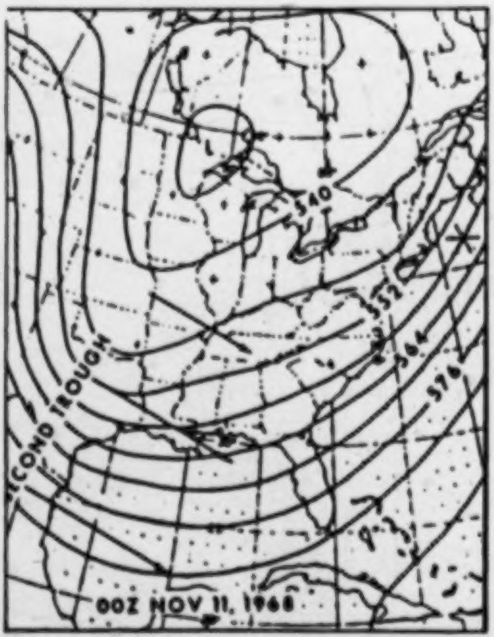
L
540
552
564
576
COND TROUGH
00Z NOV 11, 1968

Figure 3.35 500-mb chart, adapted from Petterssen and Smebye (1971).

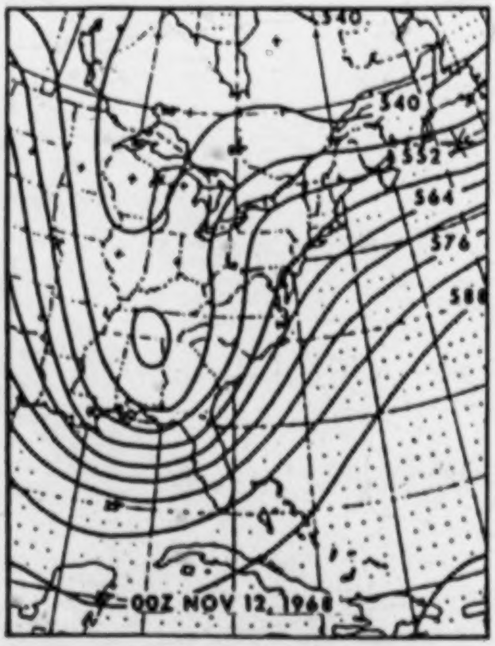
540
540
552
564
576
588
L
00Z NOV 12, 1968

Figure 3.36 500-mb chart, adapted from Petterssen and Smebye (1971).

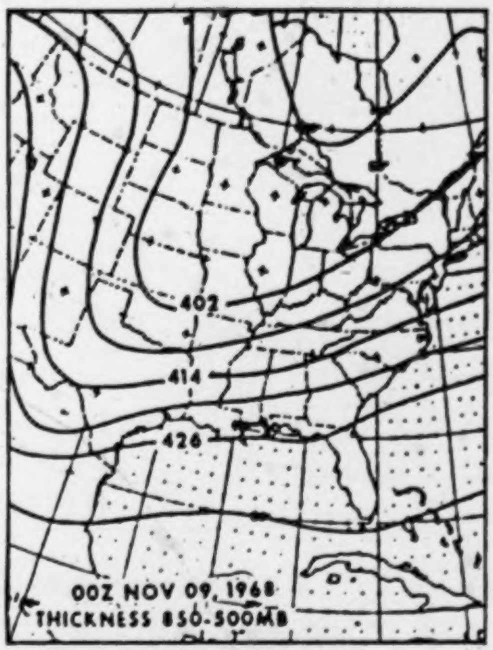
402
414
426
00Z NOV 09, 1968
THICKNESS 850-500MB

Figure 3.37 Thickness analysis for the layer 850/500 mb, adapted from Petterssen and Smebye (1971).

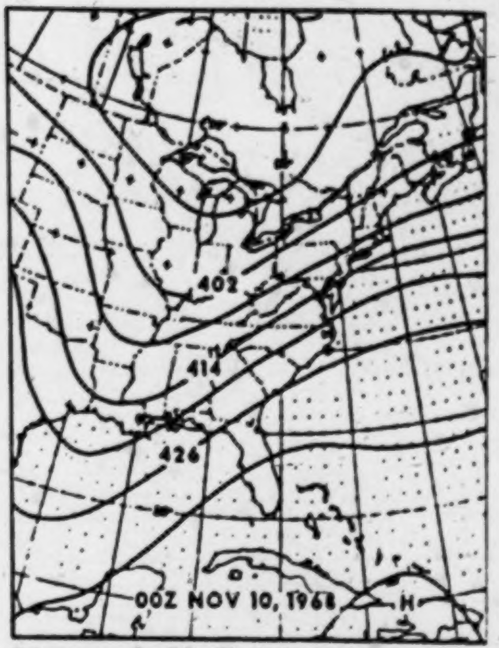
402
414
426
00Z NOV 10, 1968
H

Figure 3.38 Thickness analysis for the layer 850/500 mb, adapted from Petterssen and Smebye(1971).

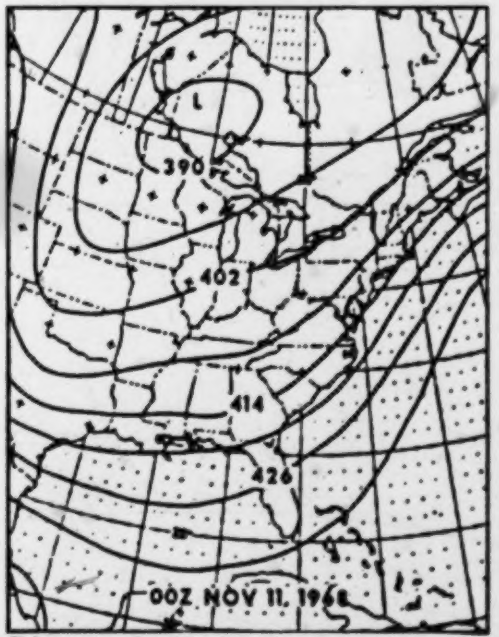
L
390
402
414
426
00Z NOV 11, 1968

Figure 3.39 Thickness analysis for the layer 850/500 mb, adapted from Petterssen and Smebye(1971).

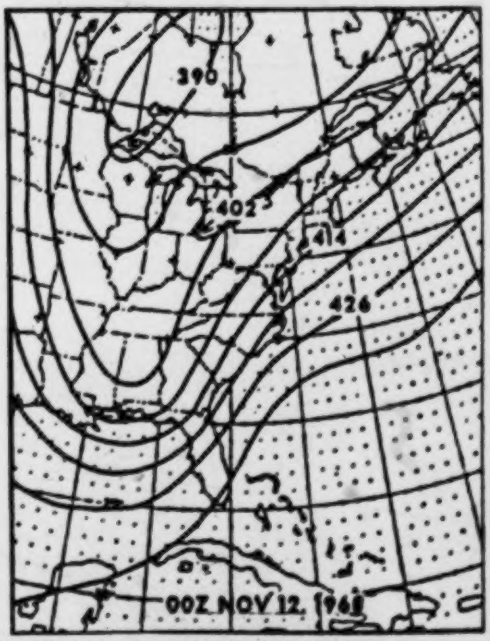
390
402
414
426
00Z NOV 12, 1968

Figure 3.40 Thickness analysis for the layer 850/500 mb, adapted from Petterssen and Smebye(1971).

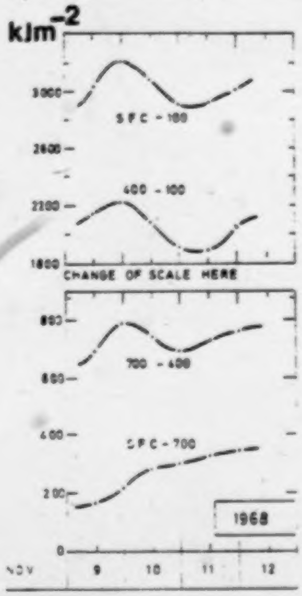

Figure 3.41 The kinetic energy analysis for different layers during the lifetime of the system, SFC : surface, adapted from Petterssen and Smebye (1971).

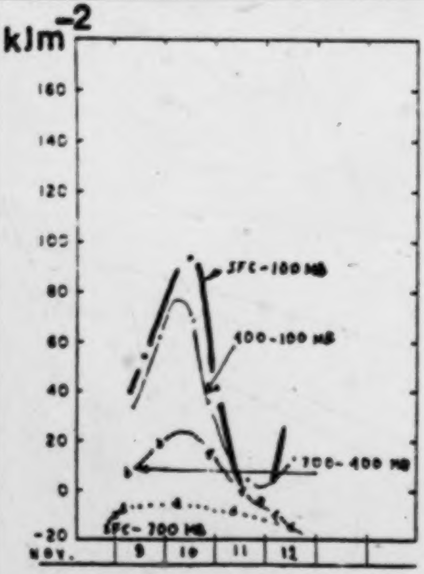

Figure 3.42 the horizontal kinetic energy distribution, adapted from Petterssen and Smebye (1971).

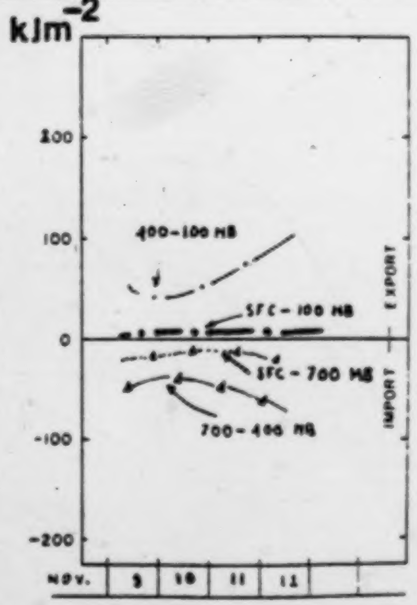

Figure 3.43 The vertical kinetic energy distribution, adapted from Petterssen and Smebye (1971).

decreases and reaches a minimum value at the time of decay. Subsequently, it increases again with the approach of the new system. The energy distribution was similar for all layers except in the lowest layer (surface-700 mb). Comparison of Figures 3.42 and 3.43 shows again the importance of the vertical transport of kinetic energy. One should note that the downward export of kinetic energy, from the top layer (400-100 mb), became less than that in the pure case, while the kinetic energy, for the layer (700-400 mb), has increased. This supports the hypothesis that low-level development took place at the expense of upper-level baroclinicity as well as the low-level baroclinicity of the surface front.

### 3.4 Zwatz-Meise's Model of Upper-Level Lows

In 1972, Zwatz-Meise introduced a model of development for upper-level lows, based on satellite and conventional data. The model is based on data from the Mediterranean Sea and Southeast Europe. The different stages of development are discussed in relation to the topography of the 500-mb surface, the surface pressure and the stability index.

By observing the cloud configuration of cut-off systems, cloud areas can be monitored. One should always be aware of the various sources of error, when correlating different parameters with either satellite data or surface reports. One source of error, not to be underestimated, is the time difference between the sources of data used. A second source is the limitation of the data available, e.g. the use of the geostrophic relative vorticity to approximate the relative vorticity field.

Showalter Index ( SI ) was used for the analysis of stability conditions. This index is defined as:

$$SI = T^{5} - T^{\cdot}$$

,where $T^{5}$ is the actual temperature at the 500-mb surface and $T^{\cdot}$ is the temperature of an air parcel lifted adiabatically from the 850-mb surface to the 500-mb level.

The index provides information about possible convective activities as follows:

-For SI > +3°C, stable conditions are expected.

-For 0°C< SI < +3°C, unstable conditions and probable showers are expected.

-For -3°C< SI < 0°C, unstable conditions and thundershowers are expected.

-For SI <-3°C, unstable conditions and heavy thunderstorms are expected.

One should be careful in areas of surface fronts or low-level inversion, since the index may be subjected to error like any other prognostic device

Zwatz-Meise's model was based on four upper-level cyclone cases, two during Winter, one in Spring and one in Fall. Winter cases show very distinct cut-off lows, whereas Spring and Fall cases lack definitive configuration. The model includes five stages of development: (i) the trough stage, (ii) the pinch-off stage, (iii) the split-off stage, (iv) the cut-off stage, and (v) the decay stage

### 3.4.1 The Trough Stage

Figure 3.44 shows the different cloud areas and their positions with respect to the flow at the 500-mb level. Two main cloud areas can be detected at this early stage. The first is an old band, marked with the letter (F), and the second consists of new developing convective clouds, marked with the letter (B). Band (F) is an old frontal band ,stratiform, formed within a southerly flow of warm air. The band is separated from the cloud area (B) and has no effect on it. (B) consists of broken cumuliform cells of different sizes. (B) occupy the central region of the upper-cold trough (L). The formation of (B) is due to a flow of cold air over the area (L). It resembles the decay stage of an extra-tropical cyclone.

The surface low, denoted by (*), precedes the upper centre (L) on the southeast side. Figure 3.44 shows also the surface front with an incipient wave. The upper flow shows the troughing stage, where the trough is elongated southward with respect to the main westerly current. A closed circulation may form at the base of the trough as shown in Figure 3.44.

In Figure 3.44, the dashed contour encircles an area with SI less than 3° C, i.e. an unstable area and with shower probability. When the system reaches this stage, weather observers usually report showers and thundershowers. Sometimes, however, discrepancies may arise between the stability index analysis and surface reports, because of time differences, insufficient data coverage, short-term frontal movements and similar meso-scale changes.

### 3.4.2 The Pinch-Off Stage

In this stage the two main cloud areas continue to develop, as shown in Figure 3.45. The cloud area (F) breaks down into two or more parts. The whole cloud area (F) moves east-ward from (B). The cloud area (B) increases in size and thickness, especially in its eastern part, and becomes more organized. The regular shape of the pattern is a reflection of the upper-level vorticity field.

The elongated trough pinches off at its neck, as indicated by the solid arrows pointing inward. More closed circulation may show up at the base of the trough. The surface low (•) approaches the centre of (L). The surface front decays and the frontal wave disappears.

In Figure 3.45, the stability index contour shifts northward without much change. Surface reports may again show thunder activity within the eastern part of (B).

### 3.4.3 The Split-Off Stage

The split-off stage is shown in Figure 3.46, with the different cloud areas as marked before. The cloud area (F) decays considerably and moves away from (B). In the meantime, (B) attains a comma-like shape with pronounced thickness and apparent size. It is centered on the southeast sector of (L). On the central and western part of (L),a new cloud area (D) develops for the first time. It is composed of open and closed cellular elements of considerable size. The overall configuration of (B) and (D) shows an organized pattern of circular or ellitical shape. Both, (B) and (D), are isolated from any other patterns and have a well-defined boundary.

The pinch-off opens up again, as indicated in Figure 3.46 by the solid arrows pointing outward. No more closed circulations form at the base of the trough. The surface low (*) approaches from (L), while the surface front continues to decay.

In Figure 3.46, SI indicates the possibility of showers within the 3° C contour. On the other hand, surface reports may indicate thundershowers within the 1° C contour, specially over the head of (B).

### 3.4.4 The Cut-Off Stage

This is a very important stage in the life history of the system. Figure 3.47 shows the different cloud areas and their relation to the upper flow. The overall cloud pattern configuration attains a circular shape and moves further eastward with respect to the centre (L). New cloud areas form while (F) vanishes completely. (B) develops vertically and moves to the northeast sector of (L). A new cloud area (C) of spiral shape forms in the northerly flow on the rear side of the elongated trough. Another cloud area, (A), develops on the northeast side of (L). It has a stratiform structure but is of lesser thickness than (C). The persistence of both (B) and (C) depends on the intensity of the cold air dome. The weak cloud area (D) continues to move toward the centre of (L); its size and structure depend on the cold air dome intensity and the type of underlying surface (water-land). For example, an irregular pattern indicates a weak cloud area.

The neck of the elongated upper trough continues to open up (Figure 3.47), and the closed circulation weakens and begins to cut-off from the main northern current. The surface low (*) moves away from the upper centre (L) and the surface front dissipates completely.

The outer stability contour in Figure 3.47 indicates stable conditions, yet, it encloses an area of dense cloud cover with possible shower activity.

### 3.4.5 The Decay Stage

This last stage has few regular features and may vary considerably from one case to another. But, common to all are the cloud areas (B) and (D), as shown in Figure 3.48. (B) decays and loses its comma shape as it decreases in size and thickness; it moves to the northwest side of (L) with its tail pointing northward. The cloud area (D) becomes more and more irregular while all other cloud areas disappear. Both (B) and (D) are no longer due to a synoptic air flow, but are largely maintained by subsynoptic-scale processes.

In Figure 3.48, the surface centre moves further away from the upper centre (L). The mid-tropospheric circulation penetrates to lower levels whereas it weakens aloft. The influence of the upper circulation diminishes while that of the low-level increases.

Showalter index yields good results at this stage. The entire area enclosed by the stability contour ( Figure 3.48 ) indicates shower activity confirmed by surface reports. The close match between the cloud configuration and SI boundary is due to the stability of the moisture field, whereas in the early stages of development, the moisture field was highly variable.

### 3.4.6 Summary and General Remarks

An upper-level cyclone is a spiral system which develops in the middle and upper troposphere. It has no corresponding low-pressure system at lower levels, in the early stages of development. In the late stages, vortexogenesis propagates downward, and may lead to the formation of a surface low. The upper cold air superimposes the cyclonic system, such that the temperature in the central area is lower than that in the surroundings. In general, upper-cold lows tend to be steered in the direction of the low-level flow as observed on the 850-mb surface.

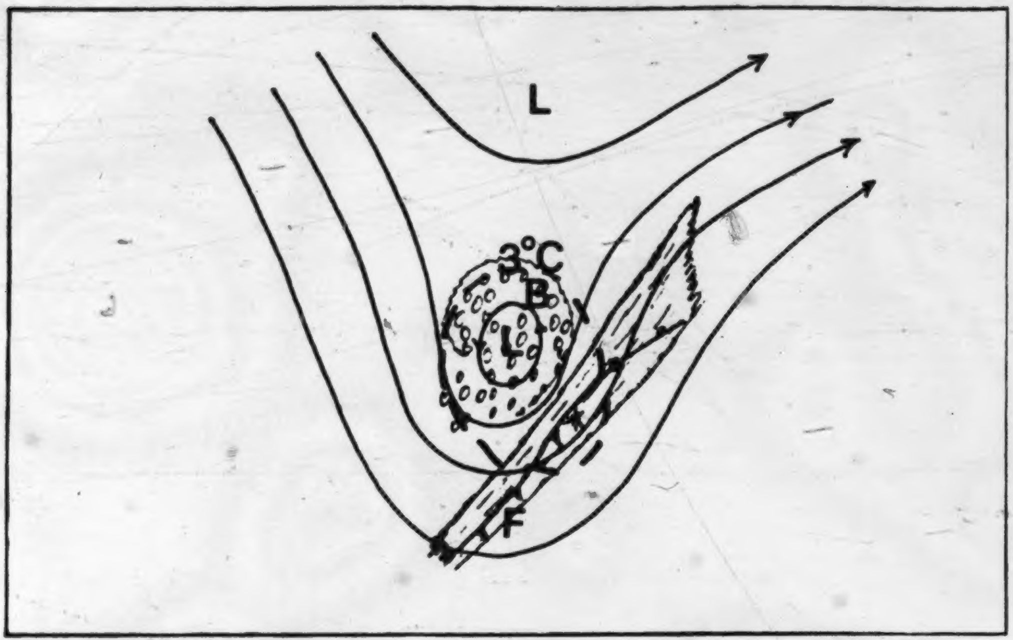

Figure 3.44 The troughing stage, solid lines: 500-mb contours, dashed line: stability index, F: frontal band, B: comma developed area and *: surface low centre.

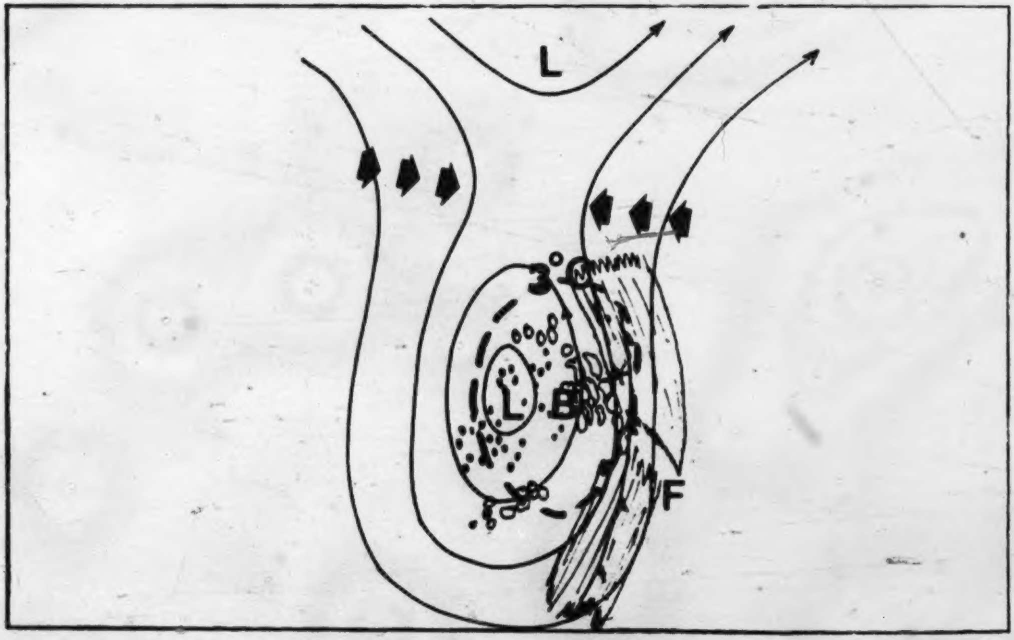

Figure 3.45 The pinching-off stage, solid lines: 500-mb contours, dashed line: stability index, F: frontal band, B: comma developed area and *: surface low centre.

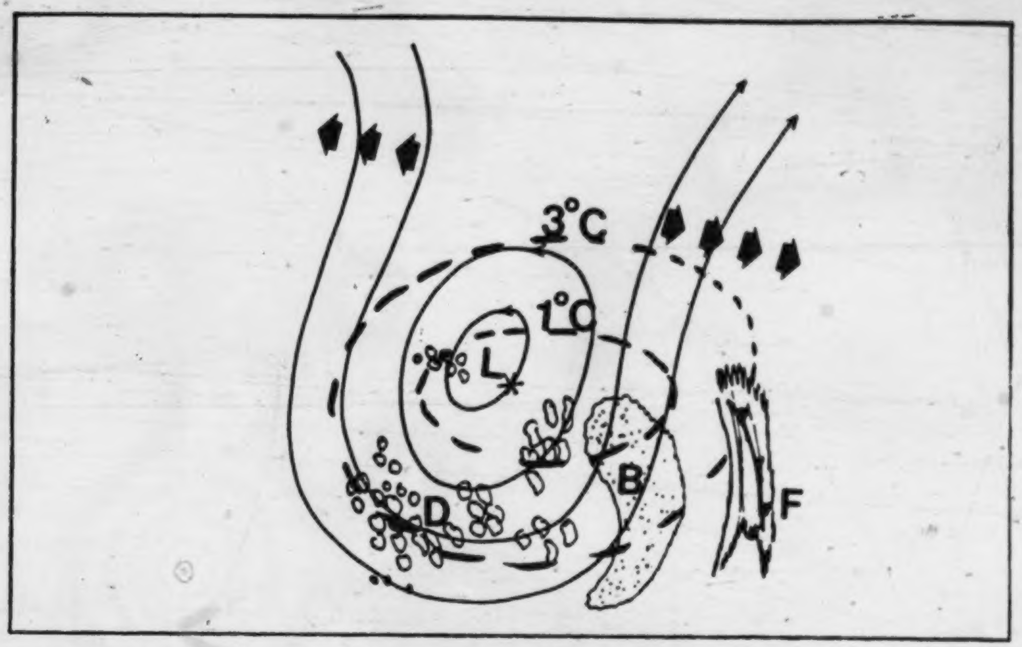

Figure 3.46 The splitting-off stage, solid lines: 500-mb contours, dashed lines: stability index, F: frontal band, B: comma developed area, D: cellular cloud area, and *: surface low centre.

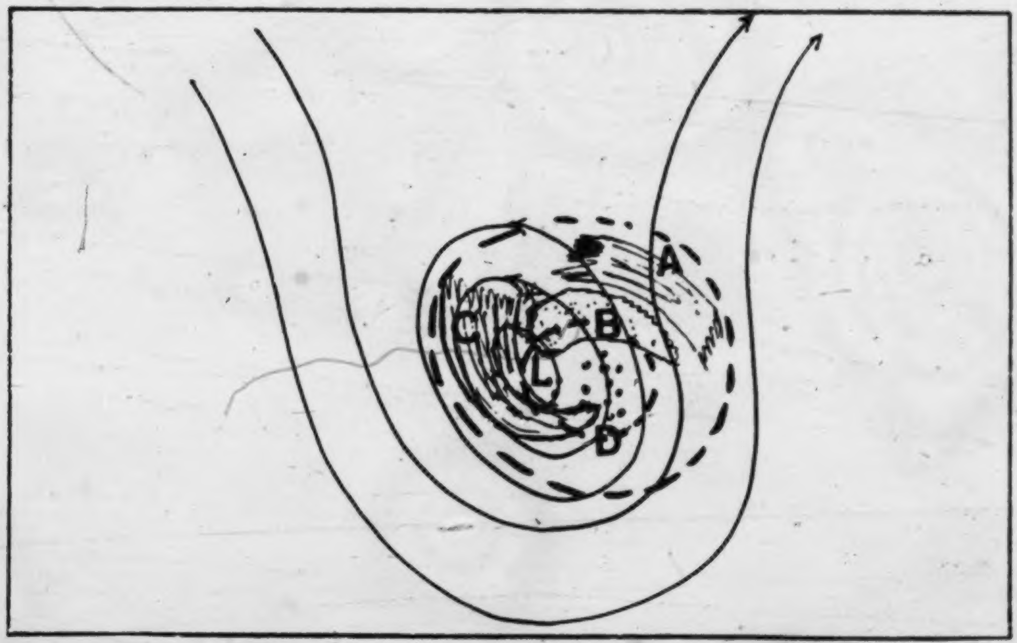

Figure 3.47 The cut-off stage, solid lines: 500-mb contours, dashed lines: stability index, B: comma developed area, D: cellular cloud area, A and C :stratiform cloud area, and *: surface low centre.

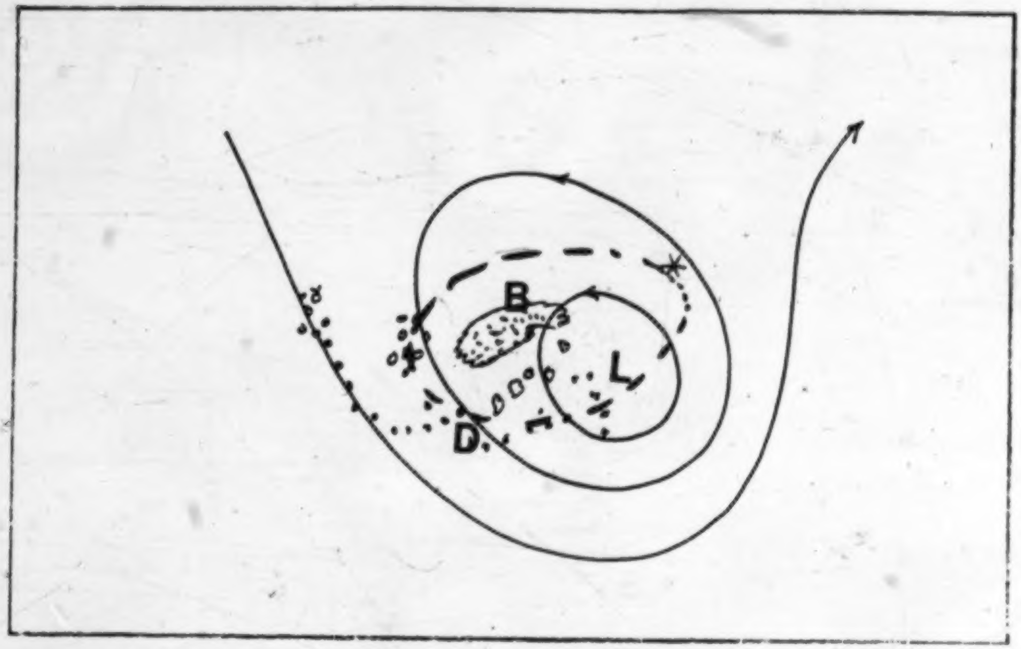

Figure 3.48 The decay stage, solid lines: 500-mb contours, dashed line: stability index, B: comma developed area, D: cellular cloud area, and *: surface low centre.

# 4. Upper-Level Low Case Studies

## 4.1 Introduction

Actual case studies of upper-level cyclogenesis and development will be presented in this chapter. The discussion will concentrate on the main features. Examples of pure and modified upper-level low cases will be discussed. Pure and modified cases were defined by Petterssen and Smebye (1971) as development without and with low-level frontal systems, respectively. In pure or modified cases, the low-level frontal development was not readily dicernable on a satellite image.

The cases are illustrated with satellite images ( visible and infrared ) and synoptic maps (500-mb and 850-mb surfaces) of scale 1:20,000,000 . On the satellite images the cloud areas are labelled as follows: (A) marks the baroclinic cirrus deck, (B) the vorticity comma, (C) denotes the deformation cirrus deck and (D) the cellular cloud area. These different cloud areas were defined before in Chapter 3, under section "Pattern of Cyclogenesis on Satellite Images ".

At the 500-mb surface, the solid isopleths are the height contours in 60 gpm intervals. Dashed isopleths represent the thickness contours for the layer 500 / 1000 mb. at 60 gpm intervals. Dashed-dotted contours define the absolute vorticity field at $2 \times 10^{-5}$ $s^{-1}$ intervals, with the numerical values enclosed within squares. The arrows indicate the jet streams at the 250-mb surface. Open arrows, marked with (2), denote the advancing newly-developed jet, while solid arrows, marked with (1), are for the old-decaying jet. On the 850-mb maps, the solid isopleths are the height contours in 60 gpm intervals, while the dashed lines are the isotherms in 5° C intervals. The frontal analysis is shown by means of conventional symbols.

In the analysis of an upper-level low, satellite data were used to identify both the initial and subsequent stages of development. The formation of the cloud area (B) was taken as the first sign of upper cold-low cyclogenesis. In synoptic analysis and diagnosis, the strengthening or weakening of a cloud system is of particular interest as the initiation process. There are three possible sources for cloud pattern development: strengthening, no change, and weakening. For the sake of simplicity "strengthening" and "no change" were considered as one class, the reason being that a developing cloud system can be effective even when unchanging. Moreover, cloud pattern development depends on several parameters, such as: (i) the sharpness of the cloud area edges, (ii) the grey scale changes on the infrared image (cloud top temperature), (iii) the spatial expansion, and (iv) the change of the cloud area configuration. The first two parameters were analysed only with difficulty and various degrees of uncertainty, but they provide a good estimate of the vertical activity of cloud area (B). On the other hand, the last two parameters, (iii) and (iv), were easily analysed. Again for the sake of simplicity, the development of the cloud area (B) was considered as an indicator for the development of the whole system. The reason for this choice is that (B) is a common cloud area present in all cases, from strong to weak.

The degree of sharpness of a cloud area edge is defined as the degree of contrast between the cloud area body and the adjoining cloud-free area, such that the contrast is a measure of cloud development, i.e. the higher the contrast the more active the cloud mass. The grey scale change is defined as the rate of increase in area of the cloud-top temperature detected on an enhanced infrared image. The configuration parameter is defined as the characteristic circulation of a cloud area. For (B) it is the cyclonic spiralling, while for (A) and (C) it is the anticyclonic circulation. Finally, the spatial expansion parameter is defined as the horizontal enlargement of a cloud area. In practice, this means that changes in cloud area are a useful and direct measure of development, i.e. the more the increase in area, the more extensive cloud development.

In considering the cloud pattern development of an upper cold-low, a combination of individual changes during a 12-hour period and a 24-hour period was considered. Thus, if a cloud system weakens within 12-hour and 24-hour periods, the system is considered to be weakening; otherwise it is considered to be strengthening.

The examination of the different cases of cold-low cloud systems (pure or modified) showed that, they may be classified as strong, moderate, and weak. A system is said to be strong if the cloud pattern attains the storm stage configuration at one stage during its lifetime. A system is considered moderate if it has, at least, a cloud area (B) of well-defined comma shape. Finally, a system is considered weak if it fails to develop a defined comma-shaped cloud area, regardless of any other cloud areas that may be present.

## 4.2 Case #1

This case took place in the period from 0000 GMT, 10 May 1983 to 1200 GMT, 14 May 1983. It represents strong upper system development where all cloud areas (A, B, C, and D) were present at one stage of development. Figures 4.1-4.29 show the sequential stages of development. The map scale, for all charts used, is 1:20,000,000 except for Figures 4.9 and 4.19. The values of vorticity are in units of $10^{-5}$ $s^{-1}$.

An upper system developed over central Nevada, moved NE-ward and decayed over Northeastern Ontario. This is an example of a modified case, where a low-level system (shown on synoptic maps only) masked the early stages until it took over in the late stage of development. The upper system developed within a cold region without any low-level warm air intrusion. It was initiated and developed within an area of cyclonic vorticity (greater than or equal to 16) but without appreciable positive vorticity advection (PVA). On the other hand the positive thermal advection was present along the periphery of the cloud pattern.

Starting with the satellite image of Figure 4.1, the first sign of formation is the appearance of an upper system over central Nevada and Idaho. The overall pattern has a regular ellipsoidal configuration. Cloud areas (A), (B), and (C) have formed at this early stage. Comparison of the visible (a) and the infrared (b) images shows the degree of activity of (B) which has attained a cyclonic circulation and is located within the vorticity contour 16. The cloud area (C) is more developed than (A), although both are stratiform sheets of clouds within anticyclonic flow not involving any jet streams. On the other hand, (A) is not associated with the low-level frontal system and there is no sign of warm air intrusion as in a typical low-level cyclogenesis. Figure 4.2 shows the corresponding 500-mb flow. A major trough over the Western Prairies, shearing off southward and forming an elongated and positively tilted trough. A weak closed circulation and a cold thermal pool are embedded within a closed positive vorticity circulation over Nevada. A new jet (2), west of the trough, is advancing toward its base, while an old jet (1) is moving

NE-ward toward Hudson Bay. On the 850-mb surface (Figure 4.3), a weak trough, extending over Nevada, contains a frontal system which is not seen on the satellite image. (B) lay northwest of the frontal system.

Twelve hours later (Figures 4.4 and 4.5), (A) and (C) weakened while (B) did not. The whole pattern moved NE-ward. According to the development assumption, stated above, the system was strengthening. (B) moved closer to the steep thickness gradient and remained within the cyclonic vorticity isopleth greater than 16. Figure 4.5 shows an increase in the cloud top height. At 500-mb level (Figure 4.6) a pinching-off is in progress at the neck of the trough. The upper flow has become symmetrical and a closed circulation has formed, in the mid-troposphere. No changes occurred in the vorticity or thermal field. The vorticity analysis did not reveal any PVA near (B), while a weak positive thermal advection (PTA) existed north of (B). Jet (2) continued advancing southward, while jet (1) moved further NE-ward without change. The 850-mb surface (Figure 4.7) shows a double system of fronts without corresponding frontal bands as can be seen in Figures 4.4 and 4.5.

Later ( in Figures 4.8 and 4.9 ), (B) developed horizontally as well as vertically and attained a comma shape while (A) decayed. From Figures 4.8 and 4.10 one should note that (B) is located within the cyclonic circulation area and not the PTA area. One can also note the first sign of the formation of cloud area (D) southwestward of (B).

In Figure 4.10, the trough neck has opened up, the cold pool advanced southward and jet (2) has wrapped itself around the base of the trough. In Figure 4.11, the frontal system has moved away from (B) while the cold air behind the second front dug southward and centered over the activity area. At this stage, the flow at the 500-mb surface shows no sign of closed circulation. Figure 4.9 was used to support Figure 4.8 because of the time difference.

Figure 4.12 shows the system development at the next stage. The upper system has attained the storm configuration and moved slowly NE-ward. In Figure 4.13, the upper low has deepened and reached the cut-off stage. The vorticity field did not change, while the thermal field continued to spread southward. The PTA area was not associated with the cloud area (B) which remained within vorticity contour 16 and the cold thermal area. Jet (2) has moved completely to the eastern side of the trough as seen in Figure 4.13. The low-level flow, shown in Figure 4.14, has reversed and a closed thermal contour has formed north of (B) but without producing a closed wind circulation.

In Figures 4.15 and 4.16 the upper system has passed its maximum intensity and weakened over the area of (B). The cloud pattern has spread over a larger area but is no longer undergoing vertical development. Again and according to the development assumption, the cloud pattern is cosidered to be strengthening. The cloud area (B) is located within cyclonic vorticity isopleth greater than 16. In Figure 4.19, the cloud band that extends over the tail of (B) is not part of the storm configuration. The whole cloud pattern has taken on the appearance of an occluded low-level system. In Figure 4.17, the 500-mb low has continued moving NE-ward and stopped deepening, as revealed by the fewer closed contours. Jet (2) has advanced northward and bent over anticyclonically. The low-level system (Figure 4.18) approached the upper system while the cold air area has expanded and centered over (B).

Twelve hours later, Figure 4.19 shows continual weakening of the cloud pattern. (B) has weakened considerably and became fragmented. Accordingly, the system is now considered weakening. At the same time, (C) has weakened and moved away from (B). The shear band (G) (described in Chapter 3) overrode the pattern to form a lambda shape.

The mid-level flow (Figure 4.20) shows considerable filling and without any closed circulation. Jet (2) has moved farther northward and acquired anticyclonic curvature. Again, (B) is located within a vorticity isopleth 16, but is not affected by the area of PVA or PTA. On the 850-mb surface (Figure 4.21), the low-level circulation is now below the upper-level system. The cold air sector has opened up and the low-level circulation is now fully established.

The next Figures 4.22 - 4.29 show how the cloud pattern, and the associated mid and low-level flow decayed rapidly. In Figure 4.22 the cloud pattern is still organized and circular. (B) is under the influence of cyclonic vorticity greater than 16. In Figure 4.27 the system lost its configuration and (B) has dissipated. In Figure 4.24, the 500-mb flow no longer has a closed circulation, but a trough has been re-established and jet (2) has moved completely NE-ward. In Figure 4.25, the low-level circulation has reached its peak intensity and the axis of the storm vortex is now close to vertical. Figures 4.26 and 4.27 show the complete decay of the cloud configuration. At this stage, it is hard to indicate the centre of activity. Figures 4.28 and 4.29 show the upper and low-level circulation during the final stage of dissipation.

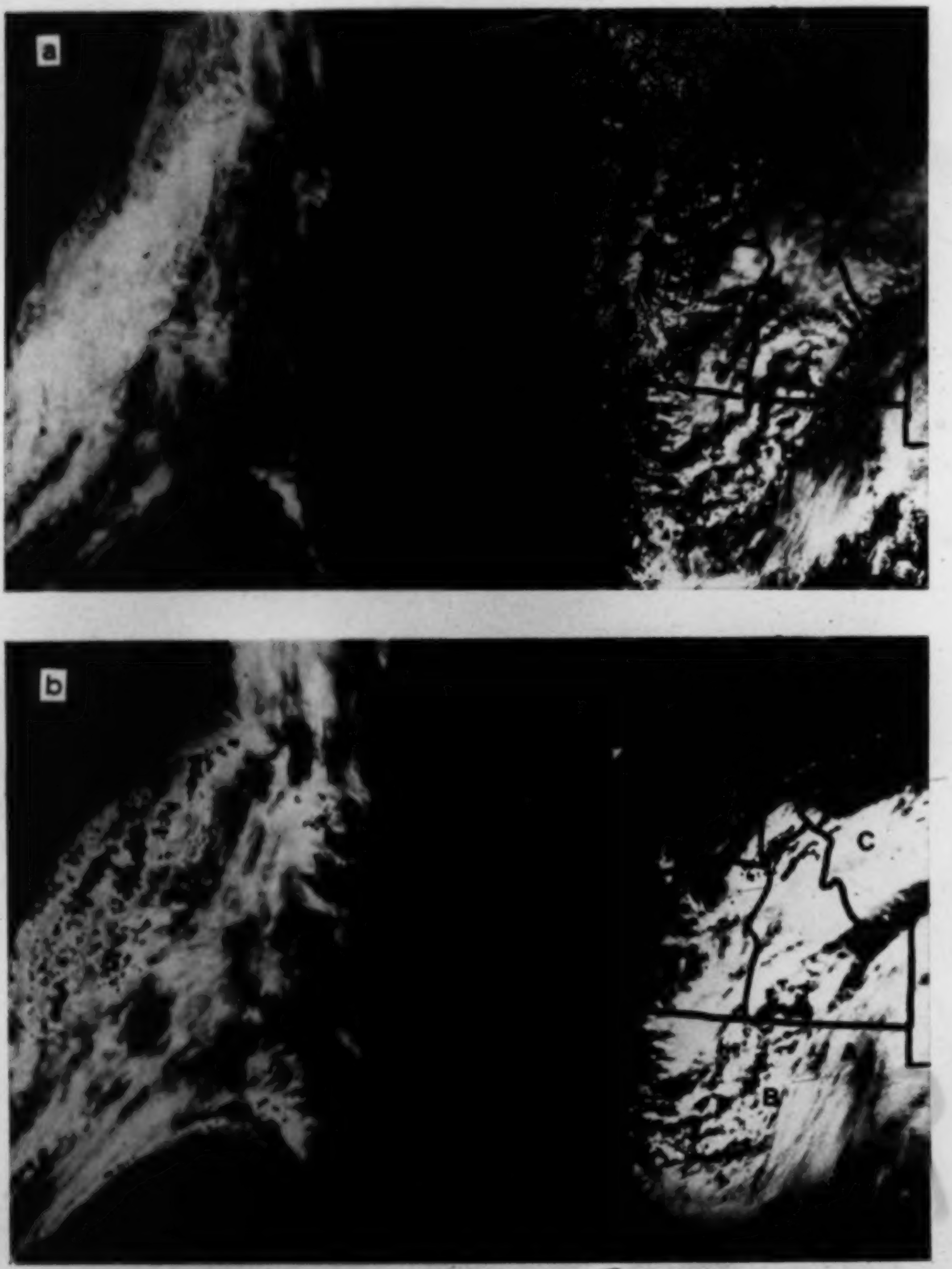

Figure 4.1 NOAA-7 satellite image, a) visible, b) infrared, 2301 GMT, 10 May 1983.

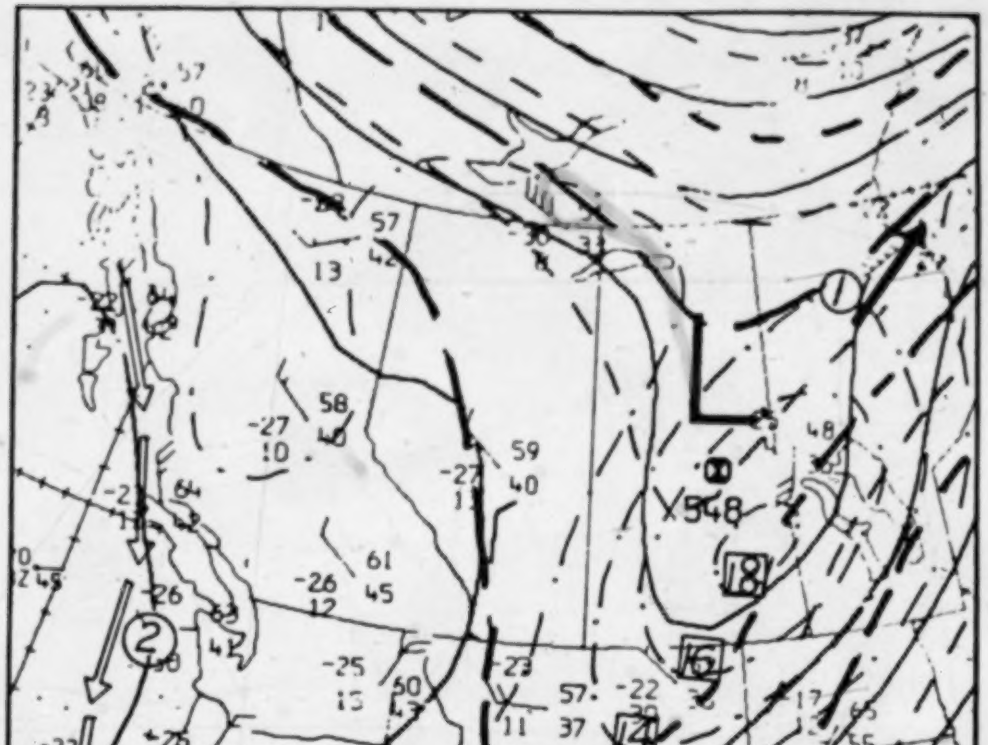
X548
18
16
14
14
16
18
552
①
②

Figure 4.2 CMC 500 mb analysis, 11 May 1983, 0000 GMT, solid lines:height contours, dashed lines: thickness field (500/1000 mb), dash-dotted: absolute vorticity ($*10^{-5}$ $s^{-1}$) and arrows: jet stream (250 mb).

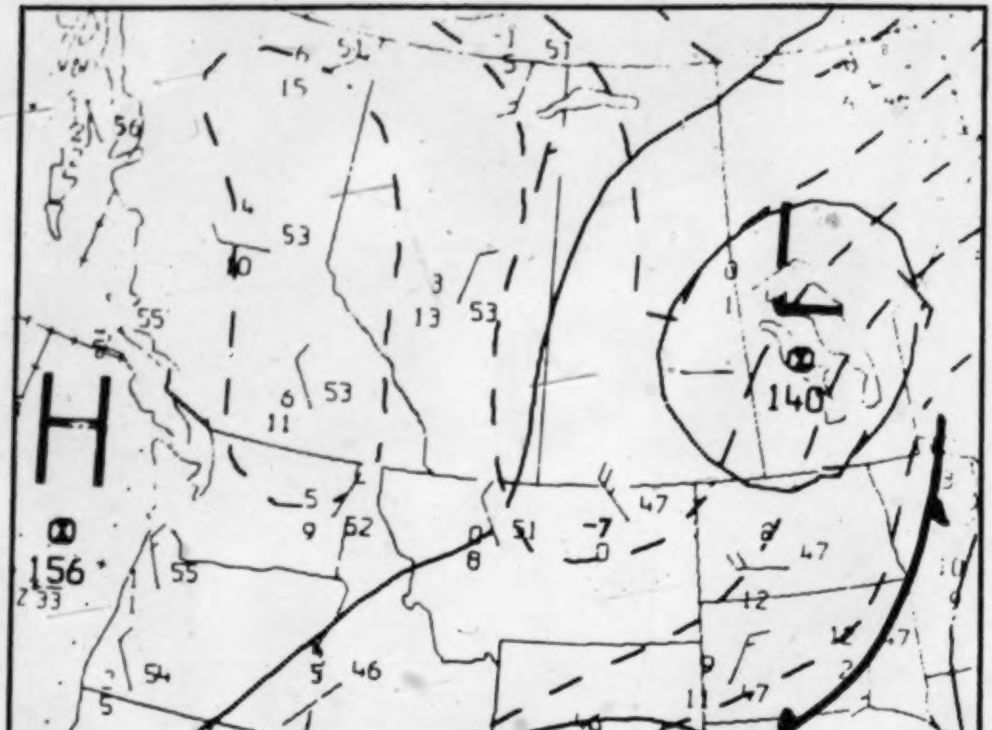
H
156
L
140
L
137

Figure 4.3 CMC 850 mb analysis, 11 May 1983, 0000 GMT, solid lines:height contours, dashed lines: isotherms.

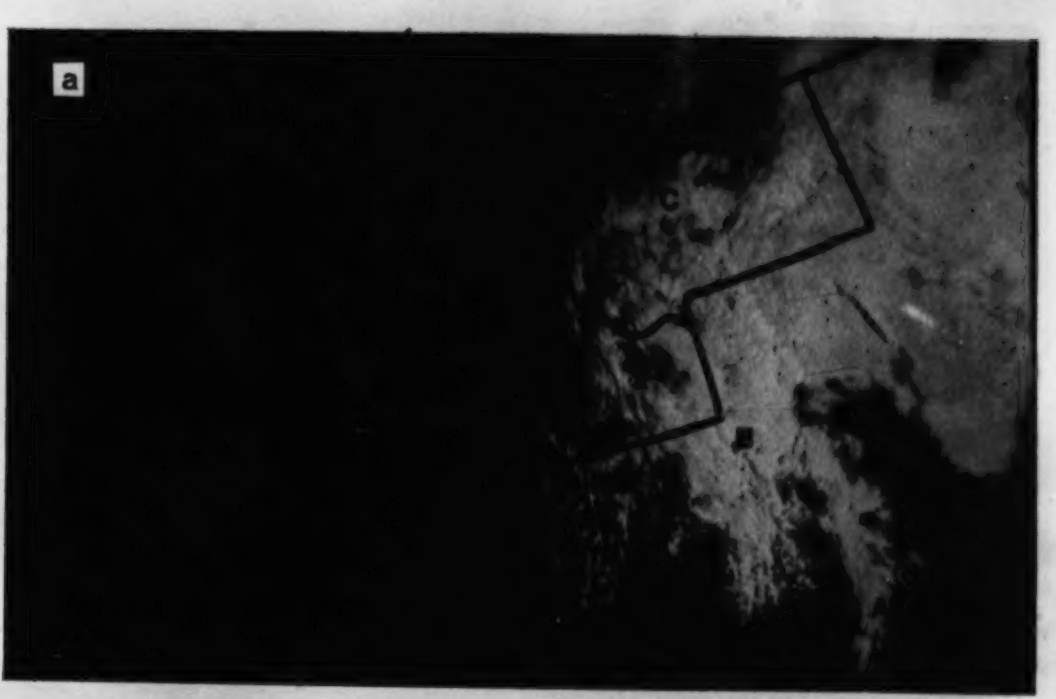

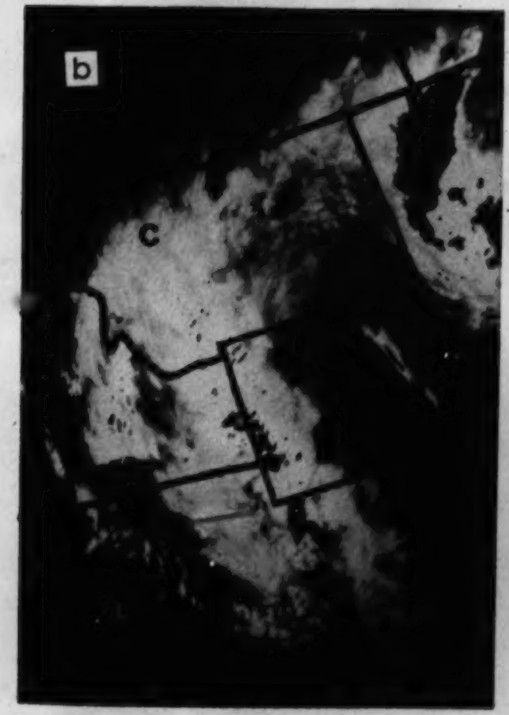

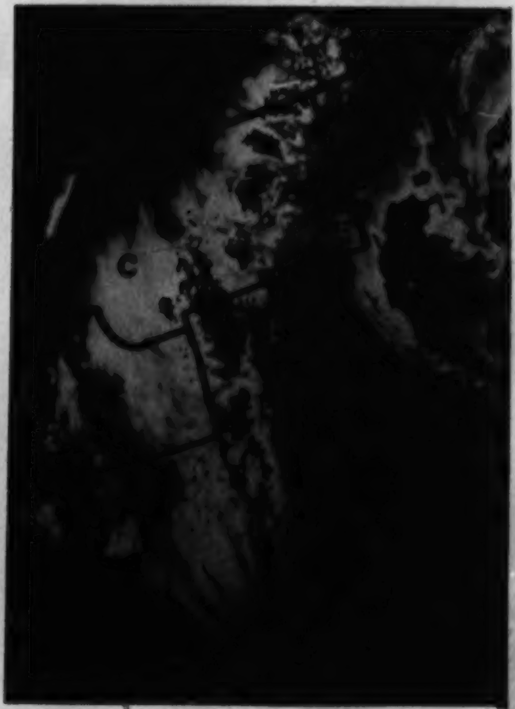

Figure 4.4 NOAA-6 satellite a) visible, b) infrared, 1545 GMT, 11 May 1983.

Figure 4.5 NOAA-7 satellite, infrared, 1115 GMT, 11 May 1983.

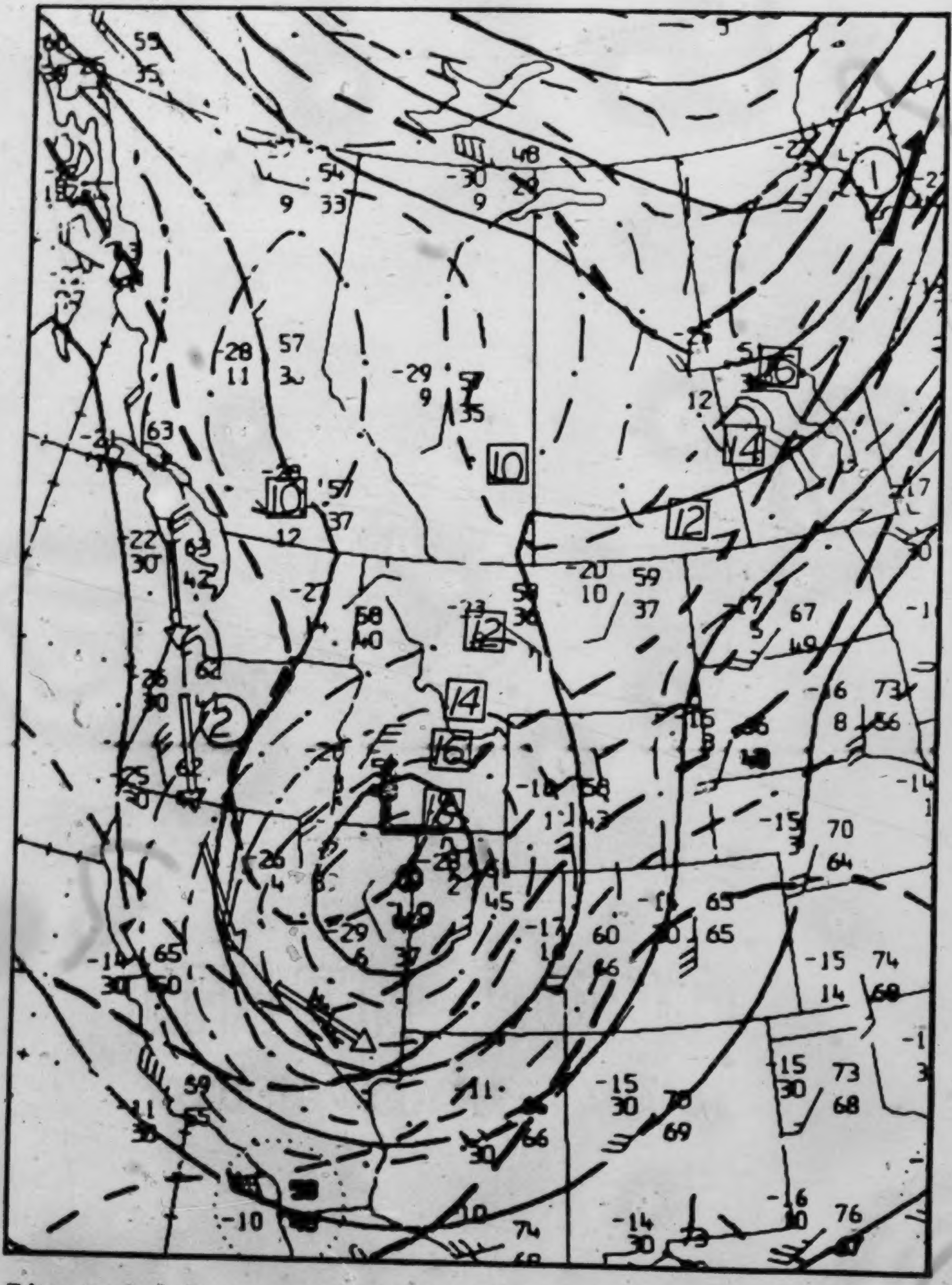
10
10
12
12
14
14
16
16
18
1
2

Figure 4.6 The same as in Figure 4.2 except for 11 May 1983, 1200 GMT.

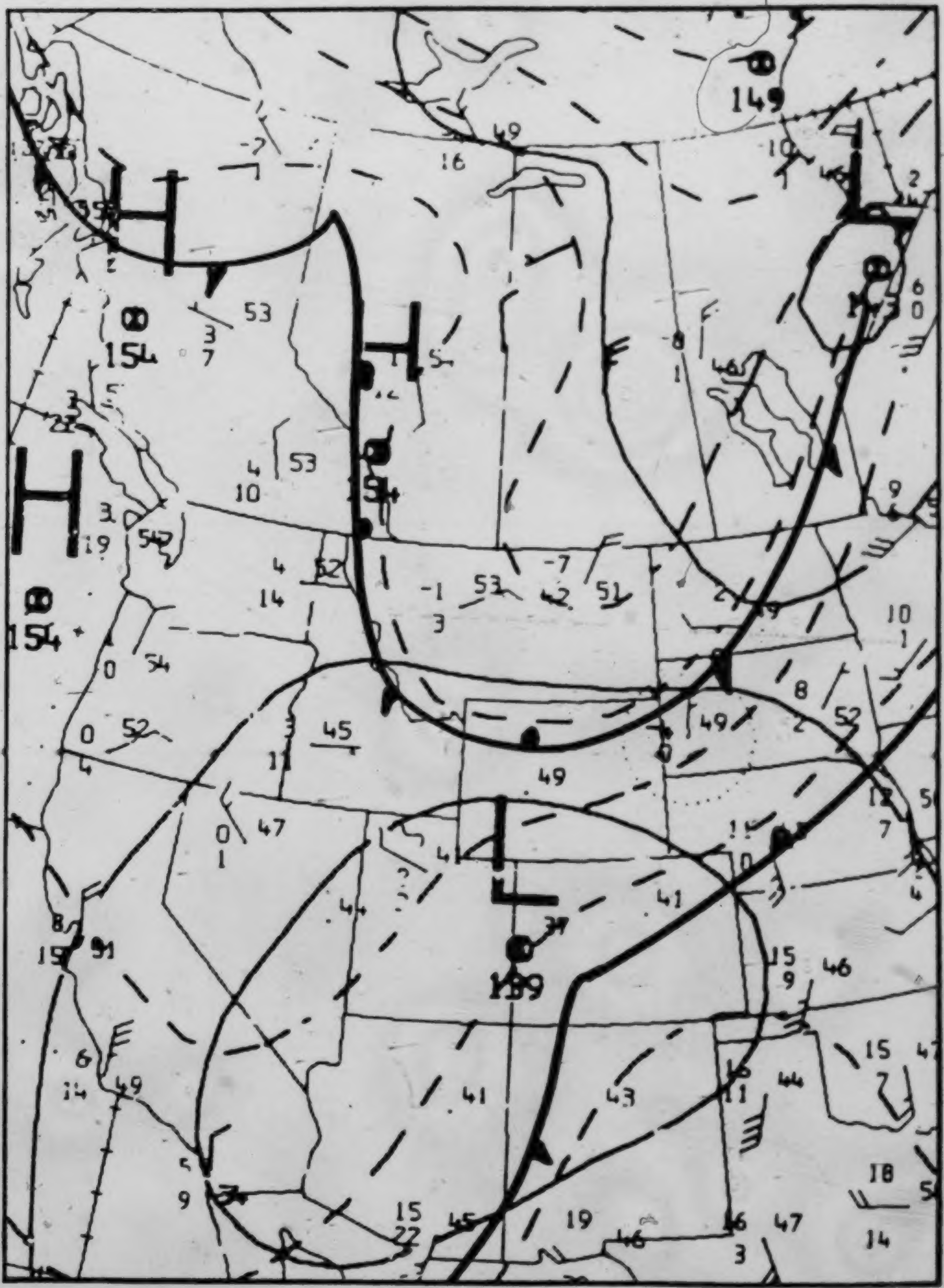

Figure 4.7 The same as in Figure 4.3 except for 11 May 1983, 1200 GMT.

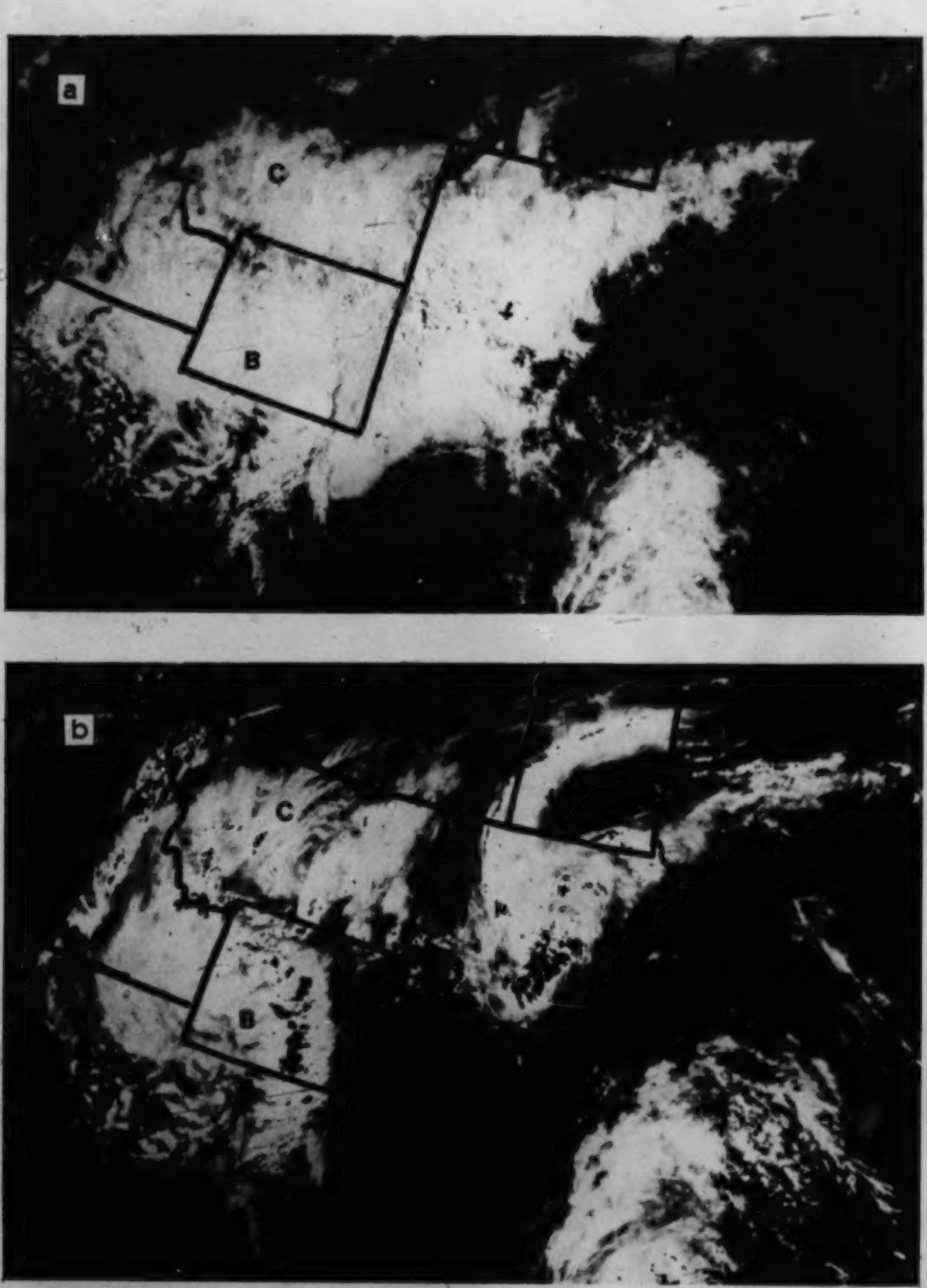

Figure 4.8 NOAA-7 satellite image, a) visible, b) infrared, 2106 GMT, 11 May 1983.

Figure 4.9 GOES-E satellite image, 100. W, visible, 0001 GMT, 12 May 1983.

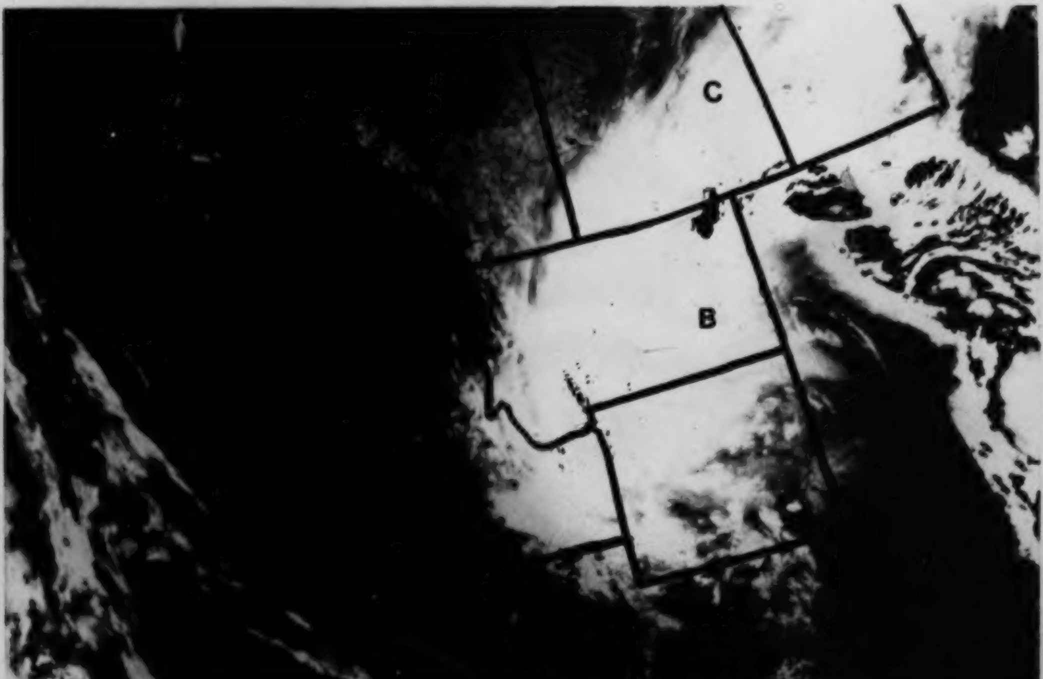

Figure 4.12 NOAA-7 satellite image , infrared 1102 GMT, 12 May 1983.

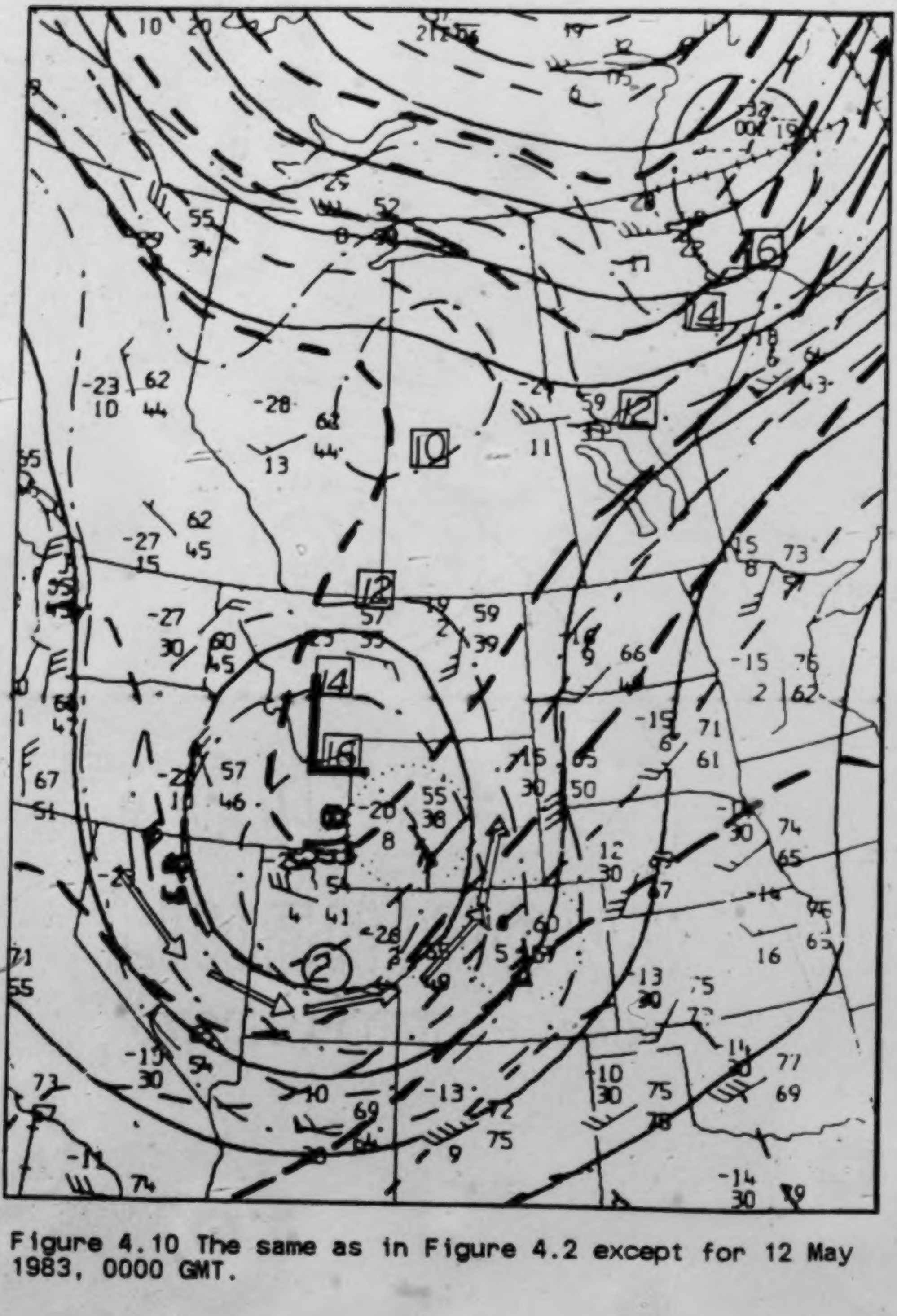

Figure 4.10 The same as in Figure 4.2 except for 12 May 1983, 0000 GMT.

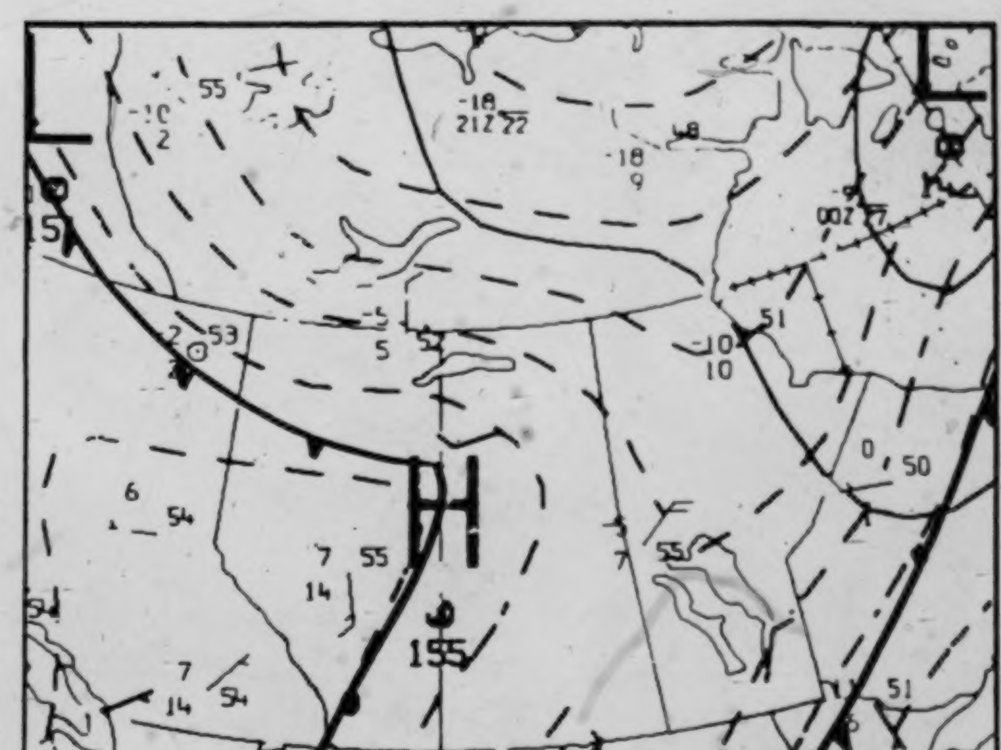
L
L
H
L
55
-10
2
-18
212 22
-18
9
48
15
2
53
-5
5
-10
10
51
0
50
6
54
7
55
14
155
55
7
14
54
51
9
30
61
-3
3
53
-5
1
57
12
52
9
0
48
13
6
54
53
46
46
48
11
48
1
8
50
2
0
14
49
52
18
44
9
135
15
49
2
-2
30
48
24
20
9
3
40
45

Figure 4.11 The same as in Figure 4.3 except for 12 May 1983, 0000 GMT.

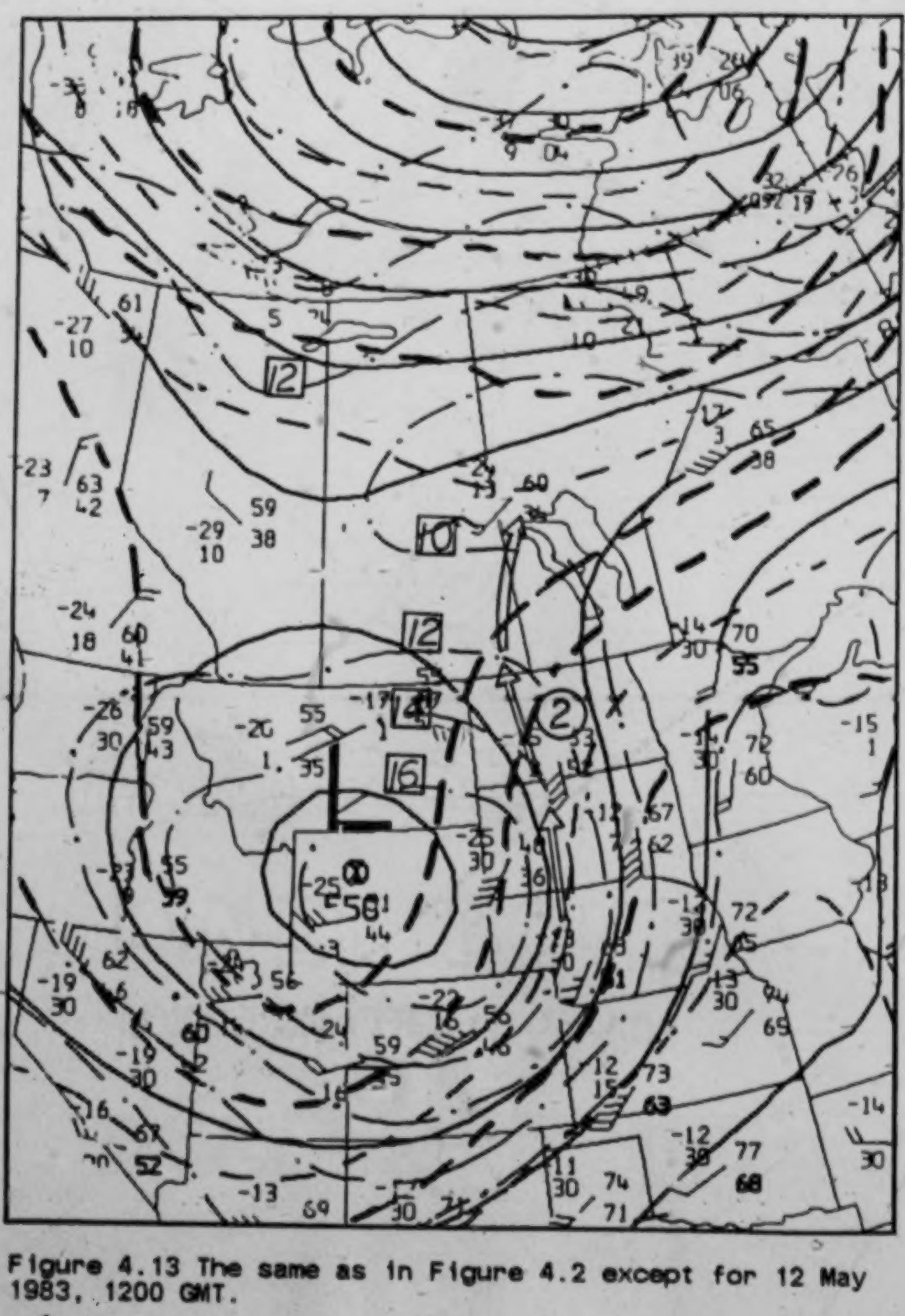
12
10
12
14
16
②

Figure 4.13 The same as in Figure 4.2 except for 12 May 1983, 1200 GMT.

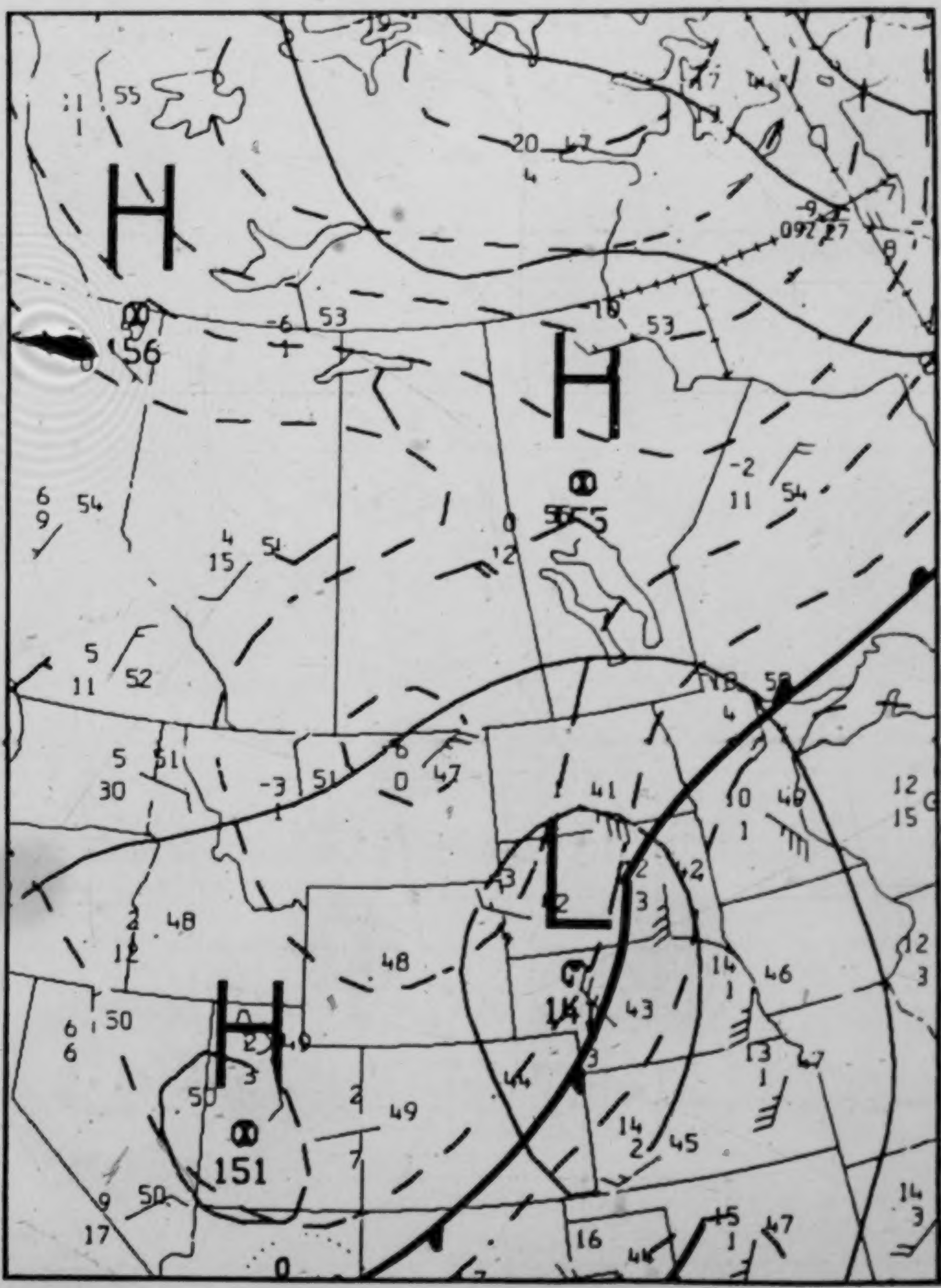
H
H
H
L
56
355
151

Figure 4.14 The same as in Figure 4.3 except for 12 May 1983, 1200 GMT.

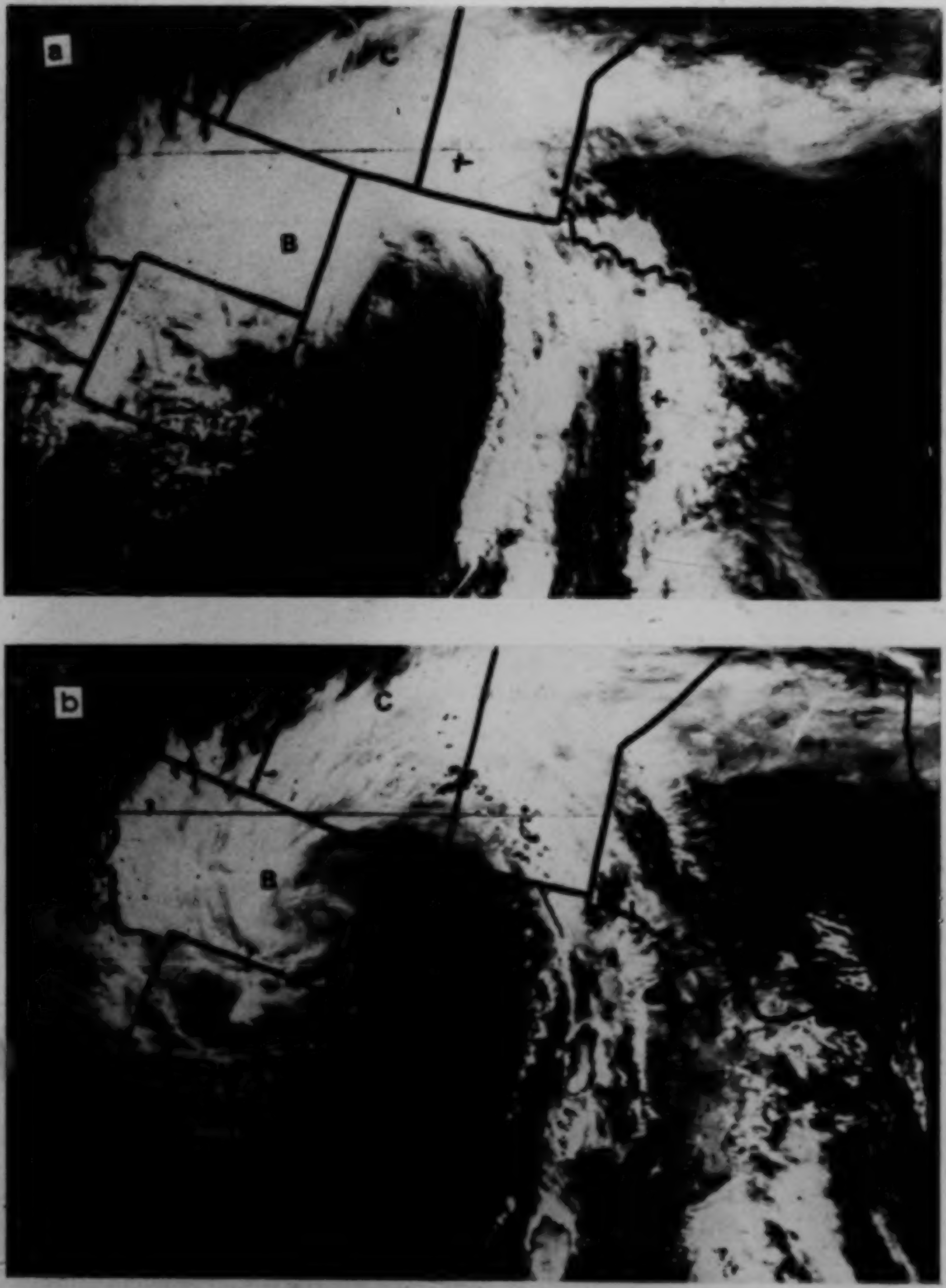

Figure 4.15 NOAA-7 satellite image, a) visible, b) infrared, 2055 GMT, 12 May 1983.

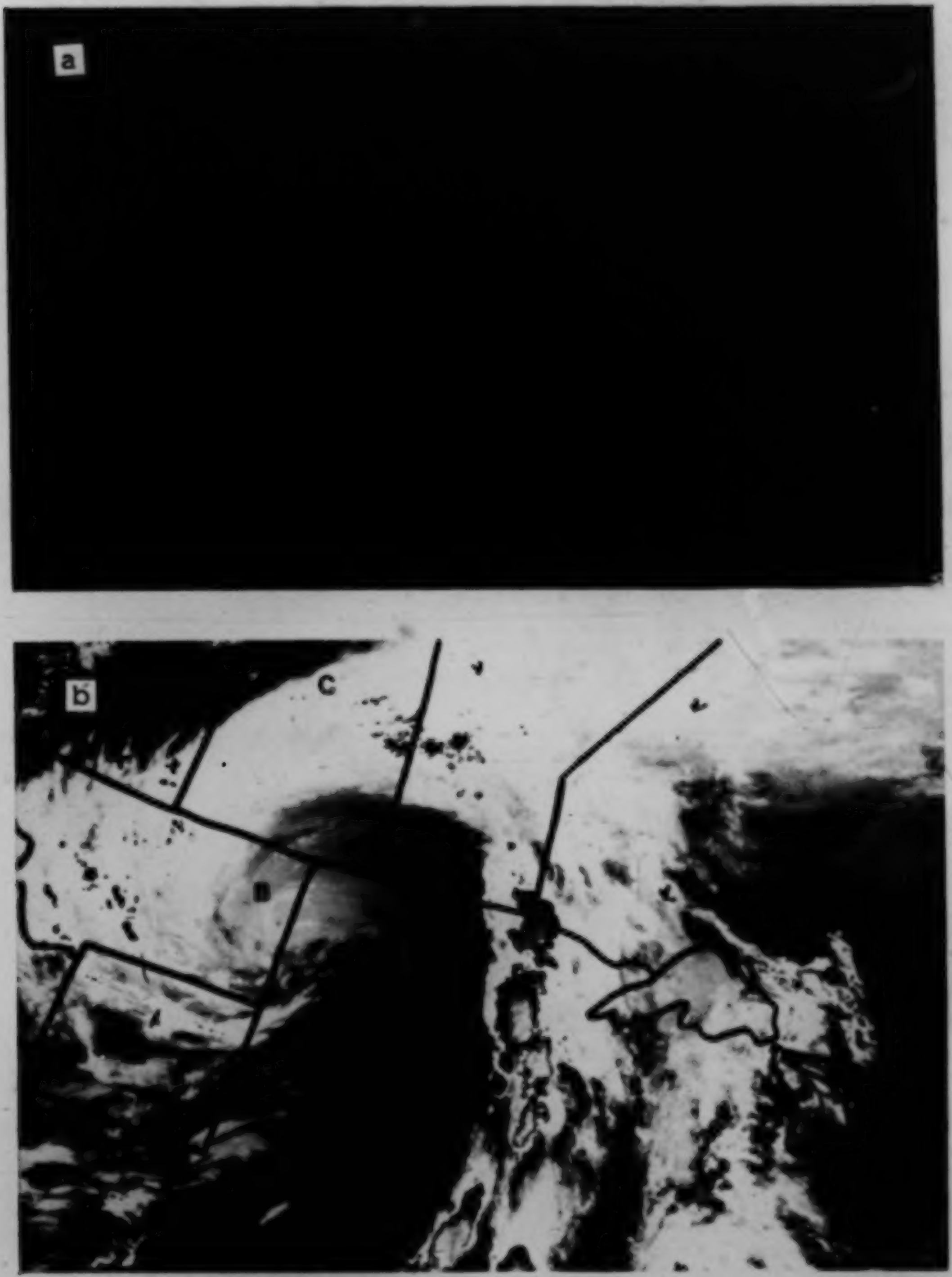

Figure 4.16 NOAA-6 satellite image, a) visible, b) infrared, 0109 GMT, 13 May 1983.

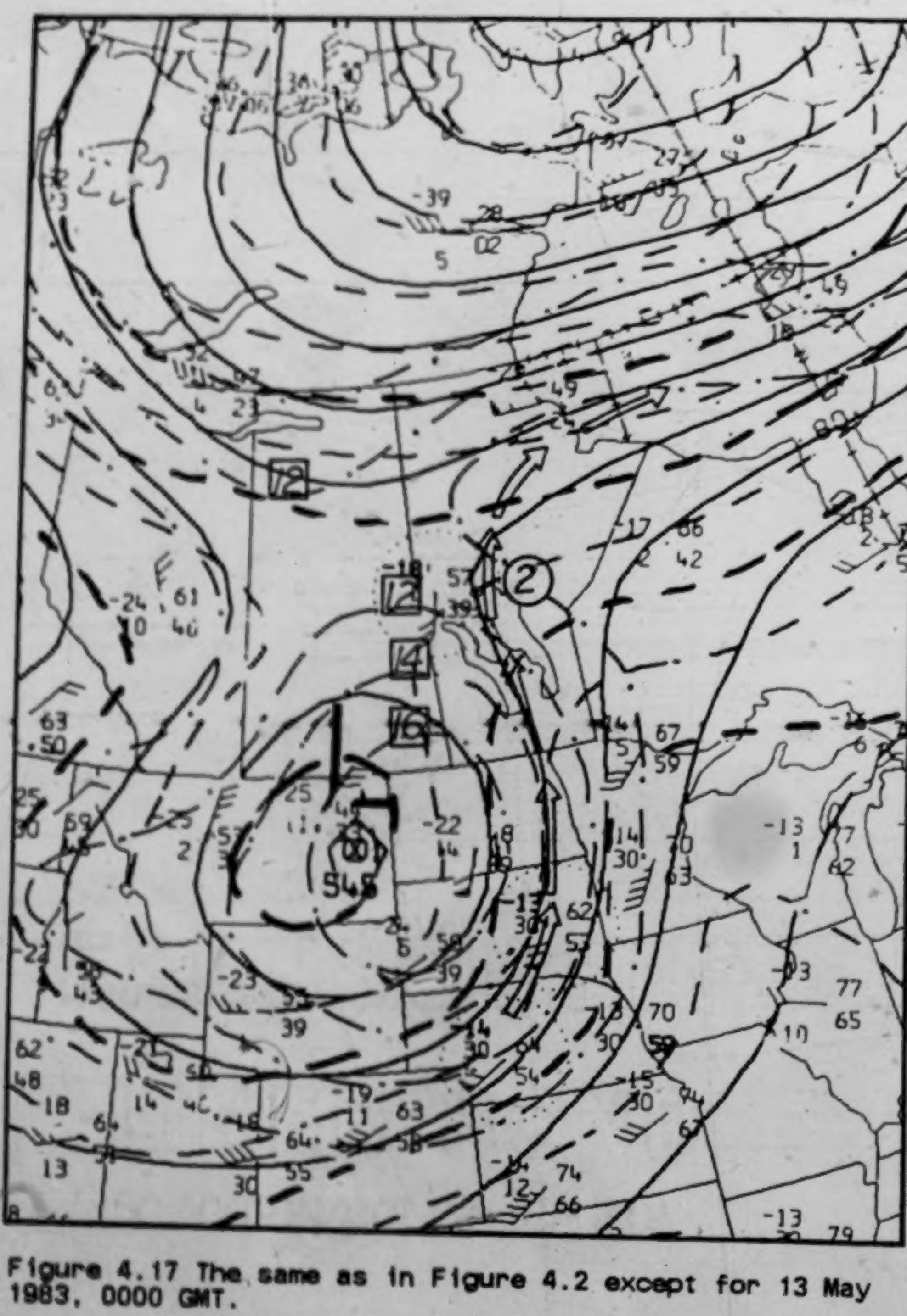

Figure 4.17 The same as in Figure 4.2 except for 13 May 1983, 0000 GMT.

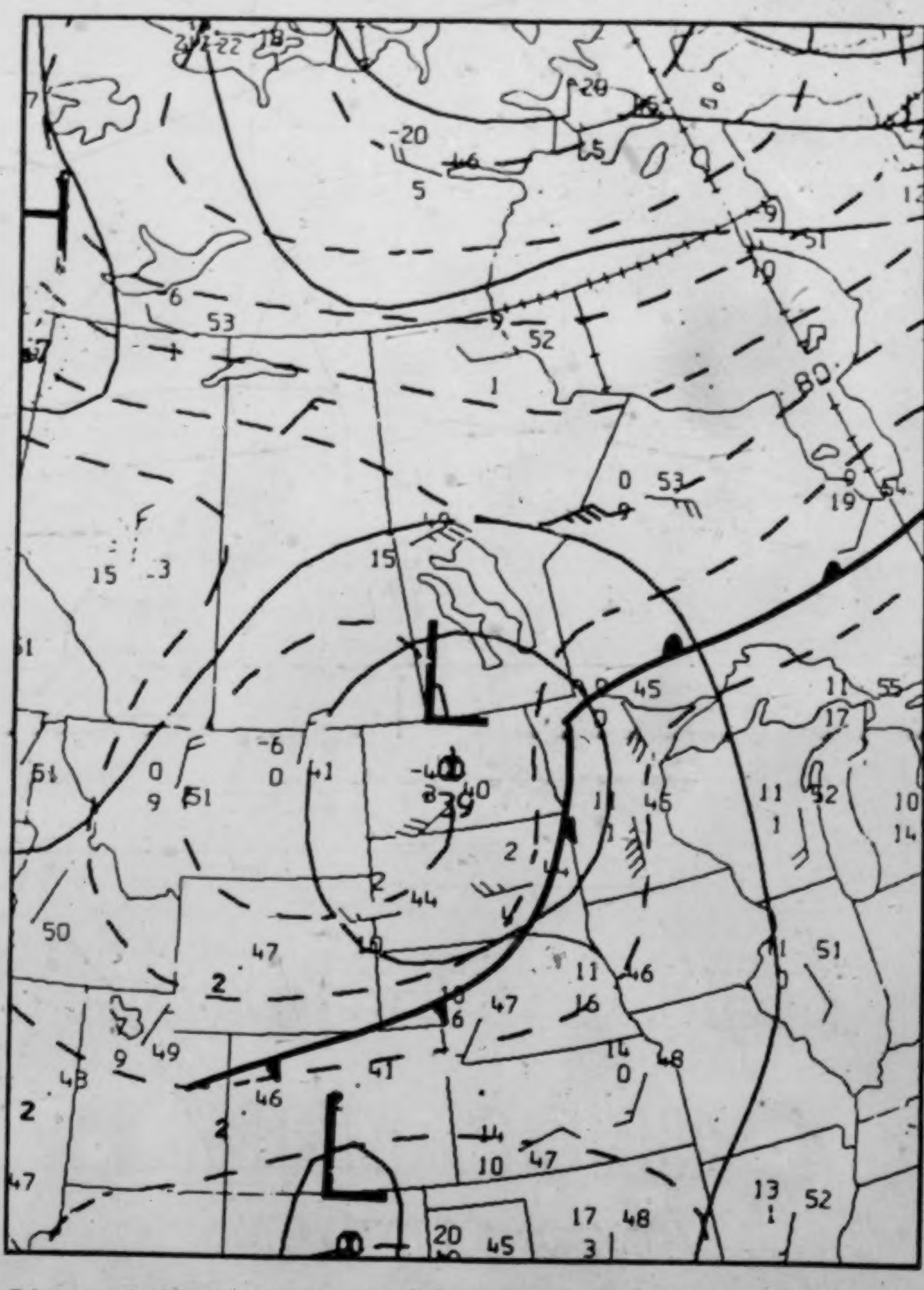

Figure 4.18 The same as in Figure 4.3 except for 13 May 1983, 0000 GMT.

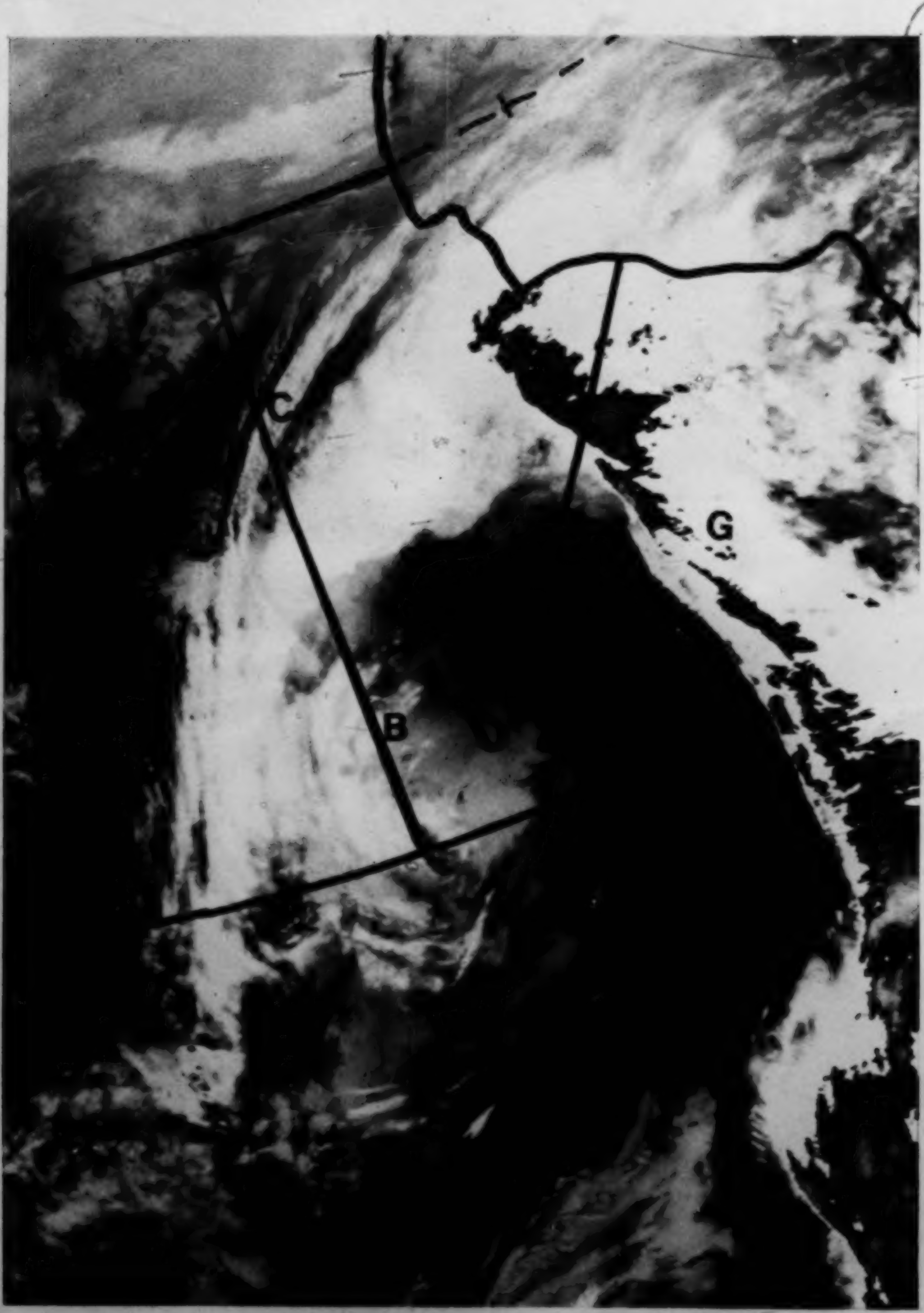

Figure 4.19 NOAA-7 satellite image , infrared, 1050 GMT, 13 May 1983.

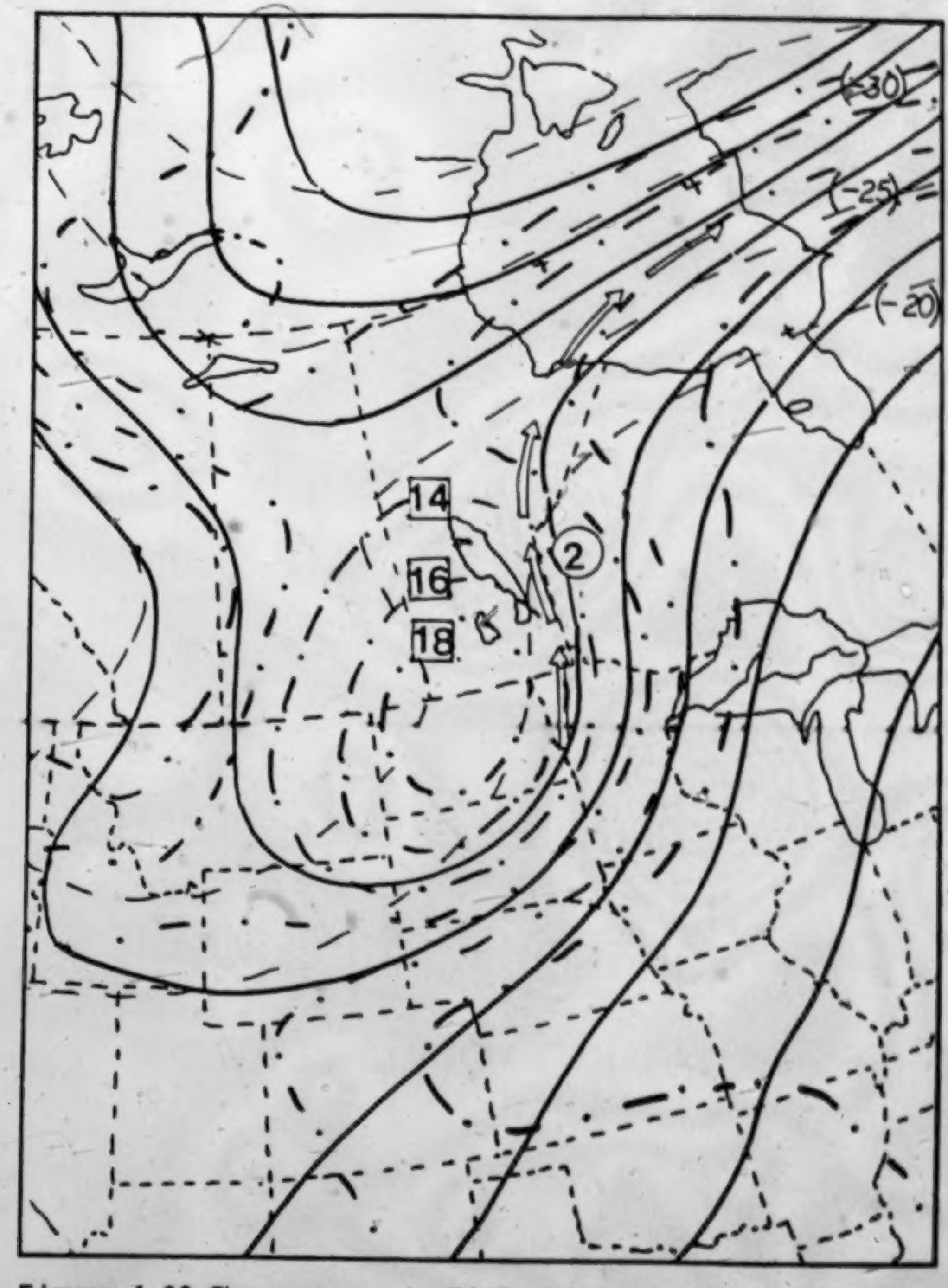
(-30)
(-25)
(-20)
14
16
18
2

Figure 4.20 The same as in Figure 4.2 except for 13 May 1983, 1200 GMT. and dashed-lines: isotherms.

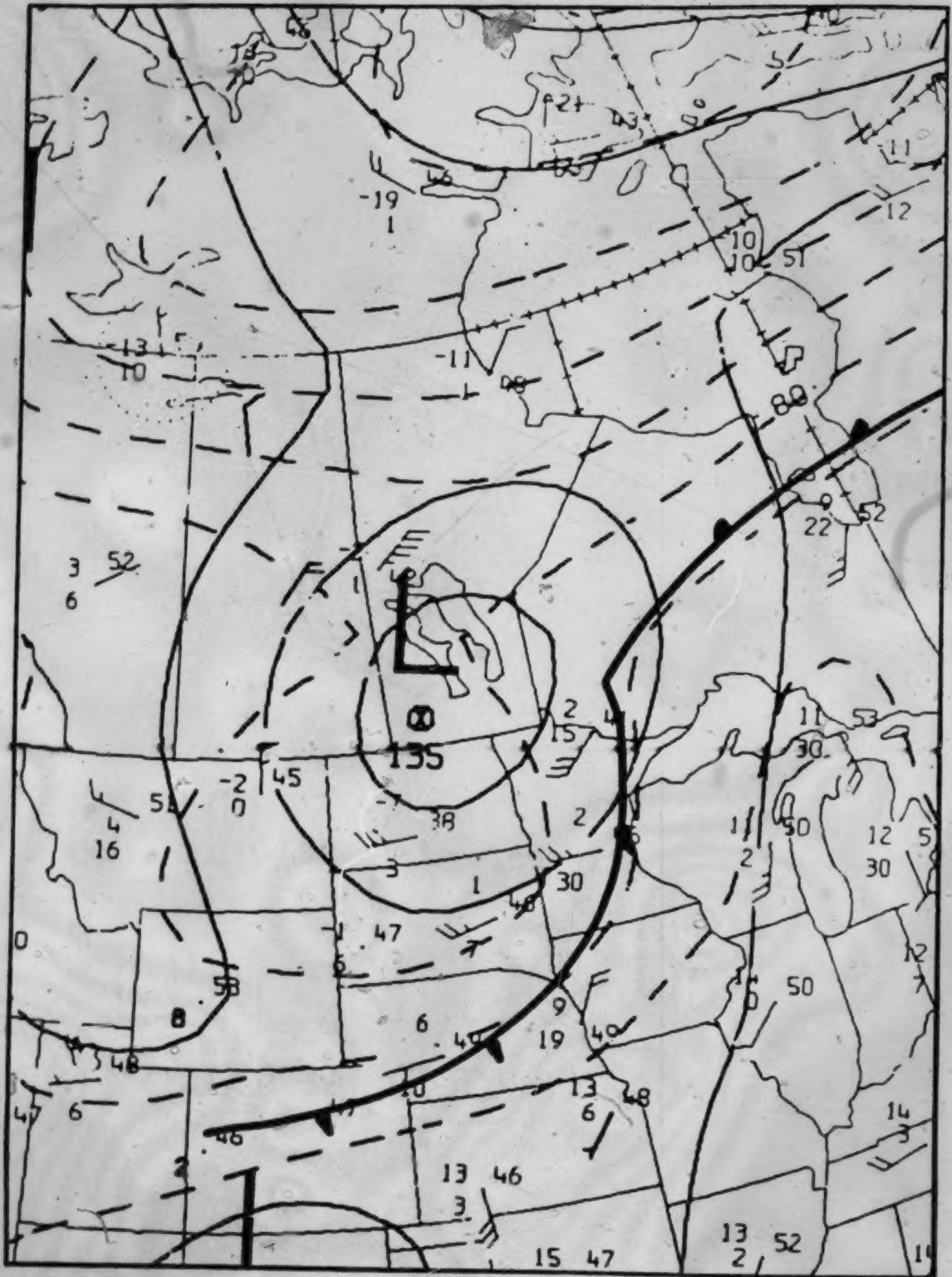
L
135
-19
1
-13
10
-11
10
10
51
12
11
3
6
52
22
52
2
15
11
53
30
-2
0
45
51
4
16
-7
38
2
1
2
50
12
30
3
1
30
48
47
6
58
8
9
19
40
50
12
6
48
13
6
48
47
6
14
3
2
46
13
46
3
13
2
52
15
47
0

Figure 4.21 The same as in Figure 4.3 except for 13 May 1983, 1200 GMT.

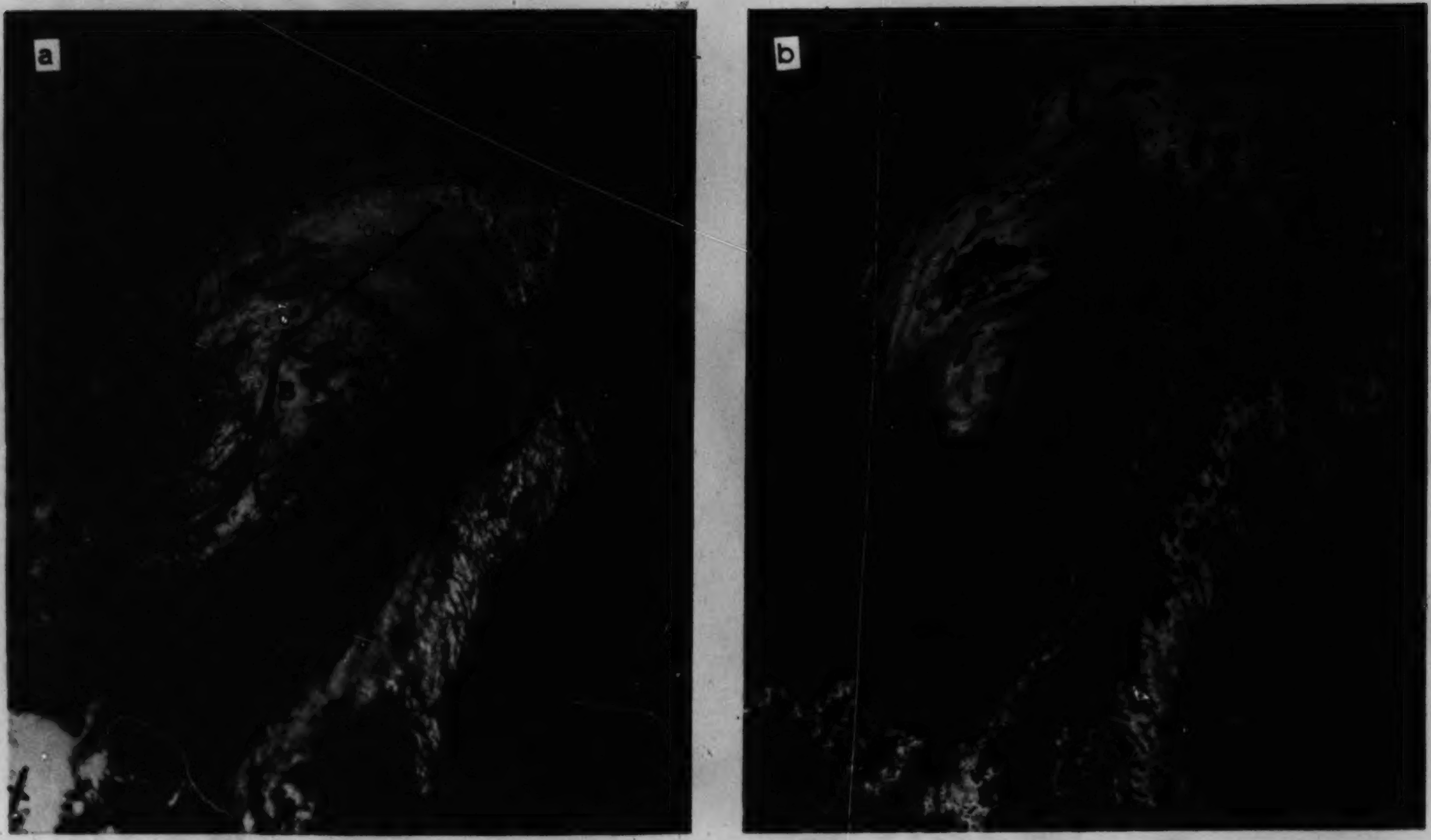

Figure 4.22 NOAA-7 satellite image, a) visible, b) infrared, 2043 GMT, 13 May 1983.

Figure 4.23 NOAA-6 satellite image, a) visible, b) infrared, 0046 GMT, 14 May 1983.

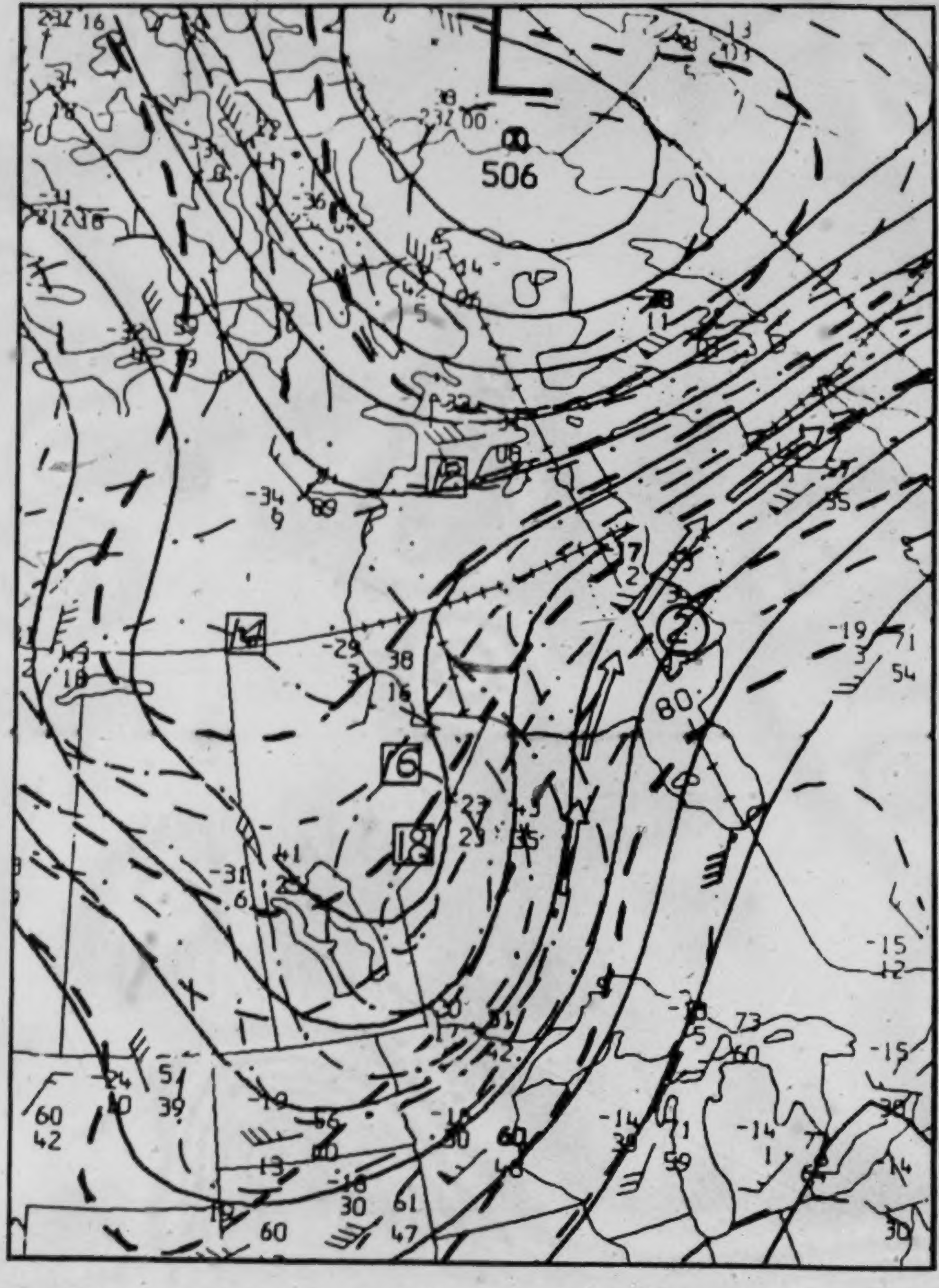

Figure 4.24 The same as in Figure 4.2 except for 14 May 1983, 0000 GMT.

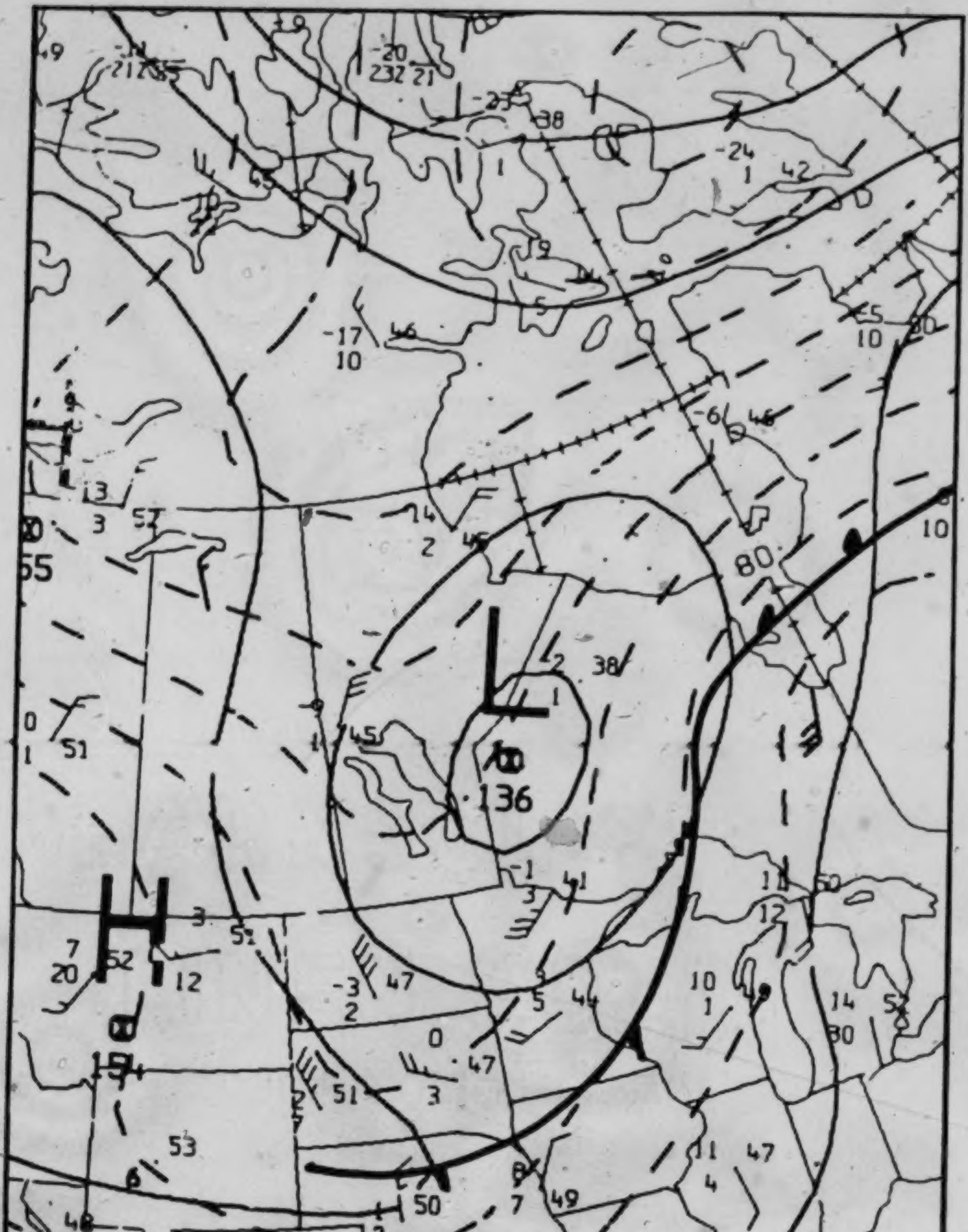
L
H
136
80
-20
232 21
-24
1 42
-17
10
-6 46
14
2 45
13
3 52
55
0
1 51
38
45
-1
3 41
7
20 52
12
-3 47
2
0
47
51
3
53
50
7 49
10
1
14
80
11
12 50
11 47
4
10
10
48
9
13
50
2
15

Figure 4.25 The same as in Figure 4.3 except for 14 May 1983, 0000 GMT.

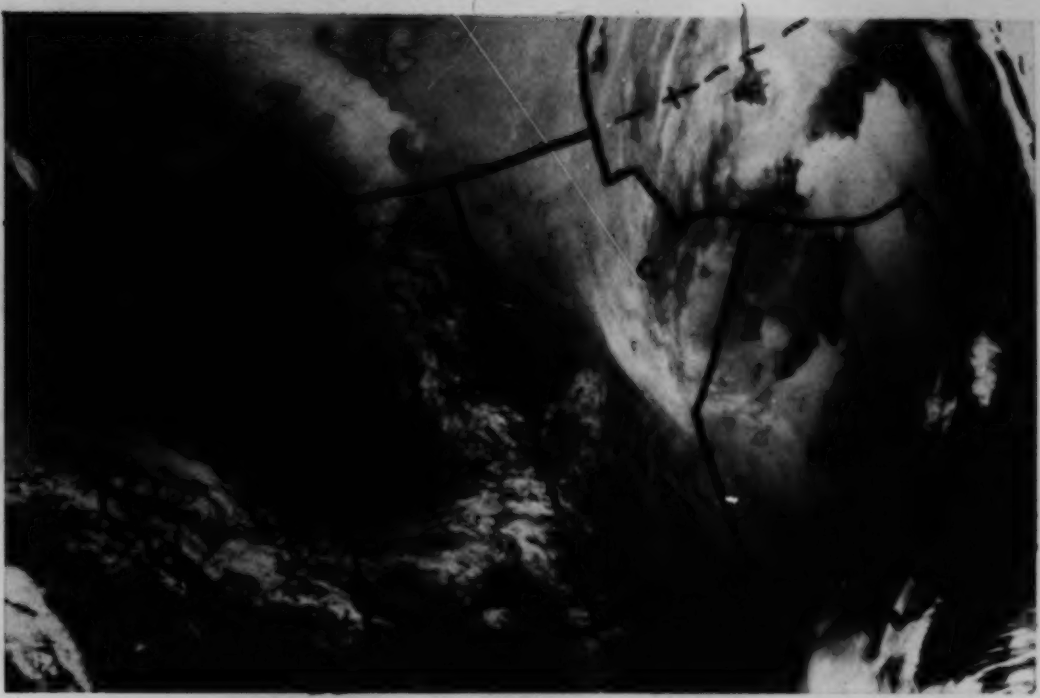

Figure 4.26 NOAA-7 satellite image,
, infrared, 1038 GMT, 14 May 1983.

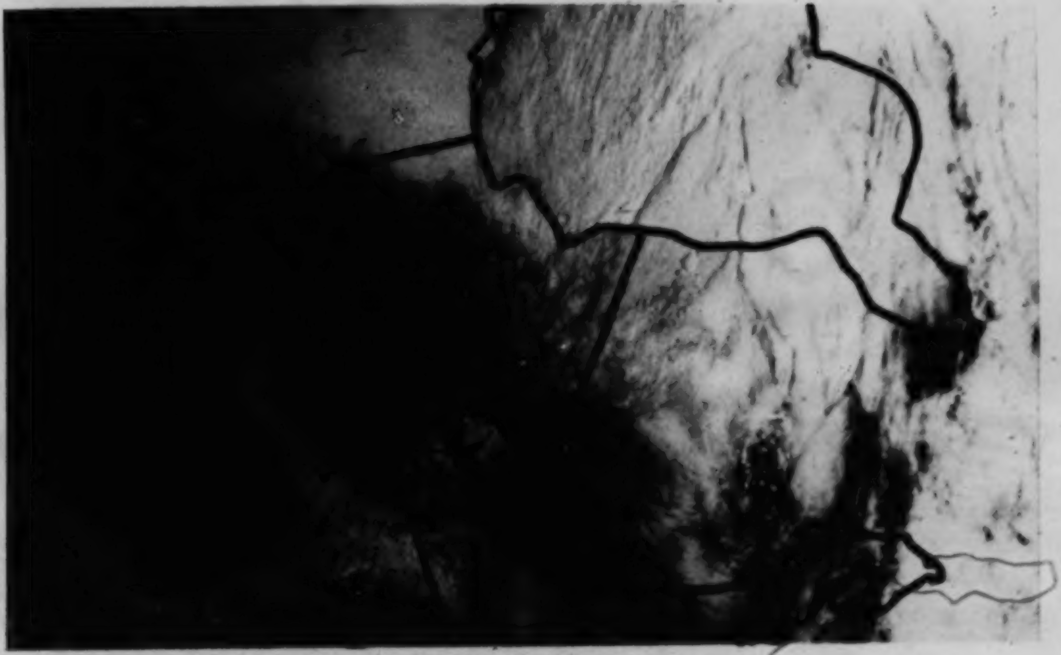

Figure 4.27 NOAA-6 satellite image,
, visible, 1434 GMT, 14 May 1983.

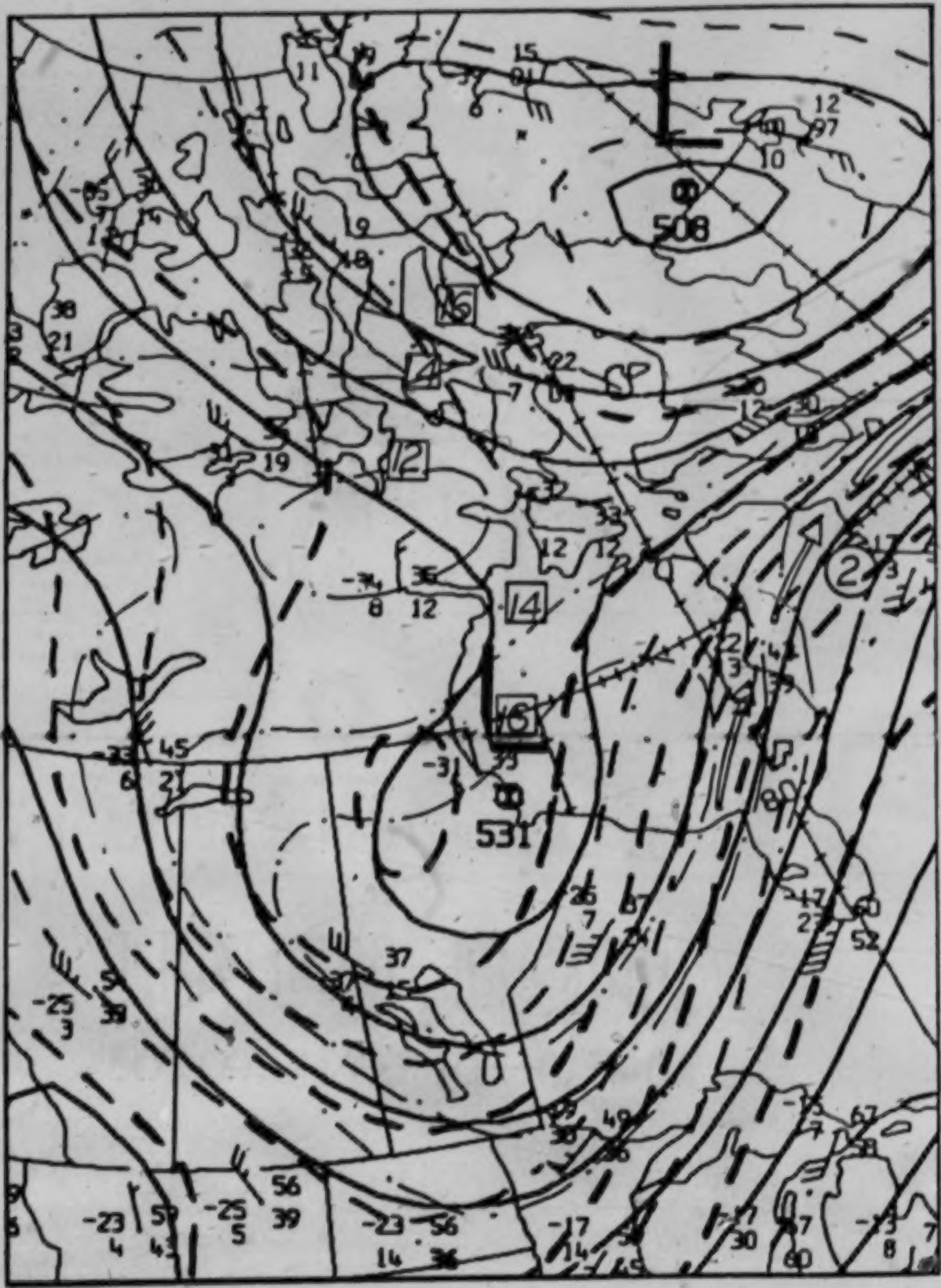
508
531
16
14
12
16
2

Figure 4.28 The same as in Figure 4.2 except for 14 May 1983, 1200 GMT.

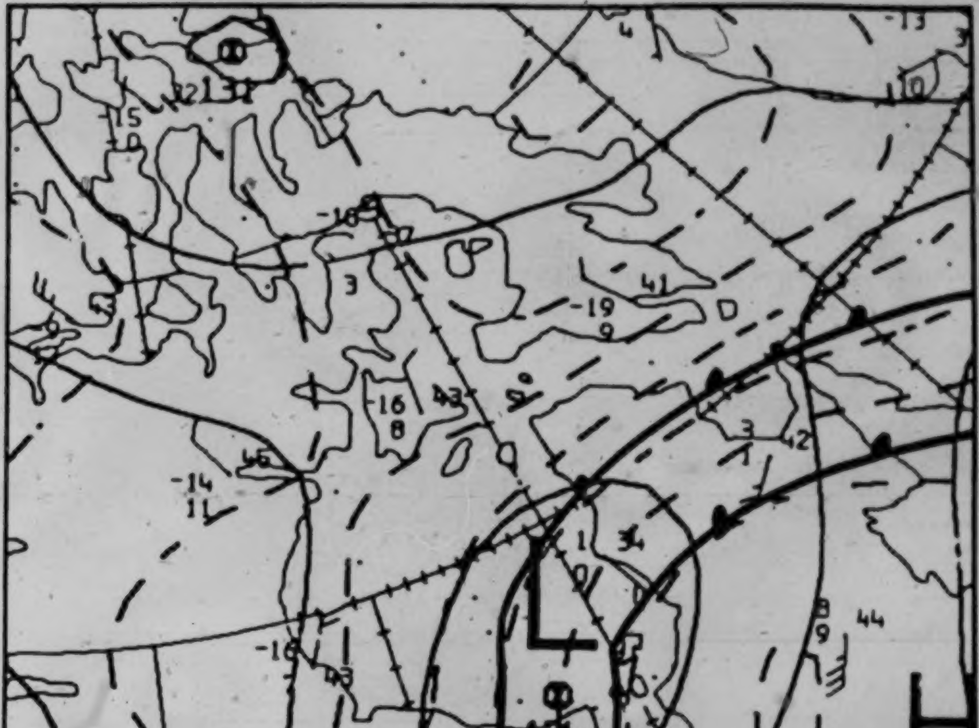
L
134
H
150
H
152
131

Figure 4.29 The same as in Figure 4.3 except for 14 May 1983, 1200 GMT.

### 4.3 Case #2

This is another example of strong development. The system was active off the West Coast and over British Columbia during the period from 1200 GMT, 22 June 1983 to 0000 GMT, 26 June 1983. The upper system development was that of a pure cold low. Lee cyclogenesis over Alberta in the late stages occurred independently of the upper system. Several cloud areas (B) have formed at various times, but only one succeeded in acquiring comma shape. In the initial stage, (B) developed within the vorticity contour greater than 16 and subsequently maintained itself within vorticity area greater than 14. No appreciable PVA or PTA was related to (B) formation. This is different from some other cases where (B) development took place within cyclonic vorticity areas greater than 16. In the early stages, conventional data indicate an upper low development which was not evident in the satellite images (Figures 4.32-4.38). This shows the need for using satellite data in connection with conventional data.

Figures 4.30, 4.34 and 4.38 show a typical upper-level development. A 500-mb trough just off and parallel to B.C. coast has dug southeastward, pinched off at the neck and formed a closed circulation west of Vancouver Island. A new jet (2) advanced towards the base of trough , wrapped around and moved on to the eastern side of the trough. The old jet (1) moved rapidly eastward and merged with the main westerly stream. The thermal structure and the vorticity field supported this. An upper cold pool and a cyclonic cell of vorticity form the core of the closed wind circulation. On the other hand (Figures 4.31, 4.35 and 4.39), a closed circulation has propagated downward with regular configuration and closed isotherm.

On the satellite images (Figures 4.32, 4.33 and 4.37) the cloud pattern did not attain any organized configuration. (A) developed on the SE-side of the trough. Several cloud areas with (B) characteristics have formed and decayed before reaching the comma shape. (B) development during that period occurred within a cyclonic vorticity area of value greater than 14.

Figure 4.40 marks a new phase of development. By 0202 GMT, 24 June 1983, the upper system initiated a new cloud area (B), vertically developed and of a considerable size and comma-shaped. Another cloud area (A) developed and masked most of (B) except for its head. (A) was associated with a jet stream, shown in Figure 4.41. (B) was located within a vorticity centre greater than 16, without any PVA or PTA near by. The 500-mb flow (Figure 4.41), a typical elongated trough , is centred just south of Vancouver Island with jet (2) on the eastern side. In Figure 4.42 no closed circulation is present at the 850-level while the low-level system moved onshore and slowly NE-ward.

Twelve hours later Figure 4.43, the 500-mb low has moved onshore and is centred over Western Washington. No change has occurred in the contour or vorticity circulation, but the thermal field has intensified. Jet (2) has moved rapidly through the downstream ridge. Figure 4.44 shows very little change in the low-level flow except that the frontal system has moved farther from the upper low area. The wind field over central B.C. is weakly cyclonic without an inner circulation. Figure 4.45 depicts a new cloud area (C) which covers most of (B). The whole pattern is considered to be intensifying.

By 2215 GMT, 24 June 1983, the system had matured. All the cloud areas have developed and merged into one pattern. The overall pattern assumes storm configuration as it reaches its maximum intensity. In Figures 4.47 and 4.48 the synoptic circulation underwent little change. The trailing edge of the cloud area (B) is now located within a vorticity contour greater than 14. In Figure 4.47 jet (2) has moved further NE-ward and the system has ceased to deepen. On the 850-mb surface (Figure 4.48), no closed contour circulation has yet been established, while the frontal system moved NE-ward.

Twelve hours later (Figure 4.49), the upper pattern did not change, appreciably, (A) merged with (B)'s tail and (D) weakened considerably. Also in Figure 4.49, the upper pattern is quite distinct from the lee cyclone which has developed over Alberta. The cloud area (B) was again located within a cyclonic vorticity area greater than 14, with no evidence of PVA or PTA. In Figure 4.50, the 500-mb closed contour pattern and the cold core have opened up while the vorticity field has shifted eastward. On the 850-mb surface (Figure 4.51), no closed circulation exists and no cold air sector develops. The frontal system associated with the lee cyclogenesis has moved farther eastward.

Figures 4.52 - 4.55 show the continual deterioration of the upper system. The cloud pattern has weakened considerably, specially (B), while the mid and low-level flow have decayed completely.

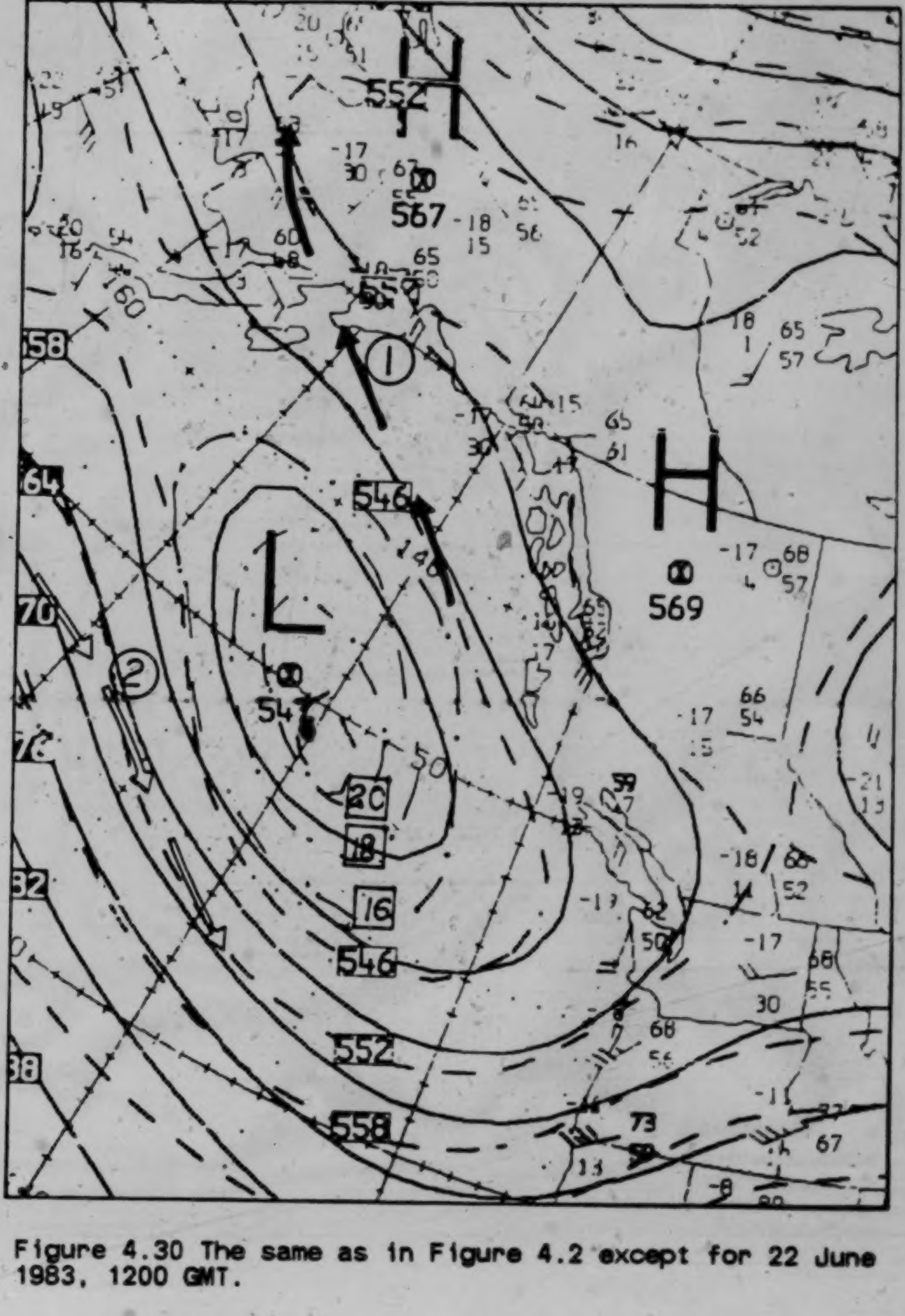
H
552
567
H
569
L
547
①
②
546
546
552
558
20
18
16
160
140
50
58
64
70
76
82
88

Figure 4.30 The same as in Figure 4.2 except for 22 June 1983, 1200 GMT.

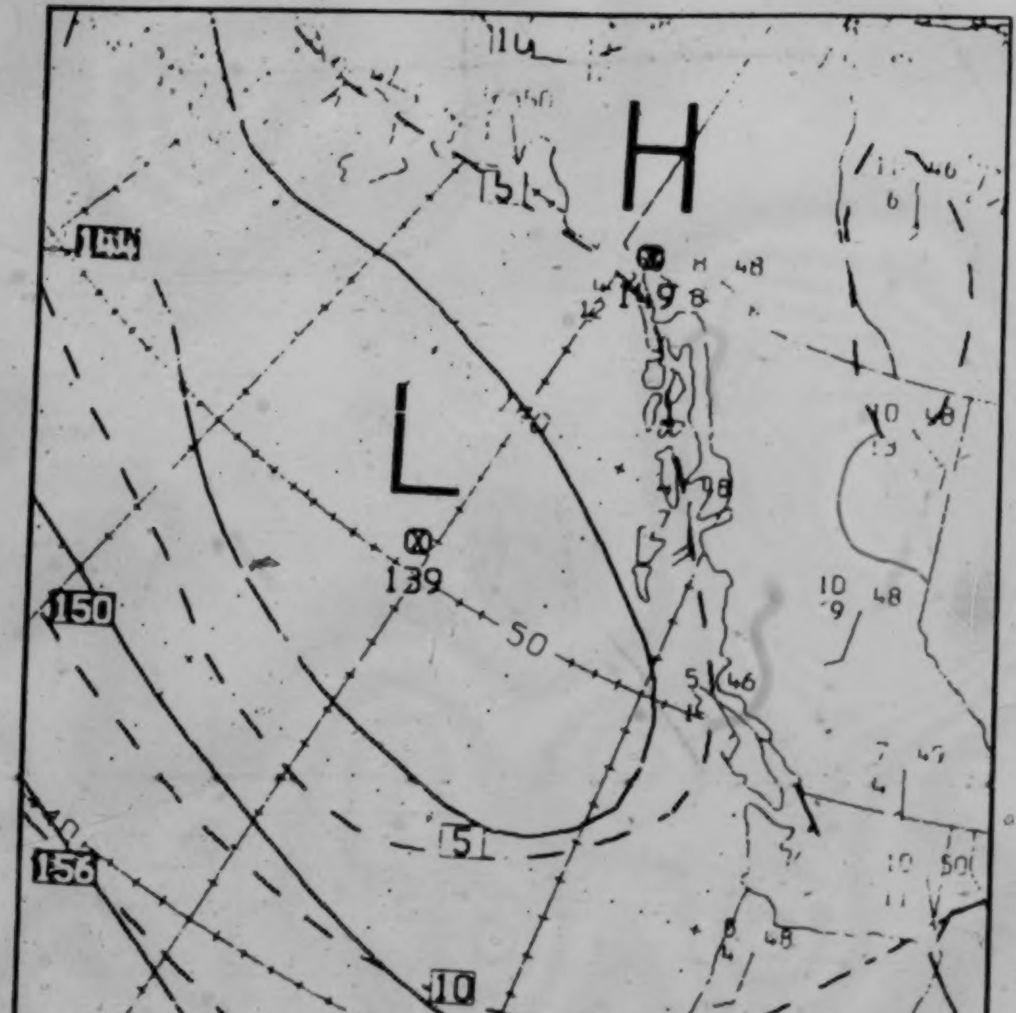
H
L
L
144
139
149
148
150
156
151
10
50

Figure 4.31 The same as in Figure 4.3 except for 22 June 1983, 1200 GMT.

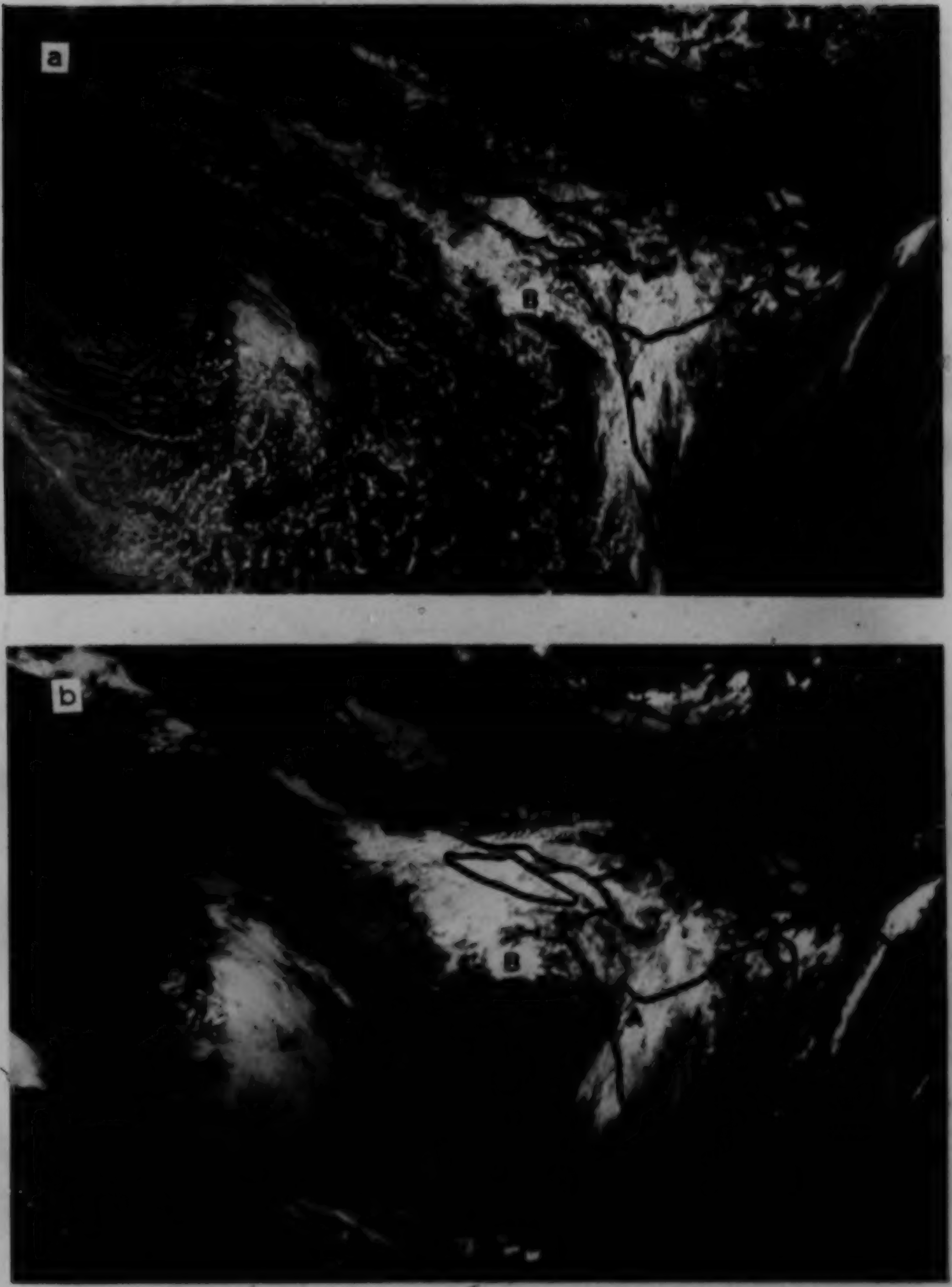

Figure 4.32 NOAA-8 satellite image, a) visible, b) infrared, 1636 GMT, 22 June 1983.

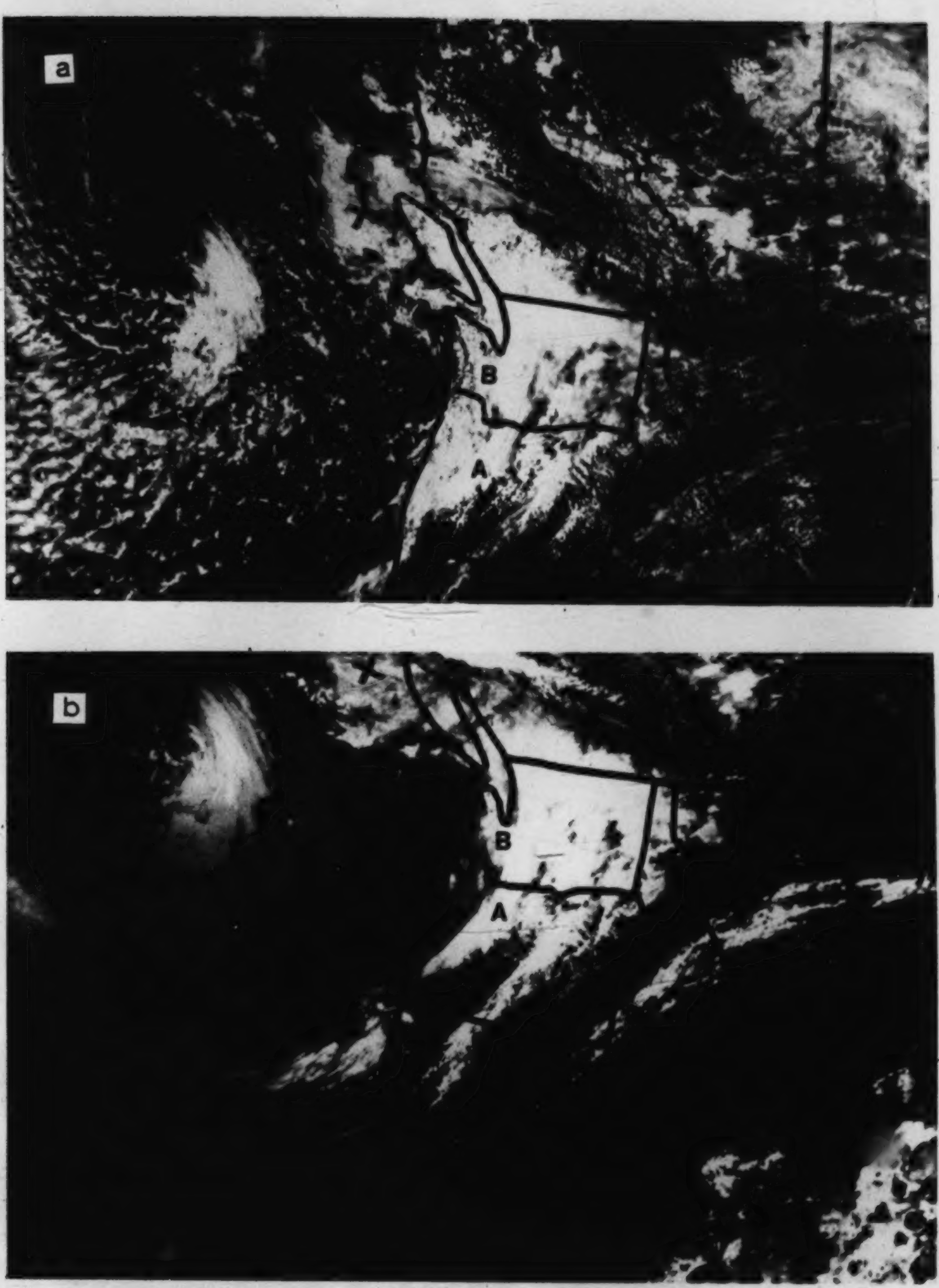

Figure 4.33 NOAA-7 satellite image, a) visible, b) infrared, 2240 GMT, 22 June 1983.

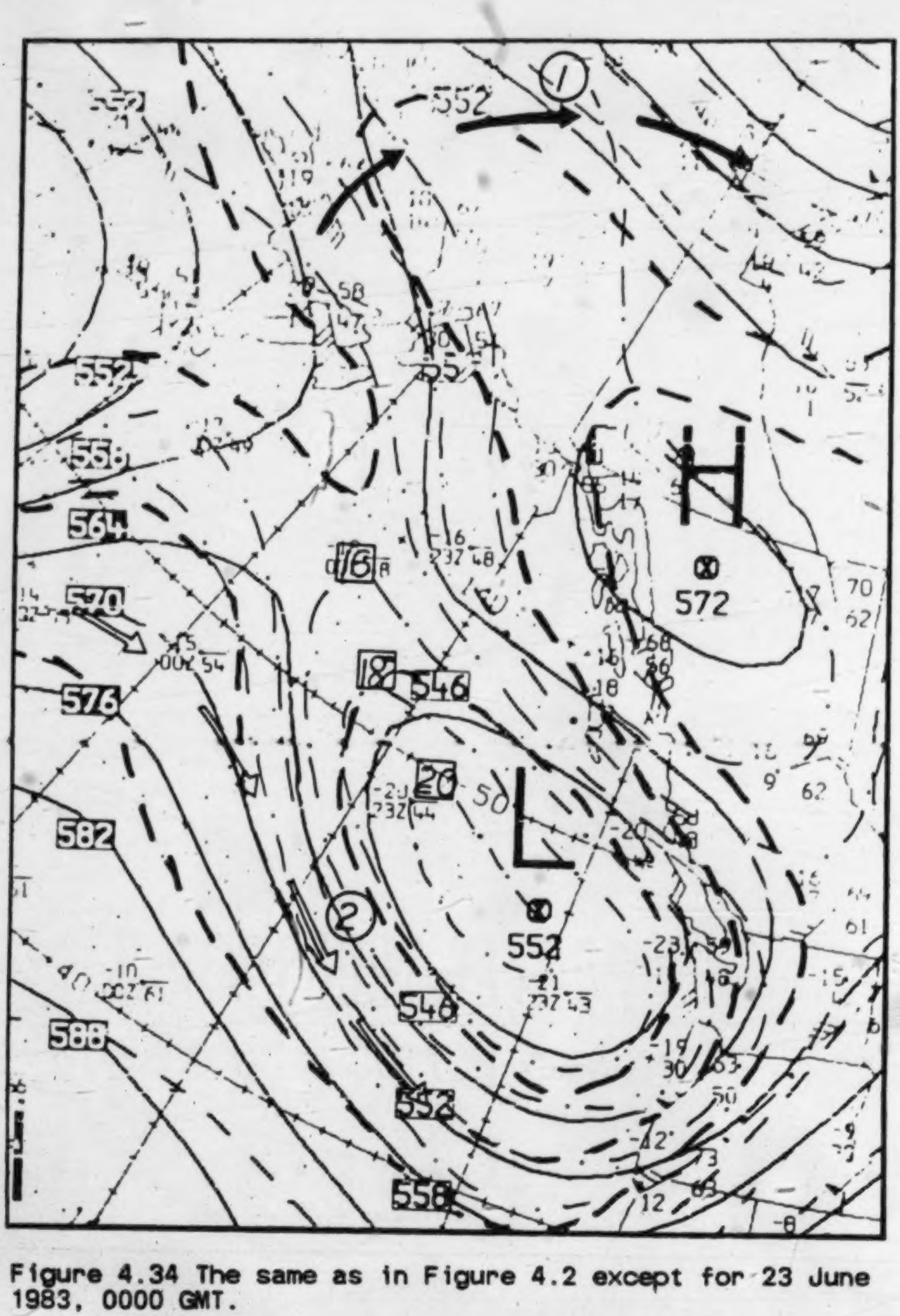
552
①
552
558
564
570
576
582
588
546
552
558
16
18
20
546
H
572
L
552
②
70
62

Figure 4.34 The same as in Figure 4.2 except for 23 June 1983, 0000 GMT.

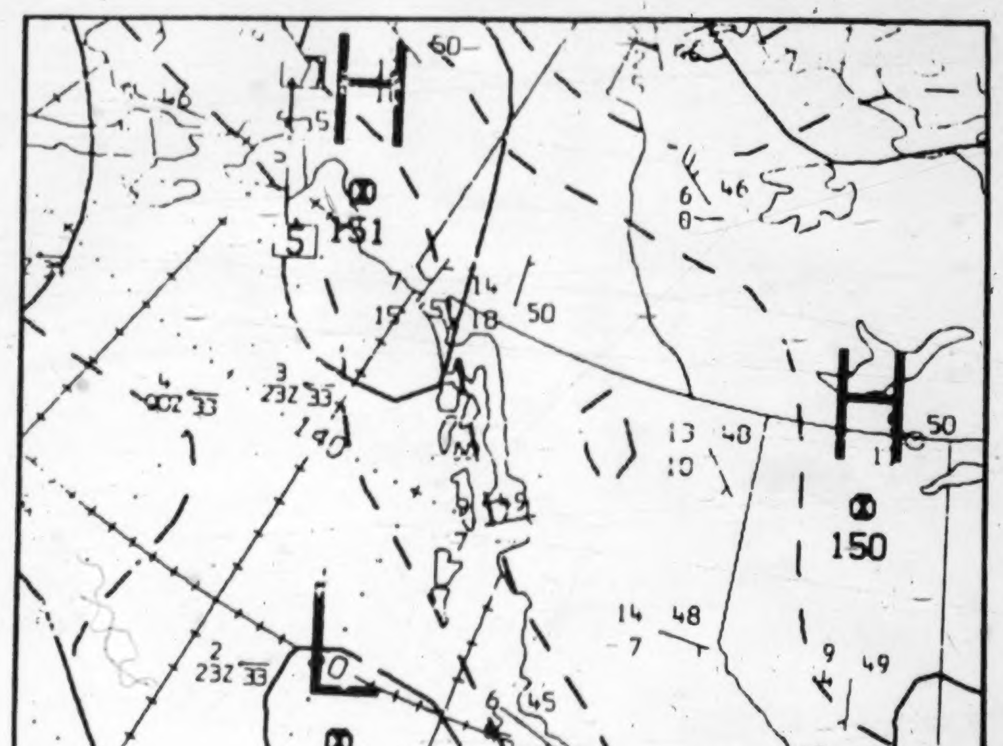
H
60
151
5
H
150
50
L
143
5
10
L
4
00Z 33
3
23Z 33
2
23Z 33
2
23Z 33
13 48
10
14 48
7
14 48
11
12 49
9 49
15 48
19 50
27
30
29
30
31
30
22Z
22Z
22Z
22Z
17
17

Figure 4.35 The same as in Figure 4.3 except for 23 June 1983, 0000 GMT.

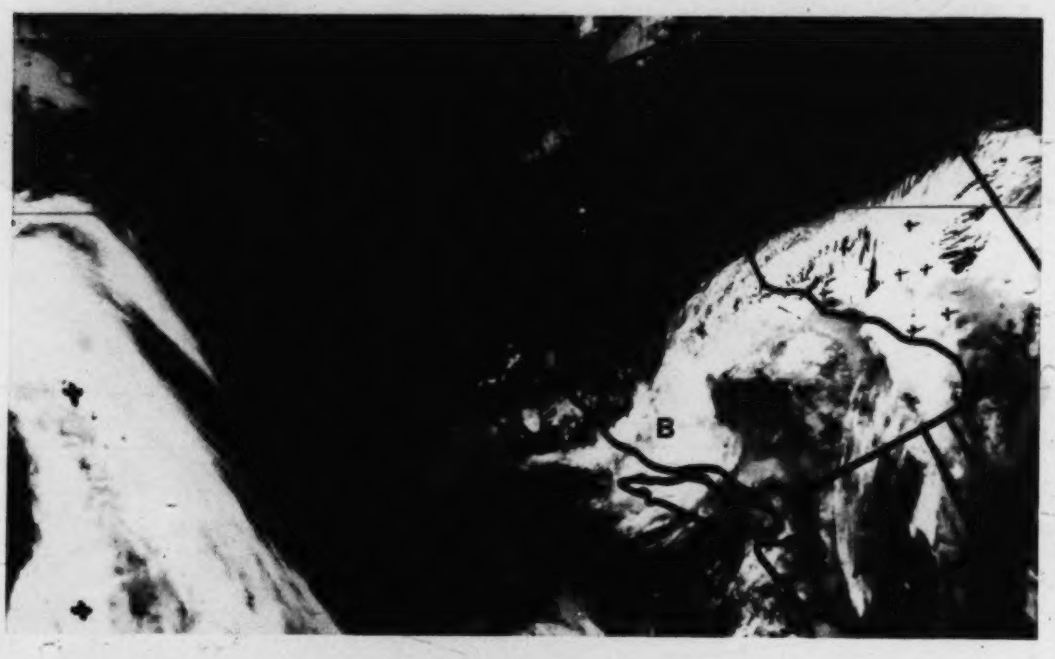

Figure 4.36 NOAA-7 satellite image , infrared, 1236 GMT, 23 June 1983.

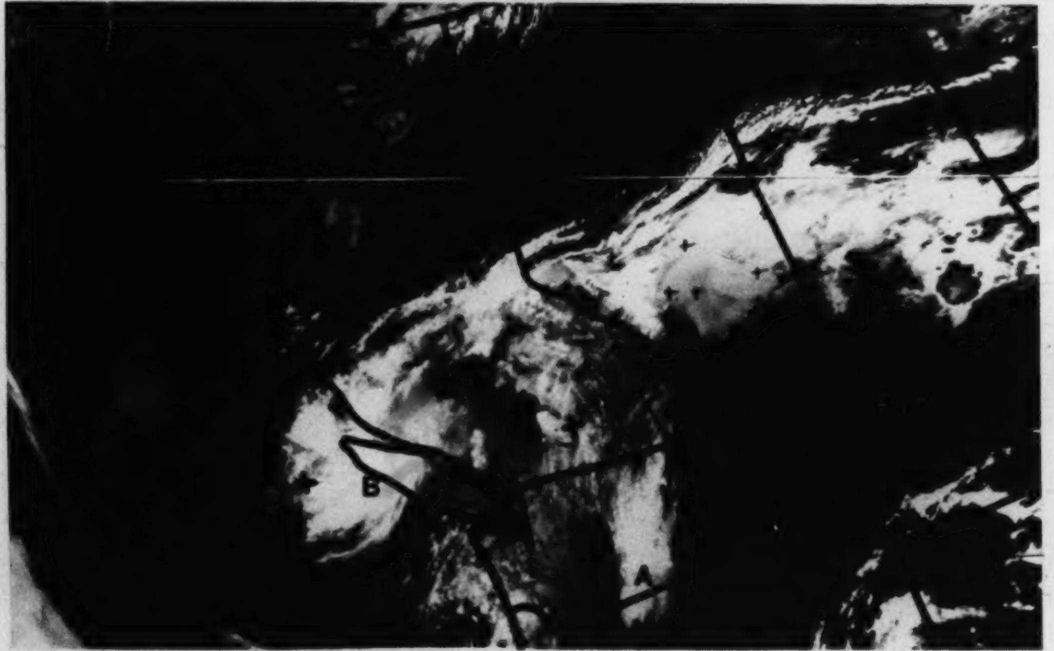

Figure 4.37 NOAA-8 satellite image , infrared, 1614 GMT, 23 June 1983.

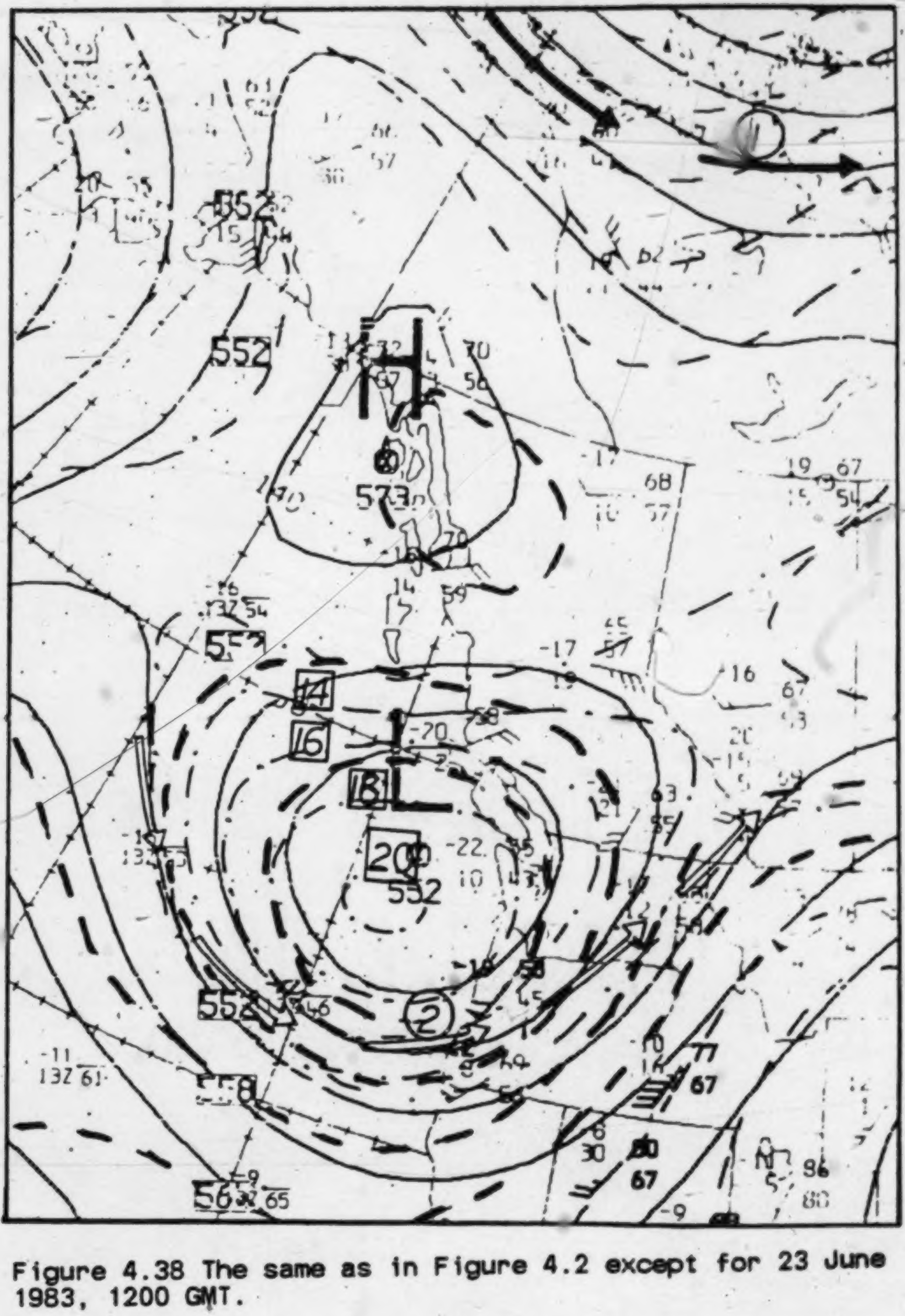
552
552
573
552
14
16
18
20
552
2
H
L

Figure 4.38 The same as in Figure 4.2 except for 23 June 1983, 1200 GMT.

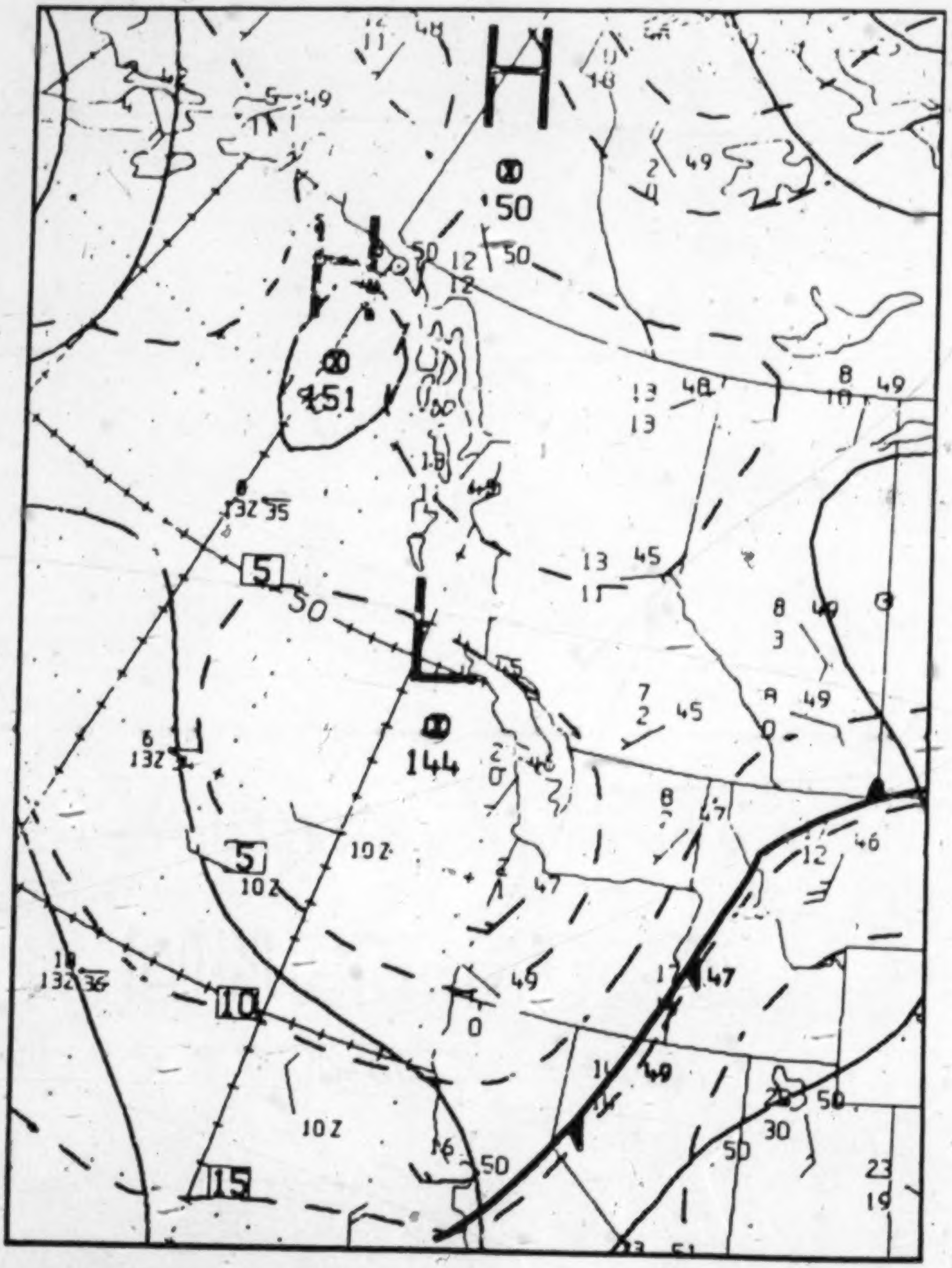
H
150
151
L
144
5
5
10
15
50

Figure 4.39 The same as in Figure 4.3 except for 23 June 1983, 1200 GMT.

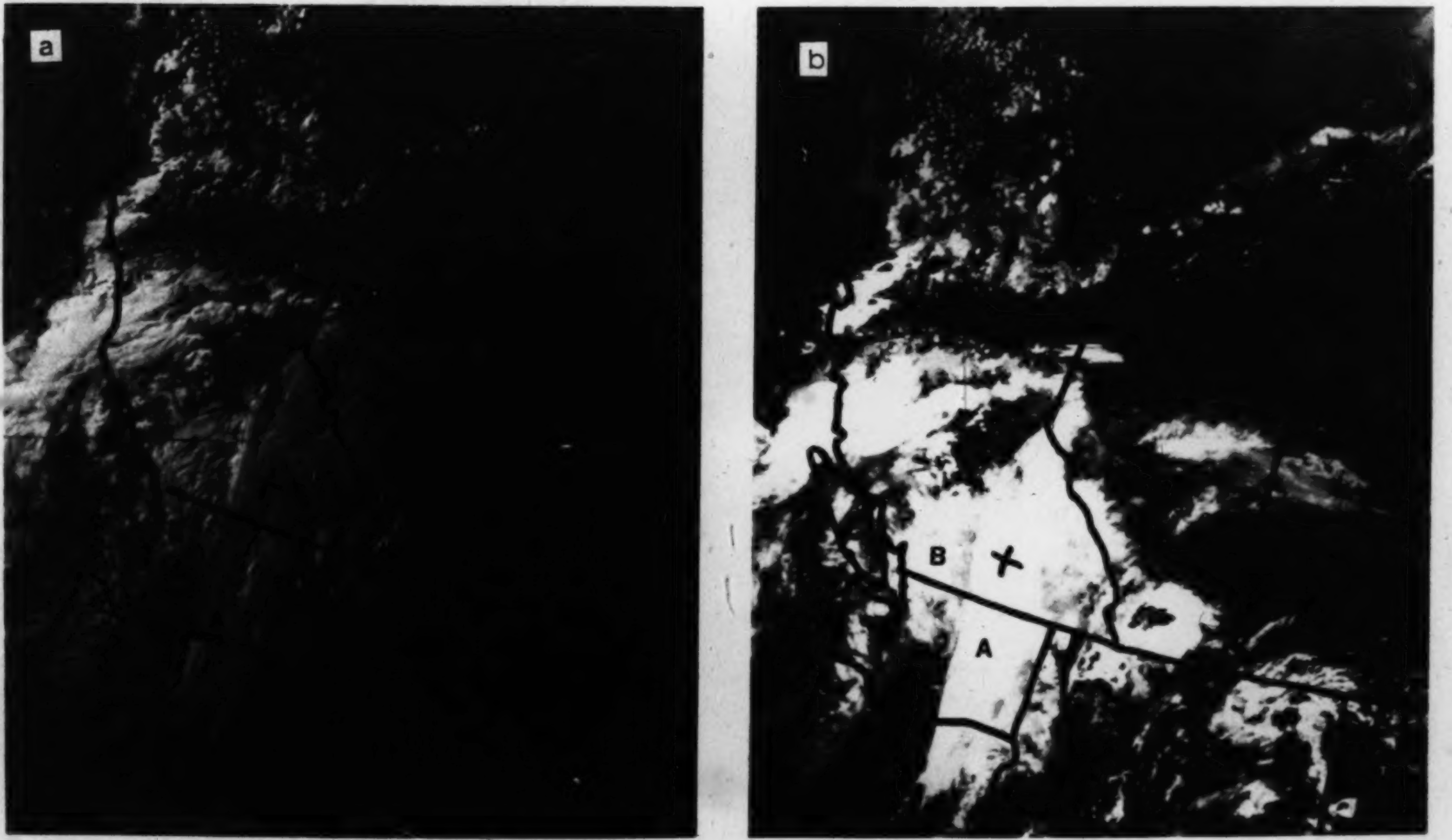

Figure 4.40 NOAA-8 satellite image, a) visible, b) infrared, 0202 GMT, 24 June 1983.

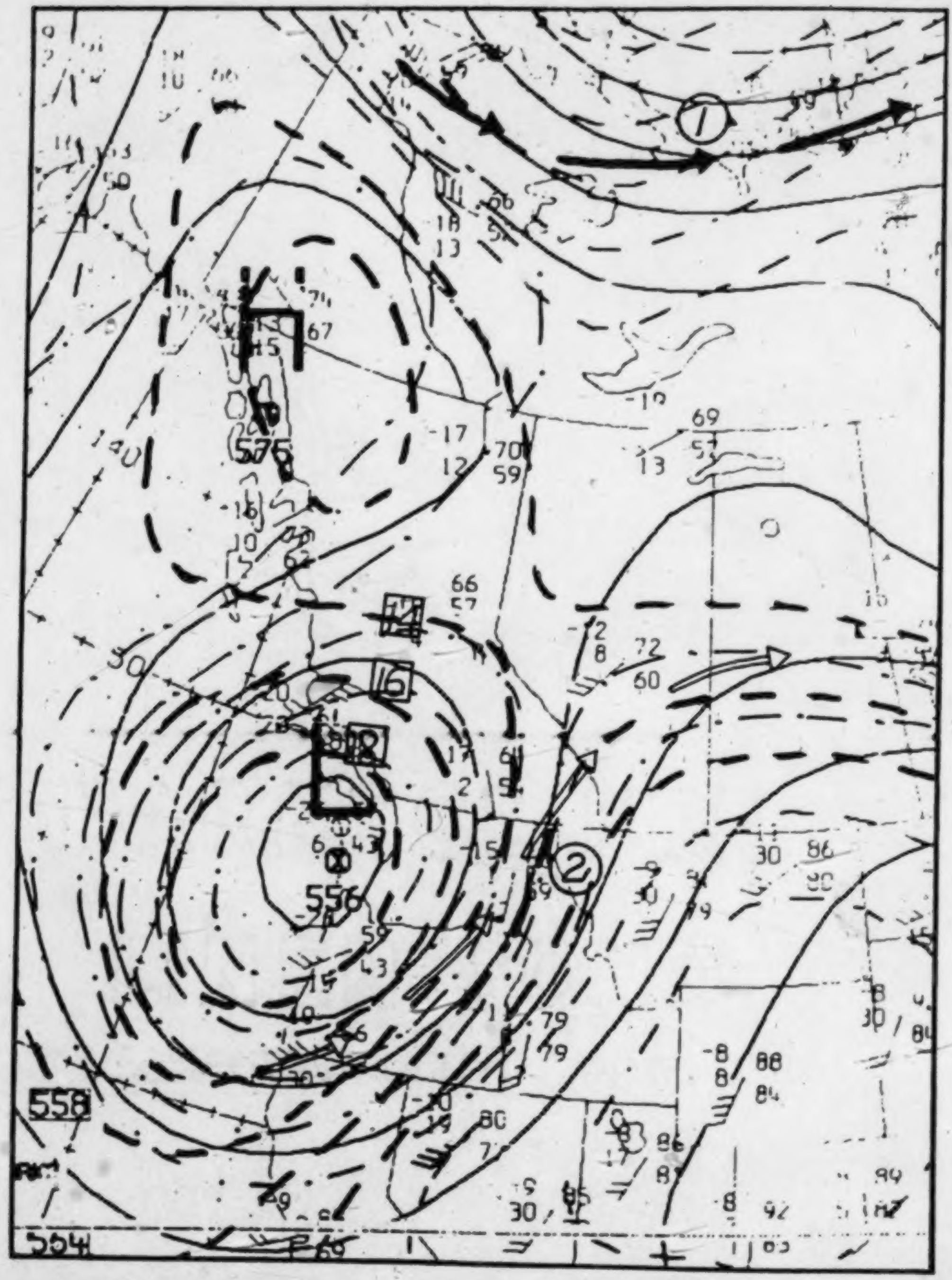
①
H
575
140
-17
12
70
59
-19
69
13
66
57
14
130
16
12
L
②
556
558
554
72
60
30
86
79
88
84
80
92
99

Figure 4.41 The same as in Figure 4.2 except for 24 June 1983, 0000 GMT.

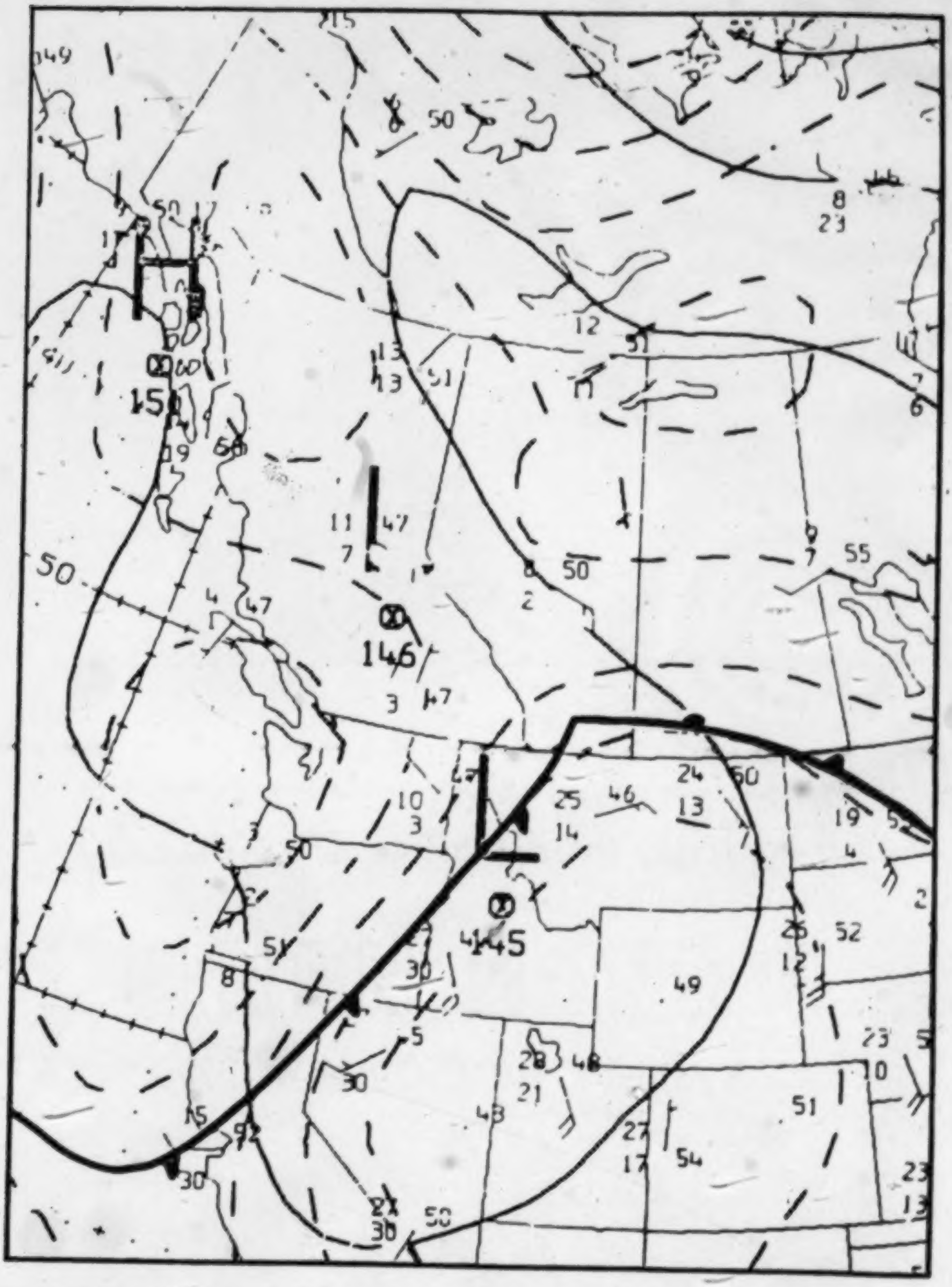

Figure 4.42 The same as in Figure 4.3 except for 24 June 1983, 0000 GMT.

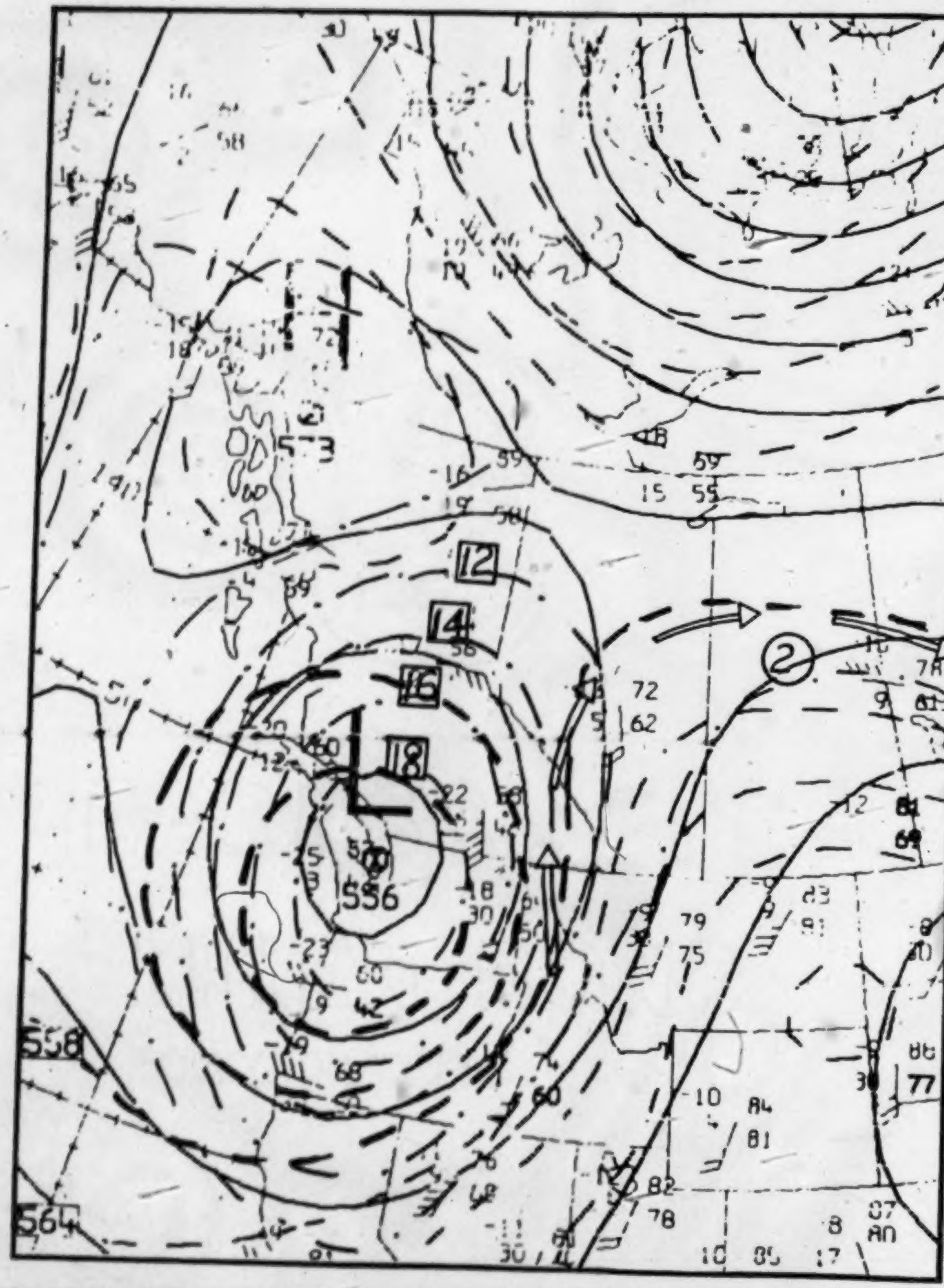

Figure 4.43 The same as in Figure 4.2 except for 24 June 1983, 1200 GMT.

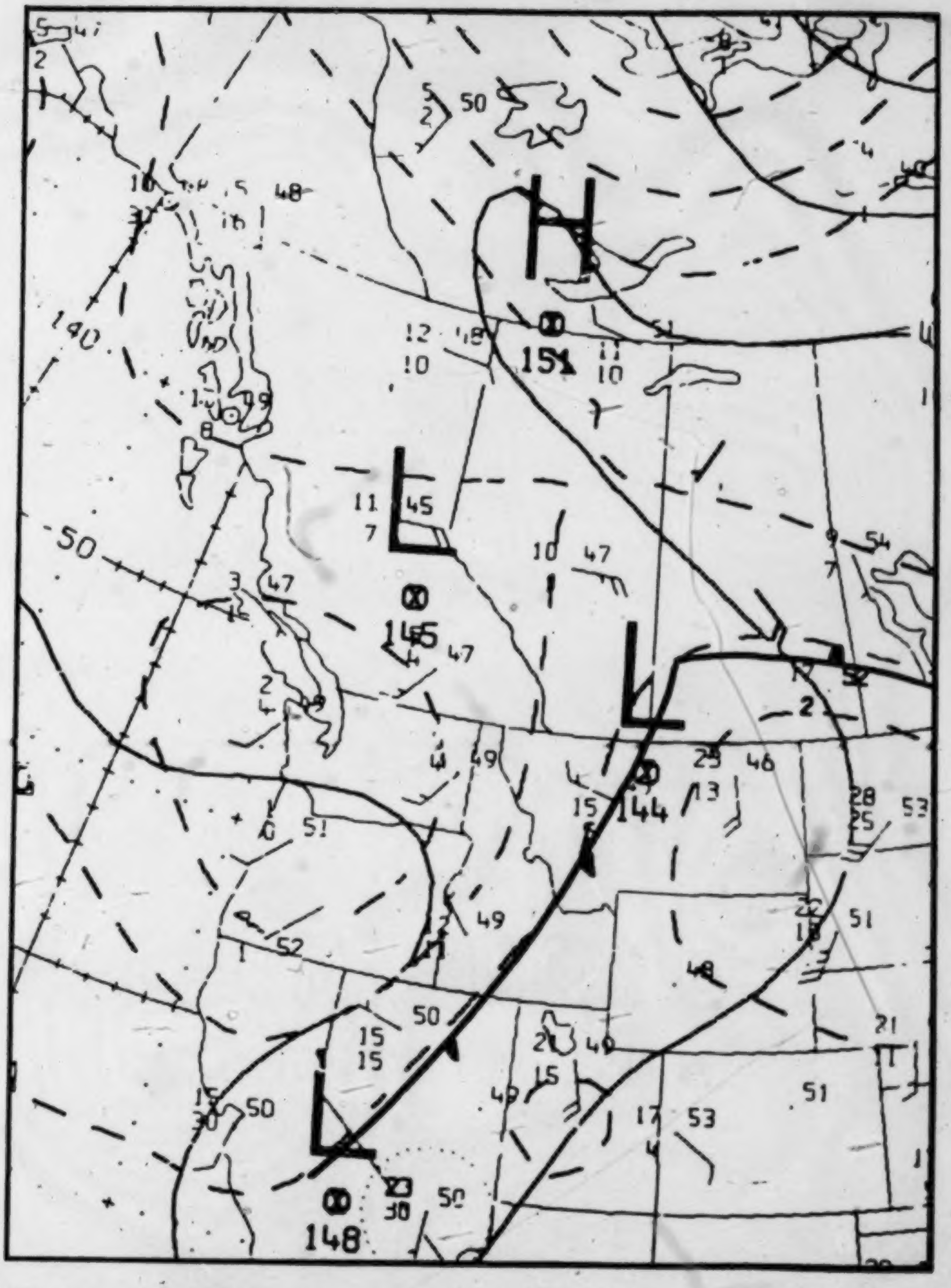
H
151
L
145
L
144
L
148
140
50

Figure 4.44 The same as in Figure 4.3 except for 24 June 1983, 1200 GMT.

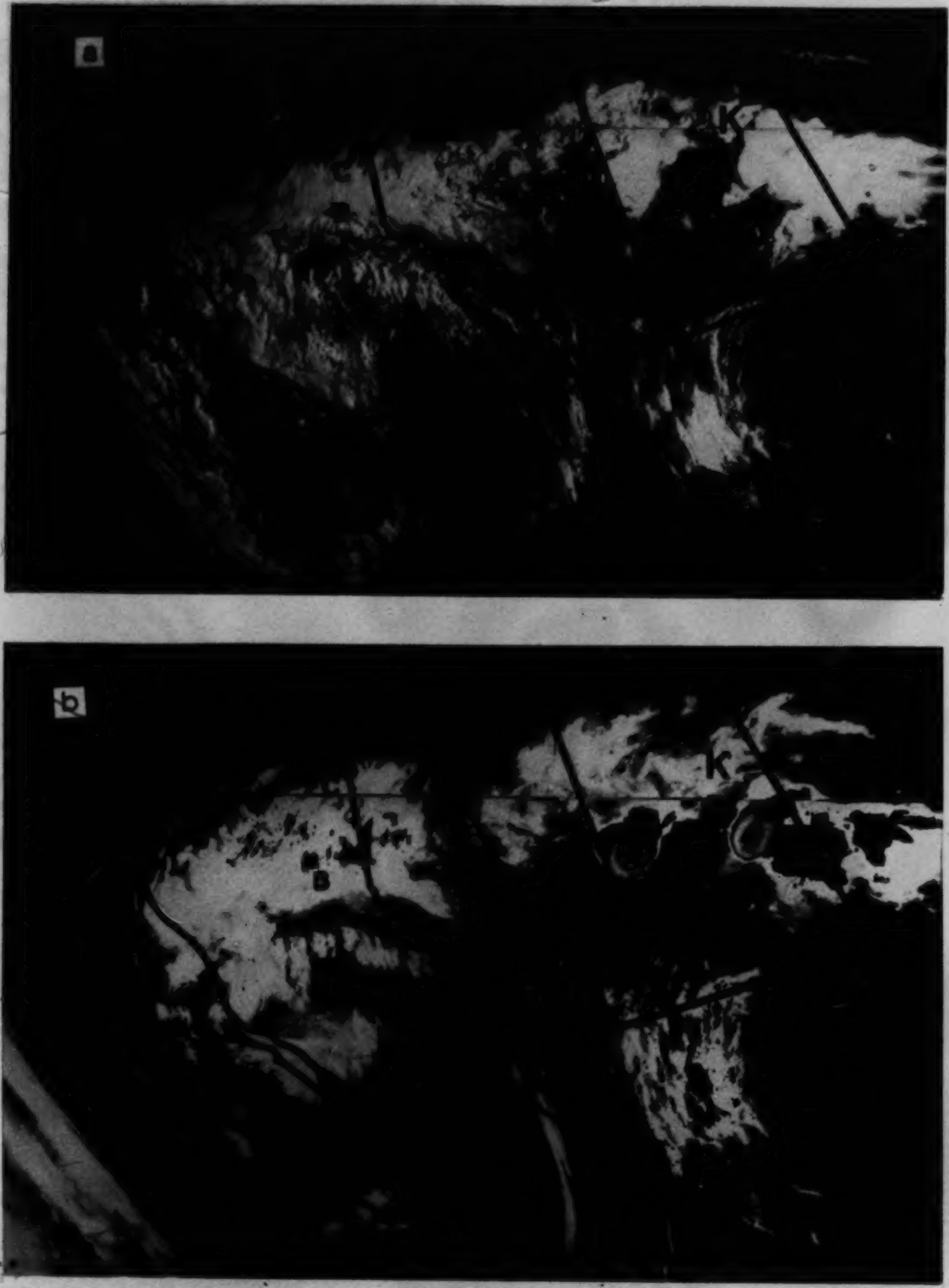

Figure 4.45 NOAA-8 satellite image, a) visible, b) infrared, 1552 GMT, 24 June 1983.

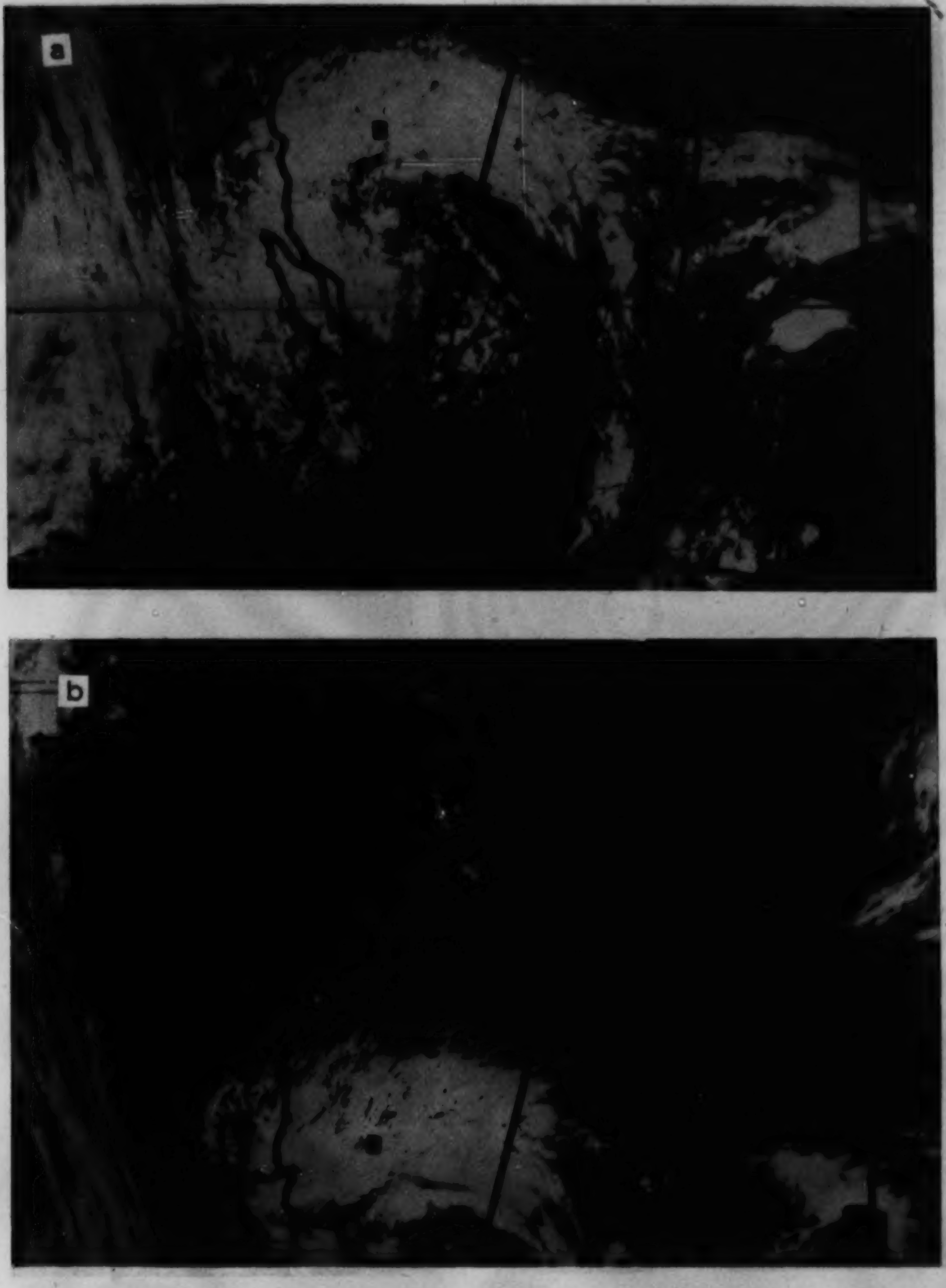

Figure 4.46 NOAA-7 satellite image, a) visible, b) infrared, 2215 GMT, 24 June 1983.

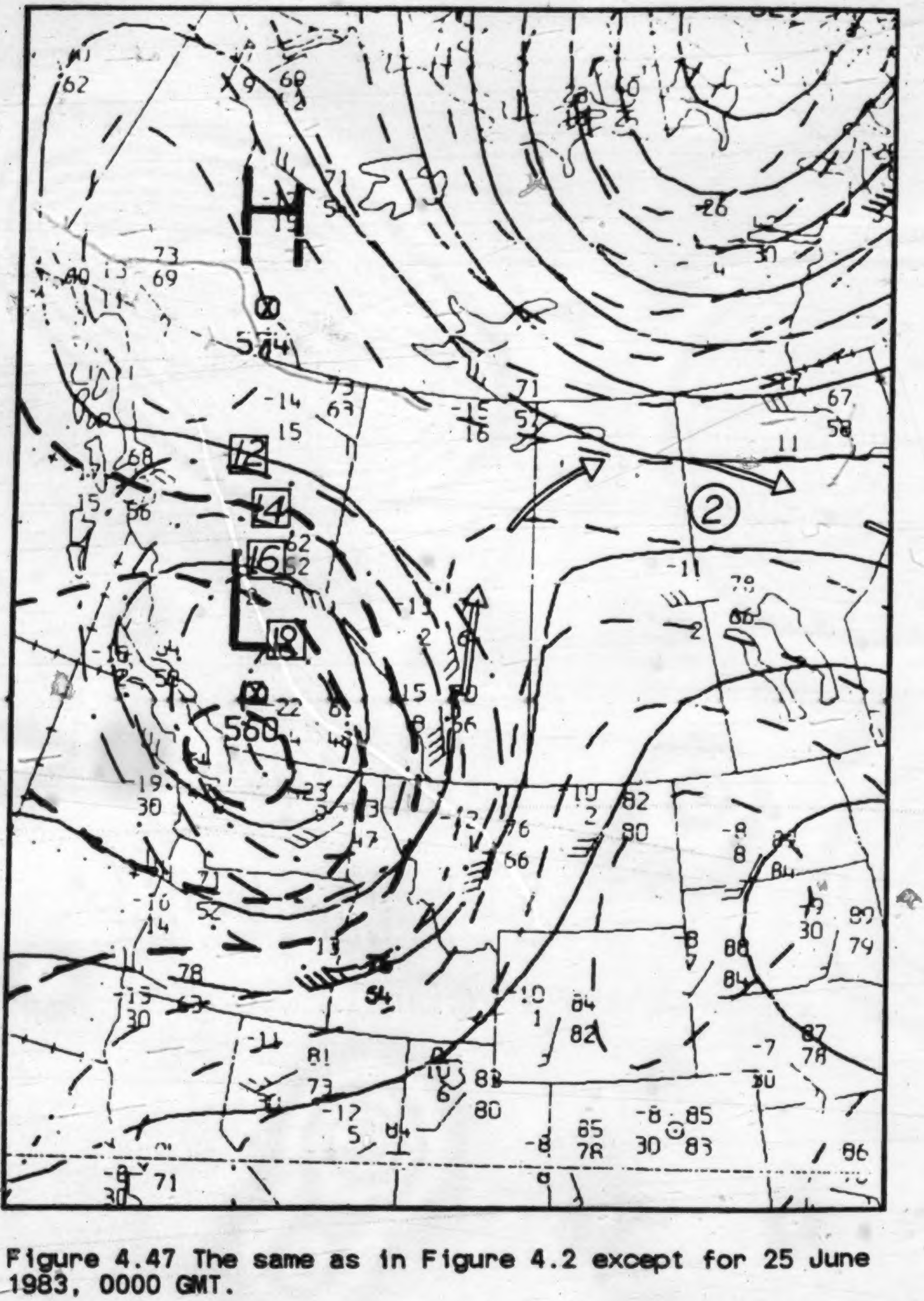
H
L
574
560
12
14
16
18
②

Figure 4.47 The same as in Figure 4.2 except for 25 June 1983, 0000 GMT.

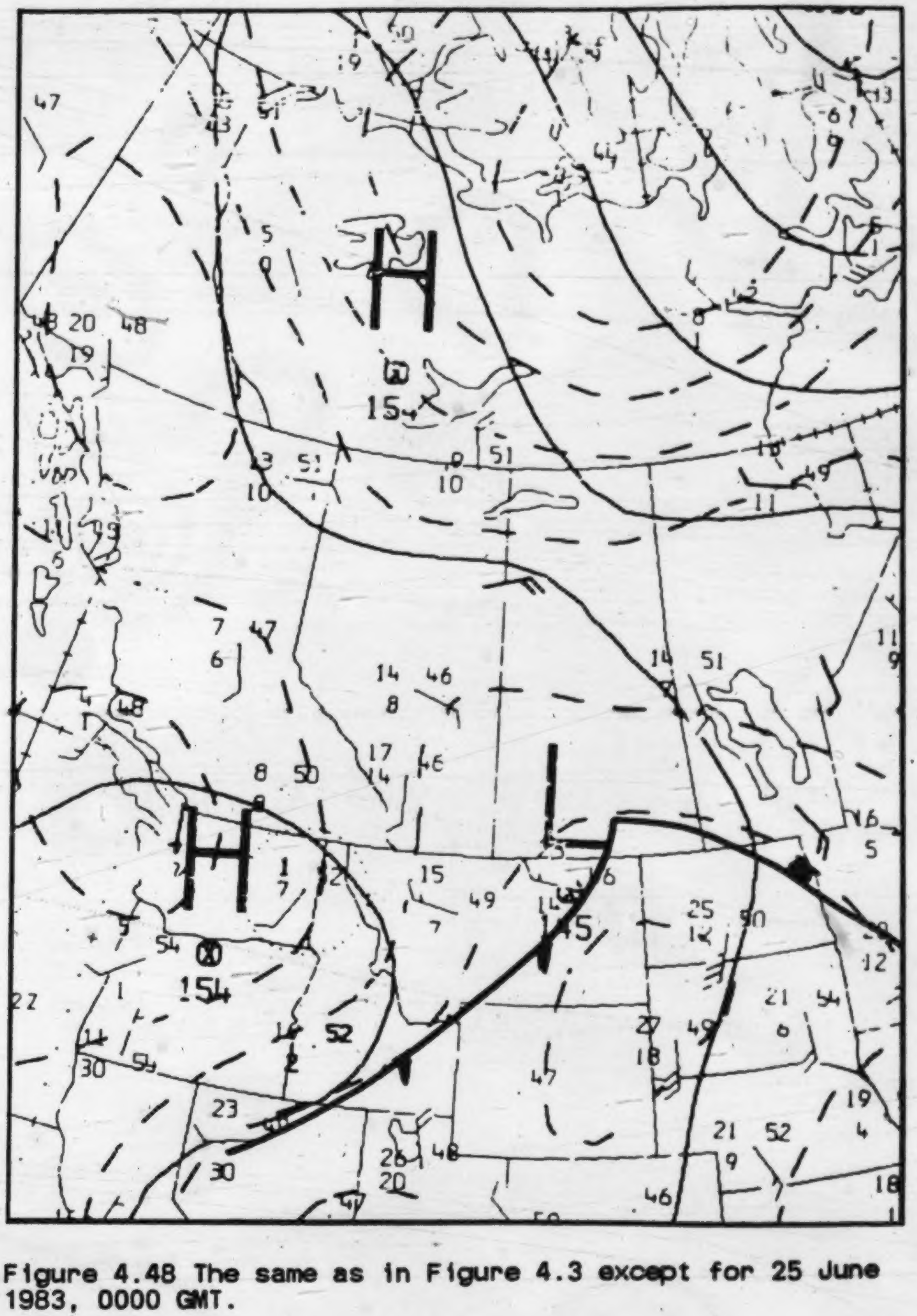

Figure 4.48 The same as in Figure 4.3 except for 25 June 1983, 0000 GMT.

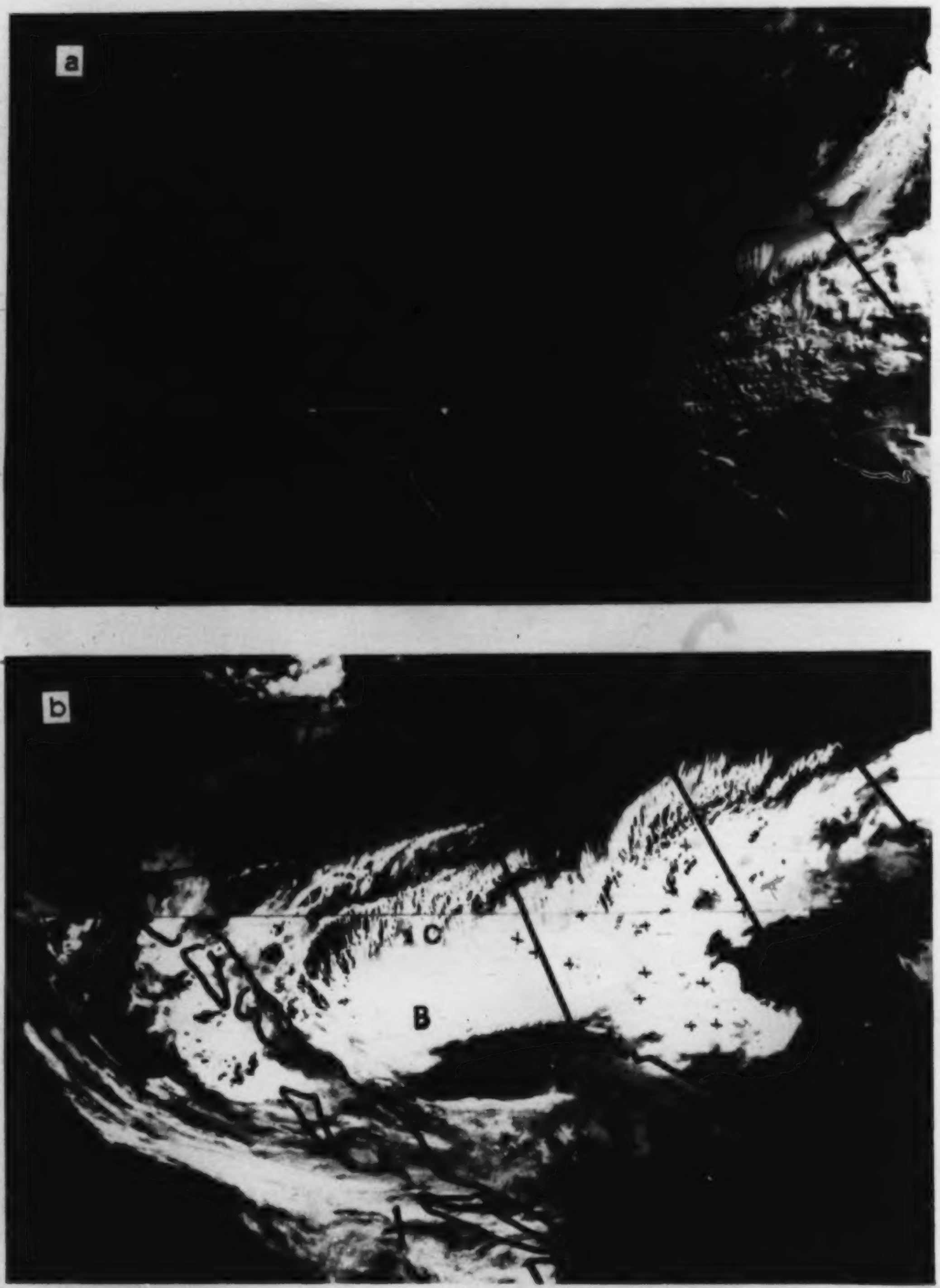

Figure 4.49 NOAA-7 satellite image, a) visible, b) infrared, 1211 GMT, 25 June 1983.

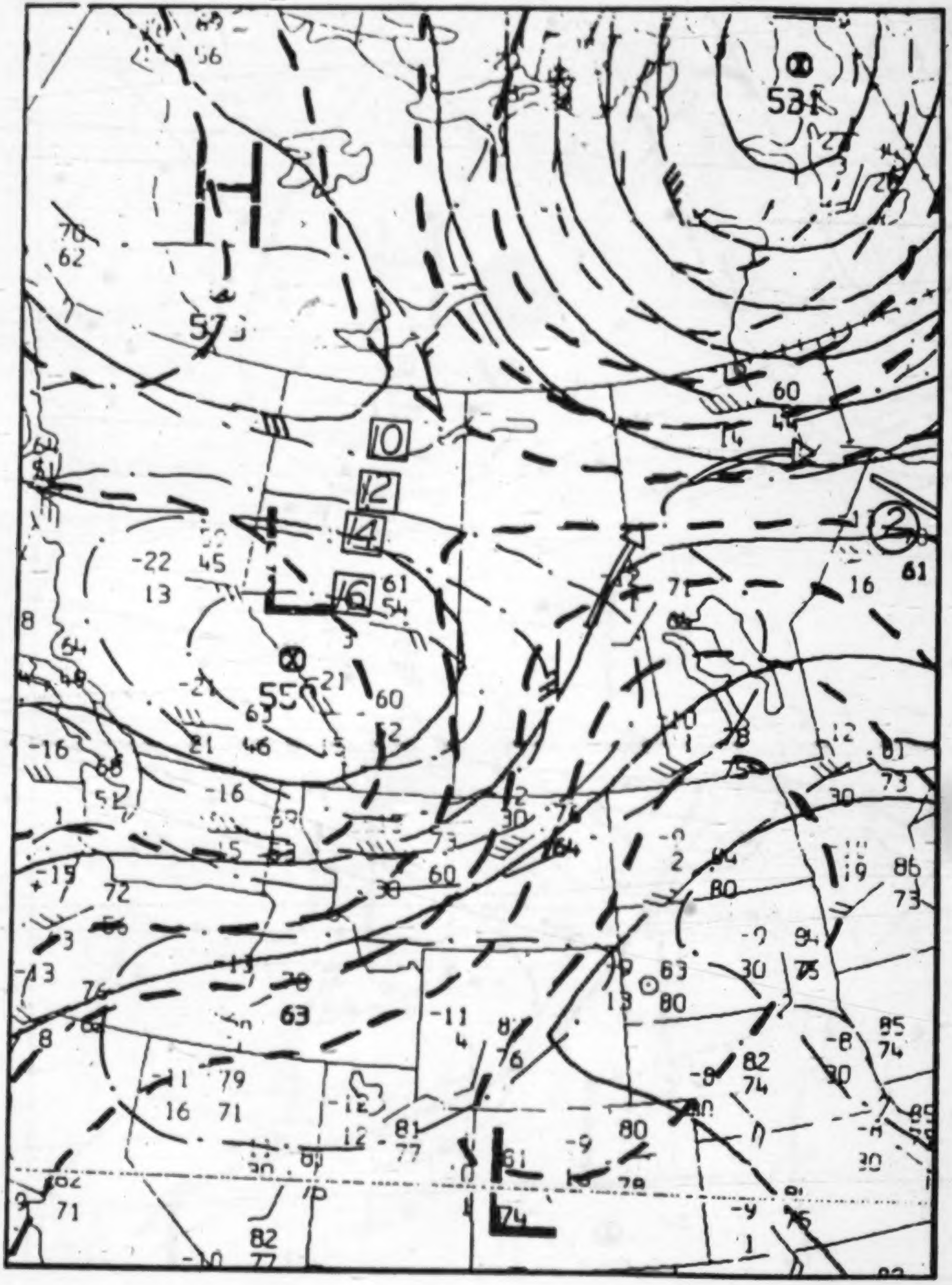
H
L
L
531
573
552
10
12
14
16
2

Figure 4.50 The same as in Figure 4.2 except for 25 June 1983, 1200 GMT.

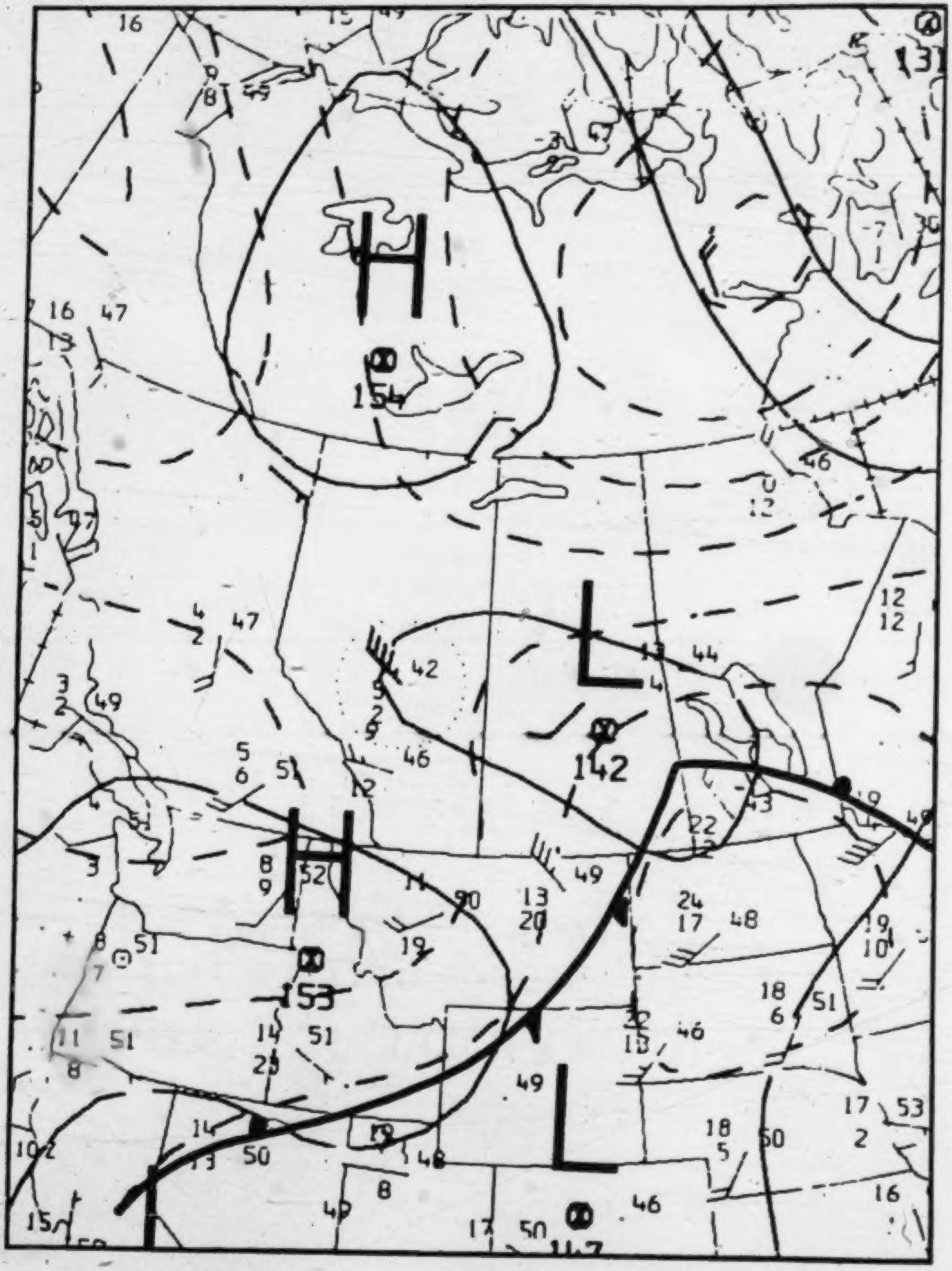
H
154
L
142
H
153
L
147
131

Figure 4.51 The same as in Figure 4.3 except for 25 June 1983, 1200 GMT.

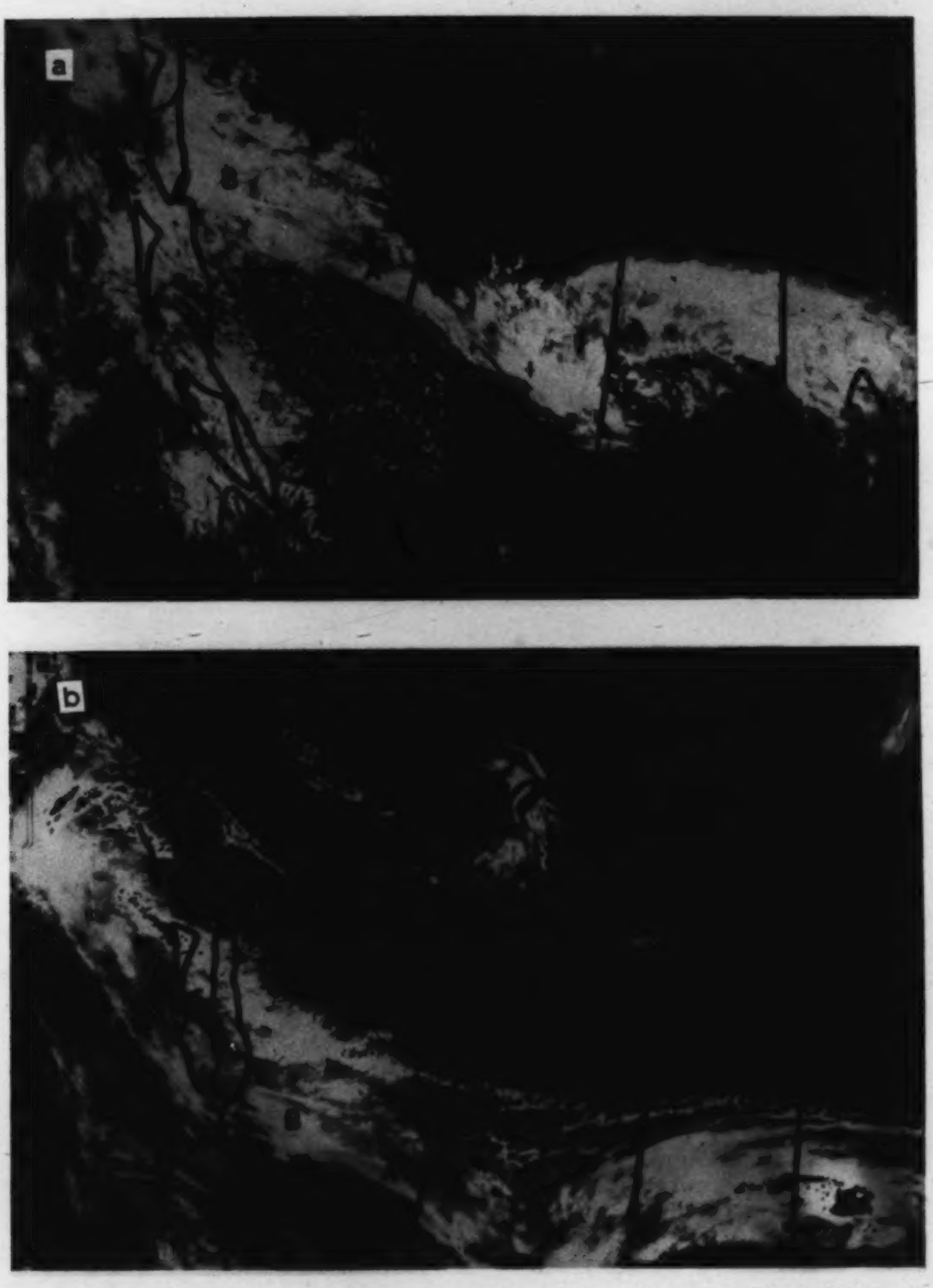

Figure 4.52 NOAA-7 satellite image, a) visible, b) infrared, 2203 GMT, 25 June 1983.

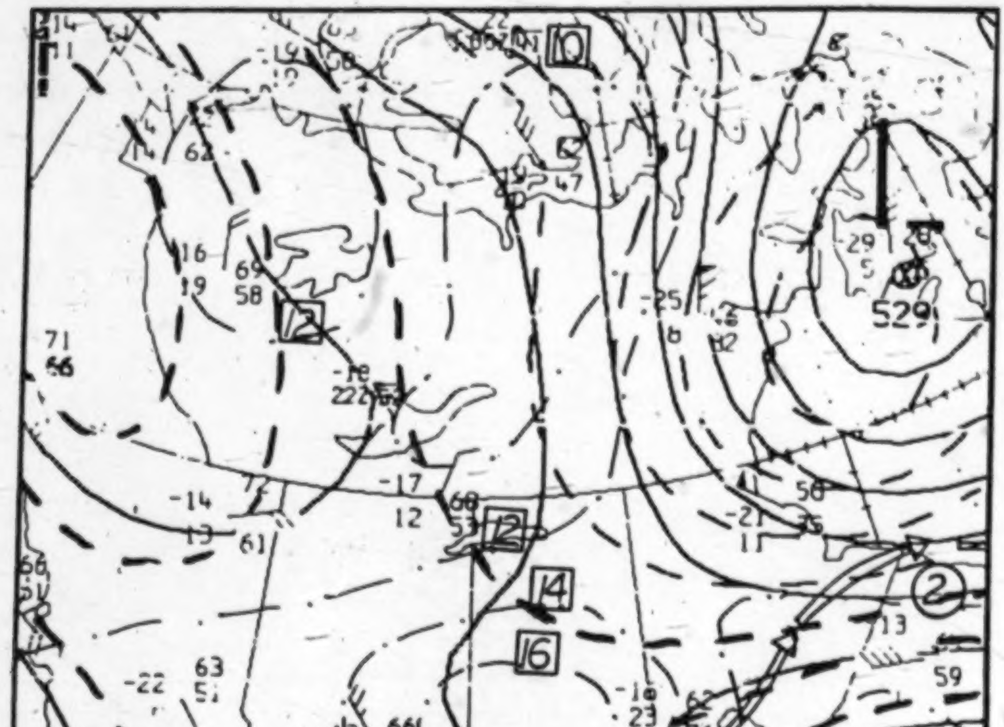
10
12
12
14
16
529
2
-25
-21
-22
-18
-17
-16
-14
-13
-12
-10
-8
-7
-6
16
19
69
58
71
66
63
57
66
57
80
77
82
78
81
78
83
78
85
77

Figure 4.53 The same as in Figure 4.2 except for 26 June 1983, 0000 GMT.

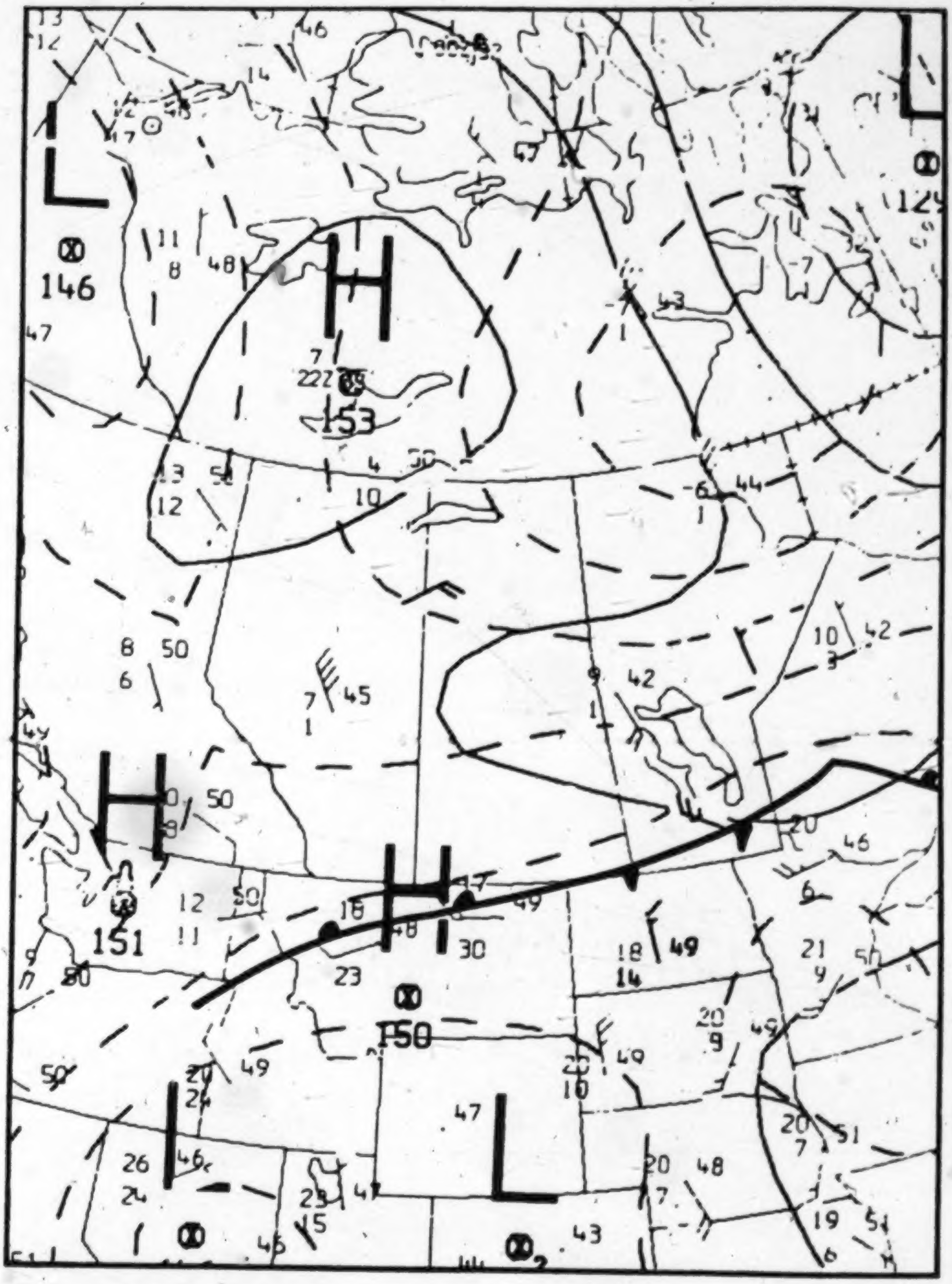
L
H
H
H
L
L
L
146
153
151
150
129

Figure 4.54 The same as in Figure 4.3 except for 26 June 1983, 0000 GMT.

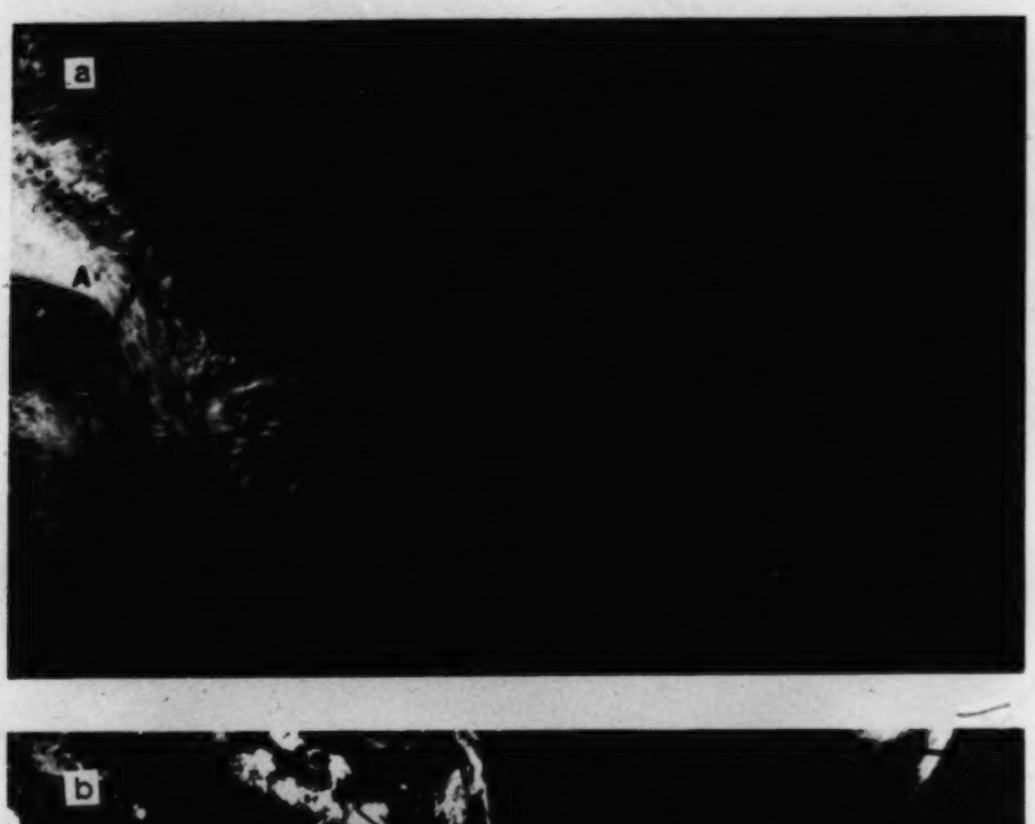

Figure 4.55 NOAA-8 satellite image, a) visible 0119 GMT, b) infrared 0119-0259 GMT, 26 June 1983.

## 4.4 Case #3

This is a pure case of moderate upper-level development, where the overall cloud pattern has failed to reach the storm stage, even though a well-defined comma has formed during the pattern's lifetime. Figures 4.56 - 4.73 depict the different phases of development. Satellite images were superior to synoptic maps, since they revealed the location and degree of activity, whereas the maps provided very little pertinent information. In the period from 0000 GMT, 16 August 1983 to 0000 GMT, 18 August 1983, an upper system formed over 60° N/ 150° W (see Figure 4.56), moved SE-ward and decayed over northern Alberta (Figure 4.73). The system evolved within an upper cold air mass without the presence of low-level warm air intrusion. It should be noted, that no pronounced troughing or pinching-off occured at the 500-mb level and that the weak contour circulation (Figures 4.56 and 4.59) did not propagate to lower levels, as in the case of typical upper-level development. The cloud area (B), however, was associated with a cyclonic vorticity area greater than 16. On the 850-mb surface (Figures 4.57 and 4.60) a weak northeasterly flow is seen to cross the Gulf of Alaska. An incipient frontal system is present on both maps, but no closed contour circulation exists. Figures 4.58 and 4.61 show the cloud pattern which has moved slowly SE-ward. (B) is still located within a vorticity area greater than 16.

A few hours later (Figure 4.62), (B) has evolved into a comma, (C) has decayed and a new cloud area (A) has formed near (B). Figure 4.65 support the continuing evolution, where a new cloud area (D) has formed as well. On the 500-mb surface (Figure 4.63), the elongated troughing has pinched-off at the neck, jet (2) continued advancing SE-ward and passed the trough base without turning to the eastern side. In Figure 4.64, the frontal system has moved southward and the cold air deepened SE-ward.

Twelve hours later, Figure 4.66, the mid-level flow has weakened considerably except in the short wave trough over Northeastern B.C., the vorticity circulation has decreased and jet (2) moved farther SE-ward. On the 850-mb surface the thermal cold ridge continued digging SE-ward. The area of activity (Figure 4.68) was covered with cold air from the 850-mb level to beyond 500-mb level. In Figure 4.68 the cloud area (A) vanished, and (B) continued non-changing, but the vorticity and the thermal fields showed no PVA or PTA near (B).

The upper pattern continued moving eastward without much change as seen in Figures 4.69 and 4.72. (B) shrank in area but was still convectively active (Figure 4.69). Figures 4.70 and 4.71 show how the upper system in the filling stage, no closed circullation exists and the vorticity field weakens. Figure 4.73 depicts the terminal stage of the upper system with only cloud areas (C) and (D) remaining.

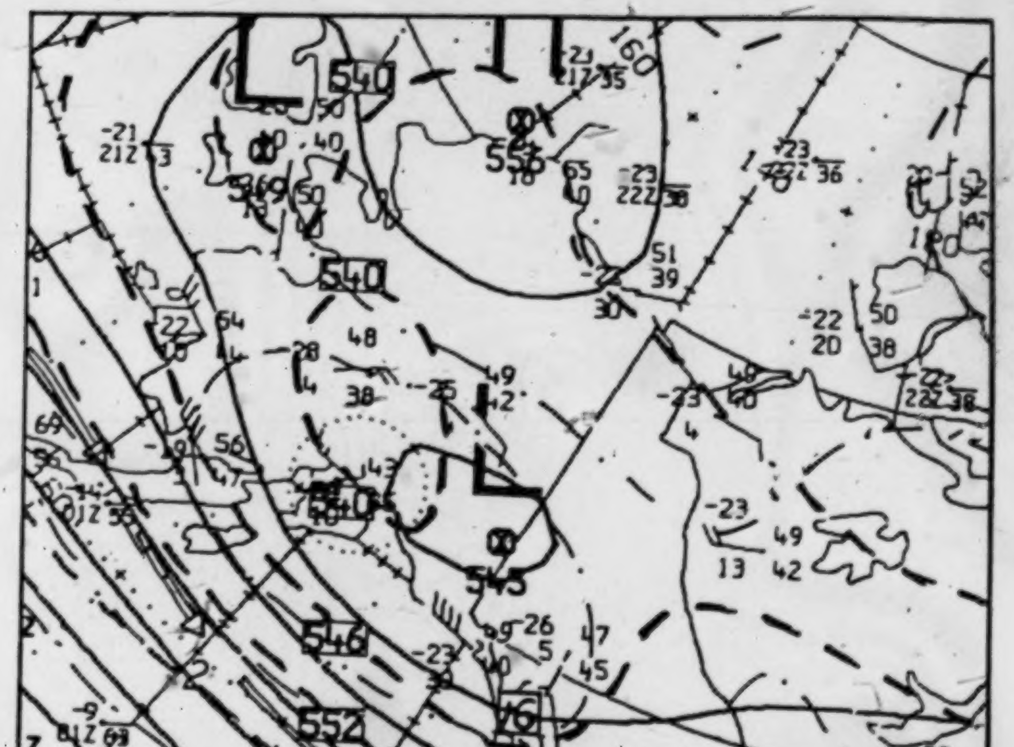

L
540
160
-21
212 35
553
-23
222 36
-23
222 38
-21
212 13
40
549
50
540
51
39
30
22
64
48
-28
38
49
42
-25
-22
20
50
38
-23
40
69
-19
56
47
-44
01Z 55
540
143
L
-23
13
49
42
545
546
-26
5
47
45
-23
552
76
-20
-9
01Z 69
558
74
56
52
-22
-12
12
-16
67
50
70
75
58
-9
00Z 64
-11
00Z 62
-15
73
68
-13
76
67
8
-12
11
14
62
-14
13
81
73
-12
83
74
3
-12
23Z 61
82

Figure 4.56 The same as in Figure 4.2 except for 16 August 1983, 0000 GMT.

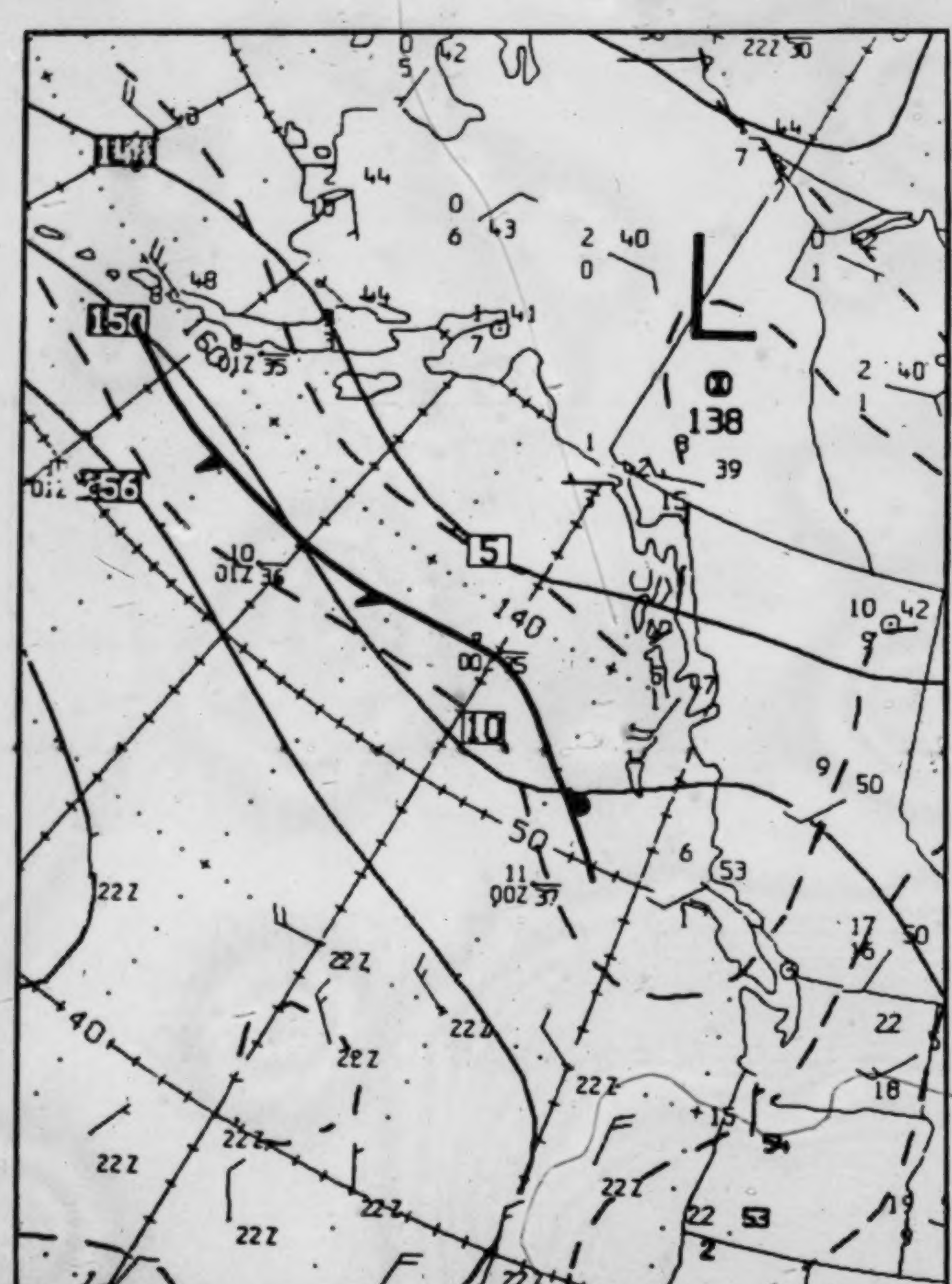
150
160
156
15
140
10
50
40
138
L
222
00Z
01Z

Figure 4.57 The same as in Figure 4.3 except for 16 August 1983, 0000 GMT.

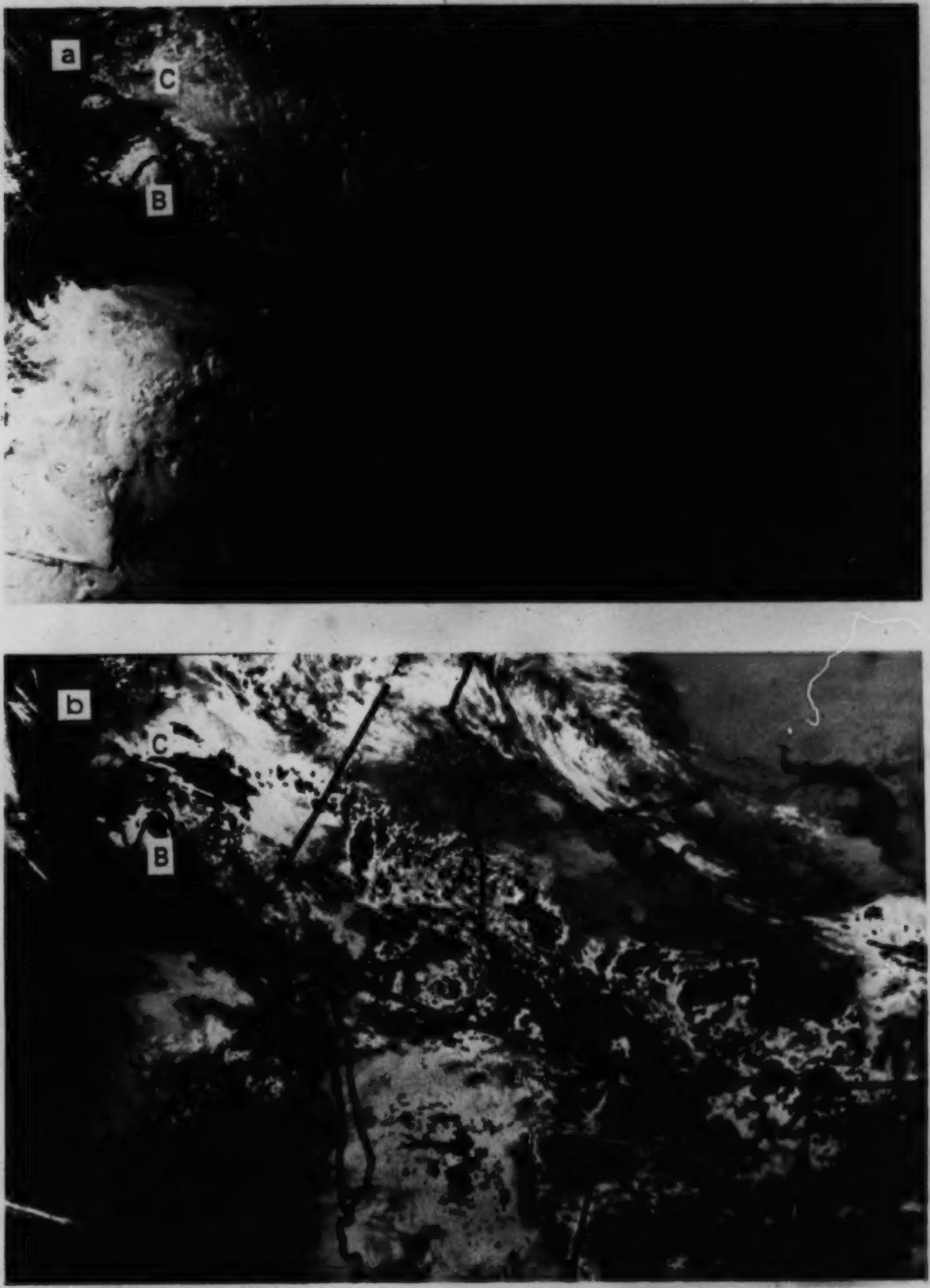

Figure 4.58 NOAA-8 satellite image, a) visible, b) infrared, 0324 GMT, 16 August 1983.

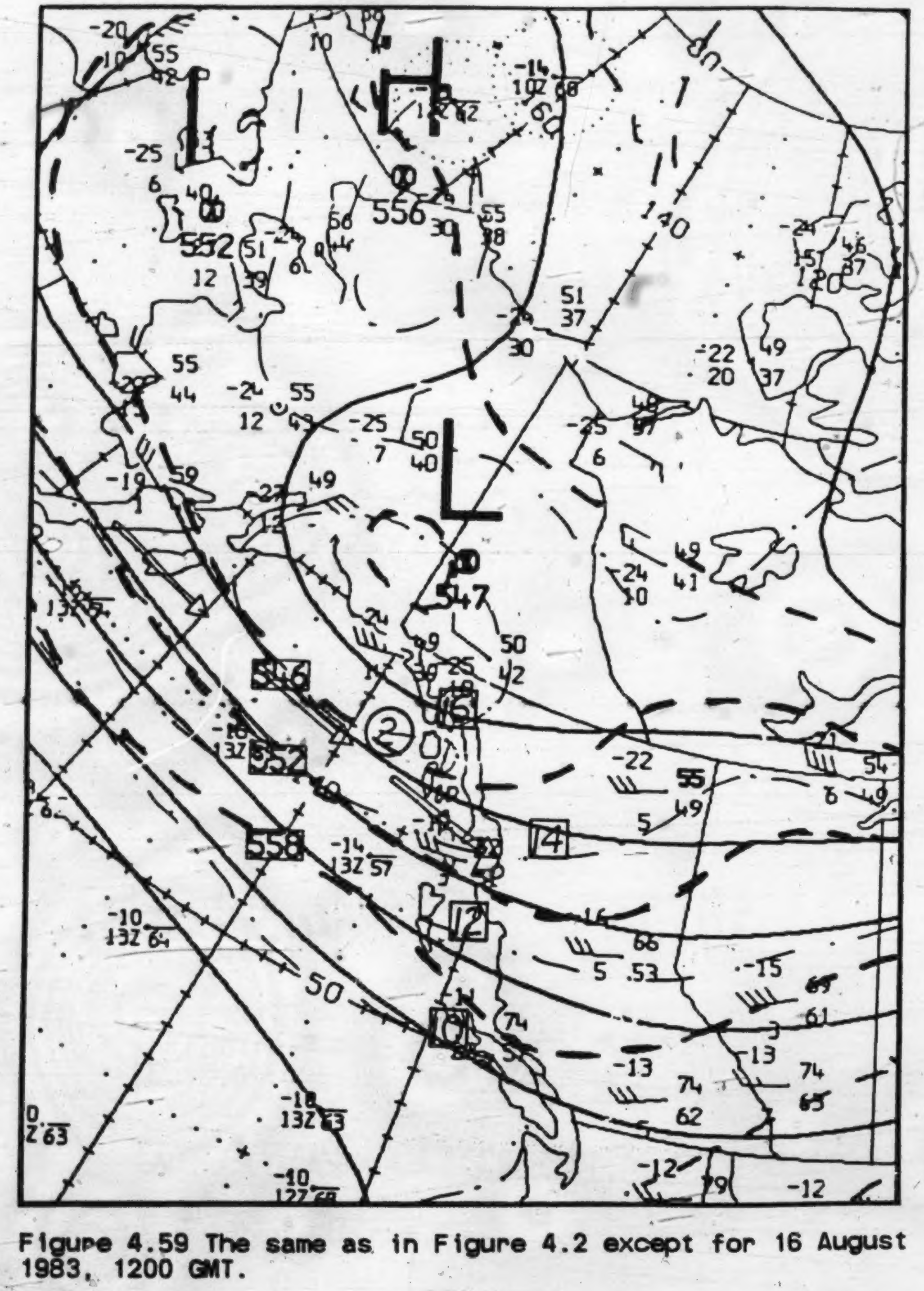
L
H
L
552
556
547
546
552
558
16
14
12
10
140
60
50
②

Figure 4.59 The same as in Figure 4.2 except for 16 August 1983, 1200 GMT.

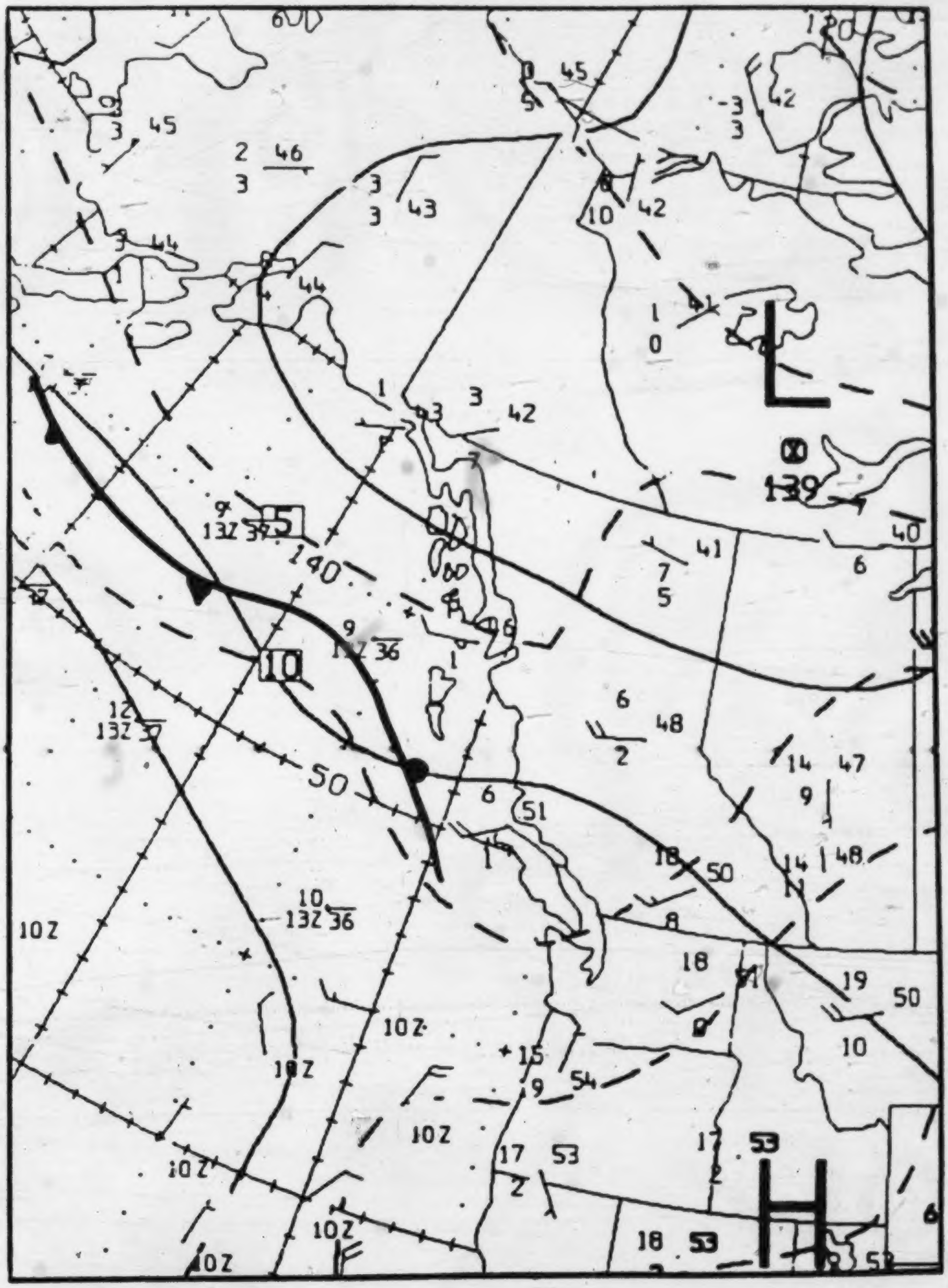
60
120
45
42
46
43
44
41
L
139
40
140
50
10
5
48
47
51
50
H
53
54
10Z
13Z 36
13Z 37

Figure 4.60 The same as in Figure 4.3 except for 16 August 1983, 1200 GMT.

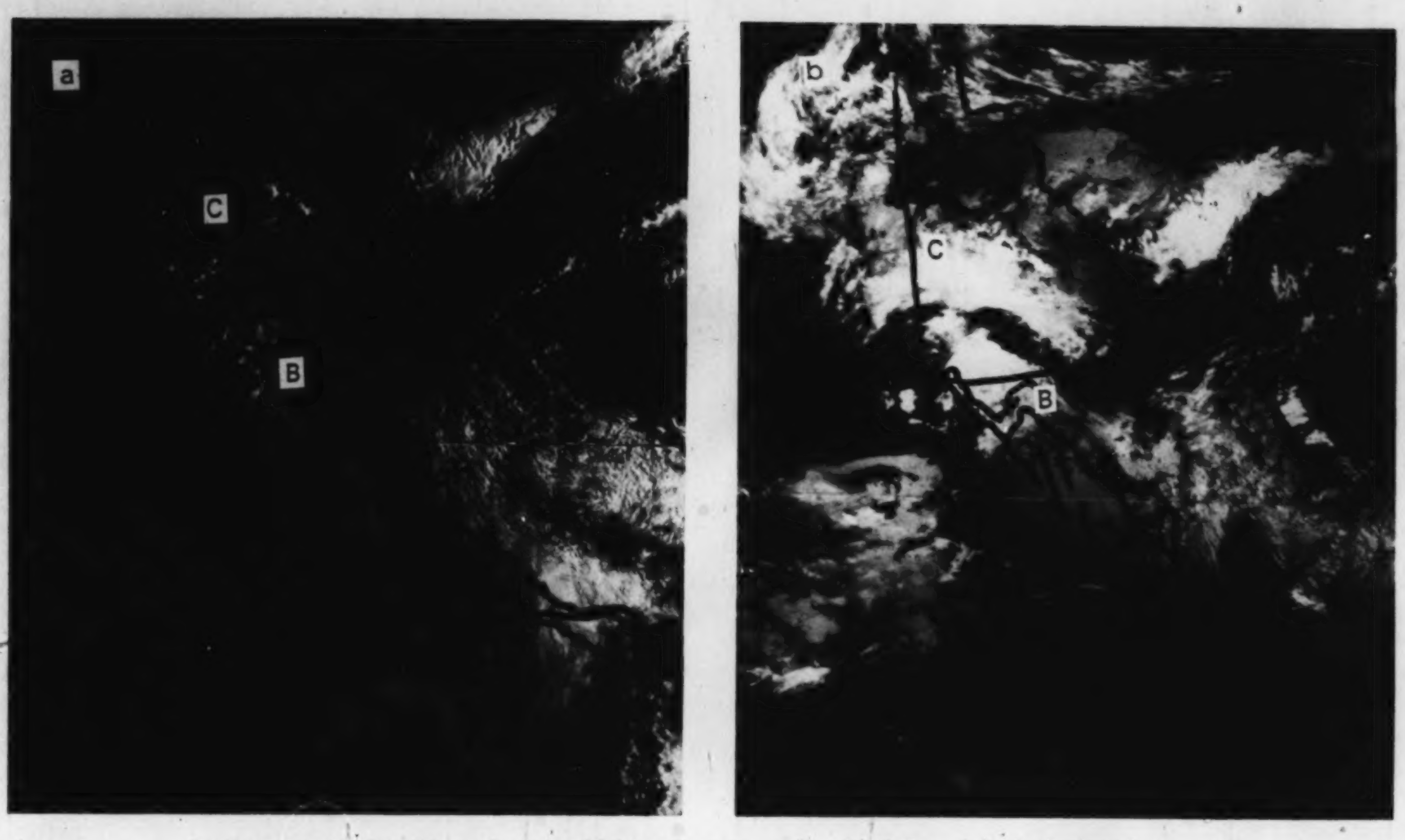

Figure 4.61 NOAA-8 satellite image, a) visible, b) infrared, 1658 GMT, 16 August 1983.

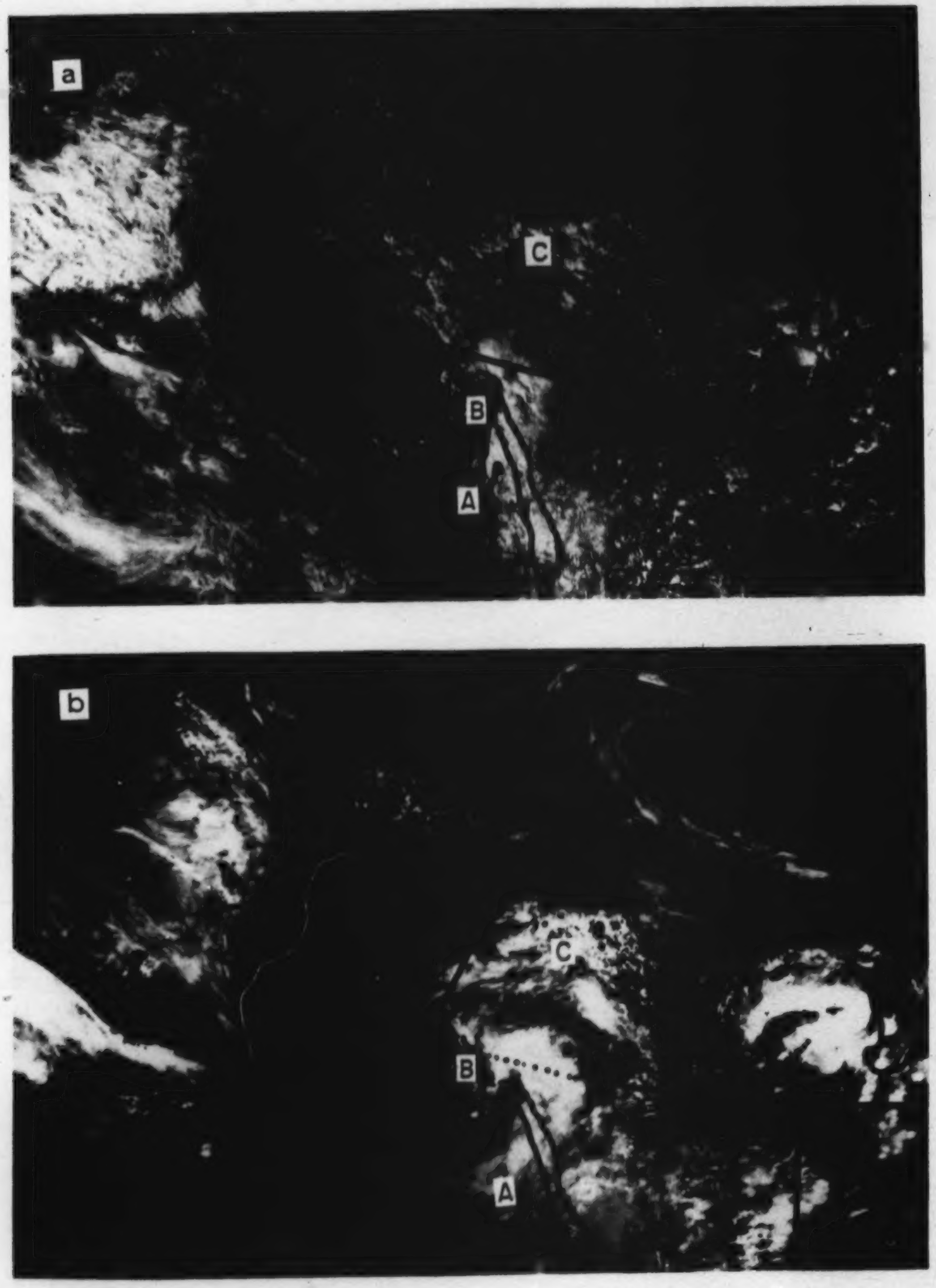

Figure 4.62 NOAA-7 satellite image, a) visible, b) infrared, 2315 GMT, 16 August 1983.

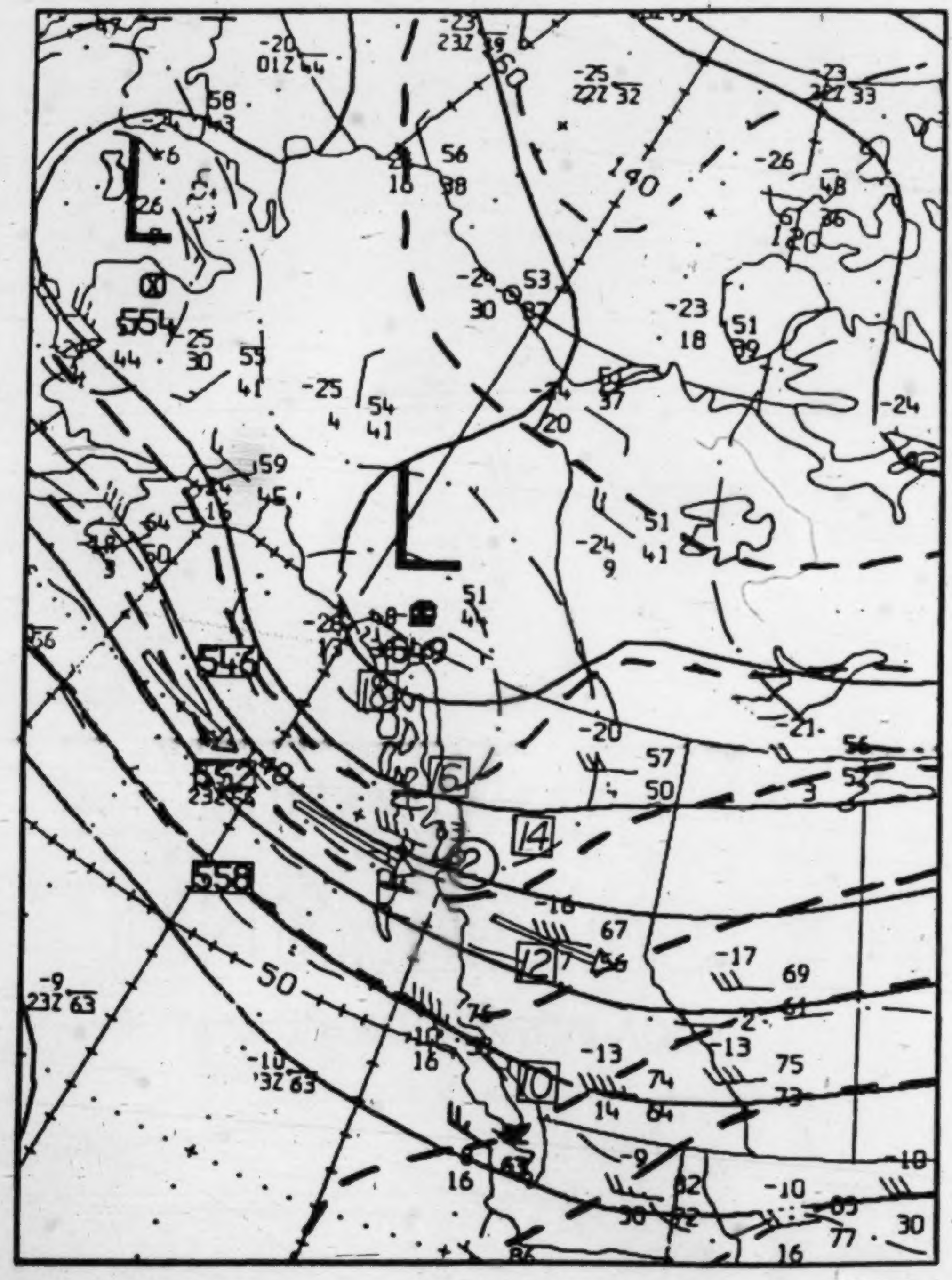

Figure 4.63 The same as in Figure 4.2 except for 17 August 1983, 0000 GMT.

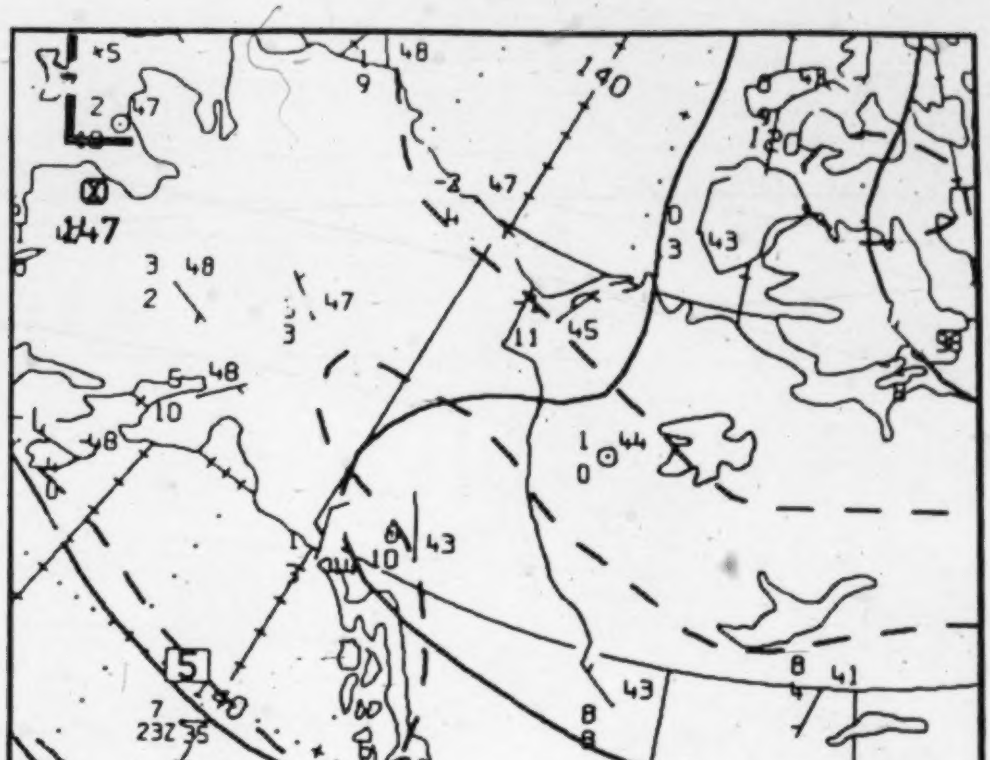
140
120
5
140
10
50
47
48
43
45
44
41
49
51
53
52
50
37
35
36

Figure 4.64 The same as in Figure 4.3 except for 17 August 1983, 0000 GMT.

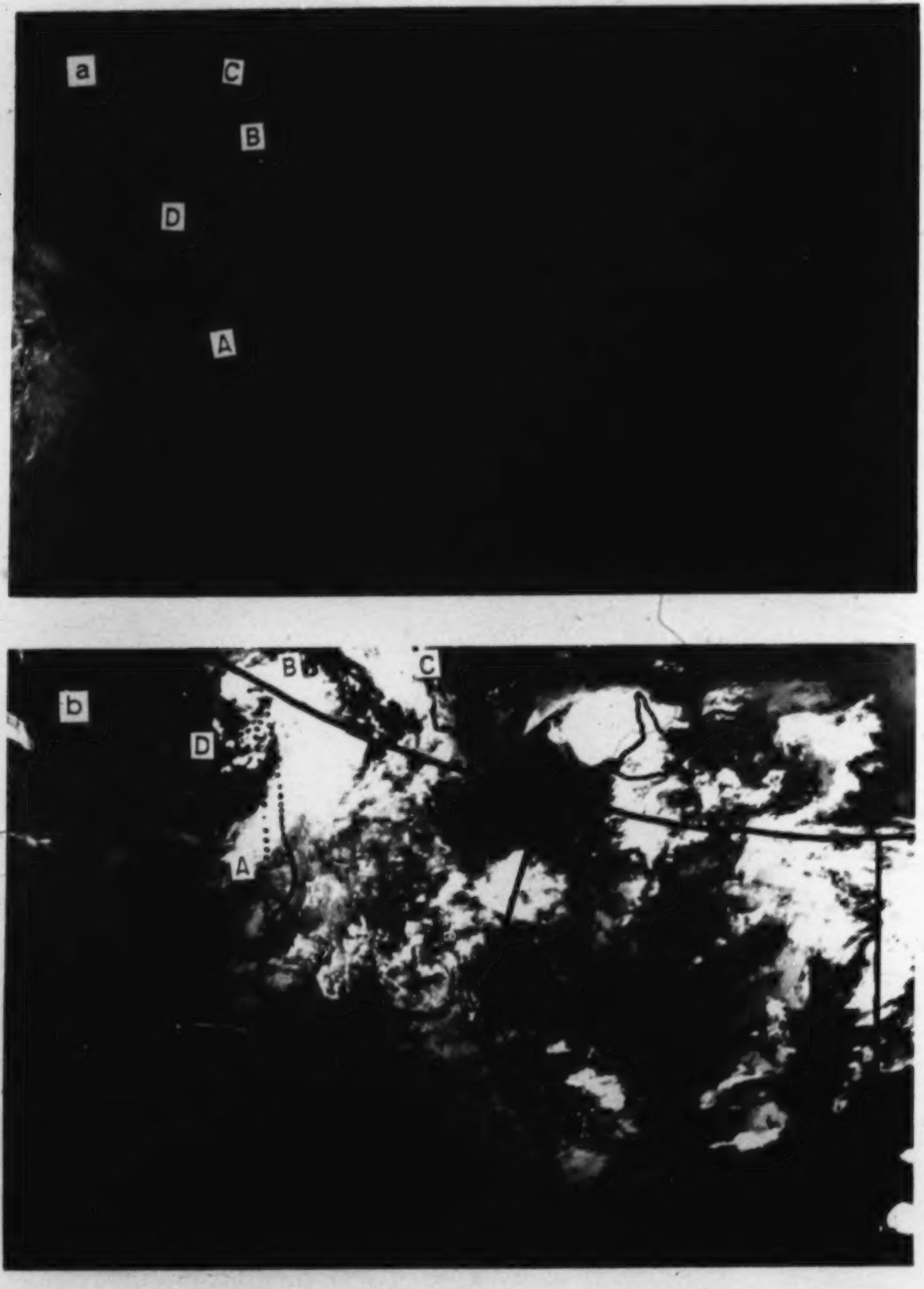
a
C
B
D
A
b
B
C
D
A

Figure 4.65 NOAA-8 satellite image, a) visible, b) infrared, 0240 GMT, 17 August 1983.

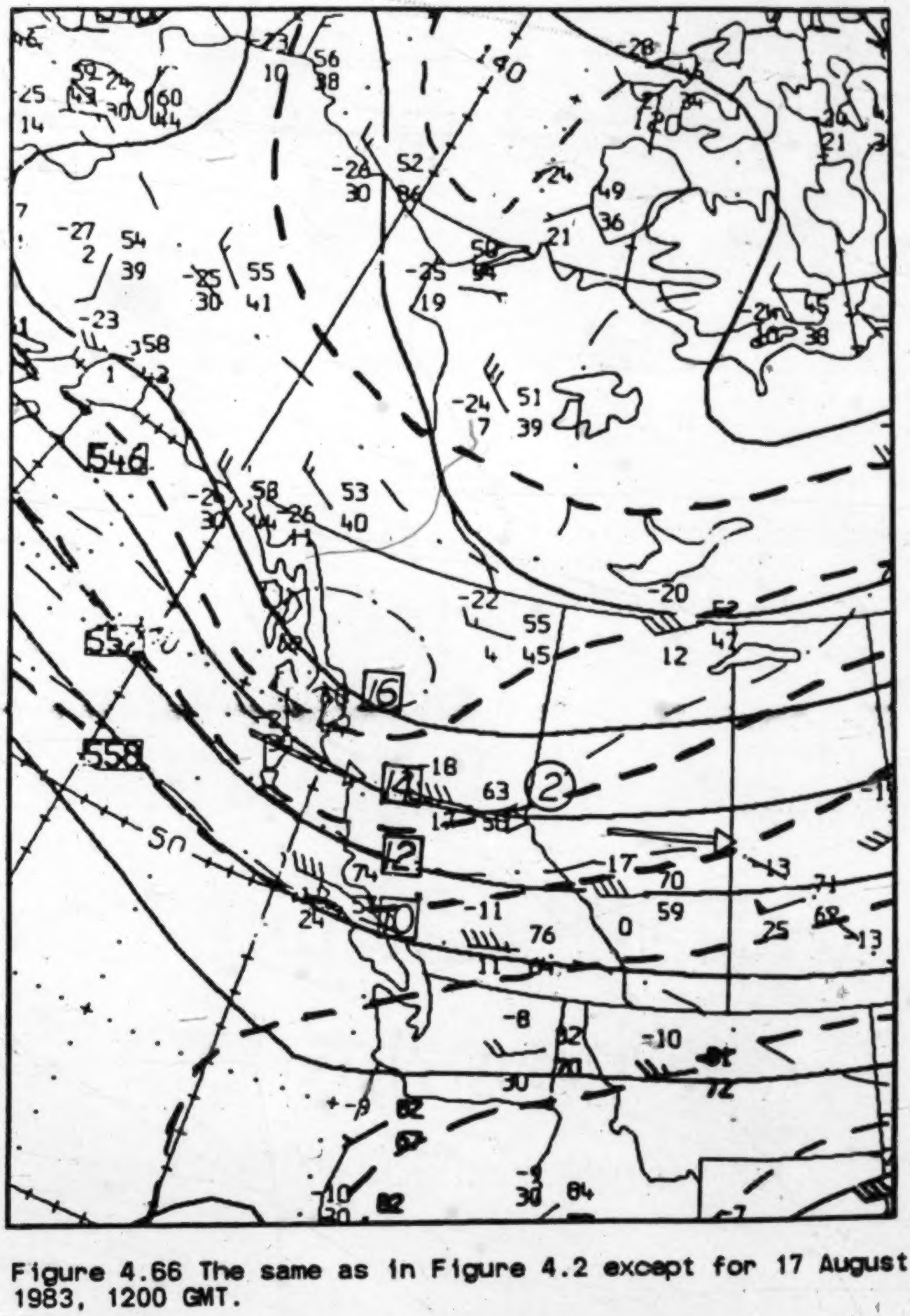
140
120
546
552
558
16
14
12
10
2
50

Figure 4.66 The same as in Figure 4.2 except for 17 August 1983, 1200 GMT.

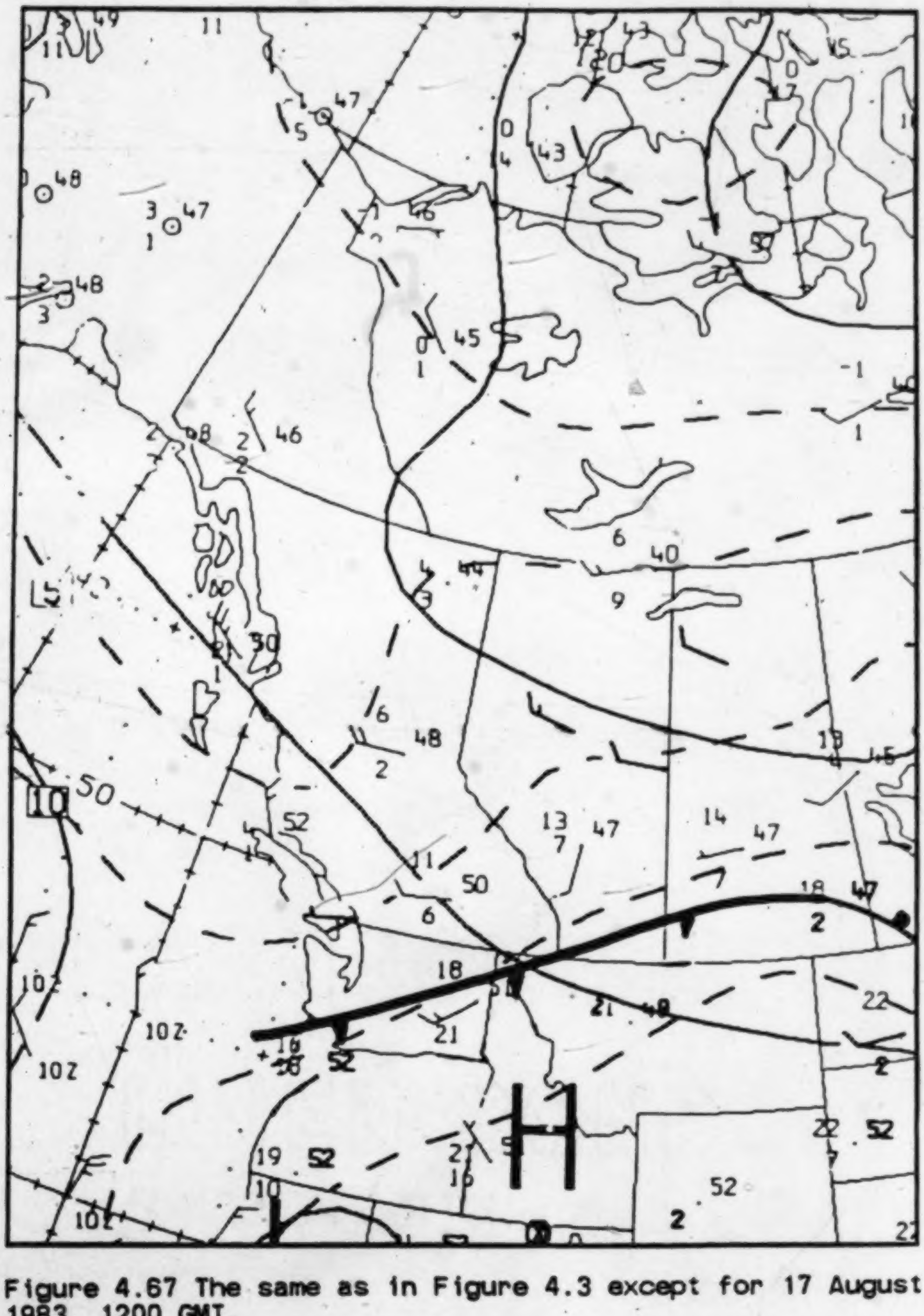

Figure 4.67 The same as in Figure 4.3 except for 17 August 1983, 1200 GMT.

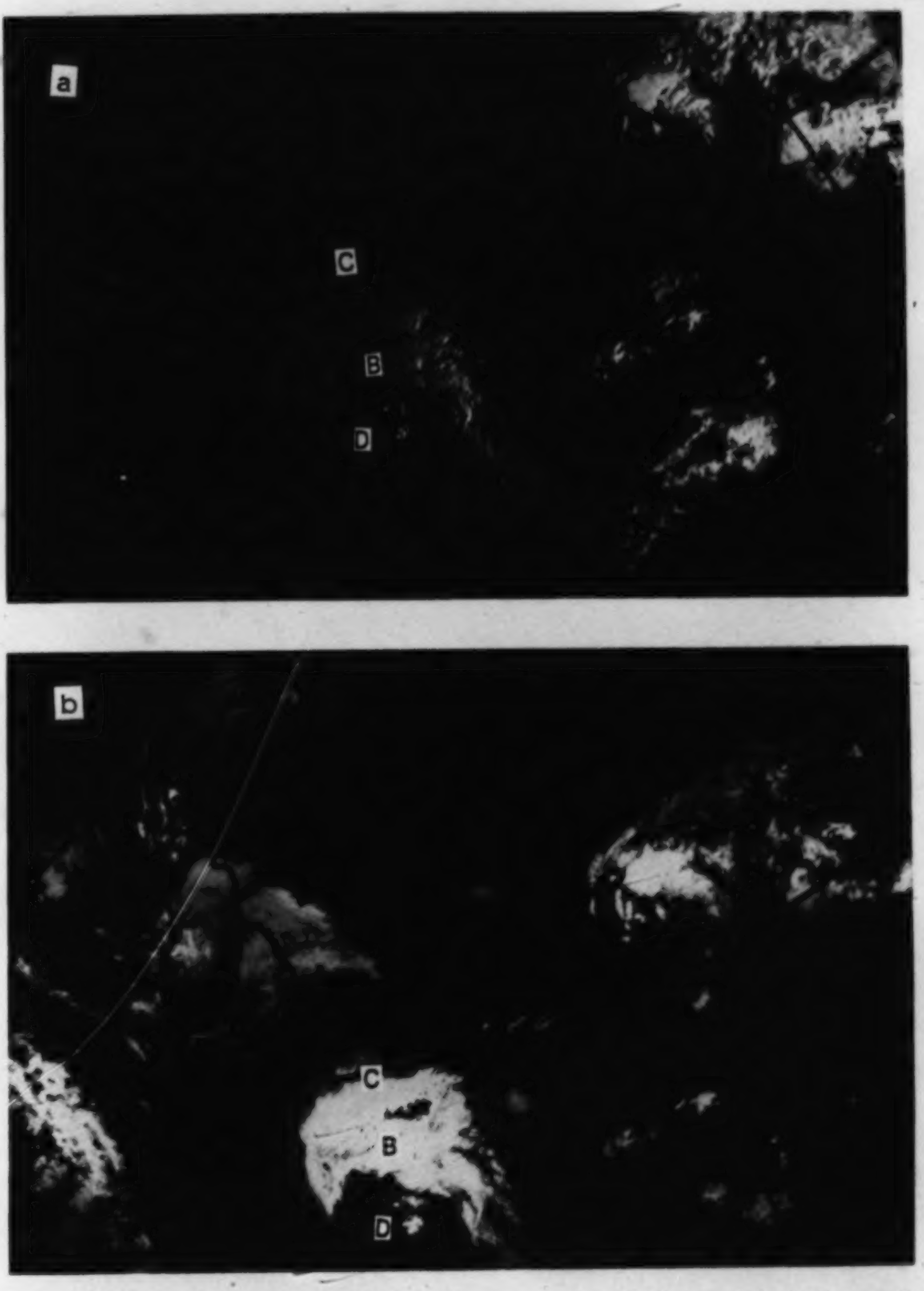

Figure 4.68 NOAA-8 satellite image, a) visible, b) infrared, 1630 GMT, 17 August 1983.

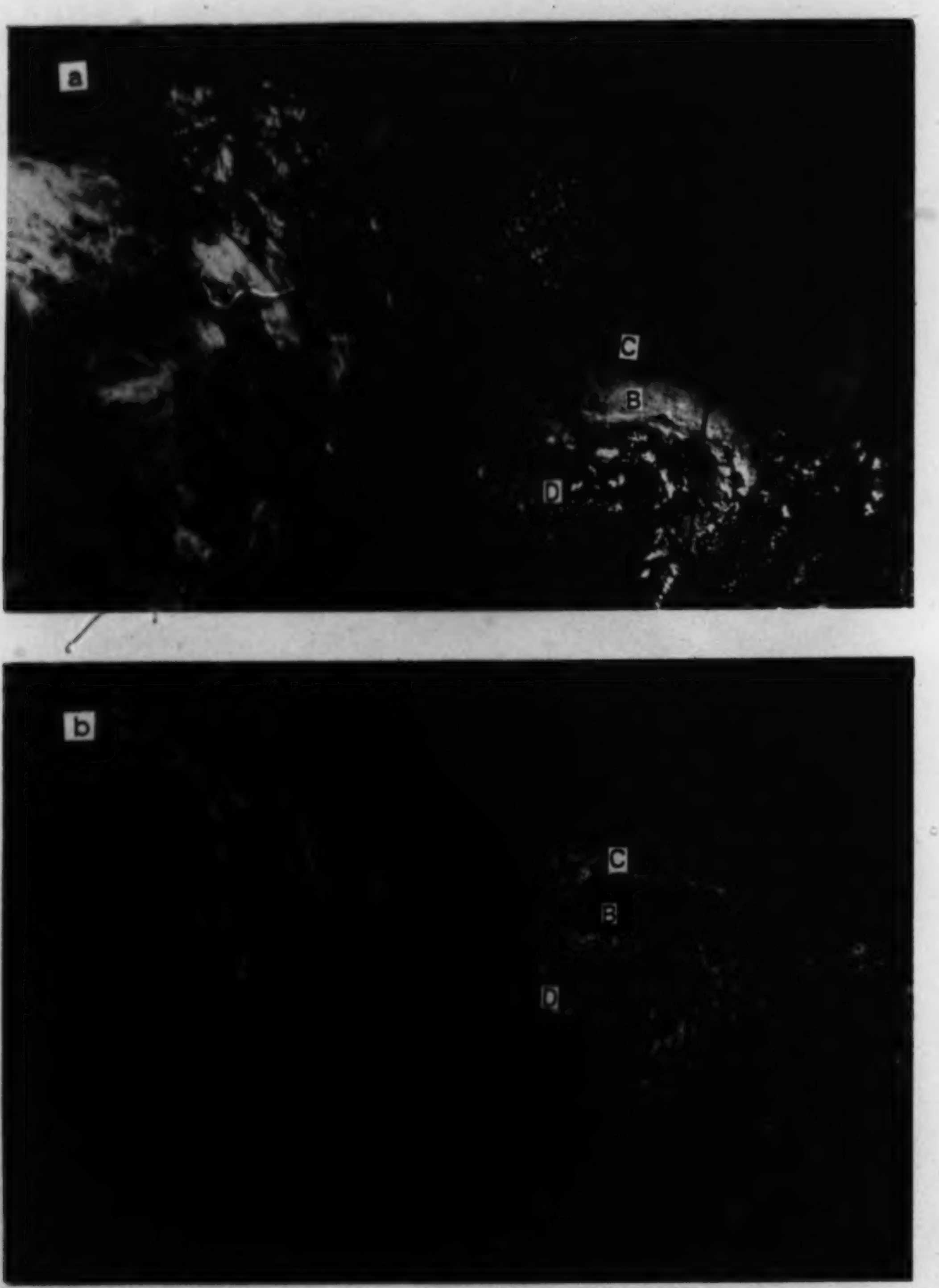

Figure 4.69 NOAA-7 satellite image, a) visible, b) infrared, 2302 GMT, 17 August 1983.

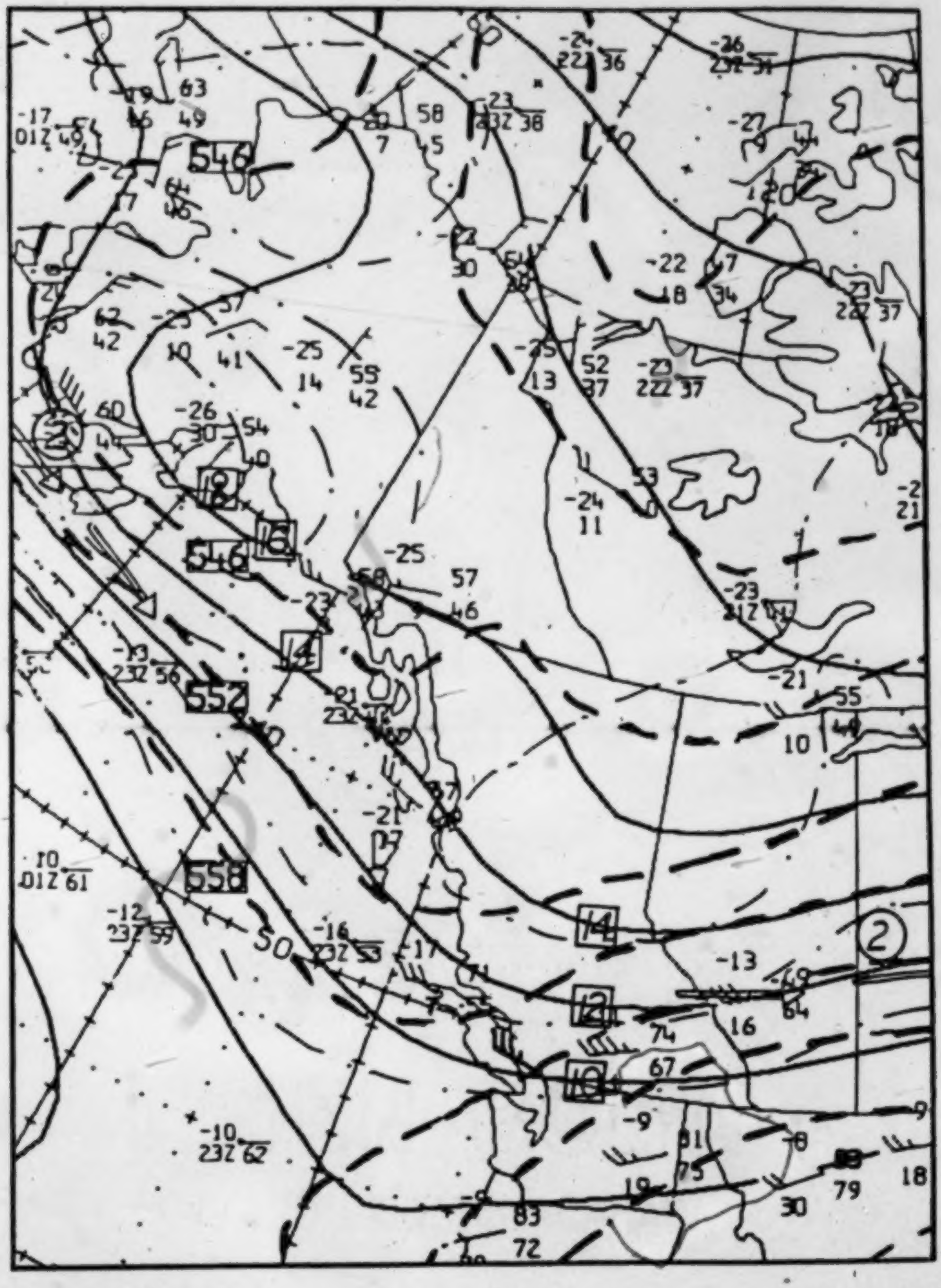
546
546
552
558
50
40
20
18
16
14
12
10
2

Figure 4.70 The same as in Figure 4.2 except for 18 August 1983, 0000 GMT.

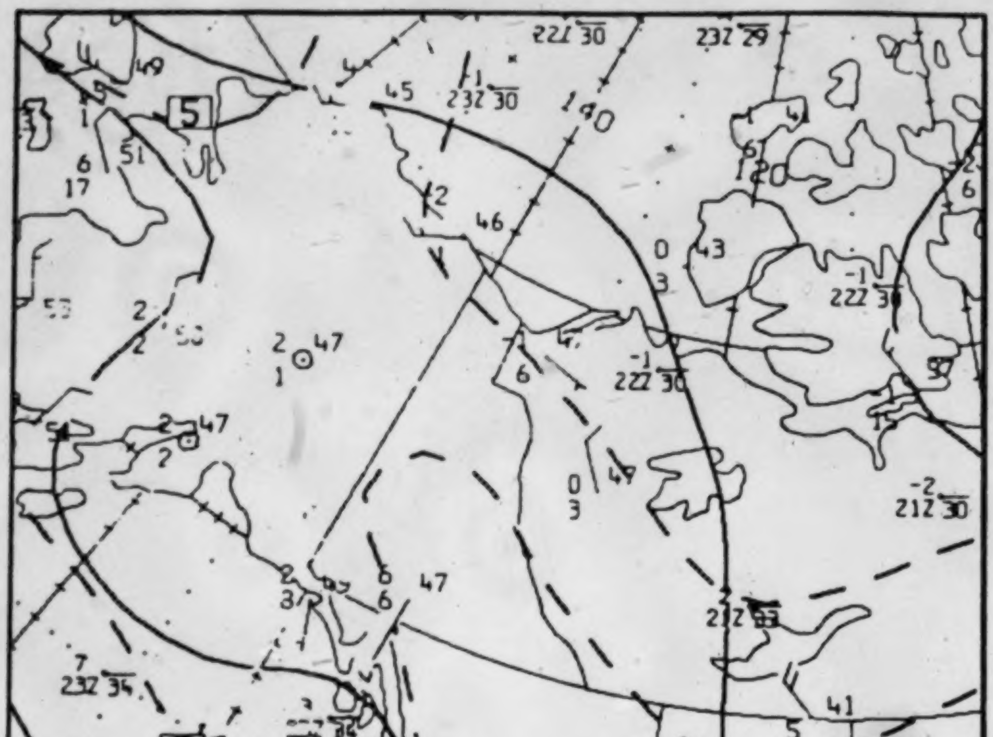
5
5
10
140
120
50
40

Figure 4.71 The same as in Figure 4.3 except for 18 August 1983, 0000 GMT.

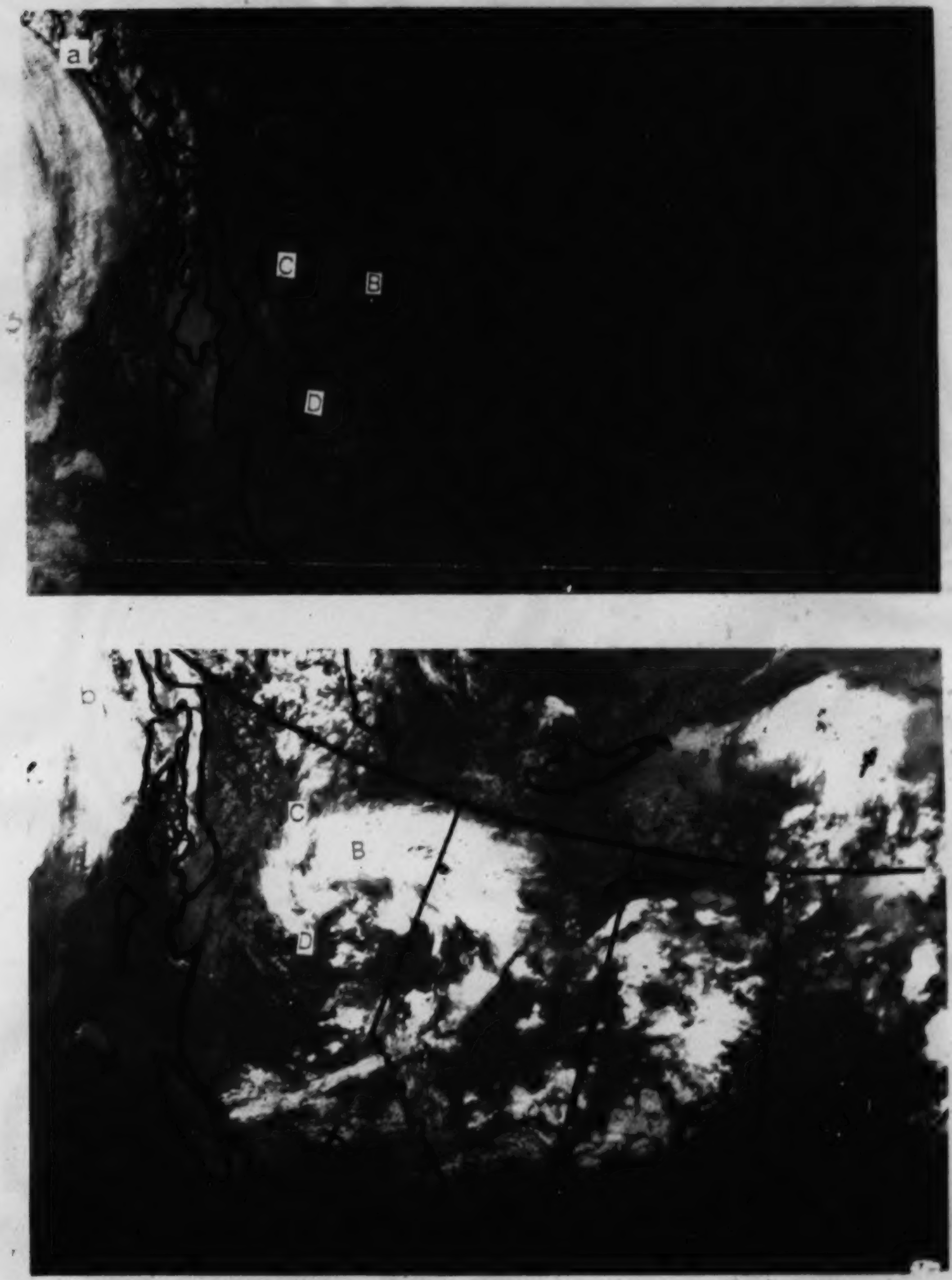

Figure 4.72 NOAA-8 satellite image, a) visible, b) infrared, 0218 GMT, 18 August 1983.

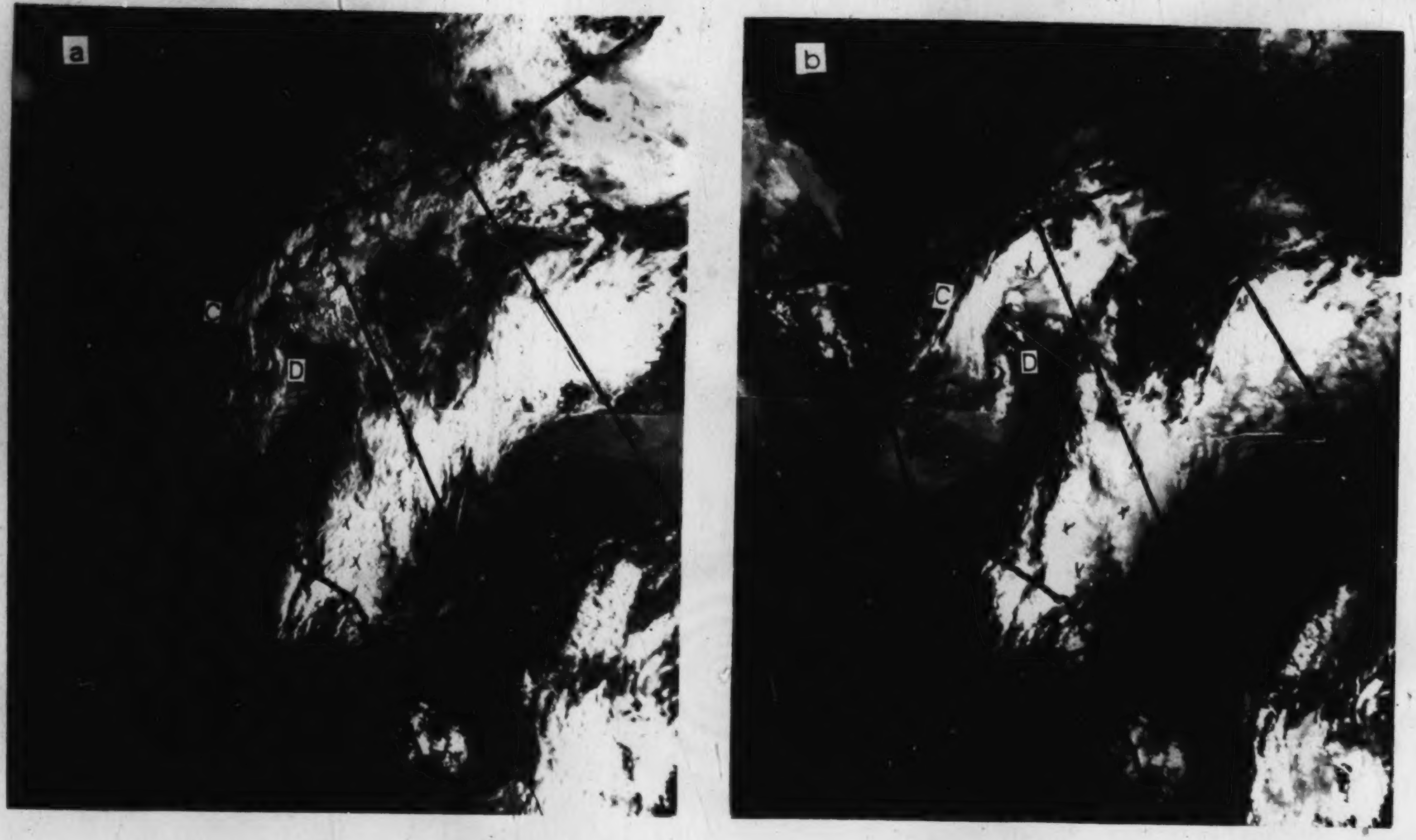

Figure 4.73 NOAA-8 satellite image, a) visible, b) infrared, 1609 GMT, 18 August 1983.

### 4.5 Case #4

This case is a second example of moderate development. The cloud pattern (Figures 4.78 and 4.82) resembles that of a storm but (B) did not gain a distinct comma shape. It is rather a modefied case where development took place at all levels at the same time. The system developed over the same area as Case #3 and also followed a similar track during the period from 1200 GMT, 18 August 1983 to 0000 GMT, 21 August 1983. The flow at low and high levels was better defined, while the jet stream track differed from that of a typical case of upper-level development. Several cloud areas (B) were initiated (see Figure 4.77) before one succeeded in developing later into a significant comma. Two other points should be noted: the cloud pattern was initiated and developed within a cold cyclonic vorticity area, and the cloud area (D) evolved into a distinct comma in the late stage (see Figures 4.81, 4.82 and 4.85).

The onset of formation can best be seen in Figure 4.69. Over an area centered at 60° N/ 150° W, convective clouds developed. Looking at the mid-level pattern in Figures 4.76 - 4.77 and taking the system motion into consideration, one will notice the quick transformation of the cumuliform clouds into a quasi-storm cloud pattern within about twelve hours. Meanwhile, the synoptic maps (Figures 4.70, 4.71, 4.74 and 4.75) reveal a similar change. On the 500-mb surface (Figures 4.70 and 4.74) the mid-level trough dug SW-ward and pinched off at the neck of the trough, while jet (2) advanced towards the trough base. On the 850-mb level (Figures 4.71 and 4.74) a closed circulation has formed and a frontal system has approached the same area. In Figure 4.77, (B) has developed within a vorticity area greater than 16.

Later, in Figure 4.78, the cloud pattern has well developed with all cloud areas (A), (B), (C) and (D) present, although (B) has not evolved into a distinct comma. This is evident from the examination of Figure 4.78 and comparison of the visible and the enhanced infrared images. Figure 4.81 supports the development process. Considering the time difference between Figures 4.78 and 4.79, (B) is located within a cyclonic vorticity area greater than 16, whereas, (A) and the tail of (B) are in a region of PVA. In Figure 4.79, a closed circulation has formed while jet (2) moved further SE-ward. On the 850-mb surface (Figure 4.80) the low has deepened gradually and a cold air sector formed as well.

Twelve hours later (Figure 4.82), the cloud pattern has lost its tight and well-defined configuration, but has regained it again by 1547 GMT (Figure 4.85). According to the development assumption, the system was still strengthening. Cloud area (B) was under the influence of PVA and within the vorticity contour greater than 14. On the 500-mb surface (Figure 4.83), the trough and jet (2) moved eastward as the formally closed circulation opened up at the neck of the trough. In Figure 4.84, the low-level circulation has also passed its maximum intensity and the closed circulation has given way to a broad trough.

The cloud pattern continued moving NE-ward without significant change (see Figures 4.86 and 4.89). Only (D) has weakened considerably and become detached from the main cloud pattern. (B) was still considered strengthening. Examination of Figures 4.87 and 4.88 shows that the upper and low-level flow has now weakened and closed circulations no longer exist at any level.

The synoptic maps in Figures 4.90, 4.91, 4.92 and 4.93 depict the continual filling of the upper system. Pictorial evidence is provided by the satellite image in Figure 4.94, where the cloud pattern has dissipated.

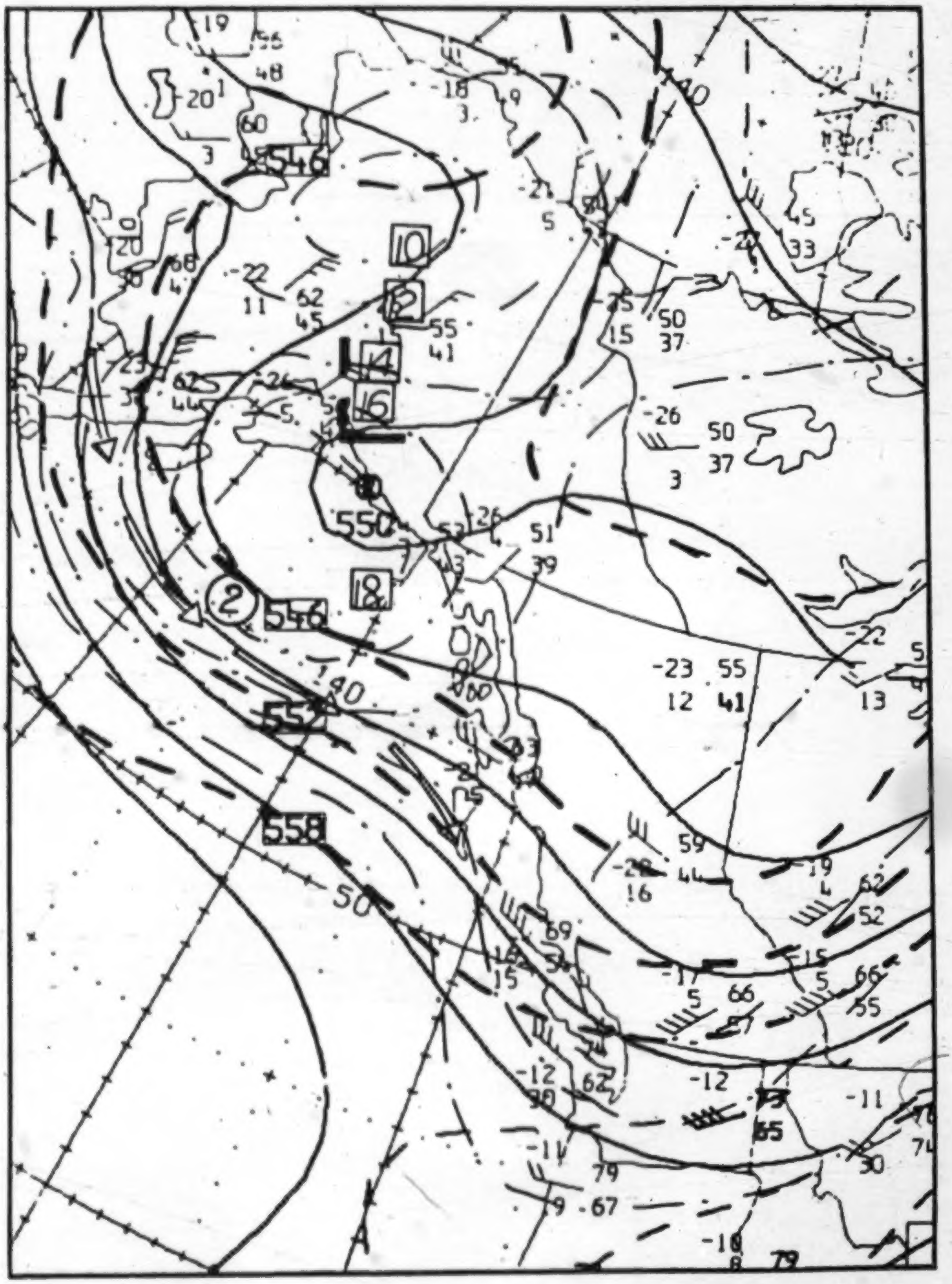
546
10
12
14
16
550
18
2
546
552
558
140
140
50

Figure 4.74 The same as in Figure 4.2 except for 18 August 1983, 1200 GMT.

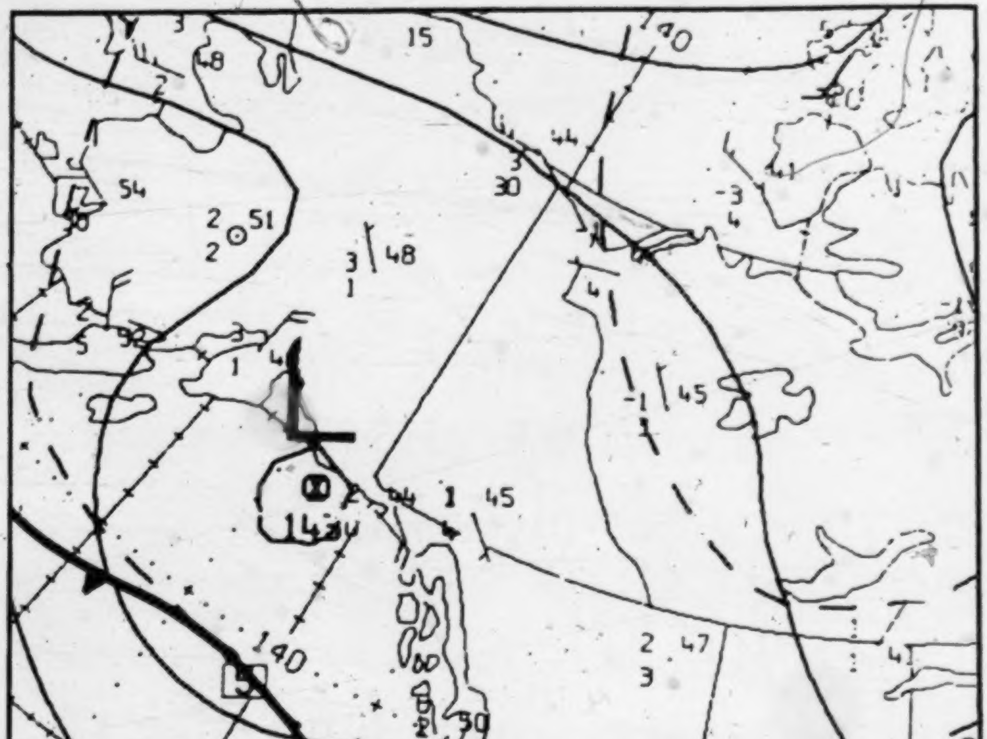
140
140
50
10
15
54
51
48
45
47
46
102

Figure 4.75 The same as in Figure 4.3 except for 18 August 1983, 1200 GMT.

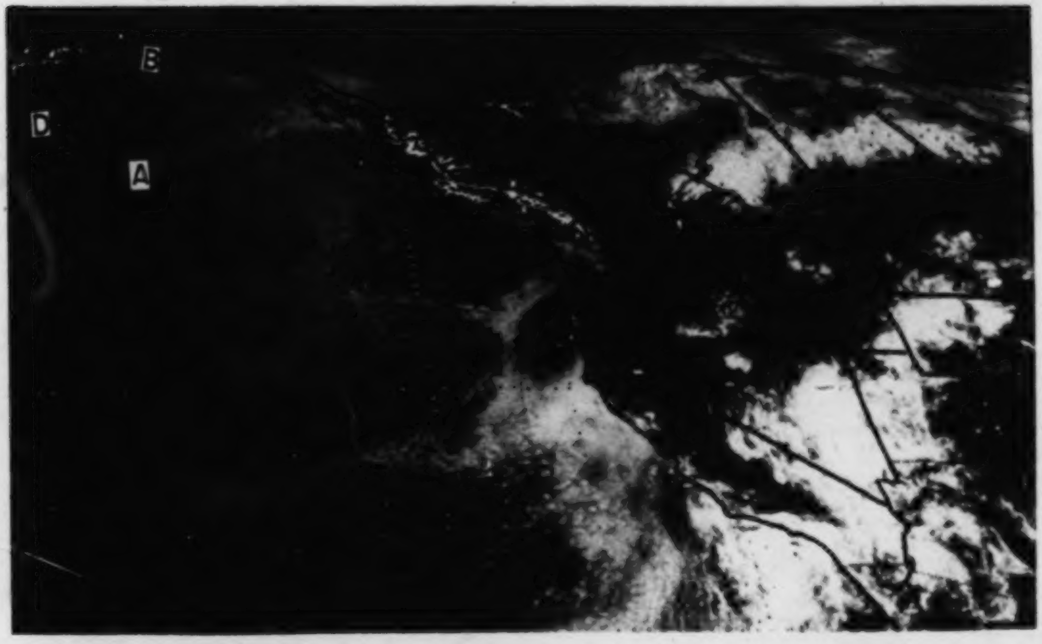

Figure 4.76 GOES-W satellite image, visible, 1515 GMT, 18 August 1983.

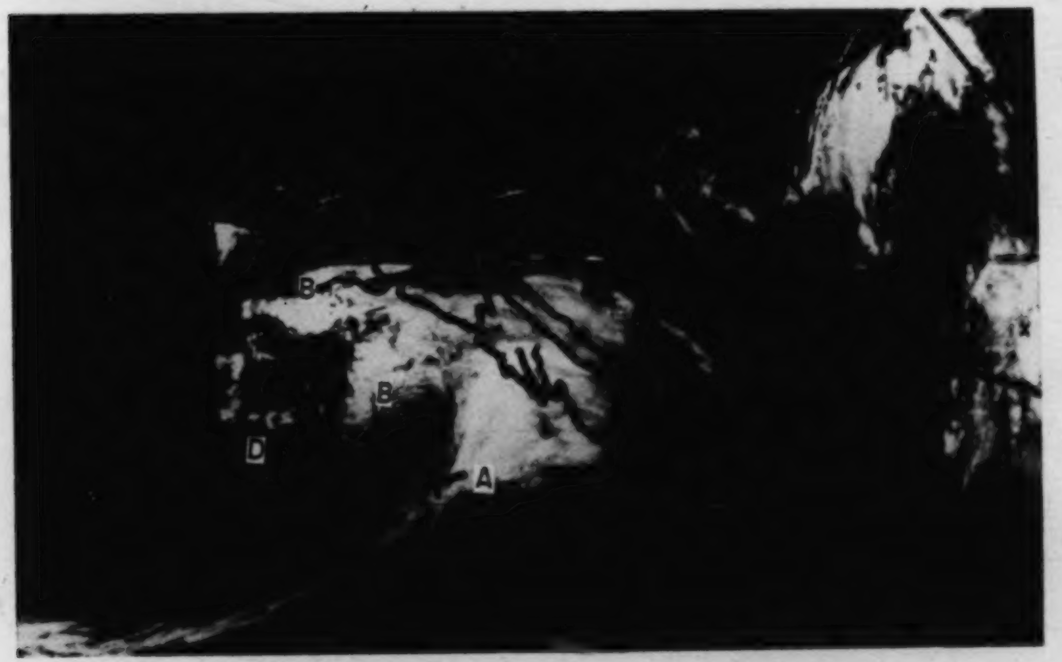

Figure 4.77 NOAA-7 satellite image, infrared, 1257 GMT, 18 August 1983.

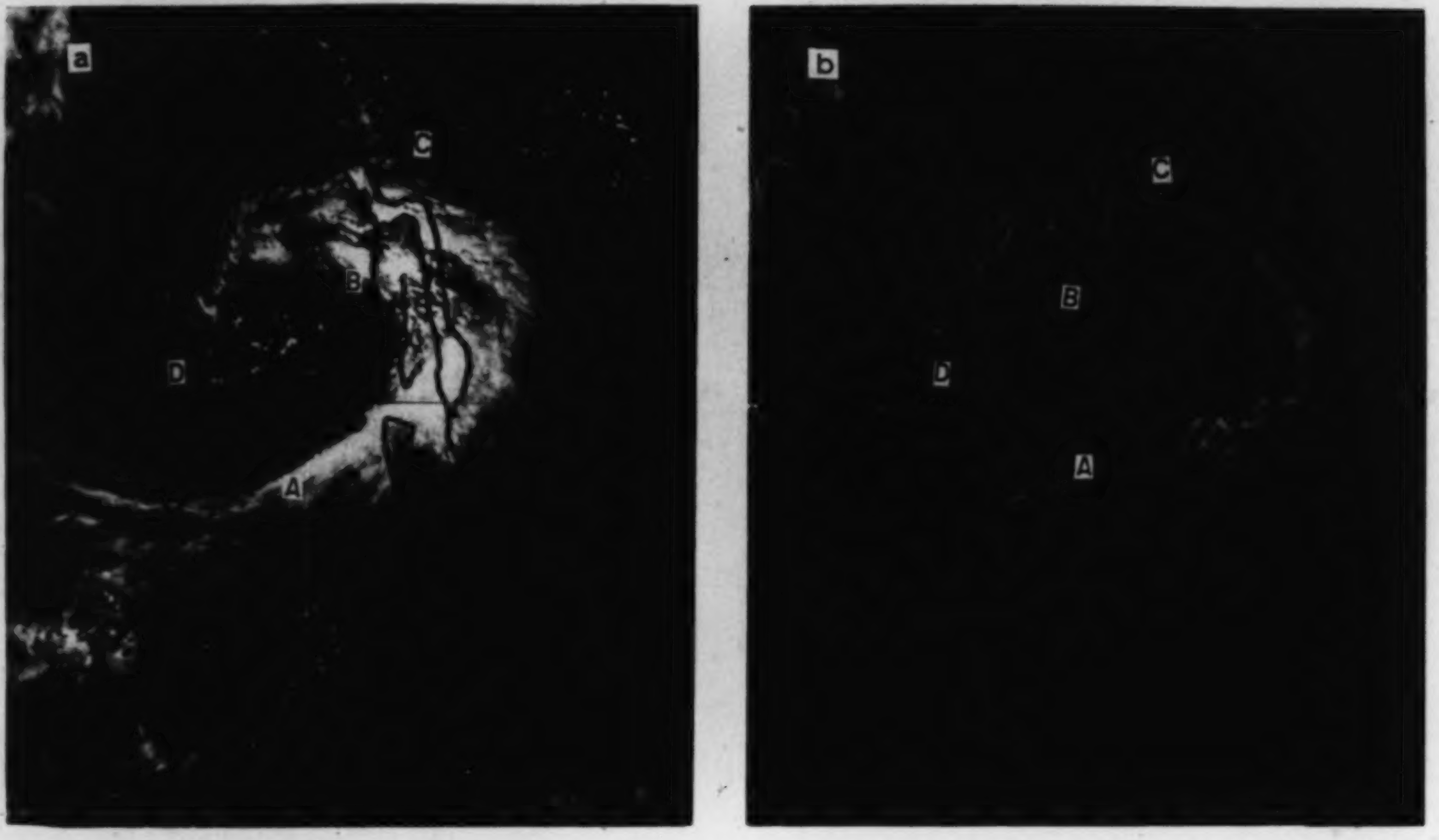
a
C
B
D
A
b
C
B
D
A

Figure 4.78 NOAA-7 satellite image, a) visible, b) infrared, 2250 GMT, 18 August 1983.

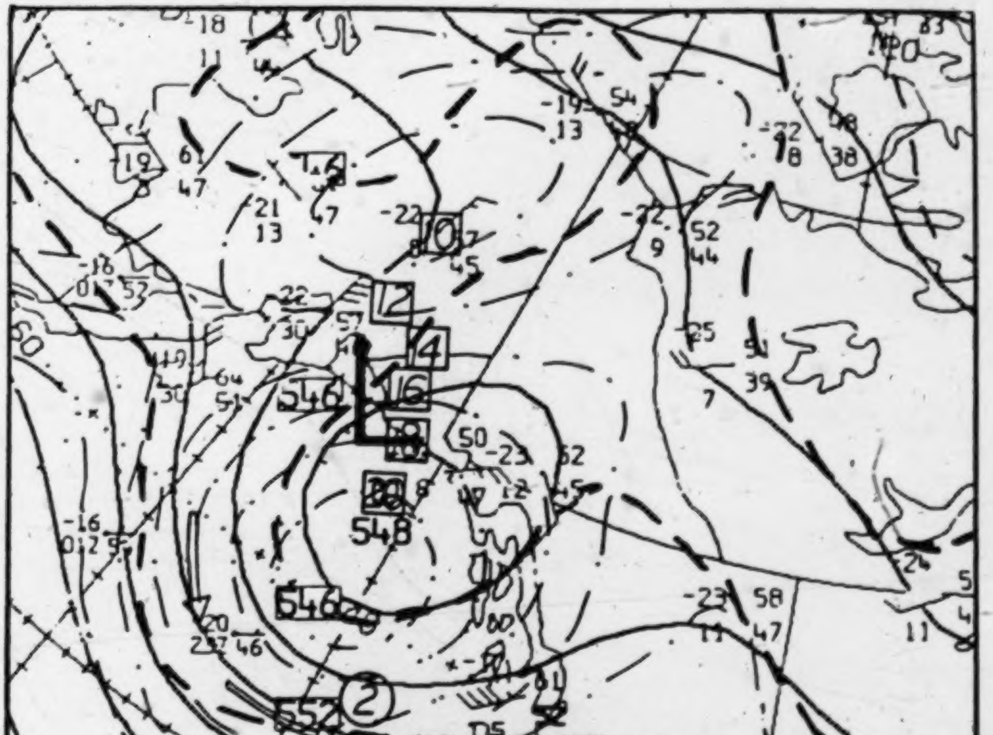
546
548
546
552
558
10
12
14
16
18
20
2
12
10

Figure 4.79 The same as in Figure 4.2 except for 19 August 1983, 0000 GMT.

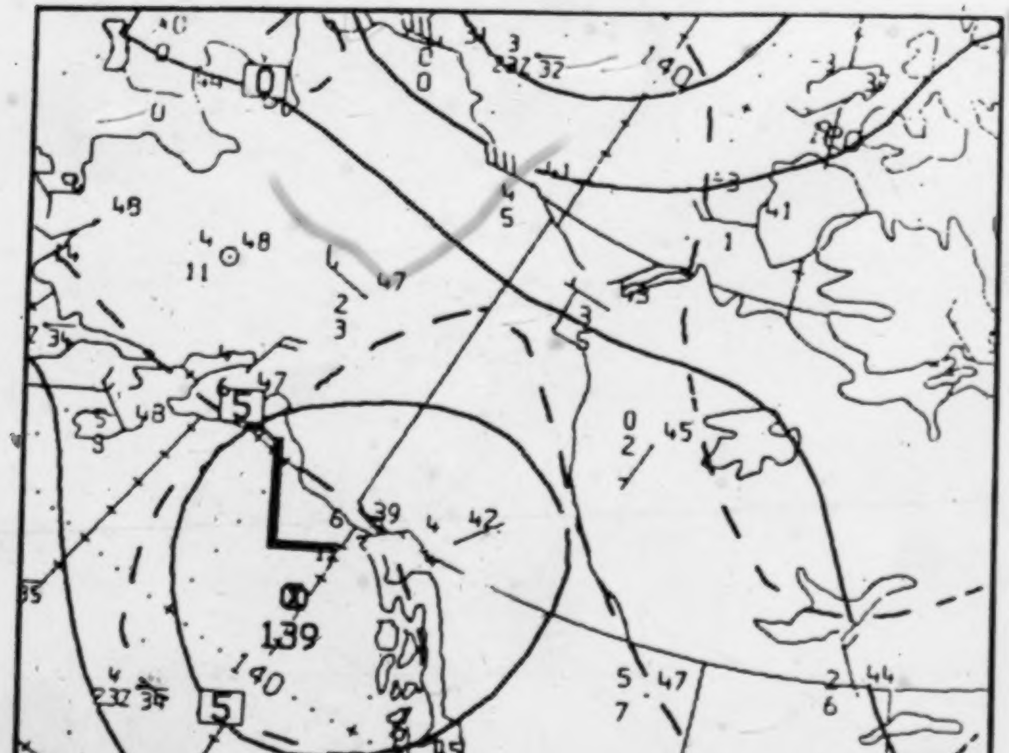
0
5
5
10
139
140
140
180

Figure 4.80 The same as in Figure 4.3 except for 19 August 1983, 0000 GMT.

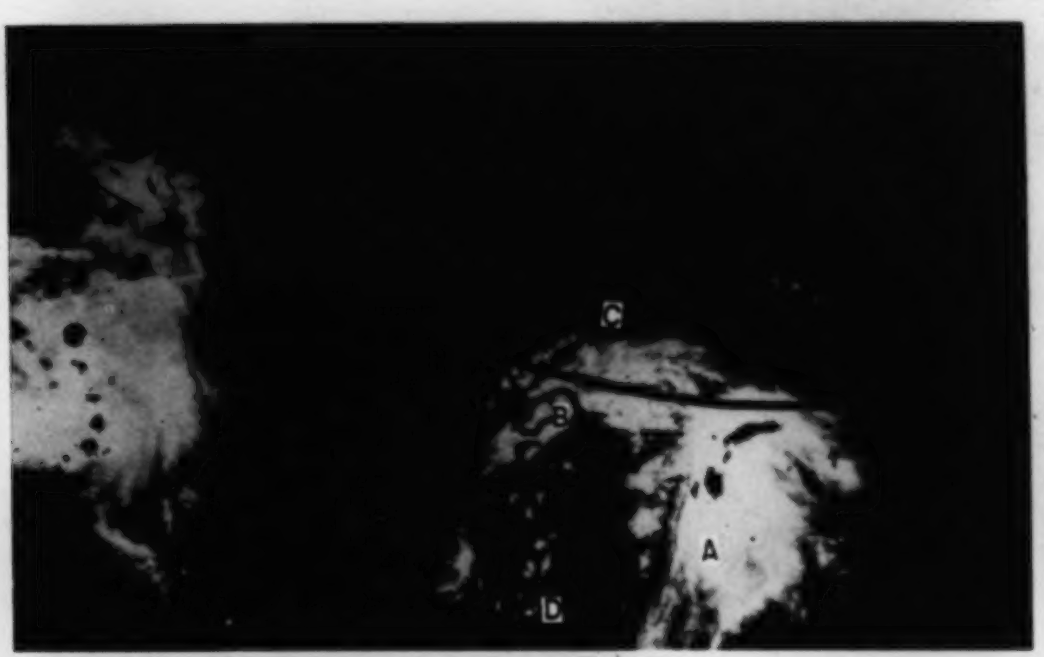

Figure 4.81 NOAA-8 satellite image , infrared, 0338 GMT, 19 August 1983.

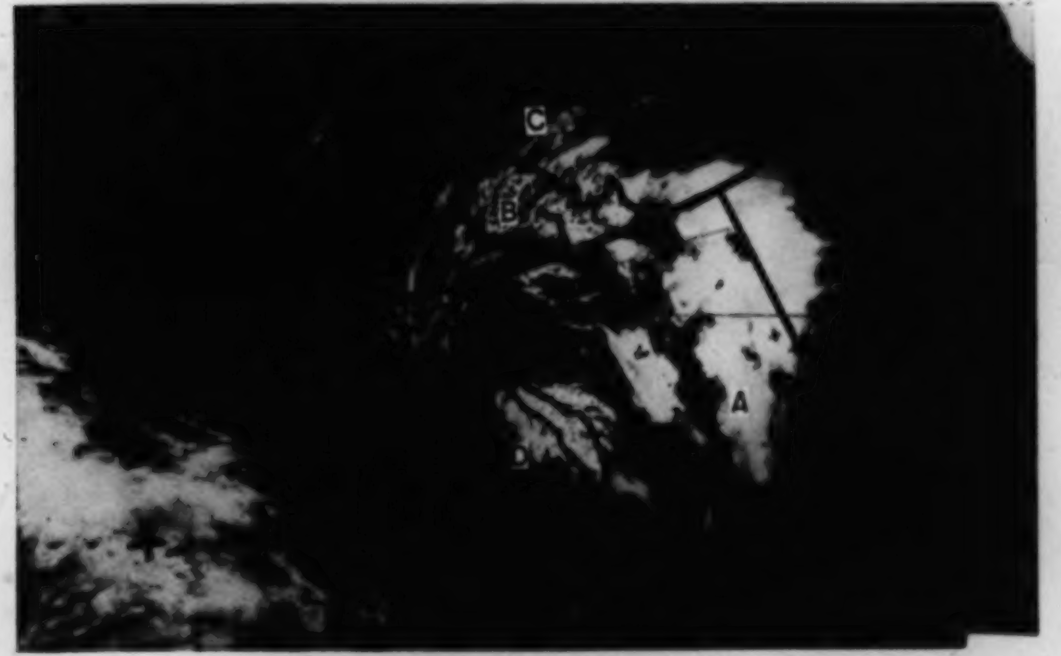

Figure 4.82 NOAA-7 satellite image , infrared, 1245 GMT, 19 August 1983.

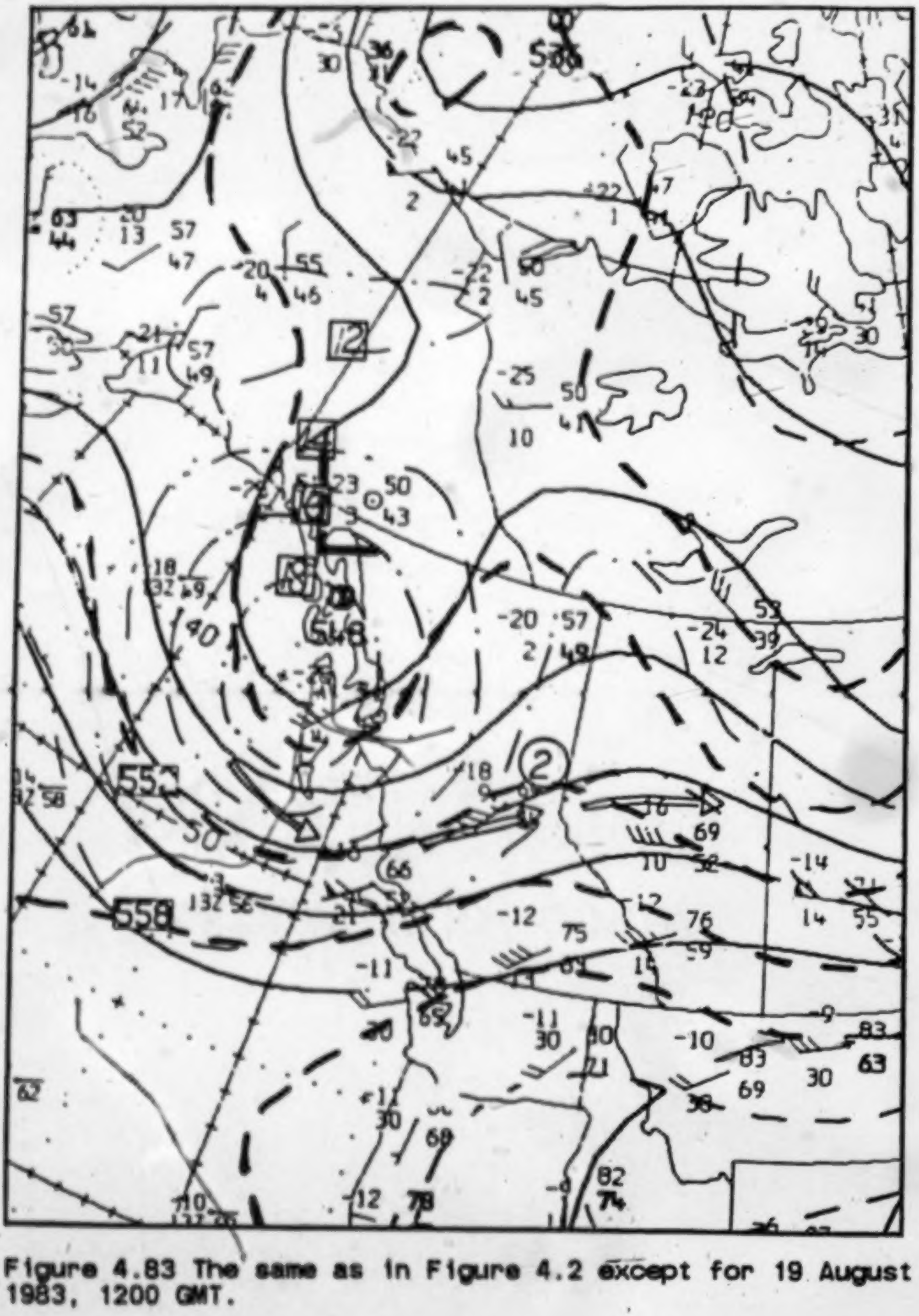

Figure 4.83 The same as in Figure 4.2 except for 19 August 1983, 1200 GMT.

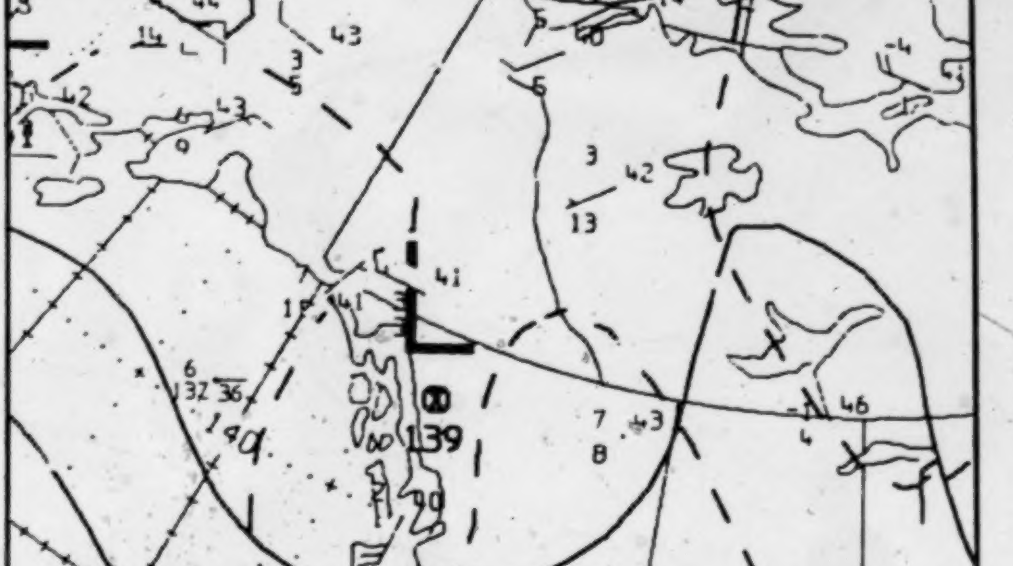
L
L
H
139
140
148
155
50
10
10
37
43
42
41
46
45
49
52
51
13Z
10Z

Figure 4.84 The same as in Figure 4.3 except for 19 August 1983, 1200 GMT.

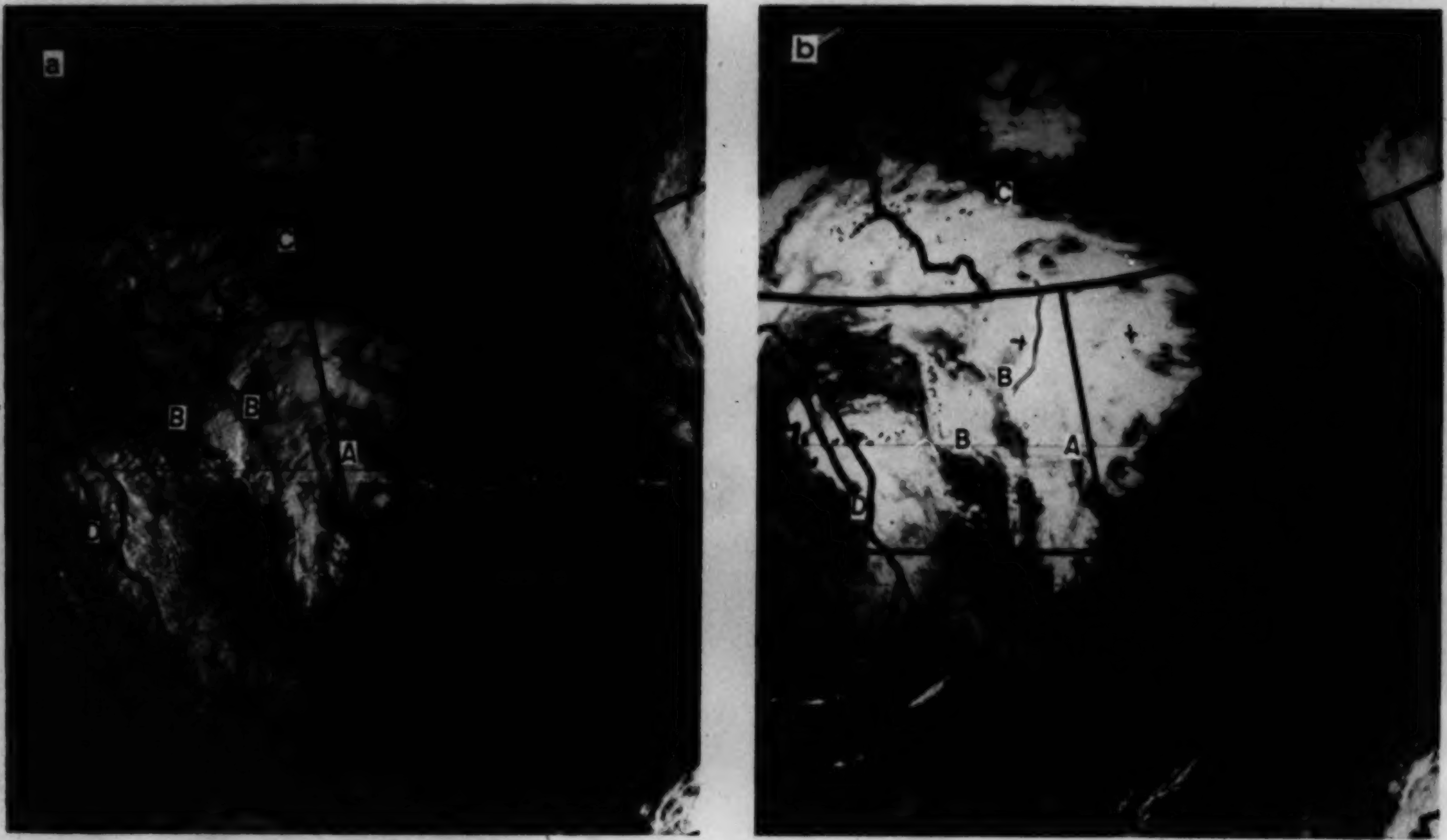
a
C
B
B
A
D
b
C
B
B
A
D

Figure 4.85 NOAA-8 satellite image, a) visible, b) infrared, 1547 GMT, 19 August 1983.

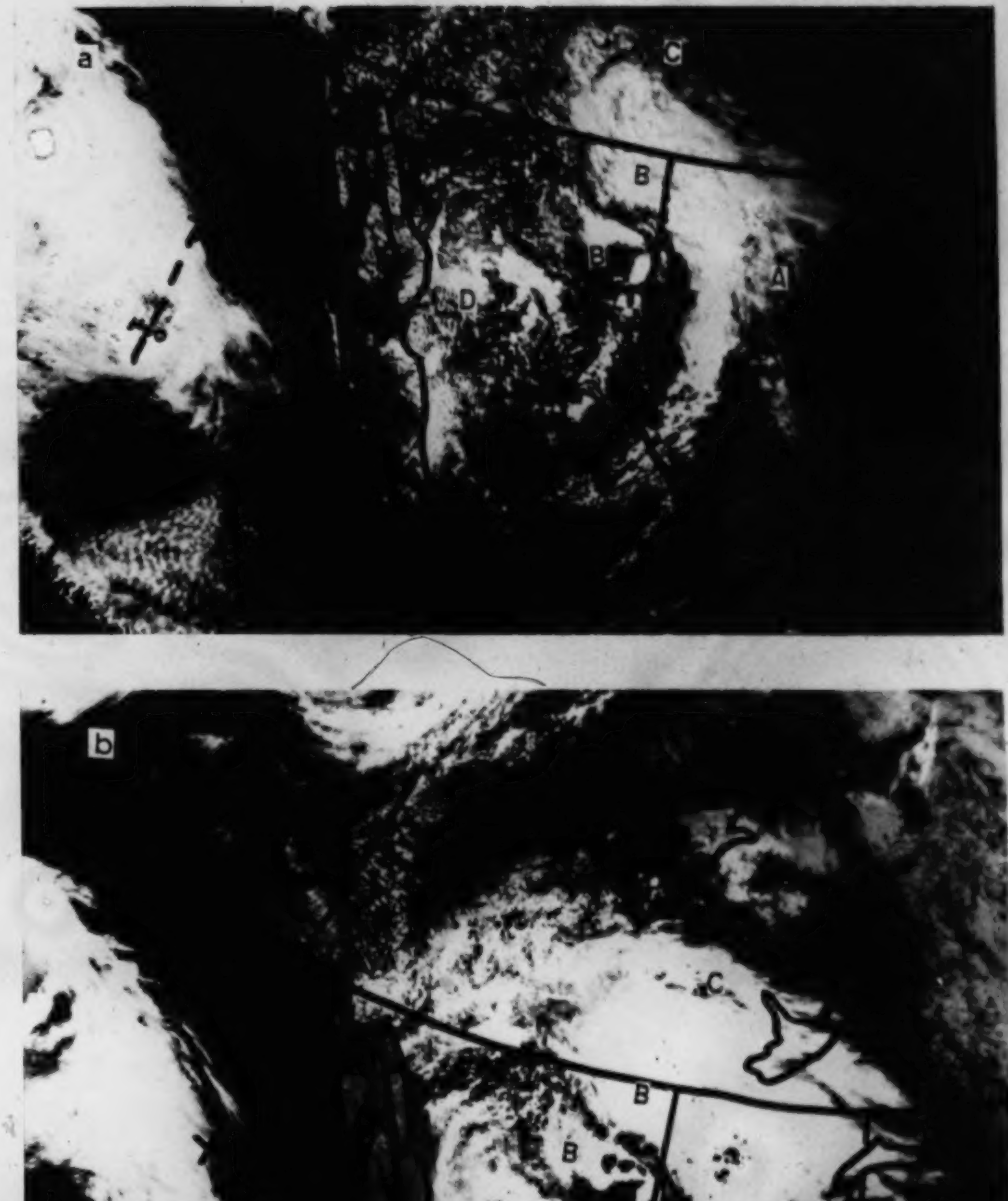
a
C
B
B
A
D
b
C
B
B
D
A

Figure 4.86 NOAA-7 satellite image, a) visible, b) infrared, 2237 GMT, 19 August 1983.

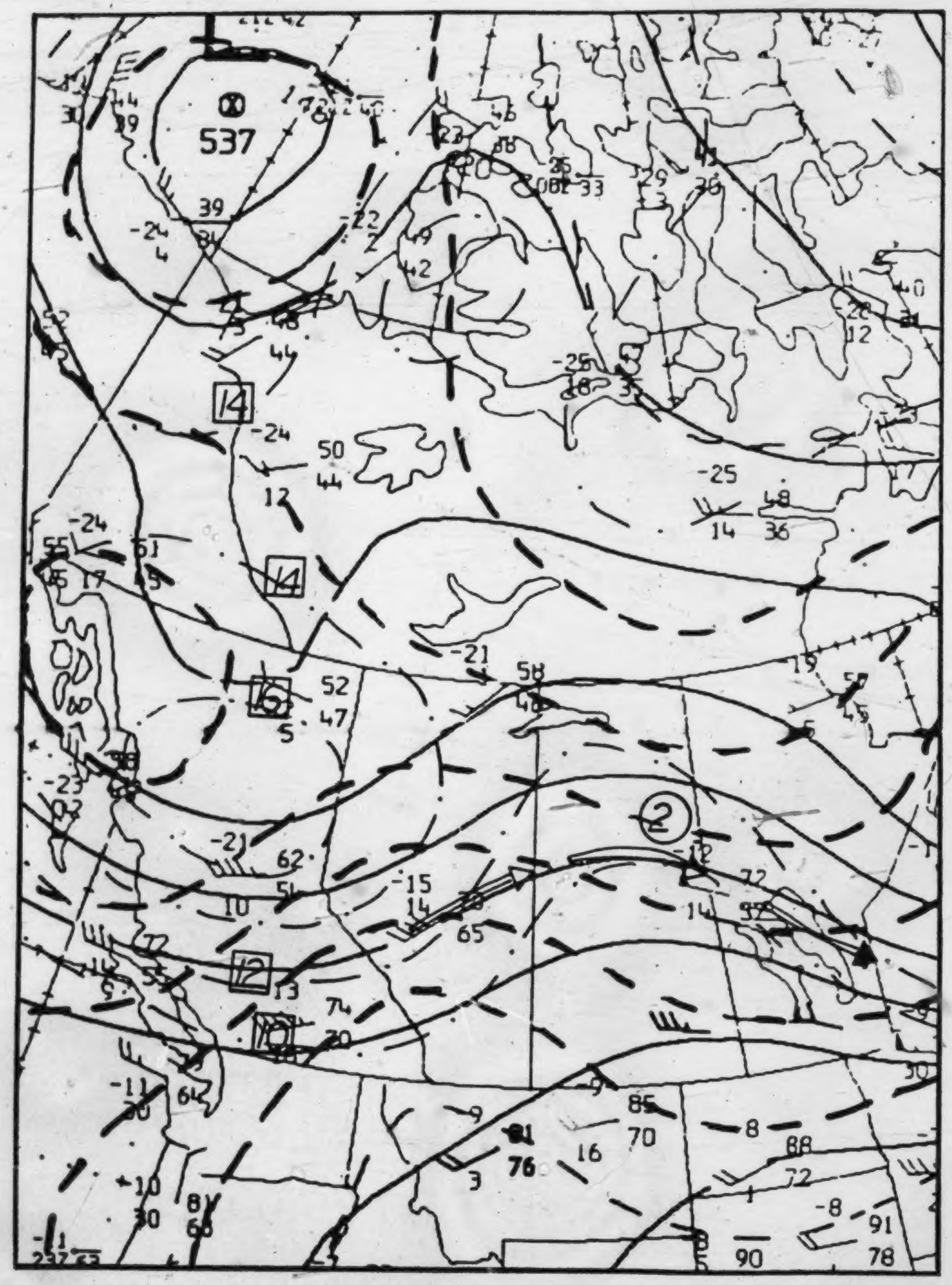
537
14
14
16
12
10
2

Figure 4.87 The same as in Figure 4.2 except for 20 August 1983, 0000 GMT.

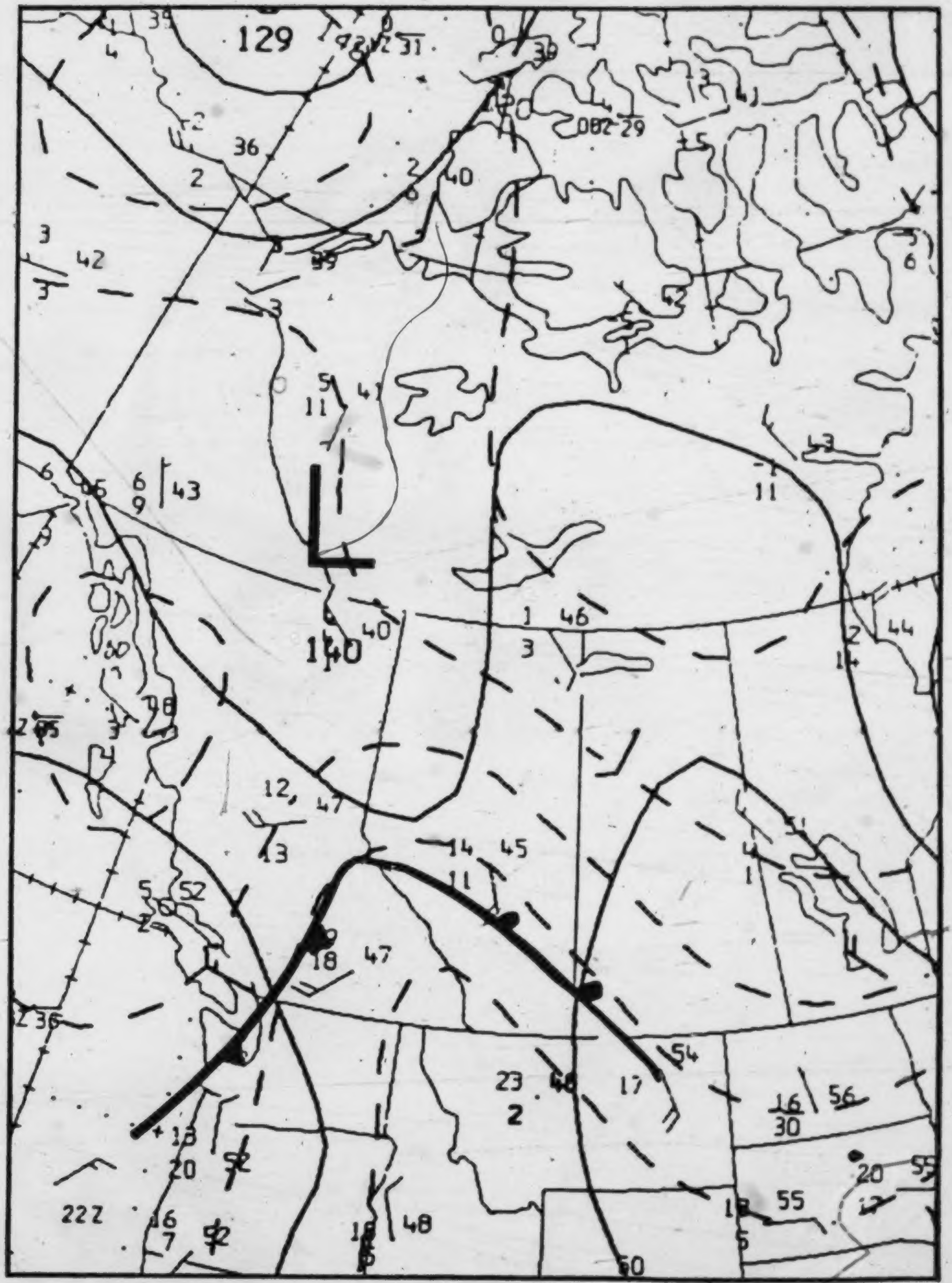

Figure 4.88 The same as in Figure 4.3 except for 20 August 1983, 0000 GMT.

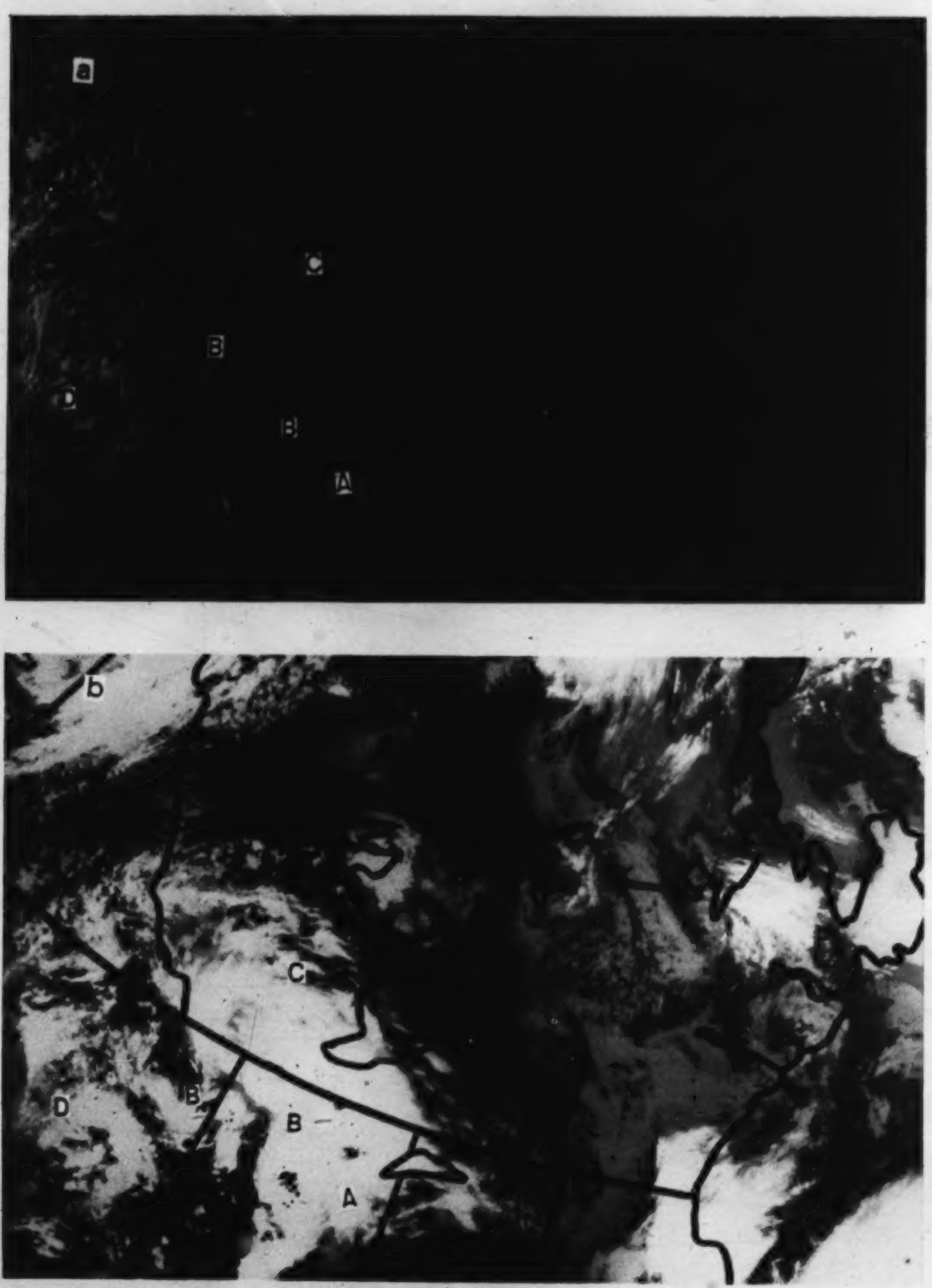
a
C
B
D
B
A
b
C
D
B
B
A

Figure 4.89 NOAA-8 satellite image, a) visible, b) infrared, 0136 GMT, 20 August 1983.

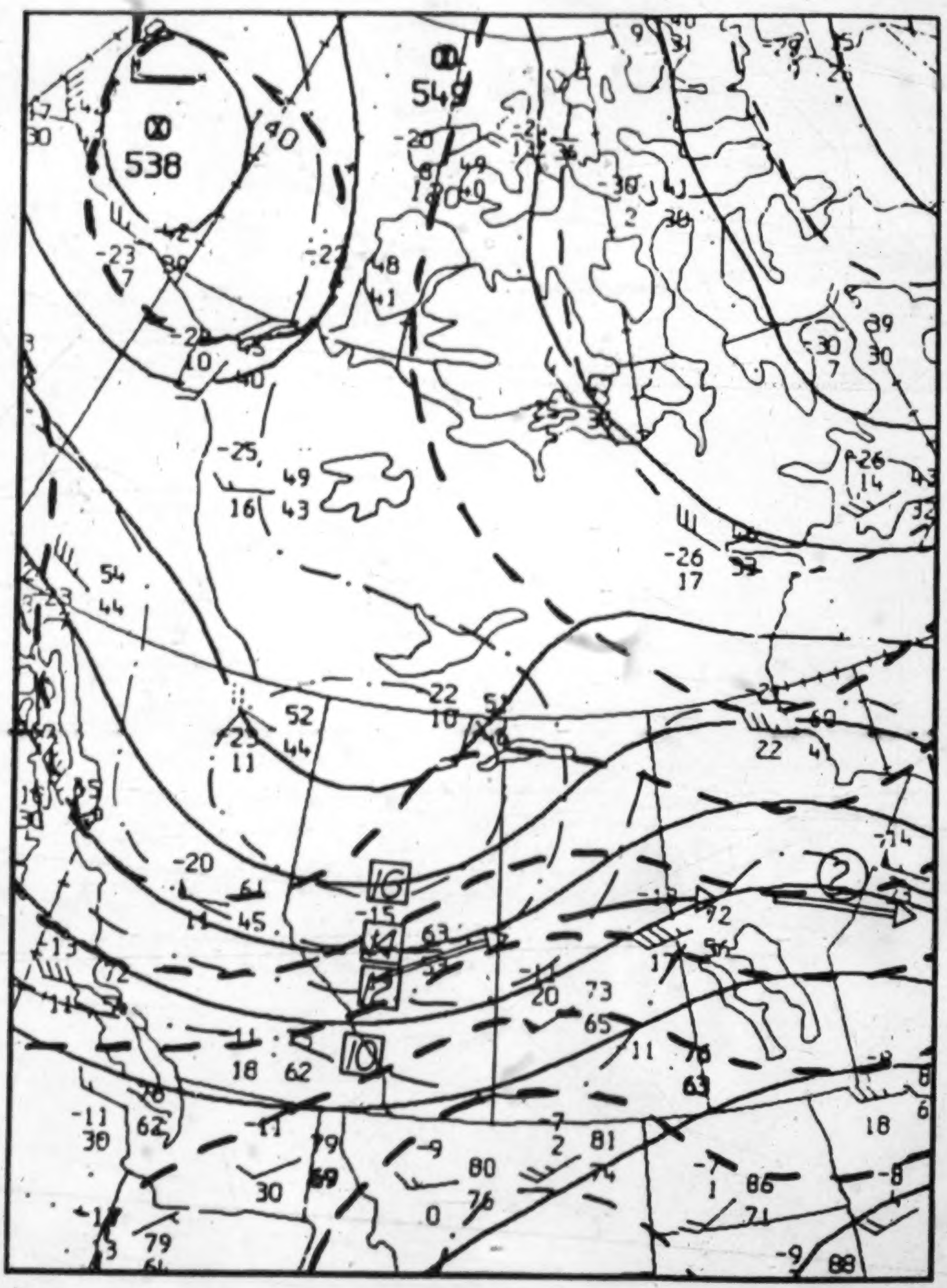
538
549
16
14
12
10
2
-25
49
16
43
54
44
52
-23
44
11
22
18
-20
61
11
45
-15
63
20
73
65
-11
18
62
-26
17
-30
7
39
30
-26
14
22
41
72
18
-11
30
62
79
69
80
76
81
74
86
71
88

Figure 4.90 The same as in Figure 4.2 except for 20 August 1983, 1200 GMT.

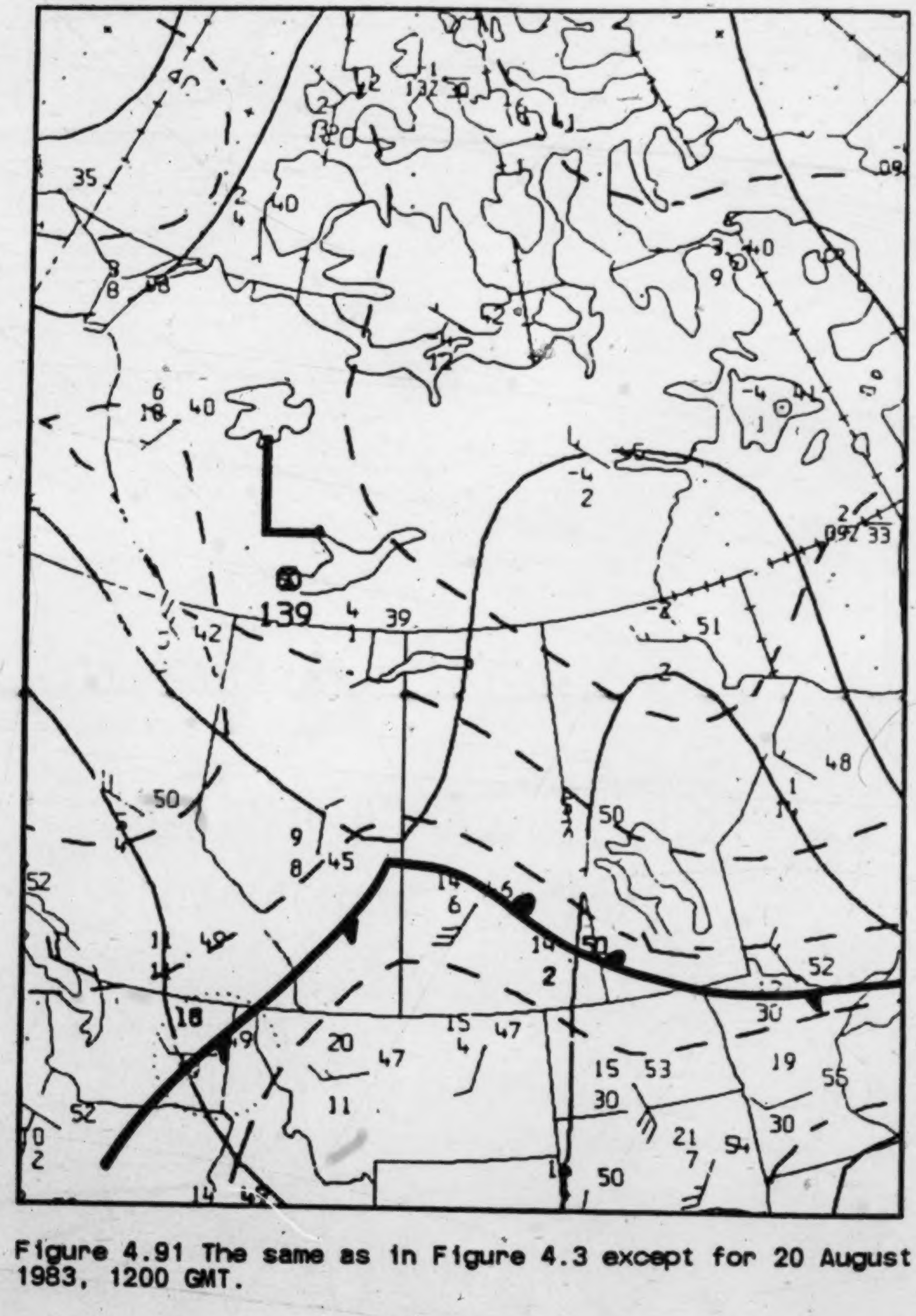
L
139
35
40
42
39
51
48
50
45
52
49
47
53
30
19
55
50
20
11

Figure 4.91 The same as in Figure 4.3 except for 20 August 1983, 1200 GMT.

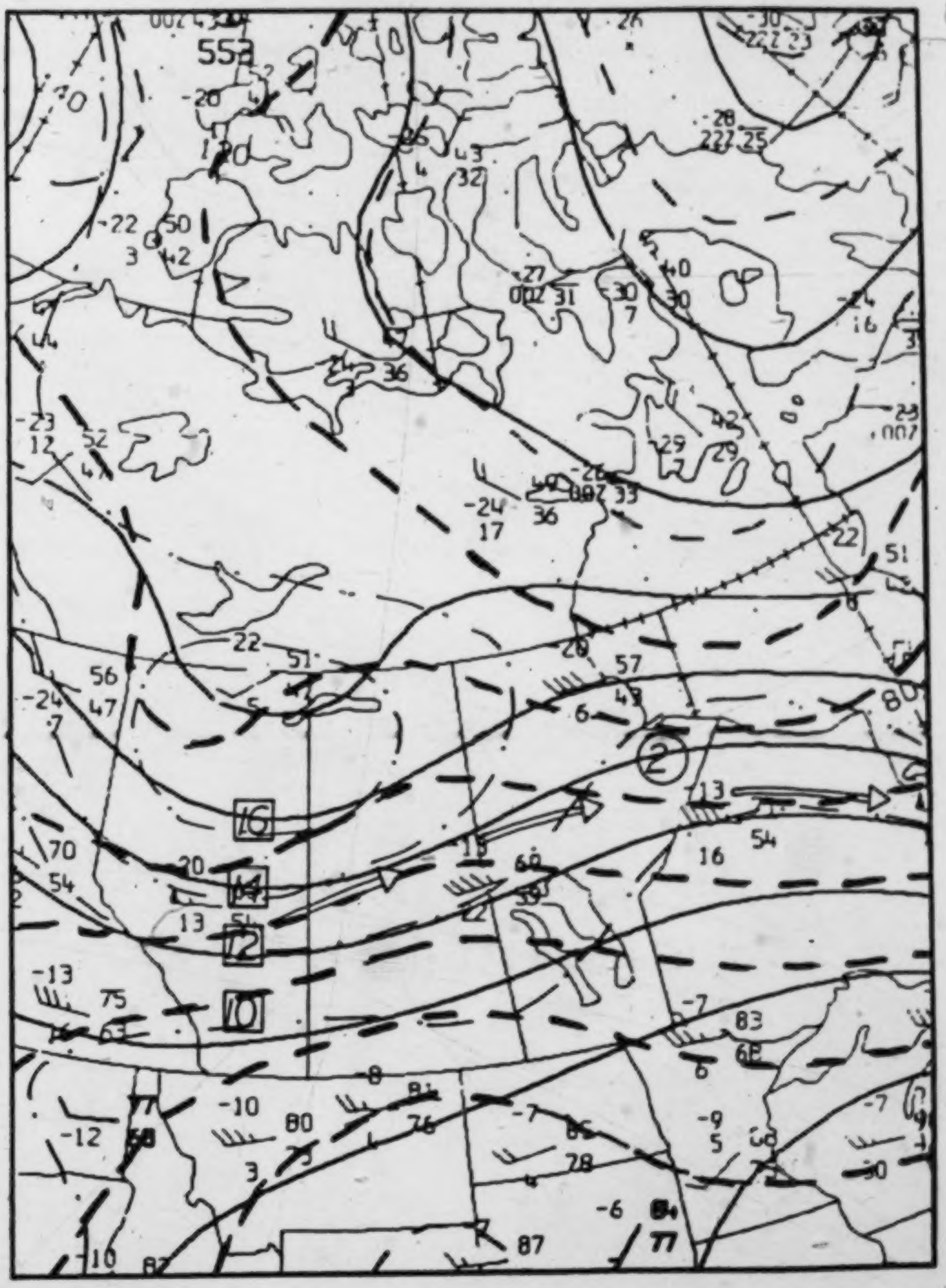
552
16
14
12
10
2

Figure 4.92 The same as in Figure 4.2 except for 21 August 1983, 0000 GMT.

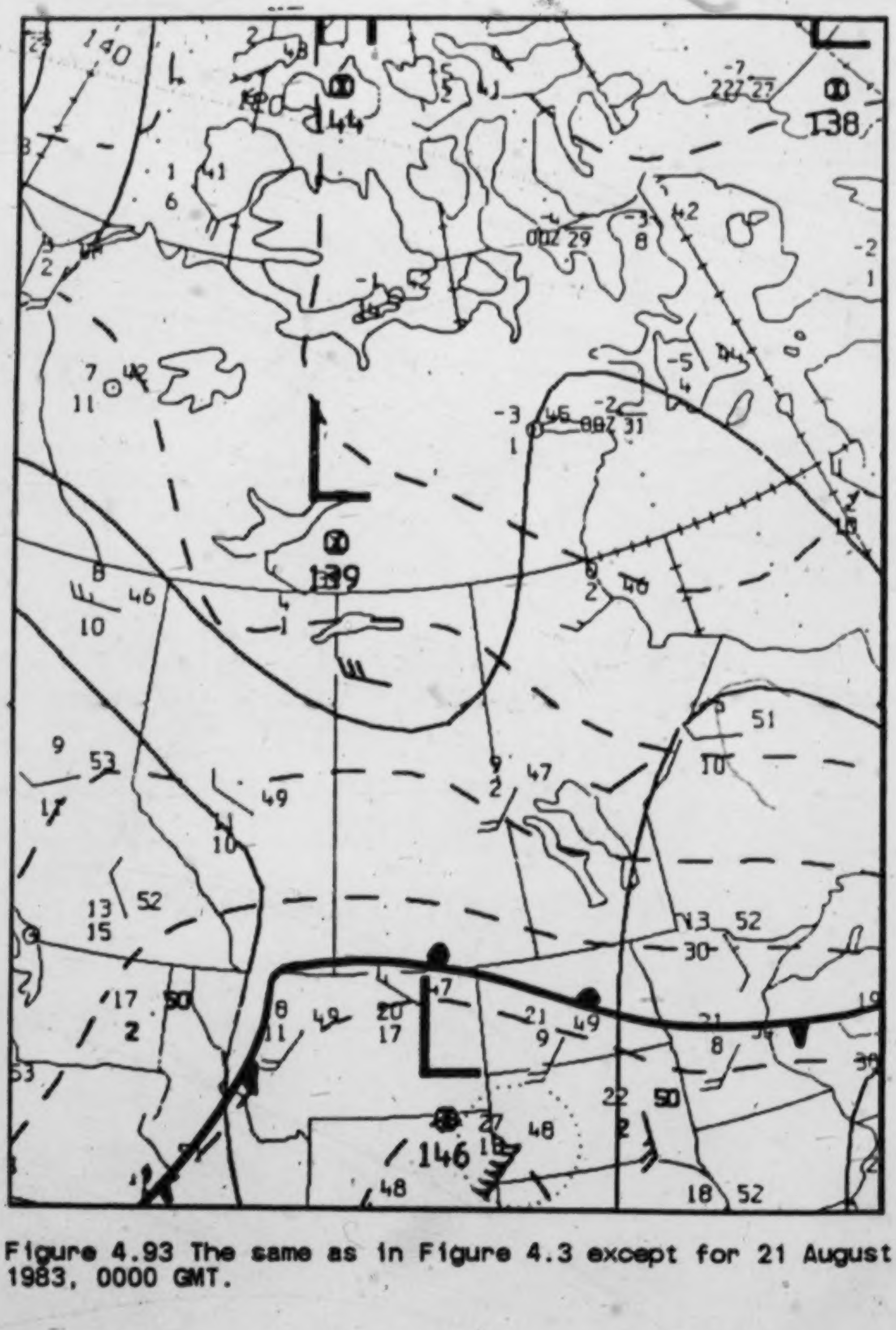

Figure 4.93 The same as in Figure 4.3 except for 21 August 1983, 0000 GMT.

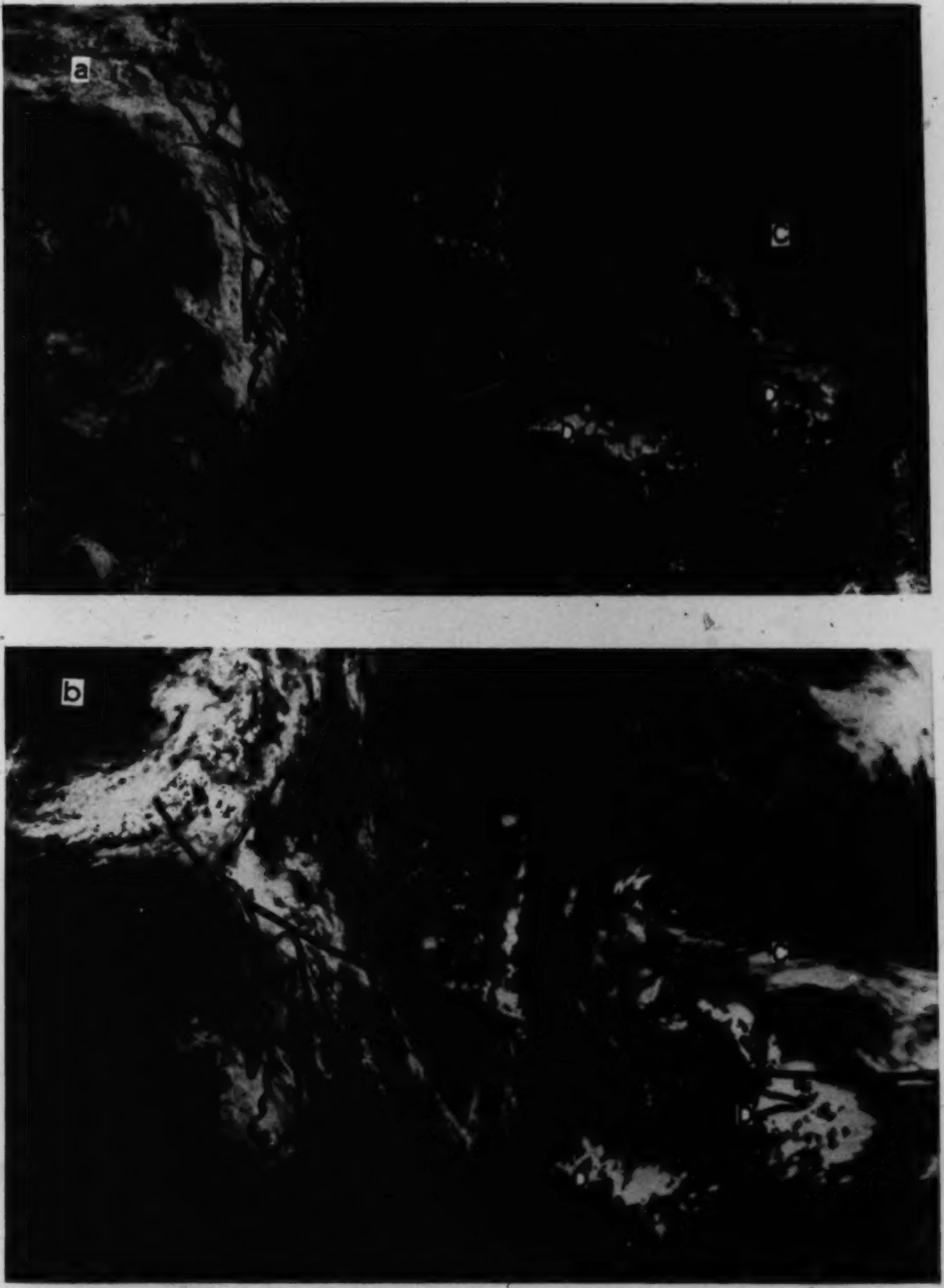

Figure 4.94 NOAA-7 satellite image, a) visible, b) infrared, 2225 GMT, 20 August 1983.

### 4.6 Case #5

This is a case of weak upper-level development, where (B) has not attained a well-defined comma shape. It is also an example of a modified upper cold low. Development took place simultaneously at all levels and a low-level warm trough covered the area of activity. Figures 4.95 - 4.110 show the different stages during the period (0000 GMT, 09 - 0000 GMT, 11 April 1983). The general configuration was very weak and lacked the tight shape of an upper cold low, but the mid and low-level flow was that for a typical upper-level development. The cloud area (B) was influenced by PVA and cyclonic circulation greater than 16.

The initial formation is shown in Figure 4.95, where (A) was weak, (B) did not attain the comma shape and (D) formed behind (B). Figure 4.96 shows a short wave trough and a pronounced jet stream at the 500-mb map, while Figure 4.97 depicts a weak northerly flow at the 850-mb level.

By 1200 GMT, 09 April (Figure 4.98), the short wave trough shifted eastward, while the vorticity circulation intensified. Jet (2) moved eastward and jet (1) advanced NE-ward. On the 850-mb surface (Figure 4.99), a closed circulation, associated with a thermal trough has formed. Five hours later (Figure 4.100), the cloud pattern became more organized, but (B) failed to evolve into a comma.

Figures 4.101 and 4.102 depict the subsequent evolution of the cloud complex. The pattern has lost its organized configuration but expanded in area, the various cloud areas have moved away from each other, and (B) weakened while under the control of a vorticity circulation less than 16. Surprisingly, Figures 4.103 and 4.104 show the continuation of a typical modified upper level development case. In Figure 4.103, one can see the pinching-off stage, while in Figure 4.104, the low-level thermal trough has progressed northwestward.

By 1200 GMT, 10 April (Figure 4.105), the 500-mb flow opened-up again, the cyclonic vorticity decreased and jet (2) advanced eastward. On the 850-mb surface

(Figure 4.106), a closed circulation has formed within the established warm intrusion. On the satellite image (Figure 4.107), the cloud pattern shows continued weakening, and the several cloud areas have decayed severely. Cloud area (B) remained however under the influence of a cyclonic vorticity area less than 16.

At 2223 GMT, 10 April (Figure 4.108) the cloud pattern dissipated. Only a few fragments of (A), (B), and (D) are left. Cloud area (B) decayed within a cyclonic vorticity region less than 16 (see Figures 4.108 and 4.109). Figure 4.110 depicts the low-level flow at the 850-mb level.

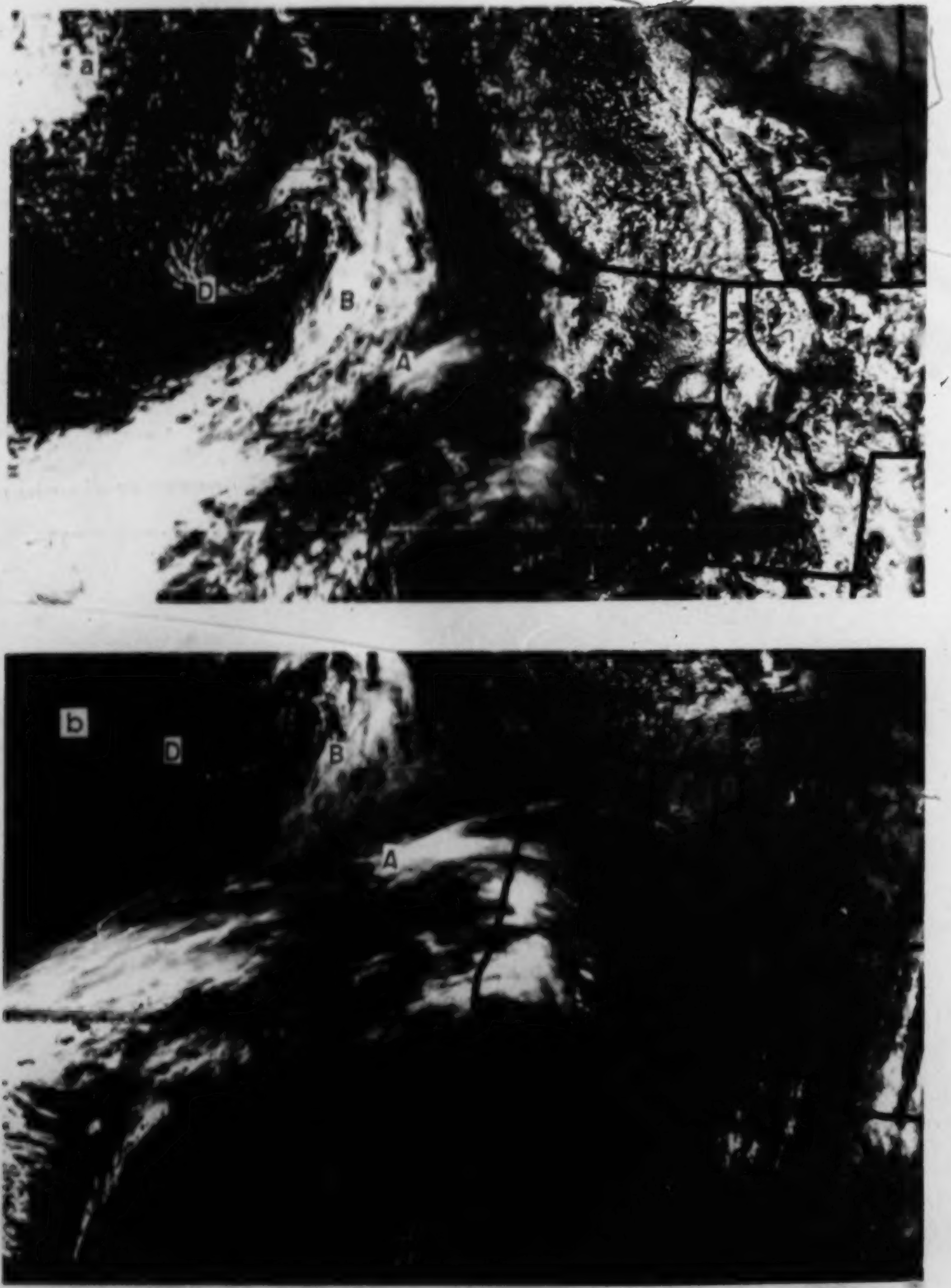

Figure 4.95 NOAA-7 satellite image, a) visible, b) infrared, 2247 GMT, 08 April 1983.

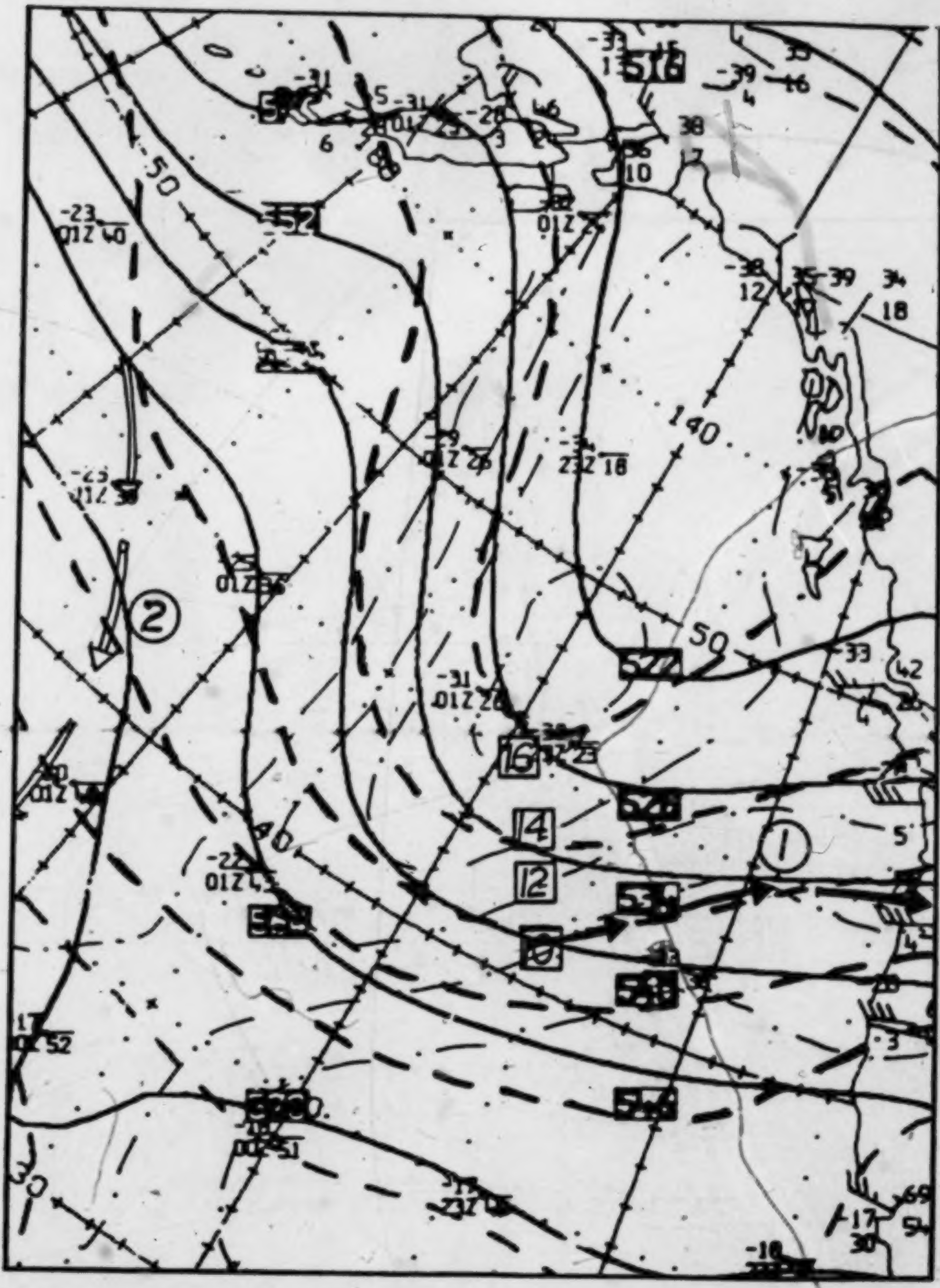
50
140
50
40
30
516
524
528
532
536
540
544
548
552
16
14
12
10
①
②

Figure 4.96 The same as in Figure 4.2 except for 09 April 1983, 0000 GMT.

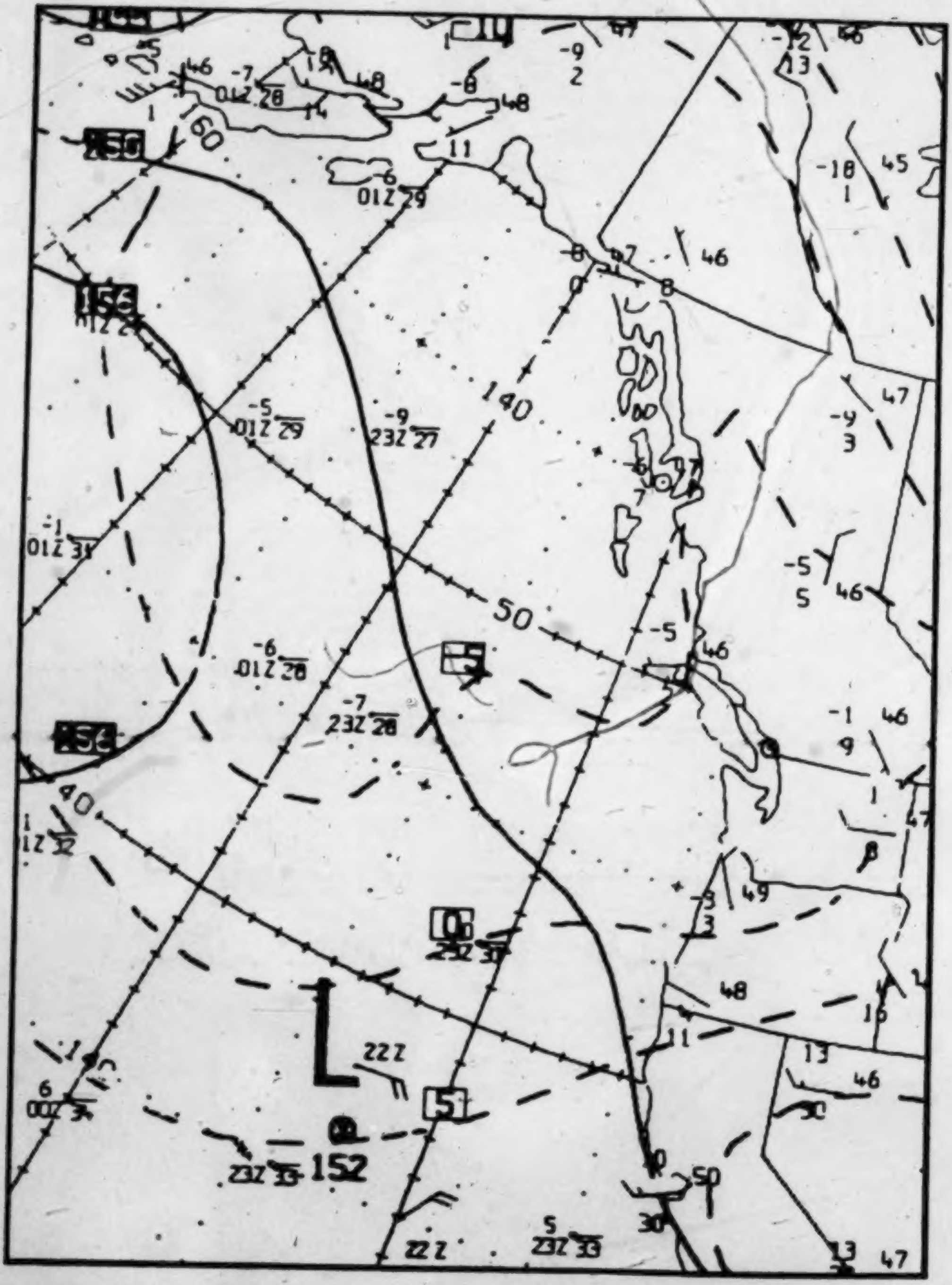

Figure 4.97 The same as in Figure 4.3 except for 09 April 1983, 0000 GMT.

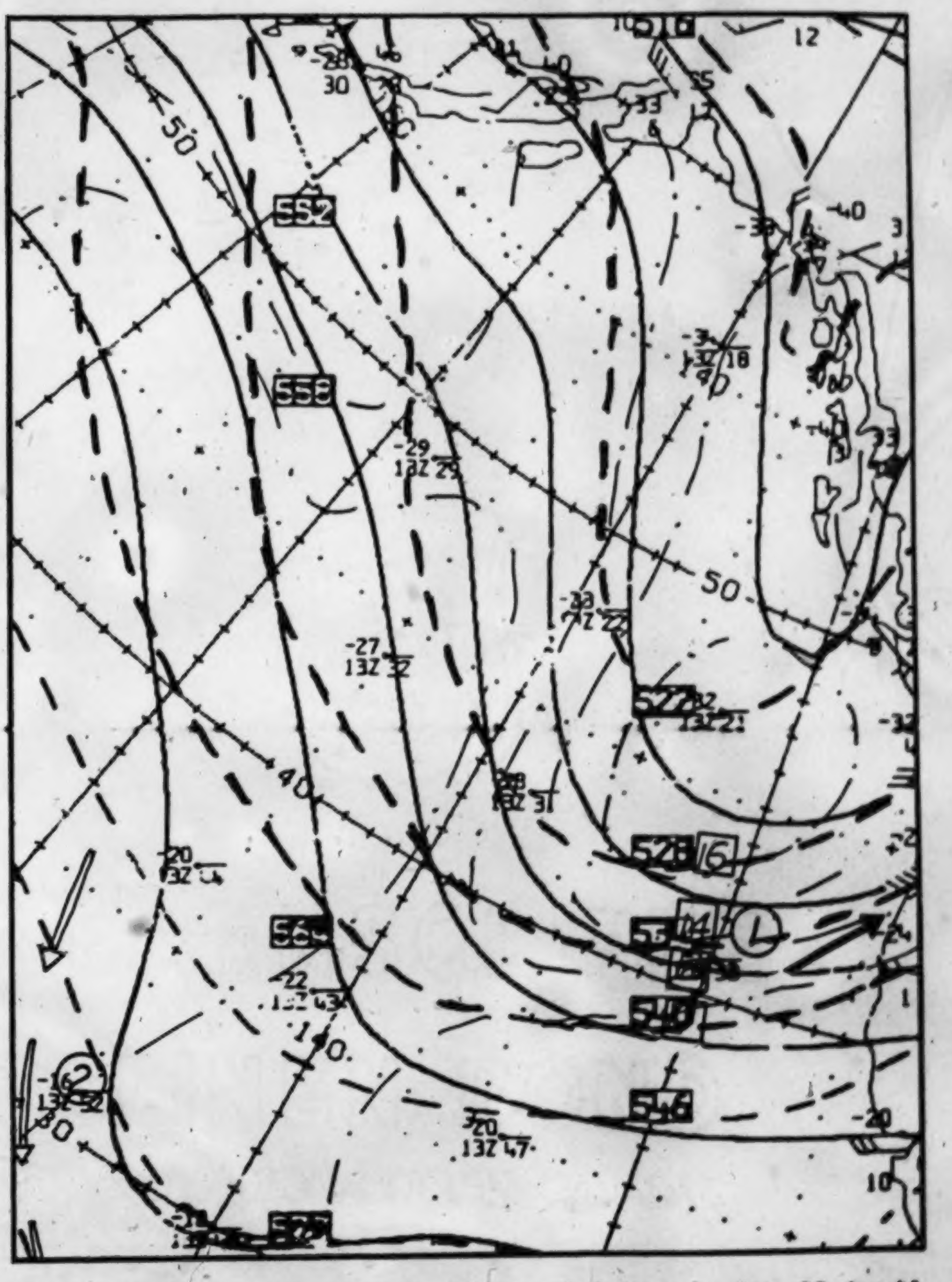
552
558
564
570
522
528
16
14
L
540
546
50
50
40
140
30
12
-40
-29
13Z 25
-27
13Z 32
-33
-20
13Z 47
-20

Figure 4.98 The same as in Figure 4.2 except for 09 April 1983, 1200 GMT.

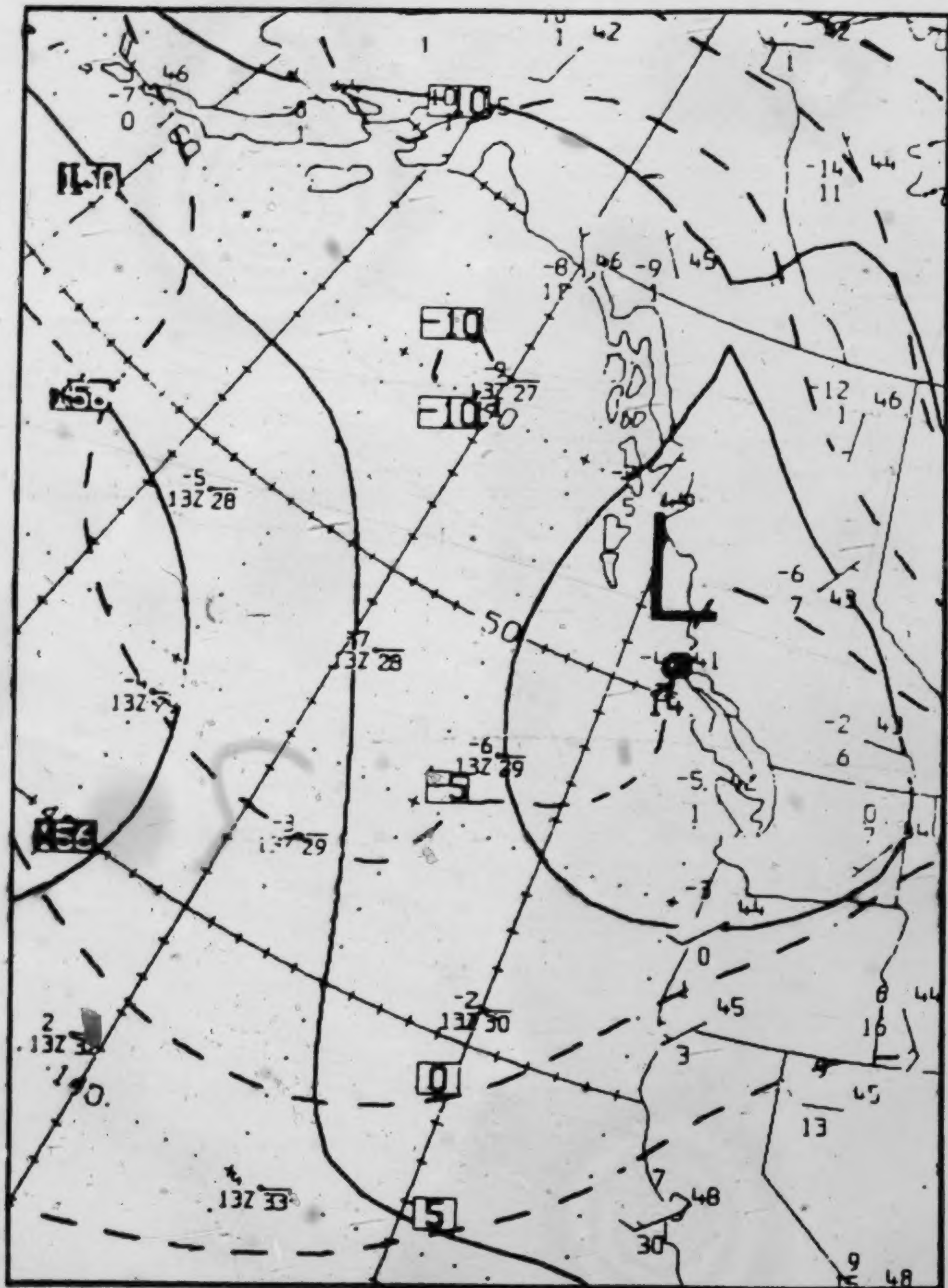
-10
-10
-10
-5
0
5
50
L
-5 13Z 28
-7 13Z 28
-9 13Z 27
-6 13Z 29
-3 13Z 29
-2 13Z 30
2 13Z 32
13Z 33

Figure 4.99 The same as in Figure 4.3 except for 09 April 1983, 1200 GMT.

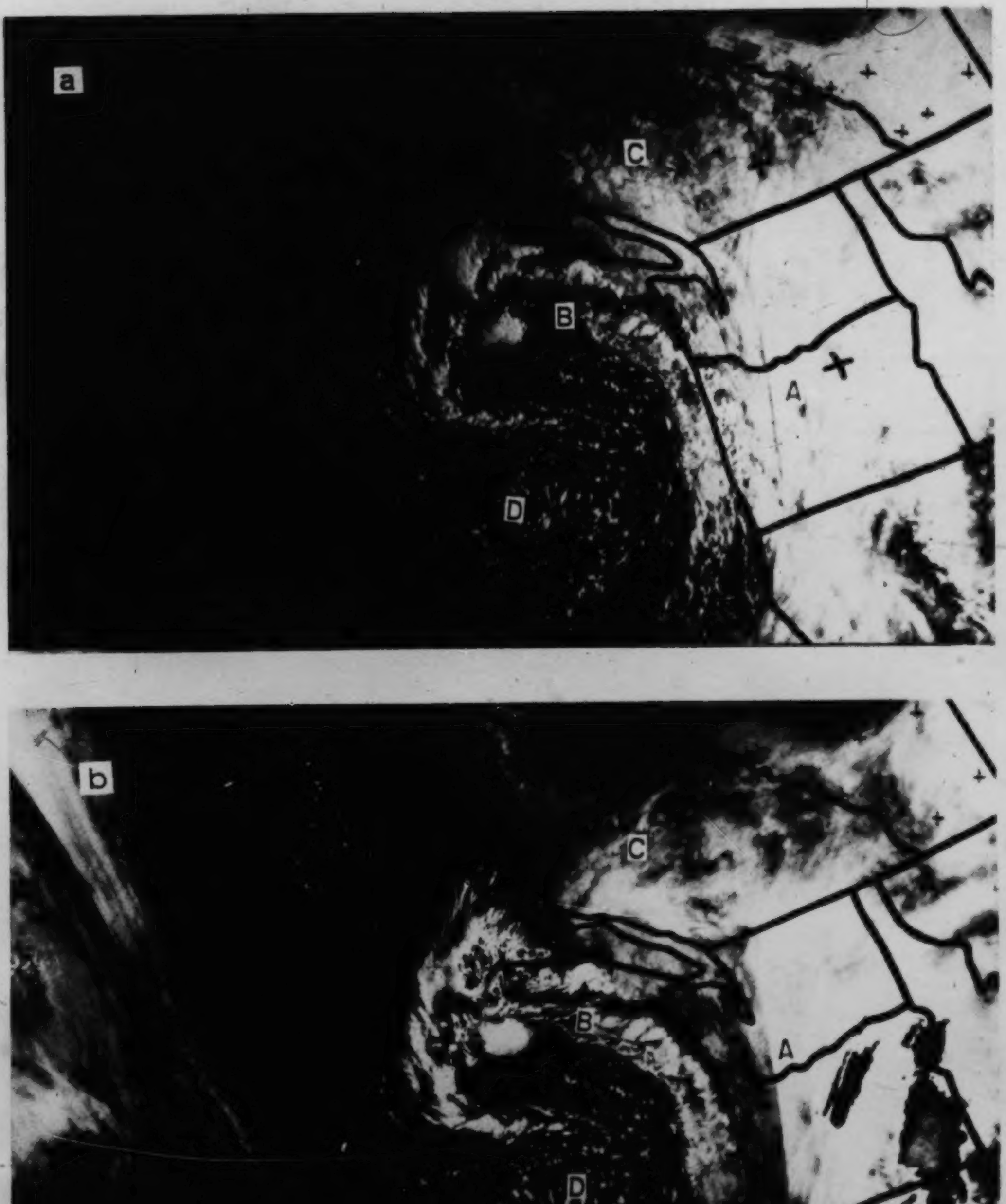
a
C
B
A
D
b
C
B
A
D

Figure 4.100 NOAA-6 satellite image, a) visible, b) infrared, 1644 GMT, 09 April 1983.

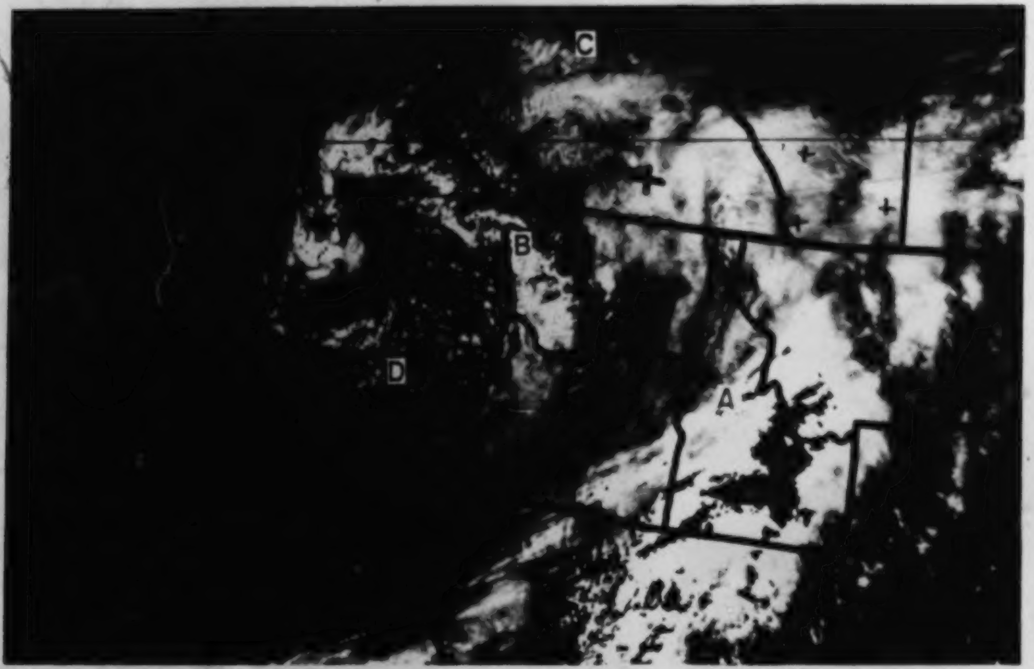

Figure 4.101 NOAA-7 satellite image , infrared, 2253 GMT, 09 April 1983.

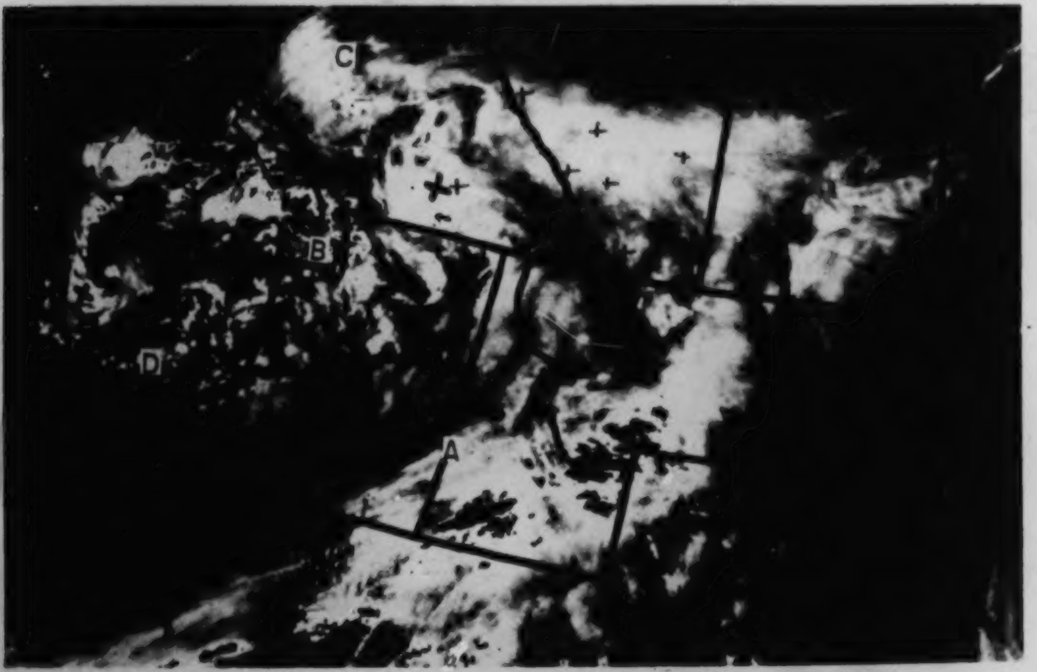

Figure 4.102 NOAA-6 satellite image , infrared, 0232 GMT, 10 April 1983.

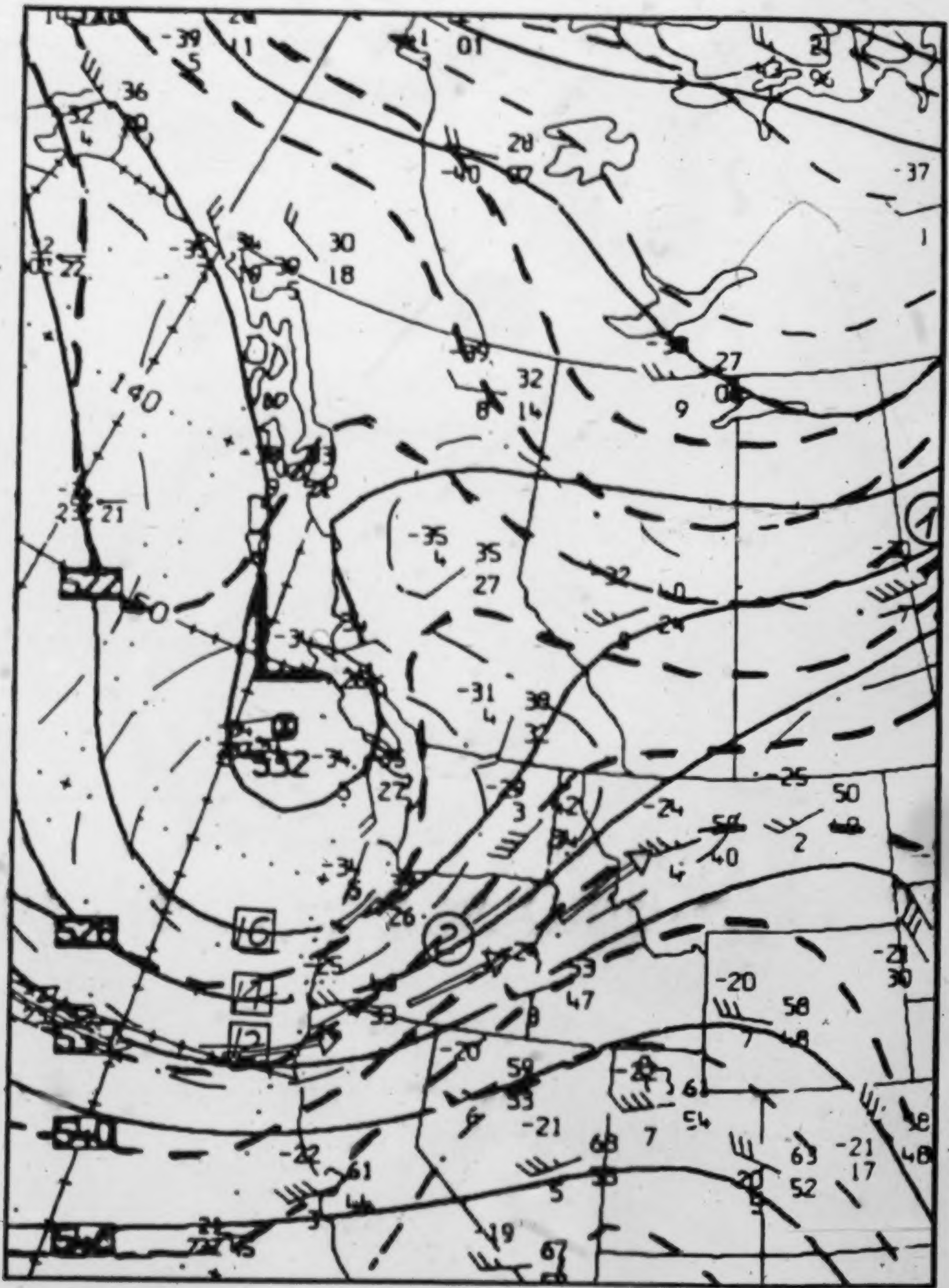
140
160
572
528
532
540
548
552
16
14
12
1
2

Figure 4.103 The same as in Figure 4.2 except for 10 April 1983, 0000 GMT.

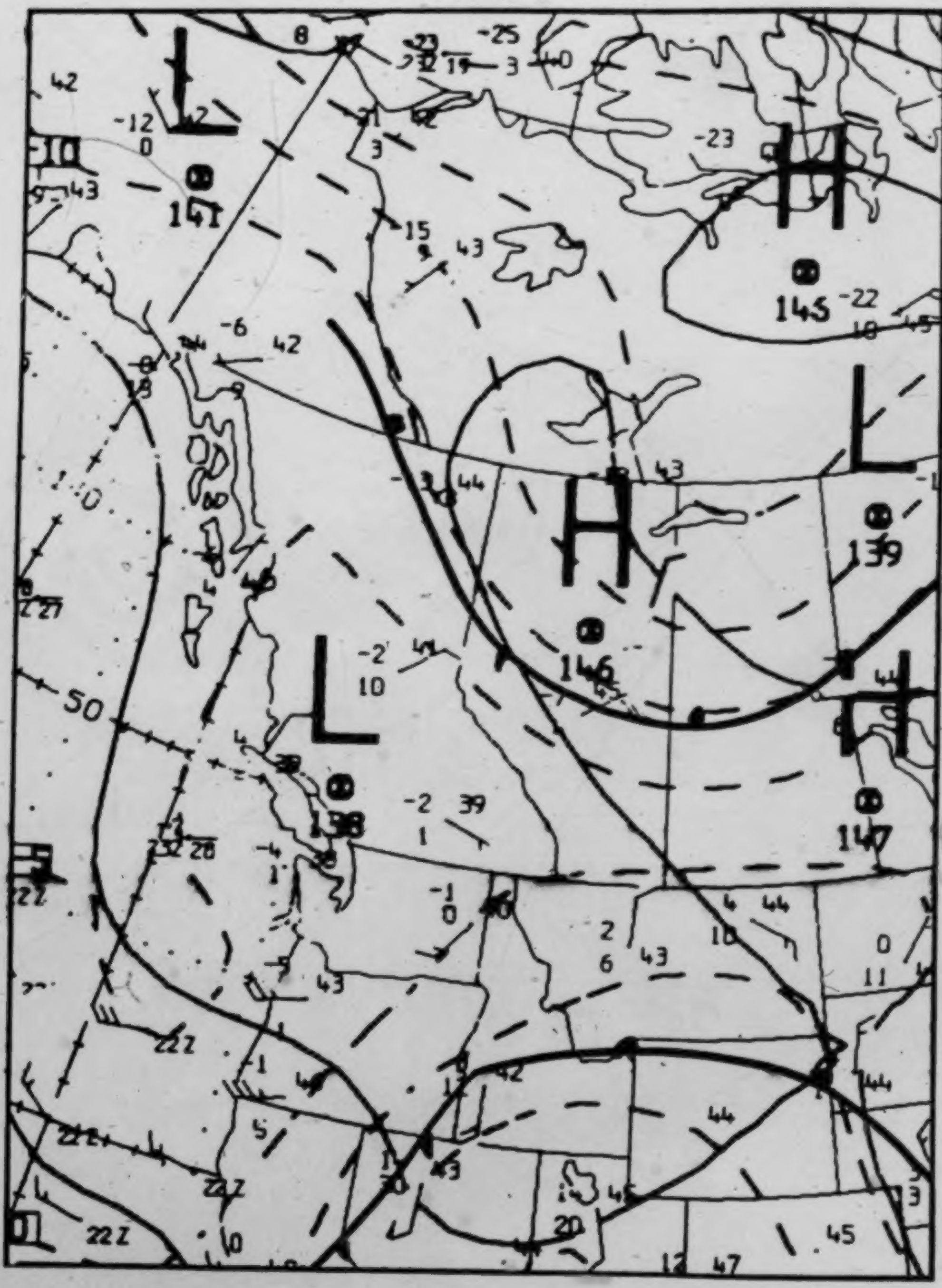
L
H
141
145
L
H
139
L
146
H
138
147
50

Figure 4.104 The same as in Figure 4.3 except for 10 April 1983, 0000 GMT.

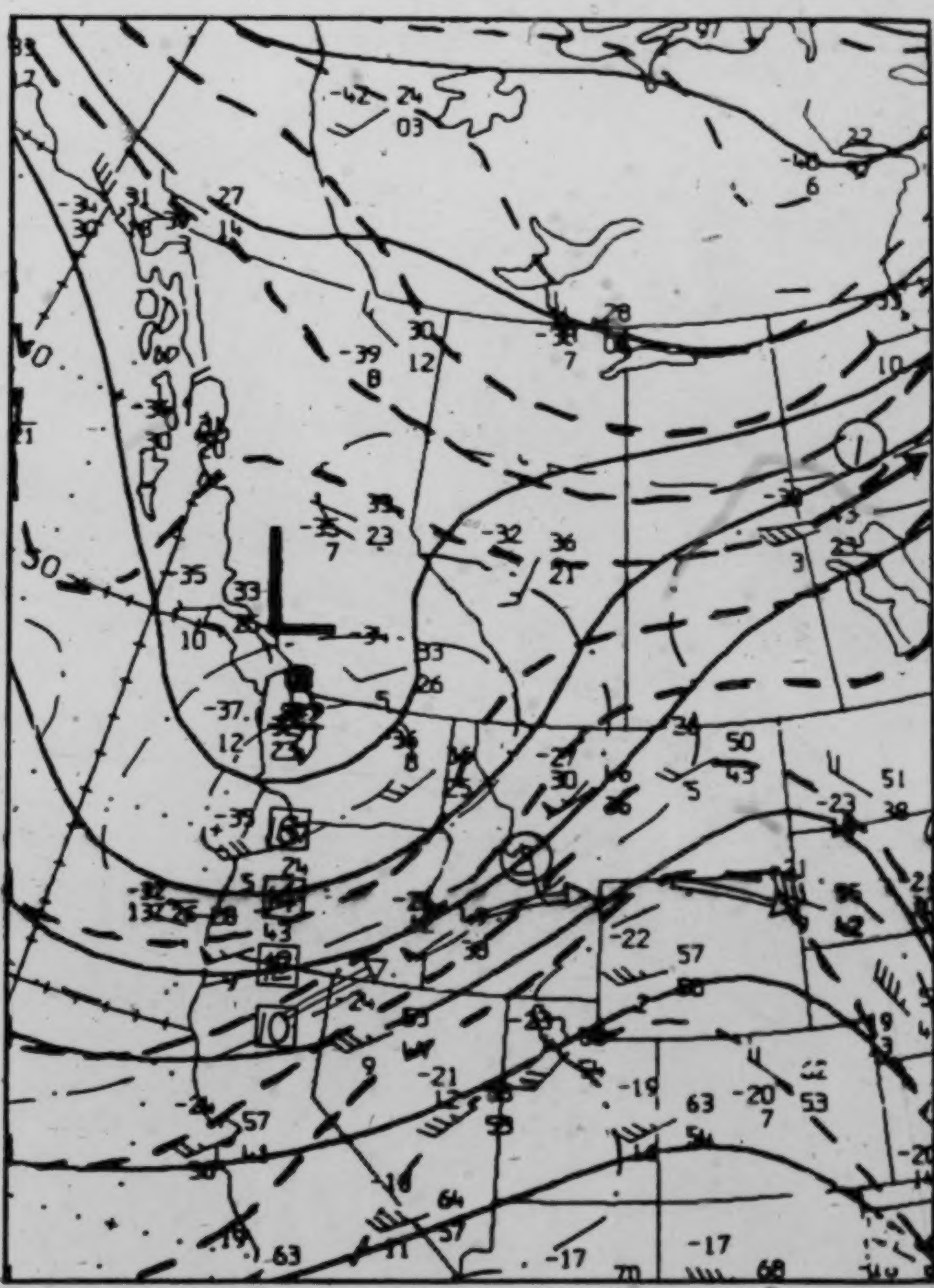

Figure 4.105 The same as in Figure 4.2 except for 10 April 1983, 1200 GMT.

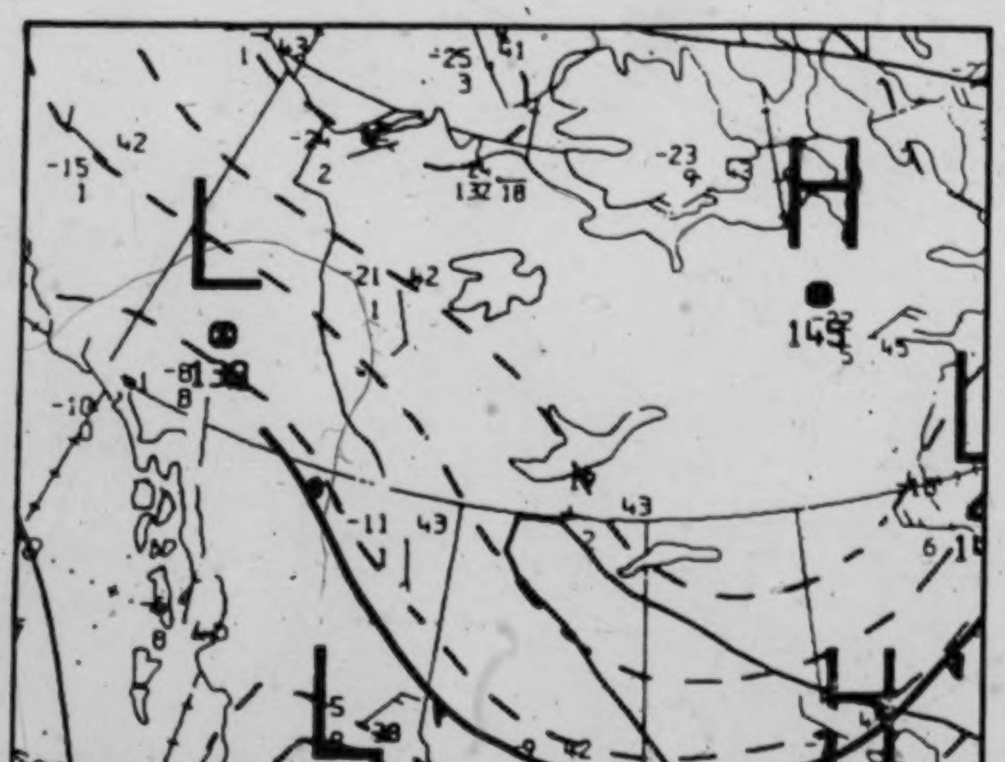
L
H
L
L
L
139
137
145
146
140
60

Figure 4.106 The same as in Figure 4.3 except for 10 April 1983, 1200 GMT.

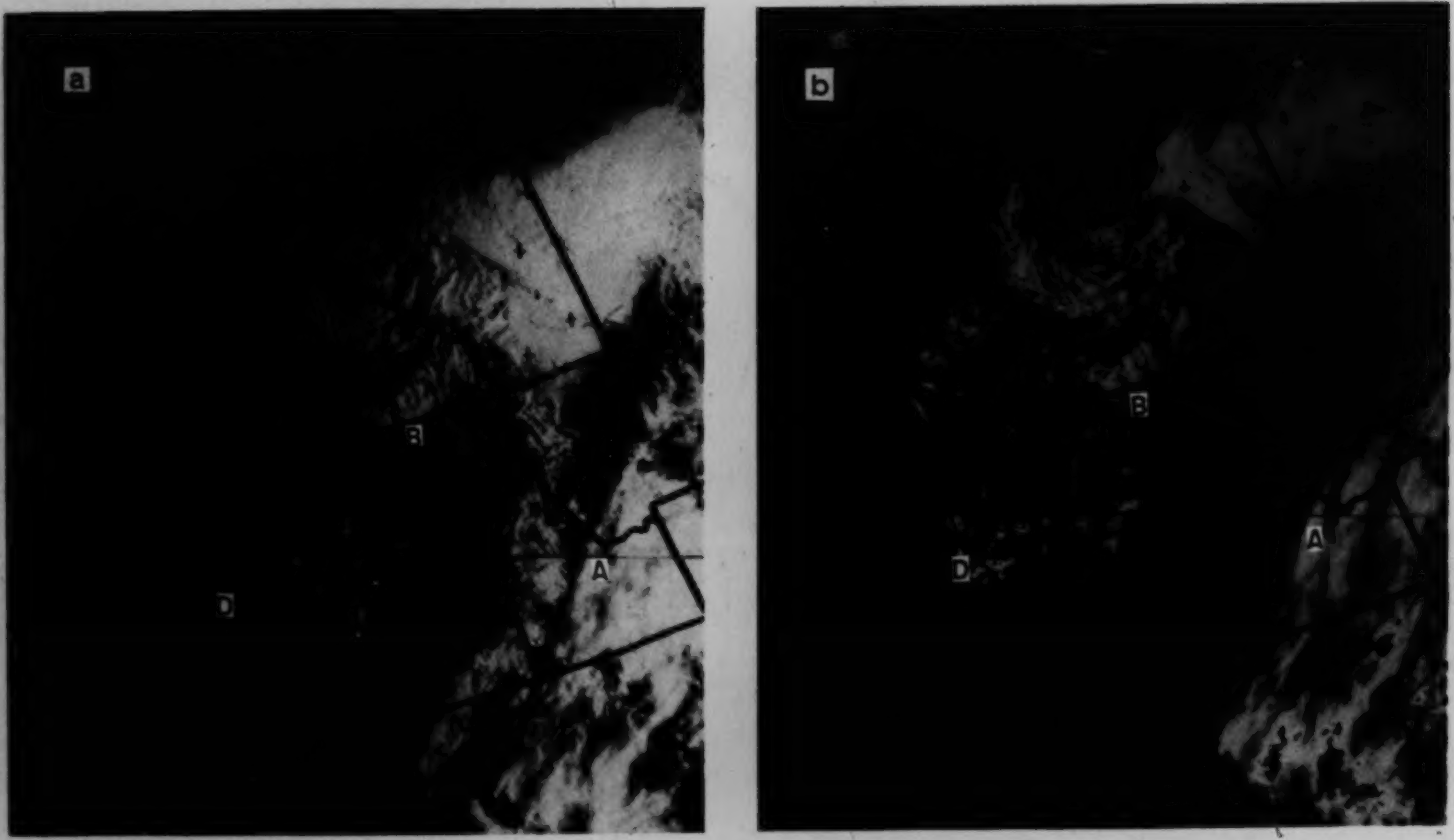

Figure 4.107 NOAA-6 satellite image, a) visible, b) infrared, 1623 GMT, 10 April 1983.

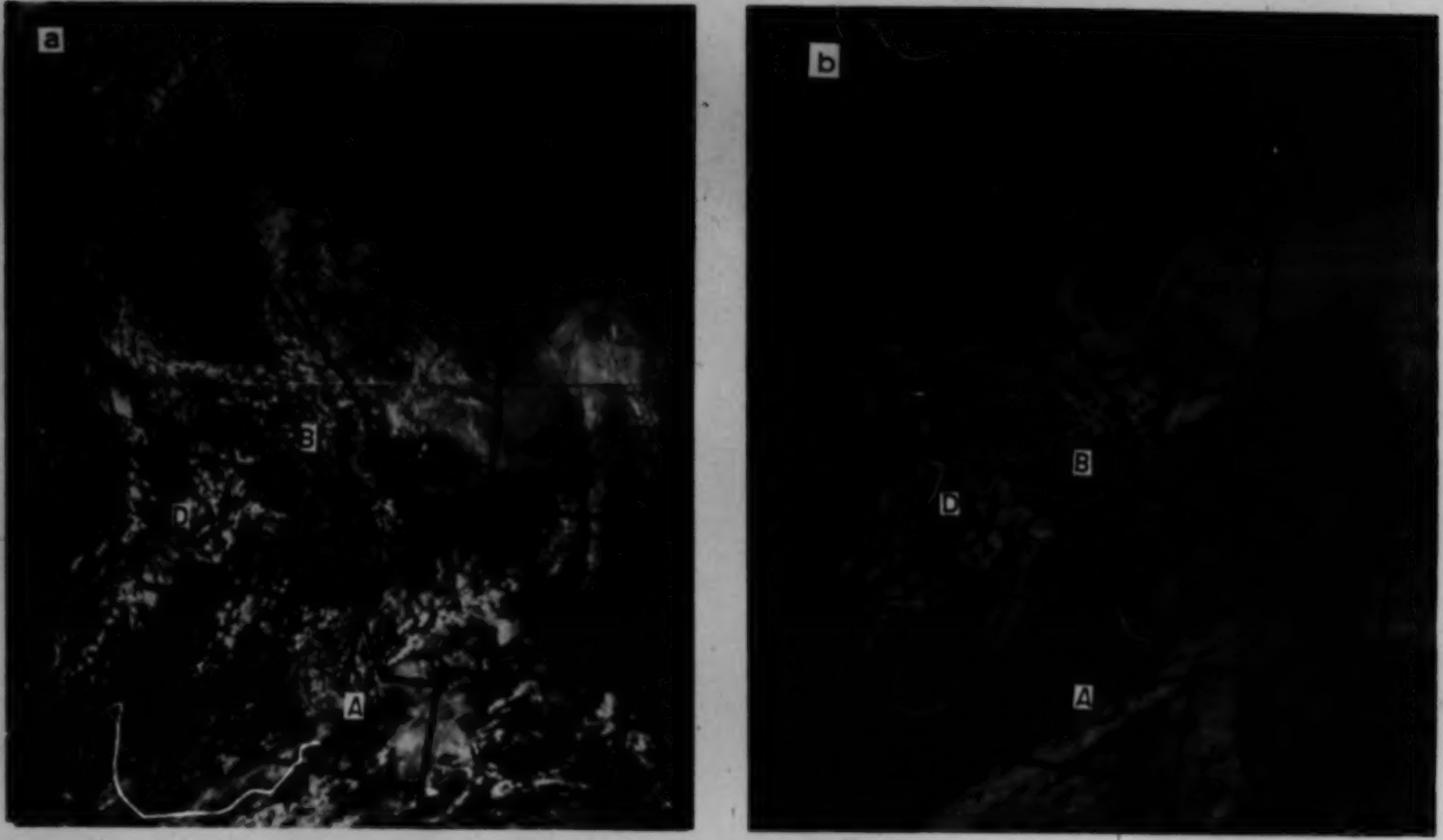

Figure 4.108 NOAA-7 satellite image, a) visible, b) infrared, 2223 GMT, 10 April 1983.

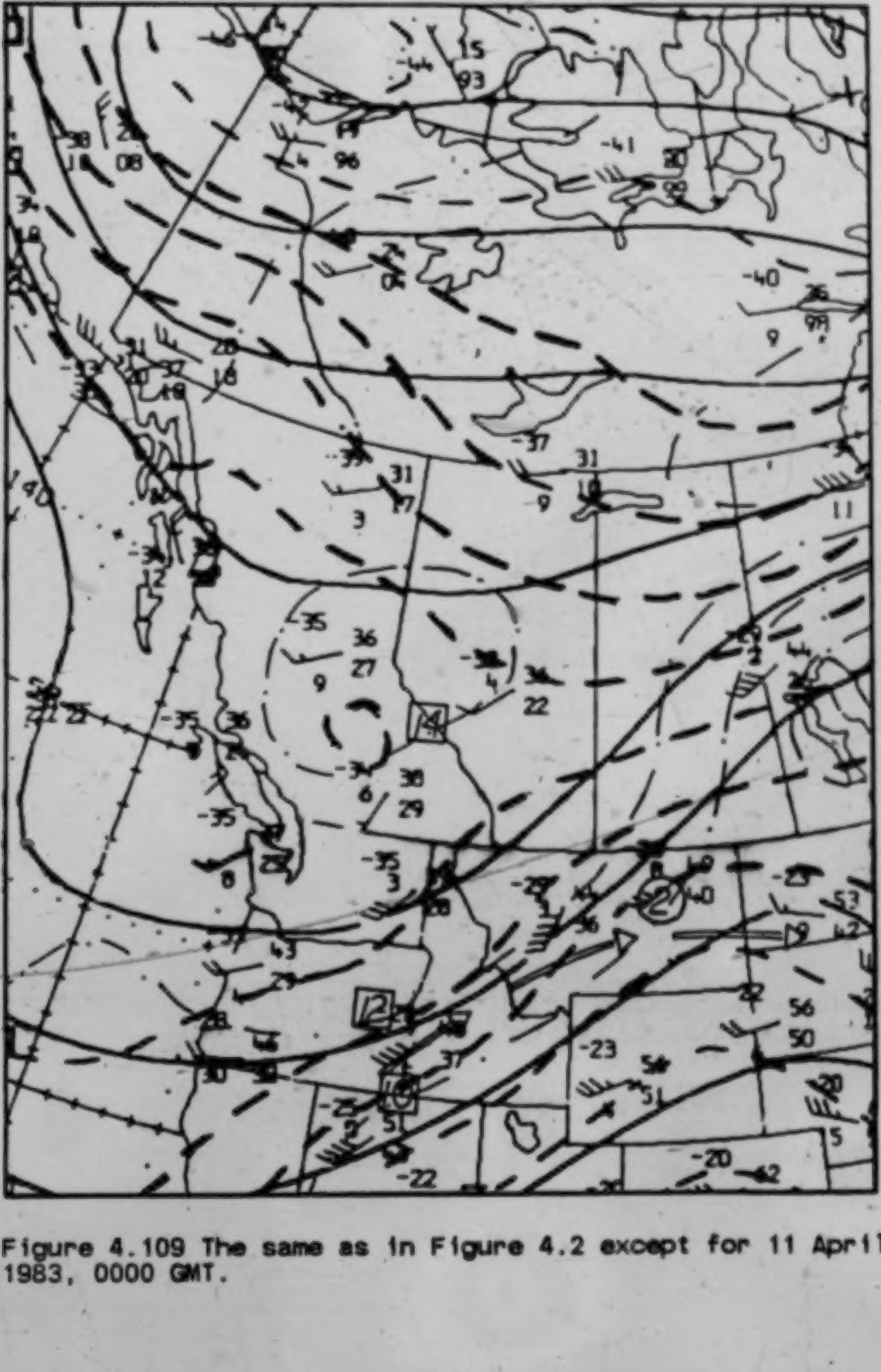

Figure 4.109 The same as in Figure 4.2 except for 11 April 1983, 0000 GMT.

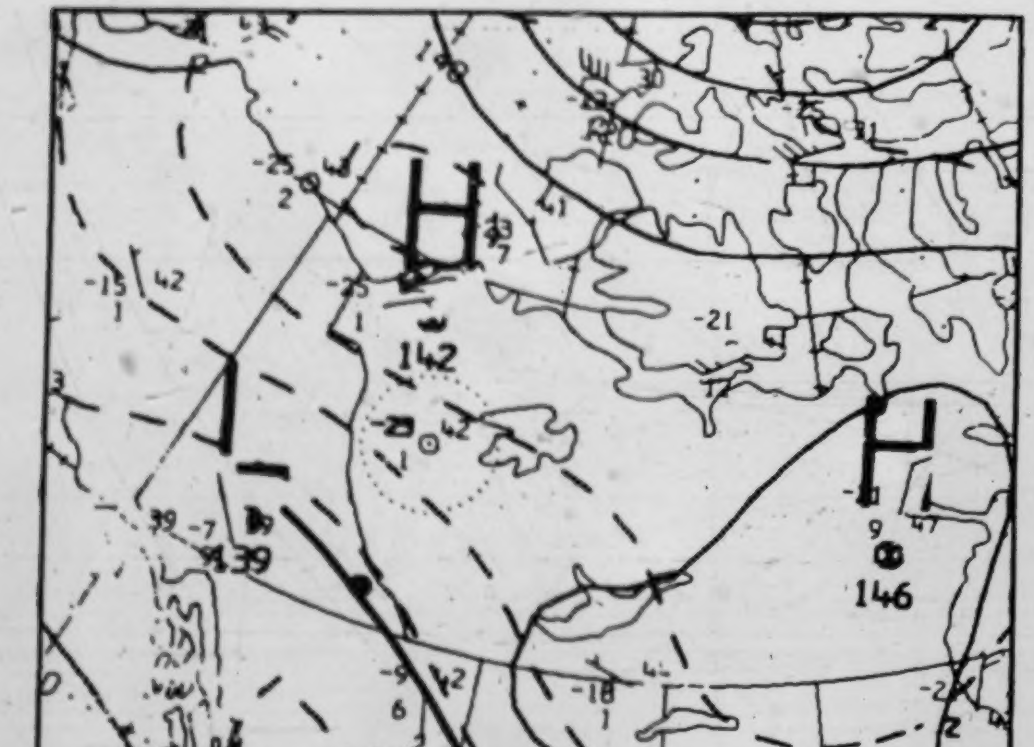
H
142
139
H
146
L
139
H
145
L

Figure 4.110 The same as in Figure 4.3 except for 11 April 1983, 0000 GMT.

### 4.7 Case #6

This, last case to be presented, is a pure case of cyclogenesis, where no surface warm intrusion or fronts existed near the critical area. It is also a weak case, since no clearly-defined pattern evolved and not even a comma developed. Figures 4.111 - 4.133 show the series of events in the formation process during the period from 0000 GMT, 23 July 1983 to 0000 GMT, 26 July 1983. The meteorological conditions such as upper-level cyclogenetic process, the thickness field, the jet stream system, the moisture source, and the associated vorticity analysis, are all favourable for strong or moderate system formation. Yet the corresponding satellite images did not support it.
In Figures 4.113, 4.116, 4.117, 4.120 and 4.123, a very weak cloud-pattern has formed over an area bounded by latitudes 50° - 55° N and longitudes 130° - 140° W. This pattern moved NE-ward and spread out as it disintegrated and finally dissipated over western B.C.

The sequence of events began at 0000 GMT, 23 July (Figure 4.111). A trough has become elongated southward. A closed thermal circulation and a closed cyclonic vorticity isopleth are located at the base of this trough. Jet (2) headed southward, while jet (1) proceeded NE-ward. On the 850-mb surface (Figure 4.112), a southerly flow is accompanied by a cold air sector. Figure 4.113 shows the cloud pattern, comprised of (B) and (C). Cloud area (B), in the pre-comma stage, is associated with the vorticity contour less than 16.

Negligible change has occured in the following twelve hours as the system moved NE-ward (see Figures 4.114, 4.115, 4.116 and 4.117).

By 0000 GMT, 24 July (Figure 4.118) a closed circulation has formed at the base of the trough, while jet (2) dug southward. The 850-mb flow (Figure 4.119) has become ill-defined. Figure 4.120 shows the upper cloud pattern which has weakened considerably.

Twelve hours later, the 500-mb flow (figure 4.121) has opened up again, the vorticity circulation weakened and jet (2) moved toward the base of the trough. The

850-mb flow (Figure 4.122) has become more ill-defined although the cold trough is still persisting over B. C. and the Yukon. Figure 4.123 shows the continuous deterioration of the cloud pattern and the dissipation of (B).

The next Figures 4.124 - 4.133 depict the persistence of the upper-flow on the synoptic maps and the continuous dissipation of the cloud pattern on the satellite images. Since (B) was assumed to be the key feature of the cloud pattern, it was difficult to track fragmenting clouds and relate them to specific features of the synoptic circulation.

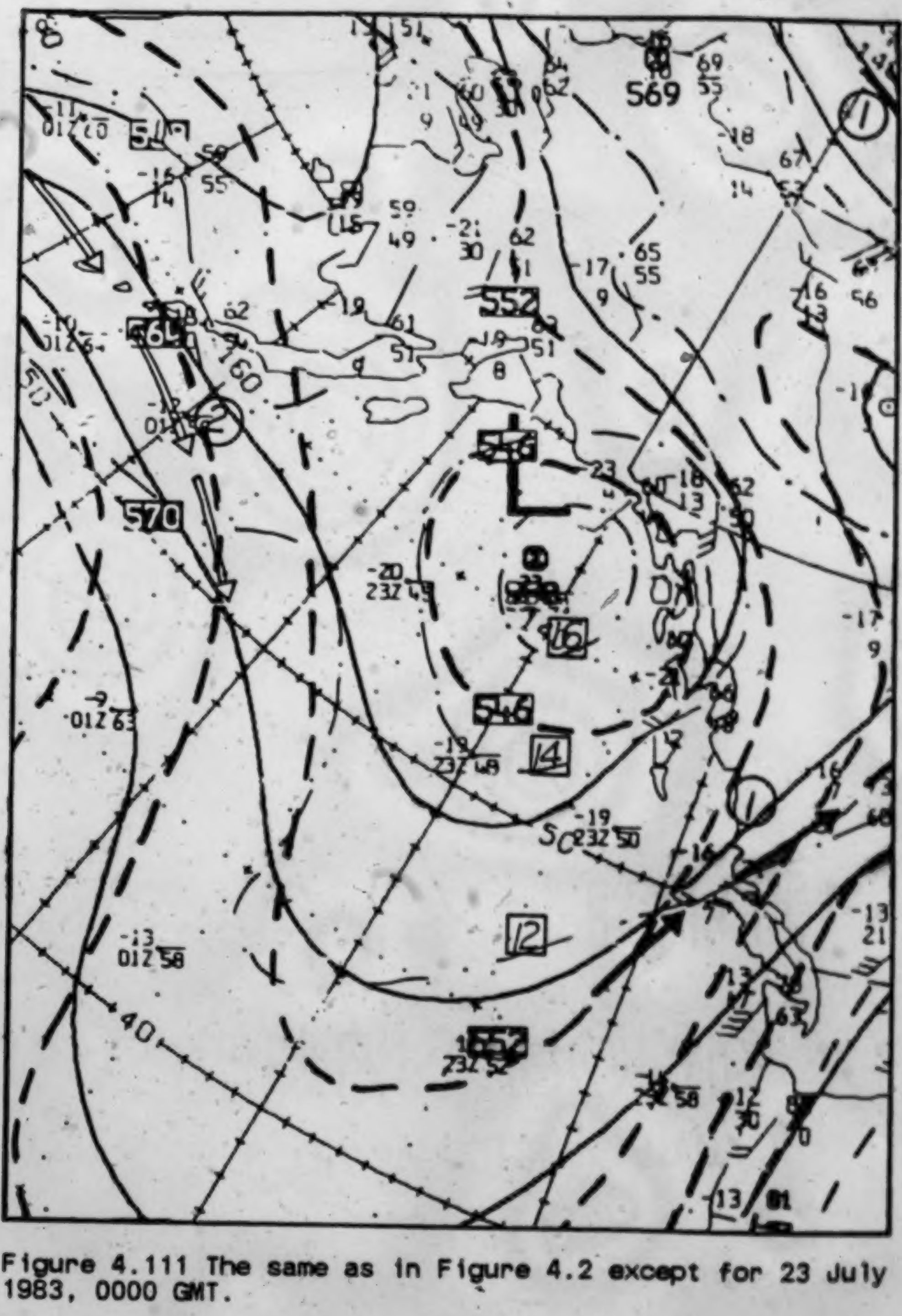
569
552
546
546
552
570
564
510
160
40
16
14
12
SC
①
②

Figure 4.111 The same as in Figure 4.2 except for 23 July 1983, 0000 GMT.

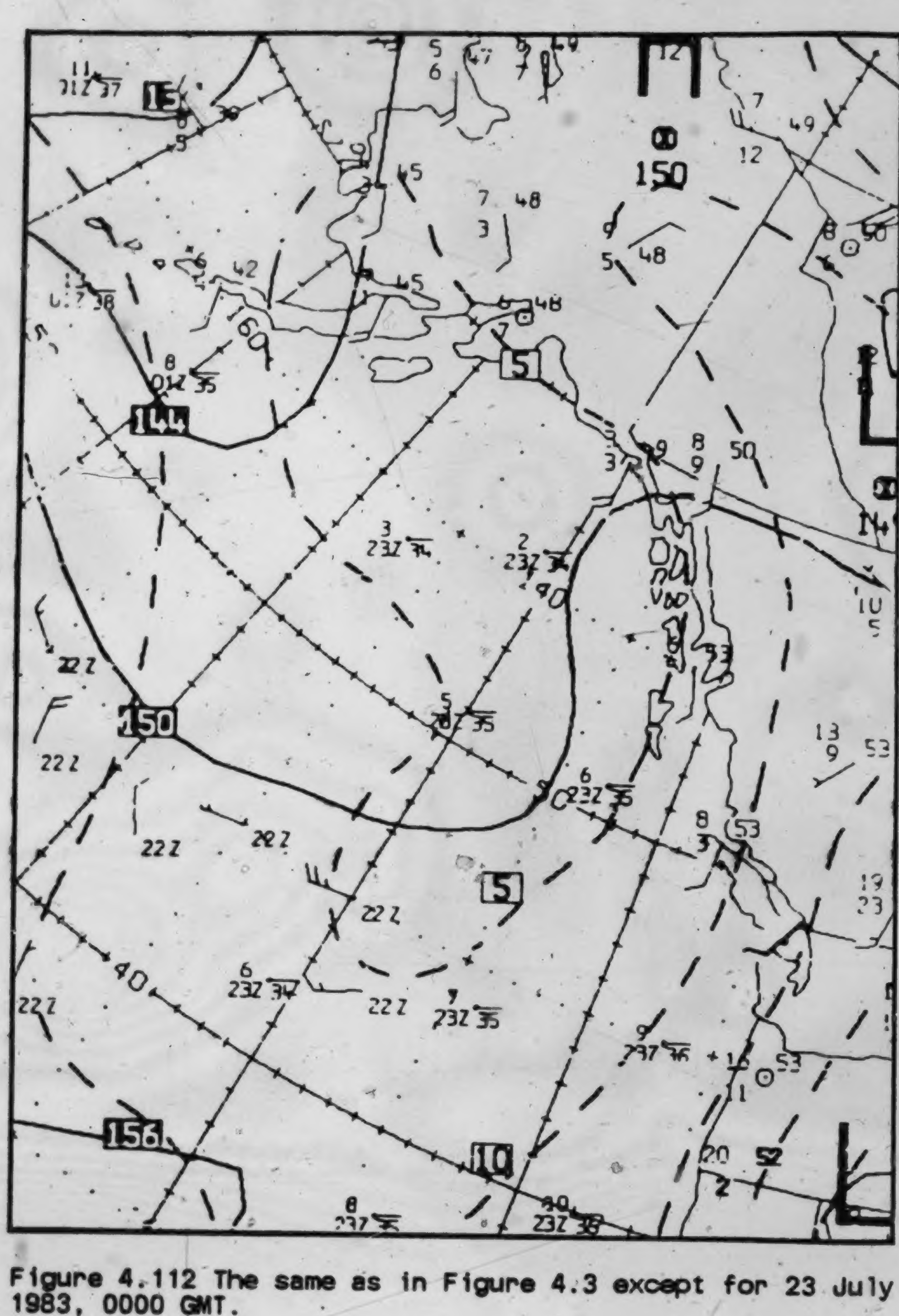
15
150
144
150
5
5
156
10
160
90
50
40

Figure 4.112 The same as in Figure 4.3 except for 23 July 1983, 0000 GMT.

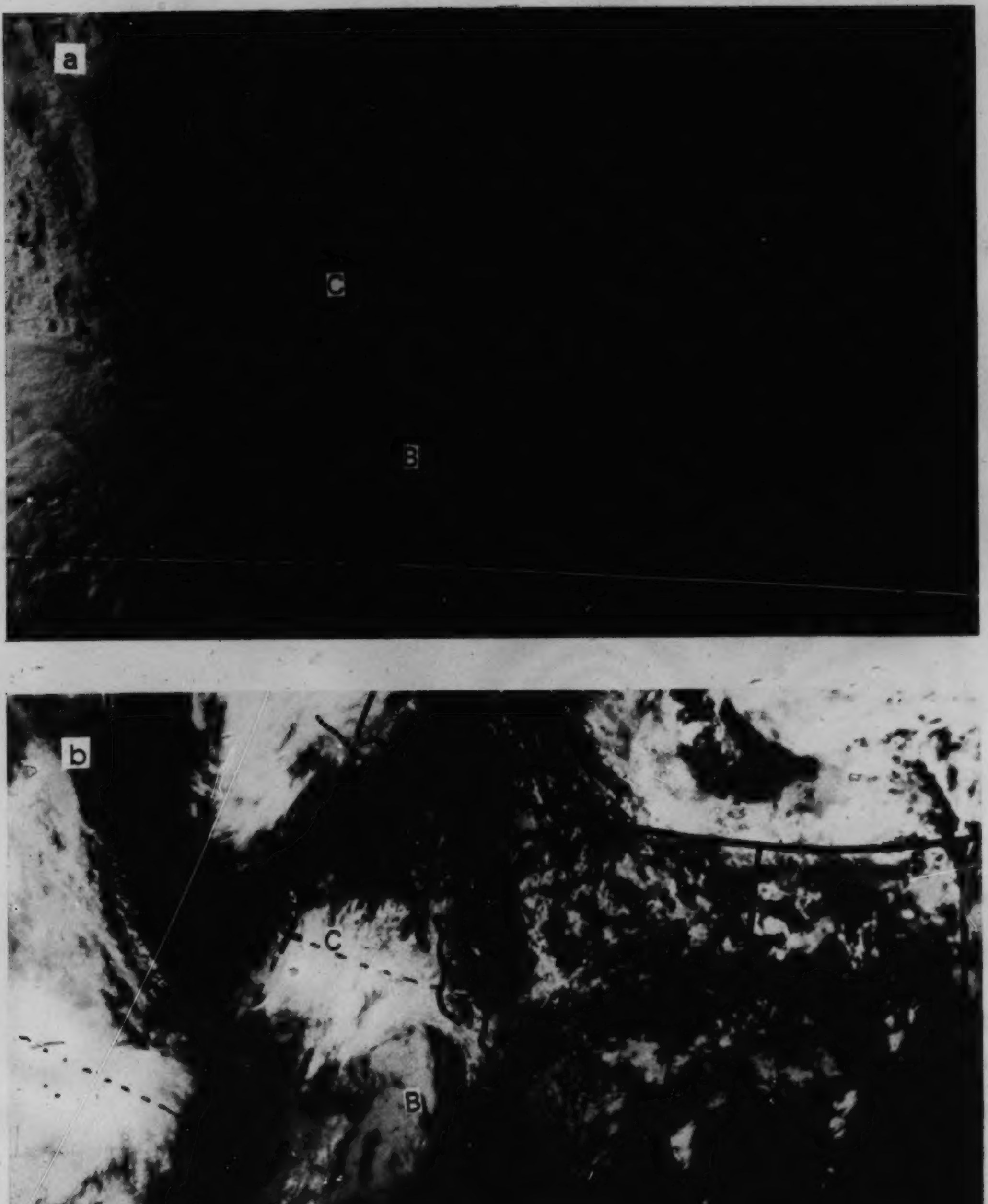

Figure 4.113 NOAA-8 satellite image, a) visible, b) infrared, 0319 GMT, 23 July 1983.

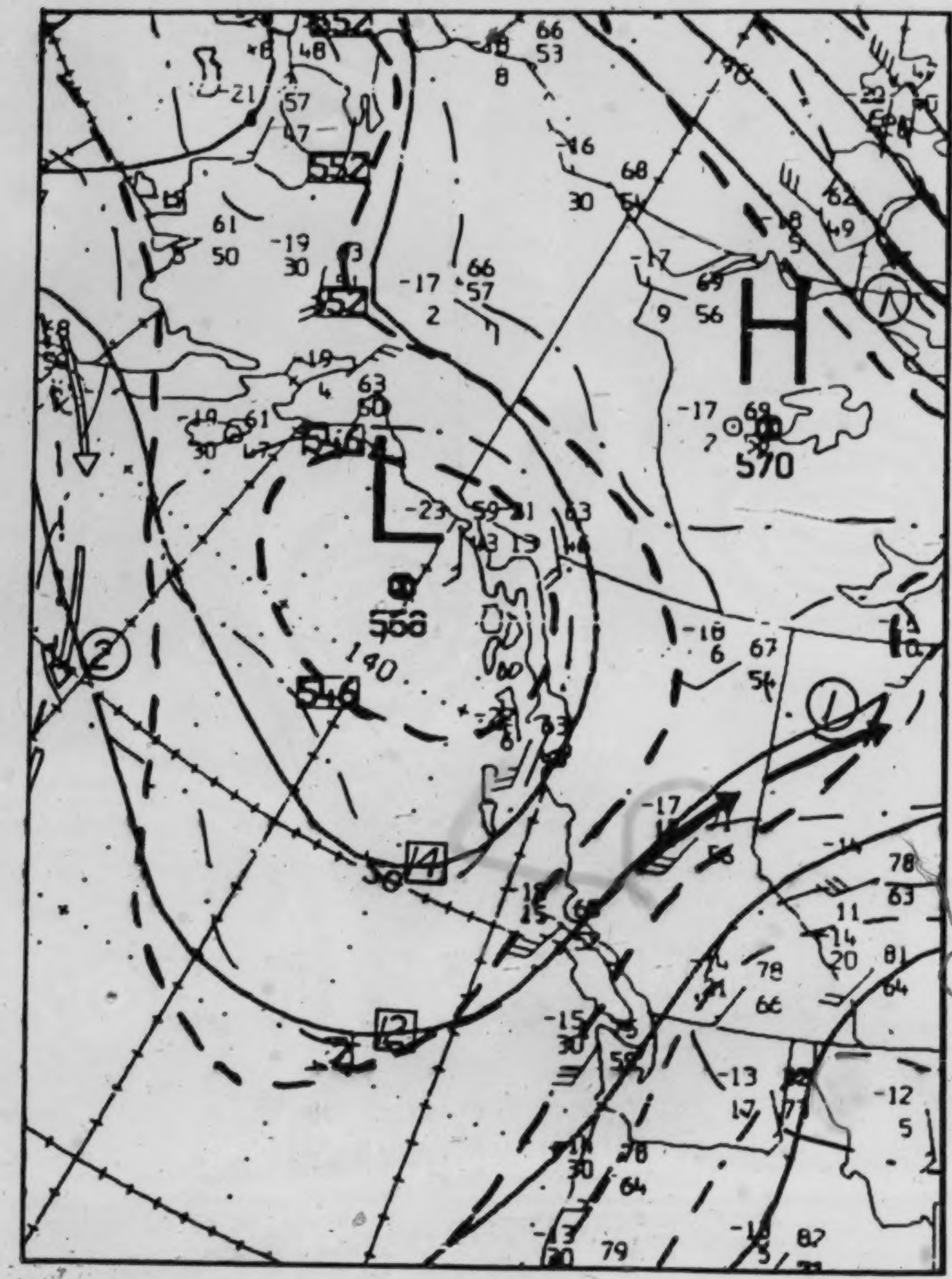
552
552
552
H
570
L
558
546
546
140
140
14
12
2
1

Figure 4.114 The same as in Figure 4.2 except for 23 July 1983, 1200 GMT.

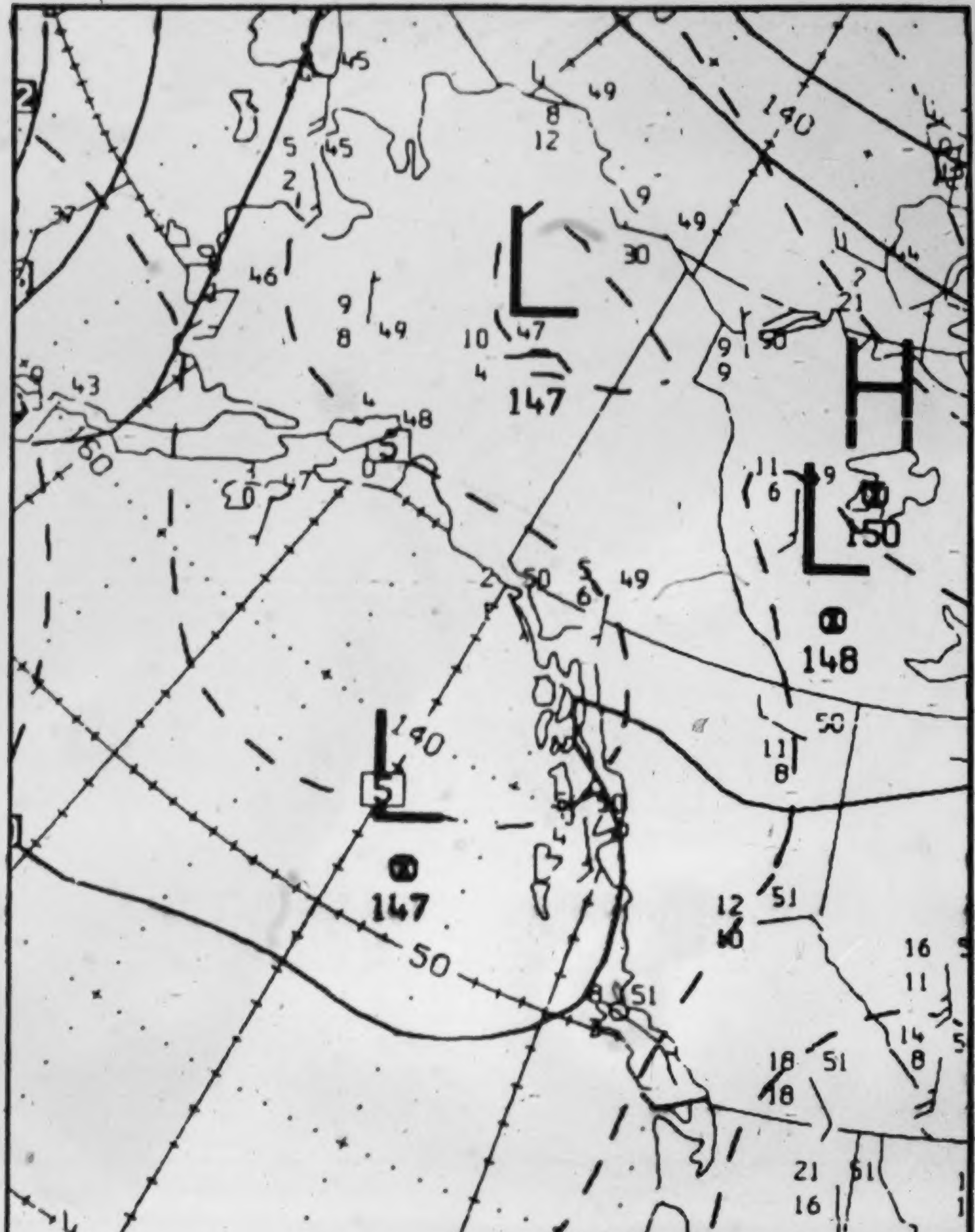
140
L
147
H
L
150
148
50
60
140
L
5
147
50

Figure 4.115 The same as in Figure 4.3 except for 23 July 1983, 1200 GMT.

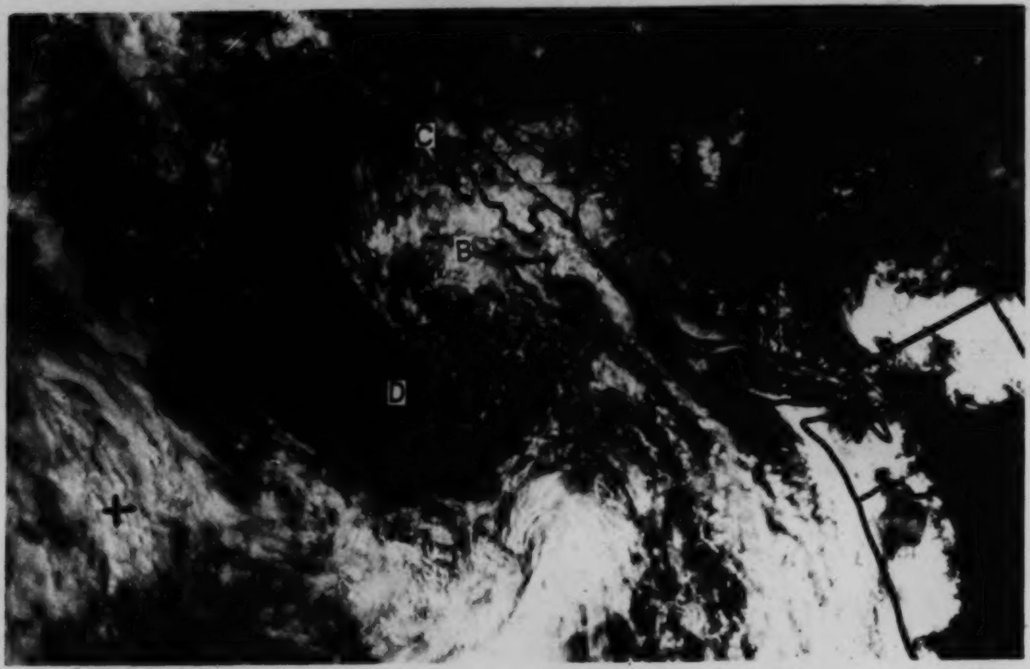

Figure 4.116 NOAA-8 satellite image , visible, 1709 GMT, 23 July 1983.

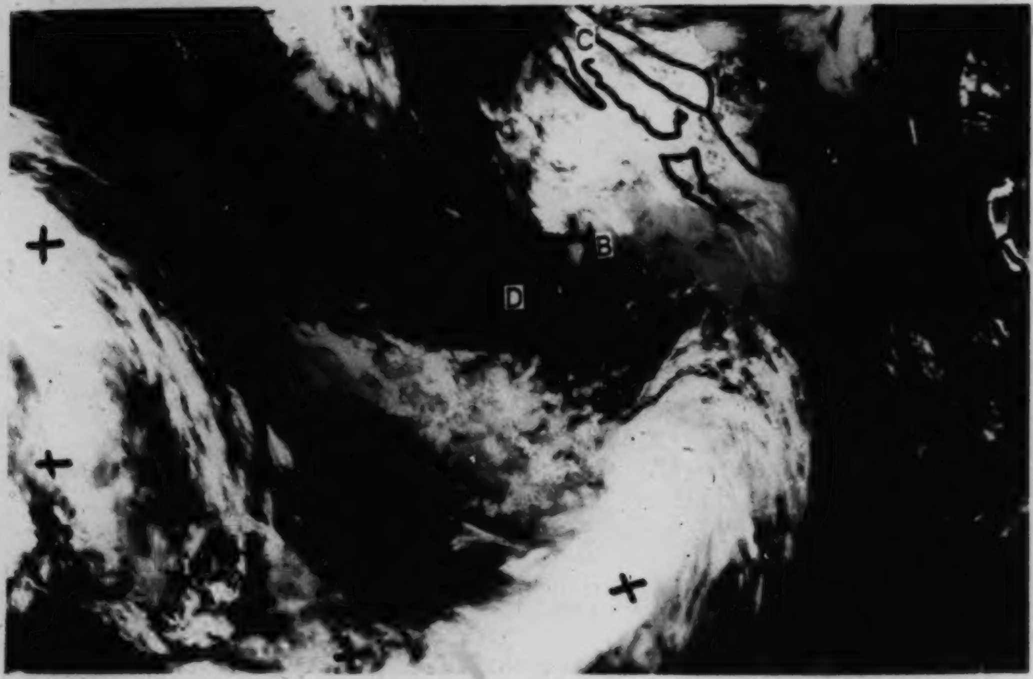

Figure 4.117 NOAA-7 satellite image , infrared, 1312 GMT, 23 July 1983.

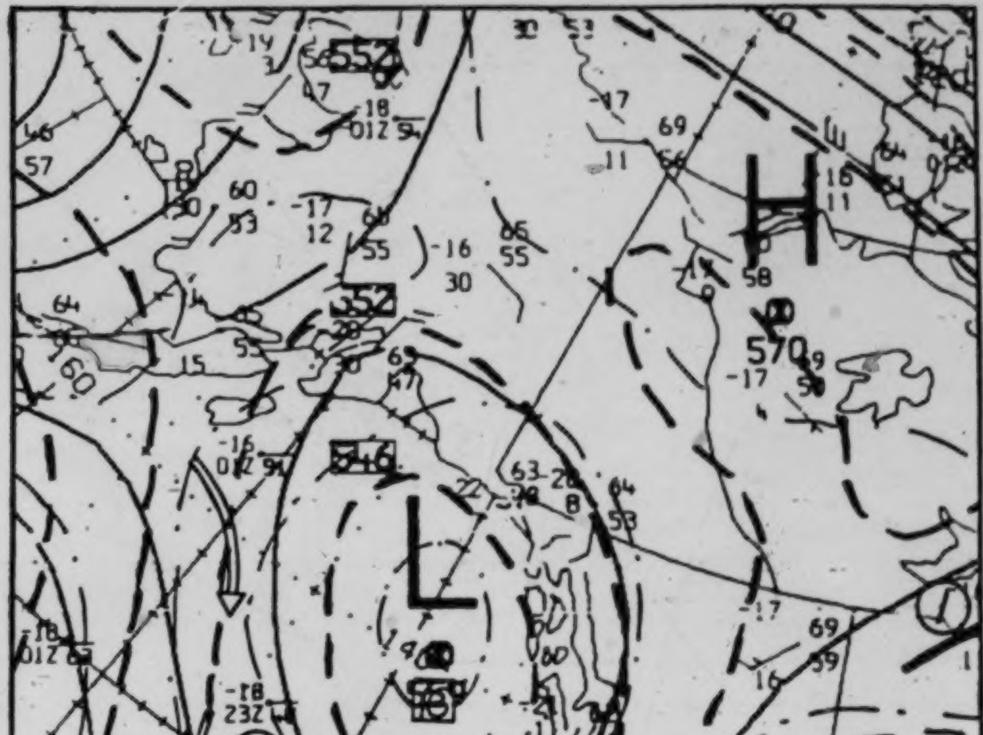
H
L
552
552
546
546
552
570
14
12
②
-18
01Z
-16
01Z
-18
23Z
-21
23Z 45
-14
23Z 56
-13
19
78
69
69
59
-17
16
10
64
79
65
85
80

Figure 4.118 The same as in Figure 4.2 except for 24 July 1983, 0000 GMT.

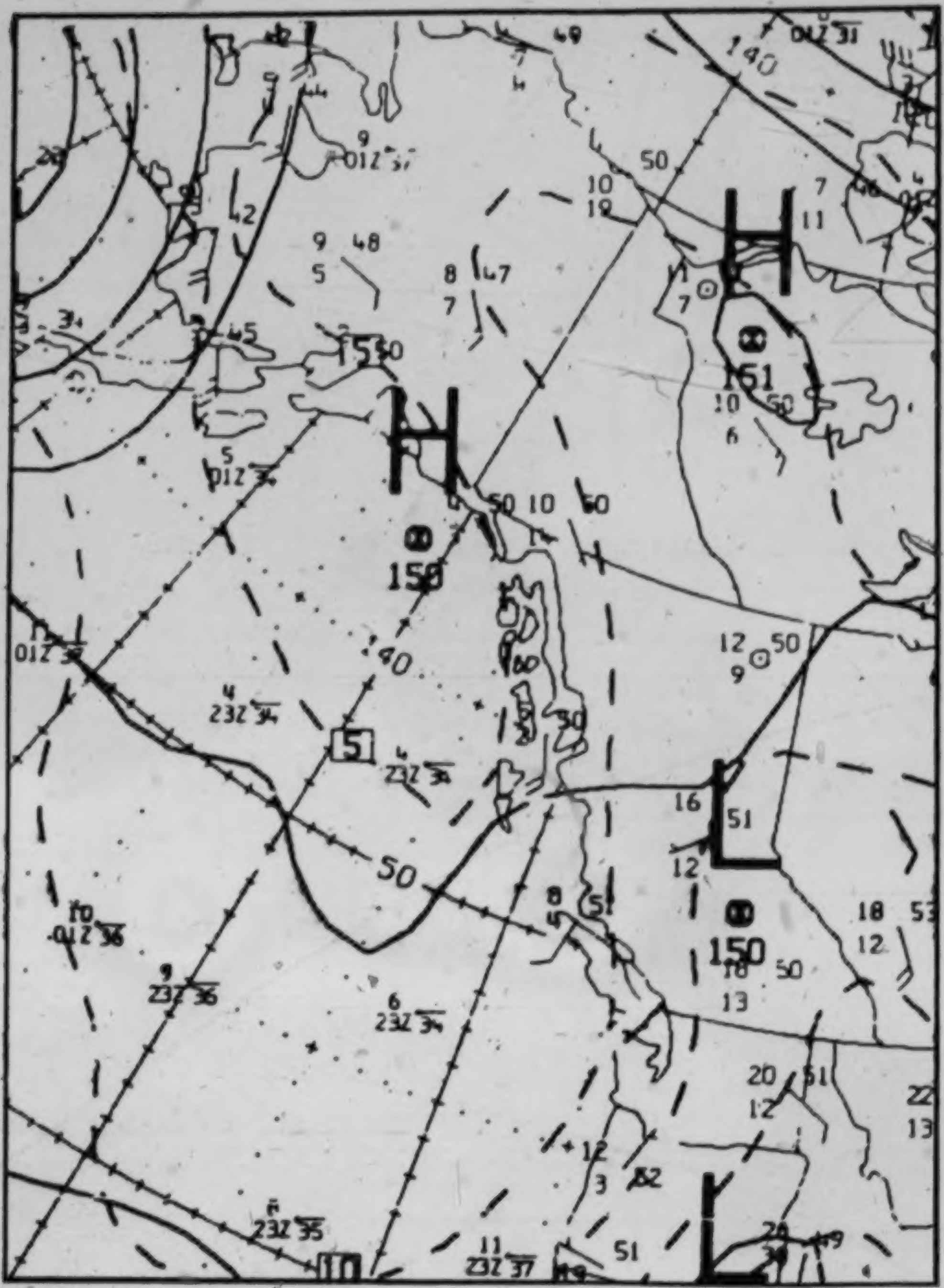
H
H
L
L
140
140
150
150
151
50
5
10

Figure 4.119 The same as in Figure 4.3 except for 24 July 1983, 0000 GMT.

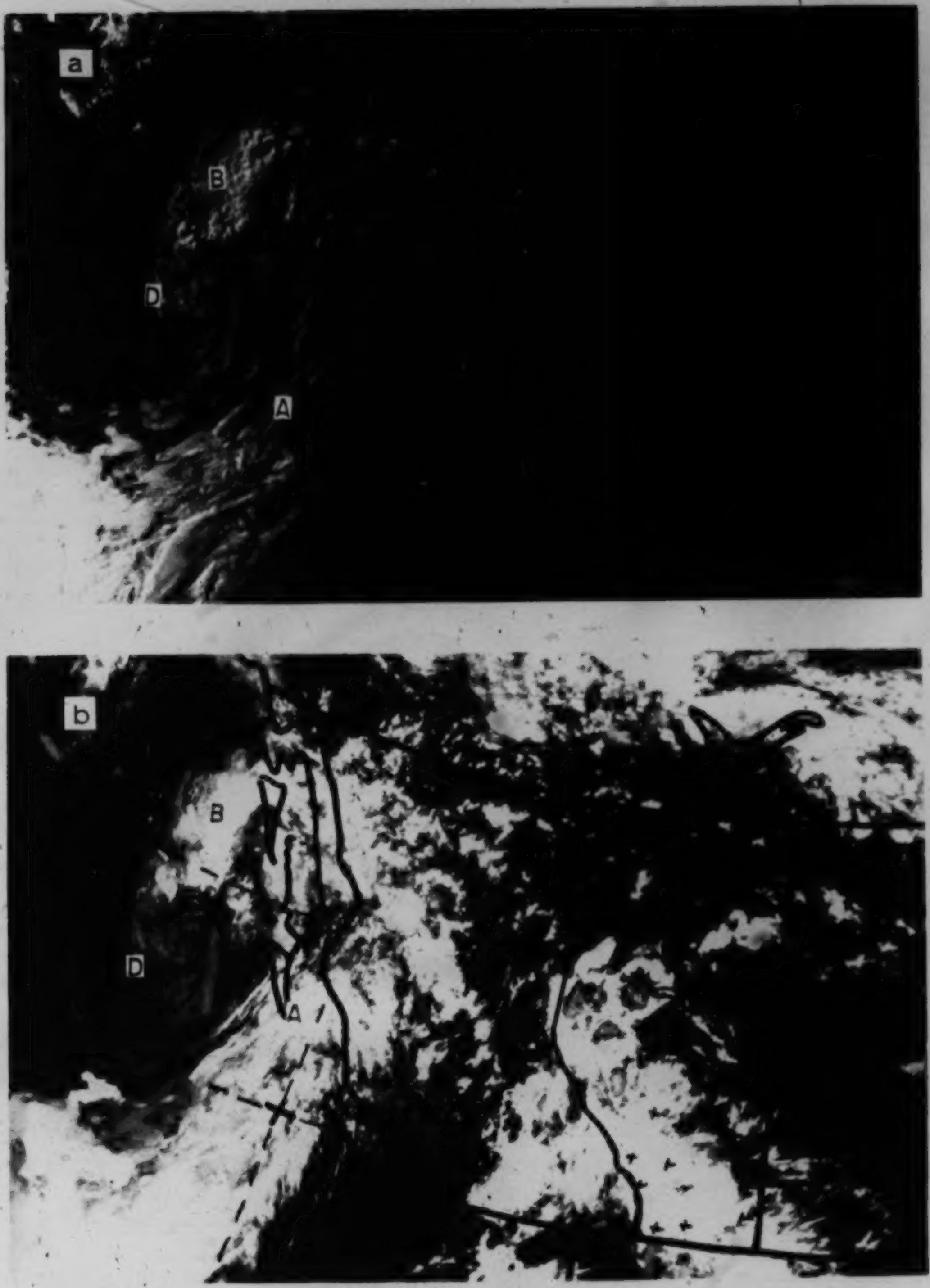

Figure 4.120 NOAA-8 satellite image, a) visible, b) infrared, 0257 GMT, 24 July 1983.

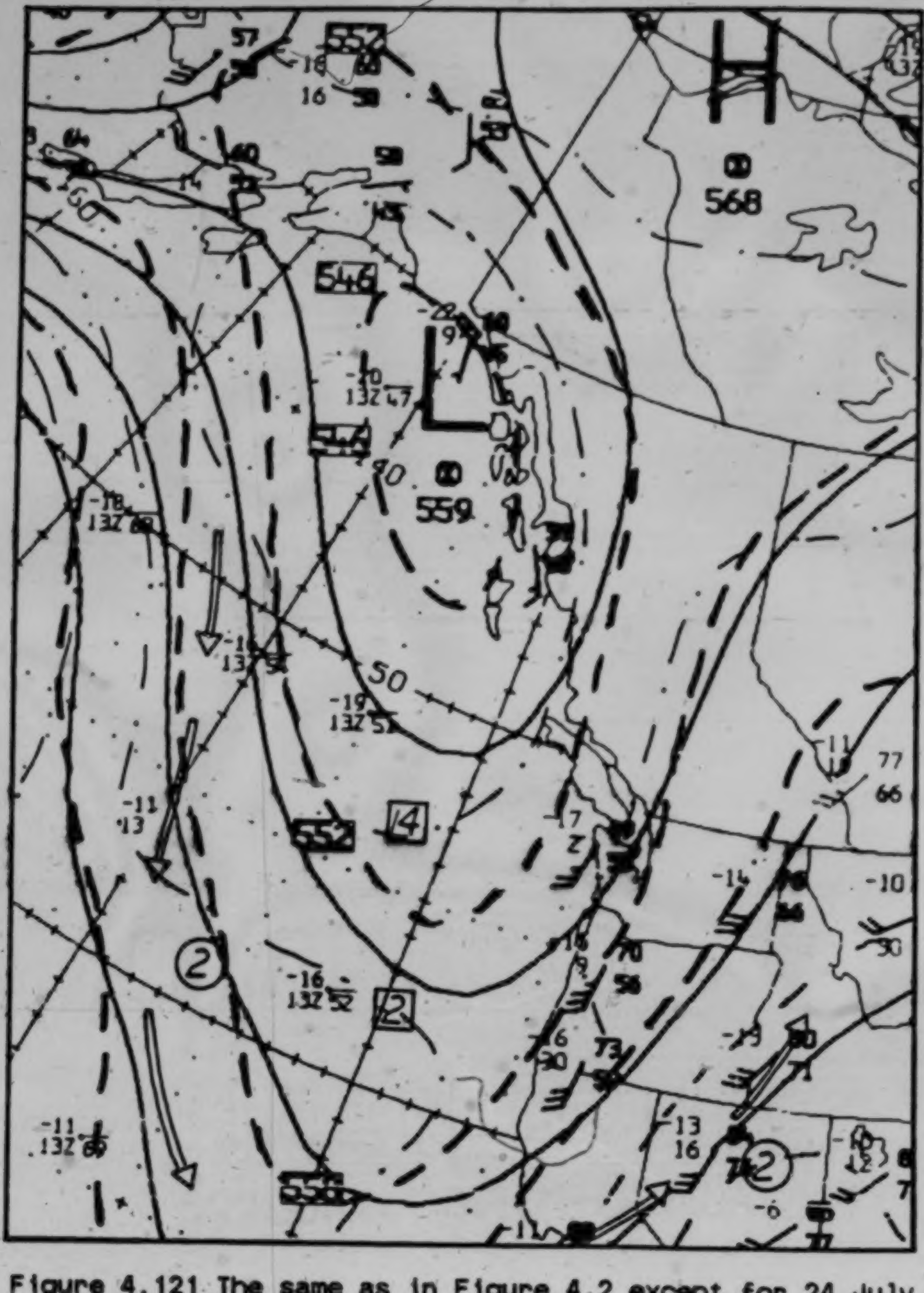
H
568
L
559
552
546
552
14
2
558
50
40
60
2
2

Figure 4.121 The same as in Figure 4.2 except for 24 July 1983, 1200 GMT.

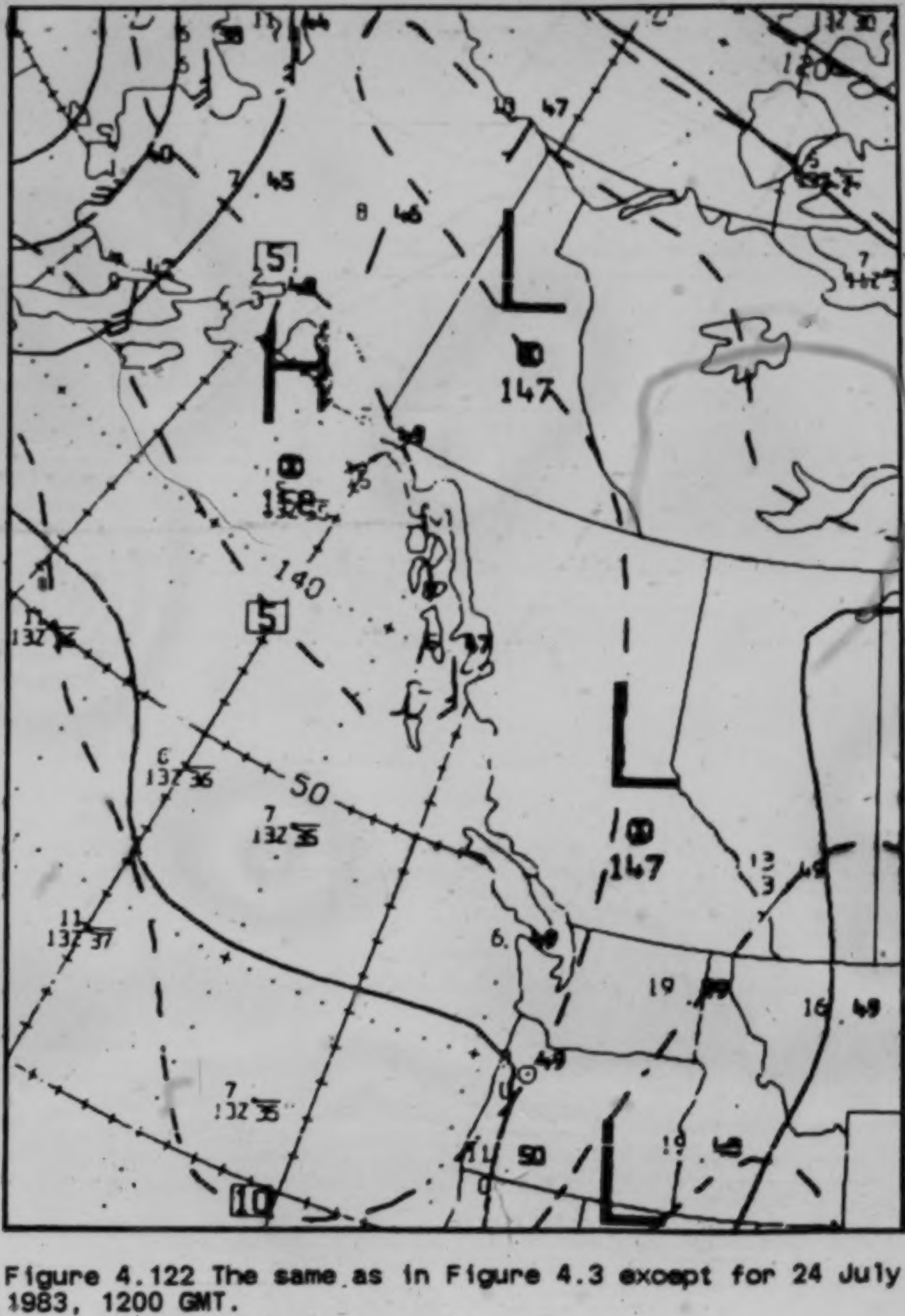
H
L
L
L
5
5
10
140
147
147
150
50
40
120

Figure 4.122 The same as in Figure 4.3 except for 24 July 1983, 1200 GMT.

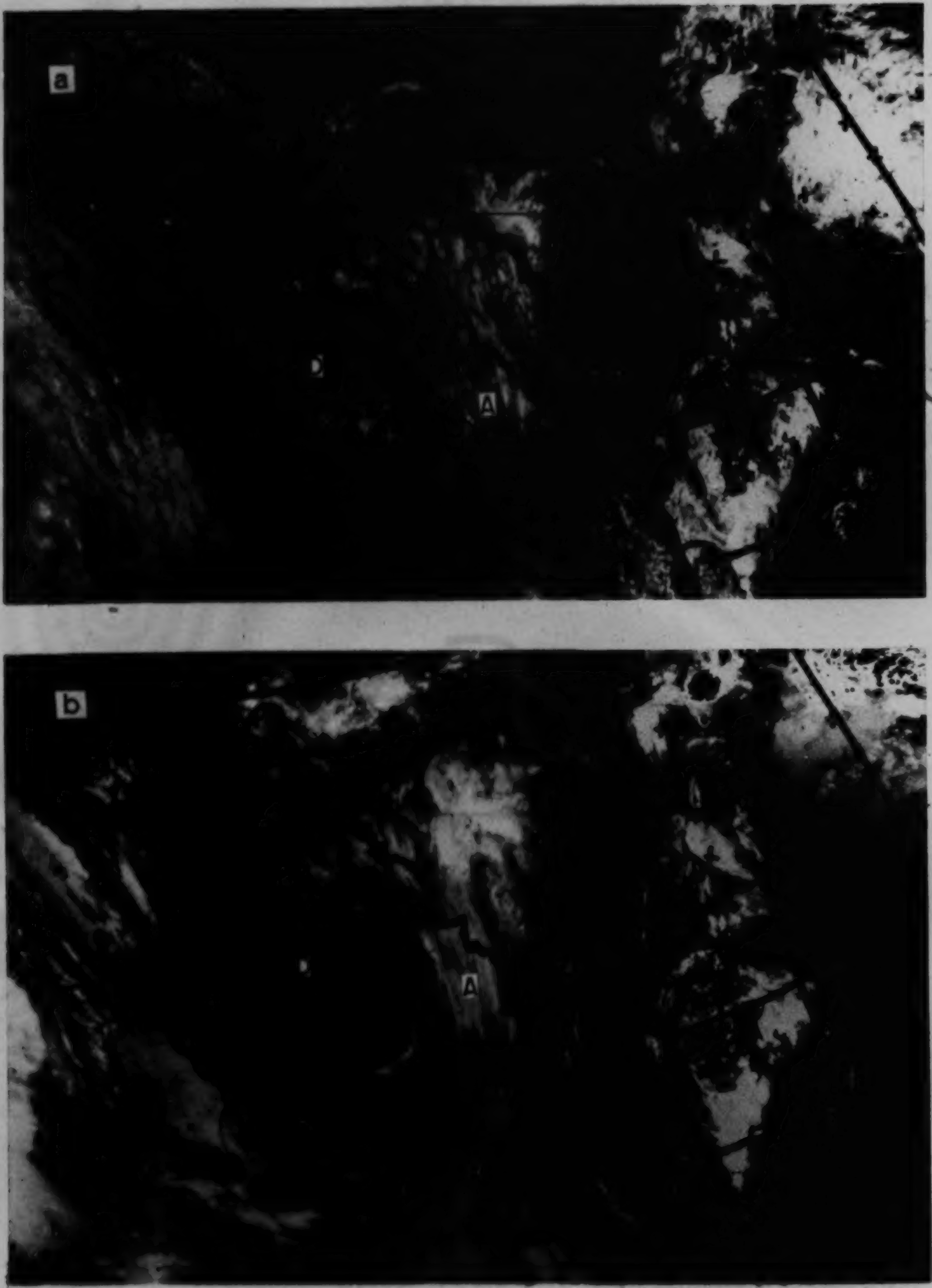

Figure 4.123 NOAA-8 satellite image, a) visible, b) infrared, 1648 GMT, 24 July 1983.

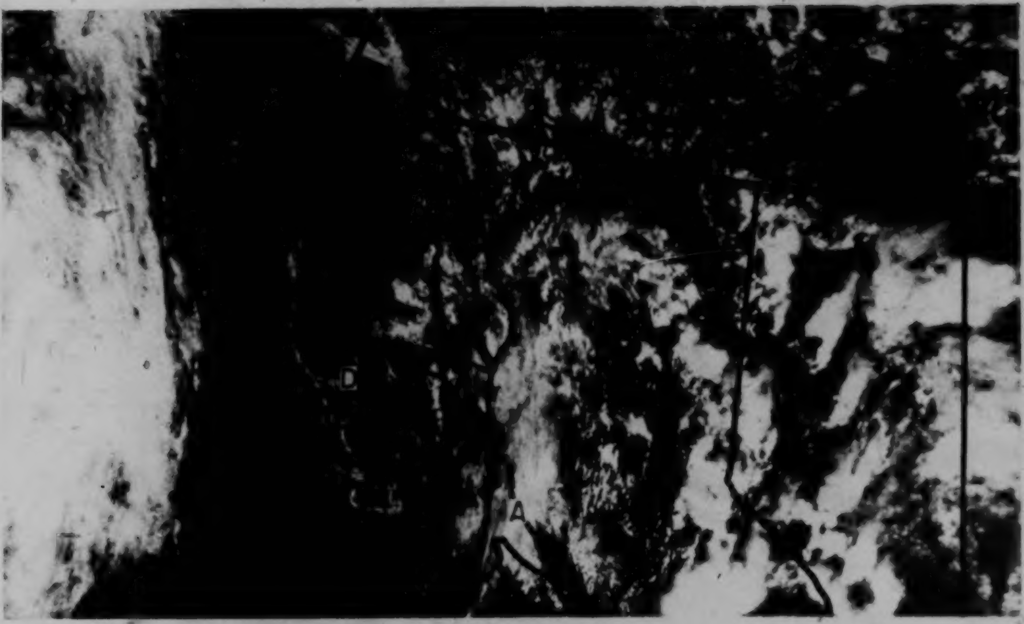

Figure 4.124 NOAA-7 satellite image , visible, 2253 GMT, 24 July 1983.

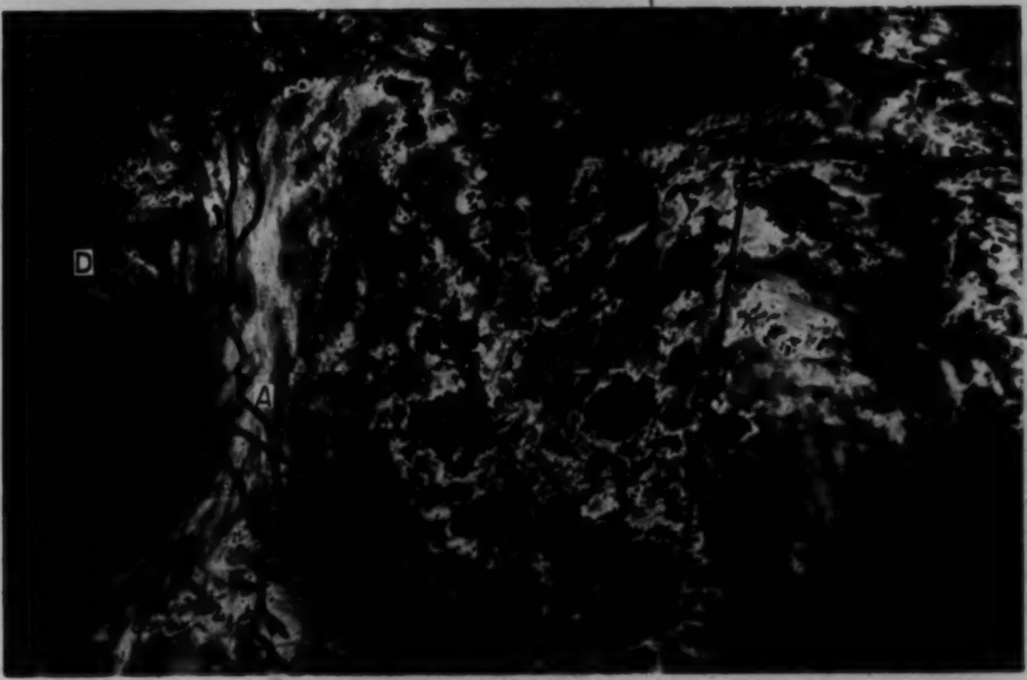

Figure 4.125 NOAA-8 satellite image , infrared, 0236 GMT, 25 July 1983.

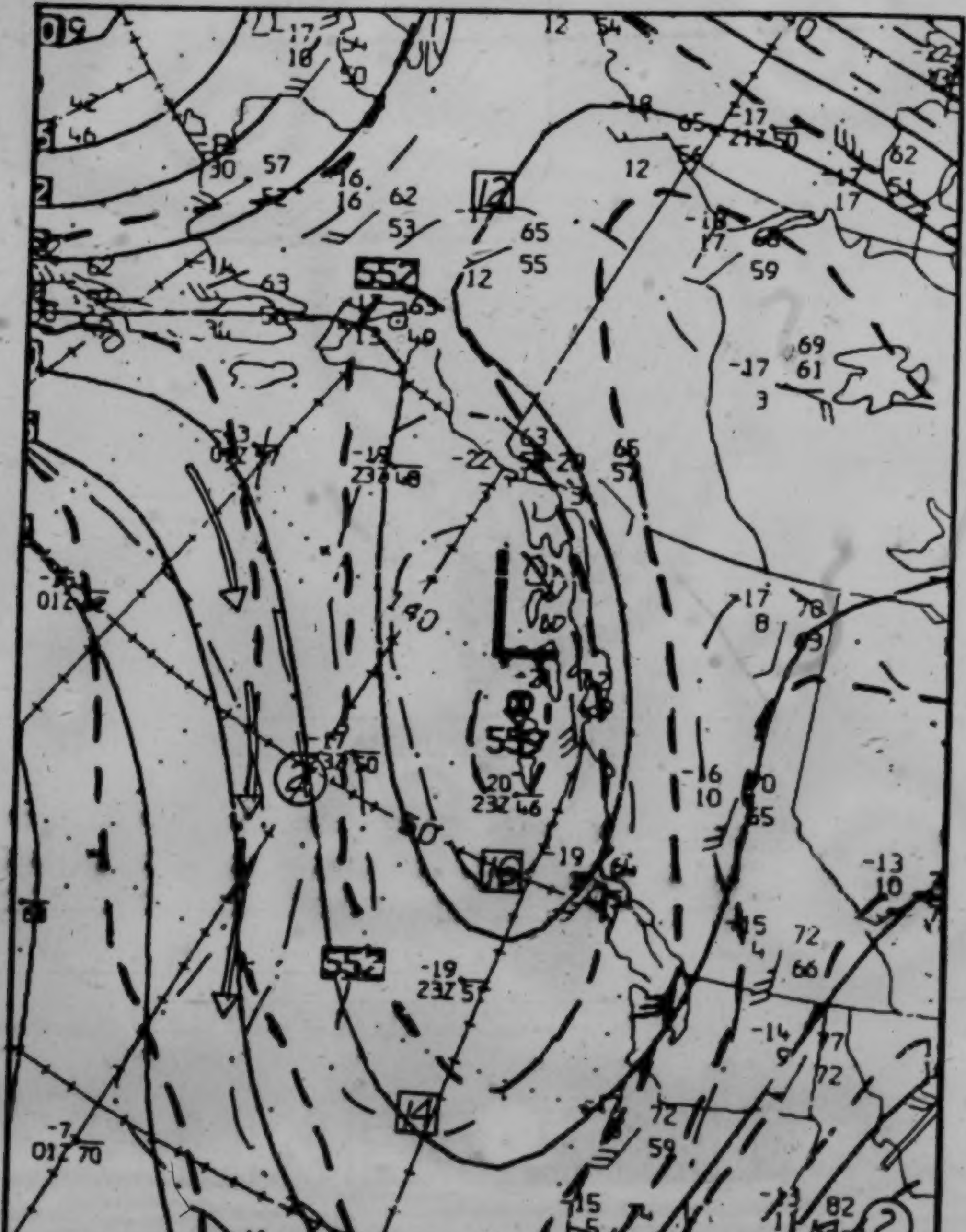
552
12
552
16
14
40
50
2

Figure 4.126 The same as in Figure 4.2 except for 25 July 1983, 0000 GMT.

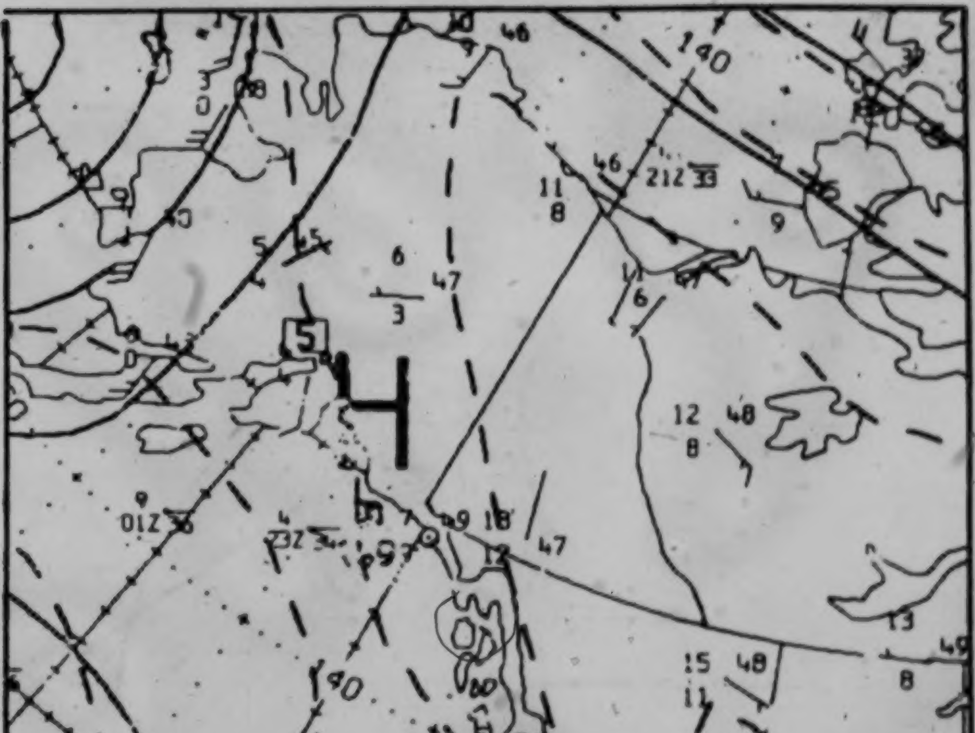
140
140
50
5
5
146
232 34
232 35
012 35
212 33
222
232 35

Figure 4.127 The same as in Figure 4.3 except for 25 July 1983, 0000 GMT.

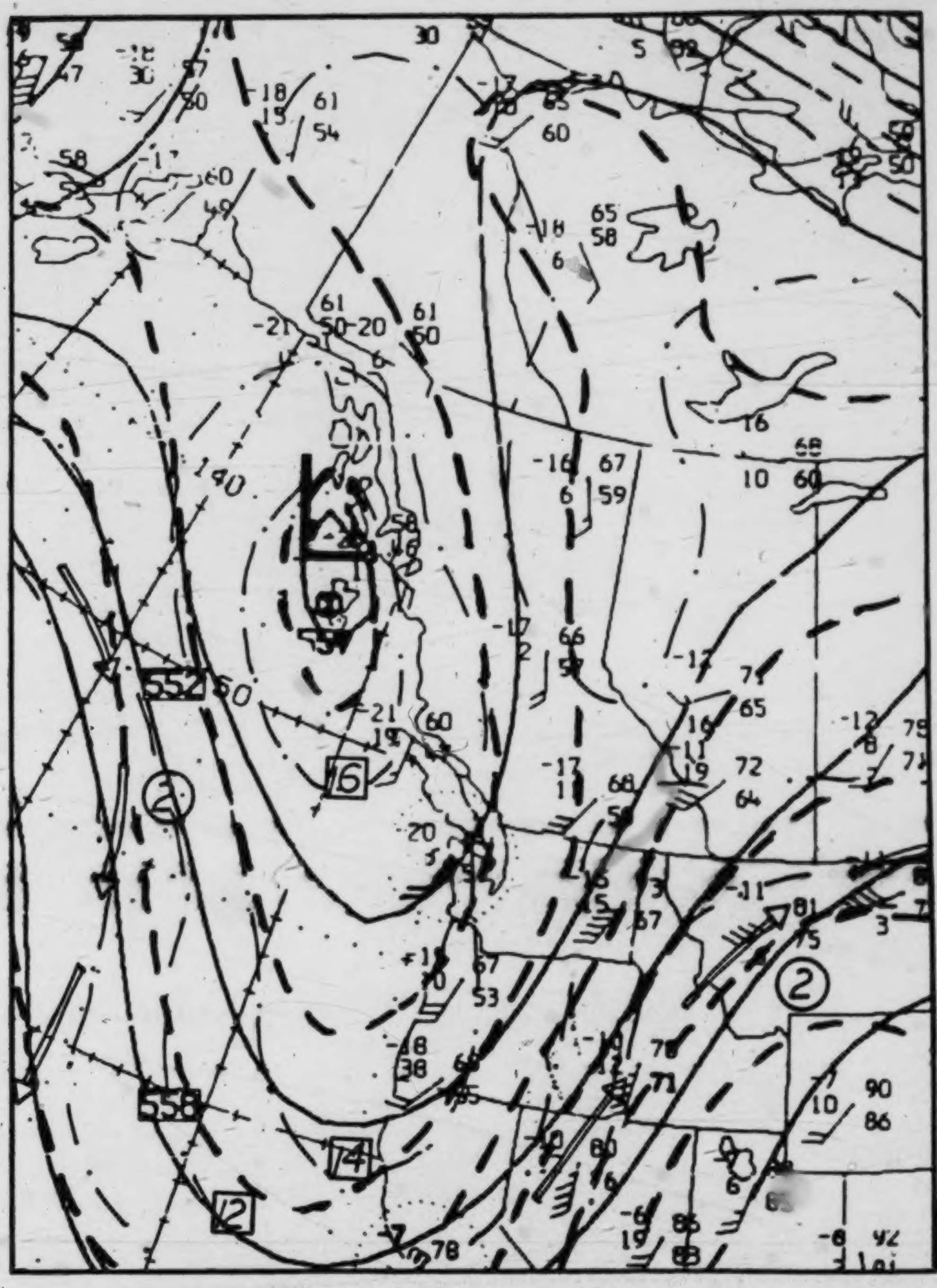
140
552
558
16
14
12
60
②
②

Figure 4.128 The same as in Figure 4.2 except for 25 July 1983, 1200 GMT.

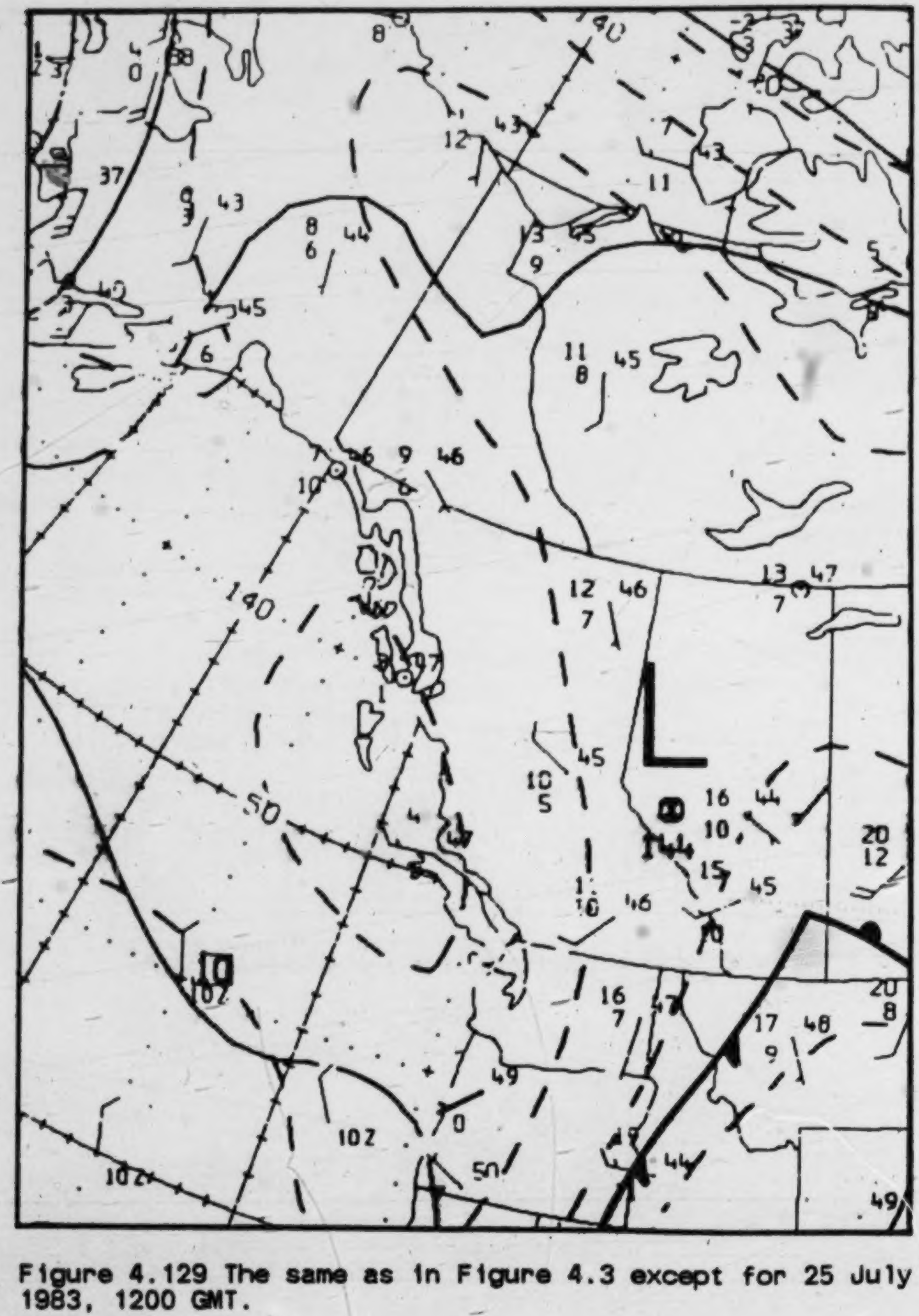
140
140
50
50
102
102
102
L
49
44
45
46
47
48

Figure 4.129 The same as in Figure 4.3 except for 25 July 1983, 1200 GMT.

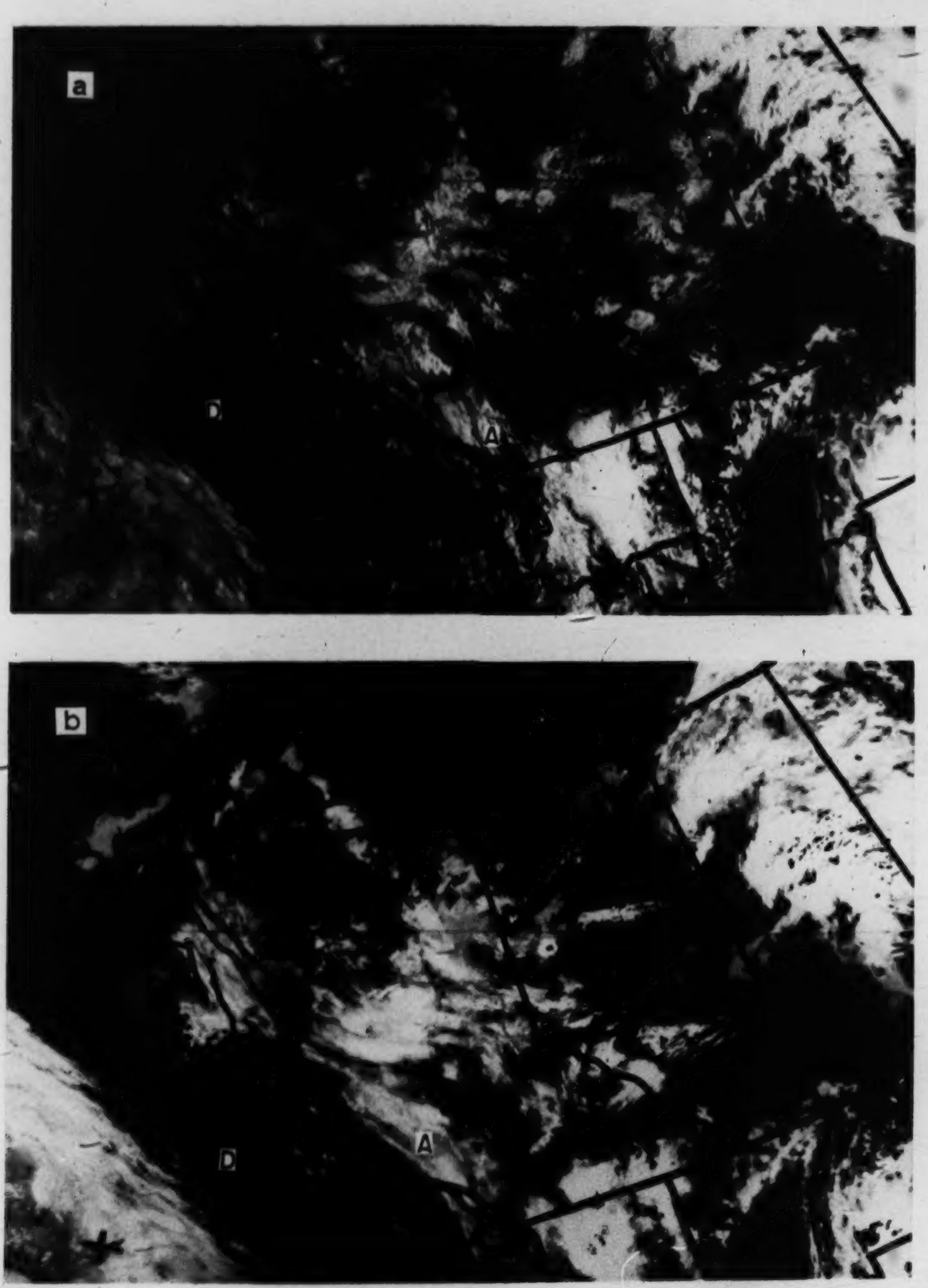

Figure 4.130 NOAA-8 satellite image, a) visible, b) infrared, 1625 GMT, 25 July 1983.

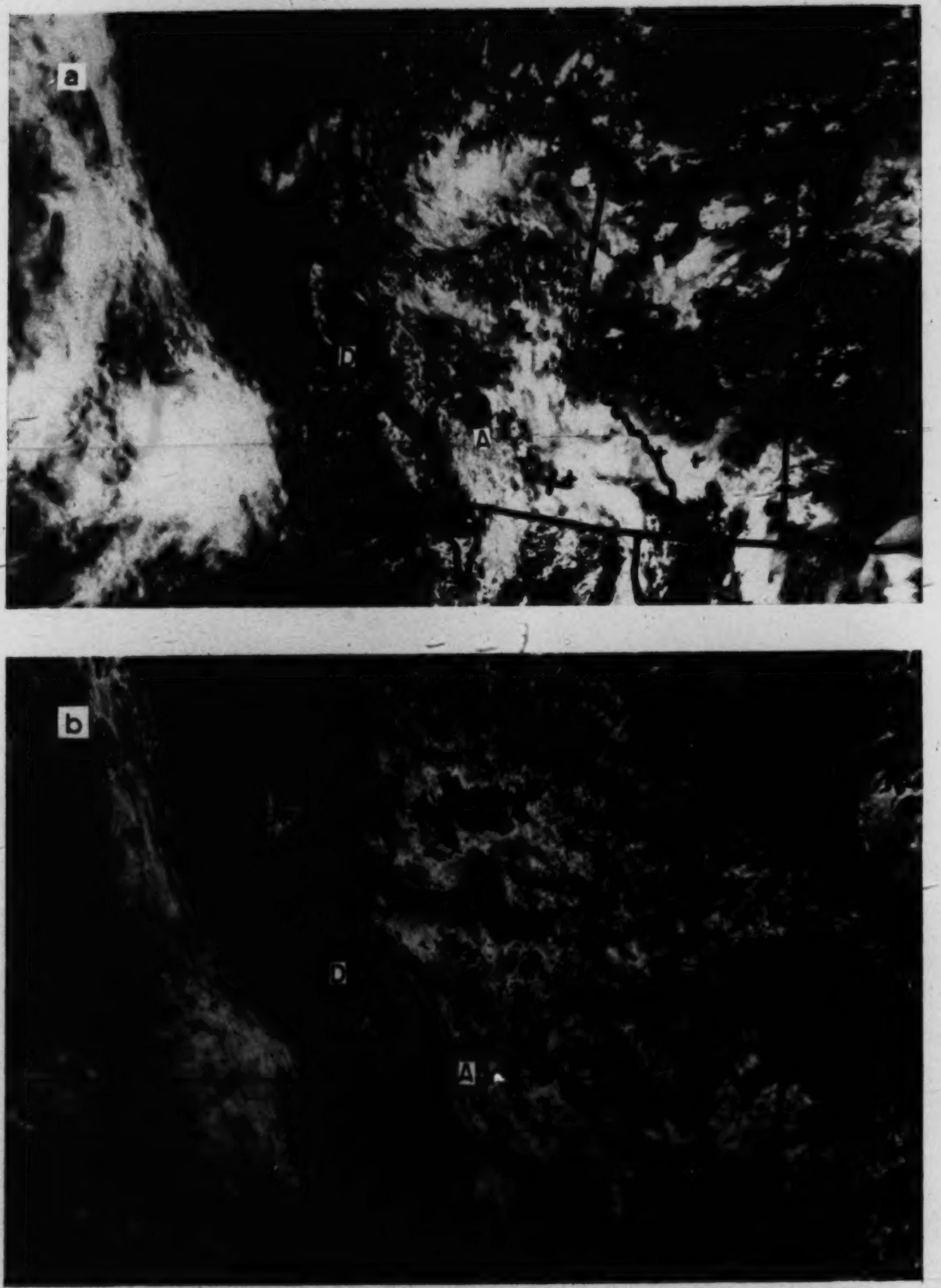

Figure 4.131 NOAA-7 satellite image, a) visible, b) infrared, 2240 GMT, 25 July 1983.

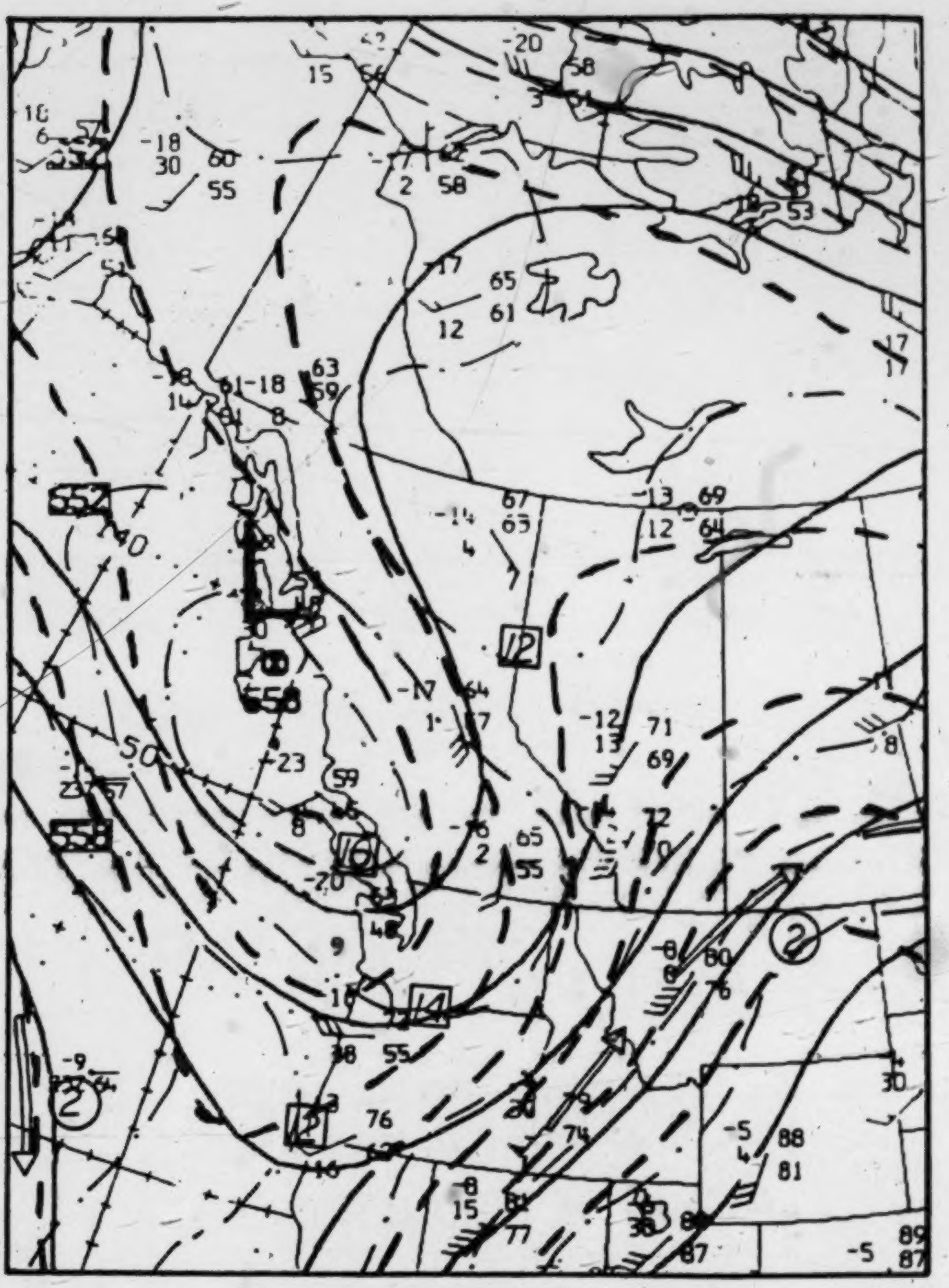
552
558
140
50
12
16
14
12
2
2
-20
58
15
-18
30
60
55
2
58
65
61
12
-17
63
59
-18
8
67
63
-14
4
-13
69
12
64
-17
64
1
57
-12
13
71
69
-23
59
8
-20
48
65
55
2
-16
72
70
-8
6
80
76
9
38
55
76
-5
4
88
81
-8
15
77
87
-5
89
87
17
17
53
30
-9

Figure 4.132 The same as in Figure 4.2 except for 26 July 1983, 0000 GMT.

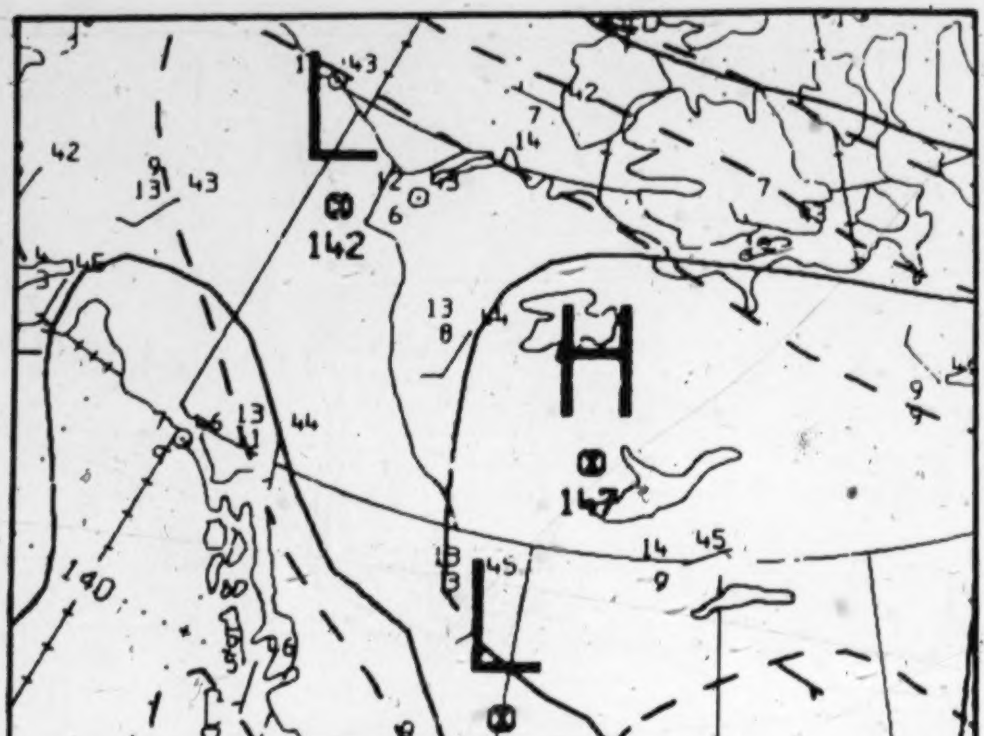
L
142
H
147
L
143
140
50
42
43
44
45
46
53

Figure 4.133 The same as in Figure 4.3 except for 26 July 1983, 0000 GMT.

# 5. Results of the Study

## 5.1 General Outline

Presented in this chapter is a summary of the principal findings of this investigation of synoptic-scale cloud patterns and development. The first part describes the general features of a synoptic cloud classification, whereas the second concentrates on the synoptic features of upper-level cyclogenesis and development.

Satellite data are sufficient to identify the various synoptic cloud patterns. Derived meteorological parameters, such as thermal gradients, vorticity, vorticity advection, etc., are useful in the sub-classification process. However in the second part, close integration of satellite and synoptic data is necessary and essential.

Since the main goal of the study concerned synoptic study, the interaction between synoptic and subsynoptic scales of development was examined only to the extent necessary for the understanding of the mechanism of development.

## 5.2 Synoptic Scale Cloud Pattern Classification

The examination of the case studies suggests that cloud patterns which attain characteristic synoptic-scale of basic dimensions can be classified into four main groups: (i) the cloud band group, (ii) the vortex group, (iii) the cellular group, and (iv) the uniform group. The length characteristic differentiates (i) and (ii) from (iii) and (iv). The curvature characteristic differentiates between (i) and (ii), and the texture characteristic differentiates between (iii) and (iv).

The cloud band group includes eight subgroups characterized by great length of the order of $10^3$ km and weak curvature of the order of $10^{-3}$ km$^{-1}$. The horizontal dimension is a common factor between the eight subgroups, whereas the vertical dimension is not. For example, jet, post-frontal, orographic, and non-frontal bands vary greatly in the vertical. The same is true for the speed of propagation, e.g. the speed of a jet band is one order of magnitude greater than that of an orographic band. The other four patterns (frontal, pre-frontal, convergence, and shear bands) satisfy the general characteristics of the group.

The vortex group includes three patterns: the low-level vortex, the upper-level vortex, and the comma cloud. They all possess significant cyclonic curvature, ranging from $2 \times 10^{-3}\,km^{-1}$ to $5 \times 10^{-3}\,km^{-1}$. The low and upper-level vortices have a defined centre of rotation, while the comma has no such identifiable centre. Despite the subsynoptic activity within a comma cloud pattern, especially in the early stages, the overall configuration of the comma enables one to consider it as a synoptic pattern.

The cellular group includes three cloud patterns: the open, the closed, and the non-organized. The development of the non-organized pattern into a comma pattern is the key for including it in this group, despite the subsynoptic development of its cloud elements. Moreover, a cellular pattern, under the influence of cyclonic circulation, may attain spiral organization for its cloud elements.

The last member is the uniform group, which has horizontal dimensions comparable to the cellular group, but the cloud pattern is more homogenous and uniform. This is most clearly shown in the case of synoptic-scale fog. This group includes the fog-low stratus pattern and the mid-level pattern. The two patterns develop under different meteorological conditions of stability and wind field but are otherwise similar in appearance on satellite images.

### 5.3 The Upper-Cold Low Model

The model for the initiation and development of an upper-level cyclone presented here is based on satellite and synoptic data for Western Canada during the spring and summer months. The objectives were to construct an upper-level model of cyclonic development and to determine the critical value of the vorticity field associated with such development. The model postulates and defines six stages of development.

The following figures will explain these different stages, where the letters (A), (B), (C), and (D) refers to the various cloud areas and have the same meaning as used before in Chapters 3 and 4. The contours outline the upper flow and the arrows represent the jet stream axes.

### 5.3.1 The Troughing Stage

Figure 5.1 shows the first stage, where the mid-level flow gives the first hint of the area of probable cyclogenesis, a pronounced amplitude. A small area of convective clouds, (B), points out the area of likely development on the corresponding satellite image. At this stage, (B) is a cumuliform non-organized cloud area of considerable thickness. The existence and advance of jet (2) all but assure the early development. Jet (2) plays the dominant role in this case, while jet (1) has no effect on the evolution process. The vertical temperature distribution within the layer 1000/500 mb (not shown), determines that (B) lies within the cold air, and on the southern part of the thermal trough. The low-level flow is usually poorly-defined except in modified strong cases. In a modified case, an incipient front or weak warm intrusion develops near (B).

### 5.3.2 The Splitting Stage

In Figure 5.2, the flow has become diffluent and is splitting into two distinct streams. Along the southern branch, associated with jet (2), upper-level cyclogenesis may be expected in the SE-corner of the trough. Jet (2) becomes more channeled and advances towards the troughing base. The trough digs farther southward acquiring usually positive or negative tilting. A closed contour circulation is not likely to appear at this stage. The vertical thermal field (1000/500 mb) becomes more centered over the trough, while the low-level flow does not show appreciable change.

Cloud area (C), composed of high and middle clouds, develops within the confluent zone as indicated in Figure 5.2. It has acquired an anticyclonic curvature and exists entirely within a confluence area of weak gradient. Appearance to the contrary, (C) is not associated with jet (1). Cloud area (B) continues its vertical development, where the rate of growth depends on stability, moisture field distribution and vertical wind shear. (B) also expands horizontally without changing its configuration, showing a regular outline in strong cases and an irregular in weak cases. Cloud area (A), composed of middle and high clouds, develops to the south of (B). It has the same general features as (C), but is not associated with jet (2). It is also more developed than (C), both in the vertical and horizontal. It is sometimes difficult to separate the troughing stage from the splitting stage.

### 5.3.3 The Pinching-off Stage

In Figure 5.3, the 500-mb flow shows the first sign of the pre-cut-off process. The trough, which has become symmetrical, is pinched-off at its neck. Jet (2) approaches the base of the trough, while jet (1) advances northeastward and merges with the westerly main flow. A weak closed wind circulation is becoming established and a closed contour circulation may appear at the base of the trough. It is not probable, at this stage, that the closed circulation propagates downward. A similar pinching-off process may affect the vertical temperature distribution.

Cloud area (C) continues farther westward with respect to the cloud pattern. The northern edge becomes better defined, as it acquires pronounced anticyclonic curvature and spirals around the core of cold air. For the first time cloud area (B) attains its comma shape (except in the weak cases), moves very slowly northward and becomes partly covered by (A).

### 5.3.4 The Cutting-off Stage

This, important phase in the life history of the upper-level storm,is ahown in Figure 5.4. All cloud areas have continued to develop and the pattern has attained pre-storm configuration. Cloud areas (A) and (C) have expanded vertically and horizontally, and both approach and cover most of (B). Cloud area (B) acquires full comma shape and moves to the cyclonic side of the advancing jet (2). Jet (2) now advances very rapidly traversing around the base of the trough.

Meanwhile, on the 500-mb surface, the pinching-off process is weakening and the contours are opening up again, but the cut-off circulation is fully established. The closed circulation, which has reached its maximum intensity, may propagate to lower levels at this stage. Throughout this phase, the flow pattern maintains its symmetrical shape and the vertical temperature distribution shows an eastward advance of the pool of cold air.

### 5.3.5 The Mature Stage

At this stage (Figure 5.5), the cloud pattern reaches its maximum development. All cloud areas are moving northeastward. The cloud pattern expands westward to the region of maximum shear. Cloud areas (A), (B), and (C) begin to merge ultimately and culminate in a very distintive lambda configuration, while cloud area (D) may develop into a separate comma or another separate system, depending on the controlling vorticity field. It is often difficult to distinguish between (C) and (A) at this stage.

At the mid-levels the flow opens up, and the closed circulation all but disappears. Meanwhile, the low-level circulation begins to intensify. Jet (2) moves completely to the eastern side of the trough and begins to curve anticyclonically as it crosses the body of the storm cloud configuration.

### 5.3.6 The Decay Stage

In this stage, the cloud pattern and the upper-level flow break down rapidly, as can be seen in Figure 5.6. The various cloud areas spread apart and move off in different directions. Cloud area (A) moves eastward, (B) and (C) move toward the west, and (D) is almost stationary. All cloud areas weaken considerably and the overall pattern loses its identity. (B) moves out and beyond the influence of jet (2).

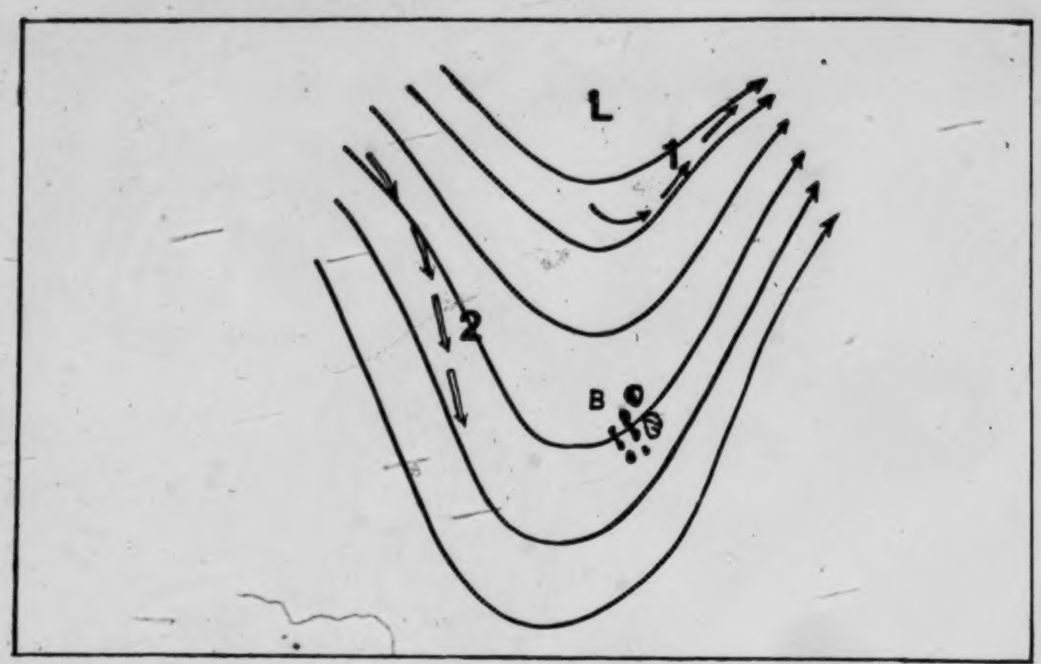

Figure 5.1 The troughing stage

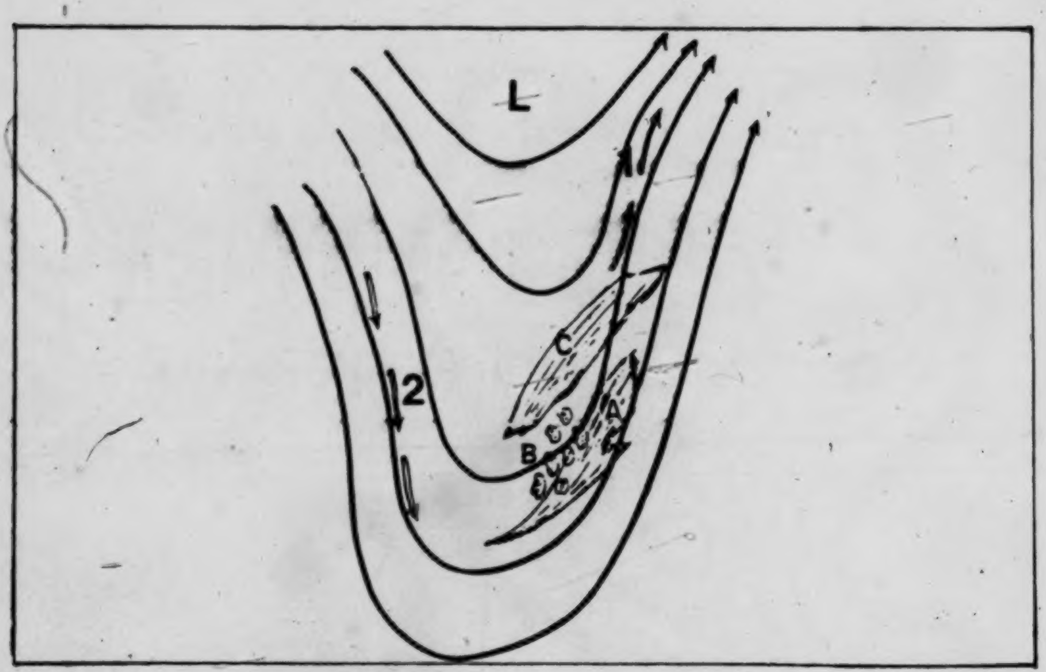

Figure 5.2 The splitting stage

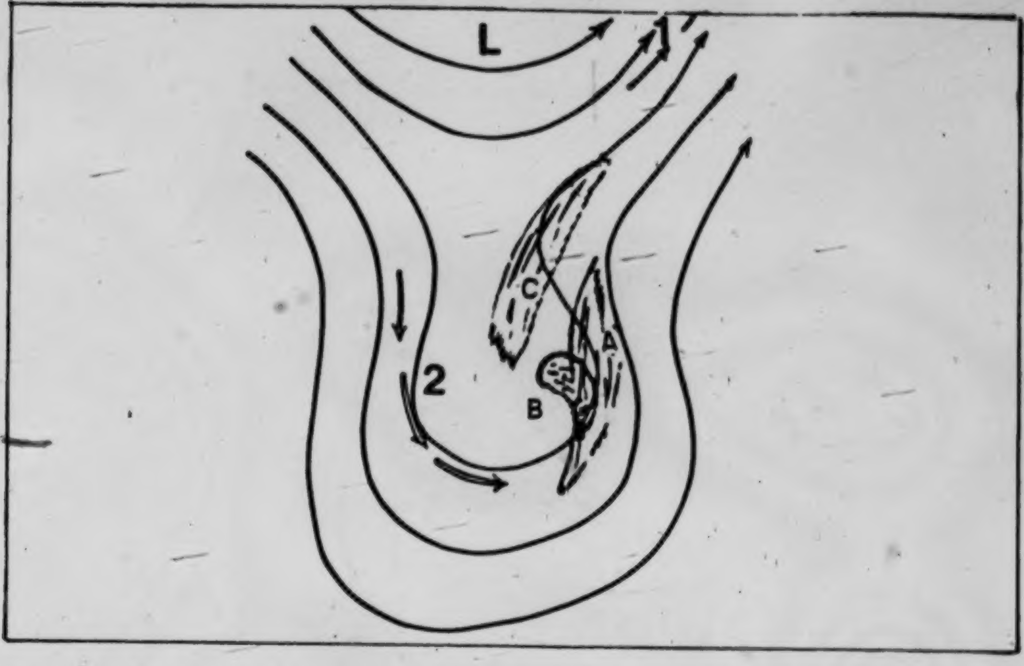

Figure 5.3 The pinching-off stage

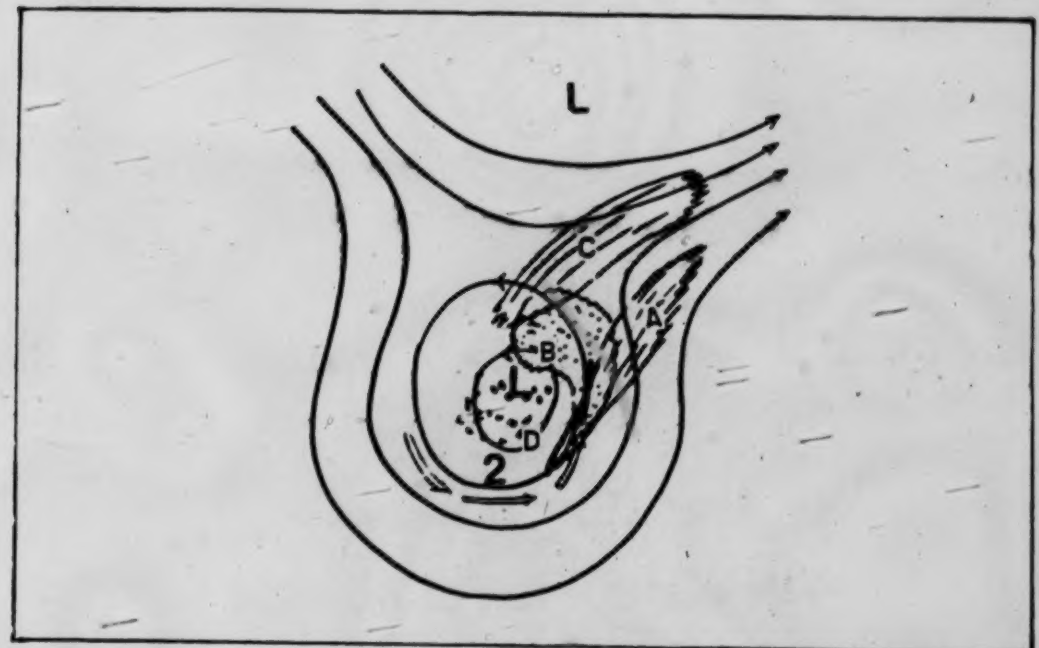

Figure 5.4 The cutting-off stage

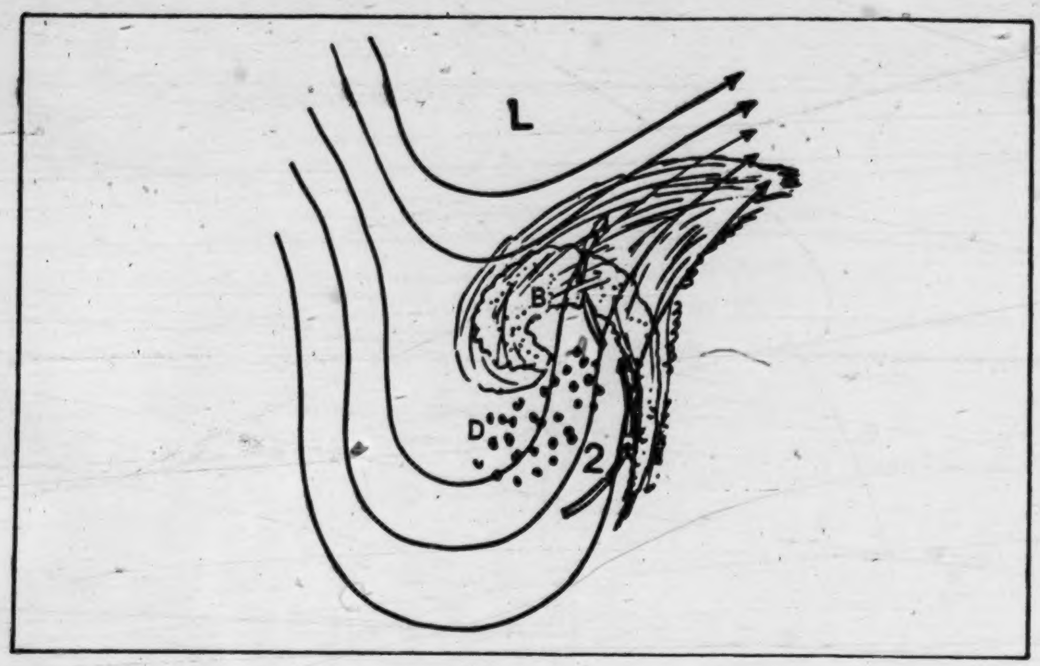

Figure 5.5 The mature stage

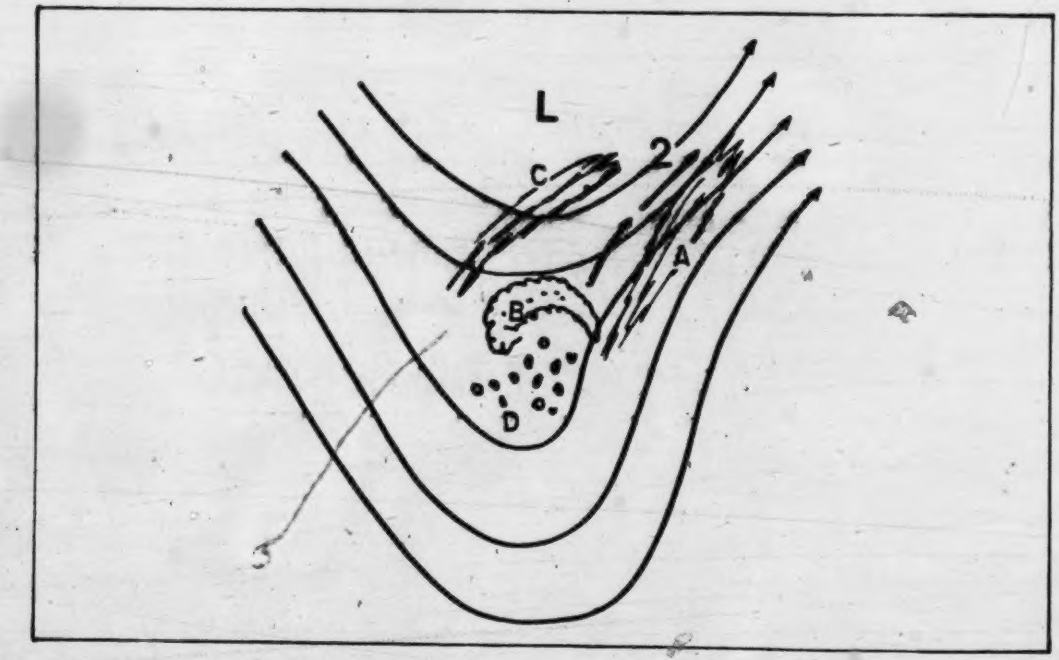

Figure 5.6 The decay stage

The upper flow opens up more and resumes the shape of a typical cold trough. Jet (2) moves rapidly eastward and merges with the main westerly flow. The cold air pool shrinks in area. At this stage, the system's persistence depends crucially on the vertical stability.

### 5.4 Results and Conclusions

The main goal of this study, the examination of the synoptic features of cloud patterns and systems, has been realized within the limitations of the project. The integration of satellite data with synoptic data in the study of cloud patterns is superior to using each one separately. Satellite images provide good resolution in space and time while synoptic observations furnish numerical values of basic meteorological parameters. The ability to identify cloud pattern regimes, based on characteristic dimensions, is a useful skill readily acquired by the analyst.

The principal criterion of classification that "any cloud system which satisfies, for a period of about 12 hours, at least the synoptic-scale horizontal dimension will be considered a synoptic system" has shown to be valid in the majority of cases examined. Zwatz-Meise's (1981) model of classification of cloud patterns can be adapted to Western Canada, if a number of modifications are made to: (i) the sub-classifying process, and (ii) the correlations between cloud patterns and corresponding parameters. In sub-classifying cloud patterns, the length, the radius of curvature, and the texture of a cloud pattern were found to be essential characteristics. Different parameters were selected to classify frontal and pre-frontal bands. In the frontal band formations the 500-mb relative vorticity, the thermal front parameter, and the surface front analyses were used to identify the degree of frontal activity. In the pre-frontal band, an active band was associated with a sharp thickness ridge (1000/500 mb), while an inactive band was associated with flat thickness ridge. This result differs from that found in Kress and Zwatz-Meise's study (1980-a) over Europe. It was also noted that more than one pre-frontal band may develop.

The classification of orographic bands was found to be difficult, since the mountainous terrain interacts with the flow in a complicated manner. Comma cloud patterns were also, at times, difficult to classify because of the large variations in size, ranging from large synoptic to small meso-scale. Non-organized cellular patterns, which may develop into a comma system, presented simillar problems because of the lack of clearly definable horizontal dimensions.

The comparison between the upper-level model and other models leads to the following considerations:

In Weldon's (1976) model, jet (2) (see Figure 5.1) plays the dominant role in development, while jet (1) does not. The splitting stage can be considered in two stages as shown in Figures 5.1 and 5.2. Jet (1) decays quickly (see Figure 5.3), while Jet (2) moves rapidly through the system after the cut-off stage (see Figures 5.5 and 5.6). Contrary to Weldon's findings, the splitting of the mid-level flow may occur in non-mountainous areas.

In Zwatz-Meise's cold-low model (1972 and 1979), summer case studies show a distinct pattern of flow development. The closed circulation is likely to develop in the fourth stage ( see Figure 5.4) and not during the first stage. The enhanced-cumuli or pre-comma cloud pattern is likely to develop in the southeast sector of the elongated trough. The cut-off (see Figure 5.4) is an important stage in the life cycle of a storm, and the various cloud areas may persist up to the decay stage, (Figure 5.6).

The comparison between the results of the present study and the Petterssen-Smebye's results published in 1971 can be summarised as follows. Good agreement exists between the different schemes classifying the upper-level lows into pure and modified systems. The examination of case studies (in Chapter 4) supports this classification with one minor difference. In pure cases of cyclonic development, a low-level front did not show up on satellite images nor on synoptic maps. Whereas, in modified cases, a low-level front was usually analysed on synoptic maps but without any corresponding support discernable on satellite images. The hypothesis that the development of comma cloud area (B) represents that for the whole upper-level system has yielded fair results. Adopting this hypothesis, a new mechanism for development may be presented:

Synoptic cloud pattern development of an upper cold-low system commences when an elongated trough with a strong absolute vorticity field spreads over an area of enhanced-cumuli clouds.

The correlation between the development of the comma cloud area (B) and the absolute vorticity field has yielded the following results:

-The absolute vorticity contour = 16 X $10^{-5}$ $s^{-1}$ can be used to distinguish between weakening and strengthening cases.

-If (B) lies within a contour greater than 16 X $10^{-5}$ $s^{-1}$, strengthening may be expected in 82 per cent of the cases.

-If (B) lies within a contour less than 16 X $10^{-5}$ $s^{-1}$, weakening may be expected in 74 per cent of the cases.

On the other hand, the correlation between the vorticity advection field or the thermal advection field and the comma cloud area (B) development was found to be poor.

Finally, upper-level low systems may be classified into three groups: strong, moderate and weak. A strong system is one at which the cloud pattern reaches storm configuration. An upper low system is said to be moderate if it develops a well-defined comma pattern, while it is said to be weak if the pattern fails to develop any discernable comma cloud area, regardless of other cloud development.

### 5.5 Suggestions for Future Studies

In order to have better understanding of the problem of upper-cold low cyclogenesis and development, it is suggested that future work be carried out on the following problems:

-The production of vorticity at higher levels, e.g. 300-mb, 200-mb.

-The dissipation of energy due to friction at lower levels.

-Objective analysis of the vorticity and thermal advections at different levels and their relation with the comma cloud area.

-Objective analysis of comma cloud area weakening or strengthening.

-The relation between the comma cloud area development and other meteorological parameters, such as the moisture field, vertical instability, and vertical motion.

# Bibliography

Anderson, R. K., Ferguson, E. W., and Oliver, V. J., 1966: The Use of Satellite Pictures in Weather Analysis and Forecasting, WMO Tech. Note #75.

Anderson, R. K., Ashman, J. P., Farr, G. R., Ferguson, E. W., Isayeva, G. N., Oliver, V. J., Parmenter, F. C., Popova, T. P., Skidmore, R. W., Smith, A. H., and Velishchev, N. F., 1973: The Use of Satellite Pictures in Weather Analysis and Forecasting, WMO Tech. Note #124.

Anderson, R. K., Ashman, J. P., Bittner, F., Farr, G. R., Ferguson, E. W., Oliver, V. J., and Smith, A. H., 1974: Application of Meteorological Satellite Data in Analysis and Forecasting, ESSA Tech. Rep. NESC. 51.

Bjerknes, J., and Solberg, H., 1922: Life cycle of cyclones and the polar front theory of atmospheric circulation. Geofys. Publikasjoner, Norske Videnskaps-Akad, Oslo 3, No. 1, 1-18.

Bjerknes, J., and Holmboe, J., 1944: On the theory of cyclones. J. Meteor, 1, 1-22.

Charney, J. G., 1948: On the scale of atmospheric motion. Geofys. Publ. , 17(2), 1-17.

Clark, J. D., 1983: The GOES user's guide, NOAA, NESDIS, U.S. Dept. of Commerce.

Dines, W. H., 1919: The characteristics of the free atmosphere, Geophys Mem., #13, London.

Hailzl, G., 1980: Ein Beispiel zur Erfassung eines Konvergenzbandes mit Hilfe von Satellitenbildern und Trajektorien, Veröffentlichungen der Zentralanstalt für Meteorologie und Geodynamik, Wien, No. 243.

Kress, Ch., and Zwatz-Meise, V., 1980-a: Ein Beispiel der Interpretation einer Wetterlage durch Satellitenbild und Diagnose-Parameter, Veroffentlichungen der Zentralanstalt fur Meteorologie und Geodynamik, Wien.

Maddox, R. A., 1980: Mesoscale Convective Complexes, BAMS, Vol. 61, No. 11, 1374-1387.

Margules, M., 1904: Über die Beziehung zwischen Barometerschwankung und Kontinuitätsgleichung. Boltzmann Festschrift. Leipzig, 585-589.

Namias, J., and Clapp, P., 1949: Confluence theory of the high-tropospheric jet stream, J. Meteor., 6, 330-336.

Orlanski, I., 1975: A rational subdivision of scales for atmospheric processes, BAMS, Vol. 56, No. 5, 527-530.

Petterssen, S., 1955: A general survey of factors influencing development at sea level, J. Meteor., 12, 36-42.

Petterssen, S., 1956: Weather Analysis and Forecasting, Vol. I, 2nd ed., McGraw-Hill Book Co.

Petterssen, S., and Smebye, S. J., 1971: On the development of extratropical cyclones, Quart. J. Roy. Meteorol. Soc., Vol. 97, 457-482.

Reed, R.J., 1979: Cyclogenesis in polar air streams, MWR, Vol. 107, 38-52.

Reinelt, E. R., Hof, P., Oracheski, D., and Broszkowski, J., 1975: Research Studies of Numerical Enhancement of APT Scanning Radiometer Data for Application to Arctic Weather and Ice Prediction, Final Report, DDS (AES), Contract OSV4-0183, U. of Alberta.

Reiter, E. R., 1963: Jet-stream meteorology, Chicago, University press.

Riehl, H., and Teweles, S. Jr., 1953: A further study on the relation between jet stream and cyclone formation, Tellus, 5(1), 66-79.

Riehl, H., 1954: The jet stream, Meteorological Monograph, AMS, Vol. 2, #7.

Scherhag, R., 1934: Die Bedeutung der Divergenz fur die Entstehung der vb-Depression. Ann. Hydrograph, Berlin, 62.

Schwalb, A., 1978: The TIROS-N/NOAA A-G satellite series, NOAA Tech. Memo. NESS 95.

The Office of the System Engineering, 1979: Geostationary operational environmental satellite/data collection system, NOAA Tech. Report NESS, 78.

Thepenier, R. M., and Gruette, D., 1981: Formation of cloud bands associated with the American subtropical jet stream and their interaction with mid-latitude synoptic disturbances reaching Europe, MWR, Vol. 109.

Weber, E. M., and Wilderotter, S., 1981: 3 WW/TN- 81/001 Tech. note, Third Weather Wing Offutt AFB NE 68113.

Weldon, R. B., 1975-1979: Part-I, Basic cloud systems, Part-II, The structure of winter storms, Part-III, The cloud patterns of short scale wave system in westerlies, Part-IV, Cloud patterns and the upper wind field, NOAA/NESS.

Wieler, J. G., 1981: The Application of Satellite and Radar Data in Thunderstorm Research, M.Sc., Thesis, U. of Alberta.

WMO, 1977 : The Use of Satellite Imagery in Tropical Cyclone Analysis, Tech. Note #153, WMO-#473.

Zwatz-Meise, V., 1972: Satellitenbilder als Hilfsmittel zur Strukterbestimmung von Hohenzyklonen, Arch. Met. Geoph. Biokl., Ser. A, 21, 373-397.

Zwatz-Meise, V., 1979: Einige Beispiele zur Interpretation nichtfrontaler Wolkensysteme in Satellitenbildern, Arch. Met. Geoph. Biokl., Ser. A, 28, 233-244.

Zwatz-Meise, V., 1979: Beispiele zur prognostischen Verwendung der Bilder von Polarbahnsatelliten, Arch. Met. Geoph. Biokl., Ser. A, 28, 349-359.

Zwatz-Meise, V., and Hailzl, G., 1980-b: Interpretation of so-called shear bands in satellite images, Arch. Met. Geoph. Biokl., Ser. B, 28, 299-315.

Zwatz-Meise, V., 1981: Use of satellite images and derived meteorological parameters for weather analysis and forecasting; Remote Sensing in Meteorology, Oceanography, and Hydrology; 412-451; Ellis Horwood Ltd.